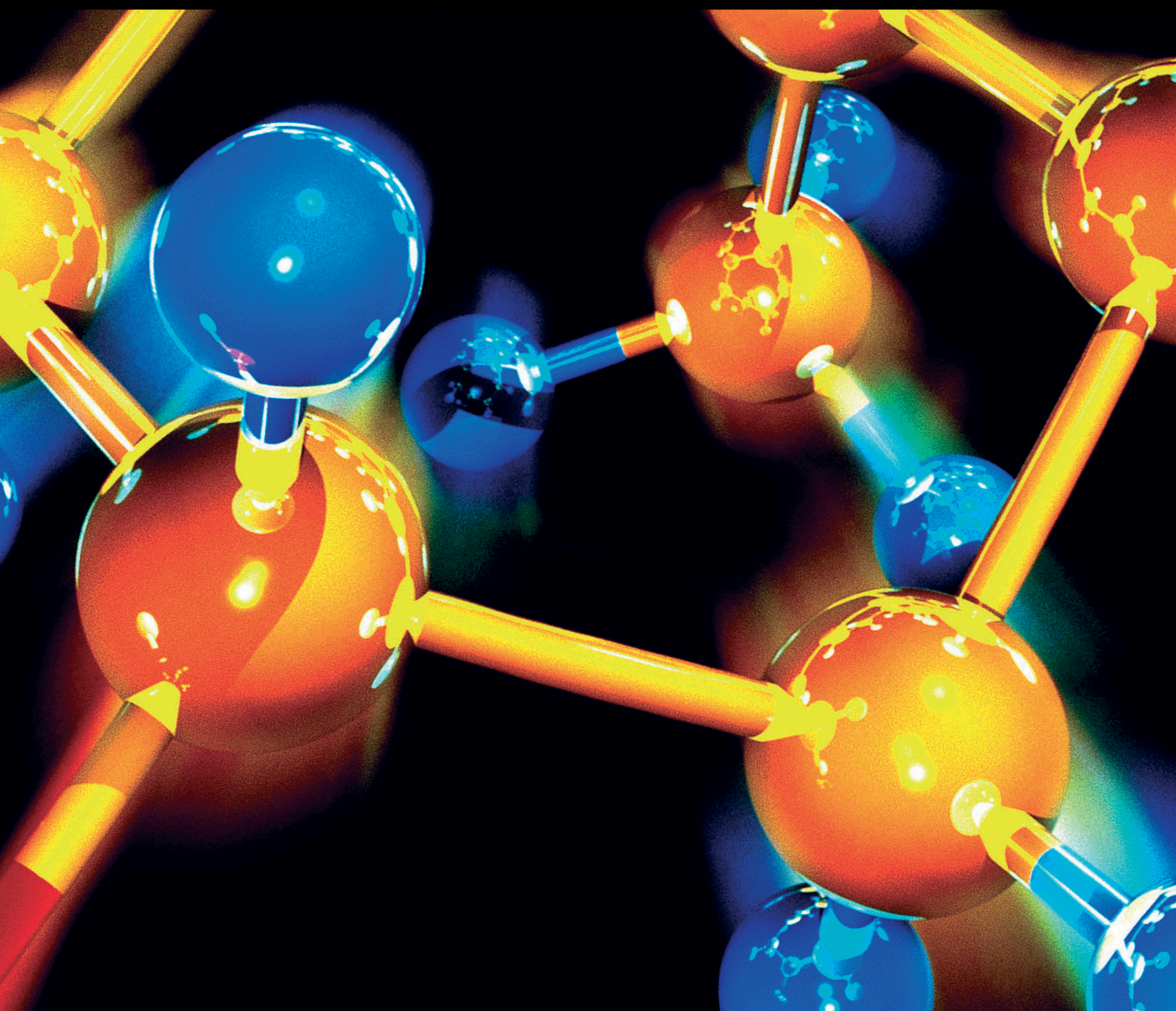


Environmental Behavior and Effects of Pollutants in Water

Lead Guest Editor: Chenglian Feng

Guest Editors: Lisa Yu, Yihua Xiao, and Chunjiang An





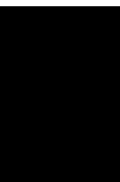
Environmental Behavior and Effects of Pollutants in Water

Journal of Chemistry

Environmental Behavior and Effects of Pollutants in Water

Lead Guest Editor: Chenglian Feng

Guest Editors: Lisa Yu, Yihua Xiao, and Chunjiang
An



Copyright © 2020 Hindawi Limited. All rights reserved.



This is a special issue published in "Journal of Chemistry." All articles are open access articles distributed under the Creative Commons Attribution License, which permits unrestricted use, distribution, and reproduction in any medium, provided the original work is properly cited.

Editorial Board


Luqman C. Abdullah, Malaysia
Daryoush Afzali, Iran
Mohammad A. Al-Ghouthi, Qatar
Shafaqat Ali, Pakistan
Claudio Cameselle, Spain
Zenilda Cardeal, Brazil
Claudia Crestini, Italy
Shayessteh Dadfarnia, Iran
Fatih Deniz, Turkey
Claudio Di Iaconi, Italy
Yingchao Dong, China
Valdemar Esteves, Portugal
Alberto Figoli, Italy
Andrea Gambaro, Italy
Wenshan Guo, Australia
Ewa Kaczorek, Poland
Mostafa Khajeh, Iran
Woojin Lee, Kazakhstan
Carlos A Martínez-Huitle, Brazil
Mehrab Mehrvar, Canada
Saima Q. Memon, Pakistan
Maurice Millet, France
Kaustubha Mohanty, India
José Morillo, Spain
Khaled Mostafa, Egypt
Pedro Avila Pérez, Mexico
Nicolas Roche, France
Stéphanie Sayen, France
Darren Sun, Singapore
Sedat Yurdakal, Turkey
Minghua Zhou, China

Contents


Environmental Behavior and Effects of Pollutants in Water

Chenglian Feng , Lisa Yu , Yihua Xiao, and Chunjiang An
Editorial (2 pages), Article ID 2639389, Volume 2020 (2020)



The Interaction Test of Binary Mixtures of Endocrine-Disrupting Chemicals Using In Vitro Bioassays

Qianqian Tang, Bingli Lei , Yun Liu, Xiaolan Zhang, Qian Liu, and Su Sun
Research Article (12 pages), Article ID 9729015, Volume 2020 (2020)




Progress in the Research of the Toxicity Effect Mechanisms of Heavy Metals on Freshwater Organisms and Their Water Quality Criteria in China

Ya-jun Hong, Wei Liao, Zhen-fei Yan, Ying-chen Bai, Cheng-lian Feng , Zu-xin Xu, and Da-yong Xu 
Review Article (12 pages), Article ID 9010348, Volume 2020 (2020)

Kinetic Study of the Adsorption of Polyphenols from Olive Mill Wastewater onto Natural Clay: Ghassoul

Safae Allaoui , Mohammed Naciri Bennani, Hamid Ziyat , Omar Qabaqous, Najib Tijani, and Najim Ittobane
Research Article (11 pages), Article ID 7293189, Volume 2020 (2020)


Assessing Redox Properties of Natural Organic Matters with regard to Electron Exchange Capacity and Redox-Active Functional Groups

Zhiyuan Xu , Zhen Yang, Hongping Wang , and Jie Jiang 
Research Article (8 pages), Article ID 2698213, Volume 2020 (2020)




Study on Treatment of Salicylhydroxamic Acid Wastewater from Tungsten Molybdenum Mineral Processing

Liping Zhang , Xin Zhang, Jun Xiang, Jingwen Xue, and Xuejing Song
Research Article (8 pages), Article ID 7125874, Volume 2020 (2020)




Molecular Signatures of Humic Acids from Different Sources as Revealed by Ultrahigh Resolution Mass Spectrometry

Shuai Qin, Chengbin Xu, Yingzi Xu, Yingchen Bai, and Fei Guo 
Research Article (11 pages), Article ID 7171582, Volume 2020 (2020)



Sources of Nitrogen Pollution in Upstream of Fenhe River Reservoir Based on the Nitrogen and Oxygen Stable Isotope

Ying Zhao , Jinhua Dang , and Fei Wang 
Research Article (8 pages), Article ID 6574210, Volume 2020 (2020)

Distributions and Sources of Sedimentary Sterols as well as Their Indications of Sewage Contamination in the Guanting Reservoir, Beijing

Xin Wen, Yijuan Bai , Shurong Zhang , Aizhong Ding, Lei Zheng, and Jian Li 
Research Article (11 pages), Article ID 3050687, Volume 2020 (2020)

Campus Sewage Treatment by Golenkinia SDEC-16 and Biofuel Production under Monochromic Light

Changliang Nie , Liqun Jiang, Ze Yu, Zhigang Yang, Qingjie Hou, and Haiyan Pei 


Research Article (9 pages), Article ID 5029535, Volume 2020 (2020)

Ranking Ecological Risk of Metals to Freshwater Organisms in Lake Taihu, China

Qi Wang , Yalin Du , Fuhong Sun , Xinmiao Deng , and Hong Chang 

Research Article (6 pages), Article ID 2536207, Volume 2020 (2020)

Aerobic Biodegradation of Four Groups of Steroid Hormones in Activated Sludge

Jiaxin Zhang, Jun Luo, and Hong Chang 








Research Article (8 pages), Article ID 1309183, Volume 2020 (2020)

Effects of Urbanization on Water Quality and the Macrobenthos Community Structure in the Fenhe River, Shanxi Province, China

Linfang Wang, Hua Li , Jinhua Dang , Ying Zhao, Yu'en Zhu, and Pengming Qiao


Research Article (9 pages), Article ID 8653486, Volume 2020 (2020)

Polycyclic Aromatic Hydrocarbons in Surface Water from Wuhai and Lingwu Sections of the Yellow River: Concentrations, Sources, and Ecological Risk

Yun Liu , Qingwei Bu , Hongmei Cao , Handan Zhang , Chuansheng Liu , Xiaofan He , and Mengqi Yun 


Research Article (8 pages), Article ID 8458257, Volume 2020 (2020)

Thyroid-Disrupting Activities of Groundwater from a Riverbank Filtration System in Wuchang City, China: Seasonal Distribution and Human Health Risk Assessment

Dongdong Kong, Hedan Liu, Yun Liu, Yafei Wang, and Jian Li 



Research Article (9 pages), Article ID 2437082, Volume 2020 (2020)

Investigating the Impact of Anthropogenic and Natural Sources of Pollution on Quality of Water in Upper Indus Basin (UIB) by Using Multivariate Statistical Analysis

Mansoor A. Baluch  and Hashim Nisar Hashmi



Research Article (13 pages), Article ID 4307251, Volume 2019 (2019)

Neglect of Temperature and pH Impact Leads to Underestimation of Seasonal Ecological Risk of Ammonia in Chinese Surface Freshwaters

Zhen-Guang Yan, Jun-Tao Fan, Xin Zheng, Shu-Ping Wang, Xiao-Shan Guo, Tian-Xu Zhang, Su-Wen Yang , and Yi-Zhang Zhang 

Research Article (7 pages), Article ID 3051398, Volume 2019 (2019)



Modeling of Flocculation and Sedimentation Using Population Balance Equation

Zhipeng Shi , Genguang Zhang , Yuzhuo Zhang, Tingting He, and Guoliang Pei

Research Article (10 pages), Article ID 9187204, Volume 2019 (2019)


Contents

Effect of Colloidal Silicate on the Migration Behaviour of Strontium in Groundwater Environment of Geological Disposal Candidate Site

Rui Zuo , Kexue Han , Rongtao Shi, Fei Ding, Li Liu, Jinsheng Wang, Yanguo Teng, Jie Yang, and Xin Liu

Research Article (11 pages), Article ID 9606121, Volume 2019 (2019)

Distribution and Bioaccumulation of Perfluoroalkyl Acids in Xiamen Coastal Waters

Zhineng Dai  and Fansheng Zeng

Research Article (8 pages), Article ID 2612853, Volume 2019 (2019)

Editorial

Environmental Behavior and Effects of Pollutants in Water

Chenglian Feng ¹, **Lisa Yu** ², **Yihua Xiao**,^{3,4} and **Chunjiang An**⁵

¹State Key Laboratory of Environmental Criteria and Risk Assessment, Chinese Research Academy of Environmental Sciences, Beijing, China

²Civil and Environmental Engineering, Temple University, Philadelphia, PA, USA

³Department of Biological and Environmental Science, University of Jyväskylä, Jyväskylä, Finland

⁴School of Environmental & Municipal Engineering, Qingdao University of Technology, Qingdao, China

⁵Department of Building, Civil and Environmental Engineering, Concordia University, Montreal, Canada

Correspondence should be addressed to Chenglian Feng; fengcl@craes.org.cn

Received 5 August 2020; Accepted 5 August 2020; Published 17 September 2020

Copyright © 2020 Chenglian Feng et al. This is an open access article distributed under the Creative Commons Attribution License, which permits unrestricted use, distribution, and reproduction in any medium, provided the original work is properly cited.

Water pollution caused by anthropogenic activities is one of the major environmental problems in the world. Persistent toxic substances can be divided into two categories, mainly persistent organic pollutants and heavy metals. Persistent toxic chemical pollutants have become a problem of global concern. They have high bioaccumulation properties and are extremely difficult to degrade. They can realize long-distance transmission. They contain carcinogenic and mutagenic factors and have strong endocrine interference. International environmental protection organizations, governments, and researchers all over the world have paid close attention to this issue. A large number of hazardous substances such as heavy metals, petrochemicals, pharmaceuticals, nanomaterials, pesticides, and herbicides are released into the aquatic environment intentionally or unintentionally during industrialization and urbanization, endangering wildlife and human health. However, there are significant differences in environmental behavior and toxicity of different types of pollutants. For example, heavy metals in water may exist in different forms, which in turn may be altered by environmental conditions such as the presence of different types of organic matter, the pH and hardness of the water system, and form transformation, thus affecting their behavior and bioavailability. The biological effects and toxicological mechanisms of organic pollutants are more complex. Some organic pollutants are hydrophobic and tend to accumulate in aquatic organisms, while others are hydrophilic and easily migrate in water. Therefore,

studies into the environmental behavior and ecological effects of these pollutants in aquatic environments are required.

This special issue aims to bring innovative articles on the environmental behavior and effects of anthropogenic pollutants in aqueous environments. It mainly includes the transport, fate, toxic effects, and environmental management of pollutants. The articles received by the journal were carefully selected, thus offering a high-quality collection. A total of 19 articles have been accepted, and several representative articles are listed below.

Y. Hong et al. review paper titled “Progress in the Research of the Toxicity Effect Mechanisms of Heavy Metals on Freshwater Organisms and Their Water Quality Criteria in China” introduced the sources, hazard levels, toxic effect mechanisms, and the current research status of water quality criteria for heavy metal pollutants in China. In addition, the focus and direction of future research on the toxic effects of heavy metals on aquatic organisms and the necessary changes in criteria were also discussed. This review paper would provide an important theoretical basis for the future research of water quality criteria and risk assessment of heavy metal pollutants.

Z. Yan et al. presented a paper on the influence of temperature and pH on the risk of ammonia nitrogen (AN). They collected the ecotoxicity and exposure data of AN in Chinese surface freshwaters in 2017. The species sensitivity distribution of AN was established, and the ecological risk of

AN in Chinese surface waters was assessed. Ecological risk assessments on AN suggested that, in summer and autumn, when the water temperature and pH are high, the risk of AN may occur at some sites with good water quality. The authors pointed out that neglecting water parameters' impact may lead to underestimation of ecological risk of AN in Chinese basins.

J. Zhang et al. presented a paper on aerobic biodegradation of four groups of steroid hormones in activated sludge. They first developed an analytical method for simultaneously monitoring four groups of 29 steroid hormones in a single water sample. Laboratory studies were then performed to investigate their aerobic biodegradation which was found to follow first-order reaction kinetics. Among all of the target hormones, halogenated glucocorticoids were more persistent than others. In addition, C-21 ester glucocorticoids were more prone to decomposition than C-17 esters. Hydrolysis did not significantly affect the decomposition of esterified steroids.

B. Lei et al. presented a paper titled "The Interaction Test of Binary Mixtures of Endocrine-Disrupting Chemicals Using *In Vitro* Bioassays." In this study, they evaluated the combined effects of estradiol valerate (EV) and other four endocrine-disrupting chemicals on the human breast MCF-7 cells by detecting the cell proliferation, intracellular reactive oxygen species (ROS) levels, and estrogen receptor alpha (ER α) protein expression using the equal concentration ratio method. The authors found that EV had the strongest effect in inducing cell proliferation. They concluded that the joint toxicity of binary mixtures of EV and other EDCs do not interact in a synergistic fashion in inducing cell proliferation, intracellular ROS levels, and ER α protein expression.

Kong et al. presented a paper on human health risk assessment of thyroid-disrupting activities of groundwater from a riverbank filtration (RBF) system in Wuchang City, China. They used TRgene yeast assay to reveal the presence of thyroid-disrupting activities in the groundwater from the RBF system. And then, they applied a novel risk assessment approach to assess the impact of thyroid hormones on humans. Their study shows that RBF systems can remove the TDCs from river water and samples collected during the dry season had higher TR antagonistic activity. These findings are highly relevant to environmental safety and human health and will provide an important scientific basis for drinking water safety.

Dai and Zeng investigated the distribution and bioaccumulation of perfluoroalkyl acids (PFAs) in the Xiamen coastal area where there were no rivers from other cities. In their study, six types of PFAs were analyzed in water, sediments, and organisms from both freshwater and seawater. The results showed that the PFA concentration in water was positively correlated with the PFA concentration in sediments. The bioaccumulation factors were also calculated with the quantity of PFAs in different trophic levels of aquatic organisms. The findings of this study can be used to support the environmental management of organic pollutants in the coastal area.

Considering the current special issue, we think the selected articles offer an ideal opportunity to update our knowledge on environmental behavior and effects of different pollutants in water environment.

Conflicts of Interest

The guest editors have no conflicts of interest to declare.


Acknowledgments

The editors thank all the authors for their contributions.

Chenglian Feng
Lisa Yu
Yihua Xiao
Chunjiang An

Research Article

The Interaction Test of Binary Mixtures of Endocrine-Disrupting Chemicals Using *In Vitro* Bioassays

Qianqian Tang,¹ Bingli Lei ,¹ Yun Liu,² Xiaolan Zhang,¹ Qian Liu,¹ and Su Sun¹

¹Institute of Environmental Pollution and Health, School of Environmental and Chemical Engineering, Shanghai University, Shanghai 200444, China

²South China Institute of Environmental Sciences, MEP, 7 West Street, Yuancun, Tianhe District, Guangzhou 510655, China

Correspondence should be addressed to Bingli Lei; leibingli@126.com

Received 9 August 2019; Revised 10 January 2020; Accepted 3 June 2020; Published 22 June 2020

Guest Editor: Lisa Yu

Copyright © 2020 Qianqian Tang et al. This is an open access article distributed under the Creative Commons Attribution License, which permits unrestricted use, distribution, and reproduction in any medium, provided the original work is properly cited.

Typical environmental endocrine-disrupting chemicals (EDCs) such as estradiol valerate (EV), diethylstilbestrol (DES), di-ethylhexyl phthalate (DEHP), mono-2-ethylhexyl phthalate (MEHP), and bisphenol A (BPA) have a strong reproductive and developmental toxicity at low concentrations. However, information on their joint toxicity is scarce. In this study, we evaluated the combined effects of EV and other four EDCs (DES, DEHP, MEHP, and BPA) on the human breast MCF-7 cells by detecting the cell proliferation, intracellular reactive oxygen species (ROS) levels, and estrogen receptor alpha (ER α) protein expression using equal concentration ratio method. The results showed that, after exposure for 24, 48, and 72 h, single EV, DES, and BPA can promote the proliferation of MCF-7 human breast cancer cells, and EV has the strongest effect in inducing cell proliferation. DEHP and MEHP cannot induce MCF-7 cell proliferation for all exposure time, while cell proliferation induced by EV was significantly attenuated by DES, BPA, DEHP, and MEHP when they mixed with EV. For intracellular ROS, single EV, BPA, DES, DEHP, and MEHP elevated intracellular ROS levels for different exposure time. Similar to the cell proliferation, DES and BPA decreased intracellular ROS levels induced by EV when they mixed with EV for 24 h. EV, DES, and BPA exposed alone or combined with EV upregulated the ER α protein expression. However, DEHP and MEHP exposed alone or combined with EV had no effect on ER α protein expression, indicating that DEHP or MEHP could attenuate ER α protein expression upregulated by EV. These results showed that the joint toxicity of binary mixtures of EV and other EDCs do not interact in a synergistic fashion in inducing cell proliferation, intracellular ROS levels, and ER α protein expression. These findings have important implications in the human risk assessments of EV mixed with other EDCs in the environment.

1. Introduction

Environmental endocrine-disrupting chemicals (EDCs) such as estradiol valerate (EV), diethylstilbestrol (DES), bisphenol A (BPA), diethylhexyl phthalate (DEHP), and mono-2-ethylhexyl phthalate (MEHP) bring up prevalent attention because they have a strong reproductive and developmental toxicity on human and various animal species at low doses [1, 2].

EV is one of the most common sources of free E2 in hormone replacement therapy [3]. In animal farming, EV is mainly applied as a growth promoter [4] and for developing a single-sex population of fish in aquaculture [5, 6]. EV may act as an endocrine disruptor and adversely affect

reproductive outcome [7]. EV has been detected in natural waters in China, and its concentration range is approximately 1–10 ng/L [8, 9]. DES was the first synthetic estrogen originally used for clinical therapy to prevent miscarriages. However, exposure to DES can cause adverse effects on male and female reproductive tracts in humans, even causing developmental anomalies in subsequent generations [10]. Though the use of DES has been banned in humans, it is still employed in livestock and aquaculture operations as a growth promoter or to produce monosex (female) populations of fish in some parts of the world [11]. DES is also quite potent in aquatic organisms such as fish and may be comparable to, or even exceed, that of 17 α -ethinylestradiol (EE2) with a predicted no-effect concentration (PNEC) in

fish lower than 1 ng/L [12]. Detectable concentrations of DES in surface water and effluents from different locations have been reported to range from slightly below 1 to greater than 10 ng/L [13–16]. BPA, as one of the high-volume chemicals produced worldwide, has wide applications in organic synthesis industry as raw material in the manufacture of plastics and epoxy resins [17]. BPA has been widely detected in various environmental media, foodstuffs, and human samples [17]. Exposure to BPA has shown low-dose effects including disturbed mammary gland development, changes in normal behavioral development, and changes in obesity associated parameters in rodents [17]. DEHP and MEHP belong to phthalates, and MEHP is metabolite of DEHP. DEHP is used in raw materials of clothing, food packaging, building, and children's products [18]. DEHP pollution has raised public concern, especially after the plasticizer incident in Taiwan in May 2011. High levels of DEHP are detected in municipal domestic waste, soil, rivers, fruits, vegetables, plastic-wrapped food, and medical devices to which people are closely related. A recent study indicated that the concentration of DEHP was 78 $\mu\text{g/L}$ in Bohai Sea (in Tianjin, China), and MEHP was also found at a relatively high concentration [19]. DEHP has been reported to have carcinogenic, mutagenic, and hepatotoxic effects [20]. These compounds can affect the reproductive health of organisms at low concentrations. However, the estrogen activity and reproductive toxicity have been extensively studied mainly based on individual EDCs. Few studies have addressed the joint effects of mixtures of these compounds on estrogen-dependent responses. Estrogen activity of these individual EDCs is relatively weak; even DEHP and MEHP present antiestrogenic activity [21, 22]; however, the "real-life" mixtures of EDCs may carry significant biological potency [18]. Therefore, the joint toxicity of complex EDCs should not be ignored and potential interactions of weakly anti- or estrogenic substances could have important implications for public health.

The estrogen-sensitive tumor cell proliferation is an ideal method for evaluating estrogenic activity of compounds [23]. Occurrence of reactive oxygen species (ROS) in estrogen-sensitive cells has been a common response of chemical estrogenic activity [24]. For environmental estrogen, it is widely accepted that a moderate increase of ROS can stimulate proliferation of estrogen-sensitive tumor cells [25, 26]. Besides, environmental estrogen can induce estrogen-sensitive cell proliferation and may increase mitochondrial ROS production by estrogen receptor α/β ($\text{ER}\alpha/\beta$) pathway [27]. In this study, we evaluate the effects of single EV, DES, BPA, DEHP, and MEHP on proliferation of MCF-7 cells to assess their estrogen activities. Among these EDCs, EV induced the highest MCF-7 cell proliferation. Its estrogenic potency is similar to estradiol (E2). To evaluate influence of other EDCs on cellular biological effects induced by EV, we further assess joint toxicity of the binary mixtures of EV and other four EDCs by measuring the cell proliferation, ROS generation, and $\text{ER}\alpha$ expression in MCF-7 cells. In order to simplify the joint toxicity experimental method, the equal concentration ratio mixing method was widely recommended in joint toxicity mechanism research of binary mixtures

[28, 29]. In this study, we also used equal concentration ratio mixing method to study joint toxicity of binary mixtures of EV and the other four EDCs. The results can provide a comprehensive understanding of binary mixture of EV and other EDCs toxicity effects.

2. Materials and Methods

2.1. Materials. E2 (estradiol), DES (diethylstilbestrol), EV (estradiol valerate), BPA (bisphenol A), DEHP (diethylhexyl phthalate), and MEHP (mono-2-ethylhexyl phthalate) were purchased from Sigma (Saint Louis, MO, USA) and were of the highest grade commercially available.

The stock solutions of all target chemicals were prepared in dimethyl sulfoxide (DMSO, 99.5%, AMRESCO, PA, USA) and were stored at -20°C . Cell Counting Kit-8 (CCK-8) was purchased from Dojindo (Kumamoto, Japan). 2',7'-Dichlorodihydrofluorescein diacetate (DCFH-DA) and tert-butyl hydroperoxide (tBHP) were purchased from Sigma (Saint Louis, MO, USA). MCF-7 breast cancer cell line was purchased from American Tissue Culture Collection (Rockville, MD, USA). All other reagents used were analytical grade chemicals from Sigma (Saint Louis, MO, USA), if not otherwise stated.

2.2. Maintenance and Treatments of MCF-7 Cells. In our previous study, cell maintenance and treatment of MCF-7 cells are described in detail [30]. The specific process is that stock cultures of MCF-7 cells were maintained in regular RPMI 1640 medium (HyClone, Logan, UT, USA) containing 10% fetal bovine serum (FBS) (Gibco, Grand Island, NY) and supplemented with 100 U/mL penicillin and 100 U/mL streptomycin (Invitrogen, Burlington, ON, Canada) in a humidified atmosphere at 37°C with 5% CO_2 . The medium was changed every 2–3 d.

The exponential growth phase cells were used for the experiments. Before each experiment, cells were starved in steroid-free (SF) medium for 24 h to minimize the basal hormonal levels during assays and allow cell adhesion. SF medium consists of phenol red-free RPMI 1640 (HyClone, Logan, UT, USA) and 5% charcoal-stripped FBS (Biological Industries, Israel) supplemented with 100 U/mL streptomycin/penicillin. 0.1% DMSO was used as the solvent control in each experiment. For ROS experiment, 400 μM tBHP was used as the positive control. In this study, we followed the methods described by Lei et al. 2017 [30]. The tBHP significantly increased intracellular ROS production and the ROS level (compared to control $\times 100$) of MCF-7 cells treated with 400 μM tBHP was $280 \pm 35.6\%$.

2.3. Cell Viability Assay. In order to study the proliferation effect of tested compounds on MCF-7 cells, CCK-8 was used to measure the viability of MCF-7 cells. The specific experiment methods were provided elsewhere [23, 30]. Briefly, the treated cells were added with the CCK-8 reagents (10 μL in 90 μL phenol red-free RPMI 1640 per well), and optical density (OD) was read with a Multiskan MK3 plate reader (Thermo Electron Corporation, Waltham, MA, USA) at a

wavelength of 490 nm. The OD value can reflect the number of living cells indirectly, and cell viability (% of control) was calculated according to the OD values of exposure group and control group.

For joint toxicity, the cells were exposed to binary mixtures of EV and the other four EDCs according to equal concentration ratio method. The corresponding cell viability was detected.

2.4. ROS Detection. Intracellular ROS were assayed using a fluorescent dye DCFH-DA. The specific experiment methods were provided elsewhere [30]. Briefly, the treated cells were incubated with 50 μL DCFH-DA (2×10^{-4} M) at 37°C for 30 min in the dark, and the fluorescence was evaluated under a fluorescence microscope (Olympus BX-51; Olympus, Japan). The intensity of fluorescence was analyzed by Image-Pro Plus 6.

For joint toxicity, the cells were exposed to binary mixtures of EV and the other four EDCs according to the equal concentration ratio method, and the corresponding ROS levels were detected according to the above method.

2.5. Western Blot. MCF-7 cells were collected after exposure to single E2, EV, DES, BPA, DEHP, DES (1–100 nM), and 0.1% DMSO (negative control) for 24 h. The specific experiment was described in our previous study [30]. Briefly, total protein samples of ER α were obtained by mammalian protein extraction reagent (M-PER). Equal amounts (20 μg) of protein samples were subjected to 10% sodium dodecyl sulfate-polyacrylamide gel electrophoresis (SDS-PAGE) and were transferred from the gels onto nitrocellulose membranes. The used specific monoclonal antibodies are anti-ER α (1:1000) and anti-glyceraldehyde-3-phosphate dehydrogenase (GAPDH) (1:2000).

To study the joint effect of binary mixtures of EV and the other four EDCs on ER α protein expression, the cells were coexposed to binary mixtures of EV and the four EDCs according to the equal concentration ratio method for 24 h. Thereafter, ER α protein samples were collected, and protein expression was analyzed.

2.6. Data Analysis. All results are expressed as the mean \pm standard deviation (SD). The differences between exposure groups and the negative control were tested using one-way analysis of variance with specific mean comparisons by Dunnett's test. Student's *t*-test was used to analyze the difference between two different exposure groups. Difference was considered significant at a *p* value <0.05. For E2 and EV, the concentration-response analyses were performed with four-parameter logistic curve regression analysis, and EC50 was calculated, which is the concentration that induces half of the maximum proliferation effect.

3. Results

3.1. The Effects of Tested Compounds on the Viability of MCF-7 Cells. The CCK-8 assay showed that E2 at all exposure concentrations and all exposure time significantly induced

cell viability except for the lowest concentration at 24 h (Figure 1(a)). The increases of cell viability presented very well dose-dependent, for the concentration range of 0.0001–1000 nM, and time-dependent manner. The EC50 values of E2 for 24, 48, and 72 h were 0.20, 0.16, and 0.059 nM, respectively. The cell viability reached the maximum value at about 1 nM and then reached a platform period. EV at all exposure concentrations and all exposure time significantly induced the viability of MCF-7 cells and presented a concentration-dependent manner at the concentration range of 0.0001–1000 nM (Figure 1(b)). Maximal induction of EV was caused by 100 nM for 24 h and 1000 nM for 48 and 72 h, and the highest proliferation ratio reached about 2.8 times that of the negative control. The EC50 values for 24, 48, and 72 h were 6.02, 0.40, and 0.33 nM, respectively.

The single effect of DES or EV and their joint effect on the viability of MCF-7 cells are shown in Figure 2. The cell viability was significantly induced by DES for all exposure concentrations for different exposure periods. When the cells were exposed to single DES (0–10000 nM), the cell viability increased from 100% to 200%. The joint effect of DES and EV on the viability of MCF-7 cells is shown in Figure 2. DES addition significantly attenuated cell viability induced by EV for three exposure periods and all exposure concentrations except for exposure concentration of 10000 nM at 24 h. In this exposure concentration and exposure time, DES addition significantly increased cell viability induced by EV. At 48 h, the cell viability induced by binary mixtures of EV and DES was the lowest, and binary mixtures of EV and DES showed antagonistic effect on the viability of MCF-7.

The single effect of BPA or EV and their joint effect on the viability of MCF-7 cells are shown in Figures 3(a)–3(c), respectively. BPA, only at the two highest exposure concentrations of 1000 and 10000 nM, significantly induced cell viability for three exposure periods. BPA significantly attenuated cell viability induced by EV when BPA mixed with EV according to equal concentrations except for 10000 nM for 24 h. At the highest exposure concentration of 10000 nM for 48 and 72 h, the binary mixtures of BPA and EV significantly inhibited cell proliferation. In addition, the binary mixtures of EV and BPA showed antagonistic effect on the viability of MCF-7 cells at 48 and 72 h.

The single effect of DEHP or EV and their joint effect on the viability of MCF-7 cells are shown in Figures 4(a)–4(c). DEHP cannot induce significant cell proliferation for three exposure periods. The binary mixtures of DEHP and EV induced significant cell viability; however, cell viability induced by the binary mixtures of DEHP and EV was significantly lower than that induced by single EV. This indicated that DEHP addition decreased cell viability induced by EV. Similarly, single MEHP or the binary mixtures of MEHP and EV cannot all induce significant cell viability for all exposure concentrations (Figure 5). This result indicated that MEHP addition completely inhibited cell viability induced by single EV.

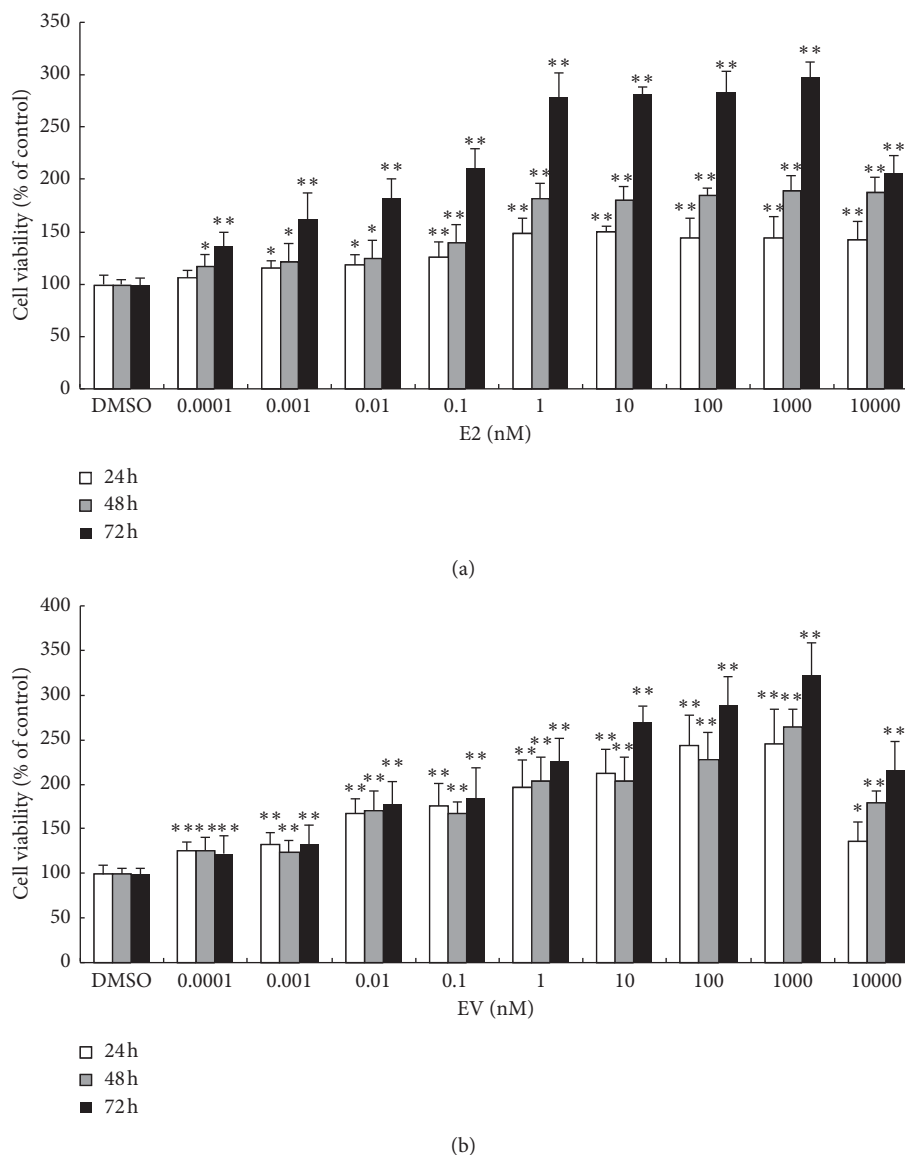


FIGURE 1: Effects of E2 (a) and EV (b) on the viability of MCF-7 cells. Data points represent mean \pm SD of three independent experiments. Asterisks show statistically significant differences with respect to corresponding negative DMSO (* $p < 0.05$, ** $p < 0.01$).

3.2. ROS Levels. As shown in Figure 6, the dose response for ROS formation is demonstrated with MCF-7 cells for individual chemicals alone or combined with EV. With the prolongation of exposure time, EV induced more ROS production. At 24 h, EV induced the highest ROS generation in MCF-7 cells. The binary mixtures of EV and other EDCs presented different change trend in inducing intracellular ROS generation for different concentrations and different exposure time.

At 24 h, the binary mixtures of EV and DES did not elevate intracellular ROS levels, while single EV significantly increased intracellular ROS levels, indicating that DES addition inhibited ROS generation induced by EV. At 1 or 3 h, the binary mixtures of EV and DES increased intracellular ROS levels, but the ROS levels induced by EV and DES mixtures were lower than those induced by single EV or DES. Similarly, at 24 h, the binary mixtures of EV and BPA cannot significantly elevate intracellular ROS levels. At 1 and

3 h, EV and BPA binary mixtures significantly increased intracellular ROS, and ROS levels induced by them were higher than those induced by single EV. The results indicated that BPA addition increased ROS levels induced by single EV for 1 and 3 h and decreased intracellular ROS levels induced by single EV for 24 h. Similarly, at 1 and 3 h, EV and DEHP mixtures significantly increased intracellular ROS levels, but the ROS levels induced by them had no significant difference between EV and DEHP binary mixtures and single EV. From the above results, at 24 h, antigenic effects of binary mixtures of EV and DES or BPA can be found in inducing intracellular ROS generation.

3.3. The Effects of Target Compounds on Protein Expression of ER α in MCF-7 Cells. To detect the effects of these EDCs on ER α protein expression in MCF-7 cells, ER α protein

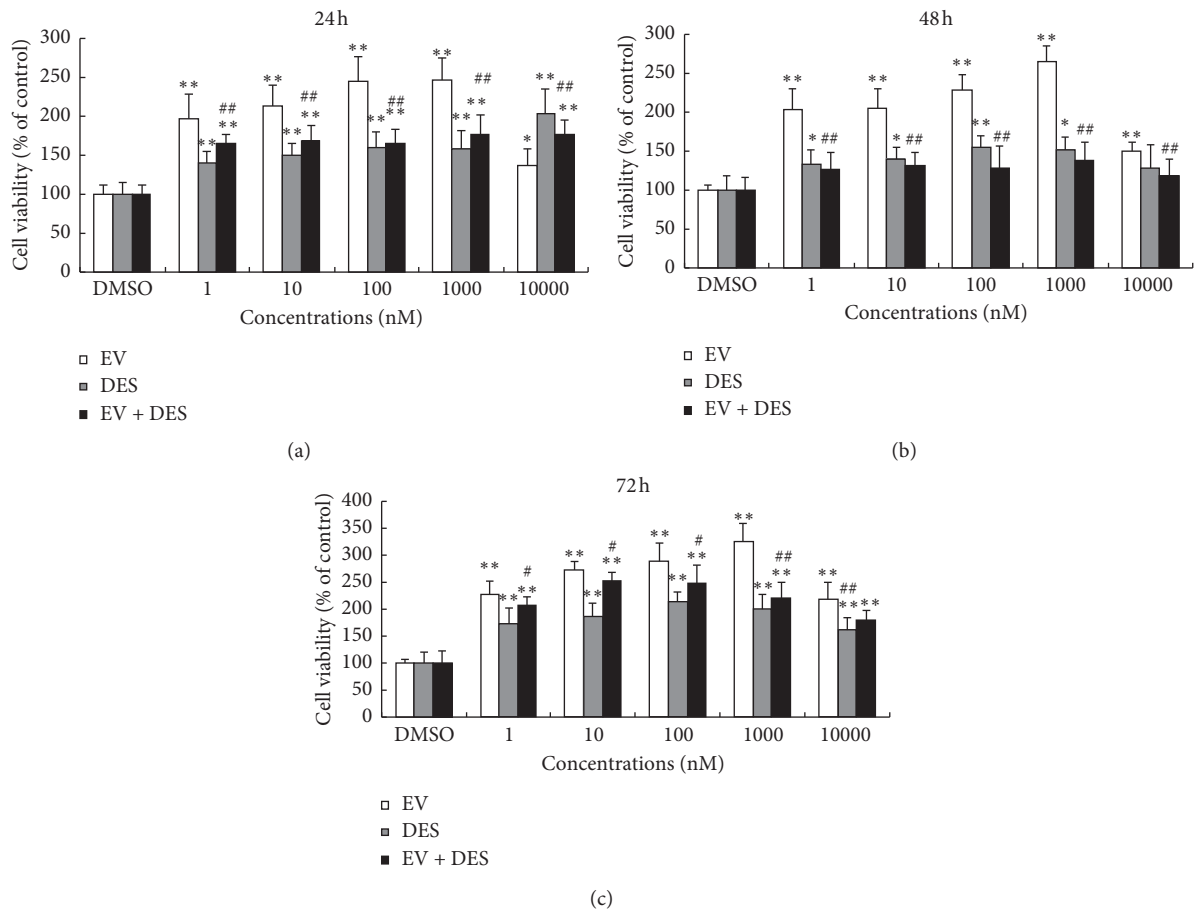


FIGURE 2: The binary joint effect of EV and DES on cell viability of MCF-7 cells. Exposure time: (a) 24 h; (b) 48 h; (c) 72 h. Data points represent mean \pm SD of three independent experiments. * $p < 0.05$, ** $p < 0.01$ compared with DMSO; # $p < 0.05$, ## $p < 0.01$, compared with EV treatment.

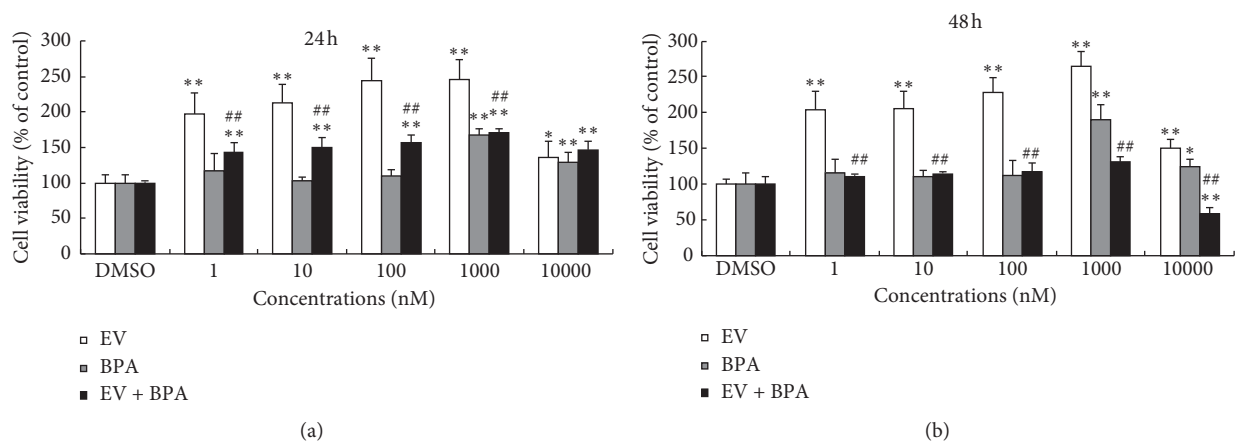
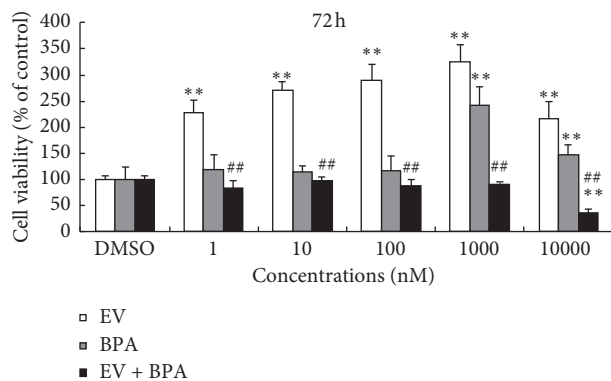
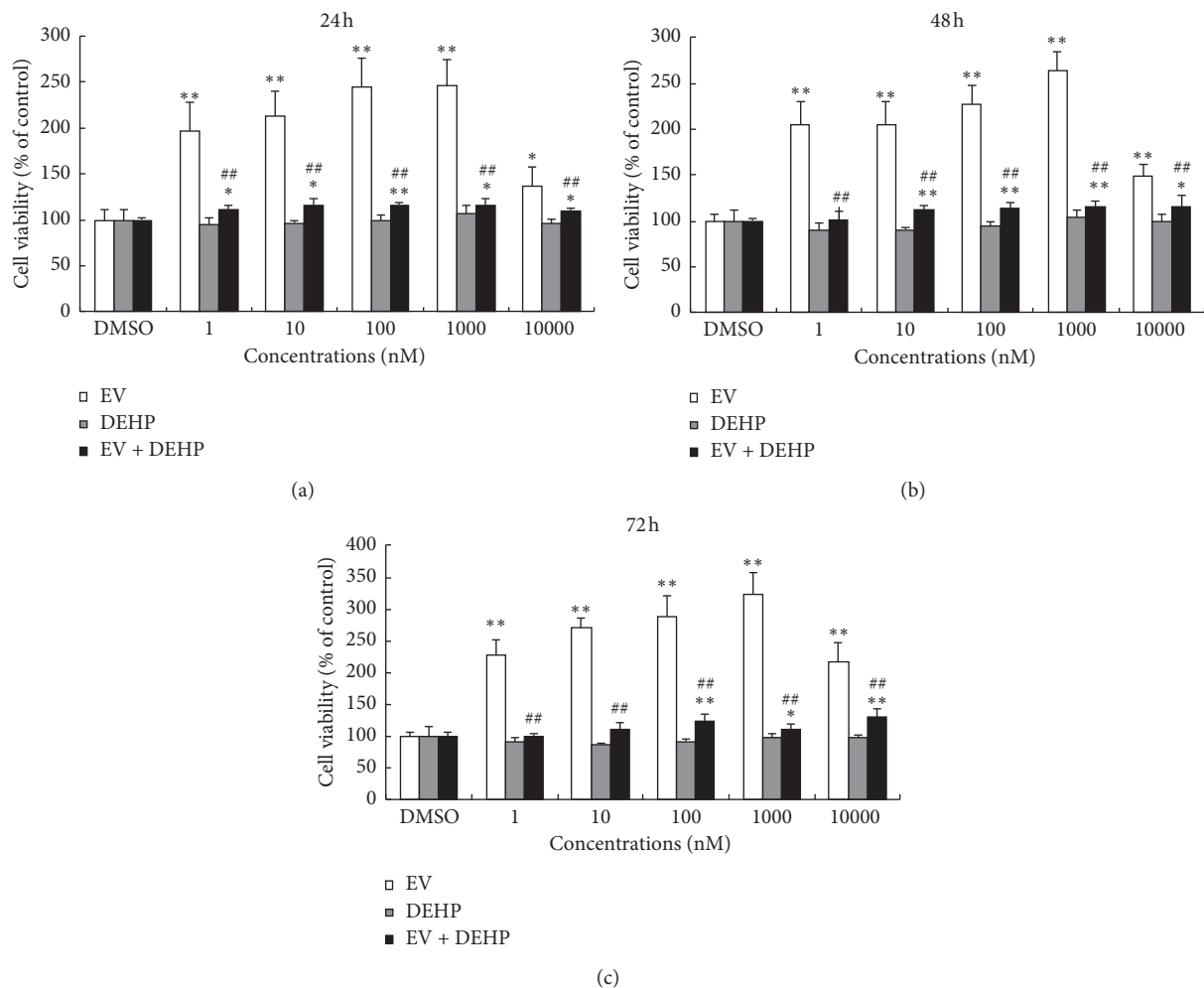


FIGURE 3: Continued.



(c)

FIGURE 3: The binary joint effect of EV and BPA on cell viability of MCF-7 cells. Exposure time: (a) 24 h; (b) 48 h; (c) 72 h. Data points represent mean \pm SD of three independent experiments. * $p < 0.05$, ** $p < 0.01$, compared with DMSO; ## $p < 0.01$, compared with EV treatment.



(a)

(b)

(c)

FIGURE 4: The binary joint effects of EV and DEHP on cell viability of MCF-7 cells. Exposure time: (a) 24 h; (b) 48 h; (c) 72 h. Data points represent mean \pm SD of three independent experiments with six replications. * $p < 0.05$, ** $p < 0.01$, compared with DMSO; ## $p < 0.01$, compared with EV treatment.

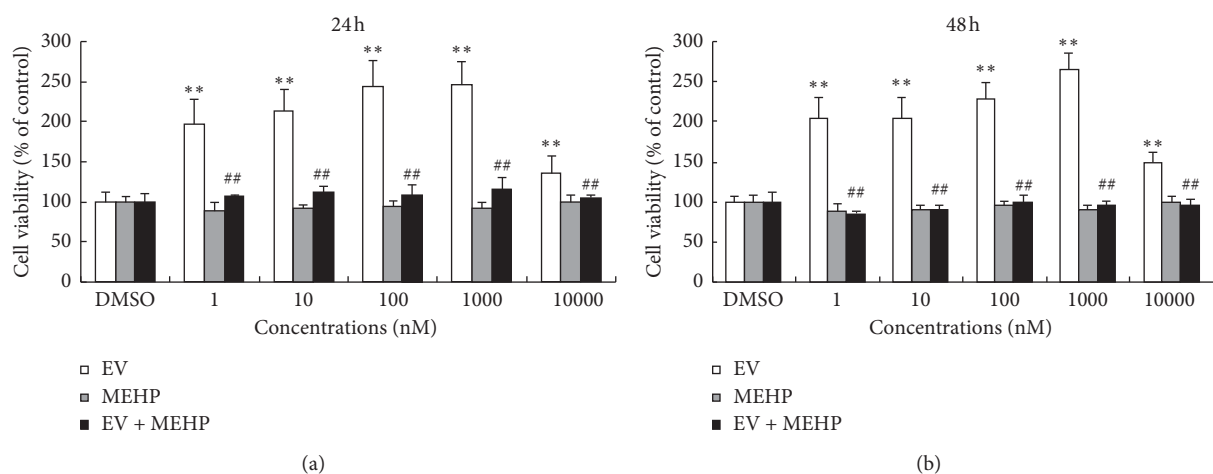


FIGURE 5: The binary joint effects of EV and MEHP on cell viability of MCF-7 cells. Exposure time: (a) 24 h; (b) 48 h. Data points represent mean \pm SD of three independent experiments with six replications. * $p < 0.05$, ** $p < 0.01$, compared with DMSO; ## $p < 0.01$, compared with EV treatment.

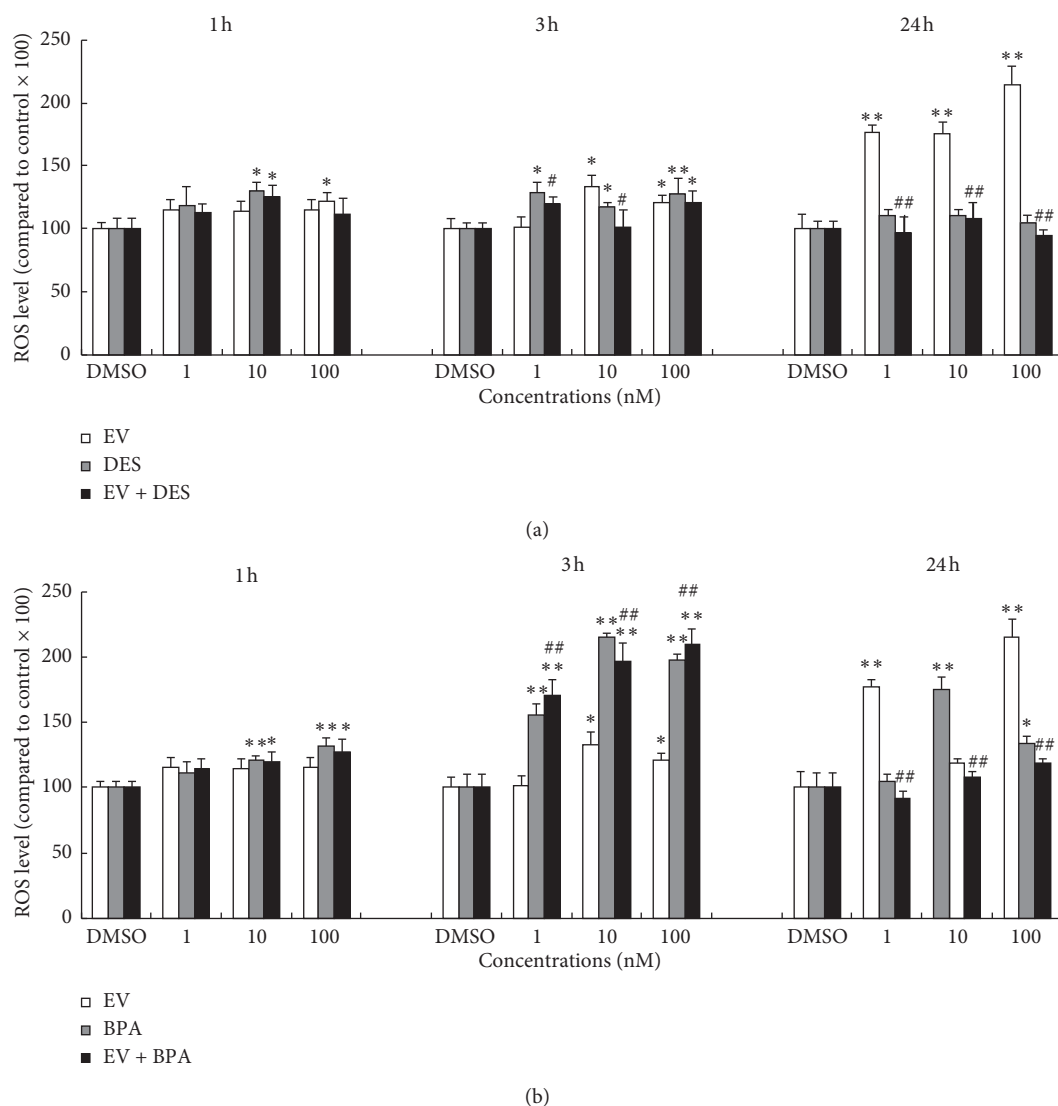


FIGURE 6: Continued.

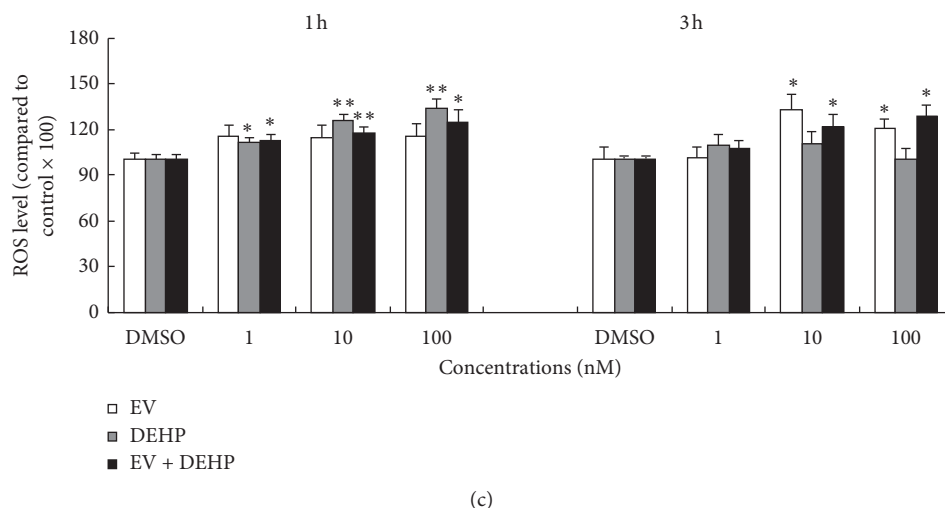


FIGURE 6: The binary joint effects of tested compounds and EV on the intracellular ROS generation in MCF-7 cells. A binary joint system of (a) DES and BPA; (b) BPA and EV; (c) DEHP and EV. Data points represent mean \pm SD of three independent experiments. * $p < 0.05$, ** $p < 0.01$, compared with DMSO; # $p < 0.05$, ## $p < 0.01$, compared with EV treatment.

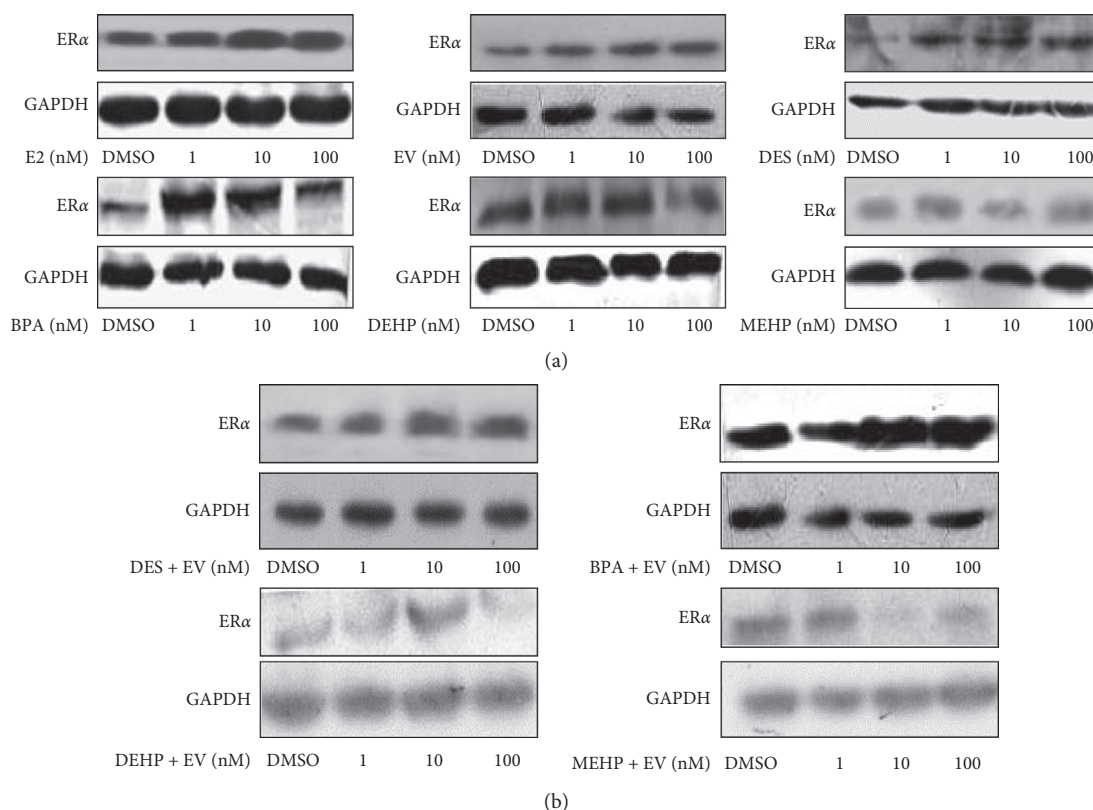


FIGURE 7: Effects of single EDCs (1–100 nM) on the expression of ER α by western blot analysis (a); joint effects of binary mixtures of EV and the other four EDCs (1–100 nM) on the expression of ER α by western blot analysis (b).

expression was analyzed by western blot. As shown in Figure 7, E2, EV, DES, and BPA upregulated the ER α protein expression, and the binary mixtures of EV and DES or BPA also upregulated ER α protein expression at the exposure concentrations of 1, 10, and 100 nM.

However, single DEHP and MEHP, and the binary mixtures of EV and DEHP or MEHP cannot all upregulate ER α protein expression, indicating that DEHP or MEHP attenuated ER α protein expression upregulated by EV.

4. Discussion

In the environment, EDCs cannot exist alone. Therefore, humans and other creatures are rarely exposed to only a single EDC, but large amounts of chemicals through a variety of ways at the same time [31]. Joint toxicity may occur when two toxic chemicals are presented in environment simultaneously [32]. When two or more pollutants act on organism, the combined effects tend to be completely different compared with a single pollutant acting on the organism [18, 33]. Usually, joint toxicity presents four forms depending on different interactions of the two compounds. Additive effect and independent effect are the result of the two compounds having no interaction or reaction, while synergistic or antagonistic effect pertains to the interaction of the two compounds, making their toxicity increscent or reductive [34].

EV, DES, BPA, DEHP, and MEHP are typical EDCs; these high production volume chemicals could be released into the ambient environment during production, storage, and transport and coexist in environment simultaneously. Although many researches were done, they focused on single EDC or a series of EDCs at a high dosage. In these EDCs, EV, DES, and BPA have estrogenic activity, while DEHP and MEHP have antiestrogenic activity [21, 22]. Generally, estrogen compounds can induce the proliferation of estrogen-sensitive tumor cells and increase the intracellular ROS levels through ER α pathway [25, 26]. Therefore, to evaluate the combined health risk of these different types of EDCs in environment, in this study, we investigated the effect of different types of EDCs on estrogenic activity of EV by detecting MCF-7 cell viability, intracellular ROS level change, and ER α protein expression. After MCF-7 cells were exposed to a series of concentration equal proportion binary mixtures of DES, BPA, DEHP and MEHP with EV for 24, 48, or 72 h, the binary mixtures of EV and the other four EDCs can significantly attenuate cell viability induced by single EV. The antagonistic effects of the binary mixtures of EV and the other four EDCs can be found by detecting cell viability. The joint effects of the binary mixtures of EV and the other four EDCs on intracellular ROS level change are totally different. At 24 h, similar to the cell viability, DES and BPA decreased intracellular ROS levels induced by EV when they mixed with EV. While at 1 and 3 h, the influence of DES, BPA, and DEHP on intracellular ROS level change induced by EV presented inconsistent results. That is to say, at some exposure concentrations, they increased intracellular ROS levels induced by EV, while, at other exposure concentrations, they decreased intracellular ROS levels. However, in general, the joint toxicity of binary mixture of EV and the other EDCs did not interact in a synergistic fashion in inducing cell proliferation and intracellular ROS levels. Ramirez et al. [34] also found that estrogenic binary mixtures of endosulfan and dieldrin did not interact synergistically in binding to ER or activating ER-mediated responses *in vitro* or *in vivo*.

Generally, the cell proliferation of estrogen-sensitive cells can give insight into estrogenic effects of environmental contaminants [35]. ER α is an estrogen nuclear receptor.

Estrogen, through binding to or activating ER α , can activate downstream signals that facilitate breast cancer cell proliferation. Both of them are generally found to be upregulated in many types of cancer and are related to cell proliferation. Numerous studies also showed that ER α signals are critical regulators of estrogen-sensitive tumor cell proliferation induced by environmental estrogen. For example, bisphenol F (BPF) can induce MCF-7 cells to proliferate by enhancing expression of proteins such as Cyclin D1 and Cyclin E1 via the ER α -dependent pathway [36]. Low concentration of BPA (1 μ M) has been shown to increase proliferation of both breast cancer cells and cancer-associated fibroblasts by an estrogen receptor-dependent pathway [37]. García et al. [38] found that environmental estrogen such as hexachlorobenzene (HCB) at low concentrations (5 and 50 nM) can increase MCF-7 cell proliferation by activating the ER α receptor. In the present study, we also found that single E2, EV, DES, and BPA can upregulate ER α protein expressions increase cell viability. In addition, the binary mixtures of EV and DES or BPA also upregulated ER α protein expression at 24 h, and their binary mixtures also increased cell viability at this exposure time. However, the binary mixtures of EV and DEHP or MEHP cannot increase the expression of ER α protein and cell viability. Some other studies also showed that DEHP and MEHP cannot activate ER α in estrogen receptor-positive cells [22, 39] and have antiestrogenic activity [22, 40]. These results showed that ER α protein expression is consistent with the results of the cell viability, which indicated that these EDCs might increase proliferation of MCF-7 breast cancer cells by activating the ER α .

However, except for ER α , EDCs can also induce estrogen-sensitive cancer cell proliferation by estrogen member receptor G protein coupled receptor 30 (GPR30) pathway [41, 42]. Moreover, there may be a crosstalk between membrane receptor such as GPR30 (nongenomic) and nuclear receptor ER (genomic) signaling pathways [43–45]. In our previous studies, we found that bisphenols such as BPF, TDP, and BPAF can induce proliferation of MCF-7 cells via interaction of ER α - and GPR30-mediated signaling pathways [23, 30, 45]. Therefore, the specific mechanism needs to further study more proteins associated with the cell proliferation such as GPR30 and its downstream signals.

Occurrence of ROS in cells has been a common response of chemical toxicity, which can damage active cellular substance, such as DNA, lipids, and proteins [46]. The redox system may be especially important during estrogen-induced cell proliferation, and different cellular signals may operate in response to varying levels of estrogen-induced ROS [47]. Many studies have found that natural or synthetic estrogen can induce ROS generation in breast cancer cells by estrogen receptor pathway, and increased ROS has been involved in both cell proliferation and carcinogenesis [25–27, 47]. However, cells have various antioxidant defense systems, consisting of both enzymatic and nonenzymatic substances, to reduce ROS levels and thus protect the cells from ROS damage [46]. When the balance between ROS and antioxidant defense system is broken, oxidative damage, or so-called oxidative stress, occurs. However, the balance

between ROS and antioxidant defense system is a dynamic process. The levels of generated ROS in intracellular are closely related to exposure concentrations and exposure time of the exposed chemicals [48]. In this study, we also found that, at different exposure concentrations and different exposure time, the intracellular ROS levels are different. The ROS generation in the binary mixtures of EV and the other four EDCs also presented different change trends at different exposure concentrations and different exposure time. The deeper reasons need further study.

5. Conclusions

Single EV, DES, and BPA can promote the proliferation of MCF-7 cells, and EV has the strongest potency in inducing cell proliferation. Cell viability induced by EV was significantly attenuated by DES, BPA, DEHP, and MEHP when they were mixed with EV. ER α signals play a key role in MCF-7 cell proliferation induced by low-concentration EDCs like EV, DES, or BPA. Single EV, BPA, DES, DEHP, and MEHP elevated intracellular ROS levels for different exposure durations. DES and BPA decreased intracellular ROS levels induced by EV when they mixed with EV for 24 h. These results indicated that the joint effects of binary mixtures of EV and other EDCs do not interact synergistically in inducing cell proliferation, intracellular ROS generation, and ER α protein expression. The results have important implications in the human risk assessments of EV coexposed with other EDCs in the environment.

Data Availability

The data used to support the findings of this study are included within the article.

Conflicts of Interest

The authors declare that there are no conflicts of interest regarding the publication of this paper.

Acknowledgments

The present work was supported by the National Natural Science Foundation of China (nos. 21777093 and 21507078), Open Foundation of Guangdong Key Laboratory of Environmental Catalysis and Health Risk Control (GKECHRC-02), and the Program for Changjiang Scholars and Innovative Research Team in University (no. IRT13078).

References

- [1] P. A. Fowler, M. Bellingham, K. D. Sinclair et al., "Impact of endocrine-disrupting compounds (EDCs) on female reproductive health," *Molecular and Cellular Endocrinology*, vol. 355, no. 2, pp. 231–239, 2012.
- [2] R. Lauretta, A. Sansone, M. Sansone, F. Romanelli, and M. Appetecchia, "Endocrine disrupting chemicals: effects on endocrine glands," *Frontiers in Endocrinology*, vol. 10, 2019.
- [3] L. M. Borgelt and C. W. Martell, "Estradiol valerate/dienogest: a novel combined oral contraceptive," *Clinical Therapeutics*, vol. 34, no. 1, pp. 37–55, 2012.
- [4] A. M. Andersson and N. E. Skakkebaek, "Exposure to exogenous estrogens in food: possible impact on human development and health," *European Journal of Endocrinology*, vol. 140, no. 6, pp. 477–485, 1999.
- [5] G. Senol, Y. Mecit, G. Kenan, and K. Turan, "Effects of oral administration of estradiol valerate on gonadal sex differentiation in the rainbow trout, *Oncorhynchus mykiss*," *Journal of Animal and Veterinary Advances*, vol. 7, no. 11, pp. 1400–1404, 2008.
- [6] Z. Chu, Y. Wu, S. Gong et al., "Effects of estradiol valerate on steroid hormones and sex reversal of female rice field eel, *Monopterus albus* (Zuiew)," *Journal of the World Aquaculture Society*, vol. 42, no. 1, pp. 96–104, 2011.
- [7] B. Lei, J. Kang, Y. Yu, J. Zha, W. Li, and Z. Wang, " β -estradiol 17-valerate affects embryonic development and sexual differentiation in Japanese medaka (*Oryzias latipes*)," *Aquatic Toxicology*, vol. 134–135, pp. 128–134, 2013.
- [8] B. Lei, S. Huang, Y. Zhou, D. Wang, and Z. Wang, "Levels of six estrogens in water and sediment from three rivers in Tianjin area, China," *Chemosphere*, vol. 76, no. 1, pp. 36–42, 2009.
- [9] W. Jiang, Y. Yan, M. Ma et al., "Assessment of source water contamination by estrogenic disrupting compounds in China," *Journal of Environmental Sciences*, vol. 24, no. 2, pp. 320–328, 2012.
- [10] A. L. Herbst, H. Ulfelder, and D. C. Poskanzer, "Adenocarcinoma of the vagina-association of maternal stilbestrol therapy with tumor appearance in young women," *American Journal of Obstetrics and Gynecology*, vol. 181, no. 6, pp. 1574–1575, 1999.
- [11] O. B. Adedeji, E. J. Durhan, N. Garcia-Reyero et al., "Short-term study investigating the estrogenic potency of diethylstilbestrol in the fathead minnow (*Pimephales promelas*)," *Environmental Science & Technology*, vol. 46, no. 14, pp. 7826–7835, 2012.
- [12] D. J. Caldwell, F. Mastrocco, T. H. Hutchinson et al., "Derivation of an aquatic predicted no-effect concentration for the synthetic hormone, 17 α -ethinyl estradiol," *Environmental Science & Technology*, vol. 42, no. 19, pp. 7046–7054, 2008.
- [13] G. Pojana, A. Gomiero, N. Jonkers, and A. Marcomini, "Natural and synthetic endocrine disrupting compounds (EDCs) in water, sediment and biota of a coastal lagoon," *Environment International*, vol. 33, no. 7, pp. 929–936, 2007.
- [14] T.-S. Chen, T.-C. Chen, K.-J. C. Yeh et al., "High estrogen concentrations in receiving river discharge from a concentrated livestock feedlot," *Science of the Total Environment*, vol. 408, no. 16, pp. 3223–3230, 2010.
- [15] L. Wang, G.-G. Ying, J.-L. Zhao et al., "Assessing estrogenic activity in surface water and sediment of the Liao River system in Northeast China using combined chemical and biological tools," *Environmental Pollution*, vol. 159, no. 1, pp. 148–156, 2011.
- [16] R. Guedes-Alons, Z. Sosa-Frerra, and J. Juan Santana-Rodríguez, "Simultaneous determination of hormonal residues in treated waters using ultrahigh performance liquid chromatography-tandem mass spectrometry," *Journal of Analytical Methods in Chemistry*, vol. 2013, Article ID 210653, 8 pages, 2013.
- [17] Y. Q. Huang, C. K. C. Wong, J. S. Zheng et al., "Bisphenol A (BPA) in China: a review of sources, environmental levels, and potential human health impacts," *Environment International*, vol. 42, pp. 91–99, 2012.
- [18] B. Huang, M. Feng, D. Li, and Y. Yang, "Antagonistic joint toxicity assessment of two current-use phthalates with waterborne copper in liver of *Carassius auratus* using

- biochemical biomarkers," *Ecotoxicology and Environmental Safety*, vol. 116, pp. 107–112, 2015.
- [19] X. Wu, H. Hong, X. Liu et al., "Graphene-dispersive solid-phase extraction of phthalate acid esters from environmental water," *Science of The Total Environment*, vol. 444, pp. 224–230, 2013.
- [20] J. C. Caldwell, "DEHP: genotoxicity and potential carcinogenic mechanisms-a review," *Mutation Research/Reviews in Mutation Research*, vol. 751, no. 2, pp. 82–157, 2012.
- [21] R. Czernych, M. Chraniuk, P. Zagożdżon, and L. Wolska, "Characterization of estrogenic and androgenic activity of phthalates by the XenoScreen YES/YAS in vitro assay," *Environmental Toxicology and Pharmacology*, vol. 53, pp. 95–104, 2017.
- [22] D.-H. Kim, C. G. Park, S. H. Kim, and Y. J. Kim, "The effects of mono-(2-ethylhexyl) phthalate (MEHP) on human estrogen receptor (hER) and androgen receptor (hAR) by YES/YAS in vitro assay," *Molecules*, vol. 24, no. 8, p. 1558, 2019.
- [23] B. Lei, S. Sun, C. Feng et al., "Bisphenol AF exerts estrogenic activity in MCF-7 cells through activation of Erk and PI3K/Akt signals via GPER signaling pathway," *Chemosphere*, vol. 220, pp. 362–370, 2019.
- [24] S.-L. Liu, X. Lin, D.-Y. Shi, J. Cheng, C.-Q. Wu, and Y.-D. Zhang, "Reactive oxygen species stimulated human hepatoma cell proliferation via cross-talk between PI3-K/PKB and JNK signaling pathways," *Archives of Biochemistry and Biophysics*, vol. 406, no. 2, pp. 173–182, 2002.
- [25] P. K. S. Mahalingaiah and K. P. Singh, "Chronic oxidative stress increase growth and tumorigenic potential of MCF-7 breast cancer cells," *PLoS One*, vol. 9, no. 1, Article ID e87371, 2014.
- [26] K. Lata and T. K. Mukherjee, "Knockdown of receptor for advanced glycation end products attenuate 17 α -ethinyl-estradiol dependent proliferation and survival of MCF-7 breast cancer cells," *Biochimica et Biophysica Acta (BBA)-General Subjects*, vol. 1840, no. 3, pp. 1083–1091, 2014.
- [27] J. Sastre-Serra, A. Valle, M. M. Company, I. Garau, J. Oliver, and P. Roca, "Estrogen down-regulates uncoupling proteins and increases oxidative stress in breast cancer," *Free Radical Biology and Medicine*, vol. 48, no. 4, pp. 506–512, 2010.
- [28] K. Lin, "Joint acute toxicity of tributyl phosphate and triphenyl phosphate to *Daphnia magna*," *Environmental Chemistry Letters*, vol. 7, no. 4, pp. 309–312, 2009.
- [29] Y. N. Gao, B. Y. Liu, F. J. Ge et al., "Joint effects of allelochemical nonanoic acid, *N*-phenyl-1-naphthylamine and caffeic acid on the growth of *Microcystis aeruginosa*," *Allelopathy Journal*, vol. 35, no. 2, pp. 249–257, 2015.
- [30] B. Lei, W. Peng, G. Xu et al., "Activation of G protein-coupled receptor 30 by thiodiphenol promotes proliferation of estrogen receptor α -positive breast cancer cells," *Chemosphere*, vol. 169, pp. 204–211, 2017.
- [31] N. Lazarevic, A. G. Barnett, P. D. Sly, and L. D. Knibbs, "Statistical methodology in studies of prenatal exposure to mixtures of endocrine-disrupting chemicals: a review of existing approaches and new alternatives," *Environmental Health Perspectives*, vol. 127, no. 2, Article ID 026001, 2019.
- [32] N. Liu, Y. Wang, F. Ge, S. Liu, and H. Xiao, "Antagonistic effect of nano-ZnO and cetyltrimethyl ammonium chloride on the growth of *Chlorella vulgaris*: dissolution and accumulation of nano-ZnO," *Chemosphere*, vol. 196, pp. 566–574, 2018.
- [33] L. Mignuez, R. Bureau, and M.-P. Halm-Lemeille, "Joint effects of nine antidepressants on *Raphidocelis subcapitata* and *Skeletonema marioi*: a matter of amine functional groups," *Aquatic Toxicology*, vol. 196, pp. 117–123, 2018.
- [34] T. Ramirez, A. Buechse, M. Dammann, S. Melching-Kollmuß, C. Woitkowiak, and B. Van Ravenzwaay, "Effects of estrogenic binary mixtures in the yeast estrogen screen (YES)," *Regulatory Toxicology and Pharmacology*, vol. 70, no. 1, pp. 286–296, 2014.
- [35] M. Shim, J.-Y. Bae, Y. J. Lee, and M.-J. Ahn, "Tectoridin from *Maackia amurensis* modulates both estrogen and thyroid receptors," *Phytomedicine*, vol. 21, no. 5, pp. 602–606, 2014.
- [36] J.-Y. Kim, H.-G. Choi, H.-M. Lee, G.-A. Lee, K.-A. Hwang, and K.-C. Choi, "Effects of bisphenol compounds on the growth and epithelial mesenchymal transition of MCF-7 CV human breast cancer cells," *Journal of Biomedical Materials Research*, vol. 31, no. 4, pp. 358–369, 2017.
- [37] M. Pupo, A. Pisano, R. Lappano et al., "Bisphenol A induces gene expression changes and proliferative effects through GPER in breast cancer cells and cancer-associated fibroblasts," *Environmental Health Perspectives*, vol. 120, no. 8, pp. 1177–1182, 2012.
- [38] M. A. García, D. Peña, L. Álvarez et al., "Hexachlorobenzene induces cell proliferation and IGF-I signaling pathway in an estrogen receptor α -dependent manner in MCF-7 breast cancer cell line," *Toxicology Letters*, vol. 192, no. 2, pp. 195–205, 2010.
- [39] C. Park, J. Lee, B. Kong et al., "The effects of bisphenol A, benzyl butyl phthalate, and di (2-ethylhexyl) phthalate on estrogen receptor alpha in estrogen receptor-positive cells under hypoxia," *Environmental Pollution*, vol. 248, pp. 774–781, 2019.
- [40] H. Yu, D. J. Caldwell, and R. P. Suri, "In vitro estrogenic activity of representative endocrine disrupting chemicals mixtures at environmentally relevant concentrations," *Chemosphere*, vol. 215, pp. 396–403, 2019.
- [41] M. Barton, E. J. Filardo, S. J. Lolait, P. Thomas, M. Maggiolini, and E. R. Prossnitz, "Twenty years of the G protein-coupled estrogen receptor GPER: historical and personal perspectives," *The Journal of Steroid Biochemistry and Molecular Biology*, vol. 176, pp. 4–15, 2018.
- [42] L.-Y. Cao, X.-M. Ren, C.-H. Li et al., "Bisphenol AF and bisphenol B exert higher estrogenic effects than bisphenol A via G protein-coupled estrogen receptor pathway," *Environmental Science & Technology*, vol. 51, no. 19, pp. 11423–11430, 2017.
- [43] Z.-G. Sheng and B.-Z. Zhu, "Low concentrations of bisphenol A induce mouse spermatogonial cell proliferation by G protein-coupled receptor 30 and estrogen receptor- α ," *Environmental Health Perspectives*, vol. 119, no. 12, pp. 1775–1780, 2011.
- [44] L.-C. Ge, Z.-J. Chen, H.-Y. Liu et al., "Involvement of activating ERK1/2 through G protein coupled receptor 30 and estrogen receptor α/β in low doses of bisphenol A promoting growth of sertoli TM4 cells," *Toxicology Letters*, vol. 226, no. 1, pp. 81–89, 2014.
- [45] B. Lei, Y. Huang, Y. Liu et al., "Low-concentration BPF induced cell biological responses by the ER α and GPER1-mediated signaling pathways in MCF-7 breast cancer cells," *Ecotoxicology and Environmental Safety*, vol. 165, pp. 144–152, 2018.
- [46] Z. Ji, Y. Zhang, J. Tian, F. Wang, M. Song, and H. Li, "Oxidative stress and cytotoxicity induced by tetrachlorobisphenol A in *Saccharomyces cerevisiae* cells," *Ecotoxicology and Environmental Safety*, vol. 161, pp. 1–7, 2018.

- [47] L. Yuan, A. K. Dietrich, and A. M. Nardulli, "17 β -estradiol alters oxidative stress response protein expression and oxidative damage in the uterus," *Molecular and Cellular Endocrinology*, vol. 382, no. 1, pp. 218–226, 2014.
- [48] B. Lei, S. Sun, J. Xu et al., "Low-concentration BPAF-and BPF-induced cell biological effects are mediated by ROS in MCF-7 breast cancer cells," *Environmental Science and Pollution Research*, vol. 25, no. 4, pp. 3200–3208, 2018.

Review Article

Progress in the Research of the Toxicity Effect Mechanisms of Heavy Metals on Freshwater Organisms and Their Water Quality Criteria in China

Ya-jun Hong,^{1,2} Wei Liao,^{1,3} Zhen-fei Yan,¹ Ying-chen Bai,¹ Cheng-lian Feng ,¹ Zu-xin Xu,² and Da-yong Xu ⁴

¹State Key Laboratory of Environmental Criteria and Risk Assessment, Chinese Research Academy of Environmental Sciences, Beijing 100012, China

²College of Environmental Science and Engineering, Tongji University, Shanghai 200092, China

³Key Laboratory of Poyang Lake Environment and Resource Utilization, Ministry of Education, School of Environmental and Chemical Engineering, Nanchang University, Nanchang 330031, China

⁴College of Biological and Chemical Engineering, Anhui Polytechnic University, Wuhu 241000, China

Correspondence should be addressed to Cheng-lian Feng; fengcl@craes.org.cn and Da-yong Xu; xdy826@ahpu.edu.cn

Received 12 October 2019; Revised 22 April 2020; Accepted 28 April 2020; Published 18 May 2020

Academic Editor: Kokhwa Lim

Copyright © 2020 Ya-jun Hong et al. This is an open access article distributed under the Creative Commons Attribution License, which permits unrestricted use, distribution, and reproduction in any medium, provided the original work is properly cited.

Water quality criteria are the scientific basis for formulating water quality standards and environmental management practices. Due to the development of urbanization and industrialization, the problem of heavy metal pollution has become a serious environmental problem. Heavy metals not only have major impacts on aquatic organisms, but also seriously threaten human health. However, the current environmental criteria refer to the maximum value limitations of environmental factors in environmental media where harmful or detrimental effects are not produced on specific protected objects. This study reviewed the sources, hazard levels, toxic effect mechanisms, and the current research status of China's water quality criteria for heavy metal pollutants. In addition, the focus and direction of future research on the toxic effects of heavy metal on aquatic organisms and the necessary criteria changes were discussed. The present study would provide an important theoretical basis for the future research of water quality criteria and risk assessment of heavy metal pollutants.

1. Introduction

Heavy metals are becoming one of the most serious environmental problems due to their persistence, biological toxicity, nondegradability, and capability of entering the food chain. In addition, heavy metal pollutants have even been found to react with some organic substances under certain conditions to convert them into even more toxic metal-organic complex pollutants [1, 2]. Aquatic organisms can accumulate and concentrate heavy metals to a certain extent. However, when the concentration and toxicity levels of heavy metals exceed the tolerance of aquatic organisms, they will produce serious toxic effects on their related indicators and even their life activities. At the same time,

genetic mutations or variations may be caused, which will result in changes in species diversity and survival rates. Since heavy metal pollutants have the potential of eventually being transmitted to humans and other advanced organisms through the food chain, they also pose serious threats to human health. For example, heavy metals are not easily eliminated after entering the human body and tend to continuously accumulate over time. Once they exceed the physiological load of the human body, they will cause physiological structural changes. These changes will then lead to acute, chronic, or long-term hazardous effects. For example, Zn, Cd, methyl Hg, Se, and Ni are teratogenic. Under environmental conditions with high concentrations of heavy metals, the ingestion of excessive amounts of heavy

metals will lead to poisoning effects with possible serious consequences [3].

In recent years, due to the major potential harmful effects of heavy metals in water on both aquatic organisms and humans, many experts and researchers have carried out intensive investigations regarding the ecological toxicity of heavy metals. In particular, the aforementioned studies have focused on the acute, subacute, and chronic toxic effects on organisms of nonessential elements, such as Hg, Cd, Pb, Cr, and As [4, 5]. In addition, some researchers have examined the toxicity or carcinogenesis of heavy metals in relationship to both humans and animals. The results revealed that the reactive oxygen produced by the stimulation of such heavy metals as Fe, Cu, Cd, Cr, Hg, Ni, and Pb can produce a series of toxic effects on organisms. These effects include lipid peroxidation and thiol protein consumption, as well as reactions with nuclear proteins and DNA which cause damage to biological macromolecular substances [6].

The water quality criteria specify the maximum concentration levels of toxic substances in water which will not adversely affect specific protected objectives under certain natural conditions. As the basis of the protection of water quality, the water quality criteria provide an important scientific basis for environmental protection agencies to safeguard aquatic ecosystems. The vast majority of water quality criteria are obtained by evaluating the species sensitivity distributions (SSD) of factors and/or impacted species [7]. At the present time, water quality criteria are indispensable scientific and theoretical foundations for environmental protection agencies to formulate water quality standards, evaluate water quality, and conduct effective water quality management processes [8]. Aquatic biological criteria refer to the maximum allowable concentrations of pollutants in aquatic environments which do not produce long-term or short-term adverse or harmful effects on aquatic organisms. These allowable concentration levels are the core components of water quality criteria [9]. Since different ecosystems have different biota, it has been observed that toxic concentrations which may be harmless to one biota may have irreversible toxic effects on another biota [10]. Therefore, aquatic biological criteria should have obvious regional characteristics [11]. Due to these differences in aquatic biota in different regions and countries, the baseline values of the same pollutants will vary depending on the objects to be protected. The United States was the first country to study water quality criteria. Since the 1960s, the United States Environmental Protection Agency (US EPA) successively promulgated water environment criteria documents and subsequently formed a relatively complete water quality criteria system [12]. In recent years, major progress has been made in the study of water quality criteria in China. A comprehensive water quality criteria system has been gradually established, which has successfully integrated aquatic biological, human health, sediment, ecological, and nutrient criteria, respectively. The key technological foundations of China's water quality criteria system have been established, such as the "3 Phyla and 6 Families;" "biological effect ratio;" "estimation of relationships among species;" "water effect ratio;" and "biological ligand model (BLM)." A

variety of Chinese aquatic biological criteria values based on indigenous biotoxicity data were determined, such as the types of heavy metals (Cd, Pb, Cu, Cr, and Zn); eutrophic substances (ammonia nitrogen); new organic pollutants (for triclosan); polycyclic aromatic hydrocarbons (phenanthrene, pyrene); and POPs (PFOS, PFOA). In addition, the sediment criteria values and ecological criteria values of various pollutants were derived. It is firmly believed that the research and establishment of water quality criteria values in China will provide scientific support for the formulation and revision of accurate and effective water quality criteria values which specifically pertain to China's national situation.

Based on the aforementioned important issues, this research study summarized the sources and potential hazards of heavy metal pollutants in water, as well as the toxic effect mechanisms of heavy metals on aquatic organisms. In addition, the status of the current research regarding the water quality criteria of heavy metals in China was examined. Then, using the obtained insights, this study also presented suggestions for the focus and direction of future research regarding the biological toxic effects of heavy metals on aquatic organisms and potential revisions to China's current criteria system. The further studies of the ecological toxic effects of heavy metals on aquatic organisms will provide important references for the evaluations of the ecological toxicity of heavy metals on aquatic organisms, as well as assisting in identifying effective environmental treatment methods for heavy metal pollution in water bodies. Therefore, the results of the present study provide an important theoretical basis for the examination of water quality standards and risk assessments of heavy metal pollution hazards.

2. Hazards of Heavy Metal Pollutants in Water Bodies

Once heavy metals enter the water body, they will cause certain toxicity to aquatic organisms. Heavy metals are defined as naturally occurring metals having atomic number (Z) greater than 20 and an elemental density greater than 5 g/cm^3 [4]. Some toxic heavy metals, such as Ni, As, Cr, Zn, Cu, Cd, Co, and Pb, have the potential to cause serious environmental damage. The ion forms of Cd^{2+} , Pb^{2+} , Hg^{2+} , Ag^+ , and As^{3+} act with biological organisms to form corresponding toxic compounds. At the present time, with the increases in the bioaccumulations and concentrations of heavy metals in environments, the toxicity characteristics of heavy metals have changed. Ligands and oxidized states play important roles in the bioavailability of heavy metals [13]. If the cumulative concentrations or effects of heavy metals reach certain limits, destruction of cell metabolism will result, and the impacts of the heavy metals will become toxic [14]. The toxic effects of metals mainly cause the functional loss of brain and nervous system functions, and serious damage to blood content, liver, spleen, kidney, viscera, and other organs. This damage results in physical weakness, hypomnesia, skin allergic reactions, hypertension, and other symptoms [15]. Therefore, based on these factors, the World Health Organize (WHO) is globally studying the toxicity

mechanism of heavy metals. In some cases, several regulatory agencies have also approved standardized limitations for the discharge of wastewater containing heavy metals. In previous related studies, researchers have also vigorously carried out examinations into heavy metal pollution hazards. As a result, new technologies for heavy metal wastewater treatments have been developed in order to achieve the goal of reducing the harmful effects of heavy metals on the environment as soon as possible [16].

There are a wide range of sources for heavy metals to enter the environment, including wastewater, waste gas, and waste residue. The known sources of heavy metals and their harmful effects on the human body are shown in Figure 1. Table 1 lists the specific hazards of some specific heavy metals on humans, as well as the current maximum harmful concentration levels (maximum contaminant level, MCL) [17] and the limitation values of the surface water environmental quality standard in China.

3. Toxic Effects and Mechanisms of Heavy Metals on Aquatic Organisms

3.1. Toxic Effects of Heavy Metals on Aquatic Organisms. Due to the close contact between aquatic organisms and water bodies, the heavy metals in the water bodies can easily enter the aquatic organisms. Heavy metals enter aquatic animals mainly through the following three ways. (1) Aquatic animals use gills and other organs to absorb heavy metal ions dissolved in water into their bodies. Then, the aquatic organisms accumulate heavy metals on skin surface cells or convey the heavy metals to various organs or tissues of the body through their blood. (2) Aquatic animals absorb heavy metals into their bodies via their digestive tracts through food intake and so on. (3) Heavy metals are absorbed through the animals' subcutaneous layers and then enter the bodies of the organisms through osmotic exchanges between the heavy metals and the impacted body surfaces of the aquatic organisms [41].

3.1.1. Bioaccumulations of Heavy Metals. Heavy metals can be enriched in organisms. Once heavy metals in the water environments enter aquatic organisms, they are not easily metabolized, decomposed, and excluded from the bodies of the animals. Besides, the heavy metals very easily accumulate in such organs as the liver and kidney of the animals. The results of the studies conducted by Olivares et al. [42] revealed that the main mechanism of heavy metal enrichment in organisms was through the combination with metal binding proteins in the mechanism bodies, such as the metallothionein. Rainbow and White [43] found that the processes involved in the uptake of heavy metals by organisms do not need to consume energy. In addition, since heavy metals are not easily excreted from the body, cumulative toxic effects may occur. Rzymiski et al. [44] studied the enrichment of different heavy metals by bivalves, and the results indicated that bivalves have very high enrichment capacities for the heavy metals Cu and Cd. Topcuoglu et al. [45] studied the content levels of heavy metals in aquatic

organisms in the Black Sea region of Turkey. The results showed that the heavy metals Pb, Cd, and Cr were the most abundant in mollusks and shellfish, while Fe and Zn were the least abundant.

3.1.2. Early Developmental Toxicity of Organisms. Heavy metals can be very toxic to organisms in the early stages of development. It has been found that during the embryonic and alevin stages of fish, they can be easily injured by heavy metal pollutants. It has been observed that once heavy metals enter the larvae, they can potentially react with nucleic acids, enzymes, vitamins, hormones, and other substances in the organisms and change chemical structures and biological activities. In addition, damage to the functions of such multiple systems as genetic development and endocrine and central nervous system development may occur. These changes may even lead to the disease and death of the affected organisms [46, 47]. García-Alonso et al. [48] found that the embryos and larvae of marine Polychaete Nereis Succinea were more sensitive to Ag, and exposure to AgNO₃ had significantly increased the lethality and aberration rates of embryos. In the studies conducted by Munley et al. [49], it was found that the early embryonic growth and egg laying rates of Fruticicolidae were inhibited after exposure to the heavy metals Co, Cu, Pb, and Ni for 28 days and 56 days, respectively. In addition, such heavy metals as Cu, Pb, and Zn have been found to significantly affect the development and hatching rates of the early embryos of aquatic organisms, leading to such consequences as delayed embryonic development [50].

3.1.3. Bio-Immunotoxicity. Heavy metals cause a certain degree of immunotoxicity to aquatic organisms by interfering with the normal function of the aquatic organism's immune organs and immune system. It is generally believed that exposure to low-dose heavy metals or short-term exposure to such metals has immunostimulation effects and can enhance the phagocytic activities of the blood cells in organisms [51, 52]. However, exposure to high-dose heavy metals or long-term exposures can significantly interfere with the phagocytic abilities of biological cells. This is mainly due to the fact that heavy metals have the ability to conjugate with cell membranes during this process, thereby changing the fluidity of the cell membranes and the permeability of ion pumps on cell membranes. The affects will include decreases in the stability of the cell membranes and decreases in phagocytic activities [53, 54]. The results of the studies conducted by Paul et al. [55] indicated immunotoxicity of Pb in freshwater fish. It was observed that Pb interfered with the bacteriophage and cell adhesion of intestinal macrophages. At the same time, the serum content levels of TNF had significantly decreased. Qin et al. [56] reported that heavy metal cadmium exposure negatively affected enzyme activities in crabs (Potamidae). In another related study, Vijayavel et al. [57] showed that Ni exposure promoted the formation and phagocytosis of superoxide anions in the haemolymph of crab but significantly inhibited phenoloxidase activities. The results of the study conducted by

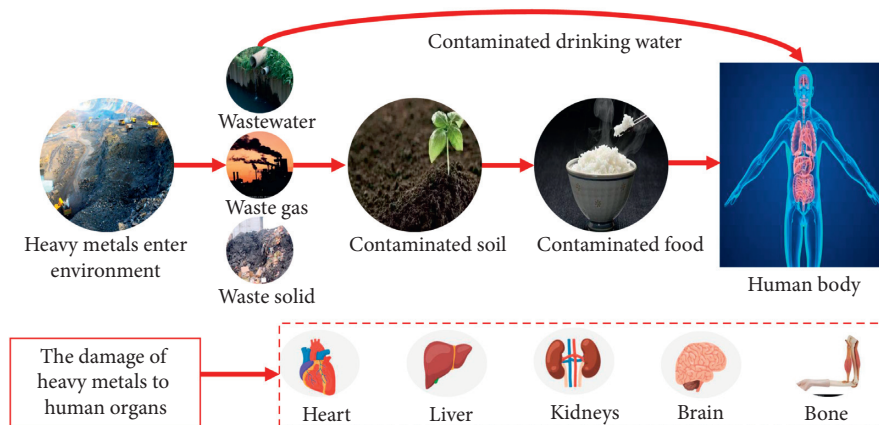


FIGURE 1: Sources of heavy metals and its hazard to the human body.

TABLE 1: Potential toxic effects of heavy metals and the current maximum harmful concentration levels (MCL) and GB3838-2002 in China.

Heavy metal	Hazards	MCL (mg/L)	GB3838-2002 in China (mg/L)	References
As	Cancer of the skin, lungs, bladder, and kidneys; cancer and other internal tumor diseases; vascular diseases and diabetes; infant mortality and weight loss of newborns; hearing loss; developmental abnormalities and neurobehavioral disorders	0.05	0.05	[18–20]
Pb	Anemia; cancer; kidney disease; neurological impairment; mental retardation; mental impairment; and behavioral problems in children	6.0×10^{-3}	0.05	[21–23]
Hg	Damage to the immunity of the renal reproductive system; damage to the blood, cardiovascular, and respiratory systems and the brain	3.0×10^{-5}	1.0×10^{-4}	[24–26]
Cd	Renal cancer damage; bronchiolitis; chronic obstructive pulmonary disease; emphysema; fibrotic bone damage	0.01	5.0×10^{-3}	[27–29]
Cr	Severe diarrhea; vomiting; pulmonary congestion; liver and kidney damage	0.05	0.05	[30–32]
Cu	Increased blood pressure and breathing; kidney and liver damage; convulsions, spasms, vomiting, and even death	0.25	1.0	[21, 33, 34]
Zn	Gastric nausea; skin irritation; spasms; vomiting; and anemia	0.8	1.0	[21, 35]
Se	Gastrointestinal discomforts; hair and nail loss; fatigue; cardiac arrhythmia; and nerve injuries	/	0.01	[36]
Ni	Dry coughing; bone, nose, and lung cancer; shortness of breath; chest tightness and chest pain; nausea and vomiting; dizziness and headache	0.2	/	[37–39]
Sb	Damage to tissue; cancer; inhibition of enzyme activities	6.0×10^{-3}	5.0×10^{-3}	[6, 40]

Chandurvelan et al. revealed that cadmium exposure increased the content of phagocytic basophils and eosinophils in mussels and caused significant DNA damage [58].

3.1.4. Genetic Mutations and Variations. Long-term exposure to water containing heavy metals can also cause mutations and mutations in the genetics of aquatic organisms. It has been determined that once heavy metals enter organisms, they become enriched and concentrated. When the dosage concentrations of heavy metals exceed a certain level or after long-term exposure to heavy metals, damage will result in the tissues and organs of the exposed organisms. In addition, large numbers of reactive oxygen species (ROS) and electrophilic metabolites will be induced, which will then combine with DNA molecules until the cells of the organisms suffer oxidation attacks in their external rings. This will lead to a series of lipid reactions in the organisms, such as peroxidation, alterations of genetic substances, and

oxidation of base ribosomes, finally resulting in cell death or the development of cancerous cells [59–61]. Hix and Augusto [62] showed that DNA becomes highly methylated when attacked by large numbers of methyl radicals induced by iron ions. The results obtained by Pfohl-Leskowicz et al. [63] also showed that heavy metal ions can significantly inhibit methyltransferase activities, and such heavy metal ions as Pb, Cu, and Zn have the ability to inhibit 5-methyltransferase activities. Also, Rossiello et al. [64] found that excessive exposure to Pb can result in low methylation of DNA.

3.1.5. Endocrine Disruption Toxicity. Heavy metals, like other endocrine disruptors, can cause some damage to the endocrine system of aquatic organisms. One of the mechanisms of heavy metal exposure which leads to such metabolic diseases as hypertension and diabetes may be that heavy metals, organochlorine pesticides, and

polychlorinated biphenyls are known typical endocrine disruptors, which can interfere with hormone synthesis and secretion and form endocrine disruptive toxicity conditions. For example, the heavy metals Cd, Mn, and Cr may increase the incidence of metabolic disorders. Moreover, exposure to metal endocrine disruptors may increase the risks of oxidative stress and mitochondrial dysfunction [65]. It has further been found that when exposed to sublethal concentrations of lead and cadmium, adult *Micropogonias undulatus* displayed significant increases or decreases in blood steroid concentrations, ovarian steroid secretion activities, and ovarian development [66]. Li et al. [67] found that corticotropin-releasing hormones, thyroglobulin, and the α and β gene expressions of thyroid receptors were significantly induced after minnow larvae were exposed to mercury for four days. Also, the content levels of thyroxine T3 and T4 were observed to have increased.

3.2. Toxicity Effect Mechanisms of Heavy Metals on Aquatic Organisms. Heavy metals can cause certain toxicity to aquatic organisms including animals, plants, and microorganisms. Some aquatic organisms live in environments containing heavy metals for long periods of time. These organisms are able to adjust their physiological and biochemical indicators in order to improve their irritability and tolerance to heavy metals. However, if fish live in water which is polluted by heavy metals for long periods of time, they will produce corresponding proteins and enzymes in their bodies in order to resist heavy metal ions, such as heat shock proteins (HSP), metallothionein (MT), transferrins (TF), glutathione transferase (GT), catalase (CAT), and superoxide dismutase (SOD), thereby reducing the cell damage caused by heavy metal exposure [68].

3.2.1. Toxicity Effect Mechanisms of Heavy Metals on Aquatic Animals. When such harmful heavy metals as Cd and Hg enter organisms, they will compete with other substances in the body. At that time, the sulfhydryl of MT can potentially react with harmful heavy metals and play an antidotal role by discharging harmful substances (such as heavy metals) from the body [69]. It has been determined that SOD can disproportionate superoxide anion radicals to produce H_2O_2 , which can then scavenge free radicals which are harmful to organisms. Also, CAT can catalyze H_2O_2 to produce harmless H_2O and O_2 . At the same time, it can synergize with SOD and POD to scavenge excess free radicals and peroxides in vivo. Xu et al. [70] found that MT expressions increased after being induced by Cd stress, which in turn resulted in the elimination of hydroxyl and peroxide, and the promotion of the mechanisms which produce stress responses in order to resist oxidation. Chen et al. [71] studied the changes of transferrin content in the livers of *Pseudosciaena crocea* under heavy metal Cd exposure. The results revealed that the Fe ions in the serum of the *Pseudosciaena crocea* had increased rapidly after being treated with heavy metal Cd ions. The maximum value was reached within 24 hours, after which it then slowly decreased and returned to its initial normal value. In another related study, Hansen

et al. [72] exposed trout (*Salmo platycephalus*) to water containing Cd and Zn for 15 days and found that the Cd and Zn in the gills of the fish were significantly absorbed. In addition, the Cd levels were found to be significantly correlated with the level of SOD transcription. It has also been observed that aquatic animals secrete abundant mucus when polluted by heavy metals, which tends to improve their tolerance to heavy metals to a certain extent [73].

3.2.2. Toxicity Effect Mechanisms of Heavy Metals on Aquatic Plants. The toxic effects of heavy metals on aquatic plants include cell membrane structural damage; inhibitions of respiration, photosynthesis, growth, and development processes; and toxicity to genetic materials. Heavy metals entering plants can change the antioxidant enzyme activities, induce ROS production, and cause oxidative damage effects. At the same time, heavy metals can interfere with the normal physiological and biochemical reactions [11, 74] of plants by interfering with the activities of transcription factors in some cells and inducing apoptosis, which severely impacts the normal vital activities of the plants. When studying the effects of Cu^{2+} stress on the growth and physiological and biochemical characteristics of *Sargassum hemiphyllum*, Fu et al. [75] found that appropriate concentrations of Cu^{2+} stress (≤ 0.05 mg/L) had a positive effect on the growth and physiological and biochemical indexes of *Sargassum hemiphyllum*. However, excessive concentrations of Cu^{2+} stress (0.05 mg/L) had negative effects on the growth of *Sargassum hemiphyllum* and its stress resistance abilities. In the studies conducted by Jian et al. [76] regarding the physiological and biochemical characteristics of the wetland plant *Ludwigia prostrata* under Cd and Pb stress conditions, it was found that the growth rates of the *Ludwigia prostrata* were significantly inhibited. In addition, the content levels of chlorophyll a, b, and chlorophyll a + b were observed to be decreased with the increases in the heavy metal concentrations, and the effects on the superoxide dismutase activities in *Ludwigia prostrata* had displayed different trends. The results of another previous study showed that the heights and root numbers of *Oenanthe javanica* were significantly reduced, and the biomass fresh weights were significantly lower, under high concentrations of Cu. At the same time, the content levels of total chlorophyll, chlorophyll a, and soluble proteins displayed downward trends [77]. In addition, the ultrastructure characteristics of the plant cells; permeability, growth, and development of the cell membranes; absorption and metabolism of the water and nutrients; photosynthesis, respiration, and antioxidant enzyme activities in vivo; and the genetic material in vivo were also seriously affected by exposure to heavy metals [78].

3.2.3. Toxicity Effect Mechanisms of Heavy Metals on Aquatic Microorganisms. Bacteria and fungi are common microorganisms in aquatic ecosystems. They are both considered to be decomposers and microconsumers of organisms. They also include primary producers, such as the photosynthetic bacteria of autotrophic bacteria. Microorganisms enhance the suitability of cells to heavy metal stress by secreting

secondary metabolites, including organic acids, glycoproteins, and polysaccharides. These extracellular metabolites combine with heavy metal ions to enhance the resistance of cells to stress. However, it has been found that heavy metal ions often cause oxidative damage to organisms, which in turn induces the production of excess oxygen free radicals, destroys the cell membranes of organisms, and damage the normal respiratory metabolic pathways of organisms [79]. Zhang et al. [79] examined the toxicity of heavy metals to *Vibrio Qinghaiensis* Q67 in the Fuyang River. It was found that the heavy metal ions inhibited the activities of reduced flavin mononucleotides and oxidized flavin mononucleotides, resulting in the transformations between them becoming abnormal. Xu [80] used white rot fungi to adsorb heavy metals, and the results showed that high concentrations of Cd stress had significantly inhibited the growth of *P. chrysosporium*, as well as causing changes in the mycelium morphology and decreases in lignin degrading enzymes (LiP and MNP). Zhou et al. [81] used the recombinant luminescent bacterium *E. coli* HB101 pUCD607 to study the singular toxicity of Zn^{2+} , Cu^{2+} , and Hg^{2+} and the combined toxicity of binary mixing systems. The experimental results showed that the sequence of toxicity of single heavy metal ions to recombinant luminescent bacterium was $Hg^{2+} > Zn^{2+} > Cu^{2+}$.

4. Water Quality Criteria of Heavy Metals for Aquatic Organisms in China

The aim of water quality criteria for aquatic organisms is to protect aquatic organisms from not have long-term or short-term adverse or harmful effects exposed to the maximum allowable concentrations of pollutants in water environments. At the present time, the two most representative international water quality criteria systems are those of the United States and the European Union. In the United States, the current water quality criteria guidance system has adopted a toxicity percentage ranking method and is considered to be a dual-value criteria system [6]. The criteria values obtained using this type of method include the criteria maximum concentration (CMC) and the criteria continuous concentration (CCC). The European Union determined its water quality criteria system by deducing the predicted no effect concentration (PNEC) [82]. In addition to the aforementioned two mainstream water quality criteria systems of the United States and the European Union, the Netherlands, Canada, Australia, and New Zealand have also developed their own respective water quality criteria programmatic documents. In China, research regarding water quality criteria started relatively late, and the initial research had only involved the collection and collation of foreign data. However, in recent years, many domestic researchers have carried out corresponding studies on water quality criteria specifically for China and have focused major attention on the aquatic biological water quality criteria of heavy metals. In this study, heavy metals copper, zinc, lead, and chromium were taken as examples to review the research progress of water quality standards for heavy metals in China.

4.1. Copper. Copper is an essential trace element for life and also one of the main elements of heavy metal pollution in water. The copper found in water mainly originates from atmospheric deposition, agricultural runoff, copper sulfate usage to control algae blooms, and the direct discharge of copper-containing industrial wastewater. Generally speaking, copper is more toxic to aquatic organisms than to humans and other terrestrial organisms, especially water fleas [83]. The toxicity of copper in natural water varies with the changes in hydrochemical properties. Although many soluble components contribute to the improvements of copper toxicity in freshwater, the main controlling factors include calcium, pH, and dissolved organic matter (DOM). These substances affect the gills of the competing cations and are related to copper toxicity through a series of geochemical processes which form various complexes in all directions. These are considered to be inferior to noncomplex biological/toxic metal ions (such as Cu^{2+}). Specifically, copper tends to be found in harder type water bodies (e.g., water bodies with higher DOM content). Calcium hardness comes from the weathering effects of rock-forming minerals (mainly carbonate rock and feldspar). Meanwhile, DOM is mainly derived from the decomposition of terrestrial and aquatic vegetation and biota [84]. There are corresponding reports currently available regarding the research conducted on the freshwater aquatic biological benchmarks of copper in China. For example, Wu et al. [85] collected and screened biological species in freshwater locations and the corresponding toxicity data by taking the freshwater aquatic ecosystems in China as the protected objects. The freshwater biological water quality criteria of copper in China were deduced by adopting an internationally accepted evaluation factor method, toxicity percentage ranking method, and a species sensitivity distribution method [6, 86, 87]. The results indicated that the baseline value of copper obtained using the evaluation factor method was $2.00 \mu\text{g/L}$. The CMC and CCC of copper obtained using the toxicity percentage ranking method were 9.10 and $5.63 \mu\text{g/L}$, respectively. The short-term and long-term dangerous concentrations of copper which would result in the protection of 95% of the species obtained using the SSD method were 30.0 and $9.44 \mu\text{g/L}$, respectively. It was found that there were some differences in the water quality criteria values of copper obtained using the aforementioned three methods. The comparative analysis results indicated that an SSD method should be recommended as the preferred method for copper benchmark deduction in China.

4.2. Zinc. Zinc is widely distributed throughout nature, and it is an essential trace element for life. However, when the concentrations of zinc exceed a certain level, it will produce certain toxicity effects on organisms. Many countries throughout the world have studied the toxicity of zinc and formulated corresponding criteria or standards [88–90]. The average daily intake of Zinc from dietary sources is approximately 10 to 15 mg, and the adult body contains approximately 2 to 3 g of zinc. Due to the low demand for zinc in organisms, when zinc concentrations exceed the

requirements, it will become a harmful substance and produce certain toxic effects. Furthermore, since zinc is far more toxic to aquatic organisms than to humans, the water quality criteria of zinc developed by various countries tend to be quite different. For example, in the newly issued criteria document of zinc issued by the EPA (US), the freshwater aquatic biological criterion of zinc is $120 \mu\text{g/L}$. Meanwhile, the human health protection standards are $7,400 \mu\text{g/L}$ (potable water + aquatic organisms) and $26,000 \mu\text{g/L}$ (only portable aquatic organisms). However, China's current water quality standards do not correspond with China's water environment characteristics [11, 91]. For example, the five types of zinc standards in the GB 3838-2002 Surface Water Environmental Quality Standard [92] are 50, 1000, 1000, 2000, and $2000 \mu\text{g/L}$, respectively, and the standard value of zinc in the GB 11607-89 Fishery Water Quality Standard [93] is $100 \mu\text{g/L}$. Wu et al. [94] collected and collated the biological species and toxicity data in freshwater areas in China. The water quality criterion of zinc for the protection of freshwater aquatic organisms in China was deduced according to several commonly used methods, including an evaluation factor method, toxicity percentage ranking method, and SSD method. The results showed that there were significant differences in the sensitivities of different organisms to zinc toxicity. For example, crustaceans had the strongest sensitivity and amphibians had the weakest sensitivity. The order of sensitivity was determined to be as follows: crustaceans > other species > fish > amphibians. Finally, it was recommended that the criteria value obtained using a toxicity percentage ranking method should be the water quality criteria value of zinc. Currently, the CMC and CCC of Zn are 89.7 and $34.5 \mu\text{g/L}$, respectively. At the same time, based on the different species sensitivity levels, the acute biological criteria values for protecting fish, crustaceans, and other invertebrates were determined to be 298.9, 67.3, and $76.9 \mu\text{g/L}$, respectively, and the chronic biological criteria values were 36.9, 12.9, and $14.8 \mu\text{g/L}$, respectively.

4.3. Lead. Heavy metals such as lead in drinking water are harmful to humans. To protect consumers, the maximum allowable concentration of lead in water has been established. Lead can cause nerve damage even when exposed to low levels of lead, especially in infants and children [95]. As a nonessential element in plant metabolism, the toxicity of lead is usually related to physiological processes, in which it interferes with the normal functions of cells to organs, including seed germination and delayed growth, water deficiency, nutritional disorders, and reduced photosynthesis, respiration, and transpiration processes [96–98]. It is known that exposure to lead can also result in the excessive production of reactive oxygen species (ROS) which potentially destroy membranes, lipids, nucleic acids, and proteins [97, 98]. In addition, the toxicity of lead is partly dependent on its biological activities, which are related to the subcellular distributions and chemical forms of plant cells [96]. For plants, the toxicity effects of lead are dependent on the concentrations and type of lead, exposure times, and the ecological types and plant species involved [99, 100]. Even

very small dosages can be toxic to organisms [101]. Although the concentrations of lead in water usually do not exceed $0.6 \mu\text{mol/L}$ [102], there have also been reports of high exposure concentrations (e.g., $4.3 \mu\text{mol/L}$) [103]. Therefore, it is of major significance to study the lead aquatic biological criteria which are suitable for the water environments of river basins in China for the protection of freshwater aquatic organisms. Kieber et al. [104] collected and screened 25 acute toxicity data cases of lead in freshwater organisms in China. In the present study, the aquatic biological criteria technology methods of the United States were used for the estimations of the aquatic biological criteria of lead in order to calculate the aquatic biological criteria of lead for freshwater organisms in China. It was determined that the criteria for lead should be 0.131 mg/L , with a chronic criterion of 0.0051 mg/L . At the same time, the criteria calculation technology of the Netherlands and Australia-New Zealand was utilized to compare the criteria calculation results. The results indicated that the criteria calculation method of the United States was relatively feasible. An ecological risk assessment for lead exposure in the Liao he River Basin was carried out using the obtained lead criteria values. The results revealed that there were certain ecological risks of lead exposure throughout most of the area.

4.4. Chromium. Hexavalent chromium (Cr^{6+}) is a typical transition metal pollutant found in wastewater which results from electroplating, leather tanning, or pigment manufacturing [105]. Cr^{6+} is a strong oxidant with cytotoxicity, mutagenicity, and carcinogenicity, which causes serious pollution effects in manufacturing wastewater. Excessive exposure to chromium may result in serious damage to many aquatic organisms, carcinogenic effects in humans, and skin irritations and corrosion [106]. Therefore, many countries rank it as a priority to control such toxic pollutants and stipulate that the maximum permissible concentration in drinking water is $50 \mu\text{g/L}$. The two valence states of Cr, Cr^{3+} and Cr^{6+} , are stable in the environment and known to have different properties. It has been found that appropriate amounts of Cr^{3+} can reduce blood sugar concentrations in human plasma, improve insulin activities, promote sugar and fat metabolism, and enhance the stress response abilities of the human body. However, Cr^{6+} is a powerful oxidant known to have strong carcinogenic, teratogenic, and mutagenic effects. It is considered to be highly harmful to organisms [107]. It is generally believed that the toxicity of Cr^{6+} is 100 times higher than that of trivalent Cr. It is precisely because of its serious biological toxicity effects that the research regarding the toxicity of hexavalent chromium has received major attention. Liao et al. [108] screened China's widespread freshwater aquatic biological species and collected the existing acute and chronic toxicity data. Then, by combining with the local toxicity data obtained in this research group's experiments, a species sensitivity ranking method, SSD method, and Australia's water quality criteria technology were used to deduce the freshwater aquatic biosafety criteria of Cr^{6+} in China [109]. Then, the double-

TABLE 2: Comparison of water quality criteria of heavy metals in China and the US EPA [12, 91].

Heavy metal	China ($\mu\text{g/L}$)		US EPA ($\mu\text{g/L}$)	
	Acute	Chronic	CMC	CCC
Zn	89.7	34.5	120	120
Cd	2.10–7.30	0.21–0.23	2	0.25
Cr	45.79	14.22	16	11
Cu	30	9.44	12	9
Hg	1.743	0.467	1.4	0.77
Pb	131	5.1	67.54	25.46

value criteria for Cr^{6+} in the freshwater aquatic organisms of China were obtained. The CMC of Cr^{6+} obtained using the three methods were 23.97, 22.84, and 29.06 $\mu\text{g/L}$, and the CCC were 14.63, 10.35, and 9.00 $\mu\text{g/L}$, respectively. On the same order of magnitude, there were some differences observed when compared with the criteria values of the United States. Therefore, it was suggested that the criteria values should be used to deduce the CMC and CCC values.

The water quality criteria of several common heavy metals in China and US EPA are shown in Table 2. By comparing with the corresponding heavy metal water quality standards of the two countries, it is found that there is a certain difference in the values of the two countries' benchmark values, which is mainly caused by the differences in biota, water quality, and species between the two countries. Therefore, water quality parameters, species distribution, and geographical factors should be considered when formulating water quality benchmarks, and it is recommended to use the BLM model.

5. Conclusions and Prospects

At the present time, experts and researchers around the world have completed a great deal of valuable research regarding the toxic effects and mechanisms of heavy metals. As a result, major achievements have been reached in the field of effective water environment quality standard systems. However, the current water quality standards in China do not efficiently combine with the characteristics of the actual water environments of the country. Currently, the toxicity effect mechanisms of heavy metals on aquatic organisms are not consistency and not comprehensive, systematic studies have not been carried out on the construction of a water environment criteria system specifically for China's national situation. Therefore, it was necessary in this study to propose an effective water quality criteria system for China on the basis of insights obtained from the mature experiences of other countries. In future research endeavors, the following points will need to be considered.

- (1) Water environmental factors such as temperature, hardness, and pH will affect the toxicity of metals; besides, emerging pollutants, such as antibiotics, microplastics (MP), endocrine disruptors (BPs), and personal care products (PPCPs), are known to be entering water bodies to form more complex systems

with heavy metals, such as particulate matter and DOM. Therefore, analyses of the corresponding toxic effects of these new types of pollutants and the subsequent impacts of the current water quality criteria should be the focus of future research; the BLM model should be considered in the derivation process of water quality criteria.

- (2) Some heavy metals found in the environment may be trace metals. However, whether or not the toxic effects of heavy metals occur during the processes of migration or transformation should be continuously tracked. In addition, corresponding models should be established to monitor, predict, and evaluate the toxic changes of heavy metals in ecosystems.
- (3) A set of systematic theories and methodologies is needed for the study of China's water quality criteria and standards. In future water quality criteria research, its theory and methodology should be continuously explored, as well as systematically studying the key scientific problems of the existing water quality criteria, in order to form a guideline document suitable for China's national conditions.

Conflicts of Interest

The authors declare that they have no conflicts of interest.

Acknowledgments

This research study was financially supported by the National Natural Science Foundation of China (nos. 41773085 and 41521003) and the China National Project of Water Pollution Control and Treatment (2017ZX07301005-001).

References

- [1] A. Maceda-Veiga, M. Monroy, E. Navarro, G. Viscor, and A. de Sostoa, "Metal concentrations and pathological responses of wild native fish exposed to sewage discharge in a Mediterranean river," *Science of the Total Environment*, vol. 449, no. 2, pp. 9–19, 2013.
- [2] S. Chowdhury, M. A. J. Mazumder, O. Al-Attas, and T. Husain, "Heavy metals in drinking water: occurrences, implications, and future needs in developing countries," *Science of the Total Environment*, vol. 569-570, pp. 476–488, 2016.
- [3] M. Rose, A. Fernandes, D. Mortimer, and C. Baskaran, "Contamination of fish in UK fresh water systems: risk assessment for human consumption," *Chemosphere*, vol. 122, no. 2, pp. 183–189, 2015.
- [4] H. Ali and E. Khan, "What are heavy metals? Long-standing controversy over the scientific use of the term 'heavy metals'—proposal of a comprehensive definition," *Toxicological and Environmental Chemistry*, vol. 100, no. 1-2, pp. 6–19, 2018.
- [5] R. J. Strong, C. J. Halsall, M. Ferenčík, K. C. Jones, R. F. Shore, and F. L. Martin, "Biospectroscopy reveals the effect of varying water quality on tadpole tissues of the common frog (*Rana temporaria*)," *Environmental Pollution*, vol. 213, pp. 322–337, 2016.

- [6] P. Morcillo, M. Á. Esteban, and A. Cuesta, "Heavy metals produce toxicity, oxidative stress and apoptosis in the marine teleost fish SAF-1 cell line," *Chemosphere*, vol. 144, pp. 225–233, 2016.
- [7] C. Feng, F. Wu, Y. Mu et al., "Interspecies correlation estimation-applications in water quality criteria and ecological risk assessment," *Environmental Science & Technology*, vol. 47, no. 20, pp. 11382–11383, 2013.
- [8] F. C. Wu, W. Meng, Y. H. Song et al., "Research progress in lake water quality criteria in China," *Acta Scientiae Circumstantiae*, vol. 28, no. 12, pp. 2385–2393, 2008, in Chinese.
- [9] U. S. EPA (Environmental Protection Agency), *Guidelines for Deriving Numerical National Aquatic Life Criteria for Protection of Aquatic Organisms and Their Uses*, Office of Research and Development, Washington, DC, USA, 1985.
- [10] L. Maltby, N. Blake, T. C. M. Brock, and P. J. Van Den Brink, "Insecticide species sensitivity distributions: importance of test species selection and relevance to aquatic ecosystems," *Environmental Toxicology and Chemistry*, vol. 24, no. 2, pp. 379–388, 2005.
- [11] F. C. Wu, W. Meng, X. L. Zhao et al., "China embarking on development of its own national water quality criteria system," *Environmental Science and Technology*, vol. 44, no. 21, pp. 7792–7793, 2010.
- [12] C. Feng, F. Wu, X. Zhao, H. Li, and H. Chang, "Water quality criteria research and progress," *Science China Earth Sciences*, vol. 55, no. 6, pp. 882–891, 2012, in Chinese.
- [13] L. Joseph, B.-M. Jun, J. R. V. Flora, C. M. Park, and Y. Yoon, "Removal of heavy metals from water sources in the developing world using low-cost materials: a review," *Chemosphere*, vol. 229, pp. 142–159, 2019.
- [14] M. Salman, M. Athar, and U. Farooq, "Biosorption of heavy metals from aqueous solutions using indigenous and modified lignocellulosic materials," *Reviews in Environmental Science and Bio/Technology*, vol. 14, no. 2, pp. 211–228, 2015.
- [15] K. Olga, S. Violetta, G. Michaela et al., "Sunflower plants as bioindicators of environmental pollution with lead (II) ions," *Sensors*, vol. 9, no. 7, pp. 5040–5058, 2009.
- [16] B. Dhir, P. Sharmila, and P. P. Saradhi, "Potential of aquatic macrophytes for removing contaminants from the environment," *Critical Reviews in Environmental Science and Technology*, vol. 39, no. 9, pp. 754–781, 2009.
- [17] S. Babel and T. A. Kurniawan, "A research study on Cr(VI) removal from contaminated wastewater using natural zeolite," *Journal of Ion Exchange*, vol. 14, no. 1, pp. 289–292, 2003.
- [18] R. Chen, C. Zhi, H. Yang et al., "Arsenic (V) adsorption on Fe₃O₄ nanoparticle-coated boron nitride nanotubes," *Journal of Colloid and Interface Science*, vol. 359, no. 1, pp. 261–268, 2011.
- [19] S. A. Ntim and S. Mitra, "Adsorption of arsenic on multiwall carbon nanotube–zirconia nanohybrid for potential drinking water purification," *Journal of Colloid and Interface Science*, vol. 375, no. 1, pp. 154–159, 2012.
- [20] M. B. Baskan and A. Pala, "Removal of arsenic from drinking water using modified natural zeolite," *Desalination*, vol. 281, pp. 396–403, 2011.
- [21] F. Fu and Q. Wang, "Removal of heavy metal ions from wastewaters: a review," *Journal of Environmental Management*, vol. 92, no. 3, pp. 407–418, 2011.
- [22] X. Qu, P. J. J. Alvarez, and Q. Li, "Applications of nanotechnology in water and wastewater treatment," *Water Research*, vol. 47, no. 12, pp. 3931–3946, 2013.
- [23] A. Salem and R. A. Sene, "Removal of lead from solution by combination of natural zeolite–kaolin–bentonite as a new low-cost adsorbent," *Chemical Engineering Journal*, vol. 174, no. 2–3, pp. 619–628, 2011.
- [24] T. Wajima and K. Sugawara, "Adsorption behaviors of mercury from aqueous solution using sulfur-impregnated adsorbent developed from coal," *Fuel Processing Technology*, vol. 92, no. 7, pp. 1322–1327, 2011.
- [25] F. D. Natale, A. Erto, A. Lancia, and D. Musmarra, "Mercury adsorption on granular activated carbon in aqueous solutions containing nitrates and chlorides," *Journal of Hazardous Materials*, vol. 192, no. 3, pp. 1842–1850, 2011.
- [26] H. Shamsijazeyi and T. Kaghazchi, "Investigation of nitric acid treatment of activated carbon for enhanced aqueous mercury removal," *Journal of Industrial and Engineering Chemistry*, vol. 16, no. 5, pp. 852–858, 2010.
- [27] Ihsanullah, F. A. Al-Khaldi, B. Abusharkh et al., "Adsorptive removal of cadmium (II) ions from liquid phase using acid modified carbon-based adsorbents," *Journal of Molecular Liquids*, vol. 204, pp. 255–263, 2015.
- [28] M. Arias, M. T. Barral, and J. C. Mejuto, "Enhancement of copper and cadmium adsorption on kaolin by the presence of humic acids," *Chemosphere*, vol. 48, no. 10, pp. 1081–1088, 2002.
- [29] G. D. Vukovic, A. D. Marinkovic, M. Colic et al., "Removal of cadmium from aqueous solutions by oxidized and ethylenediamine-functionalized multi-walled carbon nanotubes," *Chemical Engineering Journal*, vol. 157, no. 1, pp. 238–248, 2010.
- [30] Ihsanullah, F. A. Al-Khaldi, B. Abu-Sharkh et al., "Effect of acid modification on adsorption of hexavalent chromium (Cr(VI)) from aqueous solution by activated carbon and carbon nanotubes," *Desalination and Water Treatment*, vol. 57, no. 16, pp. 7232–7244, 2016.
- [31] S. S. Liu, Y. Z. Chen, L. D. Zhang et al., "Enhanced removal of trace Cr (VI) ions from aqueous solution by titanium oxide–Ag composite adsorbents," *Journal of Hazardous Materials*, vol. 190, no. 1–3, pp. 723–728, 2011.
- [32] Y. Li, Z. Jin, and T. Li, "A novel and simple method to synthesize SiO₂-coated Fe nanocomposites with enhanced Cr (VI) removal under various experimental conditions," *Desalination*, vol. 288, pp. 118–125, 2012.
- [33] M. R. Awual, M. Ismael, T. Yaita et al., "Trace copper(II) ions detection and removal from water using novel ligand modified composite adsorbent," *Chemical Engineering Journal*, vol. 222, pp. 67–76, 2013.
- [34] B. A. M. Al-Rashdi, D. J. Johnson, and N. Hilal, "Removal of heavy metal ions by nanofiltration," *Desalination*, vol. 315, pp. 2–17, 2013.
- [35] E. A. Deliyanni, E. N. Peleka, and K. A. Matis, "Removal of zinc ion from water by sorption onto iron-based nano-adsorbent," *Journal of Hazardous Materials*, vol. 141, no. 1, pp. 176–184, 2007.
- [36] R. Li, J. Q. Yang, X. J. Sun, K. L. Shi, and W. S. Wu, "Analytical methods of selenite (VI)/selenate (VI) in environmental water samples: a review," *Environmental Chemistry*, vol. 36, no. 5, pp. 939–950, 2017, in Chinese.
- [37] I. Mobasherpour, E. Salahi, and M. Ebrahimi, "Removal of divalent nickel cations from aqueous solution by multi-walled carbon nano tubes: equilibrium and kinetic processes," *Research on Chemical Intermediates*, vol. 38, no. 9, pp. 2205–2222, 2012.
- [38] Z. Reddad, C. Gerente, Y. Andres, and P. Le Cloirec, "Adsorption of several metal ions onto a low-cost biosorbent:

- kinetic and equilibrium studies," *Environmental Science & Technology*, vol. 36, no. 9, pp. 2067–2073, 2002.
- [39] Y. Omer, Y. Altunkaynak, and G. Fuat, "Removal of copper, nickel, cobalt and manganese from aqueous solution by kaolinite," *Water Research*, vol. 37, no. 4, pp. 950–952, 2003.
- [40] Y. Fan, C. Zheng, A. Huo et al., "Investigating the binding properties between antimony(V) and dissolved organic matter (DOM) under different pH conditions during the soil sorption process using fluorescence and FTIR spectroscopy," *Ecotoxicology and Environmental Safety*, vol. 181, pp. 34–42, 2019.
- [41] Y. Long, Y. J. Luo, J. Xiao et al., "Research advances in effects of heavy metals stress on fish," *Journal of Southern Agriculture*, vol. 47, no. 9, pp. 1608–1614, 2016, in Chinese.
- [42] H. G. Olivares, N. M. Lagos, C. J. Gutierrez et al., "Assessment oxidative stress biomarkers and metal bioaccumulation in macroalgae from coastal areas with mining activities in Chile," *Environmental Monitoring & Assessment*, vol. 188, no. 1, pp. 1–11, 2016.
- [43] P. S. Rainbow and S. L. White, "Comparative strategies of heavy metal accumulation by crustaceans: zinc, copper and cadmium in a decapod, an amphipod and a barnacle," *Hydrobiologia*, vol. 174, no. 3, pp. 245–262, 1989.
- [44] P. Rzymiski, P. Niedzielski, P. Klimaszuk, and B. Poniedzialek, "Bioaccumulation of selected metals in bivalves (Unionidae) and *Phragmites australis* inhabiting a municipal water reservoir," *Environmental Monitoring and Assessment*, vol. 186, no. 5, pp. 3199–3212, 2014.
- [45] S. Topcuoglu, C. Kirbasoglu, and N. Gungor, "Heavy metals in organisms and sediments from Turkish coast of the Black Sea, 1997–1998," *Environment International*, vol. 27, no. 7, pp. 521–526, 2002.
- [46] B. A. Fowler, *Handbook on the Toxicology of Metals*, Academic Press, Cambridge, MA, USA, 4th edition, 2015.
- [47] M. Tolins, M. Ruchirawat, and P. Landrigan, "The developmental neurotoxicity of arsenic: cognitive and behavioral consequences of early life exposure," *Annals of Global Health*, vol. 80, no. 4, pp. 303–314, 2014.
- [48] J. García-Alonso, N. Rodriguez-Sanchez, S. K. Misra et al., "Toxicity and accumulation of silver nanoparticles during development of the marine polychaete *Platynereis dumerilii*," *Science of the Total Environment*, vol. 476–477, no. 1, pp. 688–695, 2014.
- [49] K. M. Munley, K. V. Brix, J. Panlilio, D. K. Deforest, and M. Grosell, "Growth inhibition in early life-stage tests predicts full life-cycle toxicity effects of lead in the freshwater pulmonate snail, *Lymnaea stagnalis*," *Aquatic Toxicology*, vol. 128–129, no. 3, pp. 60–66, 2013.
- [50] A. Salvaggio, F. Marino, M. Albano et al., "Toxic effects of zinc chloride on the bone development in *Danio rerio* (Hamilton, 1822)," *Frontiers in Physiology*, vol. 7, p. 153, 2016.
- [51] M. L. Hannam, S. D. Bamber, R. C. Sundt, and T. S. Galloway, "Immune modulation in the blue mussel *Mytilus edulis* exposed to North Sea produced water," *Environmental Pollution*, vol. 157, no. 6, pp. 1939–1944, 2009.
- [52] C. J. Rickwood and T. S. Galloway, "Acetylcholinesterase inhibition as a biomarker of adverse effect: a study of *Mytilus edulis* exposed to the priority pollutant chlorfenvinphos," *Aquatic Toxicology*, vol. 67, no. 1, pp. 45–56, 2004.
- [53] L. Camus, M. B. Jones, J. F. Børseth, B. E. Grøsvik, F. Regoli, and M. H. Depledge, "Total oxyradical scavenging capacity and cell membrane stability of haemocytes of the Arctic scallop, *Chlamys islandicus*, following benzo(a)pyrene exposure," *Marine Environmental Research*, vol. 54, no. 3–5, pp. 425–430, 2002.
- [54] M. M. Grundy, M. N. Moore, S. M. Howell, and N. A. Ratcliffe, "Phagocytic reduction and effects on lysosomal membranes by polycyclic aromatic hydrocarbons, in haemocytes of *Mytilus edulis*," *Aquatic Toxicology*, vol. 34, no. 4, pp. 273–290, 1996.
- [55] N. Paul, S. Chakraborty, and M. Sengupta, "Lead toxicity on non-specific immune mechanisms of freshwater fish *Channa punctatus*," *Aquatic Toxicology*, vol. 152, no. 5, pp. 105–112, 2014.
- [56] Q. Qin, S. Qin, L. Wang, and W. Lei, "Immune responses and ultrastructural changes of hemocytes in freshwater crab *Sinopotamon henanense* exposed to elevated cadmium," *Aquatic Toxicology*, vol. 106–107, no. 1, pp. 140–146, 2012.
- [57] K. Vijayavel, S. Gopalakrishnan, R. Thiagarajan, and H. Thilagam, "Immunotoxic effects of nickel in the mud crab *Scylla serrata*," *Fish & Shellfish Immunology*, vol. 26, no. 1, pp. 133–139, 2009.
- [58] R. Chandurvelan, I. D. Marsden, S. Gaw, and C. N. Glover, "Waterborne cadmium impacts immunocytotoxic and cytogenotoxic endpoints in green-lipped mussel, *Perna canaliculus*," *Aquatic Toxicology*, vol. 142–143, pp. 283–293, 2013.
- [59] M. Waisberg, P. Joseph, B. Hale, and D. Beyersmann, "Molecular and cellular mechanisms of cadmium carcinogenesis," *Toxicology*, vol. 192, no. 2–3, pp. 95–117, 2003.
- [60] R. E. Thomas, M. Lindeberg, P. M. Harris, and S. D. Rice, "Induction of DNA strand breaks in the mussel (*Mytilus trossulus*) and clam (*Protothaca staminea*) following chronic field exposure to polycyclic aromatic hydrocarbons from the Exxon Valdez spill," *Marine Pollution Bulletin*, vol. 54, no. 6, pp. 726–732, 2007.
- [61] L. Pan, J. Ren, and J. Liu, "Effects of benzo(k) fluoranthene exposure on the biomarkers of scallop *Chlamys farreri*," *Comparative Biochemistry and Physiology Part C: Toxicology & Pharmacology*, vol. 141, no. 3, pp. 248–256, 2005.
- [62] S. Hix and O. Augusto, "DNA methylation by tert -butyl hydroperoxide-iron (II): a role for the transition metal ion in the production of DNA base adducts," *Chemico-Biological Interactions*, vol. 118, no. 2, pp. 141–149, 1999.
- [63] A. Pfohl-Leszkowicz, O. Baldacini, G. Keith, and G. Dirheimer, "Stimulation of rat kidney, spleen and brain DNA-(cytosine-5)-methyltransferases by divalent cobalt ions," *Biochimie*, vol. 69, no. 11–12, pp. 1235–1242, 1987.
- [64] M. R. Rossiello, A. M. Aresta, M. Prisco, and D. Kanduc, "DNA hypomethylation during liver cell proliferation induced by a single dose of lead nitrate," *Bollettino Della Societa Italiana Di Biologia Sperimentale*, vol. 67, no. 12, p. 993, 1991.
- [65] P. Rafa, G. Pawe, P. Malgorzata et al., "Relationship between chronic exposure to lead, cadmium and manganese, blood pressure values and incidence of arterial hypertension," *Medycyna Pracy*, vol. 61, no. 1, pp. 5–14, 2010.
- [66] B. S. Nunez and S. L. Applebaum, "Tissue- and sex-specific regulation of CYP19A1 expression in the Atlantic croaker (*Micropogonias undulatus*)," *General and Comparative Endocrinology*, vol. 149, no. 2, pp. 205–216, 2006.
- [67] Z.-H. Li, L. Chen, Y.-H. Wu, P. Li, Y.-F. Li, and Z.-H. Ni, "Alteration of thyroid hormone levels and related gene expression in Chinese rare minnow larvae exposed to mercury chloride," *Environmental Toxicology and Pharmacology*, vol. 38, no. 1, pp. 325–331, 2014.
- [68] W. Cheuk, P. Chan, and K. Chan, "Cytotoxicities and induction of metallothionein (MT) and metal regulatory

- element (MRE)-binding transcription factor-1 (MTF-1) messenger RNA levels in the zebrafish (*Danio rerio*) ZFL and SJD cell lines after exposure to various metal ions," *Aquatic Toxicology*, vol. 89, no. 2, pp. 103–112, 2008.
- [69] D.-F. Xiang, J.-Q. Zhu, S. Jin, Y.-J. Hu, F.-Q. Tan, and W.-X. Yang, "Expression and function analysis of metallothionein in the testis of *Portunus trituberculatus* exposed to cadmium," *Aquatic Toxicology*, vol. 140–141, pp. 1–10, 2013.
- [70] D. Xu, B. Yu, Y. Zhang, M. Cui, and Q. Zhang, "Metallothionein protein expression of *Crassostrea hongkongensis* response to cadmium stress," *Journal of Shellfish Research*, vol. 34, no. 2, pp. 311–318, 2015.
- [71] J. Chen, Y. H. Shi, and M. Y. Li, "Changes in transferrin and hepcidin genes expression in the liver of the fish *Pseudosciaena crocea* following exposure to cadmium," *Archives of Toxicology*, vol. 82, no. 8, pp. 525–530, 2008.
- [72] B. H. Hansen, S. Rømma, L. I. R. Sjøteland, P. A. Olsvik, and R. A. Andersen, "Induction and activity of oxidative stress-related proteins during waterborne Cu-exposure in brown trout (*Salmo trutta*)," *Chemosphere*, vol. 65, no. 10, pp. 1707–1714, 2006.
- [73] J.-S. Rhee, B.-M. Kim, C.-B. Jeong, K. M. Y. Leung, G. S. Park, and J.-S. Lee, "Development of enzyme-linked immunosorbent assay (ELISA) for glutathione S-transferase (GST-S) protein in the intertidal copepod *Tigriopus japonicus* and its application for environmental monitoring," *Chemosphere*, vol. 93, no. 10, pp. 2458–2466, 2013.
- [74] M. Sevcikova, H. Modra, A. Slaninova, and Z. Svobodova, "Metals as a cause of oxidative stress in fish: a review," *Veterinárni Medicína*, vol. 56, no. 11, pp. 537–546, 2011.
- [75] G. Q. Fu, T. T. Han, X. Y. Gong, and H. H. Huang, "Effect of Cu²⁺ stress on growth and physiological biochemical characteristics of *Sargassum hemiphyllum*," *South China Fisheries Science*, vol. 11, no. 4, pp. 34–39, 2015, in Chinese.
- [76] M. F. Jian, Y. T. Shi, T. Chen et al., "The physiological and biochemical characteristics of the wetland plant *Ludwigia prostrata* roxbunder the heavy metal pollution stress of cadmium and lead," *Journal of Jiangxi Normal University (Natural Science)*, vol. 41, no. 1, pp. 93–98, 2017, in Chinese.
- [77] J. Zhang, X. X. Zhao, X. Wang, and W. X. Lu, "Effects of cadmium stress on the growth and physiological property of *Oenanthe javanica*," *Plant Physiology Journal*, vol. 51, no. 11, pp. 1969–1974, 2015, in Chinese.
- [78] F. F. Li, *The Toxicological Effect of Lead (Pb) and Cadmium (Cd) on the Floating Plant Spirdela Polyrrhiza*, Nanjing Normal University, Nanjing, China, 2016, in Chinese.
- [79] B. W. Zhang, J. T. Zhao, E. W. Wu et al., "Water pollution characteristics of heavy metals in Fuyang River system and their toxicity to *Vibrio qinghaiensis* sp. Q67 and *Scenedesmus obliquus*," *Asian Journal of Ecotoxicology*, vol. 13, no. 1, pp. 179–189, 2018, in Chinese.
- [80] P. Xu, *Research on Heavy Metal Biosorption/accumulation by White-Rot Fungi and Fungi Tolerance/Resistance Analysis*, Hunan University, Chang Sha, China, 2016, in Chinese.
- [81] S. Y. Zhou, J. L. Zhao, G. Y. Huang, and G. G. Ying, "Toxicity and joint effects of heavy metals Zn, Cu and Hg to recombinant luminescent bacterium," *Journal of South China Normal University (Natural Science Edition)*, vol. 50, no. 1, pp. 33–37, 2018, in Chinese.
- [82] ECB (European Chemical Bureau), *Technical Guidance Document on Risk Assessment-Part II, Technical Report*, Institute for Health and Consumer Protection, Ispra, Italy, 2003.
- [83] L. Zhu, *Environmental Toxicology*, vol. 57–69, Higher Education Press, Beijing, China, 2006, in Chinese.
- [84] J. M. Morris, S. F. Brinkman, M. W. Carney, and J. Lipton, "Copper toxicity in Bristol Bay headwaters: part 1—acute mortality and ambient water quality criteria in low-hardness water," *Environmental Toxicology and Chemistry*, vol. 38, no. 1, pp. 190–197, 2019.
- [85] F. C. Wu, C. L. Feng, Y. J. Cao et al., "Aquatic life ambient freshwater quality criteria for copper in China," *Asian Journal of Ecotoxicology*, vol. 6, no. 6, pp. 617–628, 2011, in Chinese.
- [86] Canadian Council of Ministers of the Environment, *Protocol for the Derivation of Water Quality Guidelines for the Protection of Aquatic Life*, Canadian Council of Ministers of the Environment, Winnipeg, Canada, 1999.
- [87] S. A. L. M. Kooijman, "A safety factor for LC50 values allowing for differences in sensitivity among species," *Water Research*, vol. 21, no. 3, pp. 269–276, 1987.
- [88] O. N. Smirnova and E. I. Mel'nichenko, "Study of zinc and cadmium chloride toxicity using human embryo fibroblast cultures," *Gigiena Truda I Professionalnye Zabolevaniia*, no. 7, pp. 49–50, 1990.
- [89] C. Lindholmer, "Toxicity of zinc ions to human spermatozoa and the influence of albumin," *Andrologia*, vol. 6, no. 1, pp. 7–16, 1974.
- [90] Australian and New Zealand Environment and Conservation Council and Agriculture and Resource Management Council of Australia and New Zealand, *Australia and New Zealand Guidelines for Fresh and Marine Water Quality*, Anzecc and Armcanz, Canberra, Australia, 2000.
- [91] F. C. Wu, C. L. Feng, R. Q. Zhang, Y. S. Li, and D. Y. Du, "Derivation of water quality criteria for representative water-body pollutants in China," *Science China Earth Sciences*, vol. 42, no. 5, pp. 665–672, 2012, in Chinese.
- [92] State Environmental Protection Administration, *GB 3838-2002 Surface Water Environmental Quality Standards*, China Standard Publishing House, Beijing, China, 2002, in Chinese.
- [93] State Environmental Protection Administration, *GB11607-89 Fishery Water Quality Standards*, China Standard Publishing House, Beijing, China, 1989, in Chinese.
- [94] F. C. Wu, C. L. Feng, Y. J. Cao et al., "Toxicity characteristic of zinc to freshwater biota and its water quality criteria," *Asian Journal of Ecotoxicology*, vol. 6, no. 4, pp. 367–382, 2011, in Chinese.
- [95] W.-C. Lin, Z. Li, and M. A. Burns, "A drinking water sensor for lead and other heavy metals," *Analytical Chemistry*, vol. 89, no. 17, pp. 8748–8756, 2017.
- [96] R. Hu, K. Sun, X. Su, Y.-x. Pan, Y.-f. Zhang, and X.-p. Wang, "Physiological responses and tolerance mechanisms to Pb in two xerophils: *Salsola passerina* Bunge and *Chenopodium album* L.," *Journal of Hazardous Materials*, vol. 205–206, pp. 131–138, 2012.
- [97] M. M. Khan, E. Islam, S. Irem et al., "Pb-induced phytotoxicity in para grass (*Brachiaria mutica*) and Castorbean (*Ricinus communis* L.): antioxidant and ultrastructural studies," *Chemosphere*, vol. 200, pp. 257–265, 2018.
- [98] A. Kumar, M. N. V. Prasad, and O. Sytar, "Lead toxicity, defense strategies and associated indicative biomarkers in *Talinum triangulare* grown hydroponically," *Chemosphere*, vol. 89, no. 9, pp. 1056–1065, 2012.
- [99] B. Pourrut, M. Shahid, C. Dumat, P. Winterton, and E. Pinelli, "Lead uptake, toxicity, and detoxification in plants," *Reviews of Environmental Contamination and Toxicology*, vol. 213, pp. 113–136, 2011.
- [100] H. Zaier, T. Ghnaya, A. Lakhdar et al., "Comparative study of Pb-phytoextraction potential in *Sesuvium portulacastrum*

- and *Brassica juncea*: tolerance and accumulation,” *Journal of Hazardous Materials*, vol. 183, no. 1–3, pp. 609–615, 2010.
- [101] V. M. Burden, M. B. Sandheinrich, and C. A. Caldwell, “Effects of lead on the growth and δ -aminolevulinic acid dehydratase activity of juvenile rainbow trout, *Oncorhynchus mykiss*,” *Environmental Pollution*, vol. 101, no. 2, pp. 285–289, 1998.
- [102] A. Demayo, M. C. Taylor, K. W. Taylor, P. V. Hodson, and P. B. Hammond, “Toxic effects of lead and lead compounds on human health, aquatic life, wildlife plants, and livestock,” *Critical Reviews in Environmental Control*, vol. 12, no. 4, pp. 257–305, 1982.
- [103] U. S. EPA (US Environmental Protection Agency), *Environmental Criteria and Assessment Office: EPA 600/8-83-028*, U. S. Environmental Protection Agency. Air Quality Criteria for Lead, Washington, DC, USA, 1986.
- [104] R. J. Kieber, J. D. Willey, and S. D. Zvalaren, “Chromium speciation in rainwater: temporal variability and atmospheric deposition,” *Environmental Science & Technology*, vol. 36, no. 24, pp. 5321–5327, 2002.
- [105] J. J. Testa, M. A. Grella, and M. I. Litter, “Heterogeneous photocatalytic reduction of chromium (VI) over TiO_2 particles in the presence of oxalate: involvement of Cr(V) species,” *Environmental Science & Technology*, vol. 38, no. 5, pp. 1589–1594, 2004.
- [106] S. Rengaraj, S. Venkataraj, J. W. Yeon et al., “Preparation, characterization and application of Nd- TiO_2 photocatalyst for the reduction of Cr (VI) under UV light illumination,” *Applied Catalysis B Environmental*, vol. 77, no. 1-2, pp. 157–165, 2007.
- [107] Z. L. Wang and Y. L. Zhong, “Investigation progress about microelement chromium,” *China Feed*, vol. 4, pp. 16-17, 2001, in Chinese.
- [108] J. Liao, F. Liang, S. G. Yang et al., “Derivation of freshwater quality criteria for hexavalent chromium for protection of aquatic organisms in China,” *Asian Journal of Ecotoxicology*, vol. 9, no. 2, pp. 306–318, 2014, in Chinese.
- [109] G. C. Hose and P. J. Van Den Brink, “Confirming the species-sensitivity distribution concept for endosulfan using laboratory, mesocosm, and field data,” *Archives of Environmental Contamination and Toxicology*, vol. 47, no. 4, pp. 511–520, 2004.

Research Article

Kinetic Study of the Adsorption of Polyphenols from Olive Mill Wastewater onto Natural Clay: Ghassoul

Safae Allaoui ¹, Mohammed Naciri Bennani,¹ Hamid Ziyat ¹, Omar Qabaqous,¹ Najib Tijani,² and Najim Ittobane³

¹Laboratory of Chemistry-Biology Applied to the Environment, Research Team “Applied Materials and Catalysis”, Chemistry Department, Faculty of Sciences, Moulay-Ismaïl University, BP. 11201-Zitoune, Meknes 50000, Morocco

²Research Team “Membrane Materials and Separation Processes,” Chemistry Department, Faculty of Science, Moulay-Ismaïl University, BP. 11201-Zitoune, Meknes 50000, Morocco

³Research Team “Biomolecular and Macromolecular Chemistry,” Chemistry Department, Faculty of Science, Moulay-Ismaïl University, BP. 11201-Zitoune, Meknes 50000, Morocco

Correspondence should be addressed to Safae Allaoui; allaouisafae@gmail.com

Received 7 December 2019; Accepted 11 March 2020; Published 25 April 2020

Guest Editor: Lisa Yu

Copyright © 2020 Safae Allaoui et al. This is an open access article distributed under the Creative Commons Attribution License, which permits unrestricted use, distribution, and reproduction in any medium, provided the original work is properly cited.

The aim of this study is based on natural clay as an adsorbent in the elimination of polyphenols from olive mill wastewater (OMW). This clay was analyzed using XRD, SEM/EDX, FTIR, surface area measurement (BET method), thermal analysis (TGA/DTA), and X-ray fluorescence (XRF) and then used in adsorption experiments. The results reveal that the best quantity of adsorption of polyphenols is 161 mg/g at the temperature of 25°C, but they decrease at 35°C and 45°C. A great agreement with pseudo-second-order and Freundlich model is represented by kinetic and isotherms models, and several parameters such as ΔG^0 , ΔS^0 , and ΔH^0 were determined using the thermodynamic function relationship.

1. Introduction

The olive mill wastewaters (OMWs) from two-phase extraction systems are deemed to be one of the main environmental problems in region Fes-Meknes, Morocco (Figure 1), due to presence of toxic elements such as polyphenols. In 2016, Morocco generated 4000 to 5000 tonnes of OMW diverse in the rivers [1] because we used greater quantities of water which generate large volumes of the latter [2].

OMW is an environmental threat, and it became a problem that needs to be solved by the olive industry [3]. The composition of OMW may vary significantly depending on several factors: climate conditions, olive storage period, extraction process, and period of production [4].

Many physicochemical and biological techniques have been developed to treat OMW. These methods include coagulation/flocculation [5, 6], oxidation, ozonation [7], and membrane filtration [3, 7, 8]. Despite the availability of the processes above, the adsorption method is most extensively employed for treatments of the OMW.

For instance, Curi and Velioglu [9] and Azzam [10] utilized activated charcoal and natural clay for adsorption of hydroxytyrosol and other phenolic mixes from OMW.

The goal of this research is the elimination of OMW polyphenols onto a low-cost clay called ghassoul and the characterization of this material. For this purpose, the quantity of polyphenols retained has been determined at the equilibrium. The isotherms to Langmuir and Freundlich models have been described. Moreover, the kinetic of adsorption has been analyzed uses pseudo-first-order (PFO), pseudo-second-order (PSO), and Weber–Morris intra-particle diffusion (IPD) models.

2. Materials and Methods

2.1. Material. The material used is the commercial clay labelled “Ghassoul Chorafa Al Akhdar” without any further treatment, native from a site called “Ksabi” in the Province of Missouri, East of Middle Atlas (Fez-Morocco). The particles of size <63 nm are crushed and dried during 24 hours at 80°C

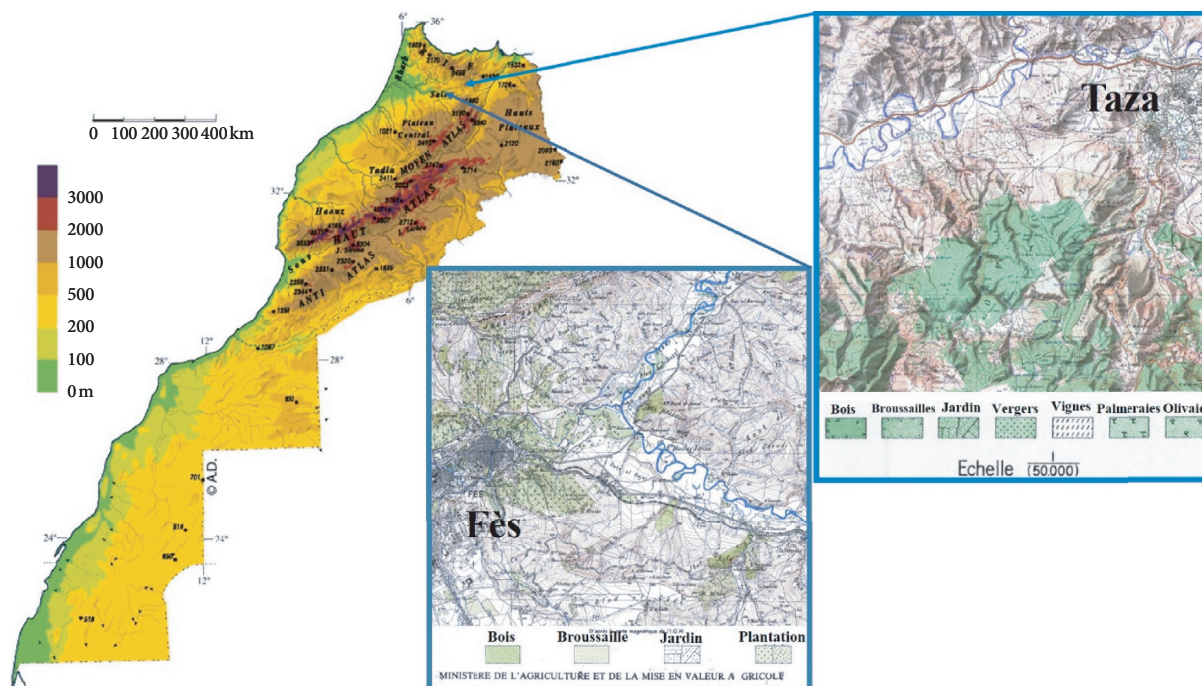


FIGURE 1: Geographical map of the origin of olive (taza) and sampling OMW (Fes), Morocco.

in the steam room. The prepared product was called Gh-B, referring to unprocessed ghassoul.

2.2. Olive Mill Wastewater and Pretreatment. The origin olive from Taza (Morocco) and the OMW was obtained from a two-phase discontinuous extraction factory in the Fes-Meknes region (Morocco) on 20 November 2018. The gathered OMW was kept in separate plastic containers until use and then treated under nitrogen stream to remove dissolved oxygen to protect polyphenols. The sample obtained was then filtered and conserved to prepare a stock solution for kinetic study.

2.3. Physical, Chemical, and Mineralogical Characterisation. The Gh-B was characterized by physicochemical techniques (XRD, FTIR, BET, DTA/TGA, SEM, EDX, and XRF).

For X-ray diffraction analysis, the Philips PW 1800 instrument has been utilized. The quickening voltage was 40 kV, the current was 20 mA, and the copper $K\alpha$ radiation was $\lambda = 1.5418 \text{ \AA}$. The spectra of the different samples were registered in an interval of 2θ (5° – 70°) with an accurate addition of 0.04° .

FTIR investigation was directed by using Fourier Transform Infrared Spectrometer (JASCO 4000), out fitted in with a detector (TGS) and a ceramic source isolated by an optical framework utilizing an interferometer of Michelson. FTIR spectra are extended somewhere in the range of 4.000 and 400 cm^{-1} .

The Micromeritics ASAP 2010 Gas Sorption System was used to measure the surface area, and both methods of BET and BJH were utilized for determination of the specific surface and the pore size.

Thermogravimetric (TGA-DTA) investigation was completed by using Shimadzu TA-60 type contraption, working under air with a direct warming rate of $10^\circ\text{C}\cdot\text{min}^{-1}$ from surrounding temperature to 600°C .

The technique of SEM-EDX was utilized to determine the morphology and elemental composition of the Gh-B.

The Gh-B dried at 105°C was analyzed by using X-ray fluorescence Philips PW 1666 type to determine the chemical composition, such as P_2O_5 , Al_2O_3 , MgO , Fe_2O_3 , BaO , and SiO_2 .

2.4. Kinetic of Adsorption of Polyphenols from OMW onto Gh-B.

Adsorption tests were done in black bottles to avoid the degradation of polyphenols. 50 mg of Gh-B with 50 mL of OMW was diluted in water (starting focus $C_0 = 30 \text{ mg}\cdot\text{L}^{-1}$). The blends were waved at temperatures of 25°C , 35°C , and 45°C during different times (20 min to 180 min). After each time, the blend is segregated by centrifugation at 3400 rpm for 8 min, and the supernatant was examined for determination of total polyphenols utilizing the Folin-Ciocalteu [11] technique and analyzed by UV-Vis spectroscopy. The absorbance at the wavelength of 760 nm was determined to calculate the leftover concentration of polyphenols (C_e , $\text{g}\cdot\text{L}^{-1}$), and amount of polyphenols adsorbed at equilibrium time (q_e , in $\text{mg}\cdot\text{g}^{-1}$) was calculated utilizing the following equation [12]:

$$q_e = \frac{(C_0 - C_e) \times V}{m}, \quad (1)$$

where C_0 is the initial concentration of polyphenols, C_e is the leftover concentration of polyphenols which are expressed by $\text{g}\cdot\text{L}^{-1}$, m (mg) is the lump of Gh-B, and V (mL) is the volume of OMW diluted.

The adsorption isotherms were done under identical conditions from those of the adsorption kinetic utilizing a larger concentration from 0 to 58 mg·L⁻¹ of polyphenols. The solutions were mixed for 3 hours until the equilibrium time was attained and then centrifuged. The determination of residual concentrations and the adsorbed amounts was done using (1).

2.5. Theoretical Background. We present in this part the expressions utilized to represent the kinetic and isotherms of the examined models.

2.6. Modelling of Kinetic Studies

2.6.1. Kinetic of PFO. The kinetic model Lagergren [13] of pseudo-first-order (PFO) is represented by the following equation:

$$\ln(q_e - q_t) = \ln q_e - K_1 t, \quad (2)$$

where q_t is the capacity adsorbed at time t ; q_e is the capacity adsorbed at balanced, which are expressed by mg·g⁻¹; and K_1 (min⁻¹) is the speed constant of PFO. K_1 and q_e can be determined by plotting $\ln(q_e - q_t)$ versus the time t .

2.6.2. Kinetic of PSO. The expression of the pseudo-second-order (PSO) model [13, 14] is represented by the following equation:

$$\frac{t}{q_t} = \frac{1}{K_2 \times q_e^2} + \frac{t}{q_e}, \quad (3)$$

where K_2 (g·mg⁻¹·min⁻¹) is the speed constant for the PSO and q_e is the quantity of polyphenols adsorbed at the balanced (mg·g⁻¹). The slope and the y -intercept are utilized to calculate K_2 of PSO and q_e .

2.6.3. Model of IPD. The determination of intraparticle diffusion models is done using equation (4) (Weber–Morris equation) [14, 15]. This model is used to determine the limiting step in the adsorption mechanism:

$$q_t = K_d \times t^{1/2} + C, \quad (4)$$

where K_d is the IPD constant in mg·g⁻¹·min^{-1/2} and C represents the value of the thickness of the boundary layer. They can both be determined from slope and the y -intercept (equation (4)).

2.7. Adsorption of Isotherm Studies. In the literature, various models have been published to compare experimental and theoretical data of adsorption isotherms. Freundlich and Langmuir models were utilized to describe isotherm adsorption.

2.7.1. Langmuir Model. The nonlinear shape of the Langmuir model [14] is expressed by the following equation:

$$\frac{q_e}{q_{\max}} = \frac{(K_L \times C_e)}{(1 + K_L \times C_e)}, \quad (5)$$

where K_L is the Langmuir constant (L·mg⁻¹), C_e is the equilibrium polyphenol concentration (mg·L⁻¹), q_e is the adsorption capacity of polyphenols at equilibrium (mg·g⁻¹), and q_m is the maximum adsorption amount for a monolayer (mg·g⁻¹). Another parameter labelled separation factor (R_L) [16, 17] is expressed in the following equation:

$$R_L = \frac{1}{1 + K_L \times C_0}, \quad (6)$$

where C_0 is the initial concentration of the adsorbate (mg·L⁻¹). R_L is the factor of separation which allows to check whether the isotherm is favorable or not provided that if the value of R_L is between 0 and 1, it confirms the validity of the Langmuir model; when R_L is close to 1 or 0, it signifies that the isotherms are linear and irreversible, respectively, and if R_L is upper to 1, it indicate that isotherm is unfavourable [16, 17].

2.7.2. Freundlich Model. The nonlinear type of the Freundlich model [15, 18] can be calculated by the following equation:

$$q_e = K_F \times C_e^{1/n}, \quad (7)$$

where q_e is the equilibrium polyphenol concentration on the ghasoul, C_e is the equilibrium polyphenol concentration of solution, K_F is the Freundlich constant, and n is the adsorption intensity characterizing the affinity of the pollutant for the adsorbent; when n is close to 1, it signifies a chemical adsorption process, and when n is greater than 1, it indicates a physical adsorption mechanism.

2.7.3. Thermodynamic Parameters of Adsorption. The enthalpy (ΔH^0), free energy (ΔG^0), and entropy (ΔS^0) thermodynamic parameters are calculated by the following relations [19]:

$$\Delta G^0 = -RT \ln(K), \quad (8)$$

$$\ln K = \frac{\Delta S^0}{R} + \frac{\Delta H^0}{RT},$$

where K_C is the equilibrium constant defined as follows:

$$K_C = \frac{C_{\text{ads}}}{C_0} = \frac{(C_e - C_0)}{C_e}, \quad (9)$$

in which C_{ads} is the adsorbed concentration (g/L) and C_0 is the initial concentration of polyphenols in OMW (g/L).

3. Results and Discussion

3.1. Physicochemical Characterization of Gh-B

3.1.1. XRD Study. XRD analyses (Figure 2) showed that Gh-B consists of three phases of clay:

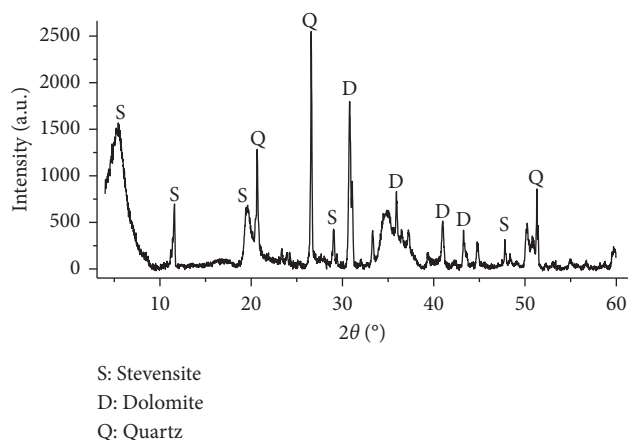


FIGURE 2: X-ray diffraction patterns of Gh-B.

TABLE 1: Chemical composition of Gh-B.

Name of compound	P ₂ O ₅	Fe ₂ O ₃	SiO ₂	BaO	MgO	MO	Al ₂ O ₃			
% of oxide	0.0325	1.544	42.965	0.0314	13.532	0.290	2.514			
Element in	S	Ca	F	Sn	As	Cu	Zn	Pb	Ag	
(%)	4.303	6.770	0.940	<LD	<LD	0.009	0.006	0.006	<LD	

LD: limit of detection.

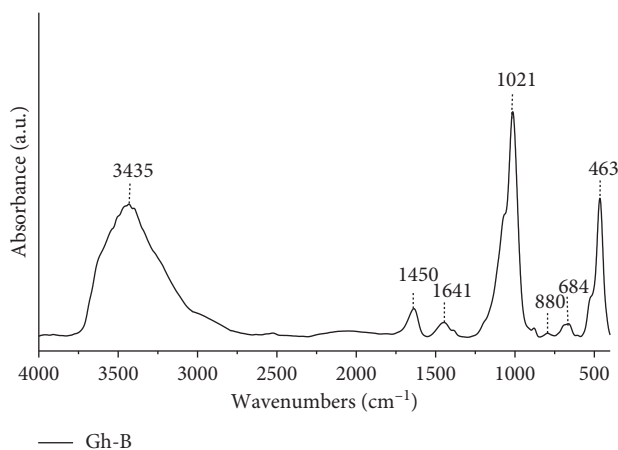


FIGURE 3: FTIR spectra of Gh-B.

- (i) Stevensite (S) observed at the $2\theta = 5.70^\circ, 11.61^\circ, 19.33^\circ, 29.43^\circ, 33.40^\circ, \text{ and } 44.84^\circ$
- (ii) Dolomite (D) observed at the $2\theta = 30.83^\circ, 34.58^\circ, 41.03^\circ, \text{ and } 35.22^\circ$
- (iii) Quartz (Q) observed at the $2\theta = 20.73^\circ, 26.52^\circ, \text{ and } 53.70^\circ$

One also notices the presence of free silica in the shape of quartz and dolomite in very small amount. On the contrary, the stevensite and magnesia poles of the smectites series are dominant in the Gh-B. These outcomes are congruent with those obtained in the literature [19–21].

3.1.2. XRF Analysis. XRF was carried out to identify the chemical composition of the minerals present in the Gh-B.

The information given in Table 1 demonstrates that the magnesium and silica oxides are available in a large quantity; the presence of alumina (Al₂O₃) is very important, and other elements are present in trace quantity. These results are in agreement with the XRD results and those cited by other authors such as Ellass et al. and Ajbary et al. [20, 21].

3.1.3. FTIR Analysis. The spectra of natural clay (Gh-B) demonstrate a large absorption band at 3437 cm^{-1} corresponding to the OH-stretching vibration of the water molecules. The bending mode of the interlayer and/or adsorbed water appears around 1641 cm^{-1} . The stretching vibrations anti-symmetric C-O around 1450 cm^{-1} show the presence of the carbonate anions ($\nu_{\text{as}}(\text{CO}_3^{-2})$) inside walls. Both vibrations of ($\nu_{\text{s}}(\text{CO}_3^{-2})$) and Al₂O₃ groups are

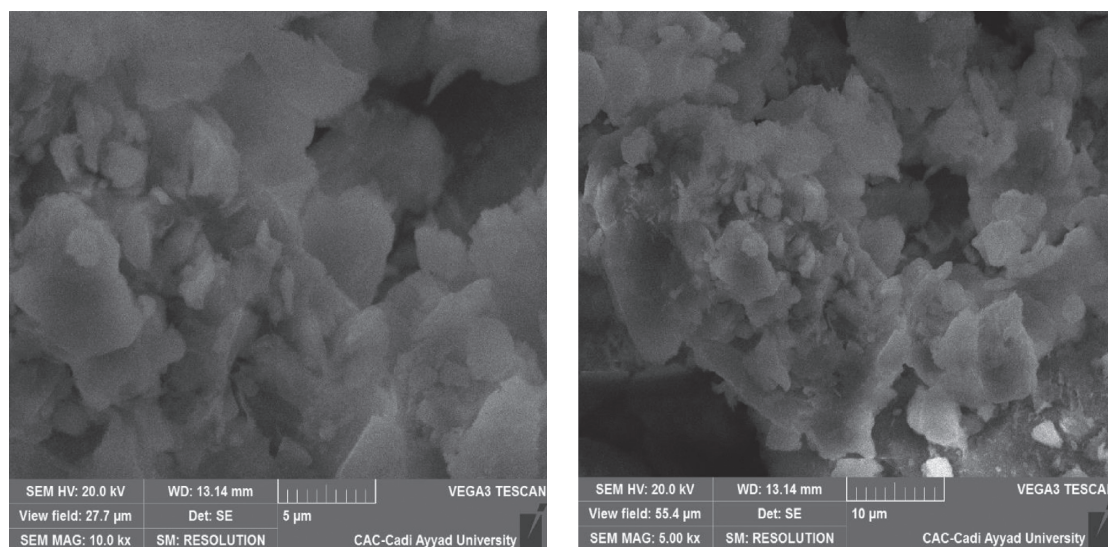


FIGURE 4: SEM images and EDX analysis of Gh-B.

TABLE 2: Chemical elements of Gh-B and their %.

Element	O	Fe	Mg	Al	Si	S	K	Ca
% masses	47.9	4	13.8	1	23.8	0.7	0.6	8.2

observed at 880 cm^{-1} . The bands which appear around 1021 , 684 , and 463 cm^{-1} are attributed to the vibrations of the SiO_2 group (Figure 3).

3.1.4. SEM/EDX and BET Analysis. SEM micrograph of Gh-B (Figure 4) shows that the morphology of the Gh-B is close to hectorite, and the particles from different sizes have the appearance of sheets which oriented parallel to each other, as indicated by Caillere and Henin [22].

The chemical elements contained in natural clay (Gh-B) were detected by EDX analysis, and the results show that Gh-B has a higher percentage of silica (Table 2) mainly due to the presence of majority of quartz followed by magnesia. These results are in agreement with XRD and XRF analysis.

Table 2 gives the chemical elements and their mass percentages determined by the EDX analysis.

The nitrogen adsorption/desorption isotherms of Gh-B show that, according to the IUPAC classification, isotherm obtained is type IV, characteristic of solid mesoporous with onset hysteresis of H3 type. After calculating using the BET method, the specific surface is $296\text{ m}^2/\text{g}$.

The pore size distribution is determined from desorption isotherm by the BJH method, shown in Figure 5. This latter shows that the pore diameter is in the order of 73 \AA and thus confirms the mesoporosity of the structure of the Gh-B.

3.1.5. Thermal Analysis (DTA/TGA). TGA/DTA thermogram (Figure 6) shows that the breakdown of Gh-B is done on three exothermic steps and one endothermic step:

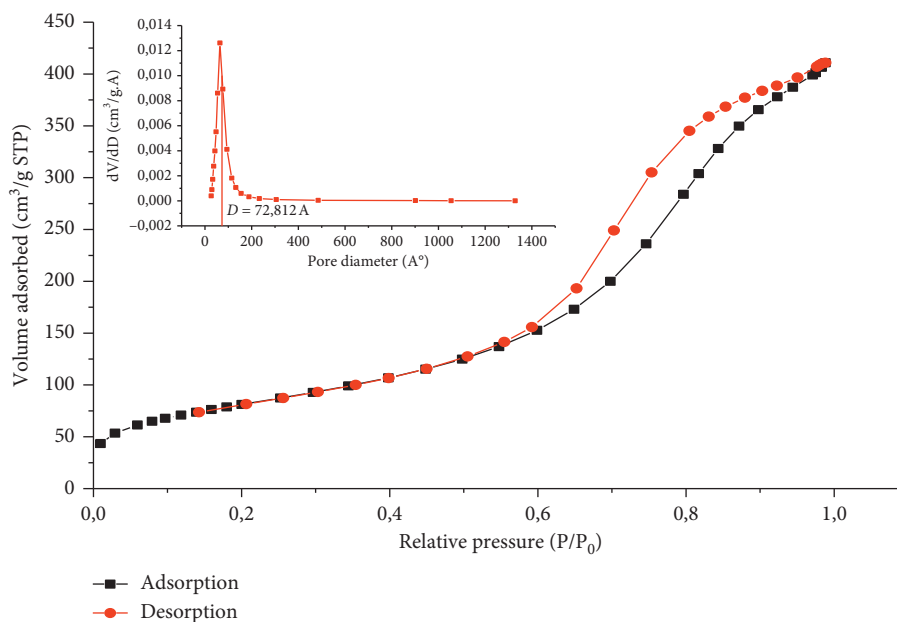


FIGURE 5: N₂ adsorption/desorption isotherms of Gh-B.

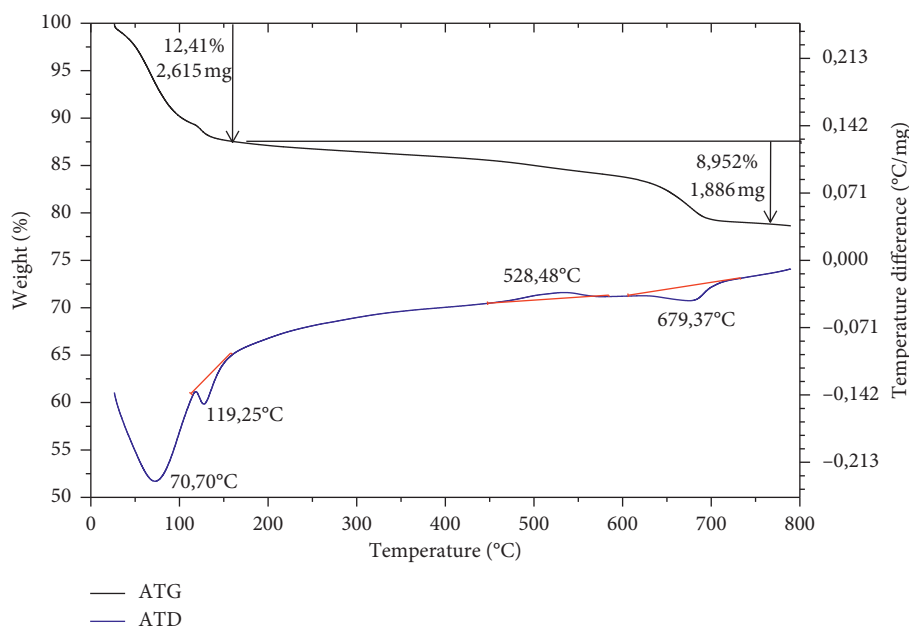
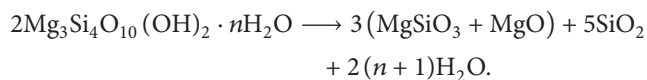


FIGURE 6: DTA and TGA plots of Gh-B.

- (i) First degradation step with loss of mass on the order of 12% due to the removal of water molecules infirm bound or adsorbed on external faces of the crystals. This step manifests itself by two distinct endothermic peaks on curve ATD at two temperatures 70.70°C and 128.95°C, respectively.
- (ii) Second loss of almost 8.95% mass at 679.37°C (ATD), which is manifested by wide and asymmetric peak corresponding to decomposition of the early mixed carbon of magnesia and the calcium.
- (iii) Exothermic pic around 528°C corresponding to allotropic transformation of the stevensite in enstatite.

That transformation of stevensite in enstatite is represented by the following equation:



(10)

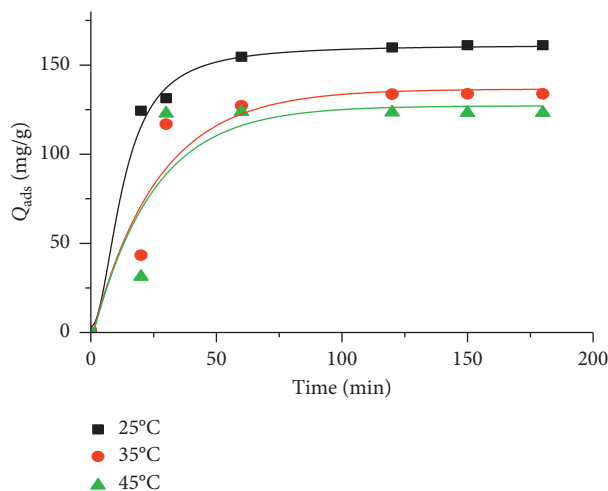


FIGURE 7: Various adsorption kinetic according to time of three temperatures.

3.2. Kinetics Adsorption. Figure 7 demonstrates that the quantity of polyphenols adsorbed at different temperatures is in the order 161 mg/g and considered important because of the high specific surface area ($296 \text{ m}^2 \cdot \text{g}^{-1}$) of Gh-B. The curves demonstrate that the adsorption kinetics is very quick at the start, due to the presence of the active sites at the start of adsorption, and the equilibrium was established after 2 h (about 60 min at 25°C). The quantities of polyphenols adsorbed onto Gh-B diminished from 161 to $123 \text{ mg} \cdot \text{g}^{-1}$ when the temperature increases from 25°C to 45°C , indicating that the temperature higher than 25°C destabilizes the force of adsorption and also decreases the interaction between Gh-B and polyphenols, and therefore, the adsorption process is exothermic. The same observation was found by De Chimie et al., works of adsorption of polyphenols from OMW by pomace olive which is utilized as an active carbon [23].

The plots of $\ln(q_e - q_t)$ and t/q_t according to time (equations (2) and (3), respectively) are obtained in Figures 8(a) and 8(b), respectively. We can wind up that polyphenols are adsorbed onto Gh-B and excellently follow-up the PSO model (Figure 8(a)). This is endorsed by these adsorbed quantities determined theoretically (q_{th}) and are very near to those obtained experimentally (q_{exp}), $R^2 = 0.99$ (Table 3).

In this study, we notice that when the temperature of the solution raises, the apparent constant of the PSO speed K_2 increased probably due to chemisorption phenomena. The same observation has been obtained in the adsorption of phenolic compounds from OMW on orange peel [24], on active carbon [25–28], onto resin [29], on onion [30], in removal of basic yellow cationic dye, [21] and in methyl violet by the same adsorbent (ghassoul) [20].

3.2.1. IPD. The plot of the adsorbed quantity q_t versus $t^{1/2}$ shows that polyphenols are adsorbed in two steps (Figure 9). The first one is quick; this is due to the transfer of polyphenols from OMW to the outside of the adsorbent. The second step is typified by a slight evolution to equilibrium,

and it represents interaction between ghassoul and polyphenols. These results validate an adsorption according to a kinetic of the PSO. However, the values of constant C are different to 0 (Table 4) that shows the rate of polyphenol adsorption onto Gh-B is not controlled only by IPD step. This results is an agreement with Valderrama et al. and Lavinia et al. [31, 32].

3.2.2. Study of Activation Energy E_a . The tracing of $\ln K_2$ as function to $1/T$ allows to determine activation energy E_a from the slope of the equation line Arrhenius. Figure 10 shows that the experimental points give a line when R^2 is very near to 1. The value of activation energy (90.622 kJ/mol) given by the slope of the Arrhenius plot demonstrates that the adsorption of polyphenols from OMW can be controlled by a chemisorption phenomenon. This phenomenon is confirmed by the obtained kinetic results. This is in accordance with the works of M. Kessoum [33] in the investigation of adsorbed polyphenols on a commercial active carbon (Picachem 150), but it is in disagreement with the results of Senol et al. [28] in the kinetic studies of biophenol adsorption onto commercial activated carbon with different particle sizes and at varied temperature. They have found the physisorption phenomenon because the values of E_a are included between 27.22 and 33.76 kJ/mol.

3.3. Adsorption Isotherms. The curves of nonlinear transforms obtained by Langmuir and Freundlich models are shown in Figure 11, and the different parameters deduced from the two models are grouped in Table 5.

In Figure 11, it is clearly demonstrated that the adsorbed quantity of the polyphenols q_{max} increases when the initial polyphenol concentration C_0 grows until the saturation. Table 5 shows a good linear correlation coefficient R^2 close to 1 for both isotherms Langmuir and Freundlich.

However, the values n from the Freundlich model for various temperatures (Table 5) are greater than 1, and the values of K_F are large, indicating that the adsorption is favorable. For the Langmuir model, the values of R_L are

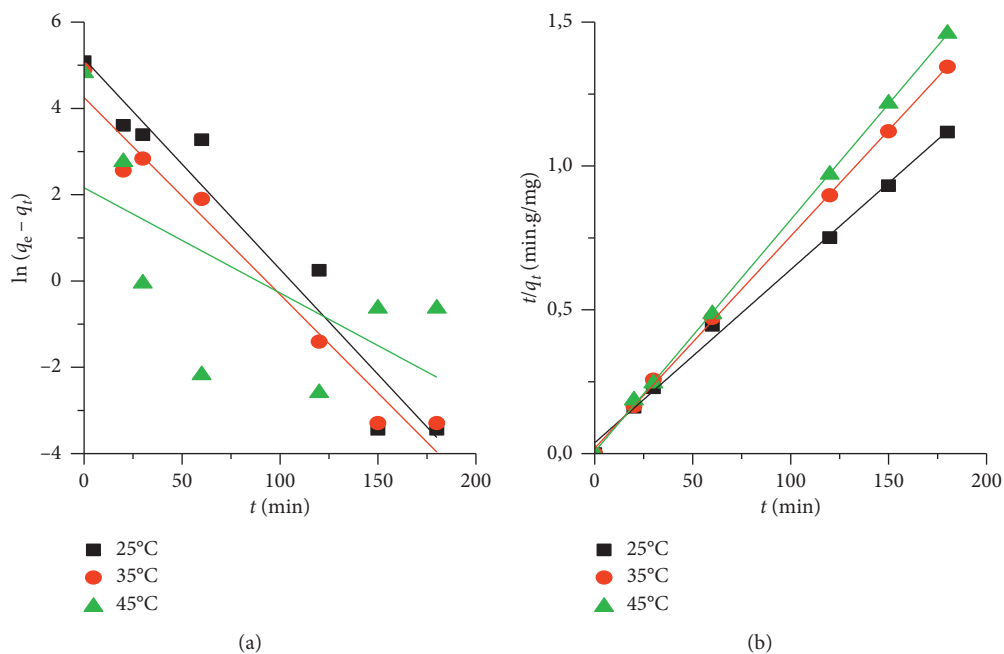


FIGURE 8: Linear portrayal of kinetic model of polyphenols adsorption onto Gh-B for both models (a) PFO and (b) PSO.

TABLE 3: PFO and PSO parameters.

T ($^{\circ}\text{C}$)	PFO model				PSO model		
	$q_{\text{ads (exp)}}$ (mg/g)	K_1 (min^{-1})	$q_{\text{ads (theorique)}}$ (mg/g)	R^2	$q_{\text{ads (theorique)}}$ (mg/g)	K_2 (g/(g·min))	R^2
25	161	0.049	171	0.872	166.113	0.001	0.999
35	134	0.046	70	0.920	135.685	0.003	0.999
45	123	0.024	8.676	0.083	124.069	0.010	0.999

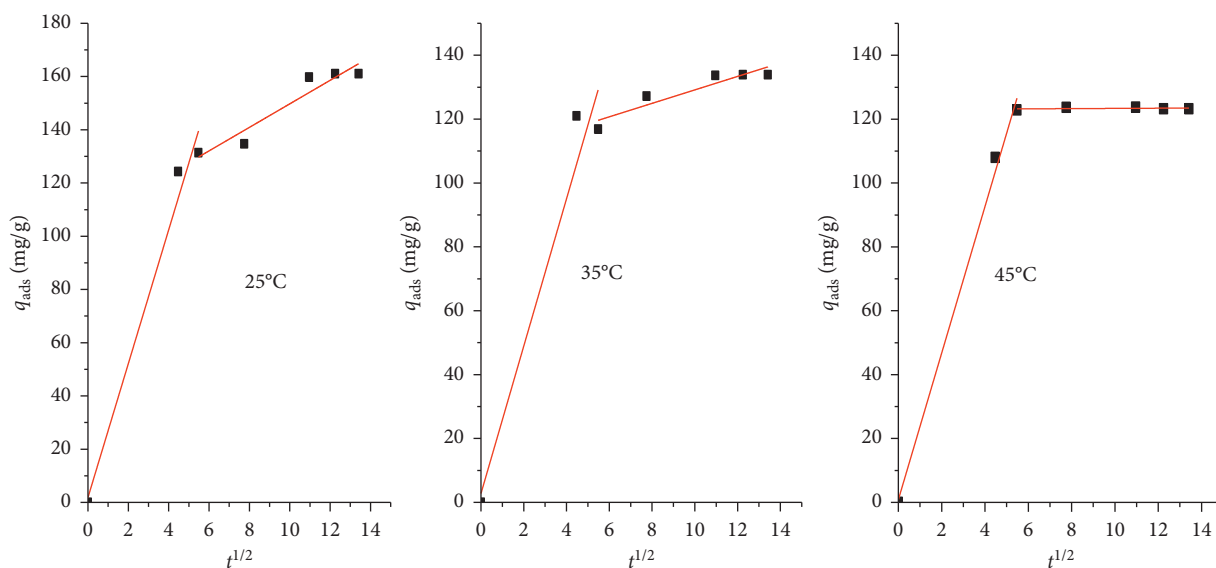


FIGURE 9: IPD plots for different temperatures.

TABLE 4: Parameters of IPD.

T ($^{\circ}\text{C}$)	Step 1				Step 2		
	C	K_d ($\text{g}\cdot\text{mg}^{-1}\cdot\text{min}^{-1/2}$)	R^2	C	K_d ($\text{g}\cdot\text{mg}^{-1}\cdot\text{min}^{-1/2}$)	R^2	
25	1.83	25.14	0.99	105.55	4.41	0.97	
35	2.76	23.07	0.98	108.06	2.10	0.96	
45	0.82	22.95	0.99	123.04	0.032	0.53	

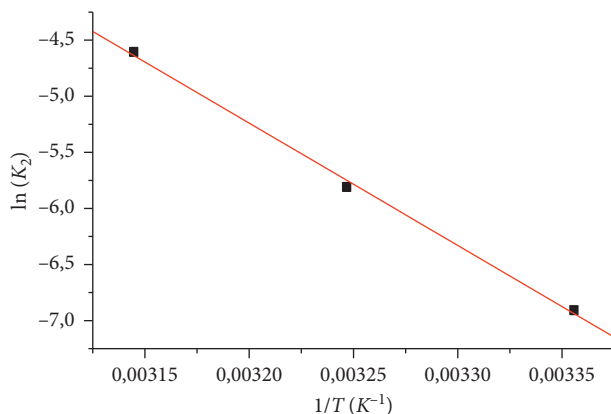


FIGURE 10: Arrhenius slope for adsorption of polyphenols.

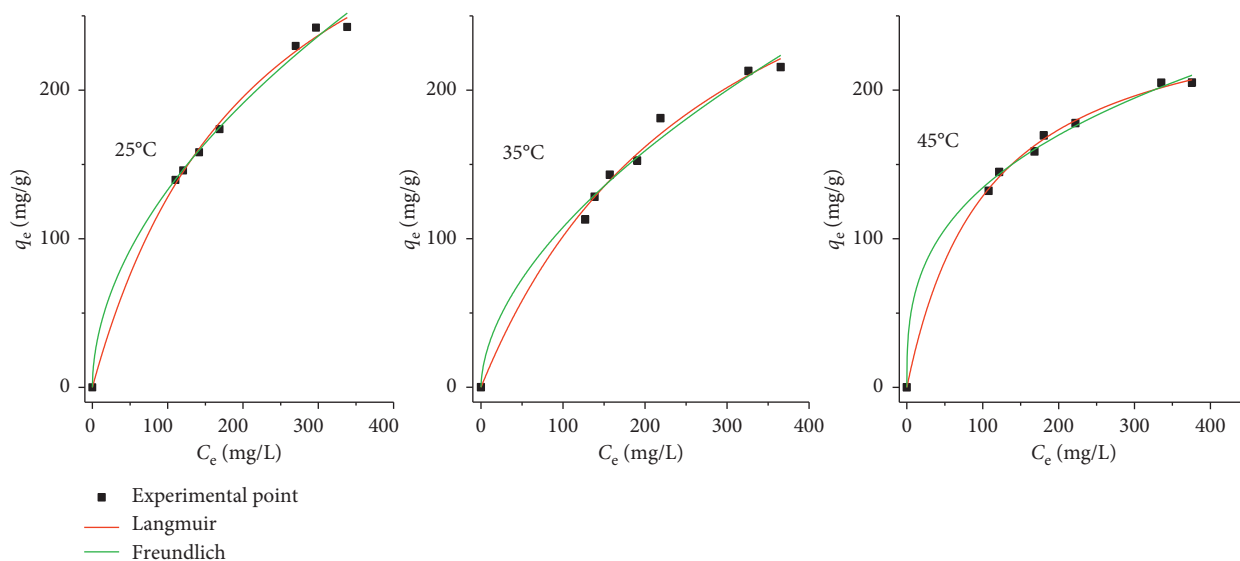


FIGURE 11: Adsorption isotherm for polyphenols onto ghassoul clay.

TABLE 5: Parameters of adsorption isotherms.

T ($^{\circ}\text{C}$)	Langmuir				n	Freundlich	
	q_{max} (mg/g)	K_L (mg/g)	R_L	R^2		K_F (mg/g)	R^2
25	411.91	4.51×10^{-3}	0.99	0.99	1.90	11.80	0.99
35	397.78	3.40×10^{-3}	0.99	0.99	1.77	8.06	0.98
45	265.81	9.38×10^{-3}	0.99	0.99	2.96	28.40	0.99

near to 1 in the concentration domain from 0 to 58 mg/L, but the amount of adsorbed q_{max} calculated from this model is much different from those found experimentally.

Therefore, the two models are favorable to describe the adsorption phenomena of polyphenols onto ghassoul clay, but Freundlich model is more suitable because the theoretical amount of polyphenols (q_{max}) calculated from the Langmuir model is very far to the experimental value for all temperatures. These results are similar to those obtained by Mounia et al. and Jedi et al. who worked on removing

phenolic compound by adsorption onto wheat bran and bentonite, respectively [33, 34].

3.3.1. Thermodynamic Parameters. The negative value of ΔH^0 (-0.14 kJ/mol) (Table 6) shows that the adsorption of polyphenols onto Gh-B is an exothermic process in accordance with the kinetic studies (q_{max} decreases with the increase in temperature). The order of the process is indicated by the negative value of ΔS^0 (-46.25 J/K·mol). The adsorption process is spontaneous because of the negative

TABLE 6: Thermodynamic parameters of adsorption of polyphenols onto Gh-B.

T (K)	ΔG^0 (kJ/mol)	ΔS^0 (J/K·mol)	ΔH^0 (kJ/mol)	R^2
298	-3.11			
308	-1.18	-46.25	-0.14	0.99
318	-0.22			

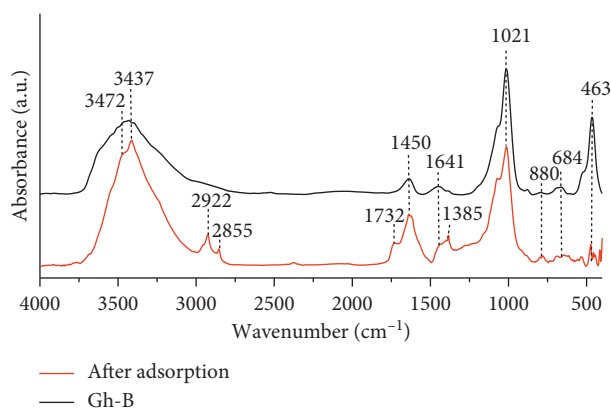


FIGURE 12: FTIR spectra of Gh-B before and after adsorption.

value of Gibbs free energy. These outcomes are identical to Makhoulouf et al. in the study of the adsorption of phenolic compounds onto mesoporous material [35].

3.4. Analysis of the Adsorption by FTIR. The spectrum of Gh-B after adsorption in Figure 12 shows new bands of vibration. A shouldering to 3472 cm^{-1} and an intense band at 3437 cm^{-1} corresponding to hydroxyl stretching vibration of free and bonded $-\text{OH}$ groups of the polyphenols, respectively. We also noted the presence of new bands at 2922 cm^{-1} and 2855 cm^{-1} corresponding to aromatic C-H and other bands at 1732 and 1385 cm^{-1} attributed to the C-O group of polyphenols (Figure 12). These results indicate the presence of polyphenols and confirmed that these compounds are adsorbed onto ghassoul.

4. Conclusion

In this study, we are interested in testing the effectiveness of natural clay “Gh-B” in the elimination of polyphenols from olive mill wastewater (OMW).

The obtained results are as follows:

- (i) The natural clay ghassoul is majority constituted of silica and magnesia. This result is in agreement with XRD, XRF, and SEM/EDX.
- (ii) The quantity of the polyphenols adsorbed at different temperature has been of order 161 mg/g , and it is considerably important because of high specific surface area ($296\text{ m}^2\text{-g}^{-1}$) of Gh-B.
- (iii) The examination of the adsorption kinetic of polyphenols onto Gh-B demonstrates that adsorption is done in two steps. The initial step is fast, and the balance comes at 2 h of contact. The next step is

typified by slow evolution to equilibrium and adsorption kinetic realized at pseudo-second-order (PSO) model.

- (iv) The experimental isotherms are preferentially described by the Freundlich model, and the thermodynamic study indicates that the adsorption of polyphenols was exothermic in nature $\Delta H^0 < 0$, ordered $\Delta S^0 < 0$, and spontaneous $\Delta G^0 < 0$.
- (v) All outcomes demonstrated that ghassoul was an effective and feeble cost adsorbent for the elimination of polyphenols from “OMW”.

Data Availability

The authors affirm that all information fundamental to the discoveries of this examination are completely accessible without limitation.

Conflicts of Interest

The authors declare that there are no conflicts of interest.

Acknowledgments

This work was done in the frame work of the project (PPR2), supported by Ministry of National Education, Professional Training, Higher Education and Scientific Research, Morocco (MENFPESRS), and National Center for Scientific and Technical Research/Rabat, Morocco (CNRST).

References

- [1] B. Zghari, F. Benyoucef, and A. Boukir, “Impact environnemental des margines sur les eaux d’oued ouessefrou: caracterisation physico-chimique et evaluation par chromatographie gazeuse couplee a la spectrometrie de masse (CPG-SM) the environmental impact of olive mill wastewater in ouessefrou,” *American Journal of Innovative Research and Applied Sciences*, vol. 2429–5396, pp. 276–291, 2018.
- [2] A. L. I. Agoumi and A. Debbarh, *Ressources en eau et bassins versants du Maroc : 50 ans de développement*, Report prepared within the framework of the “Water: Management of scarcity” organized by the Association of Moroccan Engineers of Bridges and Roads, pp. 13–62, Morocco, 2005.
- [3] B. Ibrahimoglu and M. Z. Yilmazoglu, “Disposal of olive mill wastewater with DC arc plasma method,” *Journal of Environmental Management*, vol. 217, pp. 727–734, 2018.
- [4] S. Dermeche, M. Nadour, C. Larroche, F. Moulti-mati, and P. Michaud, “Olive mill waste : biochemical characterization and valorization strategies,” *Process Biochemistry*, vol. 48, no. 10, pp. 1532–1552, 2013.
- [5] Ü. Tezcan Ün, S. Uğur, A. S. Koparal, and Ü. Bakir Öğütveren, “Electrocoagulation of olive mill wastewaters,” *Separation and Purification Technology*, vol. 52, no. 1, pp. 136–141, 2006.
- [6] T. Chatzistathis and T. Koutsos, “Olive mill wastewater as a source of organic matter , water and nutrients for restoration of degraded soils and for crops managed with sustainable systems,” *Agricultural Water Management*, vol. 190, pp. 55–64, 2016.
- [7] C. H. Neoh, Z. Z. Noor, N. S. A. Mutamim, and C. K. Lim, “Green technology in wastewater treatment technologies:

- integration of membrane bioreactor with various wastewater treatment systems," *Chemical Engineering Journal*, vol. 283, pp. 582–594, 2016.
- [8] T. Coskun, E. Debik, and N. M. Demir, "Treatment of olive mill wastewaters by nanofiltration and reverse osmosis membranes," *Desalination*, vol. 259, no. 1–3, pp. 65–70, 2010.
- [9] D. V. K. Curi and S. G. Velioglu, "Treatment of olive oil production wastes treatment and disposal of liquid and solid industrial wastes," in *Proceedings of the Third Turkish-German Environmental Engineering Symposium*, pp. 189–205, Istanbul, Turkey, June 1979.
- [10] M. O. J. Azzam, "Olive mills wastewater treatment using mixed adsorbents of volcanic tuff, natural clay and charcoal," *Journal of Environmental Chemical Engineering*, vol. 6, no. 2, pp. 2126–2136, 2018.
- [11] V. L. Singleton, R. Orthofer, and R. M. Lamuela-Raventós, "[14] Analysis of total phenols and other oxidation substrates and antioxidants by means of folin-ciocalteu reagent," in *Oxidants and Antioxidants Part A*, vol. 299, pp. 152–178, Elsevier, Amsterdam, Netherlands, 1999.
- [12] J. Huang, Y. Zhou, K. Huang, S. Liu, Q. Luo, and M. Xu, "Adsorption behavior, thermodynamics, and mechanism of phenol on polymeric adsorbents with amide group in cyclohexane," *Journal of Colloid and Interface Science*, vol. 316, no. 1, pp. 10–18, 2007.
- [13] H. Yuh-Shan, "Citation review of lagergren kinetic rate equation on adsorption reactions," *Scientometrics*, vol. 59, no. 1, pp. 171–177, 2004.
- [14] Y. S. Ho and G. McKay, "Pseudo-second order model for sorption processes," *Process Biochemistry*, vol. 34, no. 5, pp. 451–465, 1999.
- [15] T. W. Weber and R. K. Chakravorti, "Pore and solid diffusion models for fixed-bed adsorbers," *AIChE Journal*, vol. 20, no. 2, pp. 228–238, 1974.
- [16] S. Muralidharan, K. Srikrishna, and S. Subramanian, "Optimized power generation using dynamic programming," *International Energy Journal*, vol. 8, pp. 217–224, 2007.
- [17] K. R. Hall, L. C. Eagleton, A. Acrivos, and T. Vermeulen, "Pore- and solid-diffusion kinetics in fixed-bed adsorption under constant-pattern conditions," *Industrial & Engineering Chemistry Fundamentals*, vol. 5, no. 2, pp. 212–223, 1966.
- [18] Y. S. Ho and G. McKay, "Sorption of dye from aqueous solution by peat," *Chemical Engineering Journal*, vol. 70, no. 2, pp. 1227–1231, 1999.
- [19] Y. Seki and K. Yurdakoç, "Equilibrium, kinetics and thermodynamic aspects of promethazine hydrochloride sorption by iron rich smectite," *Colloids and Surfaces A: Physicochemical and Engineering Aspects*, vol. 340, no. 1–3, pp. 143–148, 2009.
- [20] K. Ellass, A. Laachach, A. Alaoui, and M. Azzi, "Removal of methyl violet from aqueous solution using a stevensite-rich clay from Morocco," *Applied Clay Science*, vol. 54, no. 1, pp. 90–96, 2011.
- [21] M. Ajbary, A. Santos, V. Morales-flórez, and L. Esquivias, "Removal of basic yellow cationic dye by an aqueous dispersion of Moroccan stevensite," *Applied Clay Sciences*, vol. 80–81, pp. 46–51, 2016.
- [22] R. M. S. Caillere and S. Henin, *Minéralogie des argiles: 2 Classification et omenclature*, Masson, Paris, France, 1982.
- [23] R. R. De Chimie, M. Ziati, F. Khemmari, and F. Didouche, "Removal of polyphenols from olive mill wastewater by adsorption on activated carbon prepared from peach stones," *Revue Roumaine de Chimie*, vol. 62, no. 11, pp. 865–874, 2017.
- [24] H. Wazani, "Etude de traitement de margine par adsorption," pp. 56–57, Faculté des Sciences Dhar Imhraz, Fés, Marocco, 2017, Master.
- [25] V. Fierro, V. Torné-Fernández, D. Montané, and A. Celzard, "Adsorption of phenol onto activated carbons having different textural and surface properties," *Microporous and Mesoporous Materials*, vol. 111, no. 1–3, pp. 276–284, 2008.
- [26] M. Abdelkreem, "Adsorption of phenol from industrial wastewater using olive mill waste," *APCBEE Procedia*, vol. 5, pp. 349–357, 2013.
- [27] A. Kumar, S. Kumar, and S. Kumar, "Adsorption of resorcinol and catechol on granular activated carbon: equilibrium and kinetics," *Carbon*, vol. 41, no. 15, pp. 3015–3025, 2013.
- [28] A. Senol, İ.M. Hasdemir, B. Hasdemir, and İ. Kurda, "Adsorptive removal of biophenols from olive mill wastewaters (OMW) by activated carbon : mass transfer , equilibrium and kinetic studies," *Asia-Pacific Journal of Chemical Engineering*, vol. 12, no. 1, 2017.
- [29] E. Ferrer-polonio, J. A. Mendoza-roca, A. Iborra-clar, and L. Pastor-alcañiz, "Adsorption of raw and treated by membranes fermentation brines from table olives processing for phenolic compounds separation recovery," *Journal Chemical Technology and Biotechnology*, vol. 91, no. 7, 2016.
- [30] S. Kühn, H. R. Wollseifen, R. Galensa, N. Schulze-kaysers, and B. Kunz, "Adsorption of flavonols from onion (*Allium cepa* L) processing residues on a macroporous acrylic resin," *Food Research International*, vol. 65, 2014.
- [31] C. Valderrama, J. Barios, M. Caetano, A. Farran, and J. Cortina, "Kinetic evaluation of phenol/aniline mixtures adsorption from aqueous solutions onto activated carbon and hypercrosslinked polymeric resin (MN200)," *Reactive and Functional Polymers*, vol. 70, pp. 142–150, 2010.
- [32] L. Luvinia, L. Cocheci, R. Pode, and I. Hulka, "Phenol adsorption using Aliquat 336 functionalized Zn-Al layered double hydroxide," *Separation and Purification Technology*, vol. 196, pp. 82–95, 2018.
- [33] M. Kessoum, V. Caqueret, O. Chedeville, B. Cagnon, S. Bostyn, and C. Porte, "Etude de la cinétique et de la thermodynamique d'adsorption de composés phénoliques en monosolutés et en mélange sur charbon actif," pp. 26–28, 2014.
- [34] A. Mounia, A. Hafidi, L. Mandi, and N. Ouazzani, "Removal of phenolic compounds from olive mill wastewater by adsorption onto wheat bran," *Desalination and Water Treatment*, vol. 52, no. 13, pp. 1–11, 2015.
- [35] M. Makhlouf, R. Hamacha, F. Villières, and A. Bengueddach, "Kinetics and thermodynamics adsorption of phenolic compounds on organic-inorganic hybrid mesoporous material," *International Journal of Innovation and Applied Studies*, vol. 3, no. 4, pp. 1116–1124, 2013.

Research Article

Assessing Redox Properties of Natural Organic Matters with regard to Electron Exchange Capacity and Redox-Active Functional Groups

Zhiyuan Xu ¹, Zhen Yang,² Hongping Wang ¹, and Jie Jiang ¹

¹Beijing Key Laboratory for Source Control Technology of Water Pollution, College of Environmental Science and Engineering, Beijing Forestry University, Beijing 100083, China

²Geomicrobiology, Center for Applied Geoscience, University of Tuebingen, Tuebingen 72076, Germany

Correspondence should be addressed to Jie Jiang; jiangjie@bjfu.edu.cn

Received 27 December 2019; Revised 16 February 2020; Accepted 11 March 2020; Published 14 April 2020

Guest Editor: Chenglian Feng

Copyright © 2020 Zhiyuan Xu et al. This is an open access article distributed under the Creative Commons Attribution License, which permits unrestricted use, distribution, and reproduction in any medium, provided the original work is properly cited.

Redox processes in groundwater play an important role in bioavailability, toxicity, and mobility of redox-active elements and contaminants. A recent study has demonstrated that low-molecular-weight fraction (LMWF) of humic substances with great number of redox-active functional groups (RAFGs) exhibits great reducing capacity. However, whether LMWF of natural organic matter (NOM) exhibits high redox capacity still remains unclear. Therefore, this study extracted Pahokee peat NOM (PPNOM) and Leonardite NOM (LNOM) from soils, and then LMWFs in these NOMs were collected using a dialysis method. Electron exchange capacities (EEC) and RAFGs of LMWF NOMs at different E_h were analyzed using a novel electrochemical method and a three-dimensional excitation emission fluorescence (3DEEM) spectroscopy. We found that the reducing capacity in LMWF PPNOM was approximately 5–6 times higher than the bulk NOM, while only 7.8% LMWF PPNOM was accounted for in the bulk NOM. An increasing in EEC (EAC + EDC, where EAC is the electron accepting capacity and EDC is the electron donating capacity) of LMWF PPNOM and LNOM with E_h reduced from -0.49 V to -0.69 V. Additionally, an obvious increase in fluorescent intensities of quinone-like fluorophores before and after being reduced LMWF LNOM is responsible for high EAC of LMWF LNOM. These findings provide a better understanding of relationship between RAFGs E_h in LMWF of NOM, further helping in predicting and protection of groundwater environment and fate of transformation and transport for redox-active contaminants in groundwater.

1. Introduction

Natural organic matters, as the most important redox-active compounds, participate in transformation and transport of redox-active elements and contaminants in biogeochemical processes in groundwater systems [1–4]. In addition, the chemical speciation, bioavailability, toxicity, and mobility of these redox-active compounds coupled with degradation of natural organic matter (NOM) [5, 6] are dependent on redox conditions. NOM can mediate electron transfer during the biogeochemical processes including microbial reduction of Fe(III) hydroxides [2, 7, 8] processed with immobilization of arsenic and phosphate [9]. The capacities of electron charging and recharging processes of NOM is related to

redox conditions (E_h) [10] and redox-active functional groups (RAFGs). NOM varies greatly in chemical and structural properties and thus change reactivity in the soil environment [11–13] that evolves from oxygen reducing to methanogenic (low reducing condition). RAFGs of NOM, including coexistence of electron donor moieties (e.g., phenolic and possibly substituted aromatic carboxylic acid groups) [14–16] and electron acceptor moieties (e.g., carbonyl-containing groups) [17–19], are responsible for cycling of electron charge-recharge within redox reactions [3, 20–25].

Quinone/hydroquinone moieties are generally considered to be the main redox-active functional groups of natural organic matter [26]. In general, NOM can be chemical and

microbial reduced, and reduced NOM facilitates electron transfer-stimulating microbial Fe[III] minerals. The extent and rate of stimulated microbial Fe[III] reduction is relating to redox property of NOM. Reducing capacities of NOM include electron accepting capacity (EAC) and electron donating capacity (EDC). NOM can be chemically reduced by H_2 in the presence of a Pd catalyst resulting in the different reducing capacities before and after being reduced. [25, 26]. Alternatively, the electrochemical reduction is a more efficient method compared to the chemical reduction [10, 27]. Previous electrochemical studies have revealed redox properties of NOM in varied redox potential range of -0.9 V – $+1.0\text{ V}$, which significantly affects transformation and electron transfer rates of pollutants in soil environments [28].

Many redox-active contaminants (such as arsenic, phosphate, and sulfate) normally are stocked in these soil nanoscale pores that have limited access to microbes [3, 21, 23, 29, 30], leading to hard transformation and transport, thus substantially arising a risk in soil groundwater health. It has been demonstrated that low-molecular-weight fractions (LMWFs) released from bulk humic substances (HSs) can exhibit great reducing capacity. The high reducing capacity of LMWF HS is attributed to LMWF HS, possessing a high amount of quinone-like fluorophores detected by three-dimensional excitation-emission matrix (3DEEM) fluorescence spectroscopy [26]. These LMWF HSs flowing into and/or out of the soil micropores ($<2\text{ nm}$) are able to significantly impact fates of transport and transformation of redox-active contaminants [26]. However, still opening questions including whether LMWF exists in natural organic matter (NOM), to which extent of electron transfer capacities of LMWF in NOMs at varied E_h in soil environment, and relationship of its RAFGs and E_h has paid a little attention.

Therefore, the aims of this study were (i) to collect different LMWFs (3500 LMWF and 14000 LMWF) and retentate from bulk NOM by means of a dialysis method with dialysis bags of molecules cutoff of 3.5 and 14 kDa; (ii) to determine electron exchange capacities (EECs) including electron accepting/donating capacity (EAC/EDC) at a varied E_h range of 0 – -0.69 V of LMWF, retentate, and bulk Pahokee peat and Leonardite natural organic matters (PPNOM and LNOM) using chemical (by H_2 and Pt/Al) and electrochemical analysis; and (iii) finally to detect redox-active functional fluorophores by 3DEEM for different molecular weight fractions of NOM at native and varied reduced E_h state (-0.49 – -0.69 V). We expected to develop a potential relationship between EEC and its RAFGs for different LMWF NOMs according to gradient E_h range of -0.49 – -0.69 V to better understand and predict fates of electron transfer process of LMWF NOM during the biogeochemistry process in soil and groundwater environments.

2. Materials and Methods

2.1. Sample Preparation and Dialysis Experiments.

Pahokee peat soil and Leonardite soil were purchased from the International Humic Substances Society (IHSS). PPNOM and LNOM were extracted from Pahokee peat soil and Leonardite soil samples (3.85 g/L) that dissolved in a

phosphate buffer solution (PP buffer; 50 mM, pH 7) to achieve final approximately total organic carbon (TOC) contents of 250 mg C/L. The NOM samples in sealed glass bottles with aluminum foil wrap were in continuous stirring for 5 days (200 rpm) to ensure fully release.

Dialysis bags were purchased from MWCO Regenerate (VISKASE, US). Before dialysis experiments, the chosen dialysis bags, MD34-3500 (pore size 1.25 nm) and MD34-14000 (pore size 2.5 nm), were prior soaked in deionized water for 24 hours. The dialysis bag containing 50 mL bulk sample was submerged in beaker with 200 mL PP buffer, and the whole device was wrapped in aluminum foil to prevent photochemical reaction. At the same time, the stirring rate was set to 200 rpm to simulate flowing rate of water in underground environment. The TOC (mg C/L) was determined by TOC-V scan analyzer (SHIMADZU).

2.2. Electrochemical Analysis with Direct Electrochemical Reduction (DER).

All electrochemical experiments were conducted in an anoxic glove box (100% N_2 atmosphere at $25 \pm 1^\circ\text{C}$). An electrolysis cell consists of (i) a platinum disk working electrode (CHI102), (ii) an Ag/AgCl reference electrode (CHI111), and (iii) a Pt wire counter electrode (CHI115, all from CH Instruments, Inc. US). The current response I was determined by CH Instruments 660E (Austin, TX). All samples were vacuumed for 3 mins, followed by purging with N_2 for 3 mins three times before electrochemical experiment. 0.1 M KCl was used as supporting electrolyte during electrochemical experiment. Each of 4 mL sample in an electrolysis cell was directly electrochemically reduced at an electrode potential of -0.49 V , -0.59 V , and -0.69 V , respectively.

2.3. Electrochemical Analysis with Direct Electrochemical Oxidation (DEO).

All setups of DEO experiments completely followed DER experiments instead of the $+0.61\text{ V}$ applied potential in DEO.

The number of transferred electrons Q_{DER} and Q_{DEO} (μmol) was calculated by an integration of the reductive and oxidative currents I over the time t (s), respectively [10]. Considering the differences in different molecular weight fractions based on TOC contents, EEC (mmol e^- /g C) of each sample was normalized to TOC:

$$Q_{DEO} = \int \frac{I_{OX}}{F} dt, \quad (1)$$

$$Q_{DER} = \int \frac{I_{RE}}{F} dt, \quad (2)$$

$$EAC = \frac{Q_{DER}}{TOC \times V}, \quad (3)$$

$$EDC = \frac{Q_{DEO}}{TOC \times V}, \quad (4)$$

$$EEC = |EAC| + |EDC|, \quad (5)$$

where F is a Faraday constant (96485 C/mol) and V (mL) is a volume of reaction samples. The EDC and I - t curve in DEO

TABLE 1: TOC contents (mg C/L) of different molecular weight fractions (including LMWF, retentate and bulk LNOM, and PPNOM, respectively) at the end of dialysis experiments.

TOC (mg C/L)	3500 Da LMWF	14000 Da LMWF	3500 Da retentate	14000 Da retentate	Bulk	% LMWF of bulk NOM (%)
PPNOM	20.57	22.44	242.70	232.10	261.80	7.8
LNOM	11.44	12.45	241.08	238.59	280.50	4.1

experiments of different molecular weight fractions of PPNOM and LNOM are shown in Figures S1 and S2 in supporting information.

2.4. Chemical Reduction. The samples were chemically reduced by H_2 with Pd/Al catalysts (palladium-coated aluminum pellets, 0.5% Pd, Merck) as chemically reduced samples. The reducing capacities of all samples before and after reduction were determined as previously described by Kappler et al. [25] and Yang et al. [26].

2.5. 3DEEM. Fluorescence spectra of all samples before and after reduction were characterized by an F-7000 fluorescence spectrophotometer equipped with both excitation and emission monochromators (Ushio Inc. Japan) with a 1500 W Xenon arc lamp as the excitation source. The fluorophores were obtained in the form of 3DEEMs via collecting a series of emission spectra over a range of excitation wavelengths, in which fluorescence intensity was presented as a function of excitation wavelength on one axis and emission wavelength on the other. To prevent reduced samples from reoxidizing, the standard 10 mm four-way quartz cell was prior purged with N_2 for 30 mins before analysis. The fluorescence spectra were analyzed as previously described by Yang et al. [26].

3. Results and Discussion

3.1. Dialysis Process and TOC Contents. Dialysis experiments were conducted within 5 days to collect different molecular weight fractions (3500 LMWF, 14000 LMWF, 3500 retentate, and 14000 retentate from bulk PPNOM and LNOM), and the results on total organic carbon TOC content among different LMWFs are shown in Table 1. The TOC results of LMWF NOM showed a continuous increase over the dialysis process (not shown), which are in agreement with our previous studies that the continuously released LMWF HS results in an increase in TOC content [19, 26]. Approximately 4.1–7.8% LMWF NOMs of bulk LNOM and PPNOM, respectively, were obtained at the end of dialysis, which was obviously higher than only 2% LMWF HA of total bulk PPHA and LHA shown in our previous study. The results suggested that NOM owned high LMWF NOM, and these LMWF NOMs occupied higher carbon contents than HA. Moreover, we found that, for both PPNOM and LNOM, TOC contents of 14000 LMWF were higher than 3500 LMWF, which suggested that 14000 LMWF NOM had more C functional groups (i.e., some electron donor and acceptor moieties: phenolic and possibly substituted aromatic carboxylic acid groups, and carbonyl-containing groups. And the number or type of RAFGs of NOM such as quinone/

hydroquinone moieties [14]) that were higher in 14000 LMWF than 3500 LMWF, but not much.

3.2. Direct Electrochemical Oxidation (DEO) and Reduction (DER) of Different Molecular Weight Fractions of PPNOM and LNOM. Quantified electron exchange capacities (EECs) including electron accepting capacity (EAC) and electron donating capacity (EDC) of different molecular weight fractions of PPNOM and LNOM were determined by electrochemical methods. The current I of different molecular weight fractions of NOM in DER and DEO experiments is shown in Figure 1 and S1, respectively. No obvious current I was detected in DEO experiments for all molecular fractions in DEO, which suggested that EDC of all LMWF, retentate, and bulk PPNOM and LNOM had no significant contribution to EEC. The I - t curve results of DER experiments showed a similar decreased tendency in current I from $77.46 \mu A$ to $11.14 \mu A$ of 3500 LMWF PPNOM/LNOM in $-0.59 V$ DER within 50 min reduction until complete final reduction. Moreover, the I - t curve of DER experiment showed a decreased tendency for all molecular fractions of both PPNOM and LNOM with a decreased E_h from $-0.49 V$ to $-0.69 V$. These results showed EAC of PPNOM and LNOM were related to environment E_h . Electron accepting moieties were distributed and concentrated in low E_h .

In addition, we found that the current I of DER experiments in LMWF molecular weight fractions showed a sharp decrease compared to that of bulk NOM with a decrease in E_h range. Bulk NOM showed a relatively higher Q_{DER} than LMWF and retentate NOM due to a high TOC in bulk NOM. This result indicated that EAC and EEC of different molecular weight fractions of NOM were highly dependent on its TOC contents.

In order to evaluate total EEC among different molecular weight fractions of NOM, EEC ($EEC = EAC + EDC$) of different molecular weight fractions was normalized to its TOC contents, referring to the number of electron transferred per gram carbon (meq e-/g C), as shown in Figure 2. Since no obvious contribution of EDC of NOM to EEC, the EAC was approximately equal to EEC according to equation (5). The EEC was significant higher in LMWF than in retentate and bulk NOM, suggesting a high electron transfer capacity of LMWF NOM. This is consistent with the previous study reported that the LMWF HA has a great reducing capacity using chemical reduction (H_2 and Pd/Al) [26]. Moreover, a small current I responded a low EEC in the low reducing potential of $-0.49 V$, while a large current I responded a high EEC in high reducing potentials. The EEC of NOM in reducing potential range of $-0.59 V$ – $-0.69 V$ accounted for up to 90% EEC in reducing potential range of $-0.49 V$ – $-0.69 V$ (Figure 2). These results indicated that

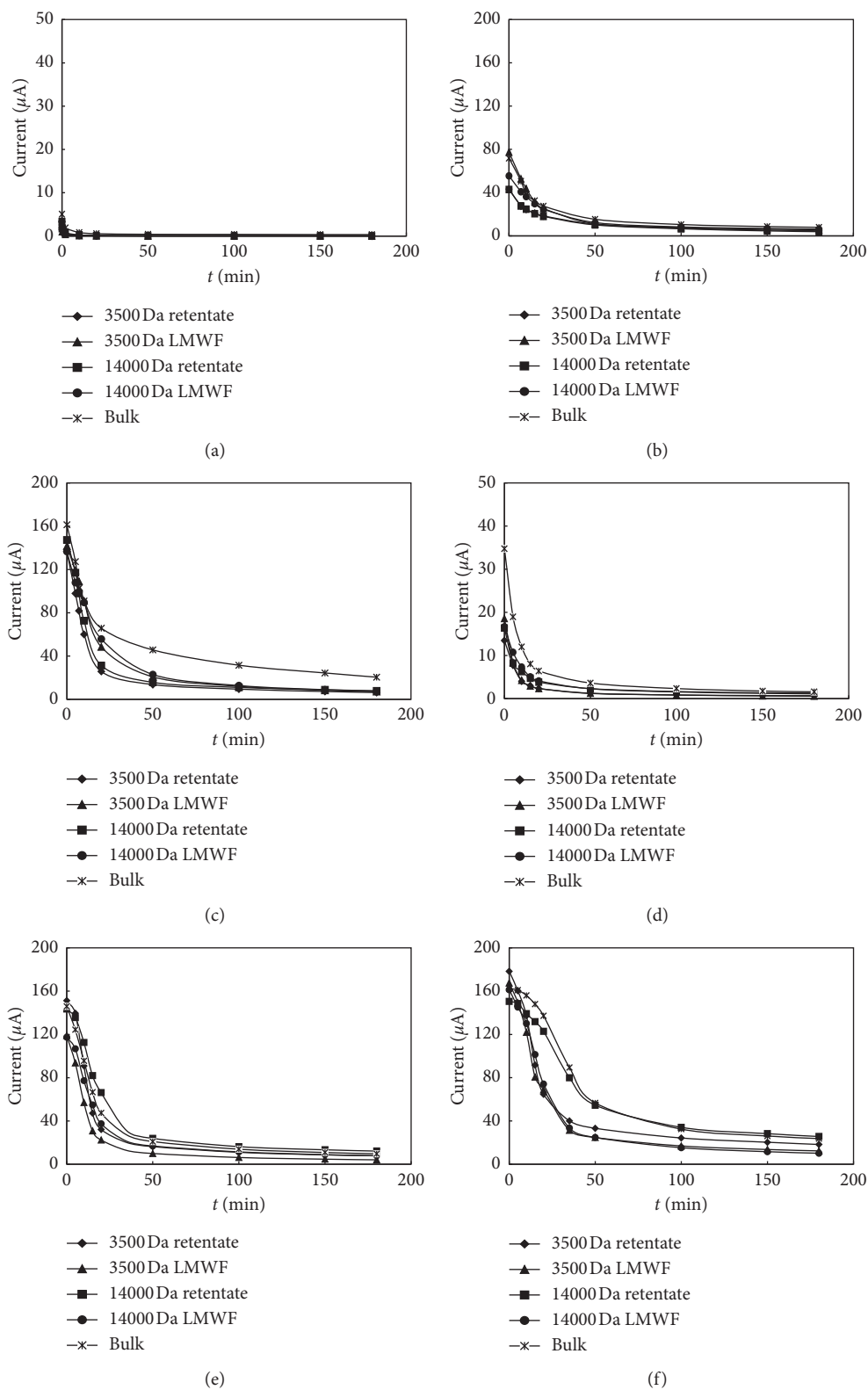


FIGURE 1: The I-t curve of different molecular weight fractions of PPNOM and LNOM in DER, which was carried out at $E_h = -0.49$ V, $E_h = -0.59$ V, and $E_h = -0.69$ V for 3 hours: (a) PPNOM -0.49 V; (b) PPNOM -0.59 V; (c) PPNOM 0.69 V; (d) LNOM -0.49 V; (e) LNOM -0.59 V; (f) LNOM -0.69 V.

electron accepting moieties of NOM was distributed mainly at a E_h range of -0.59 V– -0.69 V. Compared to PPNOM, LNOM showed a greater EEC; particularly, 3500 LMWF

LNOM had a highest EEC, suggesting 3500 LMWF LNOM had the highest amount of redox-active functional groups. Functional groups in NOM were favorable to accept

electrons rather than donate electrons; in particular, electron accepting moieties of PPNOM were fully distributed within E_h range of -0.59 V– -0.69 V. Reducing capacities of different molecular weight fractions of PPNOM were evaluated by chemical reduction (H_2 and Pt/Al), as shown in Figure 3. Reduced PPNOM showed a higher reducing capacity than that of native PPNOM, indicating that PPNOM possessed more oxidized functional groups, which is in agreement with the results shown by electrochemical analysis. LMWF PPNOM displayed a higher EAC (difference in reducing capacity between reduced state and native state) than retentate and bulk PPNOM (Figure S3), indicating that LMWF had more electron accepting moieties compared to retentate and bulk NOM.

In order to investigate the electron accepting moieties in different NOM samples, we calculated the proportion of EEC in different LMWFs and retentate of PPNOM and LNOM at different E_h of -0.49 V– -0.59 V, as shown in Table 2. Calculated EEC of PPNOM accounted for around 3.5–58.4% of total EEC for both LMWF and retentate. The result suggested that LNOM, compared to PPNOM, has higher amount of electron accepting moieties. In particular, the number of electron accepting moieties in LMWF LNOM obviously higher than in LMWF PPNOM occupied 3.5–5.4% of LNOM EEC at E_h of -0.49 V. A decrease in E_h from -0.49 V to -0.59 V was observed, which resulted in an obvious increase in proportion of LMWF of PPNOM and LNOM from 3.5–5.4% to 26.4–44.9% (Table 2). These findings indicated distribution of electron accepting moieties of LMWF NOM is dependent on its E_h range. In this study, we demonstrated that LMWF LNOM with great electron accepting moieties is responsible for a high EEC and EAC.

3.3. Characterization of Redox-Active Functional Fluorophore of LMWF NOM at Different Reducing Potentials by 3DEEM Spectroscopy. In order to clarify responsibility of redox-active functional moieties/fluorophores of LMWF LNOM to a high electron accepting capacity during the electron transfer process, RAFGs of LMWF LNOM were detected before and after reduction in different E_h ranges of -0.49 – -0.59 V using 3DEEM spectroscopy. Overall, in the native state, 3500 LMWF LNOM had a higher relative fluorescent intensity of humic-like fluorophore with quinonoid π - π^* transition compared to 14000 LMWF (Figure 4 and Table 3). These results suggested that 3500 LMWF occupied more humic-like fluorophores than 14000 LMWF LNOM. Additionally, compared to 14000 LMWF, emission wavelength (E_m) of 3500 LMWF showed a shorter E_m wavelength position accompanied with a small blue-shifting ($\Delta E_m = 5$ nm, to a shorter wavelength; Figure 4 and Table 3). This result implied that, in the native state, 14000 LMWF had a more complicate structure of redox-active functional fluorophores than 3500 LMWF.

In reduced state with -0.49 V potential, compared to native LMWF LNOM, E_m of both 3500 LMWF and 14000 LMWF LNOM shifted to a longer E_m wavelength ($\Delta E_m = 5$

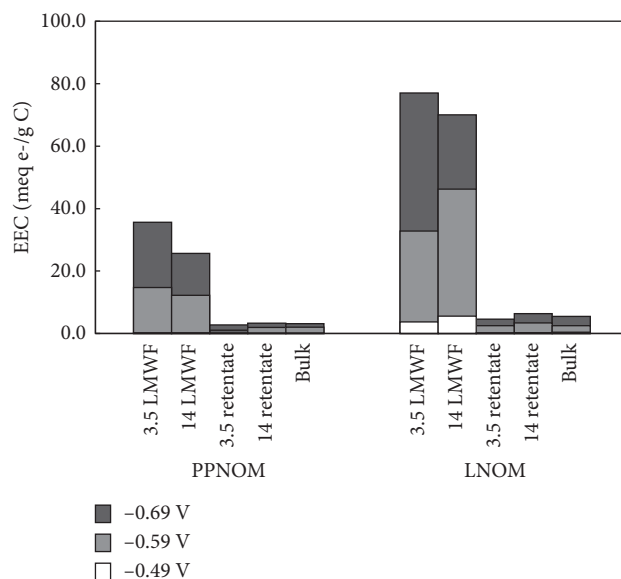


FIGURE 2: The EEC of PPNOM and LNOM.

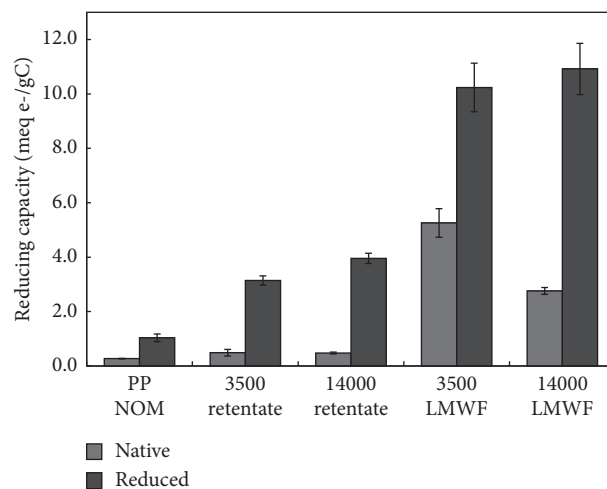


FIGURE 3: The reducing capacity of different molecular weight fractions of PPNOM in their native and reduced states. Each reduced sample was prepared by H_2 in the presence of two Pd catalysts. The reducing capacities were determined by the difference of Fe(III) before and after reacting with ferricyanide. Each data were normalized into meq e^- /g C, which is equal to mmol e^- /g C in numerical value.

or 10 nm; Figure 4 and Table 3) due to a quinonoid π - π^* transition particularly. These observations indicated that, in reduced state of -0.49 V, functional groups of LMWF changed to a more complicate structure which most likely to high level condensation in functional groups. Moreover, in reduced state of -0.59 V, E_m still slightly shifted to longer wavelengths ($\Delta E_m = 5$ nm) for 14000 LMWF and 3500 LMWF compared to native 14000 LMWF and 3500 LMWF and even to LMWF samples in reduced state of -0.49 V (Figure 4 and Table 3). These results indicated that a decrease in E_h from -0.49 V to -0.59 V for LMWF LNOM could lead to an increase in aromatic condensation of redox-active functional groups due to quinonoid π - π^* and benzenoid

TABLE 2: The proportions of EEC of PPNOM and LNOM.

Reducing potentials	3500 Da LMWF (%)	14000 Da LMWF (%)	3500 Da retentate (%)	14000 Da retentate (%)
-0.49 V	5.4	3.5	16.8	9.6
-0.59 V	44.9	26.4	41.9	58.4

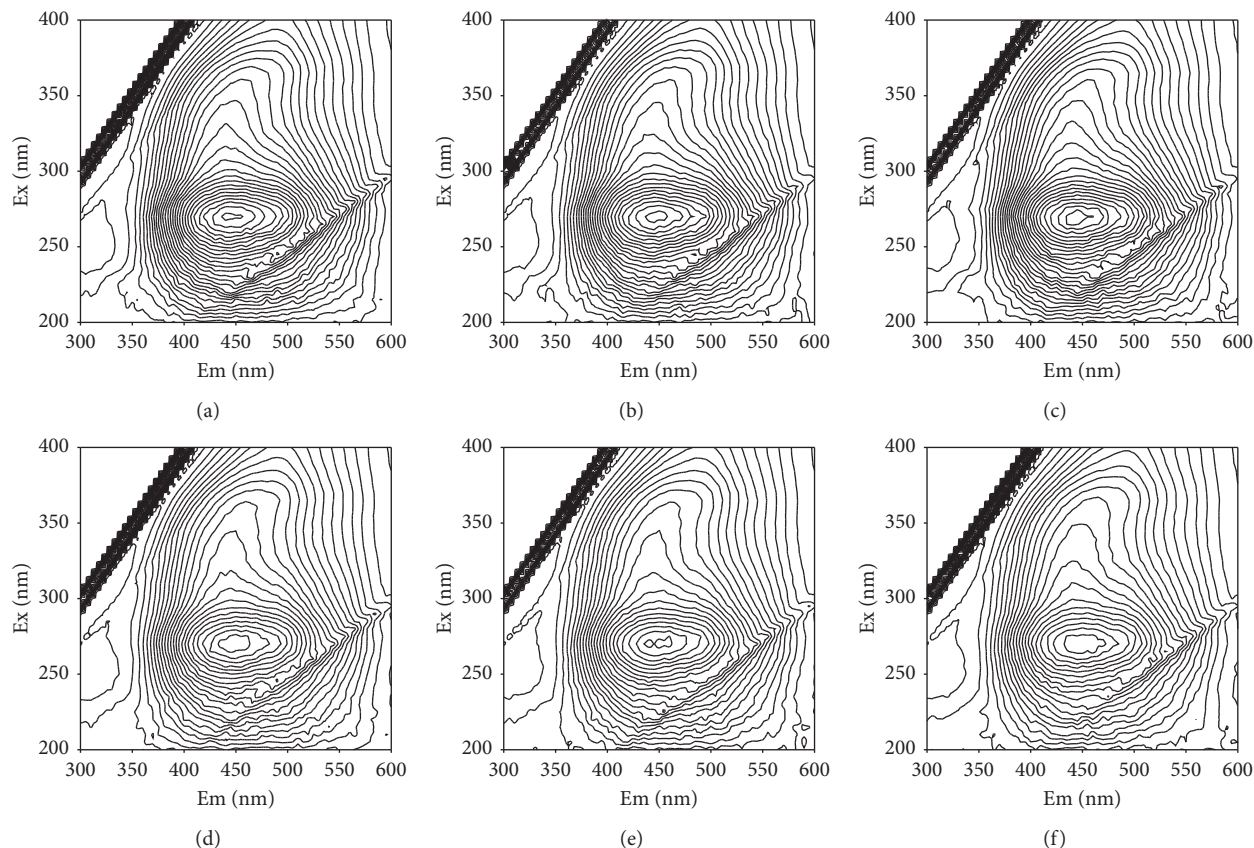


FIGURE 4: 3DEEM fluorescence spectra of LMWF of LNOM in their native, after -0.49 V and -0.59 V DER redox state: (a) 3500 LMWF native; (b) 3500 LMWF -0.49 V; (c) 3500 LMWF -0.59 V; (d) 14000 LMWF native; (e) 14000 LMWF -0.49 V; (f) 14000 LMWF -0.59 V.

TABLE 3: Fluorescence peak positions and relative fluorescence intensities of LMWF of LNOM in different redox states.

Samples	3500 LMWF				14000 LMWF			
	Ex/Em (nm/nm)	Intensity (a. u.)	Peak type	Transition section	Ex/Em (nm/nm)	Intensity (a. u.)	Peak type	Transition section
Native	270/440	1.66	Humic-like	Quinonoid π - π^*	275/455	1.40	Humic-like	Quinonoid π - π^*
-0.49 V	270/450	1.62	Humic-like	Quinonoid π - π^*	270/460	1.38	Humic-like	Quinonoid π - π^*
-0.59 V	270/445	1.69	Humic-like	Quinonoid π - π^*	270/445	1.30	Humic-like	Quinonoid π - π^*

π - π^* . In addition, after being reduced to E_h range of -0.49 to -0.59 V, 3500 LMWF had a higher relative fluorescent intensity compared to 14000 LMWF LNOM. This finding suggested that 3500 LMWF possessed a relatively low aromatic condensation but high number of quinone-like fluorophore, which was consistent with the result in respect to high EAC in 3500 LMWF LNOM using electrochemical analysis.

4. Conclusions

Redox processes impact transformation and transport of redox-active contaminants in environment, which is dependent on E_h and RAFGs of NOM. We evaluated the redox properties of NOM with respect to EECs and RAFGs. We found that the reducing capacity in LMWF PPNOM was approximately 5-6 times higher than that of the bulk NOM,

while only 7.8% LMWF PPNOM TOC accounted for bulk PPNOM TOC. An increase in EEC for LMWF PPNOM and LNOM was observed with a reduced E_h range from -0.49 V to -0.69 V. Quinone-like fluorophores in LMWF LNOM were distributed and concentrated in E_h range of -0.49 V– -0.69 V. These quinone-like fluorophores with a red-shifting in emission wavelength were observed with a reduced E_h range from -0.49 V to -0.59 V. The findings can provide a better understanding of relationship between RAFGs E_h in LMWF of NOM and thus can help to predict fates of redox-active contaminants in LMWF NOM-containing groundwater environment.

Data Availability

The experimental data used to support the findings of this study are included in the article. And more detailed data are available from the corresponding author upon request.

Conflicts of Interest

The authors declare that there are no conflicts of interest regarding the publication of this paper.

Acknowledgments

This research was supported by the Major Science and Technology Program for Water Pollution Control and Treatment of China (2018ZX07208001) and the National Natural Science Foundation of China (21677012) to J.J.

Supplementary Materials

Supplementary Figure S1: the EDC of different molecular weight fractions of PPNOM and LNOM in DEO experiments. The applied potential is $+0.61$ V. Supplementary Figure S2: the I-t curve of different molecular weight fractions of PPNOM (a) and LNOM (b) in DEO experiments, which was carried out at $+0.61$ V for 3 hours. Supplementary Figure S3: the EAC of different molecular weight fractions of PPNOM calculated by the chemical reductions and proceeding. (*Supplementary Materials*)

References

- [1] J. D. Coates, R. Chakraborty, S. M. O'Connor, C. Schmidt, and J. Thieme, "The geochemical effects of microbial humic substances reduction," *Acta hydrochimica et hydrobiologica*, vol. 28, no. 7, pp. 420–427, 2001.
- [2] Z. Struyk and G. Sposito, "Redox properties of standard humic acids," *Geoderma*, vol. 102, no. 3–4, pp. 329–346, 2001.
- [3] A. Kappler and S. B. Haderlein, "Natural organic matter as reductant for chlorinated aliphatic pollutants," *Environmental Science & Technology*, vol. 37, no. 12, pp. 2714–2719, 2004.
- [4] D. R. Lovley, J. D. Coates, E. L. Blunt-Harris, E. J. P. Phillips, and J. C. Woodward, "Humic substances as electron acceptors for microbial respiration," *Nature*, vol. 382, no. 6590, pp. 445–448, 1996.
- [5] S. Mitsunobu, T. Harada, and Y. Takahashi, "Comparison of antimony behavior with arsenic under various soil redox conditions," *Environmental Science & Technology*, vol. 25, no. 1, pp. 98–99, 2006.
- [6] J. Singh, S. D. Comfort, and P. J. Shea, "Iron-mediated remediation of RDX-contaminated water and soil under controlled eh/pH," *Environmental Science & Technology*, vol. 33, no. 9, pp. 1488–1494, 1999.
- [7] J. J. Alberts, J. E. Schindler, R. W. Miller, and D. E. Nutter, "Elemental mercury evolution mediated by humic acid," *Science*, vol. 184, no. 4139, pp. 895–897, 1974.
- [8] J. Chen, "The roles of natural organic matter in chemical and microbial reduction of ferric iron," *Science of the Total Environment*, vol. 307, no. 1–3, pp. 167–178, 2003.
- [9] J. Jiang, I. Bauer, A. Paul, and A. Kappler, "Arsenic redox changes by microbially and chemically formed semiquinone radicals and hydroquinones in a humic substance model quinone," *Environmental Science & Technology*, vol. 43, no. 10, pp. 3639–3645, 2009.
- [10] M. Aeschbacher, M. Sander, and R. P. Schwarzenbach, "Novel electrochemical approach to assess the redox properties of humic substances," *Environmental Science & Technology*, vol. 44, no. 1, pp. 87–93, 2010.
- [11] B. Gu, J. Schmitt, Z. Chen, L. Liang, and J. F. McCarthy, "Adsorption and desorption of natural organic matter on iron oxide: mechanisms and models," *Environmental Science & Technology*, vol. 28, no. 1, pp. 38–46, 1994.
- [12] C. Jie, "Fluorescence spectroscopic studies of natural organic matter fractions," *Chemosphere*, vol. 50, no. 5, pp. 0–647, 2003.
- [13] E. Z. Fratzczak, "Spectroscopic characterization of the structural properties of quinoxalinophenanthrophenazine thin films," *Journal of Materials Chemistry C*, vol. 6, 2018.
- [14] D. J. Dryer, G. V. Korshin, and M. Fabbicino, "In situ examination of the protonation behavior of fulvic acids using differential absorbance spectroscopy," *Environmental Science & Technology*, vol. 42, no. 17, pp. 6644–6649, 2008.
- [15] S. M. Phillips, A. D. Bellcross, and G. D. Smith, "Light absorption by Brown carbon in the southeastern United States is pH-dependent," *Environmental Science & Technology*, vol. 51, no. 12, pp. 6782–6790, 2017.
- [16] E. S. Boyle, N. Guerriero, A. Thiallet, R. D. Vecchio, and N. V. Blough, "Optical properties of humic substances and CDOM: relation to structure," *Environmental Science & Technology*, vol. 43, no. 7, pp. 2262–2268, 2009.
- [17] R. Del Vecchio and N. V. Blough, "On the origin of the optical properties of humic substances," *Environmental Science & Technology*, vol. 38, no. 14, pp. 3885–3891, 2004.
- [18] C. M. Sharpless and N. V. Blough, "The importance of charge-transfer interactions in determining chromophoric dissolved organic matter (CDOM) optical and photochemical properties," *Environmental Science Process Impacts*, vol. 16, no. 4, 2014.
- [19] J. Cao and J. Jiang, "Reducing capacities in continuously released low molecular weight fractions from bulk humic acids," *Journal of Environmental Management*, vol. 244, pp. 172–179, 2019.
- [20] G. R. Aiken, "Humic substances in soil, sediment, and water: geochemistry, isolation, and characterization," *Journal of Environmental Management*, vol. 142, no. 5, 1985.
- [21] G. C. Curtis and M. Reinhard, "Reductive dehalogenation of hexachloroethane, carbon tetrachloride, and bromoform by anthrahydroquinone disulfonate and humic acid," *Environmental Science & Technology*, vol. 28, pp. 2360–2365, 1994.
- [22] F. J. Stevenson, *Humus Chemistry: Genesis, Composition, Reactions*, Springer, Berlin, Germany, 2nd edition, 1982.

- [23] B. Gu and J. Chen, "Enhanced microbial reduction of Cr(VI) and U(VI) by different natural organic matter fractions," *Geochimica Et Cosmochimica Acta*, vol. 67, no. 19, pp. 3575–3582, 2003.
- [24] F. Maurer, I. Christl, B. Fulda, A. Voegelin, and R. Kretzschmar, "Copper redox transformation and complexation by reduced and oxidized soil humic acid. 2. Potentiometric titrations and dialysis cell experiments," *Environmental Science & Technology*, vol. 47, no. 19, pp. 10912–10921, 2013.
- [25] A. Kappler, M. Benz, B. Schink, and A. Brune, "Electron shuttling via humic acids in microbial iron(III) reduction in a freshwater sediment," *Fems Microbiology Ecology*, vol. 47, no. 1, pp. 85–92, 2004.
- [26] Z. Yang, A. Kappler, and J. Jiang, "Reducing capacities and distribution of redox-active functional groups in low molecular weight fractions of humic acids," *Environmental Science & Technology*, vol. 10, 2016.
- [27] M. Sander, T. B. Hofstetter, and C. A. Gorski, "Electrochemical analyses of redox-active iron minerals: a review of nonmediated and mediated approaches," *Environmental Science & Technology*, vol. 49, no. 10, pp. 5862–5878, 2015.
- [28] M. Bauer, T. Heitmann, D. L. Macalady, and C. Blodau, "Electron transfer capacities and reaction kinetics of peat dissolved organic matter," *Environmental Science & Technology*, vol. 41, no. 1, pp. 139–145, 2007.
- [29] Y. Wang, "Nanogeochemistry: nanostructures, emergent properties and their control on geochemical reactions and mass transfers," *Chemical Geology*, vol. 378–379, pp. 1–23, 2014.
- [30] A. Piepenbrock, C. Schröder, and A. Kappler, "Electron transfer from humic substances to biogenic and abiogenic Fe(III) oxyhydroxide minerals," *Environmental Science & Technology*, vol. 48, no. 3, pp. 1656–1664, 2014.

Research Article

Study on Treatment of Salicylhydroxamic Acid Wastewater from Tungsten Molybdenum Mineral Processing

Liping Zhang , Xin Zhang, Jun Xiang, Jingwen Xue, and Xuejing Song

School of Chemical and Environmental Engineering, China University of Mining & Technology, Beijing, Beijing, China

Correspondence should be addressed to Liping Zhang; haozimei77@163.com

Received 27 December 2019; Revised 8 March 2020; Accepted 18 March 2020; Published 10 April 2020

Guest Editor: Chenglian Feng

Copyright © 2020 Liping Zhang et al. This is an open access article distributed under the Creative Commons Attribution License, which permits unrestricted use, distribution, and reproduction in any medium, provided the original work is properly cited.

Salicylhydroxamic acid is an excellent collector of oxidizing ore, and it has an efficient collection performance for tungsten molybdenum ore. However, the utilization ratio of salicylhydroxamic acid is relatively low in the flotation process, and a large amount of flotation wastewater discharged might cause damage to the water environment. This study mainly compared the effects of natural sunlight degradation, ozonation, and Fenton oxidation processes on the treatment of salicylhydroxamic acid wastewater from W–Mo mineral processing. The results showed after 30 hours degradation by natural sunlight, the COD_{Cr} removal rate of wastewater was only 25.99%. When the initial pH was 8, the dosage of O₃ was 1.3 mg/L and the reaction time was 60 minutes; O₃ oxidation could remove 40.37% COD_{Cr} from wastewater, and the BOD₅/COD_{Cr} value increased to higher than 0.3 after 15 min reaction. Under the Fenton oxidation conditions such as initial pH 3, H₂O₂ dosage 0.96 g/L, and the molar ratio of H₂O₂ to Fe²⁺ 2:1, 90.43% COD_{Cr} could be removed from flotation wastewater after 90 min reaction, and the BOD₅/COD_{Cr} value was obviously improved. Fenton oxidation was a high efficient processing technology for salicylhydroxamic acid wastewater, and the effluent could meet the discharge and reuse emission standard requirements in China.

1. Introduction

W–Mo ore is one of the dominant minerals in China due to abundant reserves, high utilization value, and high economic benefits. According to the data from the China Mineral Resources Report, up to the end of 2016, the national tungsten mineral resource reserves increased by 6% to 101.955 million tons and occupied the first place in the world [1]. A large amount of flotation wastewater was produced during the mineral processing which was the absolutely necessarily tache before utilization of mineral resources Based on statistic data, the water consumption of per ton mineral with flotation is about 4~7 m³, while the gravity separation process is high to 6~15 m³ [2]. Due to the low utilization efficiency of the flotation process, large amount of flotation reagents remained in the flotation wastewater which was certainly toxic to ecological environment.

During the W–Mo ore flotation process, fatty acids, amines, citric acid, and phosphoric acid are the commonly used collectors which have the disadvantage of poor

selectivity, low flotation efficiency, and certain toxicity. Salicylhydroxamic acid is an innovative collector, which has lone pair of electrons of oxygen atom and nitrogen atom with the similar positions in the hydroxyl group structure. It is beneficial to coordinate with metal cations on the surface of tungsten ore to form chelate ring. Meanwhile, the stability of the chelate is enhanced by increasing the density of electron clouds of atomic oxygen with the α -conjugation effect, which makes the salicylhydroxamic acid to be strongly adsorbed on the mineral surface [3, 4], thus improving the mineral flotation efficiency. However, the hydroxyamidine group and a stable alkyl benzene ring in the molecular structure of salicylhydroxamic acid causes a certain degree of biological toxicity and poor biodegradability. The common treatment methods for flotation wastewater in practical engineering are natural sunlight degradation, coagulation, and flocculation, which are difficult to achieve the removal effect.

In recent years, advanced oxidation processes (AOPs) were considered as methods with application prospect to

transform nonbiodegradable pollutants into harmless substances [5]. The AOPs can effectively mineralize a variety of organic pollutants by generating highly active and nonselective free radical like hydroxyl radical ($\cdot\text{OH}$) [6]; meanwhile, the AOPs attract a wide spread attention to the treatment of industrial wastewater containing toxic organic pollutants [7]. The reaction mechanism of Fenton oxidation mainly involves the production of $\cdot\text{OH}$ by Fe^{2+} and H_2O_2 under acidic conditions [8]. The oxidation capacity of $\cdot\text{OH}$ is about $10^6\sim 10^9$ times stronger than O_3 or oxygen. The $\cdot\text{OH}$ oxidation process is nonspecific [9] and can effectively degrade residual organic contaminants in wastewater. Ozone oxidation technology is also based on the hydroxyl radical with a higher redox potential to degrade organic pollutants which can greatly shorten the reaction time [10, 11] and achieve the purpose of harmless mineralization of refractory organics [12]. There are few researches at present on the AOPs applied in salicylhydroxamic acid wastewater from W-Mo mineral processing. This study focused on the removal effect of W-Mo mineral flotation wastewater treatment with different processes such as advanced oxidation and natural photodegradation, moreover optimized process parameters, and provided reference for practical treatment project of salicylhydroxamic acid wastewater from W-Mo mineral processing.

2. Materials and Methods

2.1. Synthetic Salicylhydroxamic Acid Wastewater. The experimental wastewater prepared with salicylhydroxamic acid simulated the wastewater quality of a tungsten-molybdenum polymetallic ore tailings reservoir in Hunan province. Meanwhile, taking into account the residual ratio of the main flotation reagents in the actual flotation wastewater, the simulated wastewater was prepared with four flotation reagents such as salicylhydroxamic acid 50 mg/L, No. 2 oil 50 mg/L, sodium oleate 100 mg/L, and butyl xanthate 100 mg/L, which brought 300 mg/L COD_{Cr} concentration.

The water quality of the simulated salicylhydroxamic acid wastewater, the first-grade discharge standard in the Integrated Wastewater Discharge Standard (GB 8978), and the water quality of the reuse of urban recycling water-water quality standard for industrial uses (GB/T 19923) are listed in Table 1.

2.2. O_3 Treatment Procedure. The experimental scheme of O_3 oxidation is as shown in Figure 1. The reactor setup included a reactor made of high borosilicate glass to prevent oxidation and chemical corrosion and an ozone generator (3S-A5, China). The height, outer diameter, and inner diameter of the reactor was 1000 mm, 70 mm, and 60 mm, respectively, and the effective volume was 2.8 L. The gas distributor in the reactor was a titanium plate with about 20–30% open porosity, and the average pore size of micropores was about 17 μm .

The O_3 treatment procedure was intermittent operation. The simulated wastewater was injected into the reactor through a peristaltic pump, then turned on the ozone

TABLE 1: The water quality of simulated flotation wastewater and standard concentration limits.

Items	pH	BOD ₅ (mg/L)	COD _{Cr} (mg/L)	NH ₃ -N (mg/L)	TP (mg/L)
Simulated wastewater	9.5~10	60~70	300~350	8.5~9	<0.01
Discharge standard	6~9	30	100	15	0.5
Reuse standard	6.5~8.5	10	60	10	1

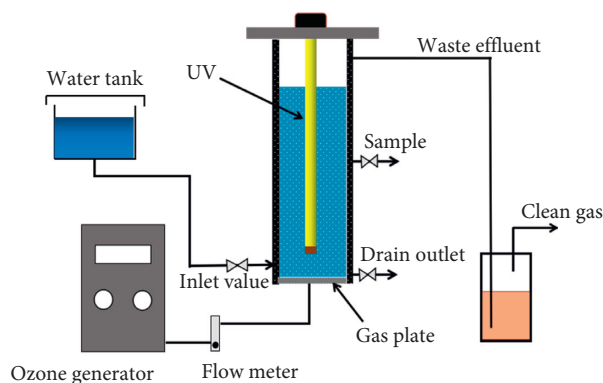


FIGURE 1: Schematic diagram of experimental devices used in O_3 oxidation.

generator, and maintained the flow rate of O_3 gas at 100 mL/min by controlling the gas flow meter. Ozone mixture was introduced into the gas distribution plate after the gas flow was stable and then adjusted the power knob of the ozone generator to control the dosage of O_3 in the range of 1~10 mg/L. A series of batch tests were employed to determine the degradation of pollutants under different stepwise reaction times, initial pH value, and O_3 dosages.

2.3. Fenton Treatment Procedure. Samples of 450 mL simulated salicylhydroxamic acid wastewater were adjusted to preselected pH value with 10% H_2SO_4 or NaOH and then put into the reactor. Different dosages of $\text{FeSO}_4\cdot 7\text{H}_2\text{O}$ and H_2O_2 (mass concentration was 30%) were added into the former solution. Samples were collected at different reaction times, and the pH was adjusted to 7~9 with 10 mol/L NaOH solution and then settled for 30 minutes. The supernatant was sampled and treated with 50°C water bath and heated for 2 hours to ensure the residual H_2O_2 in the solution completely volatilized [13]. COD_{Cr} or BOD₅ of treated supernatant was analyzed to evaluate the treatment effect.

2.4. Chemicals and Analyses. Analytical grade salicylhydroxamic acid and sodium oleate were purchased from Aladdin (Shanghai, China). Industrial grade butyl xanthate sodium and No. 2 oil were purchased from Zhuzhou mineral processing reagent company (Hunan, China). Analytical grade ferrous sulfate heptahydrate, sulfuric acid, sodium hydroxide, potassium iodide, soluble starch, and sodium

thiosulfate were purchased from Sinopharm (Beijing, China). The pH value was measured by pH meter (PHS-3C, Raytheon, China), COD_{Cr} was analyzed with UV-Vis spectrophotometer (UV3000PC, Mapada, China), BOD₅ was detected with five-day biochemistry culture method, and O₃ concentration in gas was measured by iodometry [14].

3. Results and Discussion

3.1. Degradation of Simulated Wastewater by Natural Sunlight. A beaker containing 500 mL simulated wastewater was put in natural sunshine outside and irradiated for different times. A control group was put in a place without natural light exposure. The COD_{Cr} removal ratio of the wastewater is shown in Figure 2. Natural light degradation had a limited removal effect on organic pollutants in simulated wastewater. The COD_{Cr} removal ratio increased gradually with the extension of the sun illumination time. When the sun illumination time was 30 h, the COD_{Cr} removal ratio reached the highest 25.99% mainly due to easy degradation of butyl xanthate under sunshine which was in accordance with the phenomena recorded in the literature [15]. Without sunshine radiation, the COD_{Cr} removal ratio of the control group increased to about 5% within 6 h.

In order to further explore the change in organic matter structure in the wastewater illuminated by sunlight, infrared spectrum analysis was performed on the simulated wastewater before and after sunlight degradation and the results are shown in Figure 3. Compared the infrared spectra of the wastewater before and after degradation with sunlight, the characteristic absorption peak positions did not change obviously, no new absorption peaks appeared, and the intensity of the absorption peak of the benzene ring C–C skeleton was almost unchanged; it meant that sunlight degradation could not greatly change the molecular structures of organic matters in simulated wastewater, especially the benzene ring structure could not be destroyed. Thus, natural sunlight has limited ability to degrade pollutants in the flotation wastewater, and the treated effluent could not meet the discharge or reuse standard requirements.

3.2. O₃ Oxidation Degradation of Simulated Wastewater

3.2.1. Effect of Reaction Time on Treatment. The experimental conditions were set as O₃ dosage = 2.4 mg/L and pH = 4, 6, and 10, respectively; the COD_{Cr} removal ratio of simulated wastewater by O₃ oxidation is shown in Figure 4.

The removal ratios of COD_{Cr} all rose rapidly under different pH conditions within the first 15 min of ozone oxidation reaction, and it was mainly due to the higher initial concentration of aromatic compounds, unsaturated bond-containing compounds, and heterocyclic compounds capable of providing electron groups (–OH and –NH₂) in the wastewater. Meanwhile, O₃ molecules and ·OH were electrophilic to easily oxidize the pollutants; thus, the removal ratio of COD_{Cr} increased rapidly. Prolonging the reaction time from 15 to 60 min, the COD_{Cr} removal ratio increased less than 10%. Continuously increasing the reaction time could not change the COD_{Cr} removal ratio significantly

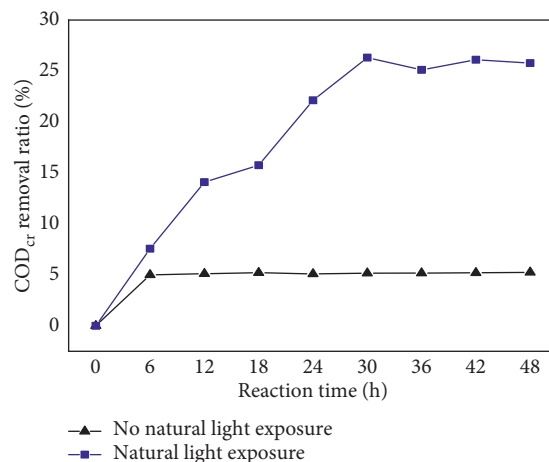


FIGURE 2: Effect of sunlight illumination time on COD_{Cr} removal.

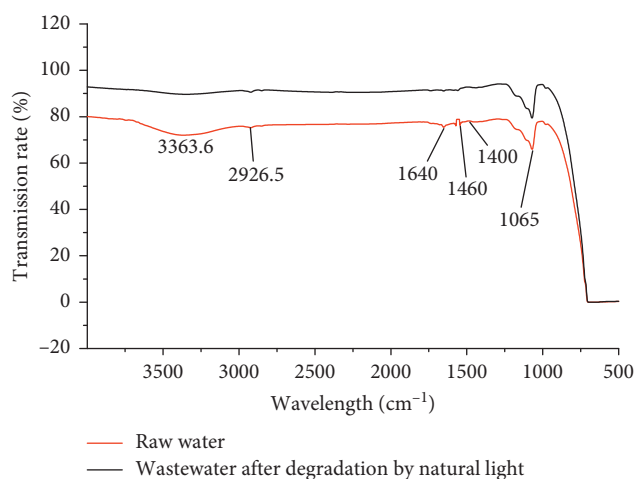


FIGURE 3: The infrared spectrum of simulated wastewater before and after natural sunlight irradiation for 48 hours.

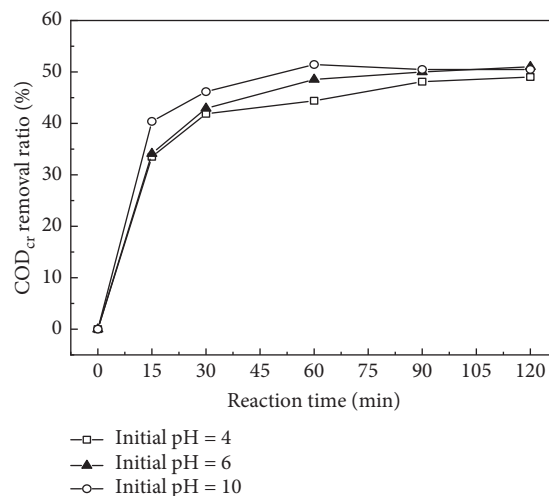
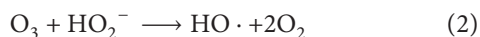
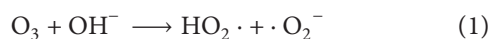


FIGURE 4: Effect of reaction time on COD_{Cr} removal by ozone oxidation.

because of the residual organic pollutants in the wastewater mainly being small organic molecules such as formaldehyde and formic acid which were difficult to be mineralized by O_3 .

3.2.2. Effect of Initial pH on Treatment. The treatment of ozone oxidation on COD_{Cr} removal was explored by controlling the dosage of O_3 2.4 mg/L, reaction time 60 min, and adjusting pH 2, 4, 6, 8, and 10, respectively, as the results in Figure 5.

The initial pH of the wastewater had a significant effect on COD_{Cr} removal by O_3 oxidation. The COD_{Cr} removal ratio reached the maximum 51.19% when pH increased from 2 to 8, but it decreased when the initial pH rose to 10. In acidic conditions, $\cdot OH$ generation was inhibited, and O_3 molecules played an active role in the oxidation process which was selective and low reaction to make the organic pollutants degradation rate slower. Under weak alkaline condition, it was more conducive to the oxidation degradation of organic pollutants in wastewater by ozone, and it should owe to the increase in the concentration of hydroxide ion as the pH value enhanced which acted as the initiator to promote O_3 molecule and generated the $\cdot OH$ through the reactions as follows:



Under the weak alkaline condition, the organic pollutants' degradation reaction is mainly based on the indirect oxidation of OH , the reaction rate was faster, and the oxidation ability was stronger, thus improving the removal effect of organic pollutants. When pH was higher to 10, on the one hand, the generation rate of $\cdot OH$ by ozone decomposition was too higher, which resulted in quenching reaction occurred among the excessive generation of radicals as $\cdot OH$ to reduce the removal efficiency of ozone on organic pollutants. On the other hand, CO_2 generated from organic pollutants mineralized could not effectively overflow from wastewater in the strong basic condition; therefore, HCO_3^- and CO_3^{2-} were the main existence forms which could quickly consume the radicals as $\cdot OH$. Meanwhile, some of the decomposition products of organic pollutants like aromatic group might inhibit the radicals generated. These factors led to the decrease in COD_{Cr} removal efficiency.

3.2.3. Effect of O_3 Dosage on Treatment. At the optimum conditions such as reaction time 60 min, pH 8, and O_3 mixture flow 100 mL/min, O_3 dosage was controlled within 1–10 mg/L by regulating the power of the O_3 generator and influent COD_{Cr} concentration 300–350 mg/L; the removal of COD_{Cr} from wastewater by ozone oxidation is displayed in Figure 6.

As the dosage of O_3 increased from 1.3 mg/L to 5.5 mg/L, the removal ratio of COD_{Cr} gradually improved from 40.37% to 55.46% and then tended to be stable by continuously adding O_3 dosage. Low dosage of O_3 produced less strong oxidation substances such as $\cdot OH$ in the wastewater which caused poorer oxidation effect and longer reaction time. With the increase in O_3 dosage, more $\cdot OH$ was produced and the oxidation rate increased. Until the O_3 dosage was added to 5.5 mg/L, the

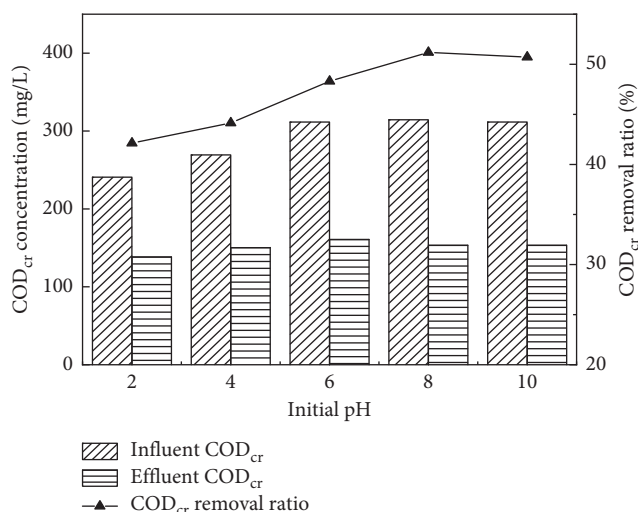


FIGURE 5: Effect of initial pH on COD_{Cr} removal by ozone oxidation.

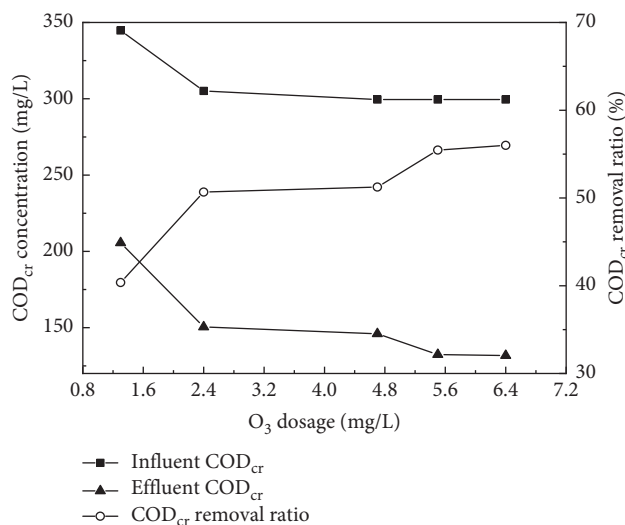


FIGURE 6: Effect of O_3 dosage on COD_{Cr} removal by ozone oxidation.

dissolved amount of O_3 molecules in the wastewater tended to be saturated, the excess O_3 gas could not be used effectively, and the effluent still could not meet the discharge or reuse standard requirements. Ozone oxidation might be an assistant treatment for flotation wastewater.

3.2.4. Effect of O_3 Oxidation on the Biodegradability of Wastewater. The biodegradability of simulated wastewater by O_3 oxidation at different times was discussed based on the experimental conditions such as O_3 dosage 1.3 mg/L and pH 8; the results are shown as Figure 7. O_3 oxidation could obviously increase BOD_5/COD_{Cr} value of wastewater to higher than 0.3 when the reaction time was 15 min and reached the maximum value 0.549 as the reaction time prolonged to 30 min. O_3 and $\cdot OH$ had a strong oxidation effect and could break down the hard-degradable organics

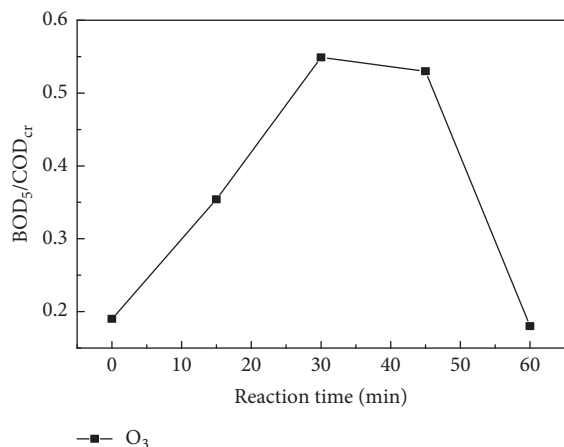


FIGURE 7: Effect of O₃ oxidation on biodegradability of wastewater.

into small-molecule intermediates by chain-breaking and ring-opening to increase the biodegradability of wastewater. As the reaction time was up to 60 min, the intermediate product from oxidative degradation played the dominant role which lead to faster degradation of BOD₅ and a corresponding decrease of BOD₅/COD_{Cr} value in the wastewater.

3.3. Fenton Oxidation of Simulated Wastewater

3.3.1. Effect of Reaction Time on Treatment. The experimental conditions of Fenton oxidation were initial pH = 4, H₂O₂ dosage = 0.48 g/L, and Fe₂SO₄·7H₂O dosage = 0.196 g/L (the molar ratio of H₂O₂ to Fe²⁺ was 5:1); the reaction time was 15 min, 30 min, 60 min, 90 min, and 120 min, respectively. The experimental results of COD_{Cr} concentration and the removal ratio are shown in Figure 8.

According to the reaction time, the COD_{Cr} removal effect of Fenton oxidation was obviously divided into two stages: COD_{Cr} removal ratio rapidly increased to more than 60% within 15 min, while the increasing trend was slowly during 15 to 120 min. In the initial stage of Fenton reaction, the catalytic reaction rate was faster and the production of ·OH was more due to the high concentration of H₂O₂ and Fe²⁺; most of the organic pollutants in the wastewater were effectively degraded. With increasing reaction time, the H₂O₂ concentration decreased which caused the reduction of ·OH generation and the degradation rate slowed down gradually. Based on comprehensive consideration of economy and efficiency, the optimum reaction time was selected as 90 min, and COD_{Cr} removal ratio reached 79%.

3.3.2. Effect of Molar Ratio of H₂O₂ to Fe²⁺ on Treatment. The initial conditions were set as pH = 4 and H₂O₂ dosage = 0.48 g/L; the dosage of FeSO₄·7H₂O was changed to different molar ratios of H₂O₂ to Fe²⁺ 1:1, 2:1, 5:1, 10:1, and 20:1, respectively. The effect of reaction time on COD_{Cr} removal ratio by Fenton oxidation is shown in Figure 9. The changing trends of the COD_{Cr} removal ratio with the reaction time at different molar ratios of H₂O₂ to Fe²⁺ had

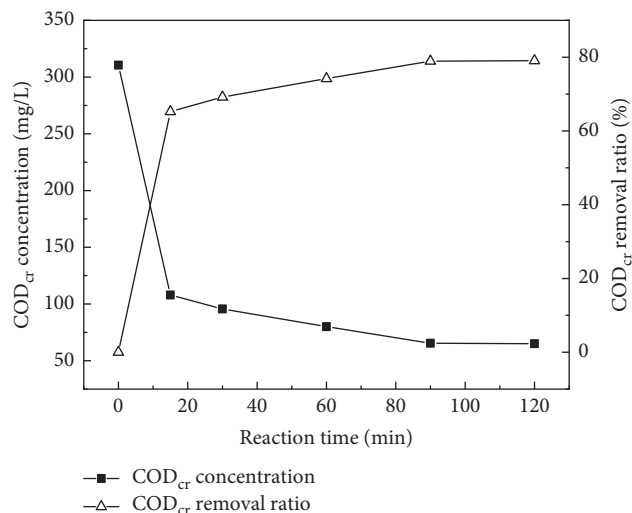


FIGURE 8: Effect of reaction time on removal of COD_{Cr} by Fenton oxidation.

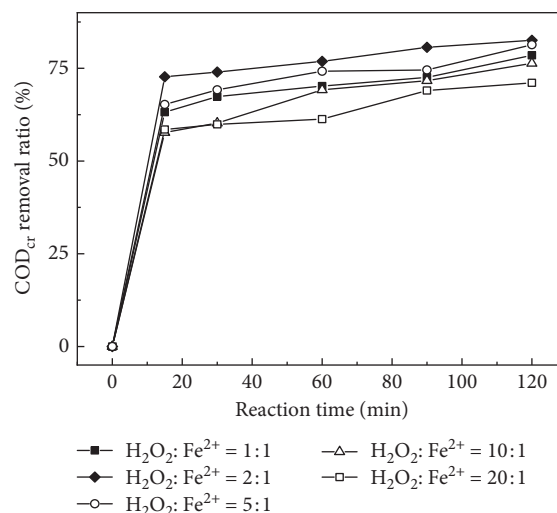
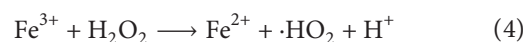
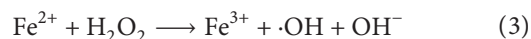


FIGURE 9: Effect of molar ratio of H₂O₂ to Fe²⁺ on COD_{Cr} removal ratio.

almost the similar tendency, within the first of 15 min reaction time; the removal ratio of COD_{Cr} increased rapidly and then improved slowly during 15 to 120 min reaction time. When the molar ratio of H₂O₂ to Fe²⁺ was 2:1 and the reaction time was 90 min, the COD_{Cr} removal ratio reached the maximum value of more than 80%.

The ·OH generation during the reaction process mainly included two stages as follows:



Fe²⁺ in the wastewater acted as catalyst. When molar ratio of H₂O₂ to Fe²⁺ was 2:1, it just met the theoretical demand for Fe²⁺ in the ·OH generation reaction, and the catalytic efficiency of Fe²⁺ and the production of ·OH could achieve

the highest level. If the molar ratio was greater than 2:1, the concentration of Fe^{2+} in the system was lower to decrease the rate of catalysis, the $\cdot\text{OH}$ yield, and the removal rate in the wastewater. When the molar ratio decreased to 1:1, the concentration of Fe^{2+} in the system was too higher, the excess Fe^{2+} would also react with $\cdot\text{OH}$ to cause redox reaction which promoted the decomposition of H_2O_2 and declined the removal efficiency of organic pollutants.

3.3.3. Effect of Initial pH on Treatment. The initial pH was one of the important factors indirectly affecting the activity and production of $\cdot\text{OH}$ and resulting in a certain limitation on the oxidative capacity of Fenton reaction [16]. The initial conditions were set as H_2O_2 dosage = 0.48 g/L, the molar ratio of H_2O_2 to $\text{Fe}^{2+} = 2:1$, and reaction time = 90 min; pH was adjusted to 2, 3, 4, 5, and 6, respectively. The experimental results are displayed in Figure 10. Fenton oxidation generally possessed a better treatment effect on wastewater with the decrease in pH. The best removal ratio of COD_{Cr} was 84.4% at initial pH = 3, and the concentration of COD_{Cr} was lower than 48.36 mg/L. As the pH value was higher than 3, the concentration of hydroxide in the wastewater increased gradually and the generation of $\cdot\text{OH}$ was inhibited; meanwhile, Fe^{2+} precipitated and affected catalytic efficiency. When the pH was lower than 3, the H^+ concentration in the system increased which inhibited the reduction of Fe^{3+} to Fe^{2+} and hindered the conversion equilibrium between Fe^{3+} and Fe^{2+} and thus reduced the efficiency of the catalytic reaction [17].

3.3.4. Effect of H_2O_2 Dosage on Treatment. The experimental conditions were selected as follows: pH = 3, the molar ratio of H_2O_2 to $\text{Fe}^{2+} = 2:1$, and reaction time = 90 min; the dosage of H_2O_2 was 0.24 g/L, 0.48 g/L, 0.72 g/L, 0.96 g/L, and 1.2 g/L, respectively. The effect of Fenton oxidation on COD_{Cr} is shown in Figure 11. When the dosage of H_2O_2 was increased from 0.24 to 0.96 g/L, the COD_{Cr} removal ratio increased rapidly from 71.63% to 90.43% and the COD_{Cr} was decreased from 85.1 mg/L to 28.7 mg/L. When the dosage of H_2O_2 was continuously increased to 1.2 g/L, COD_{Cr} removal ratio decreased obviously. When the dosage of H_2O_2 was less than 0.96 g/L, the reaction rates of equations (5) and (6) became slower and the amount of $\cdot\text{OH}$ produced decreased and reduced the removal ratio of COD_{Cr} . With the increase in H_2O_2 dosage, the concentration of $\cdot\text{OH}$ in the system increased and the degradation rate of organic pollutants accelerated. The oxidation reaction of $\cdot\text{OH}$ was not selective, the excess dosage of H_2O_2 resulted in reaction equations (3) and (4) which became the dominant reactions in the system, and H_2O_2 acted as a scavenger to reduce the concentration of $\cdot\text{OH}$ [18]:

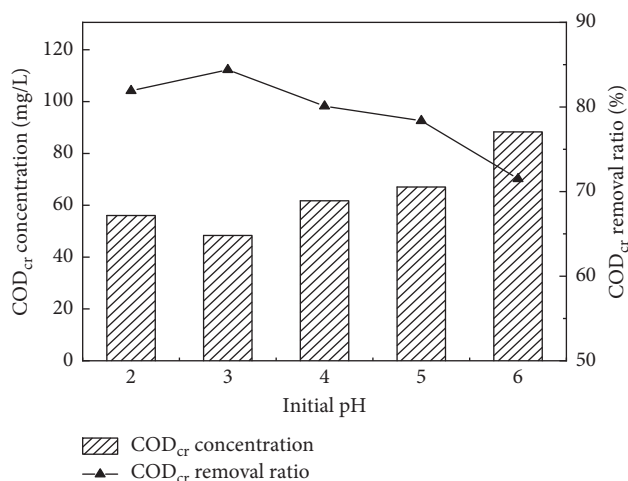
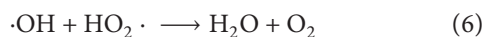
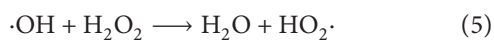


FIGURE 10: Effect of initial pH on COD_{Cr} removal.

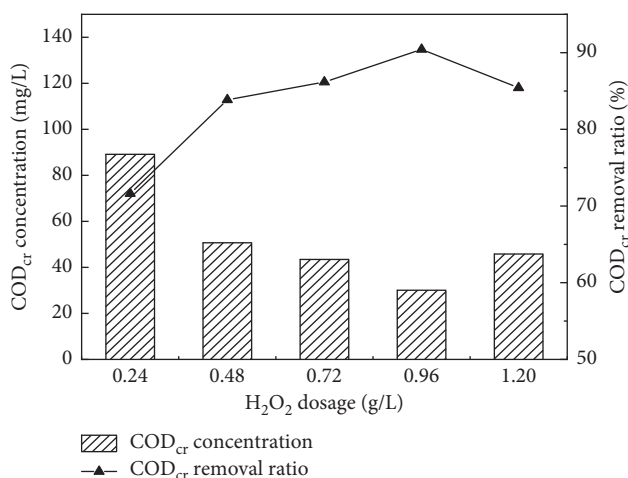


FIGURE 11: Effect of H_2O_2 dosage on COD_{Cr} removal.

3.3.5. Effect of Fenton Oxidation on Biodegradability of Wastewater. The concentrations of COD_{Cr} and BOD_5 of the simulated wastewater were 320 mg/L and 61.18 mg/L; the $\text{BOD}_5/\text{COD}_{\text{Cr}}$ was 0.19. The effect of Fenton oxidation on the biodegradability of wastewater was discussed under the experimental conditions as pH = 3, the molar ratio of H_2O_2 to $\text{Fe}^{2+} = 2:1$, and the dosage of $\text{H}_2\text{O}_2 = 0.96$ g/L; reaction time was 15 min, 30 min, 45 min, 60 min, and 90 min, respectively. The results are exhibited in Figure 12.

With the increase in reaction time, the concentrations of COD_{Cr} and BOD_5 in wastewater declined continuously. Within 60 min reaction time, the declining rate of COD_{Cr} concentration was significantly faster than BOD_5 , $\text{BOD}_5/\text{COD}_{\text{Cr}}$ value increased rapidly from 0.19 to 0.382, and the biodegradability of wastewater was improved. While the reaction time was prolonged to 90 min, $\text{BOD}_5/\text{COD}_{\text{Cr}}$ value dropped off rapidly to 0.17. Within the first 60 min reaction, difficult-to-biodegrade pollutants in the wastewater were rapidly degraded to biodegradable intermediates, and a

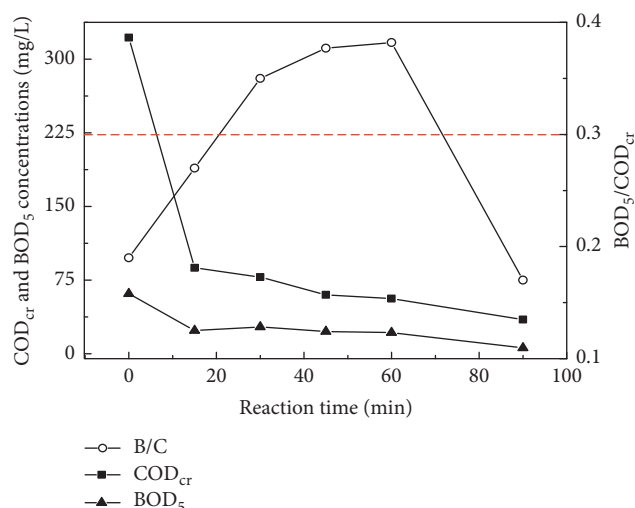


FIGURE 12: Effect of Fenton reaction time on biodegradability of wastewater.

portion was directly mineralized to CO₂ and H₂O which resulted in increased BOD₅/COD_{Cr}. Due to prolonged reaction time, the concentration of strong oxidation substances and macromolecular organic pollutants decreased, and the reaction in the system was dominated by the oxidative decomposition of intermediate products. The removal rate of COD_{Cr} was lower than the BOD₅; thus, the BOD₅/COD_{Cr} value declined.

4. Conclusions

Salicylhydroxamic acid wastewater from the W–Mo ore flotation process is difficult to be treated by coagulation-settlement technology, and the effluent is difficult to meet the requirements of the first-grade discharge standard in the Integrated Wastewater Discharge Standard (GB 8978) and the water quality of the reuse of urban recycling water-water quality standard for industrial uses (GB/T 19923). In practical engineering, tailing reservoir is generally used for a final section to treat the flotation wastewater by natural sunlight degradation, but it was proved in this paper that the degradation of natural sunlight had a limited effect on the simulated flotation wastewater, the COD_{Cr} removal ratio could reach the highest 25.99% after 48 h sun illumination, and sunlight could not degrade the mineral processing reagent with benzene ring structure. Sunlight degradation was not an effective treatment method for practical flotation wastewater. Under varied operation parameters of reaction time, initial pH, and O₃ dosage, ozonation was proved to be effective for simulated salicylhydroxamic acid wastewater, the COD_{Cr} removal ratio could reach the maximum 55.46% at the optimum experimental conditions, and the BOD₅/COD_{Cr} value increased to 0.549 after 30 min reaction. But the effluent could not reach the discharge or reuse standard, and ozonation could be the prepositive disposal combined with biochemical treatment. Ozonation is a high-power consumption treatment method, treatment cost was necessary to be considered in actual engineering, and the BOD₅/

COD_{Cr} value could be controlled as 0.35 after 15 min reaction to meet the demand of biochemical treatment. Fenton oxidation was more effective than sunlight and ozonation process, under the experimental conditions such as pH 3, H₂O₂ dosage 0.96 g/L, the molar ratio of H₂O₂ to Fe²⁺ 2:1, and the reaction time 90 min; COD_{Cr} concentration and the removal ratio in the flotation wastewater were 30.07 mg/L and 90.43%, which was far below the prescribed emission or reuse standards. Fenton oxidation could be of single-use to treat the salicylhydroxamic acid wastewater which was more simple than the ozonation process, but the consumption of H₂O₂ and Fe₂SO₄·7H₂O was large, and massive precipitate was generated which brought inconvenient operation in practical engineering.

Data Availability

The data used to support the findings of this study are available from the corresponding author upon request.

Conflicts of Interest

The authors declare that they have no conflicts of interest.

Acknowledgments

This work was supported by the National Key Research and Development Project (2018YFC0406403-1).

References

- [1] W. Liu, C. J. Moran, and S. Vink, "A review of the effect of water quality on flotation," *Minerals Engineering*, vol. 53, no. 10, pp. 91–100, 2013.
- [2] Z. G. Wang, C. H. E. N. Xiang-xiang, Y. W. Zhang et al., "New process of treatment wastewater from Lead -Zinc concentrator of Jindong mining company," *Metal Mine*, vol. 31, no. 6, pp. 126–128, 2013.
- [3] L. Che, Y. Yu, J. Pang et al., "Synthesis, properties and role mechanism of hydroxamic acid as collectors of RE mineral flotation," *Chinese Rare Earths*, vol. 25, no. 6, pp. 74–79, 2004.
- [4] W. Liu, B. Wang, and S. Dai, "Current application and development prospect of hydroxamic acid in flotation," *Non-Ferrous Mining and Metallurgy*, vol. 22, no. 4, pp. 25–27, 2006.
- [5] S. Esplugas, P. L. Yue, and M. I. Pervez, "Degradation of 4-chlorophenol by photolytic oxidation," *Water Research*, vol. 28, no. 6, pp. 1323–1328, 1994.
- [6] M. I. Litter, *Introduction to Photochemical Advanced Oxidation Processes for Water Treatment Environmental Photochemistry Part II*, pp. 325–366, Springer, Berlin, Heidelberg, Germany, 2005.
- [7] L. R. Rad, I. Haririan, and F. Divsar, "Comparison of adsorption and photo-Fenton processes for phenol and paracetamol removing from aqueous solutions: single and binary systems," *Spectrochimica Acta Part A: Molecular and Biomolecular Spectroscopy*, vol. 136, pp. 423–428, 2015.
- [8] P. T. Almazán-Sánchez, I. Linares-Hernández, V. Martínez-Miranda, V. Lugo-Lugo, and R. M. Guadalupe, "Wastewater treatment of methyl methacrylate (MMA) by Fenton's reagent and adsorption," *Catalysis Today*, vol. 220-222, pp. 39–48, 2014.

- [9] D. O. Energy, "Airborne laser induced fluorescence imaging: innovative technology summary report," Technical Reports, Office of Scientific & Technical Information, Denton, TX, USA, 1999.
- [10] S. Dai, J. Liu, W. Song et al., "Application of advanced treatment for refractory organic wastewater with ozone oxidation method," *Water Sciences and Engineering Technology*, vol. 136, no. 2, pp. 24–26, 2007.
- [11] S. Deng, M. Bai, X. Bai et al., "Characteristics and chemical reaction of hydroxyl radical," *Journal of Dalian Maritime University*, vol. 30, no. 3, pp. 62–64, 2004.
- [12] W. Jiang, X. Peng, L. Zhang et al., "Research progress in treatment of xanthate in mineral concentration wastewater by advanced oxidation technology," *Metal Mine*, vol. 498, no. 12, pp. 123–129, 2017.
- [13] X. Zhu, J. Tian, R. Liu, and L. Chen, "Optimization of Fenton and electro-Fenton oxidation of biologically treated coking wastewater using response surface methodology," *Separation and Purification Technology*, vol. 81, no. 3, pp. 444–450, 2011.
- [14] D. Zhang, Y. Wen, and X. Gao, "A comparative study on the calibration of ozone concentration with three potassium iodide methods," *Journal of Beijing University of Technology*, vol. 11, no. 1, pp. 97–103, 1985.
- [15] Z. Zhang, T. Zeng, Y. Nie et al., "Natural photolysis and photocatalytic degradation characteristics of reagent for beneficiation in gannan region," *Nonferrous Metals Engineering*, vol. 8, no. 5, pp. 50–56, 2018.
- [16] W. A. Simon, E. Sturm, H.-J. Hartmann, and U. Weser, "Hydroxyl radical scavenging reactivity of proton pump inhibitors," *Biochemical Pharmacology*, vol. 71, no. 9, pp. 1337–1341, 2006.
- [17] E. Lipczynska-Kochany, G. Sprah, and S. Harms, "Influence of some groundwater and surface waters constituents on the degradation of 4-chlorophenol by the Fenton reaction," *Chemosphere*, vol. 30, no. 1, pp. 9–20, 1995.
- [18] E. C. Catalkaya and F. Kargi, "Effects of operating parameters on advanced oxidation of diuron by the fenton's reagent: a statistical design approach," *Chemosphere*, vol. 69, no. 3, pp. 485–492, 2007.

Research Article

Molecular Signatures of Humic Acids from Different Sources as Revealed by Ultrahigh Resolution Mass Spectrometry

Shuai Qin,^{1,2} Chengbin Xu,² Yingzi Xu,¹ Yingchen Bai,¹ and Fei Guo ¹

¹State Key Laboratory of Environmental Criteria and Risk Assessment, Chinese Research Academy of Environmental Sciences, Beijing 100012, China

²School of Environmental Sciences, Liaoning University, Shenyang 110036, China

Correspondence should be addressed to Fei Guo; figoth@163.com

Received 27 December 2019; Accepted 5 February 2020; Published 1 April 2020

Guest Editor: Yihua Xiao

Copyright © 2020 Shuai Qin et al. This is an open access article distributed under the Creative Commons Attribution License, which permits unrestricted use, distribution, and reproduction in any medium, provided the original work is properly cited.

Humic acid (HA) is extremely important for understanding the geochemical cycle of pollutants in different environments. Fourier transform ion cyclotron resonance mass spectrometry (FT-ICR MS) has performed molecular-level analysis of two standard HAs from the Suwannee River (SRHA) and leonardite (LEHA) and HA from Jiufeng forest in Beijing (JFHA), which is impossible for other conventional instruments. Regardless of the source of HA, compounds containing more heteroatoms (such as nitrogen and sulfur) have a higher degree of unsaturation and aromaticity. JFHA, SRHA, and LEHA from soil, river, and leonardite, respectively, are arranged in order from the lowest to highest degree of humification, according to molecular unsaturation and aromaticity of HAs. Soil HA is more labile and contains many large molecular weight compounds with low unsaturation. Regardless of unsaturation, molecules of River HA have a homogeneous molecular mass distribution and contain many plant-derived lignin- and tannin-like compounds, which are more stable than lipid and more labile than condensed aromatics. Leonardite HA with a high degree of humification contains a large number of compounds with high aromaticity and more heteroatoms and has low lability. Our results reveal the diversity of humic acid at molecular level because of different degree of humification and the lability. These conclusions are significant for understanding the role of humic acid from different sources in pollutant transformation and the geochemical cycle at the molecular level.

1. Introduction

Humic substances (HS) are the most widespread natural organic matter (NOM) in soil, water, and sediment. HS are derived mainly from plant, organism, and animal tissues [1], while the biomaterials lost their initial structures in chemical and biological degradation. Various turnover times of humic substances that affect global carbon balance are due to inherent structural resistance to biotic decomposition and binding to minerals [2–5]. They have complex chemical structures which are more stable than their precursors and have lost their chemical properties [6]. HS can be classified into humic acid (HA), fulvic acid (FA), and humin (HM) based on the solubility [7, 8]. HA generally represents the major fraction of HS [6] and is mainly derived from typical environments rich in biochemical reactions such as soil, rivers, and leonardite.

Soil, river, and leonardite are three typical sources of HAs. Soil HAs are mainly derived from the (bio)chemical degradation of plant and animal residues and synthetic activity from microorganisms and account for 20% of the total organic matter [6, 9, 10]. Rivers play a very important role in the transformation [11, 12] and global cycling of HAs [12, 13]. Elemental composition of molecules can cause the spontaneous generation of relatively labile HAs [14, 15] or change the HA reactivity and adsorption process. Lignite (low rank coal) is the second stage of coal formation [6]. Leonardite, the most oxidized variety of lignite, is the richest source of HS [16, 17]. Leonardite-derived HA accounts for 10–80% of leonardite organic matter, depending on its maturity level [18] and is further along the diagenetic path of humification. They are much older and contain more condensed aromatics than soil HAs [6]. There are a number

of studies concerning HA derived from different types of soil [19] and rivers worldwide [11], but contrast data on the molecular composition of HA from soil, river, and leonardite are still missing. The standard samples provided by International Humic Substances Society can more accurately reflect characteristics of HA from various sources.

It is difficult to analyse HA at the molecular level due to its extreme complexity, low concentration, and high polarity [20]. There are many conventional techniques to characterize HA from a variety of sources, such as liquid chromatography-mass spectrometry (LC-MS), pyrolysis gas chromatography-mass spectrometry (GC-MS), and nuclear magnetic resonance (NMR) [21]. They provide apparent or biased information about HA and fail to dig for complete characteristics [22]. Low-resolution GC-MS and LC-MS can only analyse a small part of HA due to volatility and solubility, respectively. NMR can give the functional group information of the bulk HA but fail to give molecular-level details [20]. Fourier transform ion cyclotron resonance mass spectrometry (FT-ICR MS) is a very suitable tool for analysing HA from different sources [23]. Due to its high resolution and accuracy, it can assign unique molecular formula to thousands of compounds [24]. Moreover, as a soft ionization technology, negative ion mode electrospray ionization (ESI) has high selectivity for polar molecules in complex mixtures [25], which can avoid complex separation procedures [26].

The purpose of this work is to investigate the molecular compositions of HAs from soil, river, and leonardite using ESI FT-ICR MS. The specific objectives are to (1) compare the diversity of molecular composition between HAs from different resources and (2) discuss the lability of diverse HAs.

2. Materials and Methods

2.1. Samples and Extraction Method. Humic acid (HA) collected from Suwannee River in South Georgia (SRHA) is a standard fulvic acid sample of International Humic Substances Society (IHSS) and its serial number is 2S101F. The IHSS standard leonardite-derived HA sample (LEHA) was obtained from the Gascoyne Mine in Bowman County, North Dakota, USA [27], and its serial number is 4S102F. Leonardite was produced by the natural oxidation of exposed lignite, which was a low-grade coal. The microbial action and other chemical processes of leonardite in the natural environment are longer and more complex, and therefore LEHA has a higher degree of humification. More additional details of the source material can be found at <http://humic-substances.org/>. HA collected from Beijing Jiufeng forest soils in China (JFHA) was extracted according to the standard method recommended by IHSS. The detailed extraction method is as follows.

Take certain amount of freeze-dried soil from Jiufeng forest and thoroughly mix it with 0.1 mol/L NaOH solution to obtain mixed solution with solid-liquid ratio of 1:10. Remove the residual soil after centrifugation. The 6.0 mol/L HCl solution was added to the mixed solution to make the pH value 1 and then left to stand for 24 hours to obtain

precipitate. 0.1 mol/L KOH solution was added to the precipitate, the pH was adjusted to 13.0, and then certain amount of potassium chloride was added to adjust the solution concentration to 0.4 mol/L. After half an hour of high-speed centrifugation (10000 r/min), the supernatant was separated, and 6.0 mol/L HCl was added to adjust the pH to 1.0, and concentrated HF was added to make the concentration to 0.3 mol/L. Impurities were removed by shaking and dialysis, and the solution was freeze-dried to obtain humic acid sample.

2.2. Parameters of FT-ICR MS. The spectra of JFHA, SRHA, and LEHA were obtained using a Bruker Apex-ultra Fourier transform ion cyclotron resonance mass spectrometry (FT-ICR MS) with a 9.4 T superconducting magnet and Apollo II electrospray ion source. The operating parameters of the FT-ICR MS analysis were mainly according to the previous studies [28]. Sample solutions were continuously injected into the electrospray ion source at a flow rate of 180 $\mu\text{L}/\text{h}$ with a syringe pump. The spray shield voltage, capillary column introducing voltage, and capillary column end voltage of the negative-ion ESI were set to 4.0 kV, 4.5 kV, and -320 V , respectively. For each spectrum multiple (200–300) transient scans (collected with a 4 M Word time domain) were coadded in the m/z 200–700 mass range. The spectra were externally calibrated from a homologous series of the Suwannee River Natural Organic Matter sample (SRNOM). The mass measurement accuracy for single charged molecular ions was better than $\pm 1\text{ ppm}$. Mass peaks were exported if the signal-to-noise (S/N) ratio was greater than 6. Molecular formula assignments were limited by the following constraints for the three samples: 12C (0–100), 13C (0–2), 1H (0–100), 14N (0–3), 16O (0–30), and 32S (0–2) atoms, and only the possible element composition within $\pm 1\text{ ppm}$ mass measurement error was considered.

2.3. Molecular Indexes of Humic Acid. Normalized peak intensities (normalized to the sum of peak intensities of identified molecular formulas) were used to semiquantitatively evaluate differences in HA molecular composition [29]. The modified aromatic index (AI-mod) reflected the number of double C=C bonds, C-O bonds, and C=O bonds and was used to assess the aromaticity of compounds. AI-mod was calculated based on the assigned molecular formula (described as $\text{C}_c\text{H}_h\text{O}_o\text{N}_n\text{S}_s$) using the equation $\text{AI-mod} = (1 + c - 0.5o - s - 0.5h) / (c - 0.5o - s - n)$ [30]. The double bond equivalents (DBE) was used to assess the degree of unsaturation of compounds and calculated as follows: $\text{DBE} = c - h/2 + n/2 + 1$. Intensity weighted average values are displayed for number of carbons (C_{wa}), hydrogens (H_{wa}), oxygens (O_{wa}), nitrogens (N_{wa}), sulfurs (S_{wa}), molecular masses (m/z_{wa}), hydrogen to carbon ratios (H/C_{wa}), oxygen to carbon ratios (O/C_{wa}), double bond equivalents (DBE_{wa}), and modified aromatic indexes ($\text{AI-mod}_{\text{wa}}$). The molecular lability boundary index (MLB) is the bound when H/C is 1.5. $\text{MLB}_1\%$ which can be used to evaluate the lability of HA. When $H/C > 1.5$, the NOM constituents above MLB correspond to a more labile substance (MLB_1), and when

$H/C < 1.5$, the NOM constituents below MLB exhibit less labile and more recalcitrant characteristics (MLB_R). $MLB_L\%$ was calculated by dividing the total intensity of molecular formulas with $H/C \geq 1.5$ by the total intensity of molecular formulas [31]. Carboxyl-rich alicyclic molecules (CRAMs) which are often associated with refractory compounds are complex mixtures of carboxylated and fused alicyclic structures whose carboxyl-C: aliphatic-C ratio is 1:2 to 1:7 [32]. $CRAM\%$ was calculated by dividing the total intensity of molecular formulas with $DBE/C = 0.3-0.68$, $DBE/H = 0.2-0.95$, and $DBE/O = 0.77-1.75$ by the total intensity of molecular formulas [29]. The nominal oxidation state of C (NOSC) was used to assess the degradability of DOM [33, 34] and was calculated by using $NOSC = 4 - ((4c + h - 3n - 2o - 2s)/c)$ [34]. The assigned molecular formulas were examined using the van Krevelen diagram (v-K diagram) and modified aromatic index (AI-mod). The v-K diagram (a plot of atomic H/C and O/C) is an excellent method for graphical interpretation of large datasets and visualization of their chemical nature. Molecular formulas were further assigned to the following groups [30, 35, 36]. They are (i) polycyclic aromatics ($AI-mod > 0.66$), (ii) highly aromatic compounds ($0.66 \geq AI-mod > 0.50$), (iii) highly unsaturated compounds ($AI-mod \leq 0.50$ and $H/C < 1.5$), (iv) unsaturated aliphatic compounds ($2.0 > H/C \geq 1.5$ and $N = 0$), (v) unsaturated aliphatic compounds containing N ($2.0 > H/C \geq 1.5$ and $N > 0$), (vi) carbohydrates ($H/C \geq 2.0$ and $O/C \geq 0.9$), and (vii) fatty acids and sulfonic acids ($H/C \geq 2.0$ and $O/C < 0.9$) [37-39].

3. Results and Discussion

3.1. General Signatures of FT-ICR MS. The HAs from river, soil, and Leonardite are shown as representative spectra in Figures S1a-S1c. All HA samples have concentrated mass spectral peaks in the range of 200-700 Daltons (Da), and the overall peak shapes of SRHA and LEHA are approximately normal distribution (Figure S1). The number of assigned formulas of SRHA, JFHA, and LEHA is 3559, 2246, and 4398, respectively. The variation in the C, H, O, N, and S contents and molecular mass as well as indices based on these shows distinct differences (Table 1). There are the highest H content and lowest O and N content in JFHA, leading to the highest H/C and lowest O/C in JFHA. In addition, JFHA contains more saturated compounds with higher H/C and lower O/C (Figure 1), and its overall molecular mass is smaller (Figure S2b). This indicates that the degree of humification of JFHA is higher, because refractory humic acid fractions are marked by increases in the lipid components which have high H/C and low O/C [40]. The indexes of SRHA are relatively moderate, such as m/z_{wa} , H/C_{wa} , and DBE_{wa} . LEHA has the lowest H/C and the largest molecular mass and this may be because the condensed aromatic structure with low H/C is abundant in LEHA and has a large molecular weight. This is consistent with the previous conclusion that refractory humic acid fractions are marked by increases in the condensed aromatic components [40].

3.2. Van Krevelen Diagram Analysis. In the v-K diagram, the aromaticity of the compounds shows such a rule: the aromaticity of the compounds in lower layer is higher than that in upper layer [30]. The compound distribution of SRHA shows a rectangle in the v-K diagram, which indicates that the molecular distribution is relatively homogeneous (Figure 1). From the perspective of the number of molecular formulas and the peak magnitudes, there is no significant difference in the distribution proportion of the compounds (Table 2). The compounds are mainly concentrated in highly unsaturated compounds, accounting for 51% in terms of number of molecular formulas and 54% in terms of peak magnitudes. Highly aromatic compounds and polycyclic aromatics are ranked second and third, respectively, accounting for about 10% to 20% (Table 2).

The compounds of JFHA are mainly concentrated in the upper and lower layers, and sparse points are in the middle layer (Figure 1). In addition, from the perspective of the number of molecular formulas and peak magnitudes, the distribution of the compounds is quite different. From the number of molecule formulas, the compounds are mainly distributed in unsaturated aliphatic compounds, highly unsaturated compounds, and polycyclic aromatics, accounting for about 25%. From the peak magnitudes' point of view, the compounds are mainly distributed in unsaturated aliphatic compounds, accounting for 50%, followed by fatty acids, accounting for 25% (Table 2). By comparison, the high peak magnitudes of unsaturated aliphatic compounds and fatty acids and sulfonic acids are due to the high content of these compounds in JFHA firstly and secondly because these compounds are easily ionized in the negative ion mode of ESI FT-ICR MS [19].

The compound distribution of LEHA is a right-angled triangle in the v-K diagram; that is, the lower-layer compound is more abundant and has a wider distribution range than the upper-layer compound (Figure 1). There is no significant difference in the molecular formula number distribution and peak magnitude distribution of compounds. Obviously, the compounds are mainly concentrated in the lower layer, and the largest proportion is polycyclic aromatics, which accounts for about 50%, followed by highly aromatic compounds and highly unsaturated compounds, accounting for about 20-30% (Table 2).

DBE_{wa} for SRHA, JFHA, and LEHA are 10.02, 5.35, and 15.07, respectively, and $AI-mod_{wa}$ are 0.38, 0.17, and 0.59, respectively. These two molecular formula parameters consistently indicate that the aromaticity of LEHA is the highest among the three HAs samples, followed by SRHA, and the smallest is JFHA. This is concordant with previous research results. The DBE value increased in the progression of water-extractable organic matter from Adkins soil, labile humic acid, and refractory calcium humic acid, which indicates that as the degree of humification increases, the aromaticity of organic matter also increases [40]. The compounds that account for a large proportion of LEHA have higher degrees of unsaturation, and the most abundant compounds are polycyclic aromatics which have highest aromaticity. The presence of a large number of aromatic

TABLE 1: Molecular parameters of (a) humic acids from Jiufeng forest soil, (b) humic acids from Suwannee River, and (c) humic acids from leonardite derived from assigned molecular formulas^a.

Sample	C_{wa}	H_{wa}	O_{wa}	N_{wa}	S_{wa}	m/z_{wa}	H/C_{wa}	O/C_{wa}	DBE_{wa}	$AI-mod_{wa}$	$MLBL\%^b$	$CRAM\%^c$	NOSC
JFHA	21.63	34.60	4.62	0.04	0	368.05	1.60	0.22	5.35	0.17	75.47	8.28	-0.16
SRHA	20.07	22.16	8.19	0.54	0.01	394.22	1.10	0.42	10.02	0.38	15.33	51.91	-0.25
LEHA	23.58	19.29	8.02	0.25	0.02	434.01	0.81	0.35	15.07	0.59	7.88	18.25	-007

^aIntensity weighted average values are displayed for number of carbons (C_{wa}), hydrogens (H_{wa}), oxygens (O_{wa}), nitrogens (N_{wa}), sulfurs (S_{wa}), molecular weights (m/z_{wa}), hydrogen to carbon ratios (H/C_{wa}), and oxygen to carbon ratios (O/C_{wa}). ^{b,c}Both $MLBL\%$ and $CRAM\%$ are obtained by dividing the total intensity of the corresponding molecular formula by the total intensity of the molecular formula.

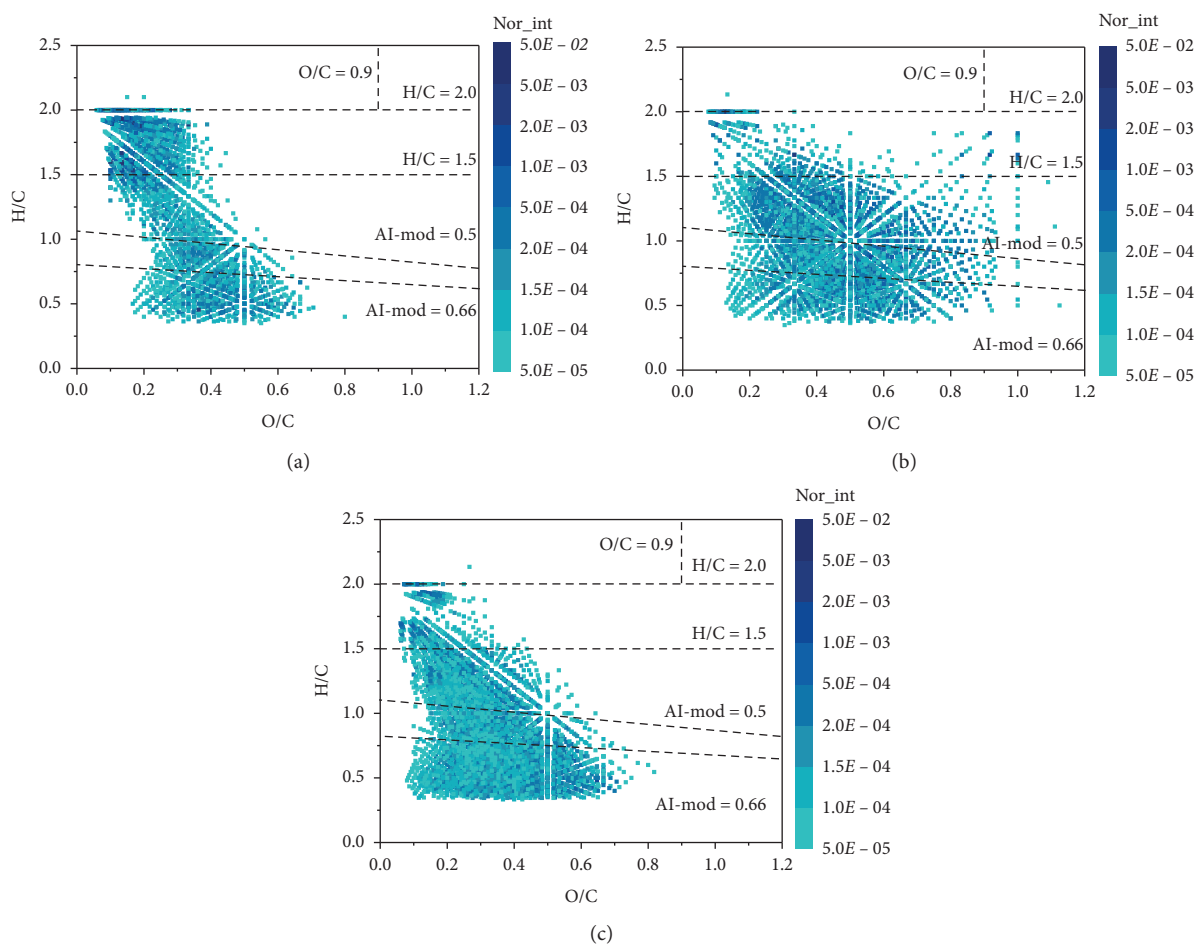


FIGURE 1: Van Krevelen diagrams from the mass spectra of (a) humic acids from Jiufeng forest soil, (b) humic acids from Suwannee River, and (c) humic acids from leonardite. The shades of color represent the peak magnitudes of the molecules. Broken lines divide the pattern into 7 areas which indicate major biomolecular compound classes: (1) polycyclic aromatics (PCAs, $AI-mod > 0.66$), (2) highly aromatic compounds ($0.66 \geq AI-mod > 0.50$), (3) highly unsaturated compounds ($AI-mod \leq 0.50$ and $H/C < 1.5$), (4) unsaturated aliphatic compounds ($2.0 > H/C \geq 1.5$ and $N = 0$), (5) unsaturated aliphatic compounds containing N ($2.0 > H/C \geq 1.5$ and $N > 0$), (6) carbohydrates ($H/C \geq 2.0$ and $O/C \geq 0.9$), and (7) fatty acids and sulfonic acids ($H/C \geq 2.0$ and $O/C < 0.9$). Nor_int is the normalization of the intensity of each molecule.

compounds indicates that LEHA is the most aromatic and has the highest degree of humification. The compounds of SRHA and JFHA are mainly concentrated in medially unsaturated compounds, which are highly unsaturated compounds and unsaturated aliphatic compounds, respectively. Highly unsaturated compounds are more aromatic than unsaturated aliphatic compounds. As a result, SRHA is more aromatic than JFHA.

DBE is roughly positively correlated with m/z among three HA samples. The compounds with DBE greater than 20 are distributed across m/z range of 450–700 DA. The number and peak magnitudes of these molecular formulas both increase in order of JFHA, SRHA, and LEHA (Figure 2). DBE is roughly negatively related to H/C among the three HA samples. The above compounds are polycyclic aromatics and highly aromatic compounds (Figure 3).

TABLE 2: Number of peaks assigned to molecular formulas having similar elemental composition to each compound group and the sum of their peak magnitudes.

Sample name	JFHA	SRHA	LEHA
Number of formulas	2246	3559	4398
Number of formulas similar to fatty acids and sulfonic acids	122 (5)	41 (1) ^a	34 (1)
Carbohydrates	0 (0)	0 (0)	0 (0)
Unsaturated aliphatic compounds containing N	0 (0)	1 (0)	0 (0)
Unsaturated aliphatic compounds	683 (30)	277 (8)	312 (7)
Highly unsaturated compounds	573 (26)	1828 (51)	1273 (29)
Highly aromatic compounds	331 (15)	788 (22)	937 (21)
Polycyclic aromatics	537 (24)	624 (18)	1842 (42)
Sum of peak magnitudes assigned to fatty acids and sulfonic acids ($\times 10^6$)	19052 (25)	2394 (4)	1120 (2)
Carbohydrates ($\times 10^6$)	0 (0)	0 (0)	0 (0)
Unsaturated aliphatic compounds containing N ($\times 10^6$)	0 (0)	3 (0)	0 (0)
Unsaturated aliphatic compounds ($\times 10^6$)	38187 (50)	6524 (11)	3681 (6)
Highly unsaturated compounds ($\times 10^6$)	6717 (9)	31135 (54)	13678 (22)
Highly aromatic compounds ($\times 10^6$)	4374 (6)	11535 (20)	12110 (20)
Polycyclic aromatics ($\times 10^6$)	7517 (10)	6600 (11)	30308 (50)
Sum ($\times 10^6$)	75847	58191	60897

^aValues in parentheses are percentages of either the corresponding number of assigned formulas or the corresponding summed peak magnitudes.

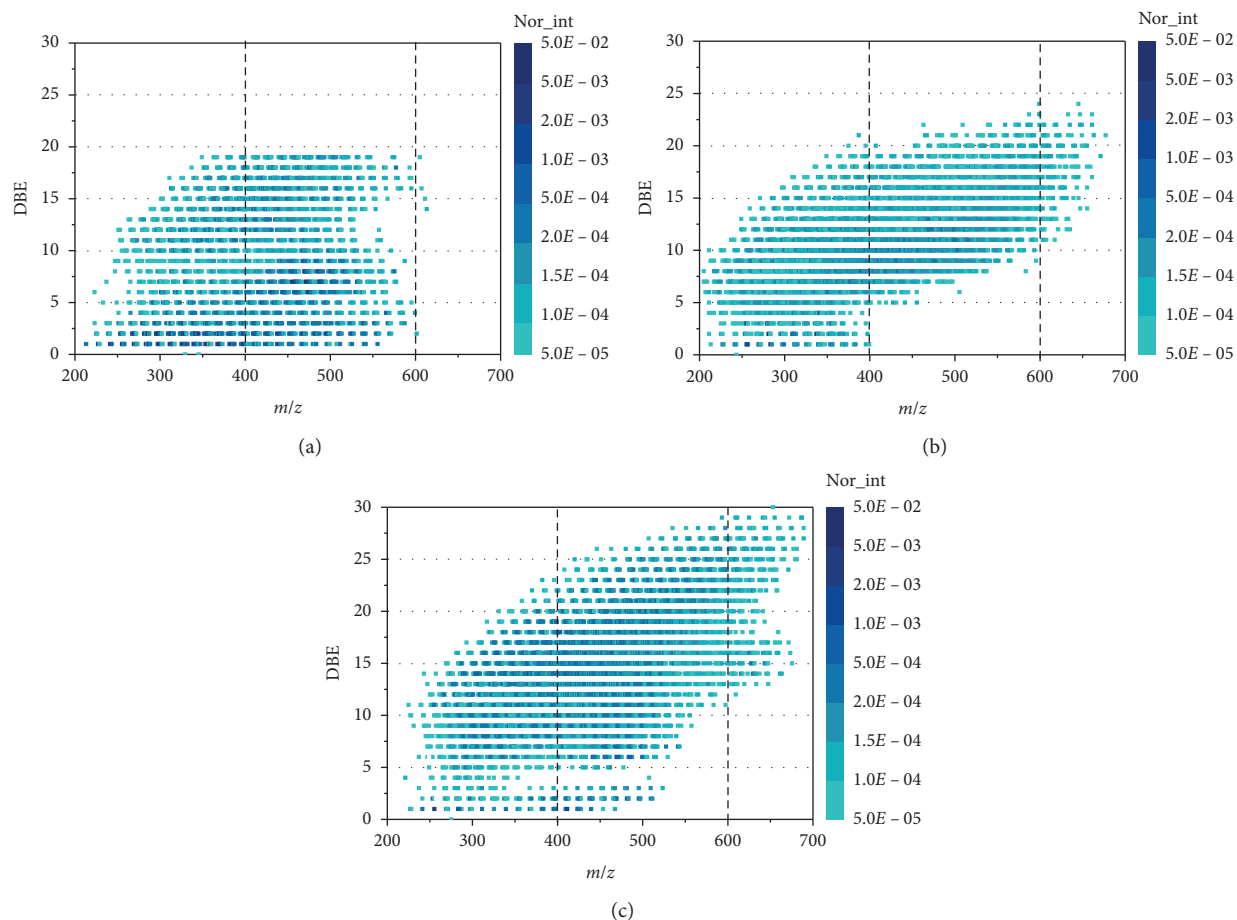


FIGURE 2: Respective DBE- m/z diagrams from (a) humic acids from Jiu Feng forest soil, (b) humic acids from Suwannee River, and (c) humic acids from Leonardite. Nor_int is the normalization of the intensity of each molecule.

Therefore, it can be inferred that the aromatic compounds with higher DBE and larger molecular mass have a significant effect on the aromaticity and humification of HA. Refractory humic acid fractions are marked by increases in

the condensed aromatic components with the highest DBE [40]. Humification processes involved in soil-derived organic matter formation are progressions where H/C ratios are steadily reduced [40] and the maximum molecular mass

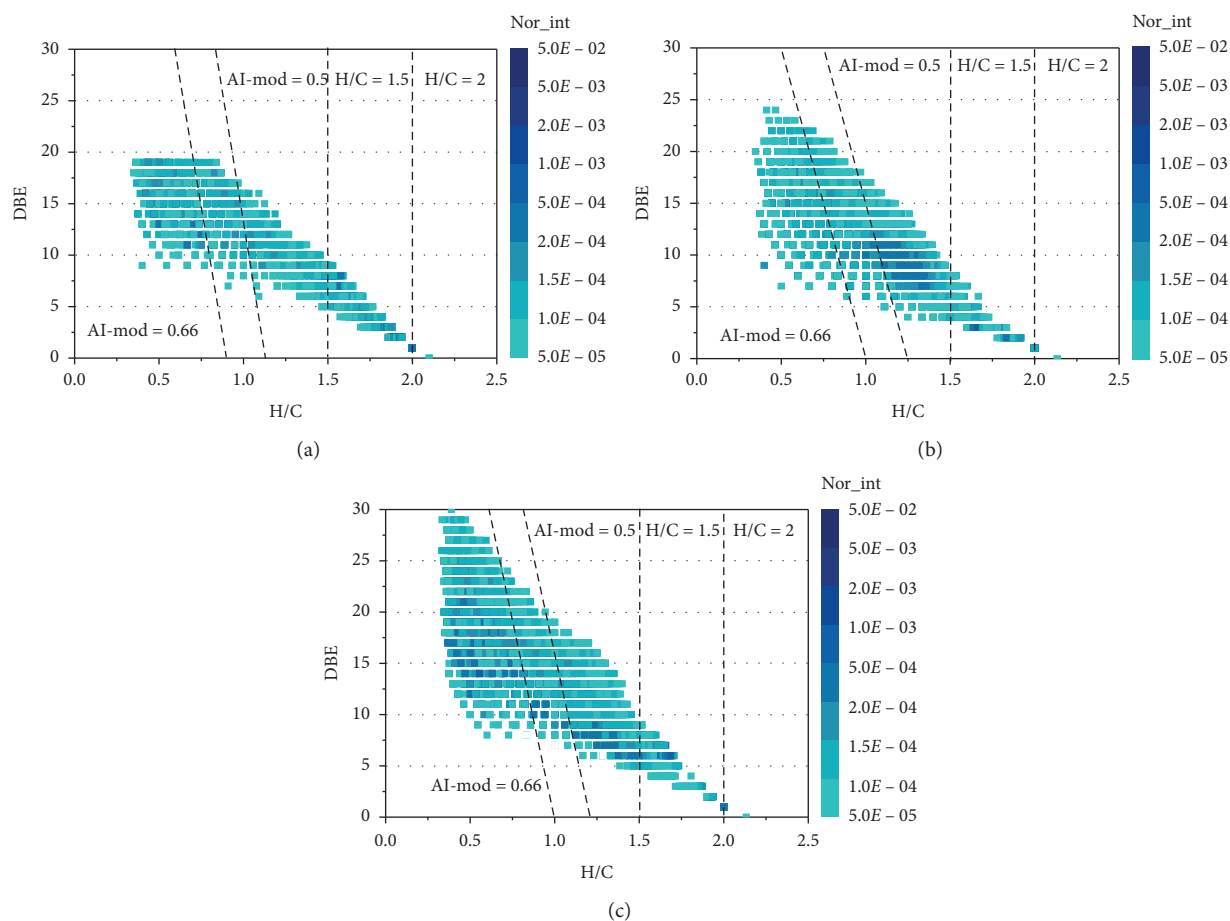


FIGURE 3: Respective DBE-H/C diagrams from (a) humic acids from Jiu Feng forest soil, (b) humic acids from Suwannee River, and (c) humic acids from Leonardite. Nor_int is the normalization of the intensity of each molecule.

of condensed aromatic components is increased [19]. There are more unsaturated aliphatic compounds in JFHA. The molecular formulas of these compounds are distributed across DBE range of 0–5 and m/z range of 400–600. That is, these compounds have low unsaturation and large molecular mass (Figure 2).

Most of molecular formulas for unsaturated aliphatic compounds ($2.0 > H/C \geq 1.5$) are distributed in the m/z range of 200–400 and a few are in the m/z range of 400–500 in SRHA. The molecular formulas for unsaturated aliphatic compounds are distributed densely in the m/z range of 200–600 in JFHA. The distribution of unsaturated aliphatic compounds in LEHA is similar to SRHA, which is sparser. It is inferred that the high content of unsaturated aliphatic compounds in JFHA has a large molecular mass. The distribution of highly unsaturated compounds and highly aromatic compounds in SRHA and LEHA is similar, while the distribution in JFHA is sparser and the distribution range is smaller. Polycyclic aromatics are distributed in the m/z range of 200–700 in LEHA, with the largest distribution range and the largest peak magnitudes. The content of polycyclic aromatics in LEHA is the highest and the molecular mass is the largest, indicating that LEHA has the strongest aromaticity [40] (Figure S2). The contribution of

aromatic compounds with larger molecular weights and higher unsaturation to the overall aromaticity of HAs is the most important.

Individual van Krevelen distribution of molecular formulas identified in each HA is included in the Supporting Information (Figure S3). Across all HAs, the assigned molecular formulas consisted primarily of C, H, and O (CHO) followed by formulas with additional N (CHON₁ and CHON₂) and S (CHOS) [11]. For these three HAs, the CHO molecular formula can make up all classes of compounds, while the CHON and CHOS molecular formulas only make up compounds with a high degree of unsaturation. CHOS molecular formula can form polycyclic aromatics and highly aromatic compounds in SRHA and LEHA. In addition, CHOS molecular formula can also form highly unsaturated compounds with relatively low unsaturation in SRHA. CHON₁ molecular formula is present in all three HAs, and the proportion is increasing according to the order of humification, namely, JFHA < SRHA < LEHA. The CHON₂ molecular formula with highest aromaticity exists in the polycyclic aromatics of JFHA and LEHA, and the aromaticity and unsaturation of the CHON₂ molecular formula are higher than the CHON₁ molecular formula, consistent with previous conclusions on FA [41]. The

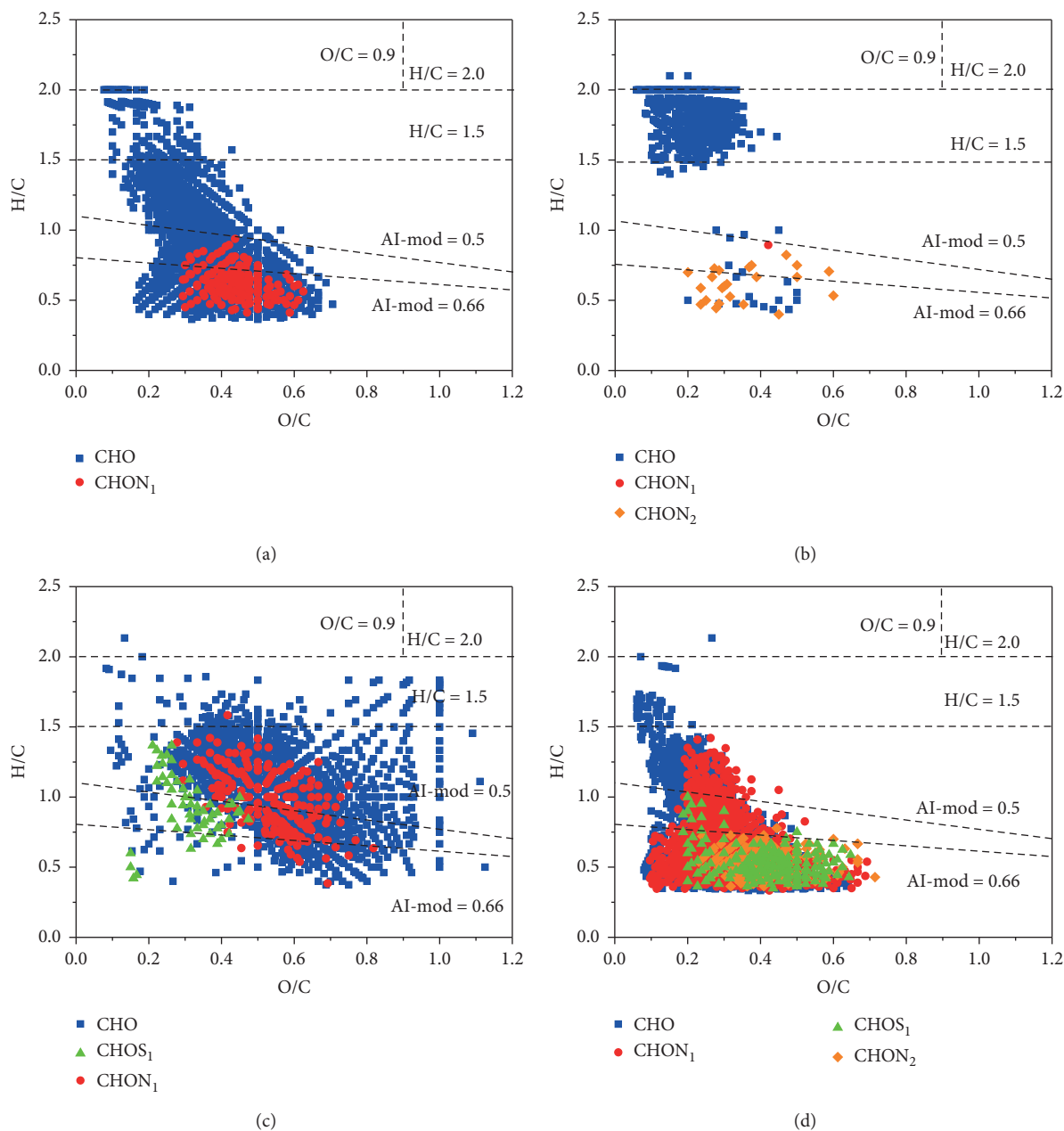


FIGURE 4: Van Krevelen diagrams of molecular formulas (a) common among all humic acid samples, (b) identified only in humic acids from Jiufeng forest soil, (c) identified only in humic acids from Suwannee River, and (d) identified only in humic acids from Leonardite. Formulas include CHO (blue), CHOS₁ (green), CHON₁ (red), and CHON₂ (orange).

aromaticity of compounds increased with the number of heteroatoms (such as nitrogen and sulfur) in the molecular formulas.

Of all formulas assigned to peaks detected by ultrahigh resolution mass spectral analysis ($n = 5329$), approximately 24% ($n = 1282$) are shared among all HA samples. The common molecular formulas consisted of the CHO molecular formulas and the CHON₁ molecular formulas. And the CHON₁ molecular formulas constituted highly aromatic compounds and polycyclic aromatics (Figure 4(a)). There is similarity in these common molecular formulas regardless of climatic regions, land use characteristics, diagenetic process

[42, 43], and other factors. The content of compounds with high aromaticity and unsaturated degree is higher than other compounds and heteroatom-containing compounds are more aromatic and unsaturated. These compounds are accumulation of a similar pool of refractory molecules [44] resulting from the removal of labile DOM components by microbial processing [45] or photodegradation [46]. There are 492 molecular formulas identified only in JFHA, and most of them are unsaturated aliphatic compounds with $1.5 < H/C < 2$ and $0 < O/C < 0.4$. Molecular formulas depleted in O and enriched in H with lower AI-mod may be derived from autochthonous sources and are generally

categorized into biolabile compound classes including carbohydrates, proteins, and lipids [20, 30]. Therefore, JFHA is mainly derived from autochthonous sources [47, 48]. These lipid-like compounds may be the products of secondary soil microbes [49]. There are 1483 molecular formulas detected only in SRHA. These compounds have higher O/C and contain more heteroatom-containing formulas (CHON_1 and CHOS_1). This indicates that SRHA has been anthropogenically impacted, such as urban region and cropland. Anthropogenic inputs to the rivers have altered in-stream DOM composition and increased the content of heteroatoms [11]. 39% of the molecular formulas are detected only in LEHA, including all classes of molecular formulas containing heteroatom, and the overall shape is a right-angled triangle. According to the order of CHO, CHON_1 , and CHON_2 (CHOS_1), the area of each class of molecular formulas becomes smaller and smaller and gradually concentrates on the lower layer of the v-K diagram, that is, the area of aromatic compounds. Therefore, the aromaticity and unsaturation of the molecular formulas containing heteroatoms are significantly higher. Molecular formulas enriched in O and depleted in H with increased AI-mod reflect terrestrial inputs from plant-derived biomacromolecules such as lignins, tannins, and carboxyl-rich acyclic molecules [20, 30, 32, 50]. Compounds containing heteroatoms (nitrogen and sulfur) are more aromatic [16], and the higher the number of heteroatoms, the stronger the aromaticity. At the same time, there is higher content for compounds containing heteroatoms in HAs with higher degree of humification.

3.3. Molecular Lability of Humic Acids. The quality of HA is determined by the mixture of different types of chemical species, including labile and recalcitrant compounds. Microbial-derived bioavailable fractions are classified as more labile organic matter, which has been correlated with high H/C and low O/C ratios in the lipid, protein, and amino sugar-like regions of the v-K diagram [48, 51–54]. Classification of less labile, more recalcitrant components from each carbon source corresponds to molecular species that cluster in more lignin-, tannin-, and black carbon-like regions of the v-K diagram [31]. The MLB_1 molecular richness ranked HAs from most to least labile as JFHA > SRHA > LEHA, whose $\text{MLB}_1\%$ is 75.47%, 15.33%, and 7.88%. JFHA represented the most purely autochthonous, microbially derived HA and has the highest contributions of more hydrogen-saturated species and labile fractions. The CRAM formulas are commonly linked with refractory compounds widely detected in diverse environments including deep ocean [32]. The structural diversity found within CRAM and its substantial content of alicyclic rings and branching contribute to its resistance to biodegradation and refractory nature [32]. The content of CRAM is SRHA, LEHA, and JFHA in order from high to low, which are 51.91%, 18.25%, and 8.28%, respectively. CRAM seems to consist mainly of the decomposition products of biomolecules, as indicated by the prevalence of its carboxyl groups and the manner of oxidation that increases with decreasing molecular size [32]. Therefore, SRHA contains plant-derived lignin- and tannin-like compounds with the relatively small molecular

mass. SRHA may have the most significance for pollutants because CRAM affected the reactivity of organic matter and the bioavailability of associated nutrients and trace metals. The nominal oxidation state of carbon (NOSC) is a formal parameter that gives information about the average oxidation state of all carbons in each chemical formula, regardless of chemical structure [33]. The NOSC ranked HAs from highest to lowest as LEHA > JFHA > SRHA, whose NOSC is -0.07 , -1.16 , and -0.25 . DOM degrades along the gradient from aromatics to aliphatics and high to low nominal oxidation states of carbon [34]. JFHA is the most labile HA because it contains a large amount of unsaturated aliphatic compounds. SRHA is easy to combine with nutrients and trace metals to affect its bioavailability. LEHA shows the highest nominal oxidation states of carbon due to higher degree of humification.

4. Conclusions

Humic acids from different sources of soil, river, and Leonardite were analyzed at the molecular level by ultrahigh resolution mass spectrometry, and thus multiple similarities and differences were found. Despite sources of HA, the compounds containing more heteroatoms (such as nitrogen and sulfur) are more unsaturated and aromatic. AI-mod and DBE consistently indicated that LEHA, SRHA, and JFHA are in order from the highest to lowest degree of humification. JFHA contained amounts of compounds with large molecular mass and low degree of unsaturation. Different classes of compounds uniformly distributed in SRHA, especially lignin- and tannin-like compounds with relatively high degree of unsaturation. LEHA contains an amount of aromatic compounds involving more heteroatoms with high degree of unsaturation and large molecular weight due to high degree of humification. Different molecular composition can cause the diversity of HA lability. JFHA is relatively labile and is prone to interact with microorganisms. The lignin- and tannin-like compounds of SRHA stem from plant-derived organic matter, which are easily combined with nutrients and trace metals to reduce the bioavailability of SRHA. LEHA is relatively less labile due to amounts of aromatic compounds. Our results reveal the diversity of HA due to different degrees of humification at the molecular level and the ways of combining with other substances because of different lability. Ultrahigh resolution FT-ICR MS is a powerful tool to address these novel hypotheses and is of great significance for studying the role of HA from different sources in the pollutant transformation and geochemical cycle at the molecular level.

Data Availability

The data used to support the findings of this study are included within the article.

Conflicts of Interest

The authors declare that there are no conflicts of interest regarding the publication of this paper.

Authors' Contributions

Shuai Qin and Chengbin Xu contributed equally to this work and Shuai Qin and Chengbin Xu are the co-first authors.

Acknowledgments

This study was sponsored jointly by the National Natural Science Foundation of China (Grant No. 331772057) and the Major Science and Technology Projects in Guangxi Province (Grant No. AA17204078).

Supplementary Materials

Figure S1 includes respective ESI FT-ICR mass spectra from (a) humic acids from Jiufeng forest soil, (b) humic acids from Suwannee River, and (c) humic acids from leonardite. Figure S2 includes respective H/C-*m/z* diagrams from (a) humic acids from Jiufeng forest soil, (b) humic acids from Suwannee River, and (c) humic acids from leonardite. Figure S3 includes van Krevelen diagrams from the mass spectra of (a) humic acids from Jiufeng forest soil, (b) humic acids from Suwannee River, and (c) humic acids from leonardite. Figure S4 includes van Krevelen diagrams of molecular formulas (a) common among in humic acids from Jiufeng forest soil and Suwannee River, (b) common among in humic acids from Jiufeng forest soil and leonardite, and (c) common among in humic acids from Suwannee River and leonardite. (*Supplementary Materials*)

References

- [1] F. J. Stevenson, *Humus Chemistry: Genesis, Composition, Reactions*, John Wiley & Sons, Hoboken, NJ, USA, 1994.
- [2] J. A. Baldock and J. O. Skjemstad, "Role of the soil matrix and minerals in protecting natural organic materials against biological attack," *Organic Geochemistry*, vol. 31, no. 7-8, pp. 697-710, 2000.
- [3] E. S. Krull, J. A. Baldock, and J. O. Skjemstad, "Importance of mechanisms and processes of the stabilisation of soil organic matter for modelling carbon turnover," *Functional Plant Biology*, vol. 30, no. 2, pp. 207-222, 2003.
- [4] E. J. W. Wattel-Koekkoek, P. Buurman, J. Van Der Plicht, E. Wattel, and N. Van Breemen, "Mean residence time of soil organic matter associated with kaolinite and smectite," *European Journal of Soil Science*, vol. 54, no. 2, pp. 269-278, 2003.
- [5] R. Mikutta, M. Kleber, M. S. Torn, and R. Jahn, "Stabilization of soil organic matter: association with minerals or chemical recalcitrance?" *Biogeochemistry*, vol. 77, no. 1, pp. 25-56, 2006.
- [6] B. Allard, "A comparative study on the chemical composition of humic acids from forest soil, agricultural soil and lignite deposit," *Geoderma*, vol. 130, no. 1-2, pp. 77-96, 2006.
- [7] J. Xu, B. Zhao, W. Chu, J. Mao, and J. Zhang, "Chemical nature of humic substances in two typical Chinese soils (upland vs paddy soil): a comparative advanced solid state NMR study," *Science of the Total Environment*, vol. 576, pp. 444-452, 2017.
- [8] J. Dai, W. Ran, B. Xing, M. Gu, and L. Wang, "Characterization of fulvic acid fractions obtained by sequential extractions with pH buffers, water, and ethanol from paddy soils," *Geoderma*, vol. 135, pp. 284-295, 2006.
- [9] L. Grasset and A. Amblès, "Structure of humin and humic acid from an acid soil as revealed by phase transfer catalyzed hydrolysis," *Organic Geochemistry*, vol. 29, no. 4, pp. 881-891, 1998.
- [10] L. Grasset, A. Amblès, and A. Pyrolysis, "Structural study of soil humic acids and humin using a new preparative thermochemolysis technique," *Journal of Analytical and Applied Pyrolysis*, vol. 47, no. 1, pp. 1-12, 1998.
- [11] S. Wagner, T. Riedel, J. Niggemann, A. V. Vähätalo, T. Dittmar, and R. Jaffé, "Linking the molecular signature of heteroatomic dissolved organic matter to watershed characteristics in world rivers," *Environmental Science & Technology*, vol. 49, no. 23, pp. 13798-13806, 2015.
- [12] J. J. Cole, Y. T. Prairie, N. F. Caraco et al., "Plumbing the global carbon cycle: integrating inland waters into the terrestrial carbon budget," *Ecosystems*, vol. 10, no. 1, pp. 172-185, 2007.
- [13] T. J. Battin, L. A. Kaplan, S. Findlay et al., "Erratum: biophysical controls on organic carbon fluxes in fluvial networks," *Nature Geoscience*, vol. 2, no. 8, p. 595, 2009.
- [14] J. Hilton, M. O'hare, M. J. Bowes, and J. I. Jones, "How green is my river? A new paradigm of eutrophication in rivers," *Science of the Total Environment*, vol. 365, no. 1-3, pp. 66-83, 2006.
- [15] S. Bertilsson and B. Jones Jr., "Supply of dissolved organic matter to aquatic ecosystems: autochthonous sources," in *Aquatic Ecosystems*, pp. 3-24, Elsevier, Amsterdam, Netherlands, 2003.
- [16] A. Y. Zhrebek, Y. I. Kostyukovich, A. S. Kononikhin, E. N. Nikolaev, and I. V. Perminova, "Molecular compositions of humic acids extracted from leonardite and lignite as determined by Fourier transform ion cyclotron resonance mass spectrometry," *Mendeleev Communications*, vol. 26, no. 5, pp. 446-448, 2016.
- [17] O. S. Yakimenko and V. A. Terekhova, "Humic preparations and the assessment of their biological activity for certification purposes," *Eurasian Soil Science*, vol. 44, no. 11, pp. 1222-1230, 2011.
- [18] L. Cavani, C. Ciavatta, and C. J. B. T. Gessa, "Identification of organic matter from peat, leonardite and lignite fertilisers using humification parameters and electrofocusing," *Bioresource Technology*, vol. 86, no. 1, pp. 45-52, 2003.
- [19] K. Ikeya, R. L. Sleighter, P. G. Hatcher, and A. Watanabe, "Characterization of the chemical composition of soil humic acids using Fourier transform ion cyclotron resonance mass spectrometry," *Geochimica et Cosmochimica Acta*, vol. 153, pp. 169-182, 2015.
- [20] R. L. Sleighter and P. G. Hatcher, "The application of electrospray ionization coupled to ultrahigh resolution mass spectrometry for the molecular characterization of natural organic matter," *Journal of Mass Spectrometry*, vol. 42, no. 5, pp. 559-574, 2007.
- [21] P. G. Hatcher, K. J. Dria, S. Kim, and S. W. Frazier, "Modern analytical studies of humic substances," *Soil Science*, vol. 166, no. 11, pp. 770-794, 2001.
- [22] J. A. Leenheer and J.-P. Croué, "Peer reviewed: characterizing aquatic dissolved organic matter," *Environmental Science & Technology*, vol. 37, no. 1, pp. 18A-26A, 2003.
- [23] S. McDonald, J. M. Pringle, P. D. Prenzler, A. G. Bishop, and K. Robards, "Bioavailability of dissolved organic carbon and fulvic acid from an Australian floodplain river and billabong,"

- Marine and Freshwater Research*, vol. 58, no. 2, pp. 222–231, 2007.
- [24] J. W. T. Blackburn, W. Kew, M. C. Graham, and D. Uhrin, “Laser desorption/ionization coupled to FTICR mass spectrometry for studies of natural organic matter,” *Analytical Chemistry*, vol. 89, no. 8, pp. 4382–4386, 2017.
- [25] Z. Fang, C. He, Y. Li, K. H. Chung, C. Xu, and Q. Shi, “Fractionation and characterization of dissolved organic matter (DOM) in refinery wastewater by revised phase retention and ion-exchange adsorption solid phase extraction followed by ESI FT-ICR MS,” *Talanta*, vol. 162, pp. 466–473, 2017.
- [26] J. M. Jarvis, A. M. Mckenna, R. N. Hilten, K. C. Das, R. P. Rodgers, and A. G. Marshall, “Characterization of pine pellet and peanut hull pyrolysis bio-oils by negative-ion electrospray ionization fourier transform ion cyclotron resonance mass spectrometry,” *Energy & Fuels*, vol. 26, no. 6, pp. 3810–3815, 2012.
- [27] Introduction to the International Humic Substances Society, <http://humic-substances.org/source-materials-for-ihss-samples/>.
- [28] K. Wang, Y. Pang, C. He et al., “Optical and molecular signatures of dissolved organic matter in Xiangxi Bay and mainstream of Three Gorges Reservoir, China: spatial variations and environmental implications,” *Science of The Total Environment*, vol. 657, pp. 1274–1284, 2019.
- [29] D. He, C. He, P. Li et al., “Optical and molecular signatures of dissolved organic matter reflect anthropogenic influence in a coastal river, northeast China,” *Journal of Environment Quality*, vol. 48, no. 3, 2019.
- [30] B. P. Koch and T. Dittmar, “From mass to structure: an aromaticity index for high-resolution mass data of natural organic matter,” *Rapid Communications in Mass Spectrometry*, vol. 20, no. 5, pp. 926–932, 2006.
- [31] J. D’andrilli, W. T. Cooper, C. M. Foreman, and A. G. Marshall, “An ultrahigh-resolution mass spectrometry index to estimate natural organic matter lability,” *Rapid Communications in Mass Spectrometry*, vol. 29, no. 24, pp. 2385–2401, 2015.
- [32] N. Hertkorn, R. Benner, M. Frommberger et al., “Characterization of a major refractory component of marine dissolved organic matter,” *Geochimica et Cosmochimica Acta*, vol. 70, no. 12, pp. 2990–3010, 2006.
- [33] T. Riedel, H. Biester, and T. Dittmar, “Molecular fractionation of dissolved organic matter with metal salts,” *Environmental Science & Technology*, vol. 46, no. 8, pp. 4419–4426, 2012.
- [34] A. M. Kellerman, D. N. Kothawala, T. Dittmar, and L. J. Tranvik, “Persistence of dissolved organic matter in lakes related to its molecular characteristics,” *Nature Geoscience*, vol. 8, no. 6, pp. 454–457, 2015.
- [35] P. M. Medeiros, M. Seidel, L. C. Powers, T. Dittmar, D. A. Hansell, and W. L. Miller, “Dissolved organic matter composition and photochemical transformations in the northern North Pacific Ocean,” *Geophysical Research Letters*, vol. 42, no. 3, pp. 863–870, 2015.
- [36] T. Šantl-Temkiv, K. Finster, T. Dittmar et al., “Hailstones: a window into the microbial and chemical inventory of a storm cloud,” *PLoS One*, vol. 8, no. 1, Article ID e53550, 2013.
- [37] M. Seidel, M. Beck, T. Riedel et al., “Biogeochemistry of dissolved organic matter in an anoxic intertidal creek bank,” *Geochimica et Cosmochimica Acta*, vol. 140, pp. 418–434, 2014.
- [38] M. Seidel, P. L. Yager, N. D. Ward et al., “Molecular-level changes of dissolved organic matter along the Amazon River-to-Ocean Continuum,” *Marine Chemistry*, vol. 177, pp. 218–231, 2015.
- [39] R. L. Sleighter, G. A. Mckee, and P. G. Hatcher, “Direct Fourier transform mass spectral analysis of natural waters with low dissolved organic matter,” *Organic Geochemistry*, vol. 40, no. 1, pp. 119–125, 2009.
- [40] T. Ohno, Z. He, R. L. Sleighter, C. W. Honeycutt, and P. G. Hatcher, “Ultrahigh resolution mass spectrometry and indicator species analysis to identify marker components of soil- and plant biomass-derived organic matter fractions,” *Environmental Science & Technology*, vol. 44, no. 22, pp. 8594–8600, 2010.
- [41] S. Qin, C. Xu, F. Guo et al., “Molecular signatures of three fulvic acid standard samples as revealed by electrospray ionization Fourier transform ion cyclotron resonance mass spectrometry,” *ChemistrySelect*, vol. 4, no. 47, pp. 13940–13946, 2019.
- [42] J. I. Hedges, E. Mayorga, E. Tsamakis et al., “Organic matter in Bolivian tributaries of the Amazon River: a comparison to the lower mainstream,” *Limnology and Oceanography*, vol. 45, no. 7, pp. 1449–1466, 2000.
- [43] J. E. Richey, R. L. Victoria, E. Mayorga, L. A. Martinelli, and R. H. Meade, “Case study 1: integrated analysis of a humid tropical region—the Amazon Basin,” in *Vegetation, Water, Humans and the Climate*, pp. 415–428, Springer, Berlin, Germany, 2004.
- [44] R. Jaffé, Y. Yamashita, N. Maie et al., “Dissolved organic matter in headwater streams: compositional variability across climatic regions of North America,” *Geochimica et Cosmochimica Acta*, vol. 94, pp. 95–108, 2012.
- [45] R. L. Sleighter, R. M. Cory, L. A. Kaplan, H. a. N. Abdulla, and P. G. Hatcher, “A coupled geochemical and biogeochemical approach to characterize the bioreactivity of dissolved organic matter from a headwater stream,” *Journal of Geophysical Research: Biogeosciences*, vol. 119, no. 8, pp. 1520–1537, 2014.
- [46] A. Stubbins, R. G. M. Spencer, H. Chen et al., “Illuminated darkness: molecular signatures of Congo River dissolved organic matter and its photochemical alteration as revealed by ultrahigh precision mass spectrometry,” *Limnology and Oceanography*, vol. 55, no. 4, pp. 1467–1477, 2010.
- [47] R. L. Sleighter and P. G. Hatcher, “Molecular characterization of dissolved organic matter (DOM) along a river to ocean transect of the lower Chesapeake Bay by ultrahigh resolution electrospray ionization Fourier transform ion cyclotron resonance mass spectrometry,” *Marine Chemistry*, vol. 110, no. 3–4, pp. 140–152, 2008.
- [48] A. C. Stenson, A. G. Marshall, and W. T. Cooper, “Exact masses and chemical formulas of individual Suwannee River fulvic acids from ultrahigh resolution electrospray ionization Fourier transform ion cyclotron resonance mass spectra,” *Analytical Chemistry*, vol. 75, no. 6, pp. 1275–1284, 2003.
- [49] T. Riedel, S. Iden, J. Geilich, K. Wiedner, W. Durner, and H. Biester, “Changes in the molecular composition of organic matter leached from an agricultural topsoil following addition of biomass-derived black carbon (biochar),” *Organic Geochemistry*, vol. 69, pp. 52–60, 2014.
- [50] N. Hertkorn, M. Frommberger, M. Witt, B. P. Koch, P. Schmitt-Kopplin, and E. M. Perdue, “Natural organic matter and the event horizon of mass spectrometry,” *Analytical Chemistry*, vol. 80, no. 23, pp. 8908–8919, 2008.
- [51] L. Chipman, D. Podgorski, S. Green, J. Kostka, W. Cooper, and M. Huettel, “Decomposition of plankton-derived dissolved organic matter in permeable coastal sediments,”

- Limnology and Oceanography*, vol. 55, no. 2, pp. 857–871, 2010.
- [52] J. D’Andrilli, C. M. Foreman, A. G. Marshall, and D. M. Mcknight, “Characterization of IHSS Pony Lake fulvic acid dissolved organic matter by electrospray ionization Fourier transform ion cyclotron resonance mass spectrometry and fluorescence spectroscopy,” *Organic Geochemistry*, vol. 65, pp. 19–28, 2013.
- [53] A. M. Grannas, W. C. Hockaday, P. G. Hatcher, L. G. Thompson, and E. Mosley-Thompson, “New revelations on the nature of organic matter in ice cores,” *Journal of Geophysical Research*, vol. 111, no. D4, 2006.
- [54] M. P. Bhatia, S. B. Das, K. Longnecker, M. A. Charette, and E. B. Kujawinski, “Molecular characterization of dissolved organic matter associated with the Greenland ice sheet,” *Geochimica et Cosmochimica Acta*, vol. 74, no. 13, pp. 3768–3784, 2010.

Research Article

Sources of Nitrogen Pollution in Upstream of Fenhe River Reservoir Based on the Nitrogen and Oxygen Stable Isotope

Ying Zhao ¹, Jinhua Dang ¹, and Fei Wang ^{2,3}

¹Shanxi Academy of Environmental Sciences, Taiyuan, Shanxi 030027, China

²School of Life Science, Shanxi University, Taiyuan, Shanxi 030006, China

³School of Physical Education, Shanxi University, Taiyuan 030006, China

Correspondence should be addressed to Fei Wang; nemo@sxu.edu.cn

Received 8 November 2019; Revised 3 February 2020; Accepted 8 February 2020; Published 31 March 2020

Guest Editor: Chenglian Feng

Copyright © 2020 Ying Zhao et al. This is an open access article distributed under the Creative Commons Attribution License, which permits unrestricted use, distribution, and reproduction in any medium, provided the original work is properly cited.

Identification of nitrate sources is important for the management of rivers. In this study, stable isotopes ($\delta^{15}\text{N}$ and $\delta^{18}\text{O}$) and a Bayesian model (stable isotope analysis in R, SIAR) were applied to identify nitrate sources and estimate the proportional contributions of multiple nitrate sources in the upstream of Fenhe River Reservoir that serves as a source of drinking water in Shanxi Province of North China. The results showed that the 86.4% of total nitrogen (TN) concentrations in the water samples exceeded the guided values of the Chinese Surface Water Environmental Quality Standard (GB 3838-2002). The influent of tributary and discharges of sewage caused the severe nitrogen pollution. SIAR was used to estimate the proportional contribution of three nitrate sources (sewage, inorganic fertilizer, and soil nitrogen). It was revealed that domestic sewage was the dominant nitrate source, and the contributions were 33%–41%. The contributions of inorganic fertilizer and soil to nitrogen load were 30%–31% and 31%–37%, respectively. Therefore, the pollution sources of nitrogen can be determined more accurately if the rules of sewage discharges are considered.

1. Introduction

As an important life element, nitrogen is the main substance used for protein synthesis during phytoplankton growth. However, water eutrophication that was caused by nitrogen and other nutrients and its harm to aquatic ecosystems have become one of the key issues of concern to society [1, 2]. Nitrate is the main form of nitrogen contaminants that occur in freshwater bodies. In recent years, the excessive use of agricultural fertilizers, the discharge of large amounts of domestic sewage, and animal manure have caused the nitrate content in freshwater bodies to be abnormally high, which poses a potential threat to the health of humans [3, 4]. In order to control the nitrogen source pollution in water bodies, identification of the pollution load caused by different sources of pollution that enter the water bodies is considered as an effective approach to help prevent and address the pollution in water bodies [5].

With the rapid development of isotope technology, nitrogen and oxygen isotope techniques ($\delta^{15}\text{N}$ and $\delta^{18}\text{O}$) are often used to determine the source of nitrate in the water body. Quantitative studies on nitrogen from different sources are carried out using mathematical models. Some frequently employed models include the stable isotope mixture model, a Bayesian model (stable isotope analysis in R, SIAR), and IsoSource model. Parnell et al. [6] established the SIAR mixture model, which used a logical priori distribution of the Dirichlet distribution established via the Bayesian framework, according to the estimated probability of the contribution rate of each source in the mixture. The model, which has been successfully applied to the analysis of nitrate sources, considered the identification of more potential sources of pollution and reduced the uncertainty of the mass mixture model. For example, it has been conducted to identify the contribution rate of different sources of nitrate nitrogen in a subtropical watershed, the groundwater,

the rainfall runoff, the river, as well as in the Three Gorges Reservoir of China [3, 7–10].

As the largest reservoir in Shanxi Province, the Fenhe River Reservoir is also the biggest centralized drinking water source in Taiyuan. The reservoir is located in the upstream section of the mainstream of the Fenhe River and has a drainage basin area of 5,268 km². At present, the daily domestic water supply in Taiyuan is about 600,000 m³/d, accounting for 43% of the total water supply. The Fenhe River Reservoir is a river-type reservoir, in which water is mainly replenished by the upstream river, and the Yellow River Transfer Project accounts for about 45% of the replenished water. This study analyzes the source of nitrates and explores the possible migration and transformation of nitrogen by analyzing the nitrogen and oxygen isotope characteristics in the water bodies. The contribution rates of nitrogen sources are estimated based on the SIAR mass mixture model. The results will facilitate the water quality control and the effective use of water resources for improved tracing and quantitation of nitrogen pollution sources in the surface water environment.

2. Materials and Methods

2.1. Study Area. The upstream of Fenhe River Reservoir has a total length of 216 kilometers and a drainage basin area of 7750 km². The Fenhe River Reservoir covers an area of 5268 km², belonging to Ningwu county, Jingle county, Lan county, and Loufan county, which accounts for 78.6% of the total area of four counties. The length of mainstream of the upper course of Fenhe River Reservoir is 122 km, and 13 tributaries are included. Each area of Honghe River, Dongnian River, Lanhe River, and Jianhe River, which were defined as the first level branches, is more than 500 km². The study area has four distinctive seasons, with an average temperature and relative humidity of 7.2°C and 60.1%. About 180–200 days in the year are frost-free. The distribution of precipitation is 465 mm, which occurred mostly from July to September. Thus, its wet season is defined between July and September, while the dry season is from November to March of the next year.

2.2. Sample Collection and Measurement. Water samples were collected at 13 sampling points in the Fenhe River Reservoir and the upstream section of the river. The specific layout and positions are shown in Figure 1. The sampling time of the wet and dry seasons is in the periods of August 21st–25th and November 15th–19th, respectively. As the aim of this study was to explore the sources of nitrogen pollution, we set the sampling sites mainly considering the influent pollutants to Fenhe River based on the state controlling sites. According to previous site investigation, there was nitrogen pollution in the middle section, and the sampling sites were less correspondingly.

The collected water samples were stored separately in 500 mL polyethylene bottles that were prerinsed with distilled water and were then put into a portable incubator for temporary storage. The water temperature (T), pH, electric conductivity (ORP), and dissolved oxygen (DO) in the water

body were measured using a portable water quality parameter tester and a portable acidometer.

The collected water samples were returned to the laboratory on the same day of collection, and 150 mL of water samples was taken and filtered with the quantitative filter paper to measure the TN, ammonium (NH₄⁺-N), nitrate nitrogen (NO₃⁻-N), and nitrite (NO₂⁻-N). These parameters were analyzed according to standard methods approved by the National Environmental Protection Agency of China [11]. TN in the digestion was measured by the alkaline potassium persulfate ultraviolet spectrophotometry. NH₄⁺-N was determined by the Nesslerization colorimetric method. NO₃⁻-N was measured by the phenol disulfonic acid ultraviolet spectrophotometric method. The concentration of NO₂⁻-N was measured by the *N*-(1-naphthyl)-ethylenediamine spectrophotometry.

The measurement of nitrogen and oxygen isotopes was conducted in the Third Oceanographic Research Institute of the Oceanic Bureau by applying MAT 253 Isotope Ratio Mass Spectrometry (Thermo Scientific Corporation). The detection process for the machine is as follows: the PAL autosampler is first used to automate sample injection, and then the N₂O in the sample is frozen and fixed by the primary cold trap in the liquid nitrogen tank. After 10 minutes, the primary cold trap leaves the liquid nitrogen tank, and the frozen and fixed N₂O is released to the secondary cold trap in the liquid nitrogen tank. After another 5 minutes, the secondary cold trap leaves the liquid nitrogen tank. The N₂O is separated from other impurity gases via a chromatographic column (with a column temperature of 45°C). The separated N₂O is transferred into the Mat 253 detector via helium gas. Under the high-energy electron impact ionization and accelerating field, the gaseous ions with different mass-to-charge ratios (*m/z*44, *m/z*45, and *m/z*46) enter the magnetic field and are separated into different ion beams. The ion beams then enter the receiver and are converted to the electric signal to measure the nitrogen to oxygen isotope ratio [12]. The values of δ¹⁵N and δ¹⁸O were obtained by referring to the international standards of atmospheric nitrogen (AIR) and standard mean ocean water (SMOW), respectively. The analysis precision for the values of δ¹⁵N and δ¹⁸O was ±0.2 and ±0.3‰, respectively, which can meet the precision requirements for the study.

2.3. The Model of Isotope Source Analysis. In this study, the SIAR isotope source analytical model was used to calculate the contribution rate of each N source. Assuming that there are *N* measured values, *J* isotopes, and *K* nitrogen sources, the SIAR model can be expressed as follows:

$$\begin{aligned}
 X_{ij} &= \sum_{k=1}^k P_k (S_{jk} + C_{jk}) + \varepsilon_{ij}, \\
 S_{jk} &\sim N(\mu_{jk}, \omega_{jk}^2), \\
 C_{jk} &\sim N(\lambda_{jk}, \tau_{jk}^2), \\
 \varepsilon_{jk} &\sim N(0, \sigma_j^2),
 \end{aligned} \tag{1}$$

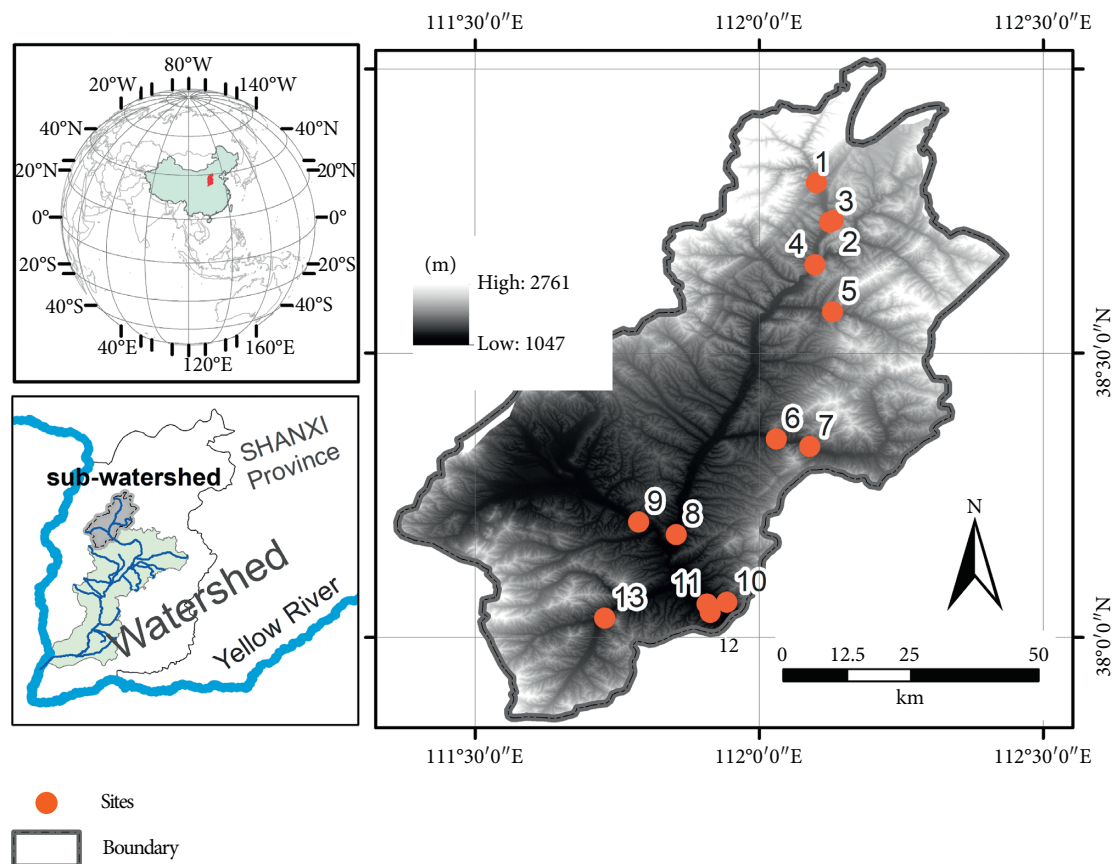


FIGURE 1: Locations of the sampling sites in study area. S1: Leiming Temple; S2: the entrance to Yellow River water diversion junction of Toumaying village; S3: the outlet of Yellow River water diversion junction of Toumaying village; S4: the junction of Honghe River; S5: Mingshuihe River; S6: Jingle county; S7: Dongnianhe River; S8: Hecha village; S9: Quli county; S10: the inlet of Fenhe Reservoir; S11: the middle part of Fenhe Reservoir; S12: the outlet of Fenhe Reservoir; S13: Jianhe River Bridge.

where X_{ij} is the ratio of the isotope i in the mixture j ($i = 1, 2, 3, \dots, N; j = 1, 2, 3, \dots, J$), P_k is the contribution rate of source k ($k = 1, 2, 3, \dots, K$), S_{jk} is the rate of isotope j in source k ($k = 1, 2, 3, \dots, K$), μ is the average value, ω is the standard deviation, C_{jk} is the fractionation coefficient of the j_{th} isotope on the k_{th} source, λ is the average value, τ is the standard deviation, ε_{jk} is the residual error, and δ is the standard deviation.

3. Results and Discussion

3.1. Nitrogen Pollution in the Upstream Section of the Fenhe River Reservoir. As shown in Table 1, in the wet period, water temperature ranged from 11°C to 25.2°C, pH was 7.83–8.85, DO concentrations were between 4.9 mg/L and 12.5 mg/L, and ORP values were 201–263 mv. However, in the dry period, pH and DO values were almost the same as that in the wet period. However, the values of temperature and ORP were lower than that in flood season.

The distribution of different forms of inorganic nitrogen during four seasons in the Fenhe River is shown in Figure 2. It can be seen that the concentrations of TN, $\text{NH}_4^+\text{-N}$, $\text{NO}_3^-\text{-N}$, and $\text{NO}_2^-\text{-N}$ during the wet season were 0.88–3.52, 0.035–0.187, 0.16–1.06, and 0.008–0.174 $\text{mg}\cdot\text{L}^{-1}$, respectively. During the dry seasons, the concentrations of TN,

$\text{NH}_4^+\text{-N}$, $\text{NO}_3^-\text{-N}$, and $\text{NO}_2^-\text{-N}$ were 0.87–10.6, 0.079–0.129, 0.28–3.01, and 0.006–0.838 $\text{mg}\cdot\text{L}^{-1}$, respectively. Figure 2 shows that 84.6% of the sampling points in the upstream of the Fenhe River Reservoir exceeded the guided values of Class III (TN for 1.0 $\text{mg}\cdot\text{L}^{-1}$) referred by Chinese Surface Water Environmental Quality Standard (GB 3838-2002) [13].

The peaks of inorganic nitrogen concentration occurred frequently at the three sampling points of S6, S8, and S9. The concentrations of the $\text{NH}_4^+\text{-N}$ and $\text{NO}_2^-\text{-N}$ in S6 were relatively high, and the concentrations of the TN and $\text{NO}_3^-\text{-N}$ in S8 reached the highest level in the wet season. As these two sampling points are located in the mainstream of the Fenhe River, the pollution was mainly from the domestic pollution caused by the untreated sewage in 13 towns along the mainstream of the Fenhe River. The concentrations of the TN and $\text{NO}_3^-\text{-N}$ at S9 were both relatively high during the wet and dry seasons. This sampling point, which was mainly affected by the tributary of the Lan River, may suffer from the incomplete treatment of the surrounding sewage treatment plants and the discharge of domestic sewage. At the sampling point S13, $\text{NH}_4^+\text{-N}$ and $\text{NO}_3^-\text{-N}$ were relatively high during the wet season. It was found that the surrounding population density was relatively dense, and a large amount of domestic sewage and livestock manure were

TABLE 1: Chemical indices in the water samples collected from the upstream of Fenhe River.

Sampling sites	Wet period				Dry period			
	T (°C)	pH	DO (mg/L)	ORP (mv)	T (°C)	pH	DO (mg/L)	ORP (mv)
S1	12.0 ± 0.6	8.23 ± 0.40	5.8 ± 0.3	257 ± 12	10.1 ± 0.5	8.52 ± 0.44	8.8 ± 0.4	164 ± 9
S2	13.0 ± 0.7	8.12 ± 0.41	11.2 ± 0.6	241 ± 13	15.5 ± 0.9	8.4 ± 0.40	16.5 ± 0.9	178 ± 9
S3	11.0 ± 0.5	8.51 ± 0.39	8.3 ± 0.4	253 ± 12	12.0 ± 0.6	8.73 ± 0.43	15.3 ± 0.8	187 ± 10
S4	14.0 ± 0.7	8.42 ± 0.44	5.5 ± 0.3	263 ± 13	18.1 ± 0.9	8.86 ± 0.46	12.3 ± 0.6	155 ± 8
S5	19.0 ± 1.03	8.25 ± 0.38	8.3 ± 0.4	254 ± 13	19.7 ± 0.9	7.83 ± 0.37	10.8 ± 0.6	155 ± 8
S6	19.0 ± 0.90	8.36 ± 0.41	12.5 ± 0.7	249 ± 11	18.5 ± 0.9	8.47 ± 0.42	6.84 ± 0.4	175 ± 10
S7	17.1 ± 0.86	8.35 ± 0.41	6.8 ± 0.4	201 ± 9	16.9 ± 0.9	8.48 ± 0.39	8.69 ± 0.4	170 ± 8
S8	14.0 ± 0.71	8.35 ± 0.47	5.5 ± 0.3	249 ± 12	18.1 ± 1.0	8.63 ± 0.48	6.38 ± 0.3	189 ± 10
S9	18.0 ± 0.83	7.83 ± 0.41	4.9 ± 0.2	252 ± 14	21.3 ± 1.0	8.07 ± 0.41	5.02 ± 0.3	161 ± 8
S10	25.2 ± 1.30	8.54 ± 0.44	9.7 ± 0.5	222 ± 12	23.5 ± 1.3	8.2 ± 0.39	10.8 ± 0.5	205 ± 10
S11	23.3 ± 1.14	8.51 ± 0.40	9.5 ± 0.5	234 ± 12	23.2 ± 1.1	8.63 ± 0.43	10.6 ± 0.6	248 ± 13
S12	23.6 ± 1.10	8.58 ± 0.43	8.6 ± 0.5	234 ± 11	22.9 ± 1.2	8.95 ± 0.46	12.5 ± 0.6	249 ± 12
S13	21.3 ± 1.12	8.85 ± 0.47	7.3 ± 0.4	246 ± 11	19.8 ± 0.9	8.85 ± 0.47	5.17 ± 0.2	184 ± 10

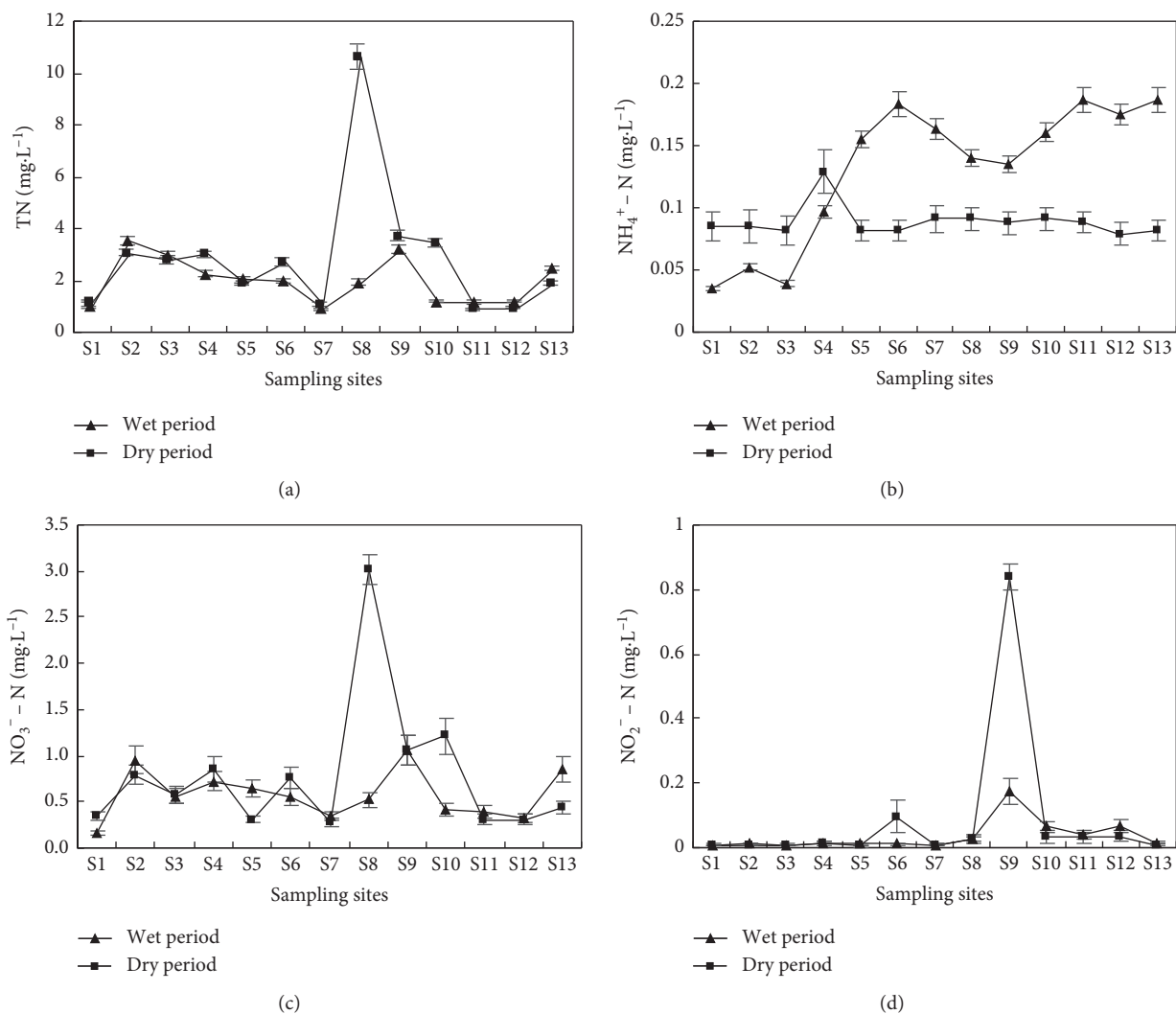


FIGURE 2: Distribution characteristics of different forms of inorganic nitrogen in study area.

directly discharged into the river without any treatment. Our previous studies also showed that the highest TN concentrations in three monitoring points of the Fenhe River

Reservoir exceeded the standard values for Class III of Chinese water quality grade scale ($1.0 \text{ mg}\cdot\text{L}^{-1}$) by 3.61 times [13]. In 2015, the concentrations of TN during the flood

season and dry season were 1.40–1.42 mg/L and 2.48–2.98 mg/L, respectively, with the TN exceeding the standard value by 1.8–4.9 times. More than 90% of the monitoring points in the upstream section of the Fenhe River Reservoir have been comprehensively polluted.

3.2. Characteristics of Nitrate Isotopes in the Upstream Section of the Fenhe River Reservoir. When using nitrate nitrogen and oxygen isotopes to identify nitrate sources in rivers, it is assuming that the nitrate nitrogen is stable in the water body. However, denitrification may change the composition of nitrate source isotopes that further affect the traceability. Therefore, understanding the existence of denitrification is a prerequisite for exploring the source of nitrate [5]. Studies have shown that if the ratio of $\delta^{15}\text{N}$ to $\delta^{18}\text{O}$ is 1.3 : 1–2.1 : 1, denitrification can take place [14]. In addition, when the DO concentrations in the water body exceeds $3.1 \text{ mg}\cdot\text{L}^{-1}$, it is not conducive to have denitrification [15]. In this study, the DO content in each sampling point was greater than $3.1 \text{ mg}\cdot\text{L}^{-1}$ during the entire sampling period, and the DO content was sufficient (Table 1). Additionally, the linear proportional relationship in the range of 1.3 : 1–2.1 : 1 was absent for the ratio of $\delta^{15}\text{N}$ to $\delta^{18}\text{O}$. Thus, it can be determined that almost no denitrification occurred in the Fenhe River.

The results of nitrate nitrogen and oxygen isotope showed that $\delta^{15}\text{N}$ during the wet season was 0.117–4.894‰, while $\delta^{18}\text{O}$ during the wet season was from –3.268 to 24.531‰ (Figure 3). During the dry season, $\delta^{15}\text{N}$ was within 0.527–4.691‰, while $\delta^{18}\text{O}$ was in the range of –0.485–21.527‰. The mean nitrate $\delta^{15}\text{N}$ during the wet and dry seasons was 2.283 and 2.710‰, respectively. The values of $\delta^{15}\text{N}$ in S9 and S5 were the lowest, whereas the values of $\delta^{15}\text{N}$ in S10 and S11 were the highest probably because the reservoir is located near Lan County that has a dense population. Therefore, S10 and S11 were more affected by domestic discharged sewage. The mean nitrate $\delta^{18}\text{O}$ during the wet and dry seasons was 5.862 and 5.891‰, respectively, and the samples with the highest values were all collected from the Jianhe River Bridge at the sampling point S13, indicating that the pollution caused by inorganic fertilizer was relatively severe at S13.

For the pollution sources of NO_3^- , the fertilizer source indicated the inorganic nitrogen in the fertilizer spread to river by precipitation or infiltration. Previous studies reported that $\delta^{15}\text{N}$ values in fertilizers vary between –6‰ and 6‰, while $\delta^{18}\text{O}$ values range from 17 to 25 [16]. NO_3^- -N derived from soil organic N is a product of bacterial decomposition of organic materials originated from degradation of plants and animal wastes [17]. The $\delta^{15}\text{N}$ values in soils (mostly organic N) frequently range from –3‰ to 8‰, and the $\delta^{18}\text{O}$ values range from 17 to 25 [18]. Atmospheric N is reported to be enriched in $\delta^{18}\text{O}$ - NO_3^- by exchanging O atoms with ozone. Literature reported that the $\delta^{15}\text{N}$ values in the atmospheric deposition range from –13‰ to 13‰, and the $\delta^{18}\text{O}$ values range from 29‰ to 58.2‰ [19, 20]. The $\delta^{15}\text{N}$ values of NO_3^- -N derived from manure and waste water generally range from 4‰ to 25‰, and the corresponding $\delta^{18}\text{O}$ values vary between –5‰ and 10‰ [21, 22].

As shown in Figure 4, the concentrations of $\delta^{15}\text{N}$ and $\delta^{18}\text{O}$ values at the sampling points of this study mainly distributed in the range of typical values of inorganic fertilizer, soil organic nitrogen, and domestic sewage area or nearby. Combining the site-investigation results of pollution sources, it can be confirmed that the nitrate nitrogen pollution in the upstream section of the Fenhe River Reservoir mainly came from the inorganic fertilizer, soil organic nitrogen, and domestic sewage.

3.3. Calculating the Contribution Rate for Each Source of NO_3^- by SIAR Model in the Upstream of the Fenhe River Reservoir. In this study, the isotope source analytical model SIAR based on Bayesian analysis was used to analyze the contribution rates of the three nitrate nitrogen sources to the upstream of the Fenhe River Reservoir. The mean isotope characteristics and variance of the three sources of pollution were derived from local sampling data. The former analysis indicated that the microbial denitrification in study area was weak. Therefore, the fractionation coefficient C_{jk} in equation (1) was assumed to be zero.

According to the output of the SIAR model, the contribution rates of the three sources of NO_3^- in the upstream section of the Fenhe River Reservoir during the wet season were in the following order, i.e., soil organic nitrogen (36.83%) > domestic sewage (32.96%) > inorganic fertilizer (30.21%). For the following dry season, however, the following order was observed as domestic sewage (40.68%) > soil organic nitrogen (31.40%) > inorganic fertilizer (27.91%) (Figure 5). The results showed that the soil nitrogen contributed a higher rate to nitrate during the wet season. It was because that the land-use types in the upstream section of the Fenhe River Reservoir in 2019 mainly consisted of farmlands, forests, and grasslands, accounting for 33.2, 30.2, and 33.1% of the total land area, respectively. Water-soluble organic nitrogen in the forest soil often plays an important role in the soil nitrogen pool. For many forests, the water-soluble organic nitrogen levels in soil are more than 100 times than the levels of NH_4^+ -N and NO_3^- -N [23, 24]. In this study, the rainfall was so high during the wet season that the water-soluble organic nitrogen entered the reservoir with water and soil loss. Then, they were converted to nitrate by nitrification. The contribution of domestic sewage to nitrate nitrogen was as high to 41% during the dry season due to the increased human activities on harvest during this period. However, the contribution of inorganic fertilizers was small (28–31%) in two periods. It can be seen that the project of “Five Water Treatment” in Shanxi Province has achieved initial success, and the nonpoint source pollution caused by planting is controlled. However, the control of rural and urban sewage discharge still needs to be further improved.

The above results were different from that reported in a subtropical watershed located in Changxing County, Zhejiang Province, by Yang et al. [7]. Their studies showed that the contribution rate of sources of manure sewage and atmospheric deposition in December was higher than that in May, while the contribution rate of sources of chemical fertilizer and soil in May was higher than that in December.

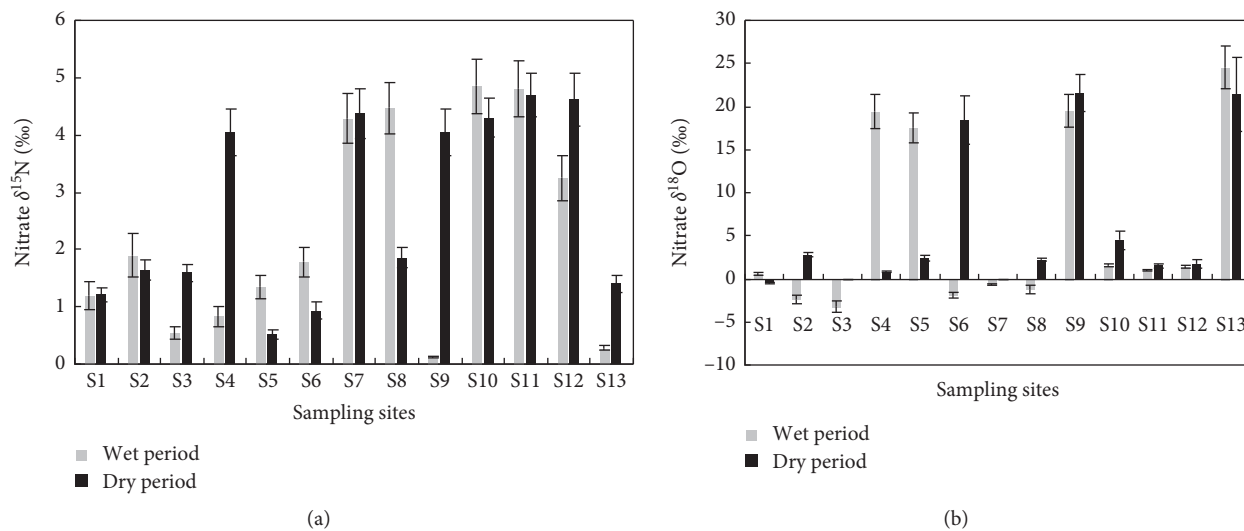


FIGURE 3: Distribution characteristics of nitrogen and oxygen isotope in the study area.

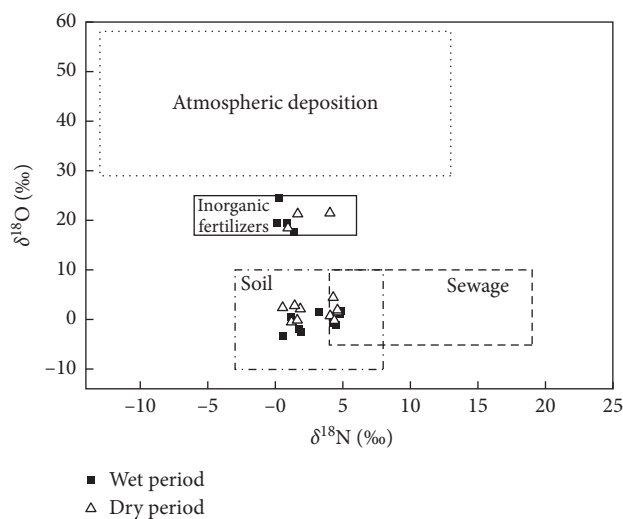


FIGURE 4: Distribution of typical and measured values of $\delta^{15}\text{N}$ and $\delta^{18}\text{O}$ for different sources of the nitrate.

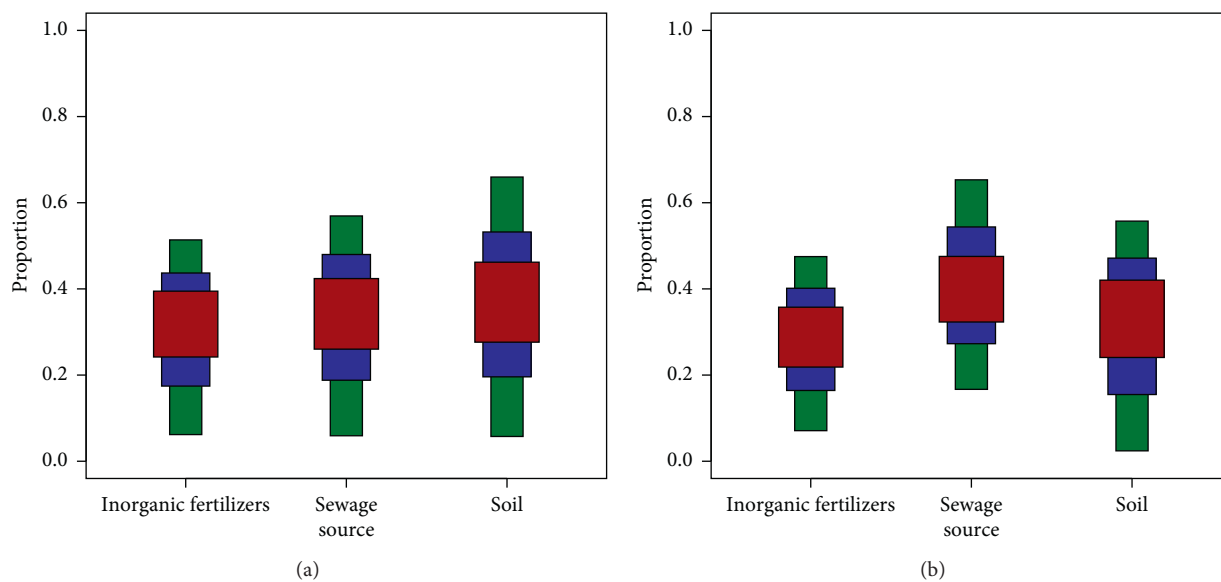


FIGURE 5: Box plots of mean probability estimates of the source contributions in the upstream of Fenhe Reservoir: (a) wet period; (b) dry period. Note: the legends of green, blue, and red referred to 50%, 75%, and 95% credibility interval, respectively.

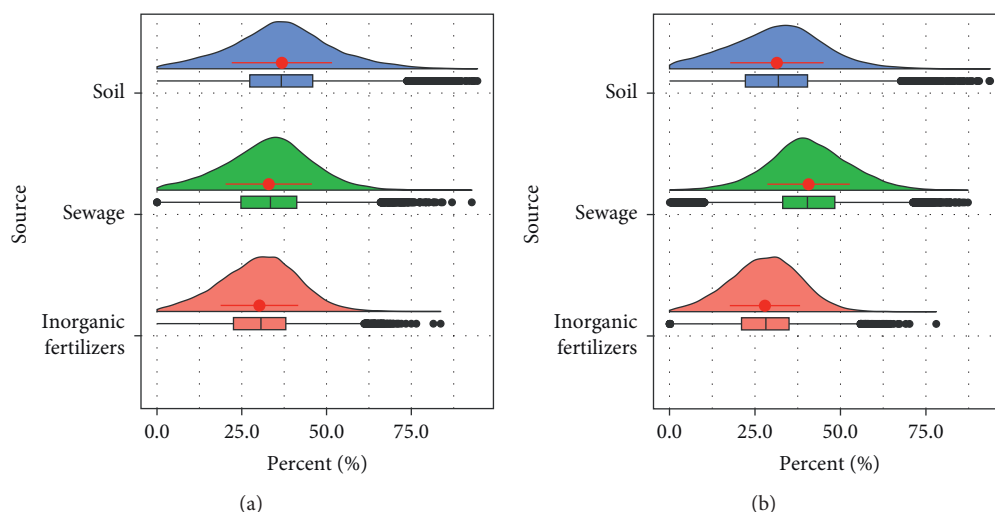


FIGURE 6: Posterior distribution of proportional contributions of three potential NO_3^- sources in the upstream of Fenhe Reservoir: (a) wet period; (b) dry period.

In December, the contribution rate of manure sewage is the highest, reaching 61%. In May, the contribution rate of fertilizer is the highest at 37%. The reasons may be related with two effects. The wet season was defined as in May, and the fertilizer is also applied in this month shortly before rice is transplanted into the field. While in Fenhe River, the wet season was in August so that the effect of fertilizer on nitrogen pollution was slight. In the watershed of Changxing County, as the N isotope signature of sewage is similar to N isotope signature of manure (mainly animal waste), these two sources were treated as one source. However, in Fenhe River, the sewage source of nitrogen pollution only indicated domestic sewage, and the manure source was not included.

To further explain the contribution of the SIAR model to each pollution source, this study provided a post hoc testing distribution diagram (Figure 6). It showed that the median, mean, and maximum posterior probabilities for different nitrate nitrogen sources were generally identical, and the post hoc probabilities were symmetrically distributed. For the posterior samples of the three nitrate nitrogen sources, their sums of the post hoc mean, median, and maximum estimated probabilities were all equal to 1.

4. Conclusions

- (1) The section with severe nitrogen pollution in the study area was mainly affected by the input of tributaries and the discharge of surrounding domestic sewage. The water quality during the wet season was better than that in the dry season. In sum, the water quality in study area was severely contaminated.
- (2) Quantitative analysis of the nitrogen and oxygen isotope of nitrate in the water body based on the SIAR model showed that the inorganic fertilizer, soil organic nitrogen, and domestic sewage were the main sources of pollution in the upstream section of the Fenhe River Reservoir. The contribution rate of

chemical fertilizers, soil organic nitrogen, and domestic sewage was 30–31%, 31–37%, and 33–41%, respectively. It was seemed that their contributions were not so far different. It may be related with the function of Fenhe River Reservoir. As the Fenhe River Reservoir is the biggest centralized drinking water source in Taiyuan, the pollution sources from industry were scare. Thus, the contributions from agricultural, domestic pollution, and soil were main pollution sources.

To establish goals of reducing nitrogen pollution in Fenhe River, a proposal was made for the development of a nitrogen control program that consists of the following elements: regulation of industrial discharges of sewage to the greatest extent practicable, reduction of rural domestic discharges from diffuse sources into the upper Fenhe River, improving the system of municipal wastewater treatment, and maintenance of a viable research program to seek maximum efficiency and effectiveness in the control of nitrogen introductions into the Fenhe River.

In this study, the SIAR model was used to study quantitatively the contribution rate of nitrate sources in the upstream section of the Fenhe River Reservoir. However, some limitations need to be considered. During the migration and transformation of water nitrogen, the nitrification and denitrification can cause the fractionation of nitrogen, which may, in turn, affect the contents of $\delta^{15}\text{N}$ and $\delta^{18}\text{O}$. In this study, C_{jk} was defined as 0 and the fractionation was neglected, which may lead to the deviations of the calculation. In future studies, the effect of the isotope fractionation should be incorporated in the SIAR model to more accurately track and quantify the nitrogen pollutants.

Data Availability

The data used to support the findings of this study are available from the corresponding author upon request.

Conflicts of Interest

The authors declare that they have no conflicts of interest.

Acknowledgments

This research was financially supported by the National Natural Science Foundation of China (no. 41601202), the Natural Science Foundation of Shanxi Province (nos. 201801D121261 and 201701D121116), and the Key Research and Development Project of Shanxi Province (nos. 201803D221002-4 and 201903D321069).

References

- [1] J. N. Galloway, A. R. Townsend, J. W. Erisman et al., "Transformation of the nitrogen cycle: recent trends, questions, and potential solutions," *Science*, vol. 320, no. 5878, pp. 889–892, 2008.
- [2] C. Wu, C. Maurer, Y. Wang, S. Xue, and D. L. Davis, "Water pollution and human health in China," *Environmental Health Perspectives*, vol. 107, no. 4, pp. 251–256, 1999.
- [3] Y. Zhao, B. Zheng, H. Jia, and Z. Chen, "Determination sources of nitrates into the Three Gorges Reservoir using nitrogen and oxygen isotopes," *Science of the Total Environment*, vol. 687, pp. 128–136, 2019.
- [4] Z. Chen, J. Chen, H. Li et al., "Sources of nitrate in Xiangshan Bay (China), as identified using nitrogen and oxygen isotopes," *Estuarine, Coastal and Shelf Science*, vol. 207, pp. 109–118, 2018.
- [5] I. Paredes, F. Ramirez, M. G. Forero, and A. J. Green, "Stable isotopes in helophytes reflect anthropogenic nitrogen pollution in entry streams at the Doñana World Heritage Site," *Ecological Indicators*, vol. 97, pp. 130–140, 2019.
- [6] A. Parnell, R. Inger, S. Bearhop et al., *SIAR: Stable Isotope Analysis in R*, 2008.
- [7] L. Yang, J. Han, J. Xue et al., "Nitrate source apportionment in a subtropical watershed using Bayesian model," *Science of the Total Environment*, vol. 463–464, pp. 340–347, 2013.
- [8] I. Matiatos, "Nitrate source identification in groundwater of multiple land-use areas by combining isotopes and multivariate statistical analysis: a case study of Asopos basin (Central Greece)," *Science of the Total Environment*, vol. 541, pp. 802–814, 2016.
- [9] Z. Jin, Q. Zheng, C. Zhu, Y. Wang, J. Jiarong, and F. Li, "Contribution of nitrate sources in surface water in multiple land use areas by combining isotopes and a Bayesian isotope mixing model," *Applied Geochemistry*, vol. 93, pp. 10–19, 2018.
- [10] C. Gong, C. Xian, Y. Su, and Z. Ouyang, "Estimating the nitrogen source apportionment of *Sophora japonica* in roadside green spaces using stable isotope," *Science of The Total Environment*, vol. 689, pp. 1348–1357, 2019.
- [11] Ouyang, *Analyzing Method for Water and Waste Water*, 3rd edition, Environmental Science Press, Beijing, China, 2002, in Chinese.
- [12] M. R. Mcilvin, M. A. Altabet, and A. Chem, "Chemical conversion of nitrate and nitrite to nitrous oxide for nitrogen and oxygen isotopic analysis in freshwater and seawater," *Analytical Chemistry*, vol. 77, no. 17, pp. 5589–5595, 2005.
- [13] SEPAC (State Environmental Protection Administration of China), *Environmental Quality Standard for Surface Water, China (GB3838-2002)*, China Environmental Science Press, Beijing, China, 2002, in Chinese.
- [14] A. Amberger and H.-L. Schmidt, "Natürliche Isotopengehalte von Nitrat als Indikatoren für dessen Herkunft," *Geochimica et Cosmochimica Acta*, vol. 51, no. 10, pp. 2699–2705, 1987.
- [15] L. A. Desimone and B. L. Howes, "Nitrogen transport and transformations in a shallow aquifer receiving wastewater discharge: a mass balance approach," *Water Resources Research*, vol. 34, no. 2, pp. 271–285, 1998.
- [16] Y.-Y. Yang and G. S. Toor, " $\delta^{15}\text{N}$ and $\delta^{18}\text{O}$ reveal the sources of nitrate-nitrogen in urban residential stormwater runoff," *Environmental Science & Technology*, vol. 50, no. 6, pp. 2881–2889, 2016.
- [17] O. Nikolenko, A. Jurado, A. V. Borges, K. Knöller, and S. Brouyère, "Isotopic composition of nitrogen species in groundwater under agricultural areas: a review," *Science of the Total Environment*, vol. 621, pp. 1415–1432, 2018.
- [18] J. Ding, B. Xi, R. Gao et al., "Identifying diffused nitrate sources in a stream in an agricultural field using a dual isotopic approach," *Science of the Total Environment*, vol. 484, pp. 10–18, 2014.
- [19] C. Kendall, E. M. Elliott, and S. D. Wankel, "Tracing anthropogenic inputs of nitrogen to ecosystems," in *Stable Isotopes in Ecology and Environmental Science*, R. H. Michener, K. Lajtha, Eds., pp. 375–449 Blackwell Publishing, London, UK, 2007.
- [20] A. Nestler, M. Berglund, F. Accoe et al., "Isotopes for improved management of nitrate pollution in aqueous resources: review of surface water field studies: review of surface water field studies," *Environmental Science and Pollution Research*, vol. 18, no. 4, pp. 519–533, 2011.
- [21] J. C. Finaly, R. W. Sterner, and S. Kumar, "Isotopic evidence for in lake production of accumulating nitrate in lake superior," *Ecological Application*, vol. 17, no. 8, pp. 2323–2332, 2007.
- [22] H. D. Freyer, "Seasonal variation of $^{15}\text{N}/^{14}\text{N}$ ratios in atmospheric nitrate species," *Tellus Series B: Chemical & Physical Meteorology*, vol. 43, no. 1, pp. 30–44, 2002.
- [23] K. Kalbitz, S. Solinger, J.-H. Park, B. Michalzik, and E. Matzner, "Controls on the dynamics of dissolved organic matter in soils: a review," *Soil Science*, vol. 165, no. 4, pp. 277–304, 2000.
- [24] J.-S. Wu, P.-K. Jiang, S. X. Chang, Q.-F. Xu, and Y. Lin, "Dissolved soil organic carbon and nitrogen were affected by conversion of native forests to plantations in subtropical China," *Canadian Journal of Soil Science*, vol. 90, no. 1, pp. 27–36, 2010.

Research Article

Distributions and Sources of Sedimentary Sterols as well as Their Indications of Sewage Contamination in the Guanting Reservoir, Beijing

Xin Wen,¹ Yijuan Bai ,¹ Shurong Zhang ,^{1,2} Aizhong Ding,^{1,2} Lei Zheng,^{1,2} and Jian Li ^{1,2}

¹College of Water Sciences, Beijing Normal University, Beijing 100875, China

²Beijing Key Laboratory of Urban Hydrological Cycle and Sponge City Technology, Beijing 100875, China

Correspondence should be addressed to Shurong Zhang; srzhang@bnu.edu.cn

Received 25 December 2019; Accepted 17 February 2020; Published 19 March 2020

Guest Editor: Chunjiang An

Copyright © 2020 Xin Wen et al. This is an open access article distributed under the Creative Commons Attribution License, which permits unrestricted use, distribution, and reproduction in any medium, provided the original work is properly cited.

In this study, domestic sewage contamination in the Guanting Reservoir, one of the major water source reservoirs of Beijing, was examined using sterols as tracing molecular markers. Nineteen sediment samples in seven cross-sections in the Guanting Reservoir were collected, extracted, and analyzed by gas chromatography-mass spectrometry (GC-MS). Seven different sterols were identified and quantified from the surface sediment samples in the Guanting Reservoir. The total sterols in sediments of the reservoir ranged from $2.78 \mu\text{g g}^{-1}$ to $40.31 \mu\text{g g}^{-1}$ with the average concentration of $13.53 \mu\text{g g}^{-1}$. Concentrations of fecal sterols, coprostanol and epicoprostanol in the Guishui River reservoir area were generally higher than in the Yongding River reservoir area. The average concentrations of coprostanol and epicoprostanol in the Yongding River reservoir area were $0.41 \mu\text{g g}^{-1}$ and $0.34 \mu\text{g g}^{-1}$, respectively. The average concentrations of coprostanol and epicoprostanol in the Guishui River reservoir area were $0.72 \mu\text{g g}^{-1}$ and $0.70 \mu\text{g g}^{-1}$, respectively. Ratios of sterols indicated higher sewage pollution in regions close to river mouths and reservoir banks. Principal component analysis (PCA) indicated three distinct sources of sterols from domestic sewage, phytoplankton, and terrestrial higher plants. This article identified the current situation of sewage contamination in sediments of the Guanting Reservoir, which could provide important references for further implementation of pollution control and basin management in the region.

1. Introduction

With strict industrial pollution control, domestic sewage discharge has increasingly become the main concern of water quality issues in many populated regions [1–4]. Sterols have been widely used as a typical biochemical marker to indicate the source of organic matter, such as domestic sewage, marine, and terrestrial source [5–7]. Compared with other microbial source tracking markers such as microorganisms (such as *E. coli*) and molecular markers (such as DNA), sterol markers have high sensitivity, high specificity, and high stability [8, 9]. Especially, with their hydrophobic properties and high persistence in the sediment, sterols are prone to be attached to particles and accumulate in sediments, and they are considered as good markers for tracing sewage contamination in sediments [10–12].

Sterols can be originated from animals, plants, and fungi. Based on their specific structures, sterols provide useful information for source specification in the aquatic environment. Animal sterols are mostly synthesized in the intestines of animals, and the precursor substances are mostly cholesterol [13]. Various types of sterols are formed by cholesterol under the action of the intestinal flora. This “fecal sterol fingerprint” can be used to evaluate the pollution of domestic sewage and trace the source of pollutants [14–16]. Particularly, coprostanol is considered as a major sign of fecal contamination, and a positive connection has been found between levels of coprostanol and abundance of fecal bacteria in previous studies [17, 18]. Moreover, various thresholds of coprostanol concentrations (such as 0.1, 0.5, or $0.7 \mu\text{g g}^{-1}$) were proposed to indicate sewage contamination in aquatic sediments [19–21]. Phytosterols are mainly found

in the seeds of plants, including sitosterol, stigmasterol, and campesterol. Among them, sitosterol and stigmasterol are important markers of terrestrial organic matter, mainly from higher plants, while campesterol is mainly derived from phytoplankton [22, 23]. Fungal sterols are mainly found in molds and mushrooms, and the most common one is ergosterol [24].

In the study of source analysis using sterols, the researchers have found that besides concentrations of individual sterols, the ratios of sterols can be used as more robust indicators to assess the sewage contamination, such as sources of pollution and treatment of sewage [25–30]. The most common ratio parameters are the ratios between coprostanol, epicoprostanol, cholesterol, and cholestanol. Coprostanol/cholesterol can indicate the pollution of domestic sewage and its pollution level. Coprostanol can be converted into epicoprostanol in the process of anaerobic treatment of domestic sewage. Hence, whether the sewage has been treated or not can be indicated by epicoprostanol/coprostanol [31]. In addition, some researchers have found that, in an uncontaminated environment, cholesterol is more likely to form cholestanol through hydrogenation [32]. Coprostanol/(coprostanol + cholestanol) can determine whether domestic sewage exist or not on water bodies.

Guanting Reservoir, an important water source of Beijing, plays a crucial role for water resources allocation and water security of Beijing city. However, human activities, such as farming and wastewater discharge in the upstream basin, are imposing a great pressure for water source protection in the Guanting Reservoir [33, 34]. Hence, it is of great significance to detect the pollution and identify the pollution sources for the protection of the Guanting Reservoir. Although studies have been widely carried out for examining water and sediment chemistry in the Guanting Reservoir, such as nutrients, persistent organic pollutants, and emerging pollutants [35–37], our current knowledge about sewage input and fecal contamination is limited. This study aims to (1) investigate the spatial distributions and sources of sedimentary sterols by combining biomarkers and statistical methods and (2) assess sewage contamination in the surface sediments of the Guanting Reservoir for providing important references for future basin management.

2. Materials and Methods

2.1. Study Area and Sampling. Guanting Reservoir is located between Beijing and Hebei province (115.43°–115.97°E, 40.19°–40.50°N), with the drainage area of 43,402 km² spanning the Inner Mongolia Autonomous Region, Shanxi province, Hebei province, and Beijing Municipality. It belongs to temperate continental monsoon climate zone, with the average annual rainfall amount of 350–500 mm, and majority of rainfall occurring in summer. In the basin, agriculture is the main land-use type. There are two rivers, Yongding River and Guishui River, discharging into the Guanting Reservoir.

In this study, there are 19 sampling points in total located in 7 cross sections in the Guanting Reservoir (Figure 1). Section S1 is located close to the dam, and sections S4 and S7

are river mouth sections of the Yongding River and the Guishui River, respectively. Table 1 shows the specific information of sampling points.

Nineteen surface sediment samples (0–10 cm depth) were collected in the Guanting Reservoir using a stainless-steel dredge sampler. Once collected, sediment samples were immediately stored on ice during transportation to the laboratory and then stored at –20°C until further analysis.

2.2. Chemicals. (3 β , 24R)-Ergost-5-en-3-ol (campesterol, >65% purity), (3 β)-stigmast-5-en-3-ol (β -sitosterol, >95% purity), and (3 β , 22E)-stigmasta-5, 22-dien-3-ol (stigmasterol, >95% purity) were purchased from Sigma-Aldrich (St. Louis, MO USA). (3 β)-Cholest-5-en-3-ol (cholesterol, >98% purity), (3 β , 5 α)-cholestan-3-ol (cholestanol, >98% purity), (3 β , 5 β)-cholestan-3-ol (coprostanol, >98% purity), and (3 α , 5 β)-cholestan-3-ol (epicoprostanol, >98% purity) were purchased from Steraloids Inc (Newport, RI, USA). 5 α -Androstan-3 β -ol (>98% purity) was obtained from Chiron Inc (Trondheim, Norway). N,O-Bis(trimethylsilyl) trifluoroacetamide (BSTFA) was obtained from TCI Inc (Tokyo, Japan). Ultra resi-analyzed n-hexane and dichloromethane were purchased from J. T. Baker Inc (Center Valley, PA, USA).

2.3. Sample Pretreatment. Prior to sterol analysis, all samples were freeze-dried, ground in a mortar, sieved at 100 μ m, and extracted.

Sterol extraction procedures were described in the previous paper by Bataglion et al. [38]. In brief, 25 g of sediment samples were spiked with a known amount of the surrogate standard (5 α -androstan-3 β -ol) and extracted by a microwave extraction system (MarsX, CEM, USA) using the mixture of n-hexane and dichloromethane (1 : 1, v/v). The extracts were concentrated to 0.5 ml using a rotary evaporator and nitrogen blowing instrument and then cleaned up by solid phase extraction (SPE) on C18 cartridges with 10 ml dichloromethane. Extracts were concentrated to near dryness under gentle nitrogen flow and derivatized with BSTFA under 70°C for 1 h.

2.4. Sterols Analysis. The sterols were quantified by gas chromatography-mass spectrometry (GC-MS). The instrument used was Agilent 7890B GC coupled with Agilent 5977A MS on the single ion monitoring (SIM) mode. There were 3 ions selected for particular sterol identification (Table 2). Samples were injected into the injector (250°C) carried by helium at a rate of 1 ml/min. The temperature gradient was with initial temperature 60°C, 15°C/min to 250°C, 1°C/min to 280°C, 5°C/min to 300°C, and hold for 10 min.

For quality assurance and quality control, the external standard method was used for quantitative analysis based on six-point calibration (1, 2, 4, 6, 8, and 10 μ g ml⁻¹). The linear regression coefficients for cholesterol, cholestanol, coprostanol, epicoprostanol, campesterol, sitosterol, and stigmasterol were 0.989, 0.979, 0.977, 0.986, 0.941, 0.992, and

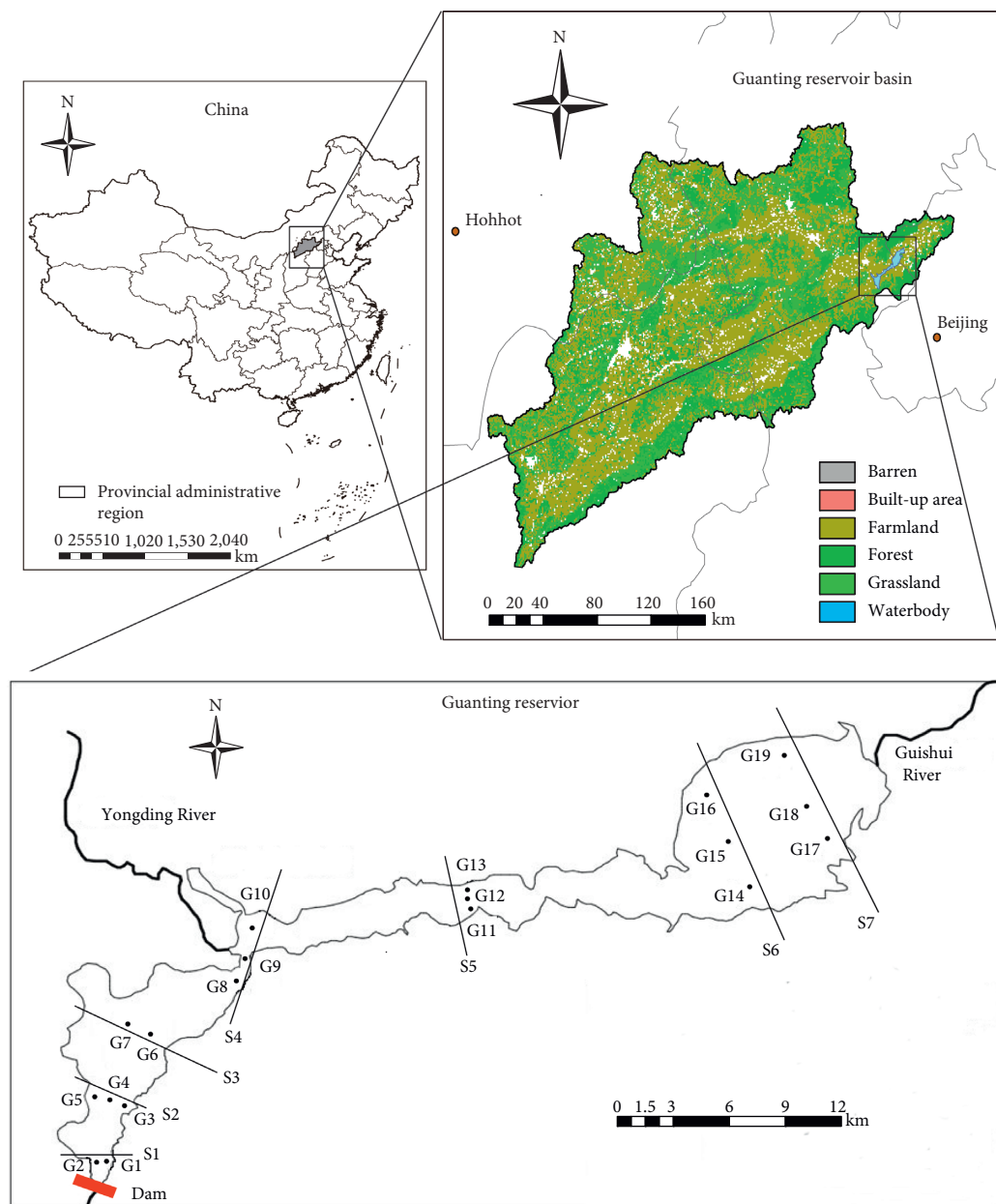


FIGURE 1: Map of sampling points in the Guanting Reservoir.

0.991, respectively. The minimum concentration of the standard curve was defined as the detection limit. According to the quantitative calibration curve, the minimum concentration was $1 \mu\text{g ml}^{-1}$, and the mass of the sediment was 25 g, so the corresponding limit of quantification for sediment samples was $0.04 \mu\text{g g}^{-1}$. The analysis precision was less than 10% for individual sterols based on three replicate analysis of a sediment sample.

2.5. Statistical Analysis. In this study, we used cluster analysis (CA) to identify the spatial distribution pattern of sterol compounds in surface sediments of the Guanting Reservoir based on various sterol concentrations of sediment samples. Also, we used Pearson correlation analysis and

principal component analysis (PCA) to examine the association between sterol compounds and identify sources of organic matter using sterols. The adaptability of PCA in our study was tested using the Kaiser–Meyer–Olkin (KMO) test. All the statistical analysis were performed by SPSS software, version 16.0 (Chicago, Illinois, US).

3. Results and Discussion

3.1. Sterol Contents and Composition Characteristics. Concentrations of the sterols in sediments of the Guanting Reservoir are shown in Table 3. The total sterols in sediments of the reservoir ranged from $2.78 \mu\text{g g}^{-1}$ to $40.31 \mu\text{g g}^{-1}$ with the average concentration of $13.53 \mu\text{g g}^{-1}$. The most abundant sterol observed was sitosterol, followed by stigmasterol

TABLE 1: General information of sampling points in the Guanting Reservoir.

Sampling area	Sampling section	Sampling point	Latitude	Altitude
Yongding River reservoir area	S1	G1	40°14.7'	115°36.12'
		G2	40°14.7'	115°35.25'
		G3	40°14.5'	115°36.18'
	S2	G4	40°14.57'	115°35.55'
		G5	40°14.58'	115°35.31'
		G6	40°16.16'	115°36.31'
	S3	G7	40°16.11'	115°35.46'
		G8	40°17.43'	115°37.20'
		G9	40°18.57'	115°37.4'
	S4	G10	40°18.16'	115°37.28'
		G11	40°21.7'	115°41.33'
		G12	40°21.11'	115°41.21'
	S5	G13	40°20.22'	115°41.2'
G14		40°20.49'	115°43.43'	
G15		40°20.55'	115°43.31'	
Guishui River reservoir area	S6	G16	40°21.6'	115°43.17'
		G17	40°21.17'	115°45.19'
		G18	40°21.28'	115°45.11'
	G19	40°21.35'	115°45.13'	

TABLE 2: Peak time and characteristic ions of sterols for GC-MS.

Sterols	Systematic name	Number of carbon	Molecular weight	Retention time/min	<i>m/z</i> for quantification and identification
Cholesterol	(3 β)-Cholest-5-en-3-ol	27	386.65	29.60	73,129,329
Cholestanol	(3 β , 5 α)-Cholestan-3-ol	27	388.67	29.91	75,129,215
Coprostanol	(3 β , 5 β)-Cholestan-3-ol	27	388.67	26.89	73,75,370
Epicoprostanol	(3 α , 5 β)-Cholestan-3-ol	27	388.67	27.19	75,215,370
Campesterol	(3 β , 24R)-Ergost-5-en-3-ol	28	400.68	28.34	43,73,129
Sitosterol	(3 β)-Stigmast-5-en-3-ol	29	412.69	36.04	57,73,129
Stigmasterol	(3 β , 22E)-Stigmasta-5,22-dien-3-ol	29	414.71	34.03	55,83,370
5 α -Androstan-3 β -ol		19	276.46	14.831	75,258,333

TABLE 3: Sterol concentrations in sediments of the Guanting Reservoir ($\mu\text{g g}^{-1}$).

Sampling point	Cholesterol	Cholestanol	Coprostanol	Epicoprostanol	Campesterol	Sitosterol	Stigmasterol	Total sterols
G1	2.93	1.00	0.28	0.44	0.09	2.88	2.04	9.66
G2	8.41	1.66	0.35	0.34	0.08	7.88	6.29	25.01
G3	0.80	0.50	0.20	0.19	0.06	0.80	0.48	3.03
G4	0.84	0.48	0.11	0.10	0.06	1.40	0.61	3.60
G5	2.63	0.83	0.57	0.33	0.15	8.03	4.69	17.23
G6	2.20	1.14	0.90	0.85	0.22	28.48	6.52	40.31
G7	1.16	0.63	0.39	0.29	0.17	2.68	2.09	7.41
G8	1.24	0.77	0.51	0.29	0.16	5.03	2.44	10.44
G9	1.35	0.57	0.71	0.41	0.17	3.08	1.06	7.35
G10	1.73	0.53	0.40	0.20	0.10	2.21	1.15	6.32
G11	1.16	0.57	0.18	0.32	0.07	1.41	0.64	4.35
G12	1.84	0.70	0.36	0.38	0.11	2.11	0.89	6.39
G13	3.22	0.71	0.37	0.32	0.11	1.73	1.19	7.65
G14	0.59	0.46	0.23	0.17	0.07	0.79	0.47	2.78
G15	7.32	2.00	1.22	1.49	0.21	1.58	1.32	15.14
G16	2.89	1.04	1.24	0.97	0.14	12.29	9.06	27.63
G17	3.01	1.26	0.55	0.67	0.11	19.50	10.58	35.68
G18	5.71	1.51	0.62	0.58	0.11	4.56	3.35	16.44
G19	2.06	0.65	0.45	0.34	0.09	4.67	2.42	10.68
Mean	2.69	0.90	0.51	0.46	0.12	5.85	3.02	13.53

and cholesterol. Concentrations of sitosterol ranged from $0.79 \mu\text{g g}^{-1}$ to $28.48 \mu\text{g g}^{-1}$, with the average concentration of $5.85 \mu\text{g g}^{-1}$. Concentrations of stigmasterol ranged from $0.47 \mu\text{g g}^{-1}$ to $10.58 \mu\text{g g}^{-1}$, with the average concentration of $3.02 \mu\text{g g}^{-1}$. As seen from Figure 2, the sum proportions of these two sterols in the total sterols were higher than 50% at most sampling points, with the maximum reaching 86.8% of the total sterols. Among phytosterols, concentrations of campesterol were very low, ranging from $0.06 \mu\text{g g}^{-1}$ to $0.22 \mu\text{g g}^{-1}$, with an average concentration of $0.12 \mu\text{g g}^{-1}$.

Cholesterol was the most abundant animal sterol, ranging from $0.59 \mu\text{g g}^{-1}$ to $8.41 \mu\text{g g}^{-1}$ with the average concentration of $2.69 \mu\text{g g}^{-1}$. The concentrations of cholestanol ranged from $0.46 \mu\text{g g}^{-1}$ to $2.00 \mu\text{g g}^{-1}$, and the average value of cholestanol was $0.90 \mu\text{g g}^{-1}$. Coprostanol was widely distributed in sediments of the reservoir, ranging from $0.11 \mu\text{g g}^{-1}$ to $1.24 \mu\text{g g}^{-1}$, with the average concentration of $0.51 \mu\text{g g}^{-1}$, which was similar to the concentrations of coprostanol in sediments of rivers of Serbia and Ulungur Lake in northern Xinjiang [39, 40]. Generally, the concentration of coprostanol has been used to assess the sewage pollution level, and the maximum threshold of sewage contamination used in previous studies was $0.7 \mu\text{g g}^{-1}$ [20, 30]. Hence, we considered $0.7 \mu\text{g g}^{-1}$ as the threshold of sewage contamination in our study. Sampling points with concentrations of coprostanol larger than $0.7 \mu\text{g g}^{-1}$ in the Guanting Reservoir were G6 ($0.90 \mu\text{g g}^{-1}$), G9 ($0.71 \mu\text{g g}^{-1}$), G15 ($1.22 \mu\text{g g}^{-1}$), and G16 ($1.24 \mu\text{g g}^{-1}$), suggesting serious sewage contamination in these regions. These sampling points were located close to river mouth regions or close to reservoir banks with leisure resorts. However, the proportion of coprostanol in the total sterol content was comparatively low, ranging from 1.4% to 9.7% with the average proportion of 4.8%. The highest coprostanol concentration detected in this study ($1.24 \mu\text{g g}^{-1}$) was much lower than that observed in some heavily polluted rivers, such as the Xiaoqing River close to Laizhou Bay in eastern China ($63.2 \mu\text{g g}^{-1}$) and the Pearl River ($53 \mu\text{g g}^{-1}$ TOC) [30, 41]. The concentrations of epicoprostanol ranged from $0.10 \mu\text{g g}^{-1}$ to $1.49 \mu\text{g g}^{-1}$, with an average of $0.46 \mu\text{g g}^{-1}$. The ubiquitous existence of epicoprostanol in sediments of the Guanting Reservoir suggested the input of treated sewage from upstream regions, which were consistent with the existence of many wastewater treatment plants in upstream cities, such as Zhangjiakou and Xuanhua.

3.2. Spatial Distribution of Sterols. According to Table 1, concentrations of coprostanol and epicoprostanol in the Guishui River reservoir area were generally higher than those in the Yongding River reservoir area. The average concentrations of coprostanol and epicoprostanol in the Yongding River reservoir area were $0.41 \mu\text{g g}^{-1}$ and $0.34 \mu\text{g g}^{-1}$, respectively. The average concentrations of coprostanol and epicoprostanol in the Guishui River reservoir area were $0.72 \mu\text{g g}^{-1}$ and $0.70 \mu\text{g g}^{-1}$, respectively. Higher coprostanol concentrations in the Guishui River reservoir area indicated that the area was more affected by sewage input from the Guishui River as well as reservoir bank areas. In sediments

that are not contaminated with feces, the content of coprostanol is approximately 1% to 2% of the total sterol content [13]. The proportions of coprostanol in the total sterol were higher than 1% throughout the Guanting Reservoir (Figure 2). Except for G2 and G17, the contents of coprostanol at other sampling points were higher than 2%, indicating that most of the Guanting Reservoir was affected with animal waste. The research data showed that the contents of coprostanol in the Yongding River mouth area were relatively higher than that of the downstream sections, reaching 9% (G6). Similar to coprostanol, the concentrations of epicoprostanol in the Guishui River reservoir area were much higher than those in the Yongding River reservoir area.

Phytosterols were the dominant types of sterols in sediments at the most of the sampling points in the Guanting Reservoir. Ratios of phytosterols to animal sterols ranged from 0.26 (G15) to 6.92 (G6) as seen in Figure 3. Except at 6 sampling points G11–G15, and G18, ratios of phytosterols to animal sterols were larger than 1 at other sampling points. Among the plant sterols, the proportion of campesterol was minor, and the concentration variation was not significant in the entire Guanting Reservoir. It has been proposed that phytosterols can be derived from municipal pollution besides their terrestrial source [40]. Hence, high proportions of phytosterols in the total sterols in the Guanting Reservoir may be partially due to sewage input.

Cluster analysis of the sterols in the sediment of Guanting Reservoir showed that the entire sediment sampling points can be divided into three groups (see Figure 4 and Table 4). Group 1, including sampling points G6 and G17, were characterized with the highest average values of the total sterol content, sitosterol content, and stigmasterol content, which were $38.00 \mu\text{g g}^{-1}$, $23.99 \mu\text{g g}^{-1}$, and $8.55 \mu\text{g g}^{-1}$, respectively. Spatially, sampling points in Group 1 were located close to the south bank of the reservoir. Group 2 included sampling points G2, G5, and G16 which were located close to the north bank of the reservoir. Group 2 generally had medium average contents of sterols except cholesterol content which was the highest among three groups. Group 3 covered the majority of the points with the lowest average content of total sterol content and individual sterols among the three groups of sampling points. Based on analysis of variance (ANOVA), three groups were significantly different in terms of the contents of the total sterol, sitosterol, and stigmasterol. Compared with Group 3, Group 1 and Group 2 had higher sterol concentrations, which suggested the enhanced input of organic matter with both naturally terrestrial source and sewage source from adjacent reservoir banks. This could be related with fish farming and small leisure resorts or restaurants along the reservoir bank, which may discharge sewage and impose important impacts on water quality of the reservoir.

3.3. Pollution Evaluation Using Sterol Ratios. Besides individual sterol contents, sterol ratio parameters are widely used to more robustly evaluate the sewage contamination [30, 40, 42]. In this study, five sterol ratio parameters were used, including coprostanol/cholestanol,

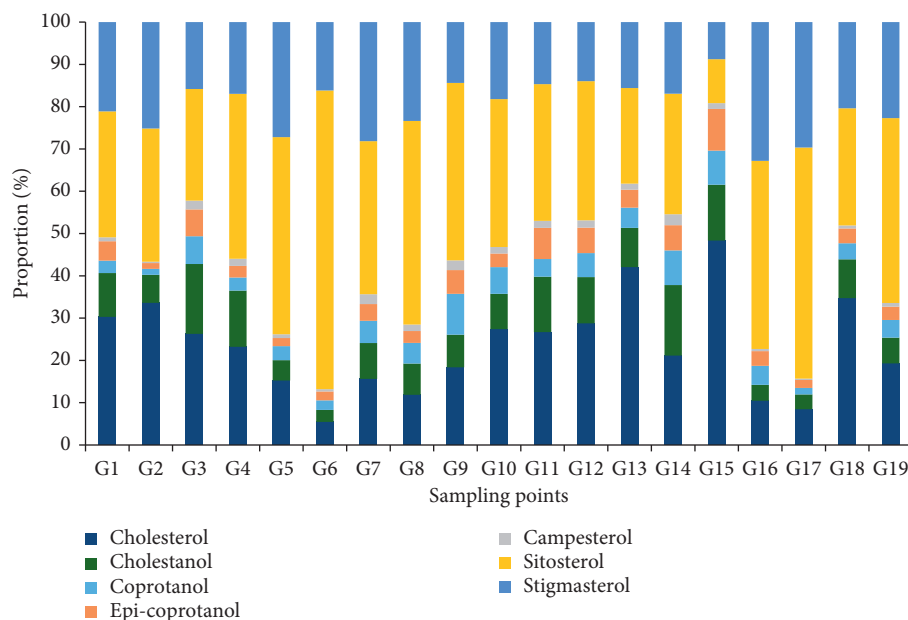


FIGURE 2: Proportions of seven sterols in total sterols in sediments of the Guanting Reservoir.

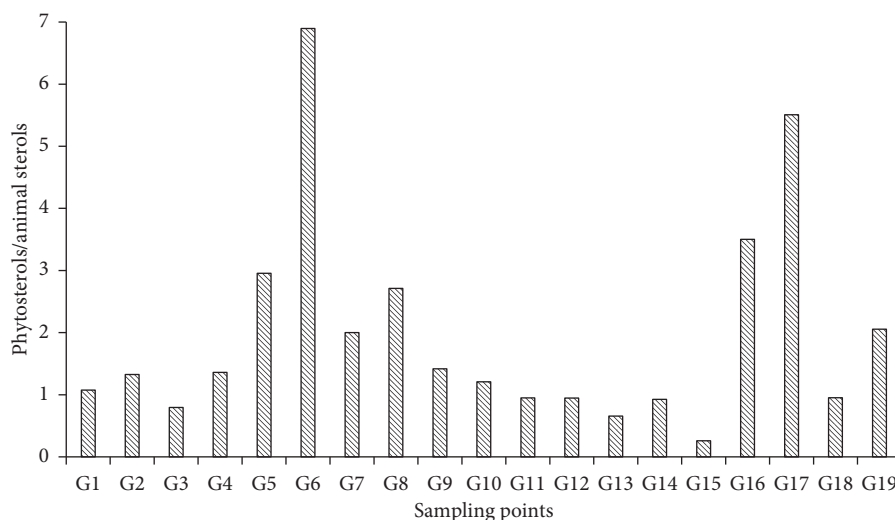


FIGURE 3: Ratios of phytosterols to animal sterols in sediments of the Guanting Reservoir.

coprostanol/(cholesterol + cholestanol), epicoprostanol/coprostanol, coprostanol/(coprostanol + cholestanol), and coprostanol/cholesterol. The distribution of the five sterol ratios is shown in Table 5.

Coprostanol/(coprostanol + cholestanol) is one of the most used indicators to determine the presence of sewage contamination. Ratio values higher than 0.7 have been commonly considered to indicate sewage contamination, while values less than 0.3 indicate no sewage contamination [19]. Except G5, coprostanol/(coprostanol + cholestanol) ratios at the sections close to dam, S1 and S2, were less than 0.3, which indicated little sewage contamination in the area far away downstream river mouths. The ratios in other areas in the reservoir were generally

between 0.3 and 0.7. The ratios of G9 and G16 were relatively high indicating more serious pollution by the animal waste. Similar studies have shown that the ratios of the majority of analyzed sediment samples were between 0.3 and 0.7, which suggested the combined input of sewage and natural sources [43, 44]. Some researchers preferred to use a lower threshold value of coprostanol/(coprostanol + cholestanol) for sewage contamination, such as 0.5 [18, 37]. In our study, sampling points G9 and G16 had ratios larger than 0.5, which suggest more serious sewage pollution in these regions. These two sampling points were also with concentrations of coprostanol larger than $0.7 \mu\text{g g}^{-1}$ having an indication of sewage pollution as discussed earlier.

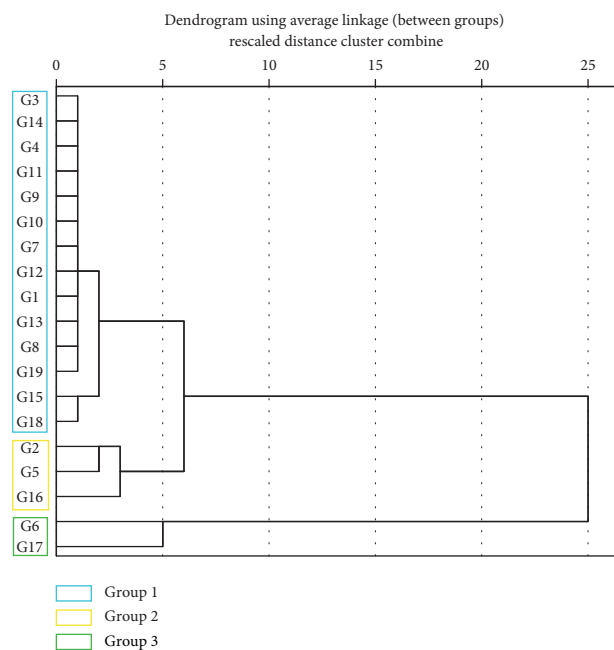


FIGURE 4: Cluster analysis results of sediment sampling points in the Guanting Reservoir.

TABLE 4: Average values of sterols of three groups of sampling points in the Guanting Reservoir based on the cluster analysis ($\mu\text{g g}^{-1}$).

Sterols	Group			ANOVA analysis		
	1	2	3	df	F	p value
Cholesterol	2.61	4.64	2.28	18	1.527	0.247
Cholestanol	1.20	1.178	0.79	18	1.573	0.238
Coprostanol	0.72	0.72	0.43	18	1.637	0.226
Epicoprostanol	0.76	0.54	0.40	18	1.185	0.331
Campesterol	0.16	0.13	0.11	18	1.02	0.383
Sitosterol	23.99	9.40	2.49	18	86.86	<0.001*
Stigmasterol	8.55	6.68	1.44	18	38.66	<0.001*
The total sterol	38.00	23.29	7.95	18	51.49	<0.001*

*The significance level p value is less than 0.05; ANOVA: analysis of variance.

Similar contamination pattern was identified using the ratio of coprostanol/(cholesterol + cholestanol). When the ratio is >0.20 , it indicates domestic sewage input, and when the ratio is <0.15 , it indicates no domestic sewage input [18, 39]. The ratios of samples at G6, G7, G8, G9, G14, and G16 were higher than 0.2, which indicated significant influence of human domestic sewage near river mouths. The ratio of other points was less than 0.15, and there was no obvious indication of domestic sewage input.

Coprostanol/cholestanol is also one of the important indicators for indicating the pollution of human sewage [13]. When the ratio is >0.50 , it indicates human sewage source. When the ratio is <0.30 , it indicates no human sewage input. Except sampling points G1–G4, G11, G14, G17, and G18, the ratios of coprostanol/cholestanol all exceeded 0.50, indicating obvious influences from human domestic sewage. The ratio values of sampling points G9 and G16 in the river mouths were especially higher. At the

most downstream section S1 close to the dam, the ratios were less than 0.30, indicating no influence by human domestic sewage. Coprostanol/cholesterol can be used to characterize different sources of pollutants with a criterion of >0.5 for human fecal inputs [45]. In the Guanting Reservoir, the ratio of G9 was greater than 0.50, indicating human fecal contamination from the Yongding River Basin.

Epicoprostanol/coprostanol can be used as an important indicator of untreated domestic sewage pollution. For sediments contaminated by raw, untreated sewage, the ratio is less than 0.20, while for sediments with no contamination or affected by treated sewage, this value increases to 0.80 [46, 47]. The ratios of most points in the reservoir were higher than 0.80, indicating that the entire reservoir area was not affected by severe untreated sewage, but the ratios of G5, G7, G8, G9, G10, G14, and G16 were between 0.20 and 0.80, indicating that in these regions near river mouths or near banks, sediments were partly affected with untreated sewage. Although there were many sewage treatment plants in the upstream regions of the Guanting Reservoir Basin, such as in cities of Zhangjiakou and Xuanhua in Heibei Province, untreated sewage discharge input from upstream river input or adjacent bank regions still existed in the Guanting Reservoir.

Through comprehensive analysis of the above sterol ratios, it can be found that in the river mouth areas and near bank regions, presences of domestic sewage were indicated. The main source in the river mouths was the upstream input from the Yongding River and the Guishui River. At the same time, because there were many locations for fish farming and small leisure resorts or restaurants along the reservoir bank, untreated domestic sewage from these reservoir bank locations may be an important source of pollution in the reservoir. Section S1 close to the dam was far away from the river mouths, and no presence of sewage contamination was identified there.

3.4. Source Discrimination Using Principal Component Analysis. In order to determine the source of sterols in sediments of the Guanting Reservoir, correlation analysis and principal component analysis were performed. Results of Pearson correlation analysis (see Table 6) showed that the correlation coefficient between cholesterol and cholestanol was 0.92, with the significance level less than 0.01, indicating these two sterols were both from the same source. Cholestanol was also extremely significantly associated with epicoprostanol, indicating these two sterols were from the same source of contamination. Coprostanol was significantly correlated with epicoprostanol, and coprostanol was significantly correlated with epicoprostanol with the correlation coefficient of 0.893. However, coprostanol was also significantly correlated with campesterol, sitosterol, and stigmasterol, with correlation coefficients 0.703, 0.466, and 0.494, respectively. The significant correlation between fecal sterols and plant sterols has also been reported by other studies [39, 48]. One reason for this phenomenon may be because plant sterols,

TABLE 5: Sterol ratio parameters in the Guanting Reservoir sediment.

Sample point	Coprostanol/ (coprostanol + cholesterol)	Coprostanol/ (cholesterol + cholesterol)	Coprostanol/ cholestanol	Coprostanol/ cholesterol	Epicoprostanol/ coprostanol
G1	0.22	0.07	0.28	0.10	1.56
G2	0.17	0.03	0.21	0.04	0.97
G3	0.28	0.15	0.40	0.25	0.97
G4	0.19	0.08	0.23	0.13	0.90
G5	0.41	0.16	0.68	0.22	0.58
G6	0.44	0.27	0.79	0.41	0.94
G7	0.38	0.22	0.62	0.34	0.75
G8	0.40	0.25	0.66	0.41	0.58
G9	0.55	0.37	1.25	0.53	0.58
G10	0.43	0.18	0.75	0.23	0.52
G11	0.24	0.10	0.32	0.16	1.76
G12	0.34	0.14	0.52	0.20	1.06
G13	0.34	0.09	0.51	0.11	0.89
G14	0.33	0.22	0.49	0.39	0.72
G15	0.38	0.13	0.61	0.17	1.22
G16	0.55	0.32	1.20	0.43	0.78
G17	0.30	0.13	0.43	0.18	1.22
G18	0.29	0.09	0.41	0.11	0.93
G19	0.41	0.16	0.69	0.22	0.76

TABLE 6: Relevance of sterols in sediments of the Guanting Reservoir.

Sterols	Cholesterol	Cholestanol	Coprostanol	Epicoprostanol	Campesterol	Sitosterol	Stigmasterol
Cholesterol	1						
Cholestanol	0.919**	1					
Coprostanol	0.417	0.602**	1				
Epicoprostanol	0.560*	0.770**	0.893**	1			
Campesterol	0.144	0.323	0.703**	0.589**	1		
Sitosterol	0.124	0.352	0.466*	0.413	0.411	1	
Stigmasterol	0.344	0.491*	0.494*	0.424	0.212	0.819**	1

such as sitosterol and stigmasterol, are also derived from municipal sewage besides their terrestrial source [40, 48]. Also, discharge of domestic sewage may lead to phytoplankton growth in the reservoir which could increase the amount of phytosterols, particularly campesterol [48]. Epicoprostanol is also significantly correlated with campesterol but had no significant correlation with the other two plant sterols. For plant sterols, the correlation coefficient between sitosterol and stigmasterol was 0.819, and the significance level was less than 0.01, indicating these two sterols had the same source, mainly from terrestrial plants input. There were no significant correlations between campesterol and other two plant sterols, suggesting that sources of campesterol were very different from sources of sitosterol and stigmasterol.

The principal component analysis method is a technique for studying the relationships between variables and extracting the main factors. Results of principal component analysis in the sediment of the Guanting Reservoir showed that three principal components were extracted from the seven sterols in this study (see Figure 5). In total, 91.97% of the total variances were explained using the three components. The load variance of PC1 was 58.05%, the load variance of PC2 was 18.60%, and the load variance

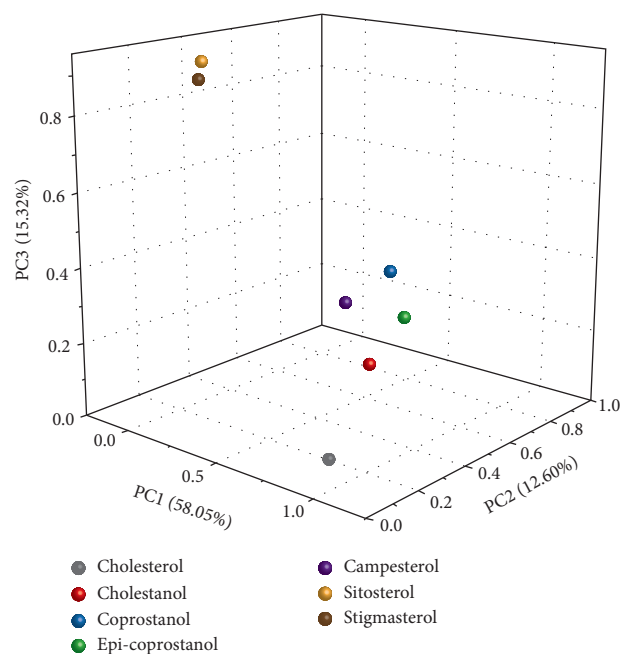


FIGURE 5: Principal component analysis of sterols in sediments of the Guanting Reservoir.

TABLE 7: Principal component analysis interpretation variables of sterols in sediments of the Guanting Reservoir.

Component	Initial eigenvalue			Extracting squares sum			Rotating squares sum		
	Sum	Variance %	Accumulation %	Sum	Variance %	Accumulation %	Sum	Variance %	Accumulation %
1	4.064	58.05	58.05	4.064	58.05	58.05	2.312	33.03	33.03
2	1.302	18.60	76.65	1.302	18.60	76.65	2.228	31.83	64.86
3	1.072	15.32	91.97	1.072	15.32	91.97	1.897	27.11	91.97
4	0.323	4.62	96.59						
5	0.160	2.29	98.88						
6	0.060	0.86	99.74						
7	0.020	0.26	100.00						

TABLE 8: Component factor matrix of principal component analysis of sterols in sediments of the Guanting Reservoir.

Sterol	Principal component		
	1	2	3
Cholesterol	0.968	0.079	0.069
Cholestanol	0.910	0.289	0.241
Coprostanol	0.371	0.821	0.289
Epicoprostanol	0.571	0.721	0.209
Campesterol	-0.004	0.921	0.129
Sitosterol	0.023	0.293	0.919
Stigmasterol	0.286	0.107	0.920

of PC3 was 15.32%. As shown in Table 7, the high load rates indicated that these three components can be used to analyze the overall sterol situation of the Guanting Reservoir sediments. The factor loadings of PCA analysis are shown in Table 8. PC1 had positive factor loadings with other sterols except for the negative correlation with campesterol, and factor loadings with cholesterol, cholestanol, and epicoprostanol were larger than 0.50, representing domestic sewage input. PC2 had positive factor loadings with all sterols, and particularly with campesterol, representing the input of phytoplankton sterols. PC3 had high factor loadings with sitosterol (0.919) and stigmasterol (0.920), representing the input from terrestrial higher plants.

4. Conclusions

In this study, domestic sewage contamination was traced using sterols for sediment samples in the Guanting Reservoir, one important water source reservoir in Beijing, China. Results revealed the spatial distribution of domestic sewage pollution in the reservoir with obvious sewage signals near river mouth regions while diminished downstream, which can provide scientific directions for sediment pollution remediation and river basin management. The use of a combined approach of sterols concentrations and diagnostic ratios of several sterols improves the determination of sterol sources in the Guanting Reservoir, which indicates sterol fingerprinting is an efficient tool for tracking sources of sewage contamination. By tracking sterols and other geochemical markers (such as fluorescent whitening agents and linear alkylbenzenes), it should provide more reliable evidence of the source and severity of sewage pollution as well as integrated river basin management.

Data Availability

The data used to support the findings of this study are available from the corresponding author upon request.

Conflicts of Interest

The authors declare that there are no conflicts of interest regarding the publication of this paper.

Acknowledgments

This study was financially supported by China National Science and Technology Major Project of Water Pollution Control and Treatment (no. 2018ZX07101005), Beijing Municipal Science and Technology Project (nos. Z170004 and Z181100005518012), and the 111 Project of China (no. B18006).

References

- [1] J. Hur and J. Cho, "Prediction of BOD, COD, and total nitrogen concentrations in a typical urban river using a fluorescence excitation-emission matrix with PARAFAC and UV absorption indices," *Sensors*, vol. 12, no. 1, pp. 972–986, 2012.
- [2] M. Taka, T. Kokkonen, K. Kuoppamäki et al., "Spatio-temporal patterns of major ions in urban stormwater under cold climate," *Hydrological Processes*, vol. 31, no. 8, pp. 1564–1577, 2017.
- [3] J. Zhi, A. Ding, and S. Zhang, "Nitrate sources and nitrogen biogeochemical processes in the Feng River in West China inferred from the nitrogen and oxygen dual isotope measurements of nitrate," *Desalination and Water Treatment*, vol. 57, no. 18, pp. 8243–8251, 2016.
- [4] S. Zhang, Y. Bai, X. Wen, A. Ding, and J. Zhi, "Seasonal and downstream alterations of dissolved organic matter and dissolved inorganic ions in a human-impacted mountainous tributary of the Yellow River, China," *Environmental Science and Pollution Research*, vol. 25, no. 18, pp. 17967–17979, 2018.
- [5] J. K. Volkman, "Sterols and other triterpenoids: source specificity and evolution of biosynthetic pathways," *Organic Geochemistry*, vol. 36, no. 2, pp. 139–159, 2005.
- [6] P. Tyagi, D. R. Edwards, and M. S. Coyne, "Use of selected chemical markers in combination with a multiple regression model to assess the contribution of domesticated animal sources of fecal pollution in the environment," *Chemosphere*, vol. 69, no. 10, pp. 1617–1624, 2007.
- [7] I. D. Bull, M. J. Lockheart, M. M. Elhmmali, D. J. Roberts, and R. P. Evershed, "The origin of faeces by means of biomarker

- detection," *Environment International*, vol. 27, no. 8, pp. 647–654, 2002.
- [8] H. Takada, F. Satoh, M. Bothner, and J. Farrington, "Anthropogenic markers: molecular tools to identify the source(s) and transport-pathway of pollutants," *Abstracts of Papers of the American Chemical Society*, vol. 212, no. 1, p. 31, 1996.
- [9] N. H. Adnan, M. P. Zakaria, H. Juahir, and M. M. Ali, "Faecal sterols as sewage markers in the Langat River, Malaysia: integration of biomarker and multivariate statistical approaches," *Journal of Environmental Sciences*, vol. 24, no. 9, pp. 1600–1608, 2012.
- [10] C. M. G. Vivian, "Tracers of sewage sludge in the marine environment: a review," *Science of the Total Environment*, vol. 53, no. 1-2, pp. 5–40, 1986.
- [11] K. O. Isobe, M. Tarao, N. H. Chiem, L. Y. Minh, and H. Takada, "Effect of environmental factors on the relationship between concentrations of coprostanol and fecal indicator bacteria in tropical (Mekong delta) and temperate (Tokyo) freshwaters," *Applied and Environmental Microbiology*, vol. 70, no. 2, pp. 814–821, 2004.
- [12] M. W. Thomes, V. Vaezzadeh, M. P. Zakaria, and C. W. Bong, "Use of sterols and linear alkylbenzenes as molecular markers of sewage pollution in Southeast Asia," *Environmental Science and Pollution Research*, vol. 26, no. 31, pp. 31555–31580, 2019.
- [13] R. Leeming, A. Ball, N. Ashbolt, and P. Nichols, "Using faecal sterols from humans and animals to distinguish faecal pollution in receiving waters," *Water Research*, vol. 30, no. 12, pp. 2893–2900, 1996.
- [14] J. A. Noblet, D. L. Young, E. Y. Zeng, and S. Ensari, "Use of fecal steroids to infer the sources of fecal indicator bacteria in the Lower Santa Ana River Watershed, California: sewage is unlikely a significant source," *Environmental Science & Technology*, vol. 38, no. 22, pp. 6002–6008, 2004.
- [15] J. W. Readman, G. Fillmann, I. Tolosa, J. Bartocci, and L. D. Mee, "The use of steroid markers to assess sewage contamination of the Black Sea," *Marine Pollution Bulletin*, vol. 50, no. 3, pp. 310–318, 2005.
- [16] K. S. Machado, S. Froehner, J. Sáñez, R. C. L. Figueira, and P. A. L. Ferreira, "Assessment of historical fecal contamination in Curitiba, Brazil, in the last 400 years using fecal sterols," *Science of the Total Environment*, vol. 493, pp. 1065–1072, 2014.
- [17] K. O. Isobe, M. Tarao, M. P. Zakaria, N. H. Chiem, L. Y. Minh, and H. Takada, "Quantitative application of fecal sterols using gas Chromatography–Mass spectrometry to investigate fecal pollution in tropical waters: Western Malaysia and Mekong Delta, Vietnam," *Environmental Science & Technology*, vol. 36, no. 21, pp. 4497–4507, 2002.
- [18] J. A. González-Oreja and J. I. Saiz-Salinas, "Short-term spatio-temporal changes in urban pollution by means of faecal sterols analysis," *Marine Pollution Bulletin*, vol. 36, no. 11, pp. 868–875, 1998.
- [19] J. O. Grimalt, P. Fernandez, J. M. Bayona, and J. Albaiges, "Assessment of fecal sterols and ketones as indicators of urban sewage inputs to coastal waters," *Environmental Science & Technology*, vol. 24, no. 3, pp. 357–363, 1990.
- [20] J. P. A. Rada, A. C. Duarte, P. Pato, A. Cachada, and R. S. Carreira, "Sewage contamination of sediments from two Portuguese Atlantic coastal systems, revealed by fecal sterols," *Marine Pollution Bulletin*, vol. 103, no. 1-2, pp. 319–324, 2016.
- [21] P. D. Nichols, R. Leeming, M. S. Rayner et al., "Comparison of the abundance of the fecal sterol coprostanol and fecal bacterial groups in inner-shelf waters and sediments near Sydney, Australia," *Journal of Chromatography A*, vol. 643, no. 1-2, pp. 189–195, 1993.
- [22] C. C. Martins, B. H. Seyffert, J. A. F. Braun et al., "Input of organic matter in a large south American tropical estuary (paranagua estuarine system, Brazil) indicated by sedimentary sterols and multivariate statistical approach," *Journal of the Brazilian Chemical Society*, vol. 22, no. 8, pp. 1341–1585, 2011.
- [23] J. K. Volkman, G. Eglinton, and E. D. S. Corner, "Sterols and fatty acids of the marine diatom *Biddulphia sinensis*," *Phytochemistry*, vol. 19, no. 8, pp. 1809–1813, 1980.
- [24] J. D. Weete, A. Maritza, B. Meredith et al., "Phylogenetic distribution of fungal sterols," *PLoS One*, vol. 5, no. 5, Article ID e10899, 2010.
- [25] P. H. Bergell, L. J. Goda, R. P. Evershed et al., "The study of molecular markers of human activity—the use of coprostanol in the soil as an indicator of human fecal material," *Journal of Archaeological Science*, vol. 21, no. 5, pp. 619–632, 1994.
- [26] T. Saeed, F. Al-Shimmari, A. Al-Mutairi, and H. Abdullah, "Spatial assessment of the sewage contamination of Kuwait's marine areas," *Marine Pollution Bulletin*, vol. 94, no. 1-2, pp. 307–317, 2015.
- [27] I. Tolosa, M. Mesa, and C. M. Alonso-Hernandez, "Steroid markers to assess sewage and other sources of organic contaminants in surface sediments of Cienfuegos Bay, Cuba," *Marine Pollution Bulletin*, vol. 86, no. 1-2, pp. 84–90, 2014.
- [28] C. C. Martins, S. N. Aguiar, E. Wisnieski, L. M. M. Ceschim, R. C. L. Figueira, and R. C. Montone, "Baseline concentrations of faecal sterols and assessment of sewage input into different inlets of Admiralty Bay, King George Island, Antarctica," *Marine Pollution Bulletin*, vol. 78, no. 1-2, pp. 218–223, 2014.
- [29] V. Campos, R. Fracácio, L. F. Fraceto, and A. H. Rosa, "Fecal sterols in estuarine sediments as markers of sewage contamination in the Cubatão area, São Paulo, Brazil," *Aquatic Geochemistry*, vol. 18, no. 5, pp. 433–443, 2012.
- [30] D. He, K. Zhang, J. Tang, X. Cui, and Y. Sun, "Using fecal sterols to assess dynamics of sewage input in sediments along a human-impacted river-estuary system in eastern China," *Science of the Total Environment*, vol. 636, pp. 787–797, 2018.
- [31] D. V. McCalley, M. Cooke, and G. Nickless, "Effect of sewage treatment on faecal sterols," *Water Research*, vol. 15, no. 8, pp. 1019–1025, 1981.
- [32] R. H. Pierce and R. C. Brown, "Coprostanol distribution from sewage discharge into Sarasota Bay, Florida," *Bulletin of Environmental Contamination and Toxicology*, vol. 32, no. 1, pp. 75–79, 1984.
- [33] Z. Yang, C. Cheng, X. Tan, R. Cheng, and M. A. Zhong, "Analysis of water environmental capacity of Guanting Reservoir and its upstream basin," *Journal of Arid Land Resources & Environment*, vol. 29, no. 1, pp. 163–168, 2015.
- [34] T. Ye, Z. Guo, Y. Qiao et al., "Remote sensing of water quality monitoring in Guanting Reservoir," *Acta Ecologica Sinica*, vol. 35, no. 7, pp. 2217–2226, 2015.
- [35] J. Li, S. Ren, S. Han, B. Lei, and N. Li, "Identification of thyroid-receptor antagonists in water from the Guanting reservoir, Beijing, China," *Archives of Environmental Contamination and Toxicology*, vol. 67, no. 1, pp. 68–77, 2014.
- [36] X. T. Wang, S. G. Chu, and X. B. Xu, "Organochlorine pesticide residues in water from Guanting reservoir and Yongding River, China," *Bulletin of Environmental Contamination and Toxicology*, vol. 70, no. 2, pp. 351–358, 2003.
- [37] J. Yang, M. Stokal, C. Kroeze et al., "Nutrient losses to surface waters in Hai He basin: a case study of Guanting reservoir and Baiyangdian lake," *Agricultural Water Management*, vol. 213, pp. 62–75, 2019.

- [38] G. A. Bataglion, H. H. F. Koolen, R. R. Weber et al., "Quantification of sterol and triterpenol biomarkers in sediments of the cananea-iguape estuarine-lagoonal system (Brazil) by UHPLC-MS/MS," *International Journal of Analytical Chemistry*, vol. 2016, Article ID 8361375, 8 pages, 2016.
- [39] X. Yao, J. Lu, Z. Liu, D. Ran, and Y. Huang, "Distribution of sterols and the sources of pollution in surface sediments of Ulungur Lake, Xinjiang," *Water Science and Technology*, vol. 67, no. 10, pp. 2342–2349, 2013.
- [40] I. M. Bujagić, S. Grujić, Z. Jauković, and M. Laušević, "Sterol ratios as a tool for sewage pollution assessment of river sediments in Serbia," *Environmental Pollution*, vol. 213, pp. 76–83, 2016.
- [41] X. Peng, G. Zhang, B. Mai, J. Hu, K. Li, and Z. Wang, "Tracing anthropogenic contamination in the Pearl River estuarine and marine environment of South China Sea using sterols and other organic molecular markers," *Marine Pollution Bulletin*, vol. 50, no. 8, pp. 856–865, 2005.
- [42] J. H. Writer, J. A. Leenheer, L. B. Barber, G. L. Amy, and S. C. Chapra, "Sewage contamination in the upper Mississippi River as measured by the fecal sterol, coprostanol," *Water Research*, vol. 29, no. 6, pp. 1427–1436, 1995.
- [43] L. G. S. M. Cordeiro, R. S. Carreira, and A. L. R. Wagener, "Geochemistry of fecal sterols in a contaminated estuary in southeastern Brazil," *Organic Geochemistry*, vol. 39, no. 8, pp. 1097–1103, 2008.
- [44] R. S. Carreira, A. L. R. Wagener, and J. W. Readman, "Sterols as markers of sewage contamination in a tropical urban estuary (Guanabara Bay, Brazil): space-time variations," *Estuarine, Coastal and Shelf Science*, vol. 60, no. 4, pp. 587–598, 2004.
- [45] R. Leeming, N. Bate, R. Hewlett, and P. D. Nichols, "Discriminating faecal pollution: a case study of stormwater entering Port Phillip Bay, Australia," *Water Science and Technology*, vol. 38, no. 10, pp. 15–22, 1998.
- [46] C. D. C. Martins, G. Fillmann, and R. C. Montone, "Natural and anthropogenic sterols inputs in surface sediments of Patos Lagoon, Brazil," *Journal of the Brazilian Chemical Society*, vol. 18, no. 1, pp. 106–115, 2007.
- [47] S. M. Mudge, M. J. A. F. Bebianno, J. A. East, and L. A. Barreira, "Sterols in the ria formosa lagoon, Portugal," *Water Research*, vol. 33, no. 4, pp. 1038–1048, 1999.
- [48] M. G. de Melo, B. A. da Silva, G. D. S. Costa et al., "Sewage contamination of Amazon streams crossing Manaus (Brazil) by sterol biomarkers," *Environmental Pollution*, vol. 244, no. 1, pp. 818–826, 2019.

Research Article

Campus Sewage Treatment by *Golenkinia* SDEC-16 and Biofuel Production under Monochromic Light

Changliang Nie ^{1,2}, Liqun Jiang,^{1,2} Ze Yu,^{1,2} Zhigang Yang,^{1,2} Qingjie Hou,^{1,2} and Haiyan Pei ^{1,2,3}

¹School of Environmental Science and Engineering, Shandong University, Qingdao 266237, China

²Shandong Provincial Engineering Centre on Environmental Science and Technology, Jinan 250061, China

³State Key Laboratory of Microbial Technology, Shandong University, Qingdao 266237, China

Correspondence should be addressed to Haiyan Pei; haiyanhup@126.com

Received 24 December 2019; Accepted 20 February 2020; Published 19 March 2020

Guest Editor: Lisa Yu

Copyright © 2020 Changliang Nie et al. This is an open access article distributed under the Creative Commons Attribution License, which permits unrestricted use, distribution, and reproduction in any medium, provided the original work is properly cited.

The integration of microalgal cultivation in wastewater can fulfill the dual roles of pollutant degradation and biomass output. Meanwhile, the LED lights with different wavelengths have a great effect on the growth and metabolism of microalgae. In this study, *Golenkinia* SDEC-16, a strain isolated for biofuel production, was evaluated to verify its potentials for campus sewage treatment and lipid accumulation under the red, green, and blue lights. The results indicated that the treated campus sewage met the first grade level in the Chinese pollutant discharge standards for municipal wastewater treatment plants within seven days under both red and blue light. The green light failed to exhibit excellent performance in nutrient removal, but facilitated the lipid synthesis as high as $42.99 \pm 3.48\%$. The increased lipid content was achieved along with low biomass accumulation owing to low effective light utilization, indicating that the green light could be merely used as a stimulus strategy. The red light benefited the photosynthesis of *Golenkinia* SDEC-16, with the maximal biomass concentration of 0.80 ± 0.03 g/L and lipid content of $36.90 \pm 3.62\%$, which can attain the optimal balance between biomass production and lipid synthesis.

1. Introduction

Microalgae act as a powerful biotechnology platform to synthesize valuable products by recovering nutrients from the culture medium [1–4]. Although the idea of biofuel production by using microalgae is not new, it is still being taken seriously, owing to the probability to alleviate global warming and inhibit the escalating price of petroleum [5]. Moreover, the algal biodiesel is an eco-friendly option where microalgae can survive in wastewater and make use of the nutrients [1, 6]. The consumption of nutrients can reduce environmental impacts and fulfill the water reclamation. In addition, the introduced wastewater can lower the requirements of microalgae on additional nutrients and freshwater compared with the conventional biofuel feedstock [7]. The dual roles of wastewater treatment and microalgal cultivation are economical.

To date, a variety of wastewater types, such as brewery wastewater [4], livestock wastewater [8–10], aquaculture sewage [11], and municipal wastewater [12] have been successfully utilized for the microalgal production. Campus sewage is one type of municipal wastewater, and the volume of discharge is vast. Campus sewage contains sufficient nitrogen, phosphorus, and organic substances, which can support microalgae growth and exerts few adverse toxic effects [13]. Given that the diversity of microalgal species, the selection of appropriate species can promote nutrient removal. In addition, the responses to the changes in the culture conditions are dependent on the specific species [1]. There remain the contemporary challenges to effective wastewater treatment and high biomass output.

Previously, we discovered that the *Golenkinia* SDEC-16, under the general culture conditions, exhibited highly

effective nutrient removal, favorable biomass output, and easily harvesting [14]. What is more, there are few relevant studies concerning varying culture conditions in the field of wastewater treatment in comparison with the widely used strains. The follow-up work needs to be carried out to enhance lipid output and maintain the concurrent high nutrient removal efficiency by *Golenkinia* SDEC-16.

Regarding the culture conditions, the monochromic LED lights emerged as an effective strategy to regulate the microalgae, and an appropriate selection of light wavelengths can facilitate the rate of nutrient remediation while descending the expenditure of energy provided by light devices [1]. Specific strains displayed different behaviors in response to the different monochromatic lights. For instance, the red light was found to give the highest growth and nutrient removal in *Chlorella vulgaris* [15]. In contrast, the blue LED light plays an outstanding role in high biomass productivity and favorable fatty acid composition for biofuel production of the green microalgae [16].

Therefore, this motivated us to evaluate the potentials of *Golenkinia* SDEC-16 for campus sewage treatment and biofuel production under the red, green, and blue lights. Our study will shed light on the effects of the monochromic light on the wastewater treatment, biomass, lipids, and fatty acids composition distinctively.

2. Method

2.1. Microalgal Strain. The microalgal strain used in the present work was *Golenkinia* SDEC-16 (GeneBank accession number: KT180320) isolated from a lake in the Quancheng Park, Jinan, Shandong Province, China. Previous cultivations of *Golenkinia* SDEC-16 were performed in the photobioreactors with BG11 liquid medium at $25 \pm 2^\circ\text{C}$ to attain healthy seed cells for further studies.

2.2. Experimental Design. Flasks with 1 L of campus sewage filtered through six layers of gauze were employed to evaluate the characteristics of wastewater treatment under red, green, and blue lights. The flasks were placed under LED lights providing red (660 nm), green (520 nm), and blue (465 nm) with intensities of approximately 1,300 lux with a photoperiod (24:0 h of light: dark period) at $25 \pm 2^\circ\text{C}$ for seven days. Continuous air aeration (1.0 L/min) was provided from an aerator through glass tubes in flasks to prevent cell sedimentation. All of the experiments were conducted in triplicate.

2.3. Nutrient Measurements. Samples were collected every day and filtered by a $0.45 \mu\text{m}$ cellulose nitrate membrane for determining the wastewater nutrients by a UV/Vis spectrophotometer (U-3010, Hitachi Co., Japan) according to the Chinese state standard testing methods [17].

Regarding the total nitrogen (TN), 1 mL of the filtrated sample was digested for 30 mins by alkaline potassium persulfate solution under 121°C and the absorptions at wavelengths of 220 and 275 nm were measured for

calculating nitrogen concentration. As for the ammonium, 1 mL of filtered samples was added with a potassium sodium tartrate solution and Nessler's reagent, and then absorption at 420 nm was read. Regarding the total phosphorus (TP), 5 mL of the filtrated sample was digested by a potassium persulfate solution (5%) under 121°C , then added 1 mL ascorbic acid solution (10%) and 2 mL ammonium molybdate solution following by determining the absorptions at 700 nm. All the concentrations were calculated according to the calibration curve and the tested sample volume. The total organic carbon (TOC) was analyzed by a TOC/TN analyzer (TOC-VCPH, Shimadzu, Japan) with 10 mL of the filtrated sample.

The initial campus wastewater characteristics were as follows: TN 61.23 ± 4.77 mg/L, ammonium 56.38 ± 2.91 mg/L, TP 4.91 ± 0.08 mg/L, and TOC 187.47 ± 6.54 mg/L. The nutrient removal efficiency (NRE) (%) could be expressed as

$$\text{NRE} = \frac{(X_i - X_0)}{\Delta t} \times 100\%, \quad (1)$$

where X_i and X_0 are the nutrient concentrations (mg/L) at the end and beginning of a batch run, respectively, and Δt (d) is the duration of the run.

Fluorescence excitation-emission matrices (EEMs) were acquired using a fluorescence spectrometry (5J2-004, Hitachi, Japan) with a 1 cm quartz cell to indicate organic composition. The spectra of filtrated samples were obtained by scanning the sample based on excitation wavelengths from 220 to 450 nm with 5 nm steps and emission wavelengths from 250 to 550 with 2 nm steps. Moreover, the scanning speed was set at 1,000 nm/min for all of the measurements.

2.4. Biomass Concentration Measurements. The microalgal growth was monitored daily by weighing the dry biomass. A 15 mL volume of microalgae solution was filtered by $0.45 \mu\text{m}$ membrane in order to remove the supernatant and then transferred to a clean and weighed aluminium foil pan, which was then dried to constant mass in a thermostatically controlled oven at 60°C for 24 h. The biomass productivity P_b (mg/L/day) and the specific growth rate μ (d^{-1}) were calculated according to dry biomass by equations (2) and (3):

$$P_b = \frac{X_m - X_0}{\Delta t}, \quad (2)$$

$$\mu = \frac{1}{\Delta t} \ln\left(\frac{X_m}{X_0}\right), \quad (3)$$

where X_m and X_0 are the concentrations of biomass (g/L) at the end and beginning of a batch run, respectively, and Δt (d) is the duration of the run.

2.5. Morphology Observation and Cell Size Measurements. Morphology of the algae strains that survived in campus sewage was observed under an optical microscope (CX31, OLYMPUS, Japan), and the microalgal diameters were

recorded using an inverted fluorescence microscope (Ti-s, Nikon, Japan). The diameter was statistically analyzed by NIS-Elements D 4.20.00 software.

2.6. Lipid Content. The lipid content was measured by solvent extraction and gravimetric method based on a reported method [18]. The harvested microalgae were freeze-dried and then ground to an approximately uniform powder for lipid extraction. Approximately 0.1 g of dry biomass powder was added with 10 mL of chloroform-methanol solution (2 : 1, v/v) in a centrifuge tube. The mixture was treated by ultrasonication (Ultrasonic Cell Crusher SCIENTZ-IIID, China) for 10 min and subsequently centrifuged at 2,000 g for 10 min at 4°C. The supernatant was transferred to a clean and dry 60 mL separatory funnel. The entire extraction process was repeated twice. After the extraction, 4 mL of sodium chloride solution (0.9%) was added into the separatory funnel to separate organic facies from hydrofacies. The mixture was shaken well for 1 min and then allowed to stand for 15 min to stratify. The volume of the lower organic phase solution was measured, and 5 mL of the solution was then transferred to a clean and weighed 10 mL glass tube. The solution in the glass tube was then evaporated under a nitrogen stream and dried in an oven at 60°C to constant mass. The lipid content (LC) was expressed as a fraction of the biomass's dry mass and calculated based on equation (4):

$$LC = \frac{(m_2 - m_1) \times V}{(5 \times m_0)}, \quad (4)$$

where m_0 (g) is the dry biomass's mass, m_1 (g) and m_2 (g) are the masses of the clean glass tube and the tube containing lipid, and V (mL) is the volume of the lower-phase.

Lipid productivity (LP, mg/L/d) was determined according to the following formula:

$$LP = P_b \times LC, \quad (5)$$

where P_b (mg/L/day) is the biomass productivity, LC (%) is the corresponding lipid content.

2.7. Fatty Acid Profile Analysis. The fatty acid composition was analyzed through the GC-MS method as described by [18]. The degree of unsaturation was calculated by fatty acid compositions using

$$ADU = \sum P_i \times N_i, \quad (6)$$

where ADU is the average degree of unsaturation of microalgae lipid, P_i is the mass fraction of each fatty acid component, and N_i is the associated number of carbon-carbon double bonds in each fatty acid component. Furthermore, the predicted properties of biodiesel could be calculated based on the ADU [18].

$$\begin{aligned} \text{Kinematic viscosity} &= -0.6316 \text{ ADU} + 5.2065, & R^2 &= 0.67, \\ \text{specific gravity} &= 0.0055 \text{ ADU} + 0.8726, & R^2 &= 0.66, \\ \text{cloud point} &= -13.356 \text{ ADU} + 19.994, & R^2 &= 0.68, \\ \text{cetane number} &= -6.6684 \text{ ADU} + 62.876, & R^2 &= 0.80, \\ \text{iodine value} &= 74.373 \text{ ADU} + 12.71, & R^2 &= 0.94, \\ \text{higher heating value} &= 1.7601 \text{ ADU} + 38.534, & R^2 &= 0.38. \end{aligned} \quad (7)$$

3. Results

3.1. Effects of Specific Lights on Wastewater Treatment. Campus sewage is rich in nutrients (e.g., organic matter, nitrogen, and phosphorus), which would pose a threat to the environment if it was not well treated before discharging to the environment. Figure 1 quantitatively depicts the remediation of campus sewage by *Golenkinia* SDEC-16 under the different monochromatic LED lights, in which the red and blue lights gave productive removal efficiencies of total nitrogen, ammonium, and total phosphorus. In particular, the red light exhibited the highest nutrient removal efficiency, with the lowest residues of 7.77 ± 0.98 and 3.31 ± 0.85 mg/L in total nitrogen and ammonium. Inferior to the red light, the total nitrogen and ammonium reduced to 9.17 ± 1.65 and 5.41 ± 0.66 mg/L under the blue light. In contrast, the green light exhibited a poor behavior of nitrogen removal, with the high residue values of 19.13 ± 1.35 and 16.73 ± 0.4 mg/L in total nitrogen and ammonium. Similar to the case of nitrogen degradation, the most effective total phosphorus removal was found upon exposure to the red and blue lights, with the values of 0.39 ± 0.06 and 0.11 ± 0.01 mg/L. The residue value of total phosphorus was 1.93 ± 0.13 mg/L under the green light.

As depicted in Figure 2, the initial total organic concentration in campus sewage was 187.47 ± 6.54 mg/L. The total organic carbon concentration fast decreased within the first two days, and the decreasing trend began to slow down and stabilized as time went on. The removal efficiencies achieved 43.46%, 40.71%, and 47.43%, corresponding to the red, green, and blue lights, respectively.

The present work also evaluated their makeup based on EEMs. The fluorescence EEMs of campus wastewater under the different monochromatic LED lights manifests in Figure 2. The raw campus sewage has a peak in fluorescence at an Ex/Em pairing of around 280/340 nm, indicating the existence of protein-like substances [19]. As time went by, the fluorescence intensity of the substances weakened and moved its position on the EEMs, indicating that the degradation of organic substances.

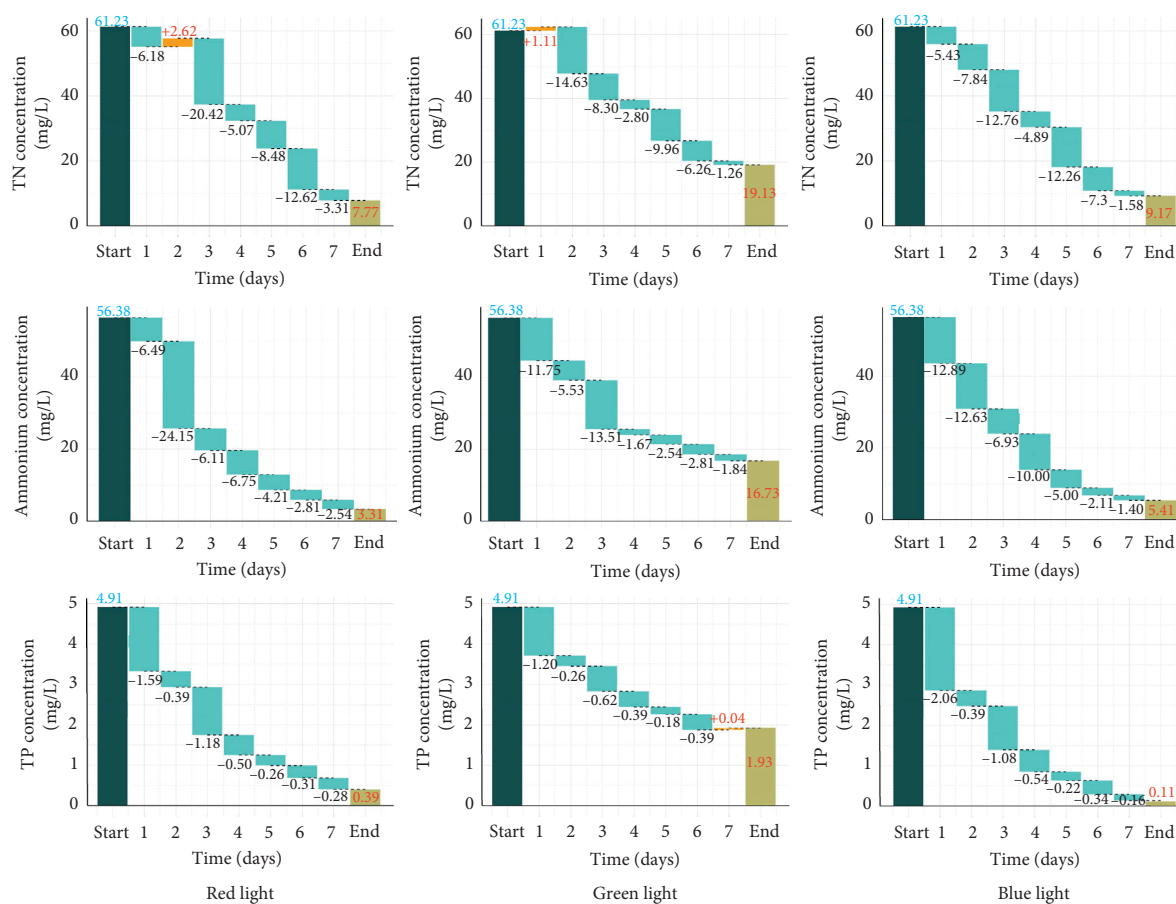


FIGURE 1: Degradation of campus sewage by *Golenkinia* SDEC-16 cultured the under red, green, and blue lights. TN represents the total nitrogen concentration; TP represents the total phosphorus concentration.

3.2. *Effects of the Different Monochromatic Lights on Biomass and Lipid Production.* *Golenkinia* SDEC-16 manifested the promising characteristics as an oleaginous candidate for bioenergy production in previous work [14]. To achieve the goal of economic production, the application into wastewater treatment coupling with biofuel production is a favorable choice. Given that the achievement of the favorable wastewater treatment, seven days was determined as the cultivation period for *Golenkinia* SDEC-16.

As shown in Figure 3, the biomass concentration in *Golenkinia* SDEC-16 vigorously grew upon exposure to the red and blue lights than the green light. The highest biomass concentration and productivity occurred under the red light, with the values of 0.80 ± 0.03 g/L and 101.27 mg/L/d. The blue light leads *Golenkinia* SDEC-16 to attain a maximal biomass concentration of 0.75 ± 0.04 g/L, average biomass productivity of 93.95 mg/L/d, and a specific growth rate of 0.29 d^{-1} . The low biomass concentration in *Golenkinia* SDEC-16 occurred under the green light, with a maximal biomass concentration of 0.55 ± 0.09 g/L, average biomass productivity of 65.60 mg/L/d, and a specific growth rate of 0.25 d^{-1} .

The lipid contents in *Golenkinia* SDEC-16 are depicted in Figure 3. The highest lipid content was attained under the green light, with a value of $42.99 \pm 3.48\%$, followed by

$36.90 \pm 3.62\%$ under the red light, and $27.93 \pm 1.95\%$ under the blue light. However, the highest lipid productivity was observed under the red light illumination (37.37 mg/L/d), benefiting from rapid biomass growth. Upon exposure to the blue light, *Golenkinia* SDEC-16 grew slower than that under the red light and accumulated less lipid in comparison to another two monochromatic LED lights, resulting in low lipid productivity. Moreover, the red light achieved superior performance about nutrient removal. With that in mind, it would be advisable to apply red light to wastewater treatment as well as biofuel production.

3.3. *Effects of Specific Lights on Fatty Acids Profile.* The fatty acid composition of the lipid in *Golenkinia* SDEC-16 in response to the monochromatic light is shown in Figure 4. The palmitic acid (C 16:0), oleic acid (C 18:1), and linoleic acid (C 18:2) dominated the compositions and were affected by the changes in light wavelengths. The palmitic acid (C 16:0) compositions were weakly affected by changes in light wavelengths, with values of 26.55%, 24.26%, and 25.77%, corresponding to the blue, red, and green lights, respectively. The red light promoted oleic acid (C 18:1) accumulation, with the highest value of 25.67%, followed by 20.54% under the green light and 18.76% under the blue light. The linoleic

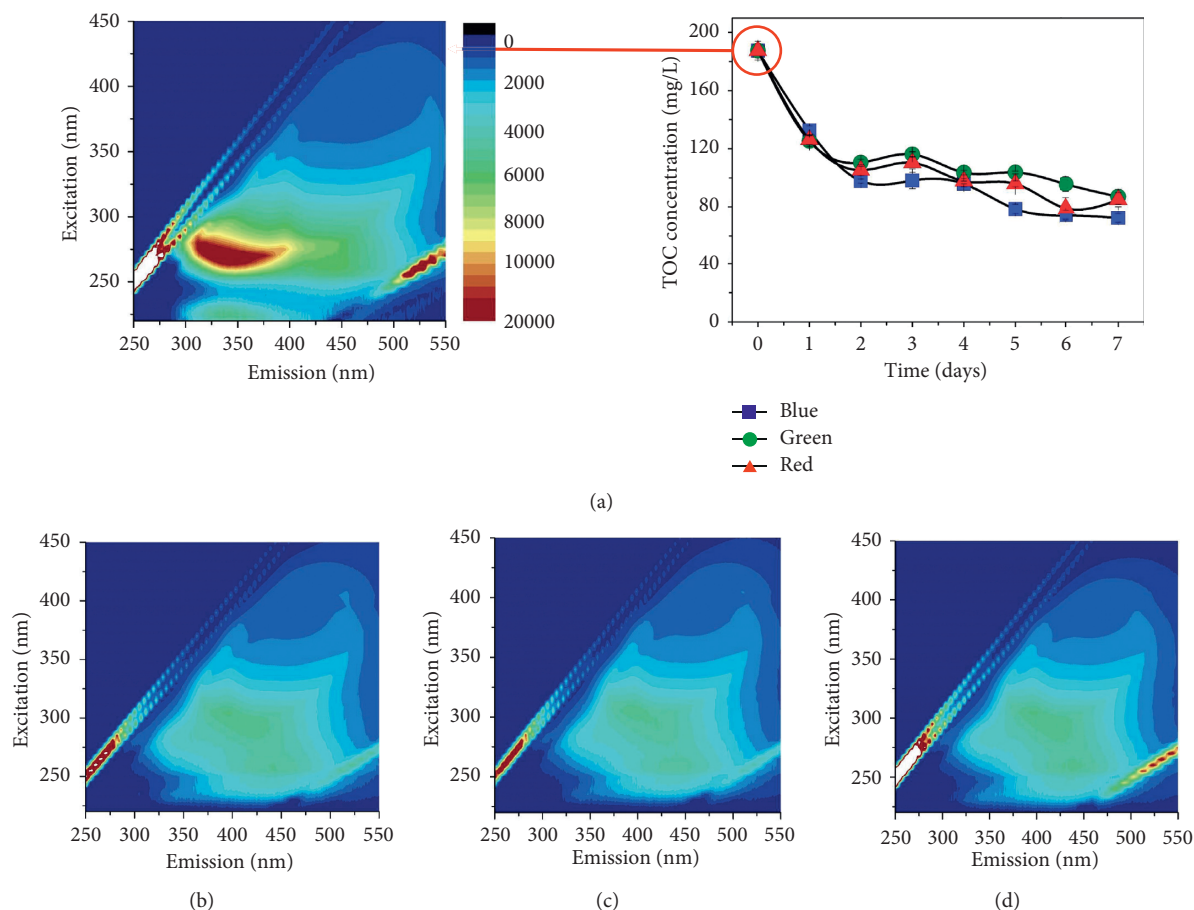


FIGURE 2: Total organic carbon (TOC) variation under irradiation with red, green, and blue lights and variation of EEMs following cultivation: initial EEM for campus wastewater (a); and EEMs on the 7th day, following irradiation with (b) red light, (c) green light, and (d) blue light.

acid (C 18:2) achieved 29.45%, 33.04%, and 32.18%, corresponding to the blue, red, and green lights, respectively. Linolenic acid (C 18:3) was only accumulated by the blue light, which accounted for 10.45%, and no observation under the green and red lights.

The low contents of palmitic acid gave rise to less than 30% of saturated fatty acids in *Golenkinia* SDEC-16 upon the exposure to the monochromatic lights. Similar to the contents of saturated fatty acids, the monounsaturated contents took up less than 30%. The polyunsaturated fatty acids take up 40.26%, 51.28%, and 32.18% of the fatty acid compositions upon the exposure to the red, blue, and green lights, respectively. The changes in the unsaturated fatty acids would affect the property of biodiesel.

3.4. Morphology of *Golenkinia* SDEC-16. The diameters were recorded at the end of the cultivation to characterize the morphology of *Golenkinia* SDEC-16 under three monochromatic LED lights. The results manifested that larger cell sizes occurred under the blue light than red and green lights, according to Figure 5. Upon the exposure to the blue light, the mean, maximum, and minimum values of the diameters were 17.65 μm , 29.8 μm , and 9.76 μm , respectively.

Smaller cell sizes occurred under the red light, with a mean of the diameter of 13.64 μm and the green light, with a mean of the diameter of 13.95 μm .

4. Discussion

In terms of nitrogen, ammonium and nitrate were the primary nitrogen sources for most plants, and both could be effectively used by microalgae. In general, the nitrate and ammonium are assimilated via different metabolic processes in microalgal cells [20]. The ammonium utilization is given priority to be taken up by microalgae on account of consuming less energy compared with other nitrogen sources [21]. The ammonium would be employed to synthesize glutamine directly with the help of ATP and enzyme. Elevated photosynthetic activity under the red and blue light would generate more electrons and ATP that would facilitate ammonium consumption.

The residual total nitrogen concentrations upon exposure to the red and blue lights met the first grade level (less than 15 mg/L) in the pollutant discharge standard for municipal wastewater treatment plants (GB T18918-2002, China). Similar to the case of the total nitrogen, the residue of ammonium concentration also met the first grade level

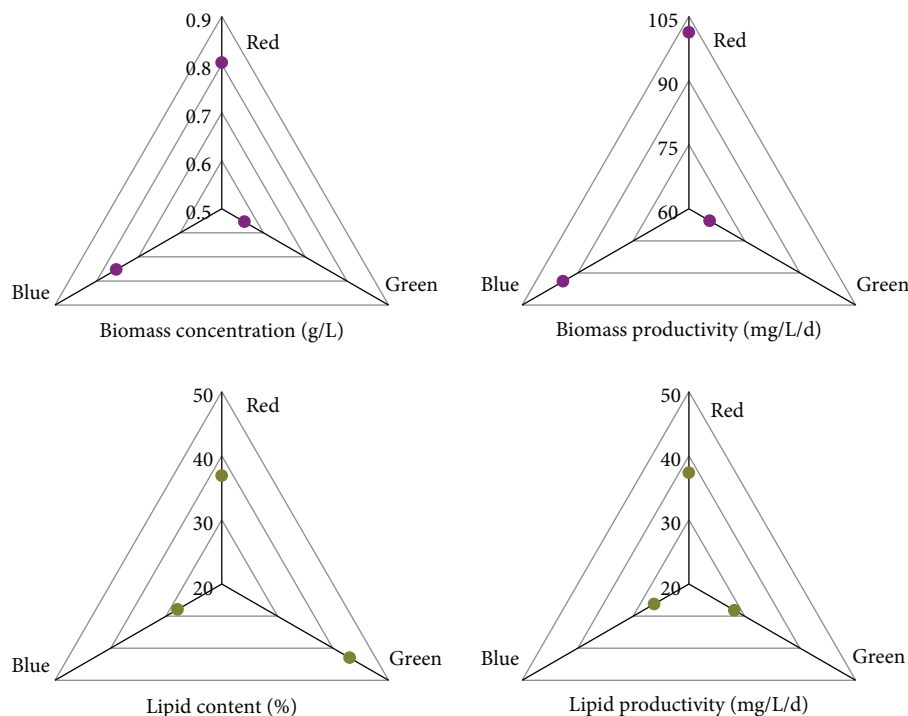


FIGURE 3: Biomass concentration and lipid contents of *Golenkinia* SDEC-16 on day 7 under red, green and blue lights.

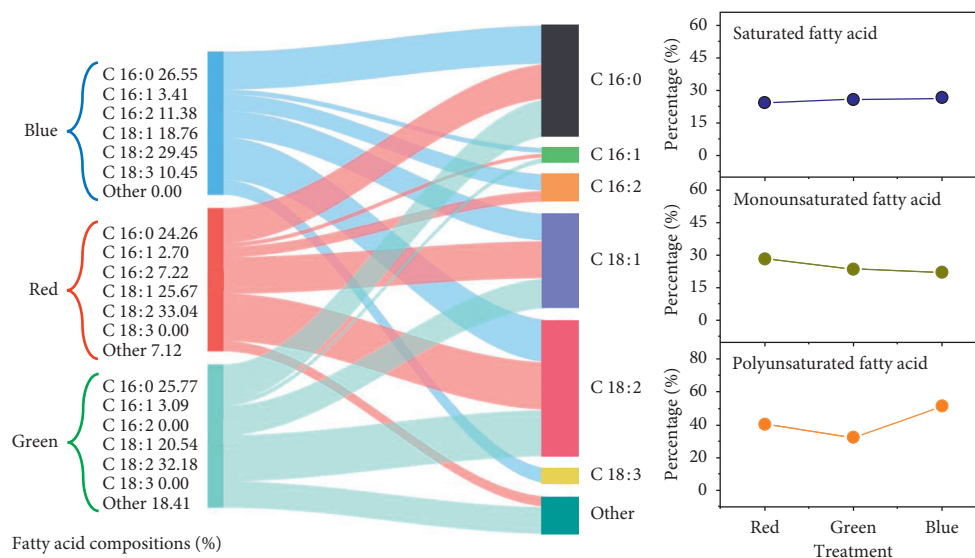


FIGURE 4: Fatty acid compositions of *Golenkinia* SDEC-16 cultivated under red, green and blue lights.

(less than 5 mg/L) in the discharge standard of pollutants for municipal wastewater treatment plants (GB T18918-2002, China) when the algae grew under the red and blue lights. In contrast, the residual total nitrogen concentration under the green light failed to achieve a good performance, which is higher than the standard value of the first grade level in the pollutant discharge standard for municipal wastewater treatment plants (GB T18918-2002, China).

Phosphorus is another vital element in microalgal metabolism and cell growth by generating ATP through phosphorylation along with adenosine diphosphate (ADP

[22]. It is commonly known that phosphorus removal efficiencies (>90%) were reported in other studies using municipal wastewater [23, 24], suggesting that *Golenkinia* SDEC-16 has a high phosphorus uptake capacity with the assistance of the red and blue lights. It is reasonable to conclude that the red and blue lights validated favorable total phosphorus removal efficiency and met the first grade level (0.5 mg/L) in the discharge standard of pollutants for municipal wastewater treatment plants.

The remaining total organic carbon concentration was still high, owing to part of the biodegradable constituents of

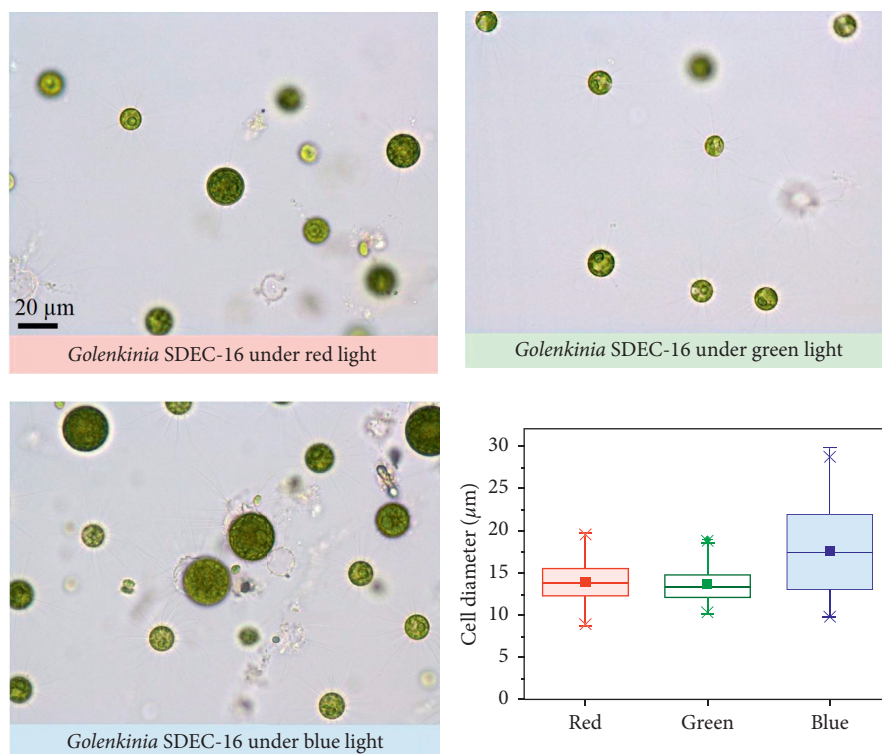


FIGURE 5: Cell sizes of *Golenkinia* SDEC-16 grown under three lights.

the effluent that could be consumed by microalgae [25]. To satisfy the ultimate discharge standard for organic waste, further intensive treatment through other wastewater treatment units would be well advised. Microalgae were able to exert organic matters, or the natural materials outflow from the dead cells, which lead to the appearance of humic or fulvic-like substances. No differences in EEMs were observed for growth under the three respective light sources, demonstrating that they had little effects on the degradation of organic substances.

In terms of the biomass concentration, it is acknowledged that the chlorophylls possess two major absorption bands at (600–700 nm) and (400–500 nm) [26]. That is the reason to explain microalgal flourishing occurred upon exposure to the red and blue light. In the present work, the red light plays an active role in promoting biomass concentration in *Golenkinia* SDEC-16. Despite, some studies concluded strains, such as *Nannochloropsis oceanica*, *Nannochloropsis salina*, and *Nannochloropsis oculata*, preferred blue light, indicating the light utilization is species-dependent. The concurrent conclusion displayed that microalgae failed to thrive under the green light, owing to ineffective energy utilization [27].

The effects on lipid synthesis by different monochromatic lights were interesting as there is not a clear general rule on the microalgal lipid synthesis. For example, *Chlorella* spp. showed the most desirable preference of lipid accumulation under blue light other than red or white light source [28]. In contrast, Ra et al. found that the green light was able to increase the lipid content of *Nannochloropsis* sp [27]. There is another study reported on the same genus of

Nannochloropsis sp that attained the highest lipid content under blue light [29]. The most top lipid content in *Golenkinia* SDEC-16 was found under the green light. It can be ascribed to a slow growth rate, which is in favor of lipid accumulation [30]. For the rewarding lipid output, we still need to consider the biomass. Retrospectively, the red light would be well advised to be applied to wastewater treatment as well as biofuel production owing to the highest lipid productivity.

The fatty acid compositions responded to the changes in wavelengths, which exerted effects on their biofuel property. Table 1 provides parameters of biodiesel based on the fatty acid unsaturated degree of the present species. There are no significant changes in biodiesel properties, except for iodine number and cloud point. The iodine number is 78.15 under the green light, which is lower than 93.69 and 89.93 under the red and blue lights, respectively. The iodine value is directly affected by the unsaturation degree of fatty acids, and the value increases with the increase in the number of double bonds [33]. The oil tends to polymerize and results in engine deposition if the iodine value increased [33].

In contrast, the cloud point is 8.19 under the green light, which is higher than 5.40 and 6.07 under the red and blue lights, respectively. Cloud point value is closely affected by the solid phase consisting mainly of the saturated methyl esters at the equilibrium point, and there are no strict specifications of the cloud point [34]. Fortunately, the standard of biodiesel still satisfied the level made by the U.S.A and Europe, indicating the application of biodiesel.

The present work also evaluated the effects of monochromatic LED lights on the morphology of *Golenkinia*

TABLE 1: Biodiesel properties of *Golenkinia* SDEC-16 cultured under the red, green, and blue lights.

Biodiesel property	Red	Green	Blue	U.S.A. (ASTM D6751-08) [31]	Europe (EN 14214) [32]
Kinematic viscosity	4.52	4.65	4.55	1.9–6	3.5–5
Higher heating value	40.49	40.12	40.40		
Cetane number	55.71	57.11	56.05	Min 47	Min 51
Specific gravity	0.88	0.88	0.88	0.85–0.90	
Iodine number	93.69	78.15	89.93		Max 120
Cloud point	5.40	8.19	6.07		

Units: kinematic viscosity, mm²/s (at 40°C); specific gravity, kg/L; cloud point, °C; iodine value, g iodine/100 g; higher heating value: MJ/kg.

SDEC-16. Similar to the observations in the reported articles, the red light tends to make microalgal cells smaller [35], while the blue light would cause the microalgal cells larger [36]. That would be explained by the differential rate of cell divisions or cell cycle progression [37]. Smaller cells were produced under the red light, owing to the early autospore release. Whereas blue light delayed the division in microalgae, resulting in producing larger size and fewer numbers of autospores [37].

5. Conclusion

Microalgal biofuel production coupling with wastewater is a promising strategy. Results revealed that campus sewage treatment under both red and blue lights was able to meet the first grade level in the Chinese pollutant discharge standards for municipal wastewater treatment plants within seven days. Regarding biofuel production, the green light facilitated lipid synthesis as high as $42.99 \pm 3.48\%$ but with low biomass concentration (0.55 ± 0.09 g/L). The *Golenkinia* SDEC-16 achieved the maximal biomass concentration, with a value of 0.80 ± 0.03 g/L as well as a lipid content of $36.90 \pm 3.62\%$, which is the promising light spectrum to attain a balance between biomass production and lipid synthesis.

Data Availability

The data used to support the findings of this study are included in the article

Conflicts of Interest

The authors declare that they have no conflicts of interest.

Acknowledgments

This research was funded by the National Science Fund for Excellent Young Scholars (51322811).

References

- [1] M. Kube, B. Jefferson, L. Fan, and F. Roddick, "The impact of wastewater characteristics, algal species selection and immobilisation on simultaneous nitrogen and phosphorus removal," *Algal Research*, vol. 31, pp. 478–488, 2018.
- [2] X. Wei and D. Jie, "Optimization to hydrothermal liquefaction of low lipid content microalgae *spirulina* sp. using response surface methodology," *Journal of Chemistry*, vol. 2018, Article ID 2041812, 9 pages, 2018.
- [3] A. Guldhe, S. Kumari, L. Ramanna et al., "Prospects, recent advancements and challenges of different wastewater streams for microalgal cultivation," *Journal of Environmental Management*, vol. 203, pp. 299–315, 2017.
- [4] D. K. Amenorfenyo, X. Huang, Y. Zhang et al., "Microalgae brewery wastewater treatment: potentials, benefits and the challenges," *International Journal of Environmental Research and Public Health*, vol. 16, no. 11, p. 1910, 2019.
- [5] S. Hena, H. Znad, K. T. Heong, and S. Judd, "Dairy farm wastewater treatment and lipid accumulation by *Arthrospira platensis*," *Water Research*, vol. 128, pp. 267–277, 2018.
- [6] J. K. Pittman, A. P. Dean, and O. Osundeko, "The potential of sustainable algal biofuel production using wastewater resources," *Bioresource Technology*, vol. 102, no. 1, pp. 17–25, 2011.
- [7] Y. Chisti, "Biodiesel from microalgae," *Biotechnology Advances*, vol. 25, no. 3, pp. 294–306, 2007.
- [8] H. Zheng, X. Wu, G. Zou, T. Zhou, Y. Liu, and R. Ruan, "Cultivation of *Chlorella vulgaris* in manure-free piggery wastewater with high-strength ammonium for nutrients removal and biomass production: effect of ammonium concentration, carbon/nitrogen ratio and pH," *Bioresource Technology*, vol. 273, pp. 203–211, 2019.
- [9] L. Luo, X. Lin, F. Zeng, S. Luo, Z. Chen, and G. Tian, "Performance of a novel photobioreactor for nutrient removal from piggery biogas slurry: operation parameters, microbial diversity and nutrient recovery potential," *Bioresource Technology*, vol. 272, pp. 421–432, 2019.
- [10] W. Zhou, Z. Wang, J. Xu, and L. Ma, "Cultivation of microalgae *Chlorella zofingiensis* on municipal wastewater and biogas slurry towards bioenergy," *Journal of Bioscience and Bioengineering*, vol. 126, no. 5, pp. 644–648, 2018.
- [11] F. Gao, Y.-Y. Peng, C. Li et al., "Simultaneous nutrient removal and biomass/lipid production by *Chlorella* sp. in seafood processing wastewater," *Science of The Total Environment*, vol. 640–641, pp. 943–953, 2018.
- [12] F. Gao, W. Cui, J.-P. Xu, C. Li, W.-H. Jin, and H.-L. Yang, "Lipid accumulation properties of *Chlorella vulgaris* and *Scenedesmus obliquus* in membrane photobioreactor (MPBR) fed with secondary effluent from municipal wastewater treatment plant," *Renewable Energy*, vol. 136, pp. 671–676, 2019.
- [13] L. Han, H. Pei, W. Hu, F. Han, M. Song, and S. Zhang, "Nutrient removal and lipid accumulation properties of newly isolated microalgal strains," *Bioresource Technology*, vol. 165, pp. 38–41, 2014.
- [14] C. Nie, H. Pei, L. Jiang, J. Cheng, and F. Han, "Growth of large-cell and easily-sedimentation microalgae *Golenkinia* SDEC-16 for biofuel production and campus sewage treatment," *Renewable Energy*, vol. 122, pp. 517–525, 2018.

- [15] K. C. Filippino, M. R. Mulholland, and C. B. Bott, "Phycoremediation strategies for rapid tertiary nutrient removal in a waste stream," *Algal Research*, vol. 11, pp. 125–133, 2015.
- [16] Y. Zhong, P. Jin, and J. J. Cheng, "A comprehensive comparable study of the physiological properties of four microalgal species under different light wavelength conditions," *Planta*, vol. 248, no. 2, pp. 489–498, 2018.
- [17] State Environmental Protection Administration, *Monitoring Method of Water and Wastewater*, China Environmental Science Press, vol. 105, pp. 246–248, Beijing, China, 4th edition, 2002.
- [18] M. Song, H. Pei, W. Hu, and G. Ma, "Evaluation of the potential of 10 microalgal strains for biodiesel production," *Bioresource Technology*, vol. 141, pp. 245–251, 2013.
- [19] W. Chen, P. Westerhoff, J. A. Leenheer, and K. Booksh, "Fluorescence excitation–emission matrix regional integration to quantify spectra for dissolved organic matter," *Environmental Science & Technology*, vol. 37, no. 24, pp. 5701–5710, 2003.
- [20] G. Markou, D. Vandamme, and K. Muylaert, "Microalgal and cyanobacterial cultivation: the supply of nutrients," *Water Research*, vol. 65, pp. 186–202, 2014.
- [21] T. Cai, S. Y. Park, and Y. Li, "Nutrient recovery from wastewater streams by microalgae: status and prospects," *Renewable and Sustainable Energy Reviews*, vol. 19, pp. 360–369, 2013.
- [22] M. E. Martínez, J. M. Jiménez, and F. El Yousfi, "Influence of phosphorus concentration and temperature on growth and phosphorus uptake by the microalga *Scenedesmus obliquus*," *Bioresource Technology*, vol. 67, no. 3, pp. 233–240, 1999.
- [23] Z. Arbib, J. Ruiz, P. Álvarez-Díaz, C. Garrido-Pérez, and J. A. Perales, "Capability of different microalgae species for phycoremediation processes: wastewater tertiary treatment, CO₂ bio-fixation and low cost biofuels production," *Water Research*, vol. 49, pp. 465–474, 2014.
- [24] K. Tuantet, H. Temmink, G. Zeeman, M. Janssen, R. H. Wijffels, and C. J. N. Buisman, "Nutrient removal and microalgal biomass production on urine in a short light-path photobioreactor," *Water Research*, vol. 55, pp. 162–174, 2014.
- [25] Q.-H. Shen, J.-W. Jiang, L.-P. Chen, L.-H. Cheng, X.-H. Xu, and H.-L. Chen, "Effect of carbon source on biomass growth and nutrients removal of *Scenedesmus obliquus* for wastewater advanced treatment and lipid production," *Bioresource Technology*, vol. 190, pp. 257–263, 2015.
- [26] A. Richmond, "Handbook of microalgal culture: biotechnology and applied phycology," in *Photosynthesis in Microalgae*, J. Masojidek, M. Koblizek, and G. Torzillo, Eds., pp. 20–39 Blackwell Publishers, Hoboken, NJ, USA, 2004.
- [27] C.-H. Ra, C.-H. Kang, J.-H. Jung, G.-T. Jeong, and S.-K. Kim, "Effects of light-emitting diodes (LEDs) on the accumulation of lipid content using a two-phase culture process with three microalgae," *Bioresource Technology*, vol. 212, pp. 254–261, 2016.
- [28] M. Izadpanah, R. Gheshlaghi, M. A. Mahdavi, and A. Elkamel, "Effect of light spectrum on isolation of microalgae from urban wastewater and growth characteristics of subsequent cultivation of the isolated species," *Algal Research*, vol. 29, pp. 154–158, 2018.
- [29] A. Vadiveloo, N. R. Moheimani, J. J. Cosgrove, P. A. Bahri, and D. Parlevliet, "Effect of different light spectra on the growth and productivity of acclimated *Nannochloropsis* sp. (*Eustigmatophyceae*)," *Algal Research*, vol. 8, pp. 121–127, 2015.
- [30] R. Huerlimann, R. de Nys, and K. Heimann, "Growth, lipid content, productivity, and fatty acid composition of tropical microalgae for scale-up production," *Biotechnology and Bioengineering*, vol. 107, no. 2, pp. 245–257, 2010.
- [31] American Society for Testing and Materials (ASTM), *Standard D6751 Standard Specification for Biodiesel Fuel Blend Stock (B100) for Middle Distillate Fuels*, ASTM, West Conshohocken, PA, USA, 2009.
- [32] European Committee for Standardization (CEN), *Standard EN 14214 Automotive Fuels Diesel Fatty Acid Methyl Esters (FAMEs) Requirements and Test Methods*, CEN, Brussels, Belgium, 2008.
- [33] G. Knothe, "Fuel properties of highly polyunsaturated fatty acid methyl esters. Prediction of fuel properties of algal biodiesel," *Energy & Fuels*, vol. 26, no. 8, pp. 5265–5273, 2012.
- [34] H. Imahara, E. Minami, and S. Saka, "Thermodynamic study on cloud point of biodiesel with its fatty acid composition," *Fuel*, vol. 85, no. 12–13, pp. 1666–1670, 2006.
- [35] C.-G. Lee and B. Palsson, "High-density algal photobioreactors using light-emitting diodes," *Biotechnology and Bioengineering*, vol. 44, no. 10, pp. 1161–1167, 1994.
- [36] P. Münzner and J. Voigt, "Blue light regulation of cell division in *Chlamydomonas reinhardtii*," *Plant Physiology*, vol. 99, no. 4, pp. 1370–1375, 1992.
- [37] D. G. Kim, C. Lee, S.-M. Park, and Y.-E. Choi, "Manipulation of light wavelength at appropriate growth stage to enhance biomass productivity and fatty acid methyl ester yield using *Chlorella vulgaris*," *Bioresource Technology*, vol. 159, pp. 240–248, 2014.

Research Article

Ranking Ecological Risk of Metals to Freshwater Organisms in Lake Taihu, China

Qi Wang ¹, Yalin Du ¹, Fuhong Sun ², Xinmiao Deng ¹ and Hong Chang ¹

¹Beijing Key Lab for Source Control Technology of Water Pollution, College of Environmental Sciences & Engineering, Beijing Forestry University, Beijing 100083, China

²State Key Laboratory of Environmental Criteria and Risk Assessment, Chinese Research Academy of Environmental Sciences, Beijing 100012, China

Correspondence should be addressed to Hong Chang; changh@bjfu.edu.cn

Received 27 December 2019; Accepted 15 February 2020; Published 9 March 2020

Guest Editor: Yihua Xiao

Copyright © 2020 Qi Wang et al. This is an open access article distributed under the Creative Commons Attribution License, which permits unrestricted use, distribution, and reproduction in any medium, provided the original work is properly cited.

Due to the persistence and the high toxicity of metals to many aquatic organisms, metals in aquatic ecosystems have attracted considerable attention. The objective of the present study was to rank metals in Lake Taihu based on the threat they pose to aquatic organisms. The method involved the assessment of the risks of metals to native aquatic organisms and the potential influence of concentration distributions. Both quotient and probabilistic methods were used to rank the risks of arsenic, cadmium, chromium, copper (Cu), mercury, manganese, nickel (Ni), lead, and zinc (Zn). Based on the probabilistic method, Cu, Ni, and Zn were the metals of great concern, with Cu posing the highest risk.

1. Introduction

With increasing urbanization and industrial development, large quantities of pollutants are discharged into aquatic environments, which, in turn, degrade wildlife habitats [1]. Therefore, a key focus of watershed management is the determination of the chemicals that pose high risks for aquatic organisms. Exposure of humans to metals is a major concern in China and globally due to their widespread occurrence and potential adverse health effects [2–4]. Metals are also highly toxic to numerous aquatic organisms, and they have attracted the attention of many researchers [5]. Several studies have demonstrated that metals pose the greatest risk to aquatic ecosystems. Johnson et al. [6] assessed the relative risks of 29 metals and organic pollutants to aquatic organisms in the Bohai region and the Yangtze and Pearl Rivers of China and found that the highest risks to aquatic ecosystems were from copper (Cu), followed by zinc (Zn) and iron (Fe). The authors also analyzed the relative risks of 71 chemicals in the UK, and the highest relative risk was associated with Cu, aluminium (Al), and Zn although at lower risk levels in [7].

Lake Taihu is China's third largest freshwater lake. Severe deterioration in species diversity and abundance has been observed in Lake Taihu, which has been attributed to habitat loss and chemical pollution [8]. Therefore, it is critical to investigate which group of chemicals should be prioritized in management efforts by identifying the chemicals posing the greatest risk to aquatic ecosystems.

Considering that previous studies have reported higher risks of metals to aquatic organisms than organic pollutants, the objective of the present study was to rank metals in the water phase of Lake Taihu based on risk to aquatic organisms. Song et al. [1] assessed the risks of metals in the surface water in the Yellow River Delta using the hazard quotient method, while Donnachie et al. [9, 10] evaluated the relative risks of metals and some organic chemicals based on proximity of the median exposure and toxicity concentrations. Although there is no perfect system, both methods are simple and transparent. However, they do not take into account spatial distribution of metal pollution and regional distributions of aquatic organisms [11, 12]. Here, we conducted an assessment of the risks of metals to native aquatic organisms in Lake Taihu, China.

2. Methods

2.1. Environmental Concentration Collection. In the present study, we searched for relevant publications using the keywords of “metals” and “taihu” and extracted available data for the following metals: “arsenic (As),” “cadmium (Cd),” “chromium (Cr),” “Cu,” “mercury (Hg),” “manganese (Mn),” “nickel (Ni),” “lead (Pb),” and “Zn.” Studies and literature that adopted inductively coupled mass spectrometry for instrumental analyses were considered. A log-normal distribution was assumed for metal concentrations, which has been adopted widely. Therefore, to convert the mean (m) and standard deviation (v) to the geometric mean (GM: e^{μ}) and geometric standard deviation (GSD: e^{σ}), the following equations were used:

$$\mu = \log\left(\frac{m^2}{\sqrt{v^2 + m^2}}\right), \quad (1)$$

$$\sigma = \sqrt{\log\left(\frac{v^2}{m^2 + 1}\right)}. \quad (2)$$

In the present study, only the metal concentration data reported in the freshwater Lake Taihu were obtained. Data from the rivers flowing into the lake, which sometimes received high amounts of polluted discharge from sewage runoff, industrial effluent, and agricultural wastewater, etc., were not included in the present study. The collected data included total water concentration measurements reported in English and in Chinese publications. English publications were obtained from the Web of Science, while the Chinese publications were mainly from the CNKI databases, in which almost all the Chinese journals, master thesis, and PhD dissertations are deposited. The period for review was from 2009 to 2019. Considering that most literature focuses on Lake Taihu hot spots such as Meiliang bay and Gonghu bay, the concentrations obtained by averaging all the data could be biased. Therefore, we divided Lake Taihu into the following seven common regions (Figure 1): Zhushan bay (area 1, Figure 1), Meiliang bay (area 2), Gonghu (area 3), middle part (area 4), southern part (area 5), and southeastern part (area 6). In the case of some literature that did not indicate sampling sites, the metal concentrations were considered as data for the entire lake (area 7). The concentrations below the limits of detection were also included by reporting them as LOD/sqrt(2).

2.2. Toxicity Data Collection. The ecotoxicity database (EOCTOX, <https://cfpub.epa.gov/ecotox/search.cfm>) by the US EPA was used as the major source of information on metal toxicity data. First, toxicity data for each metal for all freshwater species were extracted from the database. The search terms included freshwater, aquatic organisms, endpoints reflected by mortality, growth inhibition, and survival rates and reproductive rates of the species. The toxicity indices included predicted no effect concentration (PNEC), no observed effect concentration (NOEC), and maximum acceptable toxicant concentration (MATC). In the present

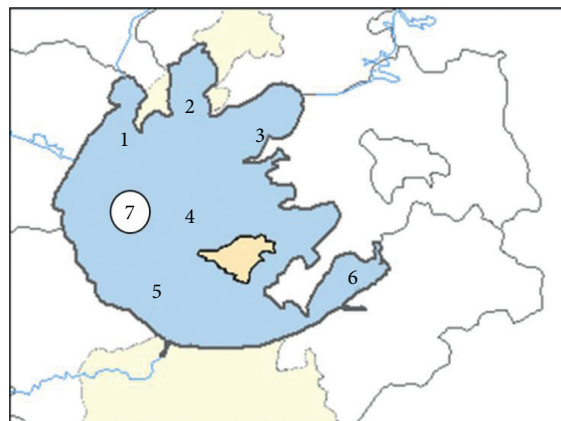


FIGURE 1: Spatial zoning in Lake Taihu. Area 1: Zhushan bay; area 2: Meiliang bay; area 3: Gonghu; area 4: middle part; area 5: south part; area 6: southeast part; area 7: the whole lake.

study, we placed an emphasis on NOEC toxicity indicators [13], and in its absence, LOEC and MATC were used as alternatives:

$$\text{NOEC} = \frac{\text{LOEC}}{2}, \quad (3)$$

$$\text{MATC} = \frac{\text{NOEC}}{\text{SQRT}(2)}. \quad (4)$$

Afterward, the toxicity data were selected for species relevant to Lake Taihu. Table 1 lists the Lake Taihu relevant species considered in this study, and they include fish, benthos, zooplanktons, phytoplanktons, and aquatic plants [14–21]. Finally, for each metal, the NOEC for an individual organism was assumed to be the GM for all eligible data for a specific organism. When multiple data were available for specific species, and the GM for all available NOECs for the species was adopted.

2.3. Risk Estimation. A two-tier approach was applied to characterize the ecological risk based on the ecotoxicological and environmental concentration data. In the first tier analysis, ecological risk was estimated based on the quotient method. For the second tier, risk was calculated using the probability approach.

2.3.1. Quotient Method. The risk (RQ) was estimated as the quotient between measured exposure concentration (MEC) and toxicity (HC_5) for each metal:

$$\text{RQ} = \frac{\text{MEC}}{\text{HC}_5}, \quad (5)$$

where HC_5 is the 5% effect concentration of the pollutant based on the species sensitivity distribution (SSD).

2.3.2. Probabilistic Method. This method is used to calculate the probability that the estimated exposure value for a metal exceeds the predicted toxicity value; that is, the overlap between the exposure concentration curve of metals in the

TABLE 1: Taihu species used for the ecotoxicity data.

Scientific name	Species group
<i>Achnanthes minutissima</i>	Algae
<i>Achnanthes lanceolata</i>	Algae
<i>Alternanthera philoxeroides</i>	Plants
<i>Anabaena doliolum</i>	Algae
<i>Anguilla anguilla</i>	Fish
<i>Atyaephyra desmarestii</i>	Crustaceans
<i>Azolla caroliniana</i>	Plants
<i>Azolla filiculoides</i>	Plants
<i>Azolla pinnata</i>	Plants
<i>Brachionus calyciflorus</i>	Invertebrates
<i>Carassius auratus</i>	Fish
<i>Carassius gibelio</i>	Fish
<i>Ceratophyllum demersum</i>	Plants
<i>Ceriodaphnia cornuta</i>	Crustaceans
<i>Ceriodaphnia dubia</i>	Crustaceans
<i>Ceriodaphnia reticulata</i>	Crustaceans
<i>Chironomus dilutus</i>	Insects/spiders
<i>Chironomus riparius</i>	Insects/spiders
<i>Chironomus tentans</i>	Insects/spiders
<i>Chironomus kiiensis</i>	Insects/spiders
<i>Chlamydomonas reinhardtii</i>	Algae
<i>Chlorella pyrenoidosa</i>	Algae
<i>Chlorella sorokiniana</i>	Algae
<i>Chlorella</i> sp.	Algae
<i>Chlorella vulgaris</i>	Algae
<i>Chlorococcum</i> sp.	Algae
<i>Chroococcus</i> sp.	Algae
<i>Chydorus sphaericus</i>	Crustaceans
<i>Clarias gariepinus</i>	Fish
<i>Clariidae</i>	Fish
<i>Cocconeis</i> sp.	Algae
<i>Corbicula</i> sp.	Molluscs
<i>Corbicula striatella</i>	Molluscs
<i>Corydoras paleatus</i>	Fish
<i>Cyclidium</i> sp.	Invertebrates
<i>Cyprinus carpio</i>	Fish
<i>Danio</i> sp.	Fish
<i>Daphnia longispina</i>	Crustaceans
<i>Daphnia pulex</i>	Crustaceans
<i>Eichhornia crassipes</i>	Plants
<i>Elliptio complanata</i>	Molluscs
<i>Elodea canadensis</i>	Plants
<i>Elodea nuttallii</i>	Plants
<i>Ephemerella</i> sp.	Insects/spiders
<i>Erythemis simplicicollis</i>	Insects/spiders
<i>Gammarus pulex</i>	Crustaceans
<i>Gammarus roeseli</i>	Crustaceans
<i>Hydrilla verticillata</i>	Plants
<i>Keratella quadrata</i>	Invertebrates
<i>Lamellidens marginalis</i>	Molluscs
<i>Lemna aequinoctialis</i>	Plants
<i>Lemna gibba</i>	Plants
<i>Lemna minor</i>	Plants
<i>Limnodrilus hoffmeisteri</i>	Worms
<i>Limnoperla fortunei</i>	Molluscs
<i>Lumbriculus variegatus</i>	Worms
<i>Mallomonas</i> sp.	Algae
<i>Mesocyclops leuckarti</i>	Crustaceans
<i>Microcystis aeruginosa</i>	Algae
<i>Moina irrasa</i>	Crustaceans
<i>Microcystis</i> sp.	Algae

TABLE 1: Continued.

Scientific name	Species group
<i>Mugil cephalus</i>	Fish
<i>Myriophyllum aquaticum</i>	Plants
<i>Navicula seminulum</i>	Algae
<i>Nymphaea spontanea</i>	Plants
<i>Oryzias latipes</i>	Plants
<i>Oscillatoria</i> sp.	Algae
<i>Palaemonetes varians</i>	Crustaceans
<i>Parachlorella kessleri</i>	Algae
<i>Parreysia corrugata</i>	Molluscs
<i>Pelteobagrus fulvidraco</i>	Fish
<i>Phragmites australis</i>	Plants
<i>Pistia stratiotes</i>	Plants
<i>Polyarthra</i> sp.	Invertebrates
<i>Potomida littoralis</i>	Molluscs
<i>Potamogeton natans</i>	Plants
<i>Salvinia minima</i>	Plants
<i>Salvinia natans</i>	Plants
<i>Scenedesmus acutus</i>	Algae
<i>Scenedesmus quadricauda</i>	Algae
<i>Scenedesmus subspicatus</i>	Algae
<i>Spirodela polyrhiza</i>	Plants
<i>Spirodela polyrhiza</i>	Plants
<i>Spirulina</i> sp.	Algae
<i>Staurostrum cristatum</i>	Algae
<i>Typha latifolia</i>	Plants
<i>Ulothrix</i> sp.	Algae
<i>Unionidae</i>	Molluscs
<i>Vorticella</i> sp.	Invertebrates

water and the density curve of the PNEC of metals. SSDs were established to describe the relationships between each species' toxicity values and their cumulative frequencies. The level of risk is calculated using the following formula:

$$\text{Risk} = \int_0^{+\infty} (f(t) - g(t))dt. \quad (6)$$

3. Results and Discussion

3.1. Exposure Level. Based on data availability, nine metals were identified: As, Cd, Cr, Cu, Hg, Mn, Ni, Pb, and Zn. Table 2 summaries the GM concentrations and GSDs of the nine metals in the seven regions of Lake Taihu. The metals were frequently detected in Lake Taihu, and the detection frequencies were in the 76% (Cd) to 99% (Cu) range. Mn was observed with the highest concentration (27473 ± 1.5 ng/L), followed by Zn, Ni, Pb, Cu, As, Cr, Cd, and Hg. The spatial distributions of the metals in Lake Taihu were influenced by local industries. As shown in Table 2, Meiliang Bay had the highest levels of Zn, Pb, and Cd. The results could be explained by the fact that Changzhou and Wujin cities, which are close to Meiliang Bay, have industries that use Zn, Pb, and Cd as stabilizers and additives in synthetic rubber and PVC materials, and therefore, high amounts of industrial wastewater are discharged into Meiliang Bay [22]. The wastewater discharged from many leather manufacturing factories in the two cities also result in the

TABLE 2: Total concentrations (ng/L) of metals in Lake Taihu.

Metal		Area 1	Area 2	Area 3	Area 4	Area 5	Area 6	Area 7	Sample number	Mean
As	GM	5950	2112	1594	3653	1745	2006	1882	132	2417
	GSD	1.08	1.37	1.44	2.5	1.71	1.41	1.5		
Cd	GM	673	806	820	772	756	785	731	282	762
	GSD	1.16	1.12	1.06	1.11	1.07	1.05	1.29		
Cr	GM	3817	22105	595	1352	1981	2668	717	280	2210
	GSD	1.22	1.15	1.05	1.06	1.1	1.08	1.28		
Cu	GM	5333	2364	2482	8180	3013	1946	4006	205	3466
	GSD	1.25	1.19	1.14	1.53	1.02	1.14	1.53		
Hg	GM	10	1	3	22	5	18	40	46	8
	GSD	3.67	1.39	6.31	7.42	3.61	6.29	2.72		
Mn	GM	41861	65836	23235	—	28418	6000	39382	105	27473
	GSD	1.45	1.64	1.59	—	1.43	1.52	1.49		
Ni	GM	16332	19477	5150	5735	13715	11216	69306	156	10002
	GSD	1.12	1.06	1.06	1.05	1.12	1.07	1.37		
Pb	GM	6597	7559	741.8	5172	14889	6993	5394	270	5233
	GSD	1.25	1.15	1.16	1.3	1.17	1.23	1.58		
Zn	GM	6143	40183	31722	21433	6076	16324	11670	177	15277
	GSD	1.86	1.04	1.15	1.48	1.31	1.59	1.68		

Area 1: Zhushan Bay; area 2: Meiliang Bay; area 3: Gonghu; area 4: middle part; area 5: south part; area 6: southeast part; area 7: the whole lake.

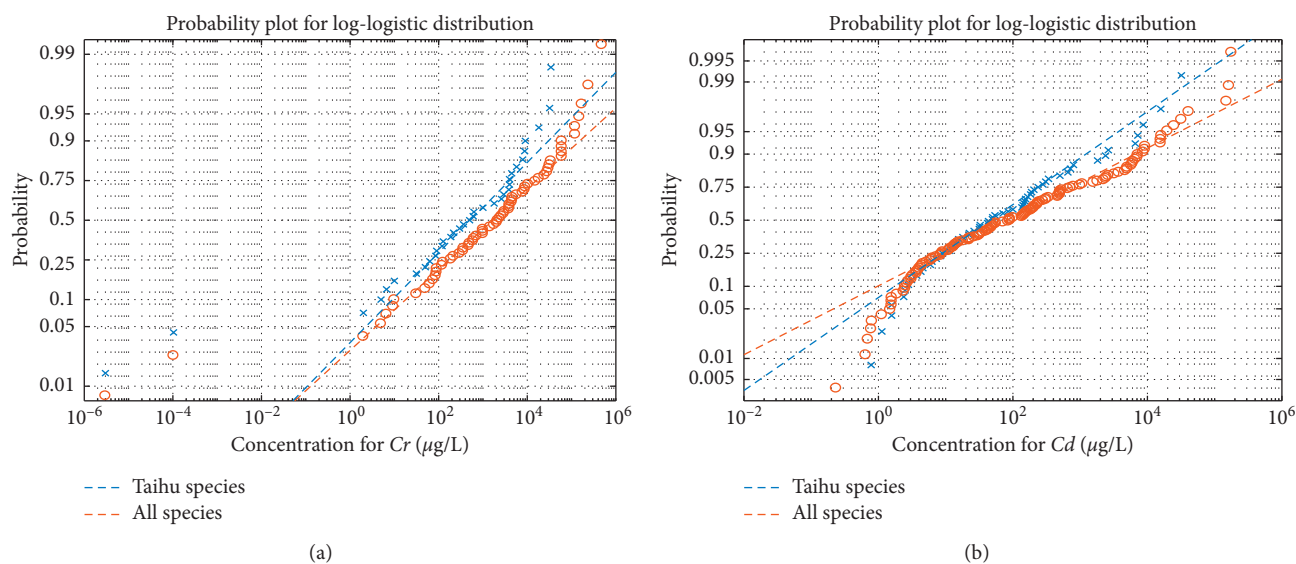


FIGURE 2: The SSD distributions of Cr and Cd for all species and Taihu species.

high Cr levels in Meiliang Bay [23]. Notably, there are much higher levels of As in Zhushan Bay and Pb in the southern part, which deserves attention.

3.2. Toxicity Assessment. Due to the numerous and sustained toxicity studies on heavy metals, a large number of toxicity data have been obtained for the metals targeted in the present study. However, some data should be eliminated because some species are not found in Lake Taihu. After filtering the data, the number of species that was confirmed to be available was 11 for As, 33 for Cd, 21 for Cr, 54 for Cu, 10 for Hg, 2 for Mn, 12 for Ni, 11 for Pb, and 24 for Zn.

In the present study, the abscissa was considered as the maximum no impact concentration and the ordinate was

considered as the proportion (%) of the affected species. Origin (OriginLab, Northampton, MA, USA) was used to illustrate the figure for obtaining the SSD curve and for fitting the model. The species composition would influence the shape and location of the SSD [24]. The different toxicity values of the Taihu species and all species indicate differences in species distribution. Therefore, difference between all the species and Taihu lake species would lead to different HC₅ values, and, in turn, different ecotoxicity effects. The SSD curves of Cr and Cd for the Taihu species and all species are illustrated in Figure 2. In contrast to the case in all species, the HC₅ value of Cr for the Taihu species was lower, while the HC₅ value of Cd was larger.

In total, 90 different species and 1436 separate ecotoxicity data points were included in the toxicity assessment of

TABLE 3: Exposure and risk results of metals in Lake Taihu.

Metal	Exposure concentration ($\mu\text{g/L}$)	HC ₅ ($\mu\text{g/L}$)	Quotient method (RQ)	Probability method (risk)
As	2.42	9.43	0.26	0.021
Cd	0.76	0.77	0.99	0.066
Cr	2.21	0.57	3.88	0.039
Cu	3.47	1.27	2.73	0.101
Pb	5.23	1.1	4.75	0.047
Mn	27.47	97.65	0.28	0.02
Hg	0.01	0.07	0.14	0.017
Ni	10	3.71	2.7	0.09
Zn	15.28	15.16	1.01	0.068

the present study. Based on the data, the SSD curves for each metal were plotted and their HC₅ values were obtained (shown in Table 3).

3.3. Risk Characterization and Ranking of Metals. The risks the metals pose to aquatic organisms could be assessed based on differences between the ecotoxicity data and environmental concentrations. When the quotient method was used, Pb, Cr, Cu, Ni, and Zn (RQ > 1) were identified as the metals posing the greatest risk to aquatic organisms. When the probability method was applied, the metals that posed high risks to aquatic organisms were Cu, Ni, Zn, Cd, Pb, and Cr. In previous reports, Cu and Zn have also been identified as the metals posing the greatest risks to freshwater ecosystems in the UK [9], in Lake Taihu, and in the Bohai Region of China [25, 26] though the studies adopted different approaches. Notably, Al, which was reported in the first or second place in the order of risk in UK river water when water chemistry is not considered, was not targeted in the present study [7, 9]. This is because the pH value in Lake Taihu is usually in the 7–8.5 range, while the most toxic Al species are found at $6\text{--}8.5\text{ pH}$ levels [9].

Each metal was initially analyzed using both the quotient and probability methods based on the data gathered in the present study. It should be noted that only seven metals were included in the present work. For other metals such as antimony and tin, we do not have both considerable measurement and local ecotoxicity data. Different forms of metals exhibit variable toxicity levels to aquatic organisms in aquatic environments. Therefore, using total metal concentrations could overestimate the risk. Another limitation is that the present work did not evaluate the influence of water physicochemical factors (e.g., pH, hardness, and DOC) on the metal bioavailability, and in turn, metal toxicity. Speciation and biotic ligand models [27] can be applied in real exposure and risk assessments at Lake Taihu, when such water chemistry factors are known. In the future, the metals could be analyzed further using the database that has been collated as ranking methodologies develop further.

4. Conclusions

The present work utilized a large amount of collected exposure and toxicity data to rank the metal ecological risk in Lake Taihu, China, based on current ecotoxicological data. The method involved the assessment of the risk posed by

metals to native aquatic organisms, and it took into account the influence of metal spatial distribution. Based on the probabilistic method, Cu, Ni, and Zn were the metals posing the greatest risk to aquatic organisms in Lake Taihu.

Data Availability

The experimental data used to support the findings of this study are included within the article. And, more detailed data are available from the corresponding author upon request.

Conflicts of Interest

The authors declare that there are no conflicts of interest regarding the publication of this paper.

Acknowledgments

This work was financially supported by the Major Science and Technology Program for Water Pollution Control and Treatment of China (No. 2018ZX07208001), the Fundamental Research Funds for the Central Universities (Nos. 2015ZCQ-HJ-02 and JC2015-02), and a grant from the Open Foundation of State Key Laboratory of Environmental Criteria and Risk Assessment, Chinese Research Academy of Environmental Sciences (No. SKLECRA2019OFP07).

References

- [1] S. Song, F. Li, J. Li, and Q. Liu, "Distribution and contamination risk assessment of dissolved trace metals in surface waters in the Yellow River Delta," *Human and Ecological Risk Assessment: An International Journal*, vol. 19, no. 6, pp. 1514–1529, 2013.
- [2] Z. Dong and J. Hu, "Development of lead source-specific exposure standards based on aggregate exposure assessment: Bayesian inversion from biomonitoring information to multipathway exposure," *Environmental Science & Technology*, vol. 46, no. 2, pp. 1144–1152, 2012.
- [3] Z. Dong, C. Liu, Y. Liu, K. Yan, K. T. Semple, and R. Naidu, "Using publicly available data, a physiologically-based pharmacokinetic model and Bayesian simulation to improve arsenic non-cancer dose-response," *Environment International*, vol. 92-93, pp. 239–246, 2016.
- [4] A. Navas-Acien, E. Guallar, E. K. Silbergeld, and S. J. Rothenberg, "Lead exposure and cardiovascular disease: a systematic review," *Environmental Health Perspectives*, vol. 115, no. 3, pp. 472–482, 2007.

- [5] W. Zhuang and X. L. Gao, "Integrated assessment of heavy metal pollution in the surface sediments of the Laizhou bay and the coastal waters of the Zhangzi Island, China: comparison among typical marine sediment quality indices," *PLoS One*, vol. 9, no. 4, Article ID e94145, 2014.
- [6] A. C. Johnson, M. D. Jürgens, C. Su et al., "Which commonly monitored chemical contaminant in the Bohai region and the Yangtze and Pearl Rivers of China poses the greatest threat to aquatic wildlife?" *Environmental Toxicology and Chemistry*, vol. 37, no. 4, pp. 1115–1121, 2018.
- [7] A. C. Johnson, R. L. Donnachie, J. P. Sumpter, M. D. Jürgens, C. Moeckel, and M. G. Pereira, "An alternative approach to risk rank chemicals on the threat they pose to the aquatic environment," *Science of the Total Environment*, vol. 599–600, pp. 1372–1381, 2017.
- [8] X. L. Wang, "Thoughts on the protection of aquatic organisms diversity in Taihu lake," *Morden Fisheries Information*, vol. 21, no. 2, pp. 22–29, 2006.
- [9] R. L. Donnachie, A. C. Johnson, C. Moeckel, M. G. Pereira, and J. P. Sumpter, "Using risk-ranking of metals to identify which poses the greatest threat to freshwater organisms in the UK," *Environmental Pollution*, vol. 194, pp. 17–23, 2014.
- [10] R. L. Donnachie, A. C. Johnson, and J. P. Sumpter, "A rational approach to selecting and ranking some pharmaceuticals of concern for the aquatic environment and their relative importance compared with other chemicals," *Environmental Toxicology and Chemistry*, vol. 35, no. 4, pp. 1021–1027, 2016.
- [11] Y. Song, *Distribution and Ecological Risk Assessment of Heavy Metals in Surface Sediments of Typical Inflow Rivers in Nansi Lake*, Shandong University, Jinan, China, 2014.
- [12] H. Y. Niu, Q. H. Wu, X. G. Chen et al., "Potential biological toxicity risk of heavy metals in the column sediments from Guangzhou section of the Pearl River," *Environmental Science & Technology*, vol. 33, no. 8, pp. 185–190, 2010, in Chinese.
- [13] L. Zheng, Z. Liu, Z. Yan et al., "pH-dependent ecological risk assessment of pentachlorophenol in Taihu Lake and Liaohe River," *Ecotoxicology and Environmental Safety*, vol. 135, pp. 216–224, 2017.
- [14] H. L. Su, *The Aquatic Biota Characteristics of Taihu Lake and its Relationship with the Derivation of Lake Water Quality Criteria in China*, Chinese Research Academy of Environmental Sciences, Beijing, China, 2011.
- [15] K. Zhao, Y. F. Zhou, Z. L. Jiang et al., "Changes of aquatic vegetation in Lake Taihu since 1960s," *Journal of Lake Sciences*, vol. 29, no. 2, pp. 351–362, 2017, in Chinese.
- [16] H. Xu, Y. J. Cai, X. M. Tang et al., "Community structure of macrozoobenthos and the evaluation of water environment in Lake Taihu," *Journal of Lake Sciences*, vol. 27, no. 5, pp. 840–852, 2015, in Chinese.
- [17] D. Li, X. W. Li, Z. C. Niu et al., "Investigation on community structure of Zooplankton in Taihu," *Journal of Anhui Agricultural Science*, vol. 42, no. 29, pp. 10173–10174, 2014, in Chinese.
- [18] Y. Chen, X. D. Hu, J. H. Zhang et al., "Phytoplankton community structure and its relationship with environmental factors in different regions of Taihu lake," *Journal of Hydroecology*, vol. 38, no. 3, pp. 38–44, 2017, in Chinese.
- [19] H. S. Xu, Y. Zhang, Y. C. Wang et al., "Spatial and temporal variation in the composition of phytoplankton species in Taihu lake," *Environmental Monitoring and Forewarning*, vol. 4, no. 6, pp. 38–41, 2012, in Chinese.
- [20] Z. G. Mao, X. H. Gu, Q. F. Zeng et al., "Fish community structure and diversity in Taihu lake," *Chinese Journal of Ecology*, vol. 30, no. 12, pp. 2836–2842, 2011, in Chinese.
- [21] Y. Chen, *Updated Study of Water Quality Criterion of Pentachlorophenol for Protection of Aquatic Organism in Tai Lake*, Nanjing University, Nanjing, China, 2014.
- [22] W. C. Qu, D. Mike, and S. M. Wang, "Multivariate analysis of heavy metal and nutrient concentrations in sediments of Taihu Lake, China," *Hydrobiologia*, vol. 450, pp. 83–89, 2001.
- [23] H. B. Yin, Y. N. Gao, C. X. Fan et al., "Distribution, sources and ecological risk assessment of heavy metals in surface sediments from Lake Taihu, China," *Environmental Research Letters*, vol. 6, no. 4, pp. 83–89, 2011.
- [24] J. Park, S. Lee, E. Lee et al., "Probabilistic ecological risk assessment of heavy metals using the sensitivity of resident organisms in four Korean rivers," *Ecotoxicology and Environmental Safety*, vol. 183, Article ID 109483, 2019.
- [25] C. Su, Y. L. Lu, A. C. Johnson et al., "Which metal represents the greatest risk to freshwater ecosystem in Bohai Region of China?" *Ecosystem Health and Sustainability*, vol. 3, no. 2, 2017.
- [26] Z. Fu, F. Chang, L. Chen et al., "Copper and zinc, but not other priority toxic metals, pose risks to native aquatic species in a large urban lake in Eastern China," *Environmental Pollution*, vol. 219, pp. 1069–1076, 2019.
- [27] D. M. Di Toro, H. E. Allen, H. L. Bergman, J. S. Meyer, P. R. Paquin, and R. C. Santore, "Biotic ligand model of the acute toxicity of metals. 1. Technical basis," *Environmental Toxicology and Chemistry*, vol. 20, no. 10, pp. 2383–2396, 2001.

Research Article

Aerobic Biodegradation of Four Groups of Steroid Hormones in Activated Sludge

Jiaxin Zhang, Jun Luo, and Hong Chang 

Beijing Key Lab for Source Control Technology of Water Pollution, College of Environmental Sciences & Engineering, Beijing Forestry University, Beijing 100083, China

Correspondence should be addressed to Hong Chang; changh@bjfu.edu.cn

Received 4 December 2019; Accepted 12 February 2020; Published 9 March 2020

Guest Editor: Yihua Xiao

Copyright © 2020 Jiaxin Zhang et al. This is an open access article distributed under the Creative Commons Attribution License, which permits unrestricted use, distribution, and reproduction in any medium, provided the original work is properly cited.

Steroid hormones in the environment have obtained considerable attention, as they can be harmful to aquatic organisms at very low concentrations. An analytical method was developed for simultaneously monitoring four estrogens, seven androgens, seven progestogens, and eleven glucocorticoids in a single water sample using liquid chromatography-electrospray tandem mass spectrometry. Laboratory studies were then performed to investigate the aerobic biodegradation of 29 steroids belonging to the four groups. The degradation of target steroids followed first-order reaction kinetics, and the degradation half-life ($t_{1/2}$) of estrogens, androgens, progestogens and glucocorticoids was 1.2–8.7 h, 0.3–1.3 h, 1.4–7.7 h, and 1.4–23.1 h, respectively. Most of the esterified glucocorticoids were more persistent than the parent compounds, but the $t_{1/2}$ for halogenated glucocorticoids was longer than that of their esterified compounds. In addition, C-21 ester glucocorticoids were more prone to decomposition than C-17 esters. Hydrolysis did not significantly affect the decomposition of esterified steroids.

1. Introduction

The presence of endocrine-disrupting chemicals (EDCs) in the environment is of wide concern throughout the world. Among EDCs, steroidal estrogens have obtained considerable attention, as they can be harmful to aquatic organisms, such as fish and amphibians, at very low concentrations [1, 2]. In addition to estrogens, other steroid hormones such as androgens, progestogens, and glucocorticoids have recently been documented to present a risk to exposed organisms [3–5]. Therefore, the occurrence and fate of steroid hormones other than estrogens in the environment deserve greater attention.

The presence of the four groups of steroid hormones and, in particular, estrogens in surface waters has been reported in multiple studies, and their concentrations were in the range of pg/L to several hundreds of ng/L [6–11]. Wastewater treatment plants (WWTPs) such as municipal and livestock WWTPs play a crucial role in restricting steroid hormones from entering riverine and coastal environments [12, 13]. Incomplete removal of these steroids in

WWTPs could result in the contamination of surface waters. Thus, it is essential to study the biodegradation of steroids by bacteria in activated sludge, particularly that of progestogens and glucocorticoids.

Microbial processes play an essential role in steroid degradation. Such processes have been particularly well documented for the microbiological degradation of estrogens and androgens [14–19]. However, for progestogens and glucocorticoids, most studies have been mainly concerned about their concentrations in WWTP influents and effluents and receiving waters. To our knowledge, few studies reported the degradation kinetics of progestogens [8, 20] and glucocorticoids [21] by aerobic sludge. Miyamoto et al. [21] studied the fate of 10 glucocorticoids upon incubation with activated sludge and revealed different degradation behaviours for structurally different glucocorticoids. However, no studies have simultaneously investigated the microbial degradation of the four groups of steroids.

This study was performed to assess the degradation of four groups of steroids, including estrogens, androgens, progestogens, and glucocorticoids, upon treatment with

activated sludge. A sensitive and reliable ultrahigh-performance liquid chromatography-tandem mass spectrometry (UPLC-MS/MS) method combined with liquid-liquid extraction (LLE) was developed for the simultaneous analysis of the four groups of steroids (including four estrogens, seven androgens, seven progestogens, and eleven glucocorticoids; see Table 1) in water samples. Due to the presence of isomers of the target steroids, effective chromatographic separation is essential for the unequivocal identification of specific compounds. Activated sludge was obtained from a working WWTP in Beijing, China. We simultaneously analyzed the degradation kinetics of 29 steroids during aerobic incubation with activated sludge and compared the rate of degradation among the four groups. This study will help understand their removal behaviour in the environment and consequently help accurately assess the risk of steroids hormones [22, 23].

2. Materials and Methods

2.1. Chemicals and Sludge Collection. Twenty-nine steroids were purchased from Sigma (St. Louis, MO, USA). Methanol, ethyl acetate, acetonitrile, acetic acid, hexane, and methylene chloride were of HPLC grade and obtained from Fisher Chemicals (Beijing, China). The activated sludge that was used as the inoculum was collected from the aerobic tank of one WWTP in Beijing, China. The slurry samples were transported back to the laboratory, stored at 4°C, and used within 24 h.

2.2. Microcosms. Aerobic microcosms were prepared by using fresh activated (aerobic) sludge. Incubation solutions containing 5% of each inoculum (v/v) were cultivated in a minimal-salt medium consisting of KH_2PO_4 (85 mg/L), NH_4Cl (5 mg/L), $\text{MgSO}_4 \cdot 7\text{H}_2\text{O}$ (22.5 mg/L), $\text{FeCl}_3 \cdot 6\text{H}_2\text{O}$ (0.25 mg/L), $\text{NaHPO}_4 \cdot 2\text{H}_2\text{O}$ (334 mg/L), $\text{CaCl}_2 \cdot 2\text{H}_2\text{O}$ (36.4 mg/L), K_2HPO_4 (217.5 mg/L), vitamins, and trace salts, including biotin (40 mg/L), folic acid (40 mg/L), riboflavin (100 mg/L), pantothenic acid (100 mg/L), para-aminobenzoic acid (100 mg/L), niacin (100 mg/L), thiamine (100 mg/L), vitamin B6 (200 mg/L), and vitamin B12 (2 mg/L). The pH of the medium was adjusted to 7.0.

2.3. Degradation Experiments. The degradation experiments were performed in two groups, including groups A (test replicates) and B (sterile controls). Each group was evaluated in three 100 mL glass conical flasks with 25 mL of media containing 1.25 mL of activated sludge. The studied compounds were spiked into the incubation media of each treatment by adding 12.5 μL of each steroid stock solution (1000 mg/L). This rendered an initial concentration of each studied compound in each treatment of 500 $\mu\text{g/L}$.

Three replicates (A1, A2, and A3) were used to monitor the degradation of each steroid at predetermined sampling time intervals (0, 0.5, 1.0, 1.5, 2.0, 3.0, 5.0, 7.0, 10.0, 12.0, 24.0, 36.0, 48.0, and 60.0 h). At each sampling time point, 1 mL of solution was removed from the same glass conical flask and transferred into a 2 mL amber glass vial to extract

the remaining compounds of interest. For the sterile controls of each treatment (B1, B2, and B3), the glass conical flasks containing incubation media were autoclaved (120°C, 30 min) three times in three consecutive days prior to experimentation, followed by the addition of 0.1 mL of HgCl_2 (100 mg/L) to maintain sterility. The target steroids were then added to each sterile control. Sterile controls for each treatment were then sampled at the same sampling points as the test groups (group A).

The treated flasks were covered with sterile sealing membranes to prevent bacteria from entering, while allowing air to circulate. The six flasks were incubated in the dark at 28°C with continuous shaking at 150 rpm to maintain aerobic conditions before sampling.

2.4. Sample Pretreatment and UPLC-MS/MS Analysis. Samples (1 mL) were collected from the incubation media (A1–A3 and B1–B3) and extracted by 1 mL of ethyl acetate three times. The mixture was thoroughly mixed before each extraction using a Vortex mixer. The extracts were dried with weak nitrogen and redissolved in 200 μL of methanol for analysis.

The LC apparatus was an ACQUITY Ultra Performance LC system (Waters, Milford, MA, USA). Separation was conducted using a Waters HSS T3 column (100 mm \times 2.1 mm, 1.8 μm , Waters, USA). The column was maintained at 40°C, and the flow rate and injection volume were 0.2 mL/min and 5 μL , respectively. The mobile phases consisted of acetonitrile containing acetic acid (0.15%, v/v) as solvent A and Milli-Q water containing acetic acid (0.15%, v/v) as solvent B. The initial gradient elution of 15% A was held for 9 min and then increased to 35% A in 4 min and 85% A in 5 min. Following the gradient elution, a final elution with 15% A was held for 4 min.

Mass spectrometry was performed using a Waters Premier XE Mass Spectrometer equipped with an electrospray ionization source (Waters). A flow injection of a standard solution of each compound was used to determine the optimum conditions for the ESI source. The average parameters were source temperature, 100°C; desolvation temperature, 350°C; capillary voltage, 3.2 kV; desolvation gas flow rate, 800 L/h; and cone gas flow rate, 50 L/h. Quantitative analyses of the target glucocorticoids were performed in the multiselected reaction monitoring (MRM) mode. Data acquisition was performed with MassLynx 4.1 (Micromass, Manchester, U. K.).

3. Results and Discussion

3.1. Method Development. The 29 steroids, including four estrogens, seven androgens, seven progestogens, and eleven glucocorticoids, were simultaneously analyzed by MS/MS in the MRM mode. The two abundant MRM transitions, cone voltage and collision energies, were optimized for each analyte by infusing the standard solutions into the mass spectrometer (see Table 1). The ESI-MS/MS analyses of glucocorticoids were operated in the negative mode, while estrogen, androgen, and progestogen were operated in the positive ion mode. The precursor ions for estrogens and

TABLE 1: Optimized instrumental and MRM conditions of the target compounds.

Analyte	Abbreviation	Mode	Precursor ion	MRM transition	CV (V)	CE (eV)	IDL ($\mu\text{g/L}$)
Estrogens							
Estrone	E1	ESI+	$[\text{M-OH}]^+$	271 > 147 ^a 271 > 197 ^b	18	10 17	2.0
α -Estradiol	α E2	ESI+	$[\text{M-OH}]^+$	255 > 159 255 > 133	35	20 20	0.20
β -Estradiol	β E2	ESI+	$[\text{M-OH}]^+$	255 > 159 255 > 133	35	20 20	1.0
Ethinylestradiol	EE2	ESI+	$[\text{M-OH}]^+$	279 > 133 279 > 159	24	16 21	1.0
Androgens							
Testosterone	T	ESI+	$[\text{M} + \text{H}]^+$	289 > 97 289 > 109	35	20 20	2.0
Methyl-testosterone	MT	ESI+	$[\text{M} + \text{H}]^+$	303 > 97 303 > 109	22	22 15	1.8
epitestosterone	ET	ESI+	$[\text{M} + \text{H}]^+$	289 > 97 289 > 109	35	20 20	1.5
Trenbolone	TBL	ESI+	$[\text{M} + \text{H}]^+$	271 > 253 271 > 199	22	18 22	1.5
Boldenone	BOL	ESI+	$[\text{M} + \text{H}]^+$	287 > 121 287 > 135	24	22 15	3.3
Dehydroepiandrosterone	DEHA	ESI+	$[\text{M} + \text{H}]^+$	271 > 253 271 > 199	28	24	2.4
cis-Androsterone	cis-ADR	ESI+	$[\text{M} + \text{H}]^+$	273 > 255 273 > 273	20	15 10	5.0
Progestogens							
Progesterone	P	ESI+	$[\text{M} + \text{H}]^+$	351 > 109 351 > 97	35	20 16	1.3
21 α -Hydroxyprogesterone	21 α -HPT	ESI+	$[\text{M} + \text{H}]^+$	331 > 108 331 > 97	28	22 21	1.0
17 α -Hydroxyprogesterone	17 α -HPT	ESI+	$[\text{M} + \text{H}]^+$	331 > 108 331 > 97	28	22 21	1.0
19-Nortestosterone	19-NT	ESI+	$[\text{M} + \text{H}]^+$	275 > 257 275 > 239	28	15 15	0.15
Medroxyprogesterone acetate	MPA	ESI+	$[\text{M} + \text{H}]^+$	387 > 327 387 > 285	28	16 16	0.20
19-Norethindrone	19-NTD	ESI+	$[\text{M} + \text{H}]^+$	299 > 231 299 > 109	24	17 24	3.0
Melengestrol acetate	MGA	ESI+	$[\text{M} + \text{H}]^+$	397 > 337 397 > 279	26	15 20	0.05
Glucocorticoids							
Cortisol	CRL	ESI-	$[\text{M-CH}_2\text{COO}]^-$	421 > 331 421 > 361	30	16 16	0.40
Cortisol 17 acetate	17-CRLA	ESI-	$[\text{M-CH}_2\text{COO}]^-$	463 > 403 463 > 373	27	11 16	0.17
Cortisol 21 acetate	21-CRLA	ESI-	$[\text{M-CH}_2\text{COO}]^-$	463 > 403 463 > 373	27	11 16	0.26
Cortisol 17-valerate	17-CRLV	ESI-	$[\text{M-CH}_2\text{COO}]^-$	505 > 455 505 > 331	20	10 16	0.12
Cortisol 21-valerate	21-CRLV	ESI-	$[\text{M-CH}_2\text{COO}]^-$	505 > 455 505 > 331	20	10 16	0.18
Betamethasone	BET	ESI-	$[\text{M-CH}_2\text{COO}]^-$	451 > 361 451 > 391	27	16 11	0.44
Dexamethasone	DEX	ESI-	$[\text{M-CH}_2\text{COO}]^-$	451 > 361 451 > 391	27	16 11	0.85
Betamethasone acetate	BETA	ESI-	$[\text{M-CH}_2\text{COO}]^-$	493 > 433 493 > 353	20	12 18	0.33
Dexamethasone acetate	DEXA	ESI-	$[\text{M-CH}_2\text{COO}]^-$	493 > 433 493 > 353	20	12 18	0.48
Cortisone	COR	ESI-	$[\text{M-CH}_2\text{COO}]^-$	419 > 331 419 > 361	30	16 16	0.60

TABLE 1: Continued.

Analyte	Abbreviation	Mode	Precursor ion	MRM transition	CV (V)	CE (eV)	IDL ($\mu\text{g/L}$)
Cortisone acetate	CORA	ESI-	$[\text{M}-\text{CH}_2\text{COO}]^-$	461 > 371	27	25	0.14
				461 > 401		16	

For all the compounds, ^a is the first MRM transition used for quantification, and ^b is the second MRM transition used for verification.

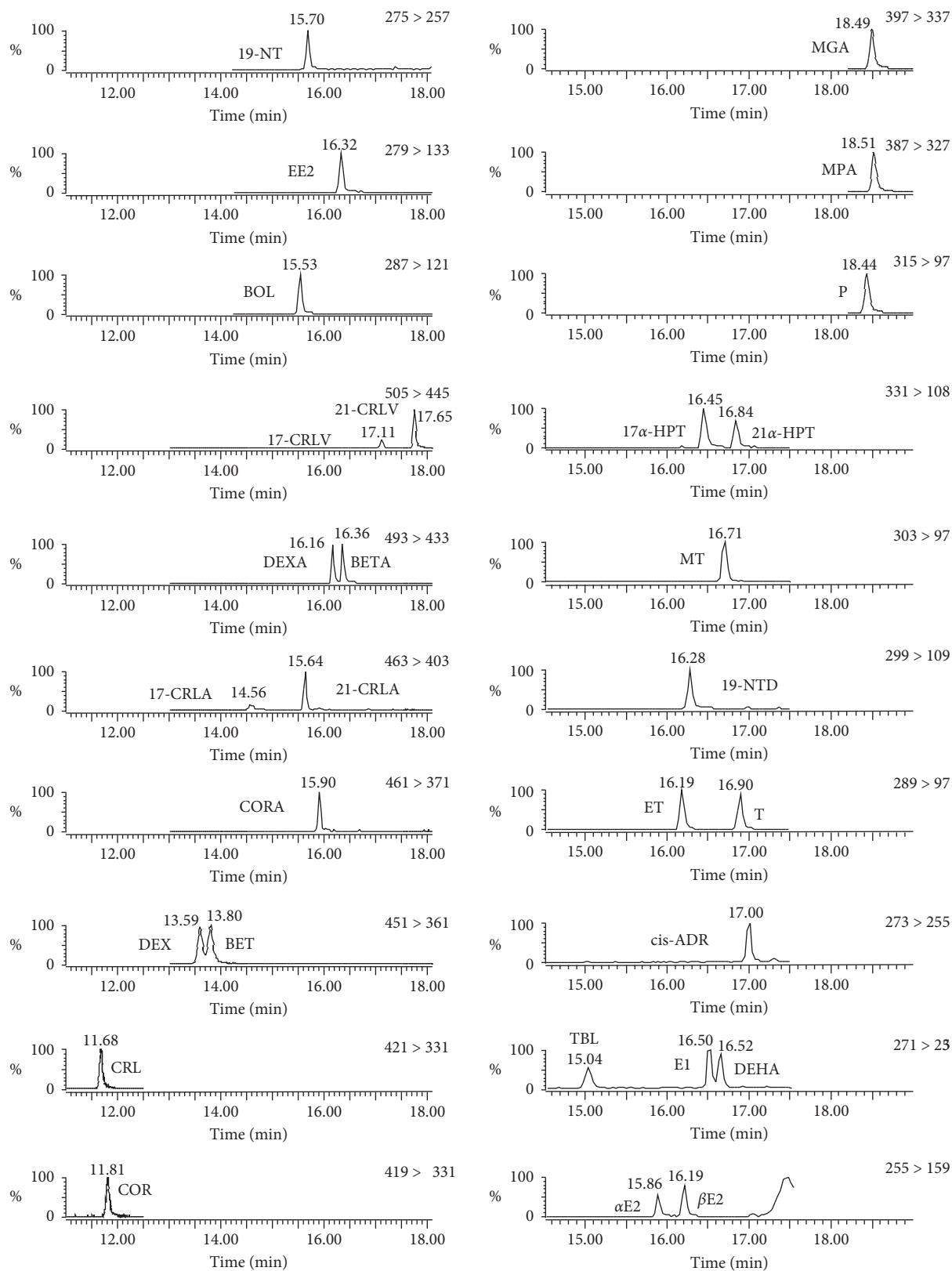


FIGURE 1: UPLC-MS/MS MRM chromatograms of target steroids.

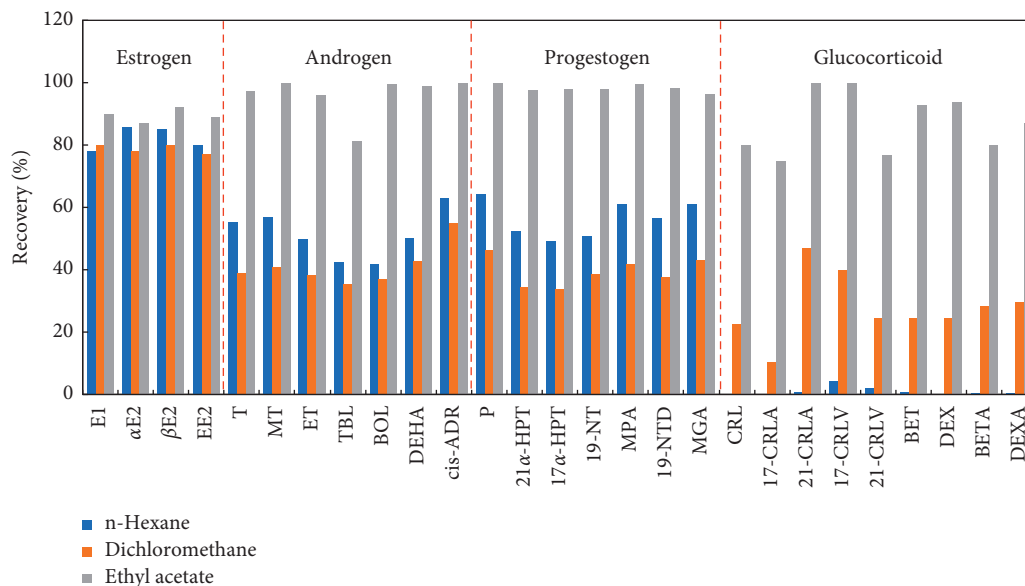


FIGURE 2: Recoveries (%) of target steroids with different elution solvents.

glucocorticoids were $[M-OH]^+$ and $[M-CH_2COO]^-$, respectively, while the precursor ions for androgens and progestogens were protonated molecular ions ($[M+H]^+$).

Chromatographic separation is important for the clear identification of the 29 target steroids because some of the target compounds were isomers with identical precursor and product ions. In this study, the use of C18 column chemistry failed to effectively separate some isomers. Thus, we also evaluated HSS T3 columns, which afforded better separation and retention of all of the target compounds. The LODs were estimated based on the peak-to-peak noise of the baseline near the peak of the analyte. The LODs were determined as the concentration with a minimum S/N ratio of 3. Figure 1 shows the UPLC-MS-MS chromatogram of the 29 steroids in less than 20 min. Very low instrumental detection limits (IDLs) were obtained for the 29 analytes (0.15–0.85 $\mu\text{g/L}$) (see Table 1).

LLE was used to extract the target steroids in the degradation experiment. Three organic solvents were evaluated, including ethyl acetate, n-hexane, and dichloromethane. As shown in Figure 2, ethyl acetate had high recoveries of estrogens, androgens, progestogens, and glucocorticoids of 87–90%, 61–100%, 96–100%, and 58–100%, respectively. In contrast, the low polar solvents, n-hexane and dichloromethane, produced very low recoveries (1–30%) for glucocorticoids, which was expected as glucocorticoids are polar compounds with log Kow of approximately 1. For estrogens, the three solvents produced similar recoveries. For androgens and progestogens, the recoveries of n-hexane and dichloromethane were 38–57%. Thus, ethyl acetate was selected as the extraction solvent for all four classes of steroids in this study.

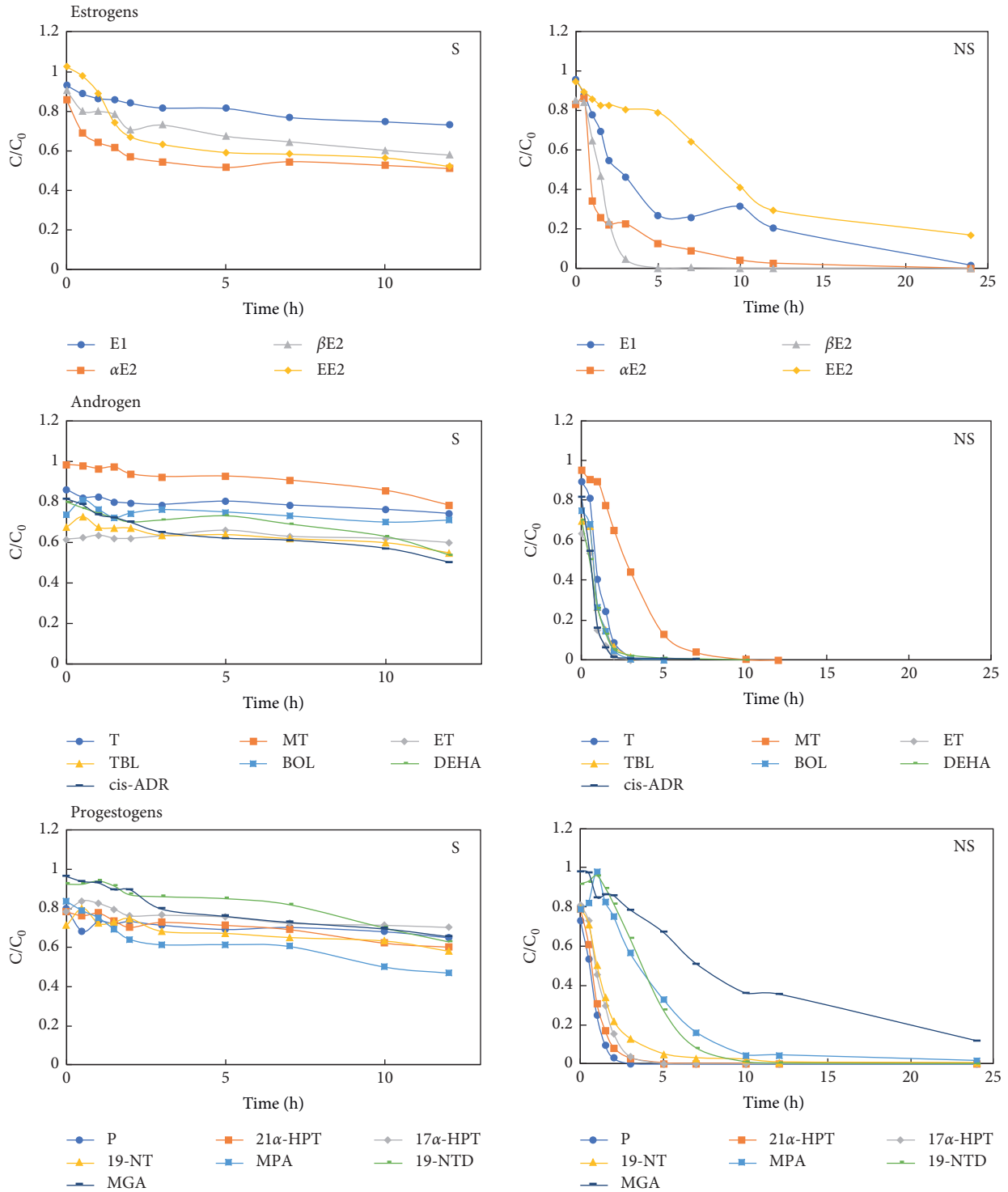
3.2. Kinetics of Steroid Biodegradation. We investigated the degradation of steroids in laboratory-scale experiments, and the degradation profiles of the 29 target compounds are shown in Figure 3. The residual steroid concentrations at 0 h are expressed

as 100%. No significant losses of the target compounds were observed in the sterile control reactions. Thus, we know that the reductions of the 29 steroids in the test groups (group A) were due to biological degradation, while the contribution from abiotic degradation, such as adsorption was very small.

For the steroids studied, aerobic biodegradation followed first-order reaction kinetics. The kinetic parameters, including half-life ($t_{1/2}$) and kinetic rate constant (k), are summarized in Table 2. The degradation $t_{1/2}$ of estrogens, androgens, progestogens, and glucocorticoids were 1.2–8.7 h, 0.3–1.3 h, 1.4–7.7 h, and 1.4–23.1 h, respectively, indicating that the degradation of androgens was the fastest, followed by estrogens, progestogens, and glucocorticoids under the same experimental conditions. Thus, compounds were all nearly fully degraded after 30 h of digestion.

The androgens were all natural hormones, which is likely why their decomposition rates were the fastest. According to the degradation curves of androgens, almost all of which were decomposed within 3 h of digestion. In addition, the $t_{1/2}$ of androgens (0.3–1.3 h) was consistent with that reported by Chang et al. [8]. Estrogens including E1, α E2, β E2, and EE2 were almost decomposed within 24 h of digestion. The decomposition rate of synthetic EE2 was much slower than that of the other three natural estrogens, which is also consistent with the results of previous studies [24–27].

Compared to natural compounds, synthetic progestogens such as MPA and MGA were also not readily degraded. The decomposition rates of glucocorticoids ranged from 1.4 h (COR) to 23.1 h (BET). It is interesting to note that most of the esterified glucocorticoids such as 17-CRLA, 21-CRLA, 17-CRLV, and 21-CRLV were more persistent relative to their parent compounds; however, this was not true for halogenated glucocorticoids, such as DEX and BET. The $t_{1/2}$ of DEX (17.3 h) and BET (23.1 h) were significantly higher than that of their esterified compounds (DEXA: 2.5 h; BETA: 2.0 h). These results may be because the decomposition of



(a)

FIGURE 3: Continued.

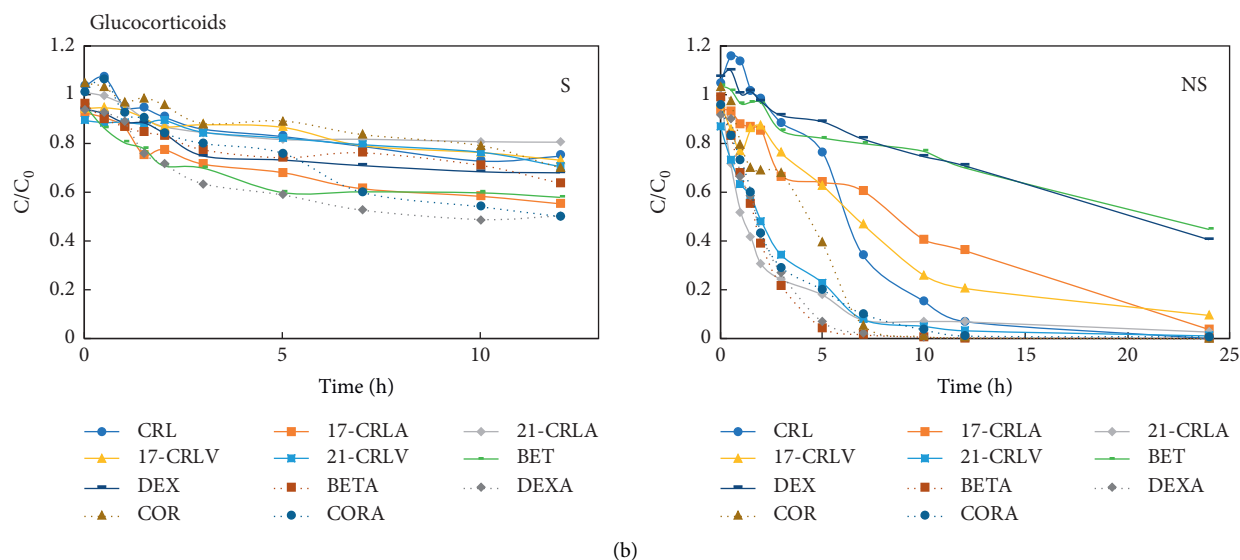


FIGURE 3: Degradation curves of steroids with 5% sludge concentrations. NS (nonsterile): slurry + steroids and S (sterile): slurry + steroids + HgCl_2 .

TABLE 2: Degradation parameters of the first-order kinetics model.

Analyte	First-order kinetics		
	k_1 (h^{-1})	$t_{1/2}$ (h)	r^2
Estrogens			
E1	0.16	4.3	0.9407
$\alpha\text{E}2$	0.26	2.7	0.9268
$\beta\text{E}2$	0.59	1.2	0.8909
EE2	0.08	8.7	0.9526
Androgens			
T	1.51	0.5	0.9466
MT	0.57	1.2	0.9817
ET	2.02	0.3	0.9762
TBL	1.35	0.5	0.9773
BLE	1.56	0.4	0.9801
DEHA	0.67	1.0	0.9710
C-ADR	0.75	0.9	0.8941
Progestogens			
P	0.28	2.5	0.9002
21 α -HPT	0.26	2.7	0.8907
17 α -HPT	0.30	2.3	0.8936
19-NT	0.49	1.4	0.9726
MPA	0.19	3.6	0.8935
19-NTD	0.28	2.5	0.9077
MGA	0.09	7.7	0.9930
Glucocorticoids			
CRL	0.28	2.5	0.9712
17-CRLA	0.12	5.8	0.9454
21-CRLA	0.15	4.6	0.9199
17-CRLV	0.10	6.9	0.9587
21-CRLV	0.20	3.5	0.9120
BET	0.03	23.1	0.9770
DEX	0.04	17.3	0.9876
BETA	0.35	2.0	0.9262
DEXA	0.28	2.5	0.8992
COR	0.48	1.4	0.9521
CORA	0.32	2.2	0.9829

halogenated glucocorticoids is more difficult than the hydrolysis of their esterified compounds. In addition, it was found that C-21 esters (21-CRLA and 21-CRLV) were prone to decomposition compared to C-17 esters (17-CRLA and 21-CRLV). Those findings are different from the recovery results reported by our recent study [11]. That study found C-17 esters were prone to hydrolysis in pure water, even under neutral conditions. Thus, hydrolysis did not significantly affect the decomposition of esterified steroids in this study.

The first-order kinetics model was applied to fit the degradation results. C_0 is initial concentration of steroids ($500 \mu\text{g/L}$); C_t is the concentrations of compounds at time t ; and k_1 is the first-order rate constant. $t_{1/2}$ can be calculated as $0.693/k_1$.

4. Conclusions

The UPLC-MS/MS method with a high selectivity and sensitivity was developed for the simultaneous determination of 29 steroids in water samples, including estrogens, androgens, progestogens, and glucocorticoids. The decomposition rate of androgens was the fastest, followed by estrogens and progestogens. The degradation of glucocorticoids was the slowest of the four groups of steroids, with DEX and BET having the longest $t_{1/2}$ among all such steroids. Hydrolysis did not significantly affect the decomposition of esterified steroids in this study.

Data Availability

The experimental data used to support the findings of this study are included in the article. And more detailed data are available from the corresponding author upon request.

Conflicts of Interest

The authors declare that there are no conflicts of interest regarding the publication of this paper.

Acknowledgments

This work was financially supported by the National Natural Science Foundation of China (Nos. 41573109 and 41322025), the Fundamental Research Funds for the Central Universities (Nos. 2015ZCQ-HJ-02 and JC2015-02), and a grant from the Open Foundation of State Key Laboratory of Environmental Criteria and Risk Assessment, Chinese Research Academy of Environmental Sciences (No. SKLECRA2019OFP07).

References

- [1] T. H. Hutchinson, G. T. Ankley, H. Segner, and C. R. Tyler, "Screening and testing for endocrine disruption in fish-biomarkers as "signposts," not "traffic lights," in risk assessment," *Environmental Health Perspectives*, vol. 114, no. Suppl 1, pp. 106–114, 2006.
- [2] J. P. Sumpter and A. C. Johnson, "Lessons from endocrine disruption and their application to other issues concerning trace organics in the aquatic environment," *Environmental Science & Technology*, vol. 39, no. 12, pp. 4321–4332, 2005.
- [3] D. G. J. Larsson, H. Hallman, and L. Forlin, "More male fish embryos near a pulp mill," *Environmental Toxicology and Chemistry*, vol. 19, no. 12, pp. 2911–2917, 2000.
- [4] T. J. Runnalls, N. Beresford, E. Losty, A. P. Scott, and J. P. Sumpter, "Several synthetic progestins with different potencies adversely affect reproduction of fish," *Environmental Science & Technology*, vol. 47, no. 4, pp. 2077–2084, 2013.
- [5] Ø. Øverli, S. Kotzian, and S. Winberg, "Effects of cortisol on aggression and locomotor activity in rainbow trout," *Hormones and Behavior*, vol. 42, no. 1, pp. 53–61, 2002.
- [6] D. W. Kolpin, E. T. Furlong, M. T. Meyer et al., "Pharmaceuticals, hormones, and other organic wastewater contaminants in U.S. streams, 1999-2000: a national reconnaissance," *Environmental Science & Technology*, vol. 36, no. 6, pp. 1202–1211, 2002.
- [7] P. Labadie and H. Budzinski, "Determination of steroidal hormone profiles along the jalle d'Eysines river (near Bordeaux, France)," *Environmental Science & Technology*, vol. 39, no. 14, pp. 5113–5120, 2005.
- [8] H. Chang, Y. Wan, S. Wu, Z. Fan, and J. Hu, "Occurrence of androgens and progestogens in wastewater treatment plants and receiving river waters: comparison to estrogens," *Water Research*, vol. 45, no. 2, pp. 732–740, 2011.
- [9] Z. Fan, S. Wu, H. Chang, and J. Hu, "Behaviors of glucocorticoids, androgens and progestogens in a municipal sewage treatment plant: comparison to estrogens," *Environmental Science & Technology*, vol. 45, no. 7, pp. 2725–2733, 2011.
- [10] X. Shen, H. Chang, D. Sun, L. Wang, and F. Wu, "Trace analysis of 61 natural and synthetic progestins in river water and sewage effluents by ultra-high performance liquid chromatography-tandem mass spectrometry," *Water Research*, vol. 133, pp. 142–152, 2018.
- [11] X. Shen, H. Chang, Y. Sun, and Y. Wan, "Determination and occurrence of natural and synthetic glucocorticoids in surface waters," *Environment International*, vol. 134, p. 105278, 2020.
- [12] M. Song, S. Chu, R. J. Letcher, and R. Seth, "Fate, partitioning, and mass loading of polybrominated diphenyl ethers (PBDEs) during the treatment processing of municipal sewage," *Environmental Science & Technology*, vol. 40, no. 20, pp. 6241–6246, 2006.
- [13] A. Muhammad, Y. Li, Y. W. Wang et al., "Occurrence, fate, and mass balance of different classes of pharmaceuticals and personal care products in an anaerobic-anoxic-oxic wastewater treatment plant in Xiamen, China," *Water Research*, vol. 123, pp. 655–667, 2017.
- [14] W. J. Barr, T. Yi, D. Aga, O. Acevedo, and W. F. Harper, "Using electronic theory to identify metabolites present in 17 α -ethinylestradiol biotransformation pathways," *Environmental Science & Technology*, vol. 46, no. 2, pp. 760–768, 2012.
- [15] Z. Li, R. Nandakuma, and N. Madayiputhiya, "Proteomic analysis of 17 β -estradiol degradation by *Stenotrophomonas maltophilia*," *Environmental Science and Technology*, vol. 46, no. 11, pp. 5947–5945, 2012.
- [16] W. Zheng, X. Li, S. R. Yates, and S. A. Bradford, "Anaerobic transformation kinetics and mechanism of steroid estrogenic hormones in dairy lagoon water," *Environmental Science & Technology*, vol. 46, no. 10, pp. 5471–5478, 2012.
- [17] O. V. Egorova, V. M. Nikolayeva, G. V. Sukhodolskaya, and M. V. Donova, "Transformation of C-19-steroids and testosterone production by sterol-transforming strains of *Mycobacterium* spp.," *Journal of Molecular Catalysis B-Enzymatic*, vol. 57, no. 1–4, pp. 198–203, 2009.
- [18] P. M. Bradley, L. B. Barber, F. H. Chapelle, J. L. Gray, D. W. Kolpin, and P. B. McMahon, "Biodegradation of 17 beta-estradiol, estrone and testosterone in stream sediments," *Environmental Science & Technology*, vol. 43, no. 6, pp. 1902–1910, 2009.
- [19] B. Khan, L. S. Lee, and S. A. Sassman, "Degradation of synthetic androgens 17 α - and 17 β -trenbolone and trendione in agricultural soils," *Environmental Science & Technology*, vol. 42, no. 10, pp. 3570–3574, 2008.
- [20] S. Liu, G.-G. Ying, J.-L. Zhao et al., "Occurrence and fate androgens, estrogens, glucocorticoids and progestagens in two different types of municipal wastewater treatment plants," *Journal of Environmental Monitoring*, vol. 14, no. 2, pp. 482–491, 2012.
- [21] A. Miyamoto, Y. Kitaichi, and K. Uchikura, "Degradation of corticosteroids during activated sludge processing," *Chemical and Pharmaceutical Bulletin*, vol. 62, no. 1, pp. 72–76, 2014.
- [22] Z. Dong, Y. Liu, L. Duan, D. Bekele, and R. Naidu, "Uncertainties in human health risk assessment of environmental contaminants: a review and perspective," *Environment International*, vol. 85, no. 12, pp. 120–132, 2015.
- [23] G. Yuan, Z. Dong, and J. Hu, "Uncertainty analysis in 2,3,7,8-tetrachlorodibenzo-p-dioxin (TCDD) cancer dose-response for three occupational cohorts," *Environment International*, vol. 88, no. 3, pp. 53–59, 2016.
- [24] S. Liu, G. Ying, and Y. Liu, "Degradation of norgestrel by bacteria from activated sludge: comparison to progesterone," *Environmental Science and Technology*, vol. 47, no. 18, pp. 10266–10276, 2013.
- [25] B. J. Robinson and J. Hellou, "Biodegradation of endocrine disrupting compounds in harbour seawater and sediments," *Science of the Total Environment*, vol. 407, no. 21, pp. 5713–5718, 2009.
- [26] X. Zhou and J. A. Oleszkiewicz, "Biodegradation of oestrogens in nitrifying activated sludge," *Environmental Technology*, vol. 31, no. 11, pp. 1263–1269, 2010.
- [27] G. Ying, S. Toze, and J. Hanna, "Decay of endocrine-disrupting chemicals in aerobic and anoxic groundwater," *Water Research*, vol. 42, no. 4-5, pp. 1133–1141, 2008.

Research Article

Effects of Urbanization on Water Quality and the Macrobenthos Community Structure in the Fenhe River, Shanxi Province, China

Linfang Wang,^{1,2,3} Hua Li ,^{1,3} Jinhua Dang ,² Ying Zhao,² Yu'en Zhu,¹
and Pengming Qiao²

¹School of Environment and Resources, Shanxi University, Taiyuan 030006, China

²Shanxi Province Research Academy of Environmental Science, Taiyuan 030027, China

³Institute of Resources and Environment Engineering of Shanxi University, Taiyuan 030006, China

Correspondence should be addressed to Hua Li; lihua@sxu.edu.cn and Jinhua Dang; 984736173@qq.com

Received 1 July 2019; Revised 15 September 2019; Accepted 25 September 2019; Published 9 March 2020

Guest Editor: Chenglian Feng

Copyright © 2020 Linfang Wang et al. This is an open access article distributed under the Creative Commons Attribution License, which permits unrestricted use, distribution, and reproduction in any medium, provided the original work is properly cited.

The relationships between land use types, water and sediment parameters, and macrobenthos community structures in the upper and middle reaches of the Fenhe River and urbanization intensity were studied. Samples were collected from 23 sampling sites. Spearman rank correlation analyses were performed to assess the relationships between the percentages of impervious area or the proportions of four land uses and the water and sediment physicochemical properties, heavy metal and polycyclic aromatic hydrocarbon concentrations in water and sediment, and biological indicators of the macrobenthos communities. Some water parameters (temperature, oxidation-reduction potential, electrical conductivity, total N concentration, total P concentration, ammonia-N concentration, and nitrate-N concentration), some sediment parameters (total N concentration, total P concentration, organic matter content, percentage of particles with diameters <2 mm, and polycyclic aromatic hydrocarbon, Cd, Cr, Cu, Ni Pb, and Zn concentrations), and some macrobenthos parameters (Berger–Parker index and percentages of collectors, tolerant taxa, and Oligochaeta) significantly positively correlated with the percentage of impervious area. Some water parameters (pH and dissolved oxygen concentration), some sediment parameters (percentage of particles with diameters >2 mm), and some macrobenthos parameters (total biomass, total number of taxa, Shannon's index, N diversity index, and percentages of Ephemeroptera, Plecoptera, Trichoptera, filterers, scrapers, and sensitive taxa) significantly negatively correlated with the percentage of impervious area. The results indicate that intensification of urbanization has strongly affected the water, sediment, and macrobenthos in the Fenhe River watershed.

1. Introduction

Effects on river basins and the use of river water have increased strongly in recent years because of urbanization. In particular, land use and land cover (principally the percentage of impervious area (PIA)) have changed [1, 2]. Continual increases in the PIA have been accompanied by decreases in the areas of farmland, forest, and grassland and the canalization of natural rivers. Increases in the PIA have also led to sharp decreases in precipitation received by soil and increases in the surface runoff coefficient and runoff volume. These changes could strongly increase the water levels in rivers after heavy rainfall, which could cause riverbanks to erode and increase the sediment loads of rivers [3]. Rainwater, domestic sewage, industrial wastewater,

surface runoff, and municipal pipeline water will be discharged into rivers after rain. Domestic sewage and some types of industrial wastewater contain large amounts of nitrogen- and phosphorus-containing compounds. Sewage and wastewater discharges into rivers can, therefore, supply excess nitrogen and phosphorus, which can negatively affect water quality and aquatic organism diversity. In such circumstances, many sensitive macrobenthos species will disappear and tolerant species will proliferate [4].

This study was focused on the effects of urbanization on macrobenthos organisms because these organisms live at the bottoms of aquatic systems, are long-lived, and move little. Changes in the macrobenthos species abundances and spatial distributions reflect environmental changes in river basins [5–7]. The intensity of urbanization in a river basin can be

expressed as the PIA (the ratio between the land area occupied by urban residences, industrial plants, commercial premises, and roads in a river basin and the total area of the basin).

This study was performed in the upper and middle reaches of the Fenhe River (Shanxi Province, China), which is the second largest tributary of the Yellow River. The effects of land-use changes caused by urbanization on water and sediment parameters and the macrobenthos community were investigated. The relationship between the macrobenthos community and land-use pattern was also investigated. The results will be useful when establishing approaches to protect river ecology in the study area as urbanization progresses.

2. Materials and Methods

2.1. Site Description. The Fenhe River, the largest river in Shanxi Province, is 716 km long. The headwater (in Ningwu County) to the Wangzhuang section (in Lingshi County) is defined as the upper and middle reaches of the river. A total of 26,210 km² of land drains into the upper and middle reaches. The Fenhe River flows south to north through Shanxi Province and has tributaries originating in Lüliang and Taihang, which are mountainous areas. The river flows through three major basins (Taiyuan, Linfen, and Yuncheng) and enters the Yellow River in Wanrong County. The Fenhe River Basin has a temperate continental monsoon climate with four distinct seasons and is in a semiarid semihumid climate-transition zone. Interannual rainfall varies strongly, and rainfall is unevenly distributed through the year. Approximately 70% of the annual rainfall occurs between June and September, mainly in heavy rainfall events. Mean annual precipitation in the whole basin is 489.3 mm, and 78.8% of this falls in the wet season. Mean annual evaporation is 2008 mm, and the mean annual air temperatures in different parts of the basin are between 6 and 13°C [8]. The sampling sites we used were mainly in the upper and middle reaches of the Fenhe River and were in the main river, primary tributaries, and secondary tributaries. Some sites were upstream and others downstream of points at which industrial wastewater or municipal sewage are discharged. A total of 23 sampling sites were selected and labeled S1–S23. The locations of the sites are shown in Figures 1 and 2.

2.2. Land Use Calculations. Spatial analysis of land use was performed using remote sensing images acquired in 2015. The images were processed, and then spatial analysis was performed using a supervised classification and visual interpretation method for the area within 3 km of each sampling site. The land uses cropland, forest, grassland, water, and construction land were used in the spatial analysis, and the distribution of each land use at each sampling site was determined.

2.3. Sample Collection and Analysis

2.3.1. Measurements of Physicochemical Indicators for Water. Water flow was measured using a current meter (LGY-II LS300-A, Beijing, China). The dissolved oxygen concentration



FIGURE 1: Location of the Fenhe River Basin.

was measured using a pen-type dissolved oxygen meter (LH-D9, Hangzhou, China). The oxidation-reduction potential was measured in situ using a pen-type oxidation-reduction potential meter (CT-8022, Qingdao, China). The electrical conductivity was measured on-site using a portable conductivity meter (LH-C661, Changzhou, China). The pH and temperature were measured on-site using a portable pH meter (PHB-4, Hangzhou, China). Other physicochemical indicators were measured using methods described in the Chinese Environmental Quality Standards for Surface Water. The total nitrogen (TN) concentration and total phosphorus (TP) concentration were determined using a potassium persulfate oxidation ultraviolet spectrophotometry method. The ammonia-nitrogen ($\text{NH}_4^+\text{-N}$) concentration was determined using a Nessler's reagent spectrophotometry method.

2.3.2. Measurements of Physicochemical Indicators for Sediment. Each sediment sample was collected using a Peterson sediment sampler and then placed in a glass bottle and stored in a refrigerator. The samples were transported to the laboratory as soon as possible after being collected and were stored at a low temperature until they were analyzed. The sediment samples were analyzed following methods described in the Soil Physicochemical Analysis document, published by

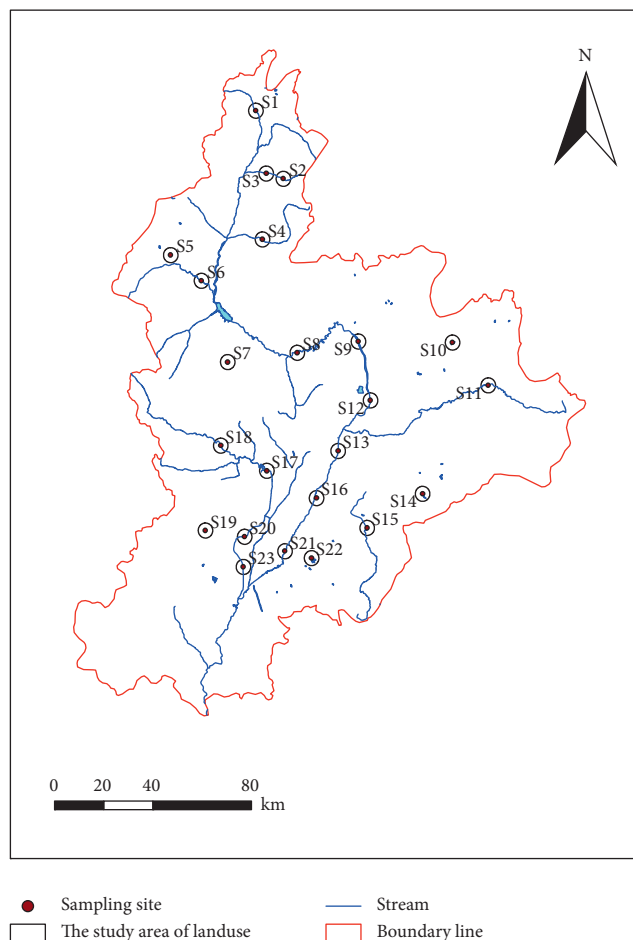


FIGURE 2: Locations of the 23 sampling sites in the upper and middle reaches of the Fenhe River.

the Institute of Soil Science, Chinese Academy of Sciences (Nanjing, China). The TN concentration was determined using a semi-micro Kjeldahl method. The TP concentration was determined using an anti-Mo-Sb spectrophotometry method. The sediment organic matter (SOM) content was determined using a potassium dichromate volumetric method. The polycyclic aromatic hydrocarbon (PAH) concentration was determined using a gas chromatography mass spectrometry method. The Cd, Cr, Cu, Ni, Pb, and Zn concentrations were determined using a $\text{HNO}_3\text{-HClO}_4\text{-HF}$ microwave digestion inductively coupled plasma mass spectrometry method. The sediment particle size distribution was determined using a method described by Dickens et al. [9].

2.3.3. Invertebrate Macrobenchos Measurements. Macrobenchos were collected using a Surber net (30 cm \times 30 cm, 500 μm mesh) when it was possible to wade into the river at the sampling site and using a 1/16 Peterson sampler when it was not possible to wade into the river. Three samples were collected at each sampling site, one from each side and one from the center of the river channel [10]. The collected material was washed using a 60 mesh sieve; then, the material retained by the sieve was placed on a white porcelain plate. The macrobenchos organisms were removed

and fixed in a 10% formaldehyde solution and then transported to the laboratory, where the species were identified and counted. The macrobenchos species were identified and the functional feeding groups classified using the publications Research on Microdrile Oligochaeta in China [11], Economic Fauna of China [12], and Identification Manual for the Larval Chironomidae (Diptera) of North and South Carolina [13]. Diversity was evaluated using Shannon's index [14]. The Berger-Parker dominance index was calculated using a method described by Xu [15]. The comprehensive (N) diversity index for the macrobenchos was calculated using a method published in the Technical Guide for Watershed Ecosystem Health Assessment [16].

2.4. Data Analysis. Analyses of variance followed by Duncan's post hoc analyses and Spearman's rank correlation analyses were used to investigate relationships between the environmental parameters and biological indicators and the land uses. The statistical analyses were performed using SPSS 19.0 software (IBM, Armonk, NY, USA). Curves were fitted to scatter plots of the PIA data and biological indicator data using Origin 8.0 software (OriginLab, Northampton, MA, USA).

3. Results

3.1. Relationships between the Physicochemical Indicators for Water and Land Use. The land uses in the areas 3 km around the sampling points are shown in Figure 3. The water flow and PIA did not correlate significantly. However, the water temperature, oxidation-reduction potential, electrical conductivity, TN concentration, TP concentration, and NO_3^- -N concentration significantly positively correlated with the PIA and percentage of cropland and significantly negatively correlated with the percentages of grassland and forest. The water pH and dissolved oxygen concentration negatively correlated with the PIA (Table 1).

3.2. Relationships between Physicochemical Indicators for Sediment and Land Use. The percentage of particles with diameters <2 mm, SOM content and TN, TP, PAH, Cd, Cr, Cu, Ni, Pb, and Zn concentrations in the sediment positively correlated with the PIA. The percentage of particles with diameters >2 mm significantly negatively correlated with the PIA, and the percentages of forest and wetland positively correlated with the PIA. The SOM content and TN, TP, Cd, Cr, and Pb concentrations positively correlated with the percentage of cropland. The TP concentration negatively correlated with the percentages of grassland and forest, and the PAH concentration negatively correlated only with the percentage of forest (Table 2).

3.3. Relationships between the Macrobenchos Community Structures and Land Use

3.3.1. Macrobenchos Community Compositions and Quantities. In total, macrobenchos from 37 genera or species were found at the 23 sampling sites in the upper and middle reaches of the Fenhe River. The macrobenchos were from 25

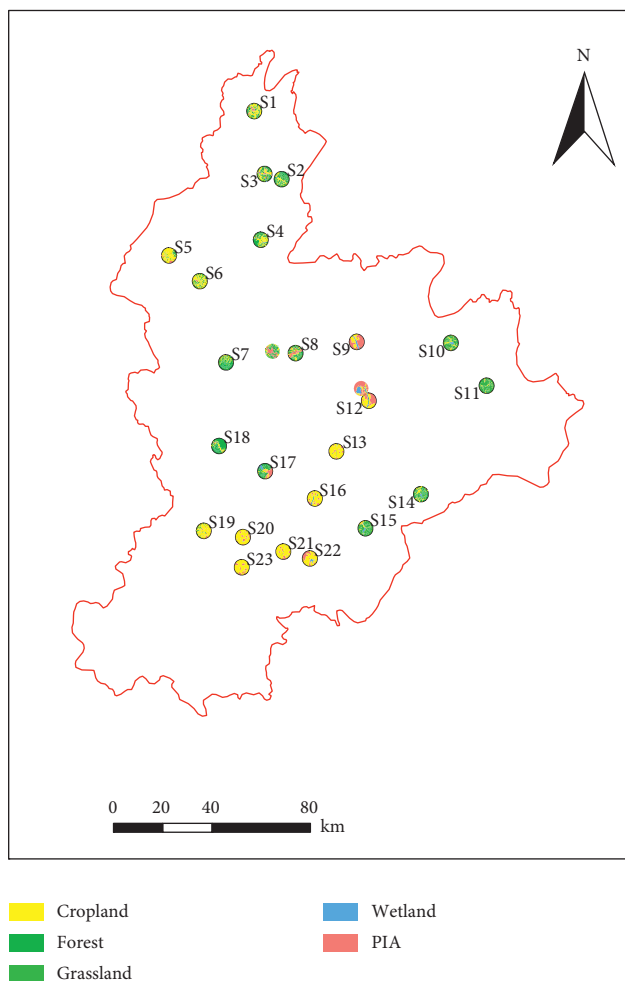


FIGURE 3: The results of spatial analysis of land use types.

TABLE 1: Environmental parameters for water at the sampling sites and the relationships between the parameters and land use.

Variable	Min	Max	Mean	SD	<i>r</i>				Percentage of impervious area (PIA, %)
					Cropland (%)	Grassland (%)	Forest (%)	Wetland (%)	
Water temperature (°C)	10.10	26.80	19.21	4.21	0.308**	-0.425**	-0.386**	0.446**	0.356**
pH	7.83	9.07	8.52	0.33	-0.191	0.257*	0.120	0.011	-0.270*
DO (mg/L)	3.02	10.80	6.82	2.03	0.235*	0.118	-0.166	-0.031	-0.271*
Flow (m/s)	0.05	3.32	0.54	0.72	-0.117	0.059	0.127	-0.027	-0.100
ORP (mv)	155.00	281.00	224.47	47.66	0.381**	-0.219*	-0.346**	0.047	0.247*
EC (μs/cm)	329.00	2000.00	1034.16	668.06	0.528**	-0.326**	-0.464**	-0.155	0.382**
TN (mg/L)	1.28	54.90	15.83	14.07	0.726**	-0.304**	-0.469**	-0.254*	0.810**
TP (mg/L)	0.01	5.66	0.93	1.49	0.630**	-0.243*	-0.450**	-0.157	0.814**
NH ₄ ⁺ -N (mg/L)	0.03	43.80	8.12	13.11	0.344**	-0.229	-0.012	-0.194	0.566**
NO ₃ ⁻ -N (mg/L)	0.02	10.30	2.20	2.34	0.334**	-0.235*	-0.371**	-0.084	0.411**

DO, dissolved oxygen concentration; ORP, oxidation-reduction potential; EC, electrical conductivity; TN, total nitrogen concentration; TP, total phosphorus concentration; NH₄⁺-N, ammonia-nitrogen concentration; NO₃⁻-N, nitrate nitrogen concentration; SD, standard deviation. * $P < 0.05$; ** $P < 0.01$.

families, six classes, and four phyla. There were nine genera or species of Annelida (24.3% of the total species), five genera or species of Mollusca (13.5% of the total species), 22 genera or species of Arthropoda (59.4% of the total species), and one

species of Turbellaria (13.5% of the total species). The dominant species in the phylum Annelida was *Limnodrilus hoffmeisteri*. In the Arthropoda phylum, 20 genera or species were in the Insecta class, and these were mainly Diptera,

TABLE 2: Environmental parameters for sediment at the sampling sites and the relationships between the parameters and land use.

Variable	Min	Max	Mean	SD	<i>r</i>				
					Cropland (%)	Grassland (%)	Forest (%)	Wetland (%)	Percentage of impervious area (PIA, %)
TN (g/kg)	0.74	1.49	1.02	0.19	0.260*	-0.240*	-0.195	0.220*	0.449**
TP (mg/kg)	0.60	1.65	0.80	0.24	0.322**	-0.216*	-0.270*	-0.037	0.219*
SOM (g/kg)	13.71	84.05	32.99	18.95	0.253*	-0.260*	-0.126	0.051	0.322**
Particle size >2 mm (%)	0.00	38.69	6.22	10.95	-0.139	-0.196	0.294*	0.307*	-0.54**
Particle size <2 mm (%)	61.31	100.00	93.78	10.95	0.139	0.196	-0.294*	-0.307**	0.54**
PAHs (mg/kg)	0.28	23.33	2.83	5.03	0.026	-0.185	-0.296*	0.206*	0.658**
Zn (mg/kg)	28.91	119.73	48.7	21.69	-0.024	-0.034	-0.183	0.276*	0.353**
Pb (mg/kg)	8.47	20.74	13.44	3.19	0.414**	-0.591**	-0.140	0.140	0.209*
Cd (mg/kg)	0.06	0.27	0.12	0.05	0.351**	-0.436**	-0.185	0.152	0.363**
Cr (mg/kg)	16.33	98.64	37.10	16.06	0.232*	-0.014	-0.439**	0.164	0.394**
Ni (mg/kg)	7.21	32.27	16.08	5.90	-0.150	-0.094	-0.165	0.573**	0.538**
Cu (mg/kg)	5.85	65.78	15.89	12.61	-0.107	-0.210*	-0.276*	0.636**	0.787**

TN, total nitrogen concentration; TP, total phosphorus concentration; SOM, sediment organic matter content; PAHs, polycyclic aromatic hydrocarbon concentration; SD, standard deviation. * $P < 0.05$; ** $P < 0.01$.

Ephemeroptera, Plecoptera, and Trichoptera. Of these, four genera or species were aquatic: Ephemeroptera, Plecoptera, and Trichoptera (EPT). *Baetis* spp. were the dominant EPT species. There were 12 genera or species of aquatic insects in the Diptera order, and *Orthocladius* sp. 1 was dominant. The most macrobenthos genera or species found at a sampling site in the upper and middle reaches of the Fenhe River was 11 at Leiming Temple (site S1).

3.3.2. Relationships between the Biological Indicators and Land Use. The macrobenthos community structure indicators and feeding function indicators correlated to different degrees with the different land use types (Table 3). The percentages of predators and shredders did not significantly correlate with the PIA. However, the biomass, total number of taxa, Shannon's index, N diversity index, and percentages of EPT, filterers, scrapers, and sensitive taxa negatively correlated with the PIA. The Berger-Parker index and percentages of collectors, tolerant taxa, and Oligochaeta significantly positively correlated with the PIA. The percentage of scrapers and the Berger-Parker index did not significantly correlate with the percentage of cropland. The biomass and percentages of collectors, tolerant taxa, Oligochaeta, and shredders significantly positively correlated with the percentage of cropland. The total number of taxa, Shannon's index, N diversity index, and percentages of EPT, filterers, predators, and sensitive taxa negatively correlated with the percentage of cropland.

Exponential lines were fitted to plots of the data for the total number of taxa, Shannon's index, Berger-Parker index, and percentage of EPT against the PIA, and the results are shown in Figure 4.

The total number of taxa, Shannon's index, Berger-Parker index, and percentage of EPT all had significant relationships with the PIAs. The total number of taxa, Shannon's index, and percentage of EPT significantly

negatively correlated with the PIAs. The percentage of EPT was generally zero when the PIA was $>8\%$. The Berger-Parker index significantly positively correlated with the PIA.

The percentages of predator and shredder macrobenthos did not significantly correlate with the PIA. However, the percentage of collectors positively correlated with the PIA, and the percentages of filterers and scrapers significantly negatively correlated with the PIA (Figure 5). The percentages of filterers and scrapers were zero when the PIA was $>3\%$. The percentage of collectors reached a maximum when the PIA was $>20\%$.

The N diversity index and percentages of sensitive taxa and tolerant taxa had nonlinear relationships with the PIA. The percentage of Oligochaeta linearly correlated with the PIA. The percentages of Oligochaeta and tolerant taxa positively correlated with the PIA. The N diversity index and percentage of sensitive taxa significantly negatively correlated with the PIA (Figure 6). When the PIA reached a particular value, the N diversity index reached a plateau and fluctuated within a small range. This indicated that the macrobenthos community only contained tolerant species and that the sensitive taxa had all disappeared.

4. Discussion

4.1. Relationships between the Environmental Parameters and the PIA. The water temperature, oxidation-reduction potential, electrical conductivity, and TN, TP, and NO_3^- -N concentrations negatively correlated with the PIA, but the pH and dissolved oxygen concentration significantly positively correlated with the PIA and percentage of cultivated land and negatively correlated with the percentages of grassland and forest. This indicated that urbanization strongly affected water quality in the river basin. The more rapid the urbanization process the more seriously polluted urban rivers will become. The "heat island effect" may

TABLE 3: Macroinvertebrate community parameters for the sampling sites and the relationships between the parameters and land use.

Variable	Min	Max	Mean	SD	<i>r</i>				
					Cropland (%)	Grassland (%)	Forest (%)	Wetland (%)	Percentage of impervious area (PIA, %)
Biomass/(g/m ²)	0.14	213.33	27.62	54.52	0.336**	-0.186	-0.105	-0.322**	-0.382**
Total number of taxa	0.00	15.57	4.3	3.58	-0.461**	0.300**	0.361**	-0.177	-0.661**
Shannon diversity index	0.00	2.27	1.11	0.70	-0.392**	0.368**	0.374**	-0.263*	-0.558**
Berger-Parker index	0.00	1.10	0.52	0.31	-0.126	0.337**	-0.167	0.069	0.705**
N diversity index	89.42	1.22	32.58	23.74	-0.385**	0.438**	0.234*	-0.239*	-0.258*
EPT (%)	0.01	1.00	0.21	0.33	-0.305**	0.450**	0.261*	0.392**	-0.419**
Collector (%)	25.81	100.00	74.05	20.78	0.308**	-0.358**	0.112	-0.066	0.76**
Filterer (%)	0.00	48.39	4.24	10.50	-0.278*	0.377**	0.177	-0.079	-0.287*
Scraper (%)	0.00	31.58	2.90	6.87	-0.065	-0.091	0.234*	0.483**	-0.535**
Predator (%)	0.00	19.23	5.21	6.71	-0.490**	0.601**	0.157	0.015	-0.186
Shredder (%)	0.00	50.00	11.82	16.96	0.489**	-0.077	-0.334**	-0.220*	-0.060
Sensitive taxa (%)	0.00	38.10	5.12	10.64	-0.400**	0.310**	0.454**	-0.023	-0.390**
Tolerant taxa (%)	0.00	100.00	55.97	37.12	0.355**	-0.377**	-0.644**	0.031	0.605**
Oligochaeta (%)	0.00	100.00	20.24	35.19	0.370**	-0.251*	-0.324**	-0.083	0.660**

EPT, Ephemeroptera, Plecoptera, and Trichoptera; SD, standard deviation. * $P < 0.05$; ** $P < 0.01$.

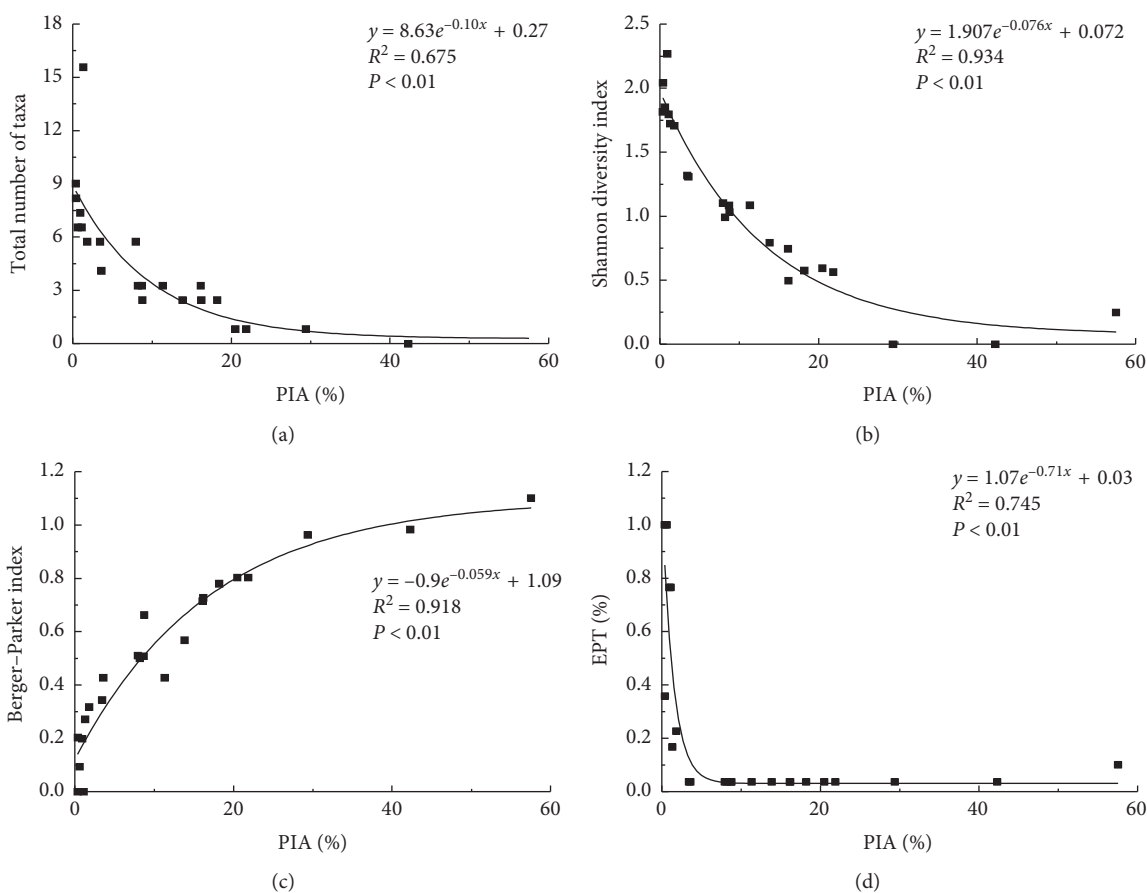


FIGURE 4: Relationships between the total number of taxa, Berger-Parker index, Shannon's diversity index, and percentage of Ephemeroptera, Plecoptera, and Trichoptera (EPT) and the percentage of impervious area (PIA) with exponential lines fitted to the data.

explain a high degree of urbanization causing high river water temperatures. Large amounts of domestic and industrial waste are discharged into the Fenhe River. This will increase the electrical conductivity by increasing the salt

concentrations and the TN and TP concentrations by increasing the amounts of nutrients entering the water. These results were consistent with the results of previous studies in China and elsewhere [7, 17, 18].

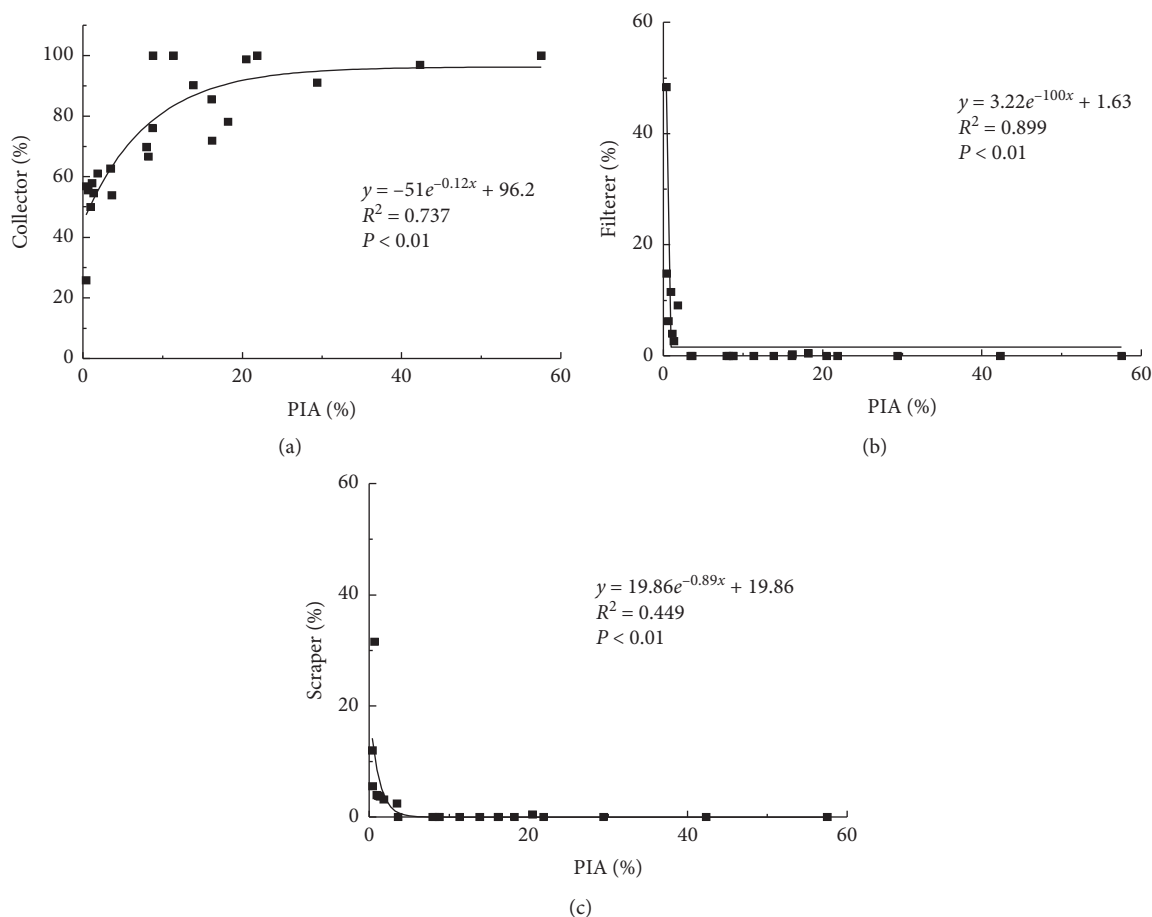


FIGURE 5: Relationships between the percentages of the macrobenthos functional groups and the percentage of impervious area (PIA).

The SOM content and TN, TP, Cd, Cr, and Pb concentrations in sediment positively correlated with the PIA and percentage of cropland probably because urbanization decreases industrial and agricultural activities and leads to increased nutrient and heavy metal emissions in rivers. These nutrients and heavy metals will form complexes and adsorb to suspended particulate matter and then enter the sediment, which will act as both a sink for and a secondary source of nutrients and heavy metals. The percentage of sediment particles with diameters <2 mm positively correlated with the PIA, and the percentage of sediment particles with diameters >2 mm significantly negatively correlated with the PIA and significantly positively correlated with the percentages of forest and wetland. This is probably because construction in highly urbanized areas will expose previously unexposed soil and, therefore, decrease the sediment particle size. Canalization of a natural river will also decrease the complexity of the river channel, increasing the proportion of fine silt. The upper reaches of the Fenhe River Basin are generally not strongly urbanized, and water flow is low and sediment mainly consists of gravel. The degree of urbanization increases downstream, and the water flow increases. This decreases the vegetation cover around the river, meaning that serious soil erosion occurs. This causes the sediment particle size to be lower in the middle than the

upper reaches of the Fenhe River. Similar conclusions have been drawn in studies in other parts of China and elsewhere [7, 17, 19]. Sediment is a source of pollutants to water. Sediment is an important reservoir of heavy metals and organic matter. If the physical and chemical properties of the aquatic environment change, nutrients, heavy metals, and persistent organic pollutants previously deposited in the sediment can be released to the overlying water, meaning the sediment is a secondary source of pollutants. The correlations between the nutrient concentrations, organic matter concentrations, and PIAs in the water and sediment samples supported this conclusion.

4.2. Relationships between the Macrobenthos Biological Indicators and PIA. The biomass, total number of taxa, Shannon's index, N diversity index, and percentages of EPT, filterers, scrapers, and sensitive taxa negatively correlated with the PIA, but the Berger-Parker index and percentages of collectors, tolerant taxa, and Oligochaeta positively correlated with the PIA. Urbanization decreased benthos diversity and biomass. A small number of pollutant-resistant groups (e.g., Oligochaeta and Chironomidae) became dominant, but sensitive taxa (represented by EPT) decreased in abundance or disappeared. Intense urbanization has caused a range of

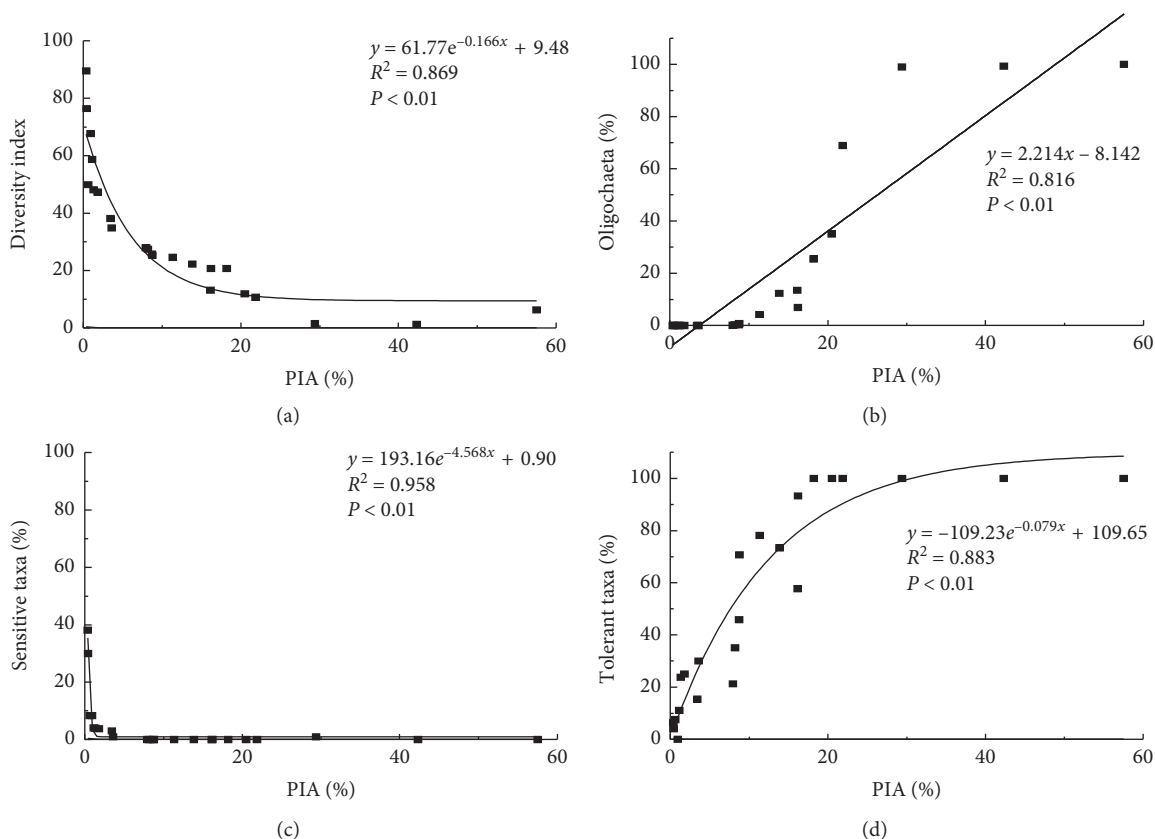


FIGURE 6: Relationships between the N diversity index and percentages of Oligochaeta, sensitive taxa, and tolerant taxa and the percentage of impervious area (PIA).

periphyton in the basin to decrease and the numbers of scrapers and filterers to decrease because of changes in the hydrological conditions and the numbers of collectors to increase because of increased nutrient loads. Similar conclusions were drawn in previous studies performed in China and elsewhere [17, 19, 20]. The total number of taxa, Shannon's diversity index, Berger-Parker index, percentage of EPT, N diversity index, and percentages of intolerant and pollutant-resistant groups nonlinearly correlated with the PIA, which was consistent with the conclusions drawn in a study performed by Liu et al. [7]. However, Li et al. [17], King [20], and others found linear correlations. The nonlinear relationships indicate that the indicators changed in one way up to a PIA threshold and then in another way above the threshold. When the PIA was $>8\%$, the percentage of EPT was zero. This was consistent with the conclusion reached in a previous study that the benthos group may be altered when the PIA is $>10\%$ or $8\%–12\%$ [21, 22]. The percentages of filterers and scrapers decreased to zero when the PIA was $>3\%$, and the percentages of gathers and collectors reached maxima when the PIA was $>20\%$.

5. Conclusions

The Fenhe River Basin, which is in the middle reaches of the Yellow River, is an important area in terms of ecological functions and grain and cotton production. The basin is

economically developed and densely populated. The basin has played an important role in the economic development of Shanxi Province. However, development has increased in recent years, and cities in the basin have expanded rapidly. Population growth and economic development in the upper and middle reaches of the Fenhe River have accelerated changes in land use. These changes have caused habitats in the upper and middle reaches of the Fenhe River to become degraded and the concentrations of pollutants in the river water and sediment to increase rapidly. This has caused the numbers of macrobenthos cleaning species to decrease sharply and the numbers of pollutant-tolerant species to increase. The macrobenthos now consists of a small number of species with unevenly distributed populations. The results of this study indicate that habitats in the upper and middle reaches of the Fenhe River are being degraded to a worrying degree.

Data Availability

All the data used to support the findings of this study are available from the corresponding author upon request.

Conflicts of Interest

The authors declare that there are no conflicts of interest regarding the publication of this article.

Acknowledgments

Funding was provided by the Key Research and Development Program of Shanxi Province (Grant nos. 201803D31211-1 and 201803D221002-4), the Natural Science Foundation Project of Shanxi Province (Grant nos. 201701D121116 and 201801D121261), the Programs for Science and Technology Development of Shanxi Province (Grant no. 20150313001-2), the Subproject of the National Key Research and Development Project (Soil Project Grant no. 2018YFC1803003), and the National Natural Science Foundation Project of China (Grant no. 41601202). The authors thank Jeremy Kamen, MSc, and Gareth Thomas, PhD, from Liwen Bianji, Edanz Group China (<http://www.liwenbianji.cn/ac>), for editing the English text of a draft of this manuscript.

References

- [1] X. Chen, X. Tu, P. Xie, and Y. Li, "Advances in the study of the human activities affecting the variation of hydrological elements," *Advances in Earth Science*, vol. 25, no. 8, pp. 800–811, 2010.
- [2] D. Wang and H. Tan, "Impact of human activities on river ecosystem," *Science Technology and Engineering*, vol. 4, no. 4, pp. 299–302, 2004.
- [3] G. Hu, J. Guo, and X. Luo, "Distribution, sources, and risk assessment of polycyclic aromatic hydrocarbons (PAHs) in surface sediments from Baiyangdian lake," *Research of Environmental Sciences*, vol. 22, no. 03, pp. 321–326, 2009.
- [4] A. P. Covich, M. A. Palmer, and T. A. Crowl, "The role of benthic invertebrate species in freshwater ecosystems-zoo-benthic species influence energy flows and nutrient cycling," *Bioscience*, vol. 49, no. 2, pp. 119–127, 1999.
- [5] Y. Zhang, L. Liu, Y. Cai, H. Yin, J. Gao, and Y. Gao, "Benthic macroinvertebrate community structure in rivers and streams of Lake Taihu Basin and environmental," *China Environmental Science*, vol. 35, no. 5, pp. 1535–1546, 2015.
- [6] A. H. Purcell, D. W. Bressler, M. J. Paul et al., "Assessment tools for urban catchments: developing biological indicators based on benthic macroinvertebrates," *Jawra Journal of the American Water Resources Association*, vol. 45, no. 2, pp. 306–319, 2009.
- [7] D. Liu, H. Yu, S. Liu, Z. Hu, J. Yu, and B. Wang, "Impacts of urbanization on the water quality and macrobenthos community structure of the tributaries in middle reach of Qiantang River, East China," *Chinese Journal of Applied Ecology*, vol. 23, no. 5, pp. 1370–1376, 2012.
- [8] H. Tomohiro, S. H. I. Jiang-hong, H. Zhang, and X.-W. Liu, "Distribution of perfluorooctanesulfonate and perfluorooctanoate in water and the sediment in Fenhe River, Shanxi province," *Environmental Science*, vol. 34, no. 11, pp. 4211–4217, 2013.
- [9] C. W. Dickens and P. M. Graham, "The South African scoring system (SASS) version 5 rapid bioassessment method for rivers," *African Journal of Aquatic Science*, vol. 27, no. 1, pp. 1–10, 2002.
- [10] X. Zhang, H. Xuan, and H. Wang, "Study on the community structure of benthic animals in different levels of rivers in Qingyi river basin," *Resources and Environment in the Yangtze Basin*, vol. 23, no. 12, pp. 1659–1664, 2014.
- [11] H. Wang, *A Study on the Small Earthworms in China*, Higher Education Press, Beijing, China, 2002.
- [12] Y. Liu, W. Zhang, and Y. Wang, *Chinese Economic Zoology (Freshwater Mollusks)*, pp. 1–134, The Science Publishing Company, Beijing, China, 1979.
- [13] J. H. Epler, *Identification Manual for the Larval Chironomidae (Diptera) of North and South Carolina*, North Carolina Department of Environment and Natural Resources, Division of Water Quality, Young Perkins, NC, USA, 2001.
- [14] J. L. Plafkin, M. T. Barbour, K. D. Porter, S. K. Gross, and R. M. Hughes, *Rapid Bioassessment Protocols for Use in Streams and Rivers: Benthic Macroinvertebrates and Fish. EPA-444/4-89-001*, US Environmental Protection Agency, Washington, DC, USA, 1989.
- [15] Z. Xu, "Zooplankton in north branch waters of Changjiang Estuary," *Chinese Journal of Applied Ecology*, vol. 16, no. 7, pp. 1341–1345, 2005.
- [16] Chinese Research Academy of Environmental Sciences, *Technical Guidelines for Valley Eco-Health Assessment*, Chinese Research Academy of Environmental Sciences, Beijing, China, 2013.
- [17] N. Li, A. Chen, C. Yang, Y. Sun, G. Ma, and Q. Ma, "Impacts of urbanization on water quality and macrobenthos community structure upstream in the Huangshui river," *Acta Ecologica Sinica*, vol. 37, no. 10, pp. 3570–3576, 2017.
- [18] T. Yuan, K. K. Vadde, J. D. Tonkin et al., "Impacts the physicochemical characteristics and abundance of fecal markers and bacterial pathogens in surface water," *International Journal of Environmental Research and Public Health*, vol. 16, no. 10, p. 1739, 2019.
- [19] C. J. Walsh, A. H. Roy, J. W. Feminella, P. D. Cottingham, P. M. Groffman, and R. P. Morgan, "The urban stream syndrome: current knowledge and the search for a cure," *Freshwater Science*, vol. 24, no. 3, pp. 706–723, 2005.
- [20] R. S. King, M. E. Baker, P. F. Kazzyak, and D. E. Weller, "How novel is too novel? Stream community thresholds at exceptionally low levels of catchment urbanization," *Ecological Applications*, vol. 21, no. 5, pp. 1659–1678, 2011.
- [21] D. Beach, *Coastal Sprawl: The Effects of Urban Design on Aquatic Ecosystems in the United States*, Pew Oceans Commission, Arlington, VA, USA, 2002.
- [22] K. F. Stepenuck, R. L. Crunkilton, and L. Wang, "Impacts of urban landuse on macroinvertebrate communities in southeastern Wisconsin streams," *Journal of the American Water Resources Association*, vol. 38, no. 4, pp. 1041–1051, 2002.
- [23] Ministry Ecology and Environment of the Peoples Republic of China and State Administration for Market Regulation, *GB3838-2002 Standards of Surface Water Environmental Quality of the People's Republic of China*, China Environmental Science Press, Beijing, China, 2002.

Research Article

Polycyclic Aromatic Hydrocarbons in Surface Water from Wuhai and Lingwu Sections of the Yellow River: Concentrations, Sources, and Ecological Risk

Yun Liu , Qingwei Bu , Hongmei Cao , Handan Zhang , Chuansheng Liu , Xiaofan He , and Mengqi Yun 

School of Chemical & Environmental Engineering, China University of Mining & Technology-Beijing, Beijing 100083, China

Correspondence should be addressed to Qingwei Bu; qingwei.bu@cumtb.edu.cn

Received 27 December 2019; Accepted 5 February 2020; Published 28 February 2020

Guest Editor: Chenglian Feng

Copyright © 2020 Yun Liu et al. This is an open access article distributed under the Creative Commons Attribution License, which permits unrestricted use, distribution, and reproduction in any medium, provided the original work is properly cited.

In this study, concentrations, sources, and ecological risk of 16 polycyclic aromatic hydrocarbons (PAHs) in 41 surface water samples collected from Wuhai and Lingwu sections of the Yellow River were investigated. The results showed that total PAH concentrations varied from 27.5 ng/L to 234 ng/L and from 135 ng/L to 265 ng/L in surface water of Wuhai and Lingwu sections, respectively. Source identification was performed by using principal component and multiple linear regression analysis. PAHs in Wuhai section of the Yellow River were mainly from coal combustion (35%) and vehicle exhausts (34%). Ecological risk of PAHs to aquatic organisms was assessed by applying the probabilistic risk assessment method. The results showed that the probabilities of exceeding the chronic toxicity for 5% of the species were 28% and 32% for PAHs in surface water from Wuhai and Lingwu sections, respectively. It has been demonstrated that there is an urgent need for environmental managers to take measures to reduce the ecological risk of PAHs in the aquatic environment in both Wuhai and Lingwu sections of the Yellow River.

1. Introduction

Polycyclic aromatic hydrocarbons (PAHs) are compounds consisting of two or more fused rings that have raised more concerns due to their persistent property and toxicity featured by considerably high direct-acting mutagenicity and carcinogenicity [1]. PAHs find their way into the environment through natural sources such as volcanoes, forest fire, and biosynthetic process. It could also be emitted from diverse anthropogenic sources such as vehicle exhausts; power plants; chemical, coke, and oil-shale industries; and urban sewage [2, 3].

It has been demonstrated that, in the process of coal mining, the treatment and storage of coal provided the basic conditions for the release of PAHs into the environment [4–9]. For example, PAHs in coal and coal waste could be leached into the mine water [10] and then enter into the aquatic environment with the discharge of mine water [11]. Therefore, the occurrence of PAHs in surface water nearby

the coal mining area has attracted lots of attention recently [5, 9, 12, 13]. However, studies on concentrations, sources, and ecological risk of PAHs in surface water of rivers located in or nearby the coal mining area are generally limited at present. Seopela et al. [9] investigated the occurrence levels and evaluated the risk of PAHs in the Loskop Dam nearby the coalmine in South Africa. They reported that the total PAH concentrations varied from 1170 ng/L to 14500 ng/L, and it was found that the occurrence of PAHs in the sediment of Loskop Dam could lead to a delay of the development and malformation of zebrafish embryo [9]. Hao et al. [12] investigated the concentrations and sources of PAHs in surface water of Fuyang River nearby the Fengfeng coal mining area. Huang et al. [5] reported that the average concentration of 16 PAHs was 427 ng/L in surface water of rivers located in Heshan coal district in Guangxi.

In the present study, we aimed to investigate the concentrations, sources, and ecological risk of PAHs in surface water of Wuhai and Lingwu sections of the Yellow River in

China. Both Wuhai and Lingwu are large coal mining bases in the northwestern China and have a long history of coal mining. Over the years, the coal mining areas in both cities have dramatically expanded. A large number of cultivated land, forest, and grassland have been occupied due to mining activities, resulting in the sharp deterioration of the local ecological environment. The Yellow River is the only surface water resource flowing through Lingwu and Wuhai. During recent years, the water resource of the Yellow River is becoming more and more stressing due to the intensive mining activities, which could also aggravate the degradation of the vulnerable ecosystem.

Therefore, we carried out a field campaign to (i) determine concentrations of PAHs in surface water collected from Wuhai and Lingwu sections of the Yellow River, (ii) identify major sources and origins of PAHs, and (iii) assess the ecological risk of PAHs to aquatic organisms by applying the probabilistic ecological risk assessment. This study would be helpful to the control of PAH risk in rivers located in or nearby coal mining areas.

2. Materials and Methods

2.1. Chemicals. The PAH mixture standard was purchased from Accustandard (USA), including naphthalene (Nap), acenaphthylene (Acy), acenaphthene (Ace), fluorene (Flu), phenanthrene (Phe), anthracene (Ant), fluoranthene (Flua), pyrene (Pyr), benzo(a)anthracene (BaA), chrysene (Chr), benzo(b)fluoranthene (BbF), benzo(k)fluoranthene (BkF), dibenzo(a, h)anthracene (DBA), benzo(a)pyrene (BaP), indeno(1,2,3-cd)pyrene (Ind), and benzo(g, h, i)perylene (BghiP). The injection standard (hexamethylbenzene, HMB) was provided by Dr. Ehrenstorfer (Germany). Phe-d10 and Chr-d12 were used as recovery standards and obtained from Accustandard (USA). All solvents, including methanol, dichloromethane, and *n*-hexane, were of HPLC grade and obtained from Fisher (USA). C18 cartridges (500 mg/6 cc) used for solid phase extraction (SPE) were purchased from Waters (USA).

2.2. Sample Collection and Analytical Procedure. A total of 30 sampling sites at Wuhai section were set up along the mainstream of the Yellow River, while 11 sampling sites were selected at Lingwu section (Figure 1). At each sampling site, approximately four liters of surface water were collected and transported to the lab immediately. All water samples were stored at 4°C and analyzed in 24 h. The sampling events were conducted in July, 2019.

The sample pretreatment method for surface water was adapted from Bu et al. [14]. In brief, approximately 2 L surface water samples (in triplicate) were filtered using a glass fiber filter (0.45 μm, Millipore, USA) prior to SPE. The sample was enriched by SPE (Supelco, USA) with the C18 cartridge that had been preconditioned with 10 mL of dichloromethane, 10 mL of methanol, and then 10 mL of ultrapure water. After enrichment, the cartridge was eluted with 10 mL of dichloromethane. The eluents were collected in a K-D concentrator and concentrated to approximately

0.5 mL under a gentle nitrogen stream. Thereafter, 20 μL of injection standards (10 μg/mL HMB) were added, and the final volume was made up to 1 mL in dichloromethane for instrumental analysis.

2.3. Instrument Analysis. Samples were analyzed by using a GC2010 gas chromatograph coupled with a QP2010 mass spectrometer (GC-MS, Shimadzu, Japan). Aliquots of sample extracts (1 μL) were introduced by the splitless injection at 280°C. Chromatographic separation of PAHs was achieved on an Rtx-5MS capillary column (length 30.0 m, i.d. 0.25 mm, film 0.25 μm, Shimadzu, Japan) over 57 min using a triple ramp oven programme (initial temperature 60°C; 20°C/min to 160°C; 3°C/min to 280°C, held for 6 min; 20°C/min to 300°C, held for 5 min). A constant flow (1 mL/min) of ultrapure helium carrier gas (99.999%) was maintained. Mass spectra were collected over the range *m/z* 50 to 500. The temperatures of the transfer line and ion source were 220°C and 250°C. Ionization of analyte was performed using the electron ionization at 70 eV. A full scan of the mixture standard containing each compound (1 μg/mL) allowed the identification of the compound peaks according to their retention times and mass spectra. Retention time locking with an internal standard was applied to ensure the reproducibility of retention time of each target compound. This was followed by data acquisition in the selective ion monitoring mode that entailed the identification of the most intense and distinct fragment ions for each compound, within a well-defined time window.

2.4. Quality Control and Assurance. Matrices-spiked control experiments were used to evaluate the method performance in parallel with each batch of samples. In brief, two liters of the contaminant-free ultrapure water were spiked with 10 μL of the PAH mixture standards (each PAH congener at 10 μg/mL), and the recovery rates of the 16 PAHs were 47%–116% (*n* = 5). Procedure blanks were run with each batch of samples to evaluate possible contamination during analysis, and levels of PAHs were below the limit of quantification (LOQ) in all cases. The LOQs of PAHs were estimated as the concentration when the signal-to-noise ratio was 10:1 (*S/N* = 10). The method detection limit (MDL) was 0.049–5.57 ng/L, assuming a final extract volume of 1.0 mL and surface water samples of 2 L. Recovery rates were also evaluated by adding the PAH mixture standard (each PAH congener at 10 μg/mL) into 2 L real surface water samples (*n* = 6) collected from Qinghe River in Beijing. The results showed that recovery rates of PAHs were 50%–104%. The average recoveries of Phe-d10 and Chr-d12 were 114% ± 4.5% and 71% ± 3.8%, respectively.

2.5. Probabilistic Ecological Risk Assessment for PAH Mixture. In this study, the probabilistic ecological risk assessment method was used to assess the hazard of PAHs to aquatic organisms in the Yellow River. Specifically, a joint probability curve (JPC) was generated through combining exposure and toxicity data [15]. The specific point on the JPC

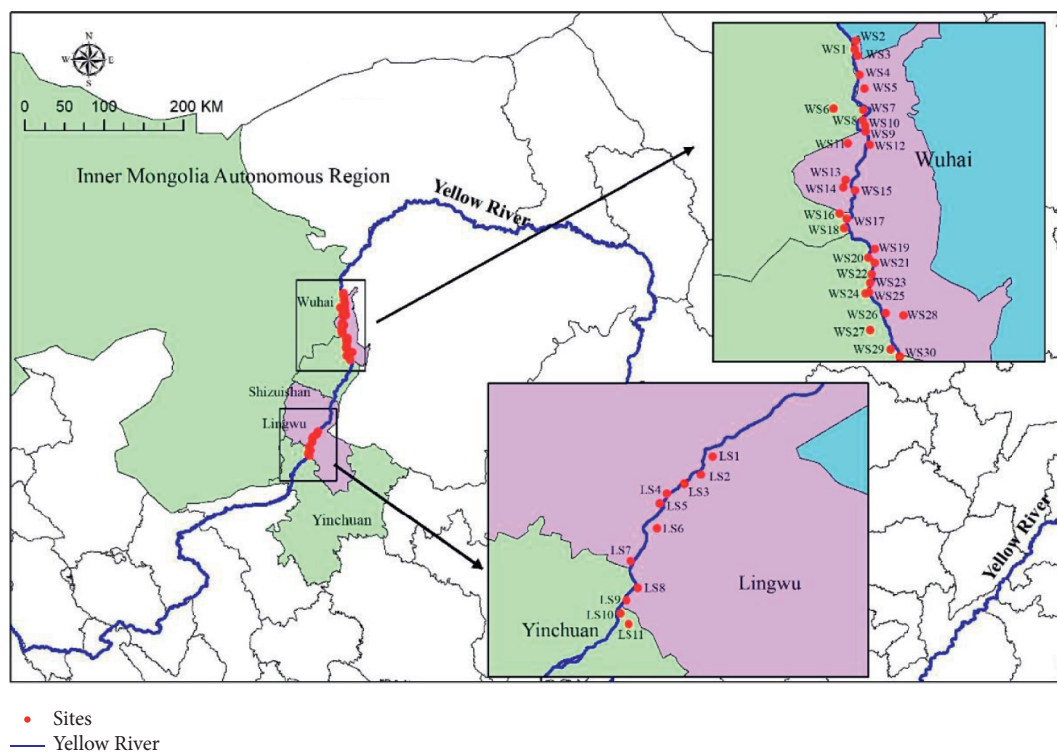


FIGURE 1: Schematic diagram showing the locations of the sampling sites in the Yellow River.

represents both the probability that the chosen fraction of species would be in danger, and the frequency with which the level of effect would be exceeded.

To reflect the additive effect of the 16 PAHs, BaP equivalency (BaP_{eq}) of PAHs was calculated based on the toxic equivalency factors (TEFs) for PAHs [16]. Then, the ecological risk of PAH mixture was evaluated. Ecotoxicology data for BaP were collected from the United States Environmental Protection Agency ECOTOXicology Database (<http://www.epa.gov/ecotox/>). All toxicity data were the no observed effect concentration (NOEC) obtained from tests conducted in a freshwater system and the data selection procedure followed principles of accuracy, relevance, and reliability [17].

3. Results and Discussion

3.1. Concentrations and Distribution. Concentrations of the 16 PAHs in surface water from Wuhai and Lingwu sections of the Yellow River are presented in Figure 2. Total concentrations of PAHs ranged from 27.5 ng/L (WS16) to 233 ng/L (WS19) in the Wuhai section of the Yellow River with a mean concentration of 162 ng/L, while PAH concentrations range from 135 ng/L (LS10) to 265 ng/L (LS6) in the Lingwu section with a mean concentration of 197 ng/L. The concentration of Nap was the highest among different congeners, accounting for 12% and 14% of the total PAH concentrations on average for Wuhai and Lingwu sections, respectively. Average concentrations of most congeners in surface water from Lingwu section were slightly higher than that from Wuhai section, except for Phe, BaA, BkF, DBA,

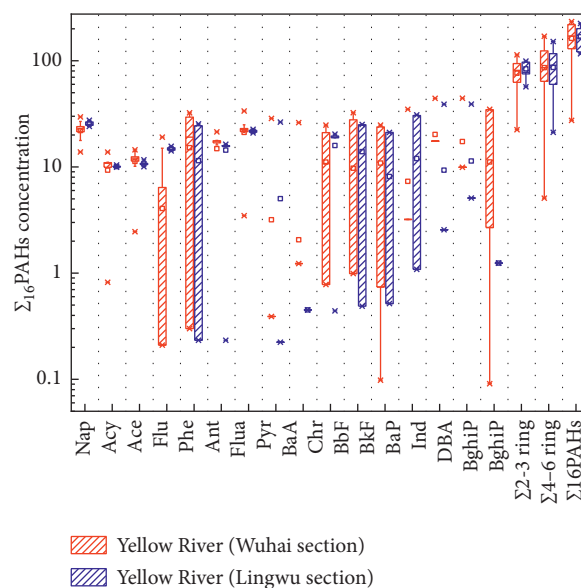


FIGURE 2: Concentrations of PAHs in surface water from Wuhai and Lingwu sections of the Yellow River.

and BghiP. In general, the compositional pattern of PAHs was in the following order for both studied areas: 3 rings > 4 rings > 5 rings > 2 rings > 6 rings (Figure 2).

We collected the available data on PAH concentrations in surface water surrounding coal mining areas from previously published literature. Through the comparison among different studies, it can be found that PAH concentrations in the present study were significantly lower than

those in the Loskop Dam (South Africa, 1170–14500 ng/L) [9], surface water of rivers in the Shilong coalmine (China, 68–8377 ng/L) [13], and rivers in the Heshan coal district (China, 199–1351 ng/L) [5]. However, PAH concentrations in surface water of rivers in the Fengfeng coalmines (China, 1.35–2.92 ng/L) [12] were significantly lower than that in our study.

Table 1 shows a comparison of PAH concentrations in surface water samples collected from rivers around China during the past decade. When compared to other studies conducted in the Yellow River watershed, our results were in the same order of magnitude to that reported for PAHs in surface water collected from Henan reach [18] and Xi'an section [19] of the Yellow River but were significantly lower than that from the Yellow River Estuary [20]. A comparison was also made to studies conducted in regions other than the Yellow River watershed (Table 1). It can be found that the mean values of the total concentration of PAHs observed in the present study were comparable to that from the Songhua River [23], the Yangtze River Delta [26], the Poyang Lake [28], Xiamen Coastal Area [30], and the Chaohu Lake [32], slightly lower than that from the Daliao River Estuary [22], the Songhua River basin [21], and the Jiangsu section of the Yangtze River [25], but significantly lower than that from the Yangtze Estuary and coastal areas [29], the Liaohe River basin [21], the Taihu Lake [27], the Huaihe River basin [21], and the Weishan Lake [31]. Moreover, our results were significantly higher than that from the Baiyangdian Lake [24], the Fujiang River [23], the Pear River [33], the Dongjiang River [33], and the Pearl River Estuary [33, 34]. Overall, PAH concentrations in surface water collected from Wuhai and Lingwu sections of the Yellow River were at moderate levels in China.

3.2. Source Apportionment

3.2.1. Sources of PAHs in Wuhai Section of the Yellow River.

Principal component analysis (PCA) was conducted to evaluate the contribution of different PAH sources, and the results are presented in Table 2, which shows the variable loadings describing the major contamination patterns and their explained variance. Note that Pyr, BaA, BaP, and Ind were not considered because of their low detection rates. Five principal components accounting for 81% of the total variance were extracted through PCA.

The first component (PC1) explained 38% of the total variance and was predominately loaded with Flua, Ace, Nap, Acy, and Ant. It has been reported that Flua and Ant were related to coal combustion-generated PAHs [2, 35–37]. Loadings of Acy and Nap have been associated with vaporization or spill of petroleum-related products [38]. Ace was one of the dominant PAHs from the coke industry and could enter into the Yellow River via industrial wastewater and atmospheric fallout [39]. Therefore, PC1 explained the compounds originating from coal combustion, spill of petroleum-related products, and the coke industry. The second component (PC2) contributed 15% to the total variance and was heavily weighted with Flu and DBA. Flu was another one

TABLE 1: Summary of concentrations (ng/L) of PAHs in surface water samples collected from rivers in China during the past decade.

Locations	<i>n</i>	Min	Max	Mean	References
Yellow River (Wuhai section)	30	27.5	234	162	This study
Yellow River (Lingwu section)	11	135	265	197	This study
Yellow River (Henan reach)	26	144	2361	662	[18]
Yellow River (Xi'an region)	6	357	2017	824	[19]
Yellow River Estuary (flood season)	8	474	1190	729	[20]
Yellow River Estuary (dry season)	8	1682	6014	2944	[20]
Liaohe River Basin	15	209	33930	4021	[21]
Daliao River Estuary	12	139	1718	486	[22]
Songhua River	7	88.6	140	—	[23]
Songhua River Basin	15	7.12	9131	759	[21]
Baiyangdian Lake	6	40.1	74	51	[24]
Fujiang River	8	43.9	81	—	[23]
Yangtze River (Jiangsu section)	15	12	3576	925	[25]
Yangtze River Delta	14	12.9	638	201	[26]
Taihu Lake	5	11000	34000	—	[27]
Poyang Lake	40	5.56	266	—	[28]
Yangtze Estuary and coastal areas	18	478	6273	1858	[29]
Xiamen coastal area	13	62	342	151	[30]
Huaihe River Basin	—	1700	7770	4386	[21]
Weishan Lake	9	5350	12970	8572	[31]
Chaohu Lake	15	95.6	370	171	[32]
Dongjiang River	8	10.9	42.3	24.9	[33]
Pearl River	8	15.4	48.1	27.1	[33]
Pearl River Estuary	20	12.9	182	45.4	[34]
Pearl River Estuary	3	11.7	18.6	15.1	[33]

n, numbers of collected samples.

TABLE 2: Rotated component matrix of studied PAHs in the Yellow River (Wuhai section).

PAHs	Components				
	1	2	3	4	5
Nap	0.912	0.195	0.014	0.158	0.086
Acy	0.884	-0.156	0.093	-0.168	-0.032
Ace	0.921	0.038	0.184	0.198	0.148
Flu	-0.055	0.861	-0.004	-0.073	0.042
Phe	0.154	-0.336	0.589	0.158	0.41
Ant	0.623	-0.038	0.5	-0.057	0.408
Flua	0.907	0.105	0.187	0.122	0.225
Chr	0.173	0.086	0.855	0.128	-0.21
BbF	0.248	0.059	0.296	0.729	-0.155
BkF	0.229	-0.047	-0.077	0.002	0.9
DBA	0.154	0.781	-0.025	0.004	-0.12
BghiP	-0.044	-0.128	-0.022	0.885	0.131
Eigenvalues	4.587	1.777	1.477	1.033	0.866
% variance	38.226	14.809	12.309	8.606	7.216
Cum. percentage	38.226	53.035	65.344	73.95	81.166

dominant PAHs from the coking process [39], while a relatively higher abundance of DBA has been identified as a marker of gasoline vehicle emissions. Hence, PC2 was

reflective of PAHs from the coking process and vehicle exhausts. The third component (PC3) characterized for 12% of the total variance. This component was heavily loaded with Chr and Phe. Chr and Phe had been identified as typical tracers of coal combustion [36]. Hence, PC3 was reflective of PAHs derived from coal combustion. The fourth component (PC4) contributed 8.6% to the total variance and was dominated by BghiP and BbF. Dominance of BghiP and BbF over other PAHs has been attributed to diesel combustion [40, 41]. Thus, PC4 was selected to represent diesel combustion source of PAHs in surface water of the Yellow River. The fifth component (PC5) was responsible for 7.2% of the total variance and weighted by BkF, Ant, and Phe. BkF has been identified as an indicator of diesel combustion [40, 41], while it has been reported that Ant and Phe were related to coal combustion [2, 36, 42]. Hence, PC5 was reflective of PAHs from coal and diesel combustion.

Using the multivariate linear regression (MLR) from PCA factor scores, the equation was calculated as follows:

$$\sum_{16} \text{PAHs} = 0.901 \times \text{PC1} + 0.408 \times \text{PC2} + 0.454 \times \text{PC3} + 0.457 \times \text{PC4} + 0.529 \times \text{PC5} (R^2 = 0.6). \quad (1)$$

Therefore, PAHs in Wuhai section of the Yellow River were originated from four major sources, and the quantitative contributions were 35% from coal combustion, 34% from vehicle exhausts, 21% from coke industry, and 11% from spill of petroleum-related products.

3.2.2. Sources of PAHs in Lingwu Section of the Yellow River.

Note that BaA, BghiP, Pyr, Ind, and DBA were not considered in the PCA because of their low detection rates. According to the results presented in Table 3, PAHs were separated into four major categories. Over 85% of the total variance of the data could be interpreted by four eigenvectors.

The first component (PC1) explained 38% of the total variance and was predominately loaded with Acy, Ace, and Flu. It has been reported that Ace and Flu were related to coke industry [39], while Acy has been related to vaporization or spill of petroleum-related products [38]. Therefore, PC1 explained the compounds originating from coking industry and spill of petroleum-related products. The second component (PC2) contributed 24% to the total variance and was heavily weighted with BbF and Flua. BbF has been recognized as an indicator of diesel combustion [40, 41], while Flua has been linked to coal combustion [2, 35–37]. Hence, PC2 was a reflection of PAHs from diesel exhaust and coal combustion. The third component (PC3) contributed 15% to the total variance and was dominated by Chr and Ant. Coal combustion could be sources of Chr and Ant [36]. Thus, PC3 was selected to represent coal combustion originated PAHs. The fourth component (PC4) was responsible for 11% of total variance and weighted by BkF and NaP. It has been pointed out that a relatively higher

TABLE 3: Rotated component matrix of studied PAHs in the Yellow River (Lingwu section).

PAHs	Components			
	1	2	3	4
Nap	0.521	-0.417	0.294	0.623
Acy	0.953	0.038	0.036	0.234
Ace	0.904	-0.026	0.295	-0.144
Flu	0.92	0.193	0.23	-0.038
Phe	-0.436	-0.786	0.191	-0.176
Ant	0.309	-0.247	0.837	-0.222
Flua	0.326	0.753	0.389	0.024
Chr	0.275	0.101	0.829	-0.031
BbF	-0.206	0.916	-0.019	0.046
BkF	-0.036	0.257	-0.166	0.926
BaP	-0.168	0.455	0.599	0.298
Eigenvalues	4.127	2.623	1.67	1.232
% variance	37.521	23.841	15.186	11.202
Cum. percentage	37.521	61.362	76.548	87.75

abundance of BkF was the marker of diesel vehicle emission [40, 41]. In the meantime, Nap was associated with vaporization or spill of petroleum-related products [38]. Hence, PC4 was representative of PAHs from petroleum-related products and diesel combustion.

PCA-MLR was performed, and the following equation was established:

$$\sum_{16} \text{PAHs} = 0.175 \times \text{PC1} + 0.043 \times \text{PC2} + 0.417 \times \text{PC3} + 0.230 \times \text{PC4} (R^2 = 0.4). \quad (2)$$

Therefore, PAHs in Lingwu section of the Yellow River were originated from four major sources and the quantitative contributions were 34% from coal combustion, 27% from spill of petroleum-related products, 24% from coke industry, and 16% from vehicle exhausts.

It should be noted that the quantitative results for source contributions should be explained with caution due to the small R^2 value of the regression, which could be caused by the limited number of data points used in the source identification. The other reasons could be the complex sources of PAHs in Lingwu section of the Yellow River, as it is well known that Lingwu was close to Yinchuan, and as well, it is one of the most important bases of coal chemical industry in the Northwestern China. More data should be collected for further analysis.

3.3. Ecological Risk Assessment. BaP_{eqs} of PAHs ranged from 0.06 ng/L to 264 ng/L in surface water in Wuhai section of the Yellow River. As for Lingwu section, BaP_{eqs} of PAHs ranged from 0.59 ng/L to 257 ng/L among different sampling sites, which was similar to that in surface water of Wuhai section. As shown in Figure 3, probabilities of exceeding the NOEC for 5% of the species were 28% and 32% for PAHs in surface water in Wuhai and Lingwu sections of the Yellow River, respectively. This indicates that ecological risks of PAHs to aquatic organisms were high in both study areas. It

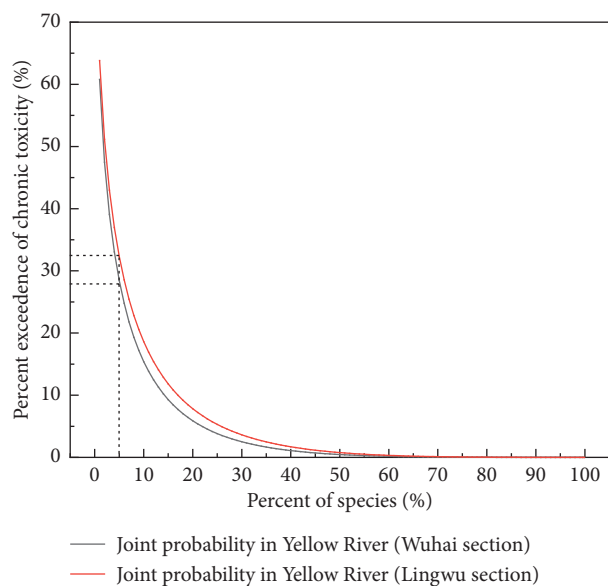


FIGURE 3: JPC of PAHs in surface water of the Yellow River.

has been demonstrated that there is an urgent need for taking measures to reduce the ecological risk of PAHs in the aquatic environment in the study areas.

However, there could be some uncertainties in the above assessing results. Other concomitants that were not taken into account may cause additive and synergistic effects, which could cause the underestimation of toxic effects [43]. For example, Wang et al. [44] reported that the joint toxic effect was observed when exposing the marine microalga to the mixture of Ant with profenofos. Moreover, the bioaccumulation and metabolism of PAHs in aquatic organisms were not being considered. In addition, collected toxic data and exposure data were limited. As emission continues, concentrations of PAHs in the aquatic ecosystem could increase.

4. Conclusions

The results showed that total PAH concentrations varied from 27.5 ng/L to 234 ng/L and 135 ng/L to 265 ng/L in surface water of Wuhai and Lingwu sections, respectively. PAHs in Wuhai section of the Yellow River were mainly from coal combustion (35%) and vehicle exhausts (34%). Results of ERA showed that the probabilities of exceeding the chronic toxicity for 5% of the species were 28% and 32% for PAHs in surface water from Wuhai and Lingwu sections, respectively. It has been demonstrated that there is an urgent need for taking measures to reduce the ecological risk of PAHs in the aquatic environment in our study areas.

Data Availability

The numerical data used to support the findings of this study are included within the article.

Conflicts of Interest

The authors declare that they have no conflicts of interest.

Acknowledgments

This work was cosupported by the National Key R&D Program of China (2017YFC0504401), National Natural Science Foundation of China (21777188), and Fundamental Research Funds for the Central Universities in China (2015QH02). Q.B. is also funded by Yue Qi Young Scholar Project, China University of Mining & Technology, Beijing (2017QN15). The authors thank Mingyue Zou, Xiaoyan Zhu, and Yali Guo for their assistance during the sample pretreatment, and Su Meng and Jihong Wu for their assistance during the instrumental analysis.

References

- [1] Y. Yang, X.-X. Zhang, and T. Korenaga, "Distribution of polynuclear aromatic hydrocarbons (PAHs) in the soil of Tokushima, Japan," *Water, Air, and Soil Pollution*, vol. 138, no. 1-4, pp. 51-60, 2002.
- [2] M. Yunker, R. Macdonald, D. Goyette et al., "Natural and anthropogenic inputs of hydrocarbons to the Strait of Georgia," *The Science of The Total Environment*, vol. 225, no. 3, pp. 181-209, 1999.
- [3] M. B. Yunker, R. W. Macdonald, R. Vingarzan, R. H. Mitchell, D. Goyette, and S. Sylvestre, "PAHs in the Fraser River basin: a critical appraisal of PAH ratios as indicators of PAH source and composition," *Organic Geochemistry*, vol. 33, no. 4, pp. 489-515, 2002.
- [4] D. Chen, Q. Feng, H. Liang, B. Gao, and E. Alam, "Distribution characteristics and ecological risk assessment of polycyclic aromatic hydrocarbons (PAHs) in underground coal mining environment of Xuzhou," *Human and Ecological Risk Assessment: An International Journal*, vol. 25, no. 6, pp. 1564-1578, 2019.
- [5] H.-F. Huang, X.-L. Xing, Z.-Z. Zhang et al., "Polycyclic aromatic hydrocarbons (PAHs) in multimedia environment of Heshan coal district, Guangxi: distribution, source diagnosis and health risk assessment," *Environmental Geochemistry and Health*, vol. 38, no. 5, pp. 1169-1181, 2016.
- [6] Z. Ouyang, L. Gao, X. Chen, S. Yao, and S. Deng, "Distribution, source apportionment and ecological risk assessment of polycyclic aromatic hydrocarbons in the surface sediments of coal mining subsidence waters," *RSC Advances*, vol. 6, no. 75, pp. 71441-71449, 2016.
- [7] B. Gao, Q. Feng, L. Zhou, H. Wu, and E. Alam, "Distributions of polycyclic aromatic hydrocarbons in coal in China," *Polish Journal of Environmental Studies*, vol. 28, no. 3, pp. 1665-1674, 2019.
- [8] R. Wang, G. Liu, C.-L. Chou, J. Liu, and J. Zhang, "Environmental assessment of PAHs in soils around the Anhui coal district, China," *Archives of Environmental Contamination and Toxicology*, vol. 59, no. 1, pp. 62-70, 2010.
- [9] M. P. Seopela, R. I. McCrindle, S. Combrinck, and T. J.-C. Regnier, "Hazard assessment of polycyclic aromatic hydrocarbons in water and sediment in the vicinity of coal-mines," *Journal of Soils and Sediments*, vol. 16, no. 12, pp. 2740-2752, 2016.
- [10] M. Hendryx, K. O'Donnell, and K. Horn, "Lung cancer mortality is elevated in coal-mining areas of Appalachia," *Lung Cancer*, vol. 62, no. 1, pp. 1-7, 2008.
- [11] F. Goodarzi and P. K. Mukhopadhyay, "Metals and polycyclic aromatic hydrocarbons in the drinking water of the Sydney basin, Nova Scotia, Canada: a preliminary assessment of their

- source,” *International Journal of Coal Geology*, vol. 43, no. 1–4, pp. 357–372, 2000.
- [12] C. Hao, Y. Huang, D. Ma et al., “Environmental behaviors of PAHs in ordovician limestone water of Fengfeng coal mining area in China,” *Environmental Monitoring and Assessment*, vol. 190, no. 12, p. 701, 2018.
- [13] C. Yang, N. Zhong, D. Chen, J. Wang, and X. Peng, “Composition and distribution characteristics of polycyclic aromatic hydrocarbons in water samples from a coal-mining area, Henan, China,” *Journal of Safety and Environment*, vol. 7, no. 1, pp. 75–78, 2007, in Chinese.
- [14] Q. Bu, D. Wang, Z. Wang, J. Gu, and N. Cao, “Removal analysis on polycyclic aromatic hydrocarbons and halogenated alkanes by water processing,” *Water & Wastewater Engineering*, vol. 37, no. 11, pp. 9–15, 2011, in Chinese.
- [15] K. Solomon, J. Giesy, and P. Jones, “Probabilistic risk assessment of agrochemicals in the environment,” *Crop Protection*, vol. 19, no. 8–10, pp. 649–655, 2000.
- [16] I. C. T. Nisbet and P. K. LaGoy, “Toxic equivalency factors (TEFs) for polycyclic aromatic hydrocarbons (PAHs),” *Regulatory Toxicology and Pharmacology*, vol. 16, no. 3, pp. 290–300, 1992.
- [17] H.-J. Klimisch, M. Andreae, and U. Tillmann, “A systematic approach for evaluating the quality of experimental toxicological and ecotoxicological data,” *Regulatory Toxicology and Pharmacology*, vol. 25, no. 1, pp. 1–5, 1997.
- [18] J.-H. Sun, G.-L. Wang, Y. Chai, G. Zhang, J. Li, and J. Feng, “Distribution of polycyclic aromatic hydrocarbons (PAHs) in Henan reach of the Yellow River, Middle China,” *Ecotoxicology and Environmental Safety*, vol. 72, no. 5, pp. 1614–1624, 2009.
- [19] W. Wang, J. Zhang, X. Li et al., “Characteristics and sources of polycyclic aromatic hydrocarbons pollution in water of Xi’an outskirts regions,” *Agricultural Research in the Arid Areas*, vol. 33, no. 5, pp. 201–206, 2015, in Chinese.
- [20] Y. Lang, Y. Jia, Z. Liu, Z. Gao, and X. Wang, “Seasonal distribution characteristics and sources of polycyclic aromatic hydrocarbons (PAHs) in water samples from the Yellow River estuary,” *Periodical of Ocean University of China*, vol. 38, no. 4, pp. 640–646, 2008, in Chinese.
- [21] G. Guo, F. Wu, H. He, R. Zhang, H. Li, and C. Feng, “Distribution characteristics and ecological risk assessment of PAHs in surface waters of China,” *Science China Earth Sciences*, vol. 55, no. 6, pp. 914–925, 2012.
- [22] B. Men, M. He, L. Tan, C. Lin, and X. Quan, “Distributions of polycyclic aromatic hydrocarbons in the Daliao River estuary of Liaodong Bay, Bohai sea (China),” *Marine Pollution Bulletin*, vol. 58, no. 6, pp. 818–826, 2009.
- [23] C. Wang, Z. Yang, X. Xia, H. Cheng, and T. Yu, “Distribution and sources of PAHs in typical Chinese rivers,” *Geoscience*, vol. 26, no. 2, pp. 400–406, 2012, in Chinese.
- [24] Y. Zhu, W. Wu, J. Wang et al., “Distribution, sources and ecological risks of polycyclic aromatic hydrocarbons in water-sediment system in lake small Baiyangdian,” *Journal of Lake Sciences*, vol. 21, no. 5, pp. 637–646, 2009, in Chinese.
- [25] H. He, G.-J. Hu, C. Sun et al., “Trace analysis of persistent toxic substances in the main stream of Jiangsu section of the Yangtze River, China,” *Environmental Science and Pollution Research*, vol. 18, no. 4, pp. 638–648, 2011.
- [26] L. Zhang, L. Dong, L. Ren et al., “Concentration and source identification of polycyclic aromatic hydrocarbons and phthalic acid esters in the surface water of the Yangtze River Delta, China,” *Journal of Environmental Sciences*, vol. 24, no. 2, pp. 335–342, 2012.
- [27] J.-X. Guo and J. Fang, “The distribution of n-alkanes and polycyclic aromatic hydrocarbons in water of Taihu Lake,” *Procedia Environmental Sciences*, vol. 12, pp. 258–264, 2012.
- [28] H. Zhi, Z. Zhao, and L. Zhang, “The fate of polycyclic aromatic hydrocarbons (PAHs) and organochlorine pesticides (OCPs) in water from Poyang Lake, the largest freshwater lake in China,” *Chemosphere*, vol. 119, pp. 1134–1140, 2015.
- [29] D.-N. Ou, M. Liu, S.-Y. Xu et al., “Distribution and ecological risk assessment of polycyclic aromatic hydrocarbons in overlying waters and surface sediments from the Yangtze estuarine and coastal areas,” *Environmental Science*, vol. 30, no. 10, pp. 3043–3049, 2009, in Chinese.
- [30] M.-L. Ya, X.-H. Wang, Y.-L. Wu, C.-X. Ye, and Y.-Y. Li, “Enrichment and partitioning of polycyclic aromatic hydrocarbons in the sea surface microlayer and subsurface water along the coast of Xiamen Island, China,” *Marine Pollution Bulletin*, vol. 78, no. 1–2, pp. 110–117, 2014.
- [31] X. Zheng, B. Han, H. Jiang, and K. Liu, “Distribution and source of polycyclic aromatic hydrocarbons in the water of aquatic product cage culture area of Weishan Lake,” *Sichuan Environment*, vol. 29, no. 6, pp. 21–24, 2010, in Chinese.
- [32] N. Qin, W. He, Y. Wang et al., “Residues and health risk of polycyclic aromatic hydrocarbons in the water and aquatic products from Lake Chaohu,” *Acta Scientiae Circumstantiae*, vol. 33, no. 1, pp. 230–239, 2013, in Chinese.
- [33] H. Li, L. Lu, W. Huang, J. Yang, and Y. Ran, “In-situ partitioning and bioconcentration of polycyclic aromatic hydrocarbons among water, suspended particulate matter, and fish in the Dongjiang and Pearl Rivers and the Pearl River Estuary, China,” *Marine Pollution Bulletin*, vol. 83, no. 1, pp. 306–316, 2014.
- [34] X.-J. Luo, B.-X. Mai, Q.-S. Yang, S.-J. Chen, and E. Y. Zeng, “Distribution and partition of polycyclic aromatic hydrocarbon in surface water of the Pearl River Estuary, South China,” *Environmental Monitoring and Assessment*, vol. 145, no. 1–3, pp. 427–436, 2008.
- [35] Y. Liu, L. Chen, Q.-H. Huang, W.-Y. Li, Y.-J. Tang, and J.-F. Zhao, “Source apportionment of polycyclic aromatic hydrocarbons (PAHs) in surface sediments of the Huangpu River, Shanghai, China,” *Science of the Total Environment*, vol. 407, no. 8, pp. 2931–2938, 2009.
- [36] P. Masclet, G. Mouvier, and K. Nikolaou, “Relative decay index and sources of polycyclic aromatic hydrocarbons,” *Atmospheric Environment (1967)*, vol. 20, no. 3, pp. 439–446, 1986.
- [37] C. Biache, L. Mansuy-Huault, and P. Faure, “Impact of oxidation and biodegradation on the most commonly used polycyclic aromatic hydrocarbon (PAH) diagnostic ratios: implications for the source identifications,” *Journal of Hazardous Materials*, vol. 267, pp. 31–39, 2014.
- [38] M. P. Zakaria, H. Takada, S. Tsutsumi et al., “Distribution of polycyclic aromatic hydrocarbons (PAHs) in rivers and estuaries in Malaysia: a widespread input of petrogenic PAHs,” *Environmental Science & Technology*, vol. 36, no. 9, pp. 1907–1918, 2002.
- [39] M. F. Simcik, S. J. Eisenreich, and P. J. Liroy, “Source apportionment and source/sink relationships of PAHs in the coastal atmosphere of Chicago and Lake Michigan,” *Atmospheric Environment*, vol. 33, no. 30, pp. 5071–5079, 1999.
- [40] C. K. Li and R. M. Kamens, “The use of polycyclic aromatic hydrocarbons as source signatures in receptor modeling,” *Atmospheric Environment. Part A. General Topics*, vol. 27, no. 4, pp. 523–532, 1993.

- [41] A. Motelay-Massei, D. Ollivon, B. Garban, K. Tiphagne-Larcher, I. Zimmerlin, and M. Chevreuil, "PAHs in the bulk atmospheric deposition of the Seine river basin: source identification and apportionment by ratios, multivariate statistical techniques and scanning electron microscopy," *Chemosphere*, vol. 67, no. 2, pp. 312–321, 2007.
- [42] F. Tian, J. Chen, X. Qiao et al., "Sources and seasonal variation of atmospheric polycyclic aromatic hydrocarbons in Dalian, China: factor analysis with non-negative constraints combined with local source fingerprints," *Atmospheric Environment*, vol. 43, no. 17, pp. 2747–2753, 2009.
- [43] B. Wang, G. Yu, J. Huang, Y. Yu, H. Hu, and L. Wang, "Tiered aquatic ecological risk assessment of organochlorine pesticides and their mixture in Jiangsu reach of Huaihe River, China," *Environmental Monitoring and Assessment*, vol. 157, no. 1–4, pp. 29–42, 2009.
- [44] Y. Wang, X. X. Tang, and Y. Q. Li, "The joint toxic effect of anthracene and profenofos on marine microalga," *Experiment & Technique*, vol. 24, no. 4, pp. 5–7, 2000, in Chinese.

Research Article

Thyroid-Disrupting Activities of Groundwater from a Riverbank Filtration System in Wuchang City, China: Seasonal Distribution and Human Health Risk Assessment

Dongdong Kong,¹ Hedan Liu,¹ Yun Liu,² Yafei Wang,¹ and Jian Li ¹

¹Engineering Research Center of Groundwater Pollution Control and Remediation, Ministry of Education, College of Water Sciences, Beijing Normal University, Beijing 100875, China

²South China Institute of Environmental Science, MEE, No. 7 West Street, Yuancun, Guangzhou 510655, China

Correspondence should be addressed to Jian Li; lijian@bnu.edu.cn

Received 25 July 2019; Accepted 11 December 2019; Published 7 January 2020

Guest Editor: Lisa Yu

Copyright © 2020 Dongdong Kong et al. This is an open access article distributed under the Creative Commons Attribution License, which permits unrestricted use, distribution, and reproduction in any medium, provided the original work is properly cited.

The recombinant thyroid hormone receptor (TR) gene yeast assay was used to evaluate thyroid disruption caused by groundwater from the riverbank filtration (RBF) system in Wuchang City, China. To investigate seasonal fluctuations, groundwater was collected during three seasons. Although no TR agonistic activity was found, many water samples exhibited TR antagonistic activity. The bioassay-derived amiodarone hydrochloride (AH) equivalents ranged from 2.99 to 274.40 $\mu\text{g/L}$. Water samples collected from the riverbank filtration system during the dry season had higher TR antagonistic activity. All samples presented adverse 3,3',5-triiodo-L-thyronine (T3) equivalent levels, ranging from -2.00 to $-2.12 \mu\text{g/kg}$. Following exposure to water samples with substantial TR antagonist activity, predicted hormonal changes in humans of different gender and age ranged from 0.65 to 1.48 $\mu\text{g/kg}$ of T3, being 47% to 231% of normal. No obvious difference was found between genders or among age groups. Overall, the results revealed that the RBF system could remove the thyroid-disrupting chemicals in the river water to some extent. Considering the varying degrees of risk to human health, further treatment is needed to remove the potential thyroid-disrupting chemicals in pumping water after riverbank filtration to ensure drinking water safety.

1. Introduction

Thyroid hormones (THs) are essential for normal growth, development, and metabolism of organisms; an imbalance in TH levels may have significant consequences for human health [1]. There is accumulating evidence that thyroid-disrupting chemicals (TDCs) disrupt TH homeostasis by interfering with the synthesis, release, transport, metabolism, and clearance of THs [2–6]. There are numerous potential routes of human exposure to TDCs, including contaminated air, water, soil, and diet [7]. TH-disrupting activity has been found in industrial effluents, sediment extracts, water sources, and even in drinking water in China [8–12]. Therefore, TDCs have become a potential threat to human health and aquatic ecosystems in China.

A riverbank filtration (RBF) system refers to a primary water treatment method in which river water filters across the riverbed and transports as the underlying groundwater toward the production wells [13, 14]. The water is decontaminated naturally via chemical, biological, and physical processes, including filtration, sorption, and biodegradation during its subsurface passage [15]. Thus, water from pumping wells is generally cleaner than water collected directly from the river in terms of reduced turbidity, microbial contaminants, natural organic matter, organic trace pollutants, and pharmaceutical residues [14, 16, 17]. The RBF system, as a reliable and cost-efficient approach for groundwater supplies, has been promoted worldwide over the past several decades [18], especially in cases where river water is unsuitable or directly contaminated (e.g., accidental contaminant release).

In an RBF system, the quality of groundwater from the collector well can be significantly affected by the river water because of variation in river discharge and quality [19]. Significant seasonal water quality changes have been documented with saturated riverine groundwater infiltration flow paths [14]. Currently, the criteria for the quality of groundwater derived from an RBF system focus on the redox milieu and related geochemical processes [20]. Knowledge is lacking regarding the toxicological effects of water samples, as well as public health risk (i.e., thyroidal and estrogenic endocrine disruptions).

To date, there is no definitive risk assessment (RA) tool for endocrine-disrupting chemicals (EDCs) [21]. There are challenges to RA in hazard characterization, exposure assessment, dose-response assessment, and risk characterization [22, 23]. More specifically, effective exposure to EDCs is complex to calculate; limitations in epidemiological and toxicological studies restrict reliable data for RAs [21]. Plotan et al. implemented a new RA method for human health by comparing the levels of exposure from samples with the established 17β -estradiol acceptable daily intake (ADI) and estimated daily consumption of estradiol through drinking water and an omnivorous diet [7]. Using this approach, new toxicological findings (i.e., endocrine disruption and mixture toxicity) could be integrated; RA values can be calculated with respect to different receptors by gender and age, which is effective in the assessment of estrogenic chemicals in the environmental medium [7].

Despite the wide RBF application for groundwater supplies in developed countries, China has few RBF systems and mainly relies on surface sources for drinking water [13, 24, 25]. Considering the substantial potential of RBF use in many large cities along major rivers, the Chinese government recently initiated a feasibility study of RBF treatment in several demonstration cities in the framework of improving the safety of the drinking water supply in China. Wuchang City was chosen as one of the pilot sites because of its location adjacent to the Lalin and Mangniu Rivers, which are tributaries of the Songhua River. As such, it satisfied the requirements for RBF system installation. The objectives of this study were to (1) quantify and characterize thyroid-disrupting activity and (2) perform a human health risk assessment for groundwater samples from the pumping wells in an RBF system in Wuchang City, China.

2. Materials and Methods

2.1. Chemicals. 3,3',5-Triiodo-L-thyronine (T3, 95%) and dimethylsulfoxide (DMSO, 99.5%) were purchased from Sigma Chemical (St. Louis, MO, USA). Amiodarone hydrochloride (AH) was purchased from Shanghai Pharmaceutical (Shanghai, China). The stock solutions of all chemicals were prepared in DMSO.

2.2. Sample Collection and Processing. There was significant seasonality in the Lalin and Mangniu Rivers caused by summer (June to September) precipitation, which accounted for approximately 70% of total annual rainfall. In winter

(December to March), the frozen period lasted for almost four months [26, 27].

Based on the seasonal variability in the targeted rivers, seven sampling locations were established for water sample collection during the dry season (October 2014), thawing period (April 2015), and wet season (July 2015). SW1 and SW7, located in the Lalin River and Mangniu River, respectively, represented the water quality of these rivers. GW2-GW6, collected from shallow groundwater, represented the groundwater conditions (Figure 1).

Each water sample (4L) was collected in a precleaned amber glass bottle and stored at 4°C until further analysis. All samples were treated within 24 h. After being filtered through glass fiber filters (0.7 μ m, Millipore, MA, USA), the water sample was extracted via solid-phase extraction using an HLB cartridge (500 mg, Waters Corp., MA, USA) [9]. Then, the resultant extracts were dried under a nitrogen stream and redissolved in 0.2 mL DMSO. Three concentration levels of test solutions were obtained by 2-fold dilution of extracts and the residues were stored at -20°C before performing the bioassay. Milli-Q water with a conductivity of 18.2 Ω was used as procedural blanks.

2.3. The Recombined TR Gene Yeast Assay. The yeast strains transfected by the TR gene were developed in our laboratory. The yeast was produced with a yeast two-hybrid assay system and selected by growth on synthetic dextrose (SD) medium (lacking tryptophan and leucine, SD/-Leu/-Trp) according to the methods previously described [28].

The recombined TR gene yeast assays, including agonistic and antagonistic activity tests, were conducted as described in the previous report [9, 29]. We followed the methods of Kong et al. [29]. T3 and AH were selected as the positive controls for agonistic activity and antagonistic activity against TR, respectively. Each experimental group included the sample, positive control, negative control (DMSO), and procedural blank. All experiments were performed in triplicate, and means of results were used for optimization. The β -galactosidase activity was calculated by equations reported by Gaido et al. [30].

2.4. Cytotoxicity. In order to ensure that the obtained results from bioassays were caused by real agonistic/antagonistic responses rather than cytotoxicity, viability was also measured in cells exposed to water samples at the maximum assay concentration. We followed the methods of Kong et al. [29]. Yeast cells were plated similarly to that in the original assay and exposed for 2 h to the medium in the presence of water samples. The change in cell density (OD_{600}) in the assay medium was used to represent cell viability spectrophotometrically. The results were assumed as noncytotoxic when the ratio ($OD_{600\text{-exposure medium}}/OD_{600\text{-blank medium}}$) ranged from 80% to 120%.

2.5. Data Analysis. The bioassay-derived equivalent concentration was calculated by comparing the agonistic/antagonistic activity of the water samples with the concentration of the standard chemicals [31]. Exposure assessment was based on the equation in the previous report [7]:

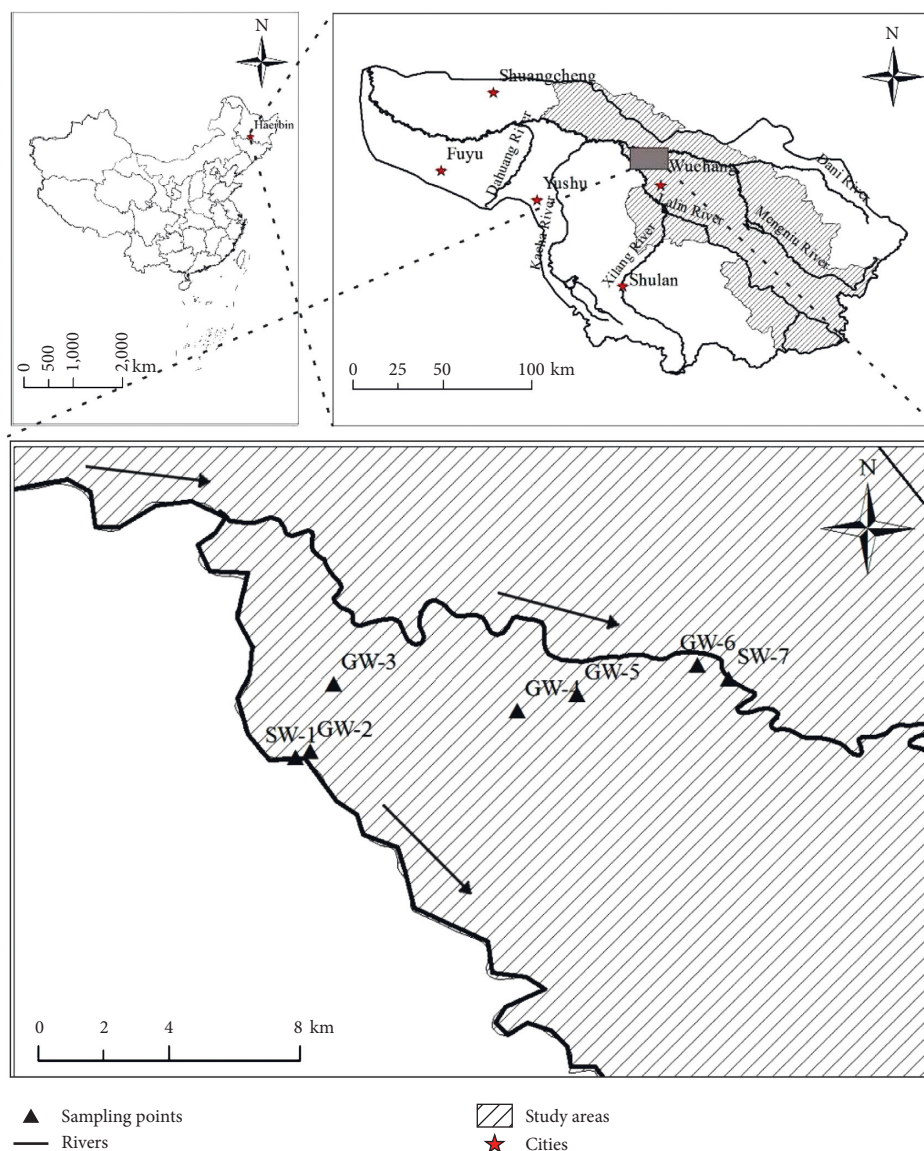


FIGURE 1: Sampling locations in Wuchang City, China.

TR agonist activity (ng/kg body weight, BW/day)

= Sample equivalent T3 concentration (ng/L)

$$\times \text{Dilution factor} \times \frac{\text{Daily dose (L/day)}}{\text{Average body weight, ABW (kg)}} \quad (1)$$

TR antagonistic activity (ng/kg BW/day)

= (Sample equivalent T3 concentration ng/L

– Concentration of added T3 ng/L) (2)

$$\times \text{Dilution factor} \times \frac{\text{Daily dose (L/day)}}{\text{ABW (kg)}}$$

It was assumed that the average adult body weight was 60 kg and the average daily dose of drinking water was 2 L/

day, as suggested by the United States Environmental Protection Agency. The T3 spike concentration was set at 5.00×10^{-6} mol/L, which is equivalent to 3.25 ng/L on the plate and was sufficient to determine potential antagonistic effects. The dilution factor was 0.02 in this study. Statistical analysis was performed using SPSS (version 19.0, SPSS Inc., Chicago, IL, USA) by *t*-test. A *p* value less than 0.05 was reported as significant.

3. Results

3.1. Cell Viability and System Credibility. To examine the β -galactosidase inhibition induced by the interaction of TDCs with TR, we tested the proficiency of the bioassay system as described in Appendix A. These results suggested that the water samples did not suppress the TR gene expression (Appendix A, Figure A1). To account for stimulatory or toxic matrix effects on yeast, we determined cytotoxicity values. The results revealed no significant

changes in cell viability, indicating that noncytotoxicity was found in these samples (Appendix A, Figure A2). The blank samples did not disrupt the TR.

3.2. TR Agonistic/Antagonistic Activity. TR agonistic activity of the water samples was not detected by the yeast assay (Figure 2). All water samples from the targeted area in different seasons exhibited TR antagonist potency (Figure 3). Higher concentrations of TR antagonists were found in river water (SW-1 and SW-7) samples during every sampling season. The TR inhibition rating of SW-7 was 44.32% during the wet season, 31.71% during the thawing period, and 28.54% during the dry season, which was higher than that of other samples. Similar to SW-7, other samples of river water exhibited higher TR antagonist potency. TR antagonistic activities were also found in groundwater samples, ranging from 9.00% to 25.91%, although the maximum inhibition rate of GW-6 during the wet season was 40.41%. The corresponding AH equivalents (AEQ) ranged from 2.99 to 274.40 $\mu\text{g/L}$ AH (Figure 4).

In addition, significant seasonal changes in TR antagonistic activity were found in the collected water samples. In the SW-1, SW-7, and GW-6 samples collected during the wet season, TR antagonist potency values were higher than those in the other two seasons ($p < 0.05$), whereas the GW-2, GW-3, GW-4, and GW-5 samples collected during the dry season had higher TR inhibition rates ($p < 0.05$, Figure 3).

3.3. RA Results. Based on the RA procedure, a risk assessment was performed that compared the levels of exposure in the samples with the suggested sum of T3 and thyroxine (T4) as shown in Table A1 (Appendix A) [32]. The potential effect on human daily exposure to T3 antagonistic activity in various groups, by gender and age, was also determined.

All samples collected from the targeted area exhibited adverse T3 equivalent levels, ranging from -2.00 to $-2.12 \mu\text{g/kg}$ T3 (Figure 5). Exposure to the water samples presented the greatest TR antagonist activity and predicted hormonal changes in various groups ranged from 0.65 to 1.48 $\mu\text{g/kg}$ T3 (Table 1) with the percentage value ranging from 47% to 231% (Table 2). The river water samples from wet season had the highest mean TR antagonist activity, accounting for 61–231% times the normal T3 and T4 levels in humans. Compared with the samples of river water, the water samples after riverbank filtration had lower TR antagonist effects. However, no obvious difference was observed in the TR antagonist effects between genders or among age groups ($p > 0.05$).

4. Discussion

4.1. TR-Disrupting Activities. Although no TR agonist activity was detected, most of the water samples from the targeted area showed TR antagonistic activity in a concentration-dependent manner, which was similar to the results obtained in other studies [9, 12, 33, 34]. Thus, TR antagonist activities in the water samples were notable and more common than TR agonist activities [12]. The AH

equivalent of water samples ranged from 2.99 to 274.40 $\mu\text{g/L}$, which was comparable with the results of the previous analysis of TR antagonist activity using recombinant yeast assays in aquatic environments in China (Table 3).

Higher TR inhibiting activities were found in the river water (SW-1 and SW-7). Some compounds have been reported to be strong TR antagonists, such as phthalate esters and phenols [35], which have been detected in rivers and drinking water supplies [11, 36]. These might be important sources of thyroid-disrupting activities in the targeted river. Previous studies demonstrated that di-n-butyl phthalate (DBP) was the predominant contributor to thyroid antagonist activity in drinking water in China [9, 11, 37]. DBP has also been detected in the Songhuajiang River with concentrations ranging from 1.69 to 11.80 $\mu\text{g/L}$ [38], which is higher than the lowest observed effective concentration.

Water quality monitoring in riverbank filtration systems has concentrated on common chemical indices, and relevant toxicological data are limited. As far as we know it was the first time to investigate the thyroid-disrupting activities of groundwater after riverbank filtration in China. The results showed that water samples from pumping wells exhibited lower TR antagonist activity than those from river, which indicated that riverbank filtration removes potential TR antagonists to some extent. Many studies have demonstrated that riverbank filtration technology was efficient in reducing turbidity, microcystins, inorganic chemical constituents, and synthetic organic compounds [16, 19], some of which have been identified as potential TDCs [35]. For example, it has been reported that the nitrate and turbidity concentrations were lower in the riverbank-filtered water than in the river water at a riverbank filtration site in the Daesan-Myeon area in the Republic of Korea [19].

Furthermore, the TR antagonist activities of groundwater exhibited a positive correlation with the distance from the pumping wells to the river. The further from the river, the lower the TR antagonist activity, which is in agreement with findings from the previous study on riverbank filtered water quality [39]. The distance between the pumping well and the river affects the travel time in the riverbank filtration system, with prolonged travel times for farther distances and shortened travel times for nearby wells. Previous research demonstrated the positive effect of increased travel time on contaminant removal [13, 40]. For instance, study regarding flooding impacts on RBF systems showed that increased abstraction rates and a high transmissivity aquifer facilitate rapid water quality recoveries [13]. The above results revealed that the RBF system could remove TDCs in the river water to some extent and their removal efficiency was positively related to the distance from the river. This study could serve as a reference for addressing the optimal positions of riverbank filtration wells before initiating field studies.

4.2. Seasonal Variation. The TR antagonistic activity of the water samples showed obvious seasonal variation. Factors, such as precipitation and temperature, varied among seasons and could impact the quantity and quality of river

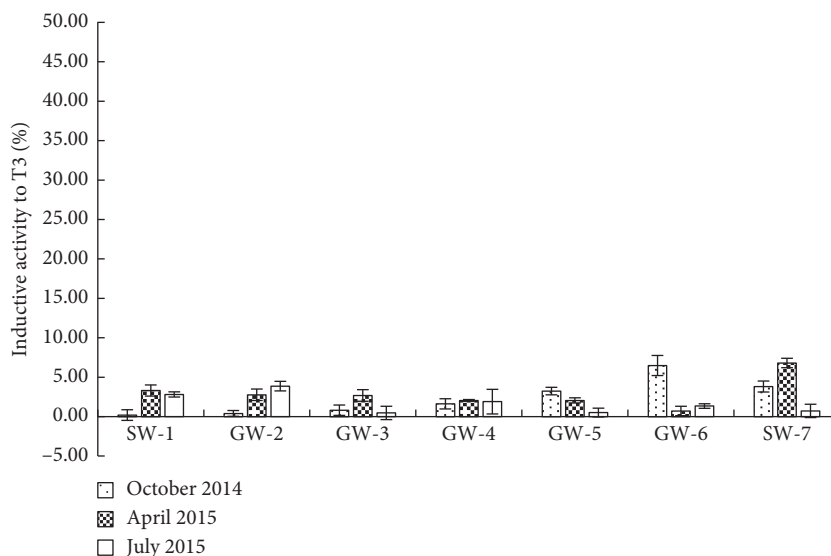


FIGURE 2: Induction of β -galactosidase activity by water samples using recombinant TR gene yeast assay.

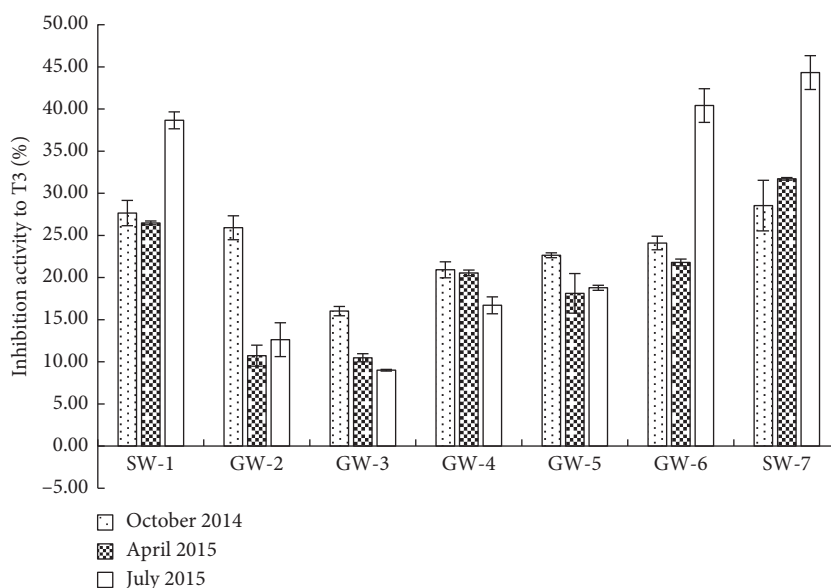


FIGURE 3: Inhibition of β -galactosidase activity by water samples using recombinant TR gene yeast assay.

water and corresponding groundwater by influencing the flow convergence process, contaminant inputs into water bodies, and redox conditions during underground passage [41].

The RBF samples GW-2, GW-3, GW-4, and GW-5, collected in the dry season, had higher TR antagonistic activity, which corroborated the scenario developed by Sprenger et al. [40]. The sensitive climatic factors influenced contaminant removal by modifying the redox conditions and travel time during underground passage. Droughts promoted anaerobic conditions during RBF passage and caused the breakthrough of pathogens, metals, suspended solids, dissolved oxygen content, and organic micro-pollutants [40]. Some EDCs were thought to experience

significant degradation under aerobic conditions [42]. Bisphenol A, atypical TDC, was found to degrade effectively under aerobic conditions during RBF passage. Our findings regarding oxidation-reduction potential of water samples tested in situ (data not shown), in addition to flow data from the literature [43, 44], support the hypothesis that under drought conditions, TDC concentration is expected to increase in the pumping water because of decreased removal efficiency under anoxic conditions [40].

In addition, high TR antagonist activity was also found in water samples collected during the thawing period. Therefore, it is necessary to investigate water samples during this time, especially for rivers with a long thawing period.

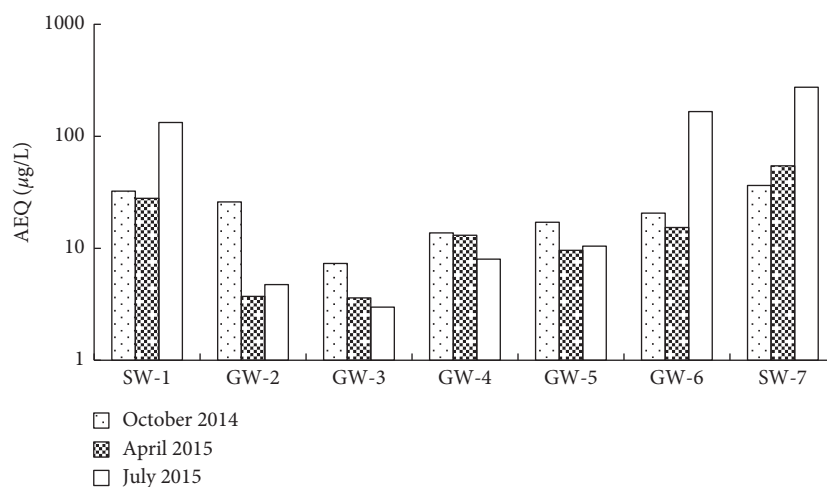


FIGURE 4: Thyroid-disrupting potency of water samples collected from the riverbank filtration system in Wuchang City, China. AEQ: amiodarone hydrochloride equivalent level.

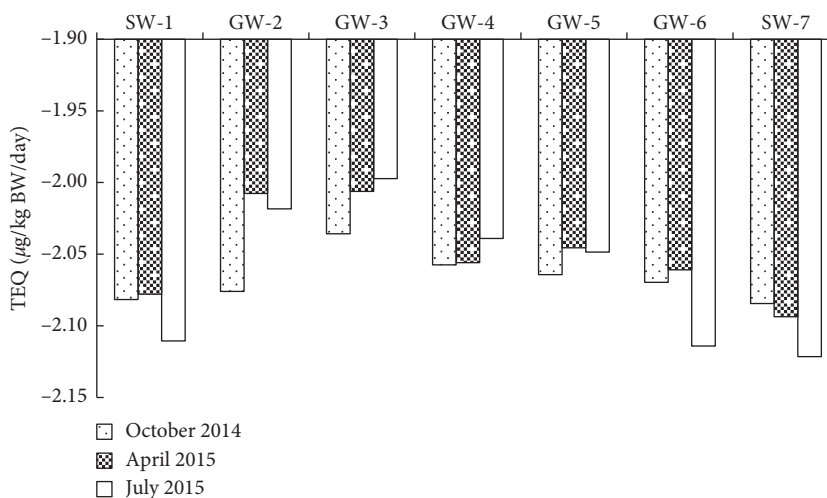


FIGURE 5: Thyroid-disrupting potency of water samples collected from the riverbank filtration system in Wuchang City, China. TEQ: T3 equivalent activity, BW: body weight.

TABLE 1: Predicted hormonal changes in various groups caused by exposure to the mean level of detected thyroidal antagonist activity in river water and groundwater samples ($\mu\text{g}/\text{kg}$).

		Male			Female			
		20–44 years	45–59 years	60–90 years	20–44 years	45–59 years	60–90 years	
River water	October 2014	Min	-0.75	-0.76	-0.74	-0.74	-0.77	-0.70
		Max	-1.40	-1.42	-1.42	-1.37	-1.44	-1.35
	April 2015	Min	-0.75	-0.76	-0.74	-0.75	-0.77	-0.70
		Max	-1.40	-1.42	-1.42	-1.37	-1.45	-1.35
	July 2015	Min	-0.78	-0.79	-0.77	-0.78	-0.80	-0.73
		Max	-1.43	-1.45	-1.45	-1.40	-1.48	-1.38
Groundwater	October 2014	Min	-0.73	-0.74	-0.72	-0.72	-0.75	-0.68
		Max	-1.38	-1.40	-1.39	-1.35	-1.42	-1.33
	April 2015	Min	-0.70	-0.71	-0.69	-0.70	-0.72	-0.65
		Max	-1.35	-1.37	-1.37	-1.32	-1.40	-1.30
	July 2015	Min	-0.71	-0.72	-0.70	-0.71	-0.73	-0.66
		Max	-1.36	-1.38	-1.38	-1.33	-1.41	-1.31

TABLE 2: Percentage of predicted effects on T3 levels through exposure to the mean level of detected thyroidal antagonist activity in the river water and groundwater samples.

Percentage	Antagonistic activity predicted effect (%)					
	River water			Groundwater		
	October 2014	April 2015	July 2015	October 2014	April 2015	July 2015
<i>Male</i>						
20–44 years	56–204	56–204	58–209	54–200	52–197	53–198
45–59 years	57–213	57–214	60–218	56–210	54–206	54–207
60–90 years	55–213	55–213	58–218	54–209	52–206	52–207
<i>Female</i>						
20–44 years	56–192	56–192	58–197	54–189	52–185	53–186
45–59 years	59–226	59–227	61–231	57–223	55–219	56–220
60–90 years	51–184	51–184	53–189	49–181	47–178	48–179

TABLE 3: Analysis of TR antagonist activities using recombinant yeast assay in an aquifer in China.

	AEQ ($\mu\text{g/L}$)	Reference
This study	2.99~274.40	
Datansha WWTP	ND~170.00	[8]
Gaobeidian WWTP	16.20~425.00	[10]
Beixiaohe WWTP	3.29~175.00	[10]
Guanting Reservoir	21.00~2150.00	[12]
Yangtze River	123.60~1332.00 ²	[34]
Yangtze River	166.08~684.00 ²	[33]

²The TR antagonist activities were described as DBP equivalent level in the original article. The calculation from DBP equivalent level to AH equivalent level was described in Section 3 of Supporting Information. AEQ: amiodarone hydrochloride (AH) equivalent level.

4.3. RA Based on the Toxicological Data. During traditional RA, concentrations of the identified contaminants from chemical analysis were used to characterize the potential risk, which does not directly reflect the real toxicological effects of these chemicals on human health [21–23, 45]. In this study, the RA was performed based on toxicological data rather than concentrations of individual chemicals, which provided a new methodology to calculate the risks of environmental mixtures. Results indicated that this novel RA method was effective for the quantification and characterization of TR antagonists in water samples and these data could provide useful information on drinking water safety [7]. Moreover, it should be pointed out that TR antagonist potency was found in the water samples from the river and pumping wells in the targeted area, which posed varying degrees of risk to human health, based on gender and age class. Because riverbank filtration wells are often the first step in a multibarrier concept to provide drinking water, further treatment is needed to remove the potential TDCs to ensure drinking water safety [40, 46].

There are some uncertainties in the RA approach. Firstly, some compounds could cause thyroid hormone disruption through different modes of action [4]; however, in this study, only the disrupting effect caused by TR activation was evaluated by the *in vitro* bioassay. As a result, the real biological effect in the environmental medium might be underestimated. Moreover, there were significant differences between the *in vitro* and *in vivo* potency of individual TDCs because of metabolic stability. Thus, their *in vitro* thyroid-

disrupting activities might not necessarily correspond to adverse *in vivo* effects. In addition, physiological data regarding thyroid hormones are limited. In this study, the recommended T3 and T4 concentrations reported by Ma et al. [32] were used to compare with the possible intake of TDCs from the water samples through the direct drinking pathway. Because of the above limitations, it should be noted that the main purpose of our study was not to derive strict guideline values, but to better understand the possible risk to human health from the groundwater in these regions.

5. Conclusions

This study revealed the presence of thyroid-disrupting activities in the groundwater from riverbank filtration systems, as well as in the river water by a recombinant TR gene yeast assay, and presents their hypothetical impact on thyroid hormones in humans using a novel risk assessment approach. The main conclusions include (1) the RBF system removed the TDCs from the river water to some extent and their removal efficiency was positively related to the distance from the river; (2) the RBF samples collected during the dry season had higher TR antagonistic activity because of decreased removal efficiency under anoxic conditions; (3) the novel RA approach, comparing the T3 equivalent levels with the normal T3 and T4 levels in humans, could be promoted as an effective method to assess the EDCs in the environmental matrix. These findings are highly relevant to environmental safety and human health. It warrants further research on drinking water use from riverbank filtration systems.

Data Availability

The data used to support the findings of this study are included within the article as well as the supplementary information files.

Conflicts of Interest

The authors declare no conflicts of interest.

Acknowledgments

This research was funded by the National Key R&D Program of China (2018YFC1800901), the China Scholarship Council

(201606045023), the National Natural Science Foundation of China (41001351), and the Major Science and Technology Program for Water Pollution Control and Treatment (2014ZX07201-010).

Supplementary Materials

A1: inhibition activity of β -galactosidase by organic extracts of water samples. A2: cytotoxicity of the organic extracts of water samples. A3: the levels of T3 and T4 in different age and gender groups. (*Supplementary Materials*)

References

- [1] K. Onigata, "Thyroid hormone and skeletal metabolism," *Clinical Calcium*, vol. 24, no. 6, pp. 821–827, 2014.
- [2] M. Boas, U. Feldt-Rasmussen, and K. M. Main, "Thyroid effects of endocrine disrupting chemicals," *Molecular and Cellular Endocrinology*, vol. 355, no. 2, pp. 240–248, 2012.
- [3] A. Buha, B. Antonijević, Z. Bulat, V. Jačević, V. Milovanović, and V. Matović, "The impact of prolonged cadmium exposure and co-exposure with polychlorinated biphenyls on thyroid function in rats," *Toxicology Letters*, vol. 221, no. 2, pp. 83–90, 2013.
- [4] A. J. Murk, E. Rijntjes, B. J. Blaauboer et al., "Mechanism-based testing strategy using in vitro approaches for identification of thyroid hormone disrupting chemicals," *Toxicology in Vitro*, vol. 27, no. 4, pp. 1320–1346, 2013.
- [5] A. Arukwe, M. Olufsen, N. Cicero, and M. D. Hansen, "Effects on development, growth responses and thyroid-hormone systems in eyed-eggs and yolk-sac larvae of atlantic salmon (*Salmo salar*) continuously exposed to 3,3',4,4'-tetrachlorobiphenyl (PCB-77)," *Journal of Toxicology and Environmental Health, Part A*, vol. 77, no. 9–11, pp. 574–586, 2014.
- [6] G. W. Louis, D. R. Hallinger, M. J. Braxton, A. Kamel, and T. E. Stoker, "Effects of chronic exposure to triclosan on reproductive and thyroid endpoints in the adult Wistar female rat," *Journal of Toxicology and Environmental Health, Part A*, vol. 80, no. 4, pp. 236–249, 2017.
- [7] M. Plotan, C. T. Elliott, C. Frizzell, and L. Connolly, "Estrogenic endocrine disruptors present in sports supplements: a risk assessment for human health," *Food Chemistry*, vol. 159, pp. 157–165, 2014.
- [8] J. Li, Z. Wang, M. Ma, and X. Peng, "Analysis of environmental endocrine disrupting activities using recombinant yeast assay in wastewater treatment plant effluents," *Bulletin of Environmental Contamination and Toxicology*, vol. 84, no. 5, pp. 529–535, 2010.
- [9] N. Li, D. Wang, Y. Zhou, M. Ma, J. Li, and Z. Wang, "Dibutyl phthalate contributes to the thyroid receptor antagonistic activity in drinking water processes," *Environmental Science & Technology*, vol. 44, no. 17, pp. 6863–6868, 2010.
- [10] N. Li, M. Ma, K. Rao, and Z. Wang, "In vitro thyroid disrupting effects of organic extracts from WWTPs in Beijing," *Journal of Environmental Sciences*, vol. 23, no. 4, pp. 671–675, 2011.
- [11] W. Shi, X. Hu, F. Zhang et al., "Occurrence of thyroid hormone activities in drinking water from eastern China: contributions of phthalate esters," *Environmental Science & Technology*, vol. 46, no. 3, pp. 1811–1818, 2012.
- [12] J. Li, M. Li, S. Ren, C. Feng, and N. Li, "Thyroid hormone disrupting activities of sediment from the Guanting reservoir, Beijing, China," *Journal of Hazardous Materials*, vol. 274, pp. 191–197, 2014.
- [13] M. J. Ascott, D. J. Lapworth, D. C. Gooddy, R. C. Sage, and I. Karapanos, "Impacts of extreme flooding on riverbank filtration water quality," *Science of the Total Environment*, vol. 554–555, pp. 89–101, 2016.
- [14] L. Sharma, J. Greskowiak, C. Ray, P. Eckert, and H. Prommer, "Elucidating temperature effects on seasonal variations of biogeochemical turnover rates during riverbank filtration," *Journal of Hydrology*, vol. 428–429, pp. 104–115, 2012.
- [15] S. Mustafa, A. Bahar, Z. A. Aziz, and S. Suratman, "Modelling contaminant transport for pumping wells in riverbank filtration systems," *Journal of Environmental Management*, vol. 165, pp. 159–166, 2016.
- [16] Y. Bai, X. Ruan, F. Wang, G. Antoine, and J. P. van der Hoek, "Sulfonamides removal under different redox conditions and microbial response to sulfonamides stress during riverbank filtration: a laboratory column study," *Chemosphere*, vol. 220, pp. 668–677, 2019.
- [17] K. P. Kowalski, H. T. Madsen, and E. G. Søgaard, "Comparison of sand and membrane filtration as non-chemical pre-treatment strategies for pesticide removal with nanofiltration/low pressure reverse osmosis membranes," *Water Science and Technology: Water Supply*, vol. 14, no. 4, pp. 532–539, 2014.
- [18] J. Regnery, J. Barringer, A. D. Wing, C. Hoppe-Jones, J. Teerlink, and J. E. Drewes, "Start-up performance of a full-scale riverbank filtration site regarding removal of DOC, nutrients, and trace organic chemicals," *Chemosphere*, vol. 127, pp. 136–142, 2015.
- [19] J.-H. Lee, S.-Y. Hamm, J.-Y. Cheong et al., "Characterizing riverbank-filtered water and river water qualities at a site in the lower Nakdong river basin, Republic of Korea," *Journal of Hydrology*, vol. 376, no. 1–2, pp. 209–220, 2009.
- [20] M. Rudolf von Rohr, J. G. Hering, H.-P. E. Kohler, and U. von Gunten, "Column studies to assess the effects of climate variables on redox processes during riverbank filtration," *Water Research*, vol. 61, pp. 263–275, 2014.
- [21] V. Futran Fuhrman, A. Tal, and S. Arnon, "Why endocrine disrupting chemicals (EDCs) challenge traditional risk assessment and how to respond," *Journal of Hazardous Materials*, vol. 286, pp. 589–611, 2015.
- [22] P. W. Harvey and D. J. Everett, "Regulation of endocrine-disrupting chemicals: critical overview and deficiencies in toxicology and risk assessment for human health," *Best Practice & Research Clinical Endocrinology & Metabolism*, vol. 20, no. 1, pp. 145–165, 2006.
- [23] A. Beronius, A. Hanberg, J. Zilliacus, and C. Rudén, "Bridging the gap between academic research and regulatory health risk assessment of endocrine disrupting chemicals," *Current Opinion in Pharmacology*, vol. 19, pp. 99–104, 2014.
- [24] B. Hu, Y. Teng, Y. Zhai, R. Zuo, J. Li, and H. Chen, "Riverbank filtration in China: a review and perspective," *Journal of Hydrology*, vol. 541, pp. 914–927, 2016.
- [25] Y. Zhu, Y. Zhai, Y. Teng et al., "Water supply safety of riverbank filtration wells under the impact of surface water-groundwater interaction: evidence from long-term field pumping tests," *Science of the Total Environment*, 2019, In press.
- [26] S. Wang, Y. Wang, L. Ran, and T. Su, "Climatic and anthropogenic impacts on runoff changes in the Songhua river basin over the last 56 years (1955–2010), Northeastern China," *Catena*, vol. 127, pp. 258–269, 2015.
- [27] M. Exner-Kittridge, P. Strauss, G. Blöschl, A. Eder, E. Saracevic, and M. Zessner, "The seasonal dynamics of the

- stream sources and input flow paths of water and nitrogen of an Austrian headwater agricultural catchment,” *Science of the Total Environment*, vol. 542, pp. 935–945, 2016.
- [28] J. Li, M. Ma, and Z. Wang, “A two-hybrid yeast assay to quantify the effects of xenobiotics on thyroid hormone-mediated gene expression,” *Environmental Toxicology and Chemistry*, vol. 27, no. 1, p. 159, 2008.
- [29] D. Kong, Y. Wang, J. Wang, Y. Teng, N. Li, and J. Li, “Evaluation and characterization of thyroid-disrupting activities in soil samples along the second Songhua river, China,” *Ecotoxicology and Environmental Safety*, vol. 133, pp. 475–480, 2016.
- [30] K. W. Gaido, L. S. Leonard, S. Lovell et al., “Evaluation of chemicals with endocrine modulating activity in a yeast-based steroid hormone receptor gene transcription assay,” *Toxicology and Applied Pharmacology*, vol. 143, no. 1, pp. 205–212, 1997.
- [31] W. Shi, S. Wei, X.-X. Hu et al., “Identification of thyroid receptor ant/agonists in water sources using mass balance analysis and Monte Carlo simulation,” *PLoS One*, vol. 8, no. 10, Article ID e73883, 2013.
- [32] R. Ma, H. Huang, Y. Yan et al., “Influence factors on serum thyroid hormone level in health people,” *Journal of Sichuan University (Medical Science Edition)*, vol. 46, no. 4, pp. 611–614, 2015, in Chinese.
- [33] W. Shi, X. Wang, G. Hu et al., “Bioanalytical and instrumental analysis of thyroid hormone disrupting compounds in water sources along the Yangtze river,” *Environmental Pollution*, vol. 159, no. 2, pp. 441–448, 2011.
- [34] X. Hu, W. Shi, F. Zhang et al., “In vitro assessment of thyroid hormone disrupting activities in drinking water sources along the Yangtze river,” *Environmental Pollution*, vol. 173, pp. 210–215, 2013.
- [35] J. Li, M. Ma, and Z. Wang, “In vitro profiling of endocrine disrupting effects of phenols,” *Toxicology in Vitro*, vol. 24, no. 1, pp. 201–207, 2010.
- [36] N. Liu, Y. Wang, Q. Yang et al., “Probabilistic assessment of risks of diethylhexyl phthalate (DEHP) in surface waters of China on reproduction of fish,” *Environmental Pollution*, vol. 213, pp. 482–488, 2016.
- [37] J. Li, S. Ren, S. Han, and N. Li, “A yeast bioassay for direct measurement of thyroid hormone disrupting effects in water without sample extraction, concentration, or sterilization,” *Chemosphere*, vol. 100, pp. 139–145, 2014.
- [38] D. Gao, Z. Li, Z. Wen, and N. Ren, “Occurrence and fate of phthalate esters in full-scale domestic wastewater treatment plants and their impact on receiving waters along the Songhua river in China,” *Chemosphere*, vol. 95, pp. 24–32, 2014.
- [39] C. Ray, T. W. Soong, Y. Q. Lian, and G. S. Roadcap, “Effect of flood-induced chemical load on filtrate quality at bank filtration sites,” *Journal of Hydrology*, vol. 266, no. 3–4, pp. 235–258, 2002.
- [40] C. Sprenger, G. Lorenzen, I. Hülshoff, G. Grützmacher, M. Ronghang, and A. Pekdeger, “Vulnerability of bank filtration systems to climate change,” *Science of the Total Environment*, vol. 409, no. 4, pp. 655–663, 2011.
- [41] S. Yu, Z. Xu, W. Wu, and D. Zuo, “Effect of land use types on stream water quality under seasonal variation and topographic characteristics in the Wei river basin, China,” *Ecological Indicators*, vol. 60, pp. 202–212, 2016.
- [42] G.-G. Ying, S. Toze, J. Hanna, X.-Y. Yu, P. J. Dillon, and R. S. Kookana, “Decay of endocrine-disrupting chemicals in aerobic and anoxic groundwater,” *Water Research*, vol. 42, no. 4–5, pp. 1133–1141, 2008.
- [43] China Water & Power Press, *China Water Resource Yearbook*, China Water & Power Press, Beijing, China, 2015, in Chinese.
- [44] China Meteorological Administration, *China Meteorology Yearbook*, China Meteorological Administration, Beijing, China, 2015, in Chinese.
- [45] G. Medema and P. Smeets, “Quantitative risk assessment in the water safety plan: case studies from drinking water practice,” *Water Science and Technology: Water Supply*, vol. 9, no. 2, pp. 127–132, 2009.
- [46] J. Hollender, J. Rothardt, D. Radny et al., “Comprehensive micropollutant screening using LC-HRMS/MS at three riverbank filtration sites to assess natural attenuation and potential implications for human health,” *Water Research X*, vol. 1, Article ID 100007, 2018.

Research Article

Investigating the Impact of Anthropogenic and Natural Sources of Pollution on Quality of Water in Upper Indus Basin (UIB) by Using Multivariate Statistical Analysis

Mansoor A. Baluch  and Hashim Nisar Hashmi

Faculty of Civil and Environmental Engineering, University of Engineering & Technology, Taxila, Pakistan

Correspondence should be addressed to Mansoor A. Baluch; mansoorbaluch@gmail.com

Received 16 June 2019; Accepted 12 September 2019; Published 16 November 2019

Guest Editor: Lisa Yu

Copyright © 2019 Mansoor A. Baluch and Hashim Nisar Hashmi. This is an open access article distributed under the Creative Commons Attribution License, which permits unrestricted use, distribution, and reproduction in any medium, provided the original work is properly cited.

Water quality of the Indus River around the upper basin and the main river was evaluated with the help of statistical analysis. In order to analyze the similarities and dissimilarities for identifying the spatial variations in water quality of the Indus River and sources of contamination, multivariate statistical analysis, i.e., principle component analysis (PCA), cluster analysis, and descriptive analysis, was done. Data of 8 physicochemical quality parameters from 64 sampling stations belonging to 6 regions (labeled as M_1 , M_2 , M_3 , M_4 , M_5 , and M_6) were used for analysis. The parameters used for assessing the water quality were pH, dissolved oxygen (DO), oxygen reducing potential (ORP), electrical conductivity (EC), total dissolved solids (TDS), salinity (%), and concentration of arsenic (As) and lead (Pb), respectively. PCA assisted in extracting and recognizing the responsible variation factors of water quality over the region, and the results showed three underlying factors including anthropogenic source pollution along with runoff due to rain and soil erosion were responsible for explaining the 93.87% of total variance. The parameters which were significantly influenced by anthropogenic impact are DO, EC, TDS (negative), and concentration of Pb (positive), while the concentration of As, % salinity, and ORP are affected by erosion and runoff due to rain. The worst pollution situation for regions M_1 and M_6 was due to the concentration of As which was approximately 400 $\mu\text{g/l}$ (i.e., 40 times higher than minimum WHO recommendation). Furthermore, the results also indicated that, in the Indus River, three monitoring stations and five quality parameters are sufficient to have a reasonable confidence about the quality of water in this most important reserve of Pakistan.

1. Introduction

One of the most influential elements regarding environment concerns all over the world is the anthropogenic distribution, e.g., sewage discharge into the river, reclamation process of the land, and climate change due to atmospheric deposition effects [1]. In the recent years, much attention is paid by various researchers in assessing the quality of surface water because of its direct connection not only with human beings but also with other species [2]. The major factors affecting the quality of river water usually are morphology of the basin and regional atmosphere along with climate change, and both natural and anthropogenic effects are responsible for governing these effects [3]. Wastewater from human activities like from industries, agriculture, and

natural degradation, e.g., weathering, affects water quality impede not only for drinking purpose but also not fit for agriculture and other utilization. Clean water is an imperative part for the affluence of human society, but the major serious environmental problem of the last century was the vandalization of the land aquatic system [4]. The most harmful pollution to the surface water bodies is due to the role of increasing contamination from industrial and urban wastewater along with the runoff from the agricultural land. The characteristics of the surface contaminations are considered as a nonpoint source, while industrial and municipal discharges are considered as a main point source due to the influenced responsibilities of water pollution [5–7]. Precipitations due to the climate change, surface flow, ground water flow, and the flow due to the pump are the major ones

responsible for the discharge of the river along with the pollutant concentration on the surface water [5]. It is therefore an effective, long lasting monitoring protocol because the surface water needs an essential knowledge of hydromorphological, hydrochemical, and hydrobiological characteristics [8]. There are other important variations, e.g., spatial and temporal variations. For such kinds of variation monitoring, there should be some conceptual and essential estimations of the surface water quality [9], and some standards, e.g., here in this study, such as FAO-29 guidelines and WHO recommendations (given in Table 1) were utilized for assessing the water quality.

Researchers have utilized number of techniques and methods to unveil the possible hidden sources of pollutions for various rivers around the world. For example, in another study, Aalami et al. [10] implemented the structured best management practices (BMPs) to define quantity-based sustainability index (SI). They had done this to link the water quality with the outflow of reservoir. Couto et al. [11] figured out the trace element distribution and their possible sources while defining the pollution indices, i.e., geoaccumulation (Igeo) and enrichment factor (EF) during the investigation for anthropogenic pressure of Ave River Portugal. Rahman et al. [12] investigated the drinking water sources in the southwest coastal area of Bangladesh and found that the availability of trace metals originated both from natural and anthropogenic sources. Salam et al. [13] utilized inductively coupled plasma-optical emission spectrometry (ICP-OES) for estimating the trace elements and found that the concentrations of heavy metals at downstream of Perak River water were higher than the concentrations of upstream at the Perak River Basin, Malaysia. Barceló et al. [14] investigated the waters from Uzunçayır Dam (Tunceli), Turkey, and concluded that the water of this dam is safe for agriculture and household use. Das Sharma et al. [15] assessed the heavy metal concentration at Kolleru lake in Andhra Pradesh, India, with multiple index values and revealed the fact that the lake was influenced anthropogenic input. Bhuyan et al. [16] assessed the water quality of the old Brahmaputra River and figured that hidden sources including industrial effluents, municipal wastes, and agricultural activities are responsible for degradation of water quality of the Old Brahmaputra River. The Gorganrood River water quality was also evaluated with new WQI, and it was found that the parameters that were directly affected due to anthropogenic impact were given more weights to assess the quality of water [17]. Sediment and suspended particulate matters of the Tadjan River (southern part of the Caspian Sea) were analyzed, and the major sources of pollution were pulp and paper mill, dairy factory, and municipal sewage [18].

A few notable studies are also present in the literature about the water quality and trace elements present in the Indus River. These studies disclosed the fact that the concentrations of toxic heavy metals are higher in the Indus River [19–21]. The Pakistani environment is badly affected by geochemical pollution through natural processes, i.e., deposition of alluvial material through floods in the Indus Delta, volcanic eruptions, as well as anthropogenic activities such as sewage irrigation, animal manure, along with

fertilizers and pesticides. This contaminated soil can lead to high levels of various trace elements, including As in the Indus River [22]. Although aforementioned studies pointed about the higher concentration of As and other toxic heavy metals in Indus River water, unfortunately no real effort has been made for assessing the actual hidden sources of pollution. It is therefore, during this multivariate statistical technique, utilized to divulge the actual sources of pollution of the Indus River.

1.1. Background Literature. Multiple multivariate statistical techniques are used to estimate the different parameters of surface water quality index with morphological status of land. The techniques used are the hierarchy cluster analysis, principal component analysis, and discriminate analysis, respectively. These statistical techniques allow estimating multifaceted data matrices for understanding the quality of surface water quality in a better way and also permit for distinguishing the possible factors having significant influence on the water system. Statistical technique also provides a tool for water flow management system along with the solution of pollution issues. It has also been used for characterizing and evaluating the parameters between surface and the fresh quality of water and helpful for exploring the effect of anthropogenic sources on the spatial and temporal variations river quality [23–25].

Pejman et al. [26] have used cluster analysis (CA), principal component analysis (PCA), and factor analysis (FA) for calculating the seasonal and spatial variations effects on the water quality of Haraz Basin. During the four seasons, i.e., summer and autumn of 2007 and winter and spring of 2008, sets of eight water quality parameters were collected and analyzed by CA and PCA. According to results, the parameters, which were significant on one season, may not be significant on the other season. Mustapha and Abdu [27] investigated the water quality parameters for the Jakara River. They have used multiple linear regression and principal component analysis (PCA) to identify the most influential parameter responsible for water pollution. Furthermore, they used PCA to figure out the origin of quality parameters which serve in identifying the hidden pollution sources. Bhattacharyya et al. [28] have used principal component analysis (PCA)/factor analysis (FA) and cluster analysis (CA) along with correlation analysis multivariate statistical technique for calculating the water quality index of the Damodar River in India. The study revealed the existence of some harmful chemicals within the river. PCA/FA interpreted the major responsible factors for affecting the water quality were geogenic and anthropogenic factors. Shrestha and Kazama [29] used cluster analysis (CA), principal component analysis (PCA), factor analysis (FA), and discriminant analysis (DA) for the evaluation of spatial/temporal variations and huge complex water quality index for the Fuji River Basin. Around twelve parameters were evaluated at thirteen different sites. FA analysis indicated that the major responsible parameters for degrading the quality of the water system were discharge and organic pollutions. More recently, Khan et al. and Zafar et al. [30, 31]

TABLE 1: Irrigation water quality framework guidelines along with WHO recommended concentration of As in $\mu\text{g/l}$.

Potential water quality problem	Units	None	Degree of restriction on using slight to moderate	Severe
Salinity (affects α on water availability)				
E_{c_w}	dS/m	<0.7	0.7–3.0	>3.0
Or				
TDS	mg/l	<450	450–2000	>2000
Infiltration (affects infiltration rate of water into the soil and evaluates using E_{c_w} and SAR together)				
SAR				
= 0–3 and E_{c_w} =		>0.7	0.7–0.2	<0.2
= 3–6		>1.2	1.2–0.3	<0.3
= 6–12		>1.9	1.9–0.5	<0.5
= 12–20		>2.9	2.9–1.3	<1.3
= 20–40		>5.0	5.0–2.9	<2.9
Specific ion toxicity (affects sensitive crops)				
Sodium (Na^+)				
Surface irrigation	SA	<3	3–9	>9
Sprinkler irrigation	me/l	<3	>3	
Chloride (alpha^-)				
Surface irrigation	Me/l	<4	4–10	>10
Sprinkler irrigation	Me/l	<3	>3	
Boron (B)	Mg/l	<0.7	0.7–3.0	>3.0
Trace elements				
Miscellaneous effects (affects susceptible crops)				
Nitrogen ($\text{NO}_3^{2-}-N$)	mg/l	<5	5.0–30	>30
(Overhead sprinkling only) pH	me/l	<1.5	1.5–8.5	>8.5
		Normal range		
		6.5–8.4		
As concentration	$\mu\text{g/l}$	<10	>50	

have used the multivariate statistics for assessing the effluent discharge on the irrigation water and Indus River water quality in KPK, Pakistan, and found that effluent discharge results in the severe degradation of water quality for irrigation purpose. Moreover, using PCA and CA, they conclude that the Indus River is found strongly affecting city effluent in KPK Province of Pakistan. In short, multivariate statistics has been used by number of researchers for analysis of water quality over the years in order to obtain useful information about required number of monitoring stations, pollution sources, and spatial and temporal variations assessment [32–34].

2. Materials and Methods

2.1. Information about Monitoring Parameters and Stations. Researchers [35] have discussed the frequently used parameters for characterizing the quality of water which includes the important physical and chemical parameters. Physical parameters are temperature, pH, electrical conductivity (EC), total dissolved solvents (TDSs), and salinity, while the chemical parameters are dissolved oxygen (DO), oxygen reducing potential (ORP), COD, BOD, anions (Cl^- , Cl^- , NO_3^- , SO_4^{2-} , and PO_4^{3-}), and toxic heavy metals (Cd, Pb, and As).

The 8 physicochemical parameters which include pH, TDS, EC, DO, ORP, salinity, and concentration of As and Pb were chosen based on the available literature and data [36] for applying multivariate statistics. The data of 64 samples

collected from 6 regions of upper Indus Basin and main Indus River were originally taken by Ahmad et al. The data [36] were utilized for the analysis of water quality over the region and obtaining useful information about the required number of monitoring stations, pollution sources, and spatial variations assessment. The six regions were labeled as M_1 to M_6 monitoring stations with the following details:

- (i) M_1 : Gilgit to Khunjerab pass
- (ii) M_2 : Gilgit to Chitral
- (iii) M_3 : Gilgit to Nalter
- (iv) M_4 : Gilgit to Deosai plain
- (v) M_5 : Skardu to Gilgit
- (vi) M_6 : main Indus River

All regions with marked sample collection points are shown in Figure 1.

3. Statistical Analysis

All the analyses are made while using XSTAT software (trial version) and Microsoft Excel version 2007.

3.1. Hierarchy Cluster Analysis. Cluster analysis is basically a cluster of multivariate database whose basic operation is to provide tools for assembling objects based on individual parametric characteristics. The primary method for classifying objects in cluster analysis is that every object is similar



FIGURE 1: Map showing the six regions of the Indus River with marked samples collection point.

comparatively to the other object with respect to predefined descriptive criteria. The resulting outcomes of cluster object correspond to high-internal homogeneity and also very high-external heterogeneity in order to differentiate between relevant and irrelevant variables. Therefore, variables in a cluster analysis must be supported through conceptual considerations. The common approach for analyzing similarities relationship between the samples through whole data set is hierarchical agglomerative clustering and is normally illustrated by a dendrogram. The main aim of this study is to calculate a relationship between individual cluster to identify the similarity and dissimilarity between each samples of monitoring sites. Dendrogram tells the parametric mean value for every sampling site. There are three statistical groups comprising all the calculating values:

- (1) Group A: this cluster could be regarded as generally less polluted areas. There should be low or moderate industrialization and urbanization. Consequently, the human effect also should be very low.
- (2) Group B: generally, this type of cluster could be regarded on highly polluted areas such as industrial sites. Pollutants in the sample from industrial sites generally are involved from industrial wastewater treatment plants along with sewage wastewater from agriculture activities.
- (3) Group C: this cluster could be viewed as generally moderate-contaminated (MC) sites. These locales may get contamination from nonpoint sources

3.2. Principal Component Analysis (PCA). PCA is a linear combination of factors, which intended to change the first factors into new, uncorrelated factors (axes), called as

principal components. The new axis lies along the direction of the maximum variance. PCA is not only used to normalize factors for the sack of comparison between the samples but also to find the factors of pollutants that influence each sample. In PCA, there is a new cluster of factors called a rotation of axis involved that is used to divide the original variables into groups. It is applied to find a compositional influential factor involved in each sample.

PCA provides certain explanation for the most valuable factor which depicts the full information set interpretation. PCA summaries the statistical correlation between the compositions among the water samples with least reduction of information. The following equation is used to express the principal component analysis:

$$Z_{ij} = a_{i1}x_{1j} + a_{i2}x_{2j} + \dots + a_{im}x_{mj}, \quad (1)$$

where Z is the component score, a is the component loading, x is the measured value of a variable, i is the component number, j is the sample number, and m is the total number of variables.

4. Results and Discussion

4.1. Descriptive Measures of River Water Quality Data. The XSTAT software (trial version) was employed in this study for PCA and CA of water quality data after normalizing the data to unit variance and zero mean following the approach reported in [37]. Due to high-dispersion-measured quality parameter's data for all regions (i.e., M_1 – M_6), as shown in Figure 2, it is extremely difficult to rely on either mean value or variance for assessing the water quality. Therefore, coefficient of variation (CV) of quality parameters focused in this study is calculated from the ratio

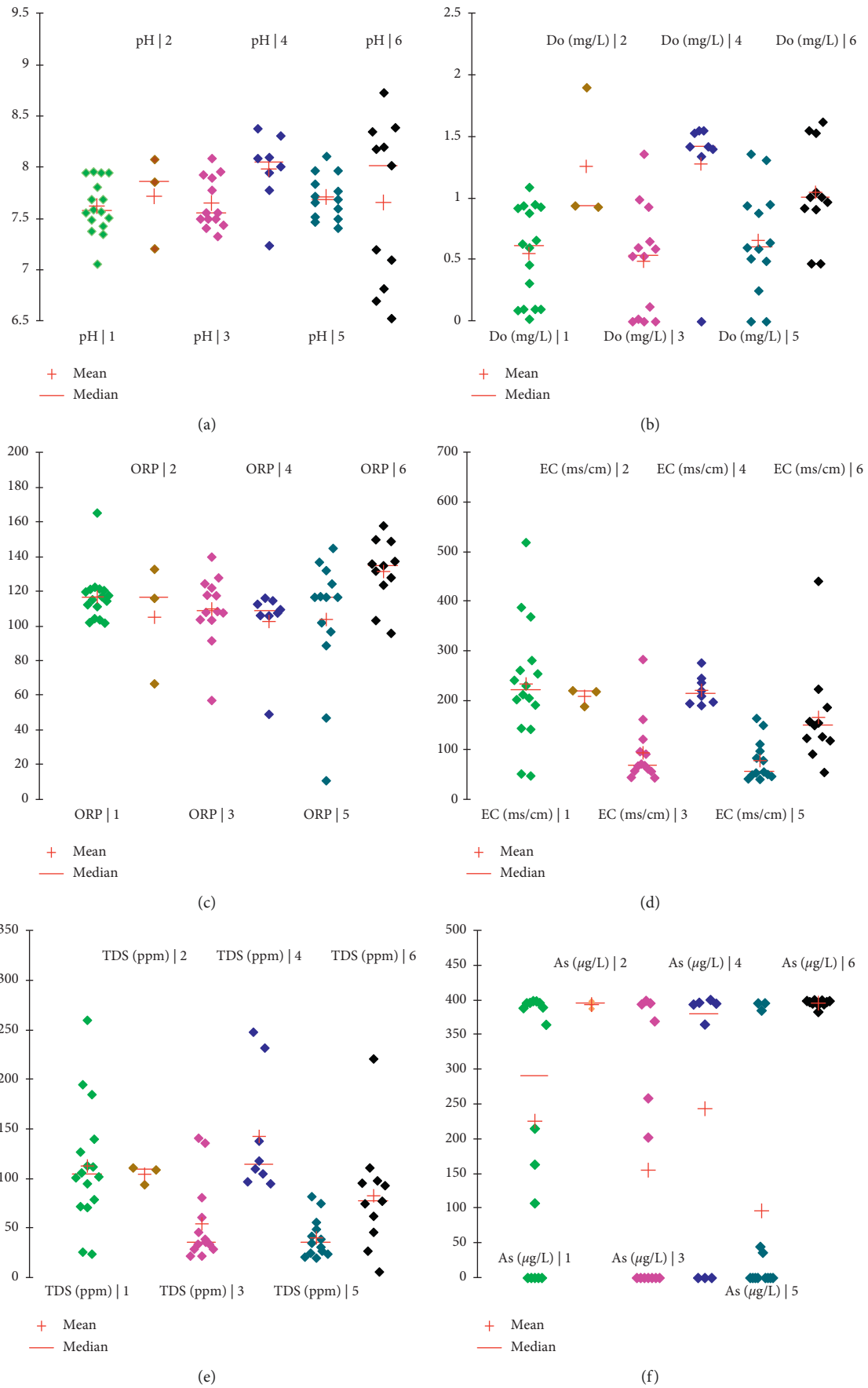


FIGURE 2: Descriptive analysis of water quality data.

of standard deviation to mean calculated. The range, mean, median, dispersion, and standard deviation of each quality parameter is shown in Figure 2 in the form of descriptive data representation, while CV is given in Table 2.

The mean and median values of pH at observation points ranging from M_1 to M_5 overlap each other, while there is a slight difference with median having a higher value than for the main Indus River (i.e., M_6 observation station). This suggests that pH do not vary much, and smaller CV values point to fact that spatial effects on pH are minor on relative scale. These findings are consistent with the findings reported in literature [33, 38]. Heavy rainfall might be responsible for this consistency because it is the “only” common factor in abovementioned studies. DO, ORP, EC, TDS, % salinity, and As and Pb concentration have higher dispersion of data at all active observations sites/stations/point as evident from Figure 2(a)–2(f) thus giving high values of CVs (see Table 2). The highest CVs of almost all the aforementioned physicochemical parameters are observed at M_3 , while the highest mean and median values of DO and TDS are observed at M_4 , and ORP, As, and Pb are observed at M_6 . The mean and median values of As and Pb are also significant higher at all stations along with the higher values of CVs. Largest variations in the mean values of “DO” and “ORP” point to the high level of organic pollutants from various sources and decomposition [33, 37, 39]. Highest mean and median values of As from the start of the Indus River suggest that it is polluted with the traces of As from the start and increases with flow when it remains in the upper Indus Basin. However, at the main Indus River, its concentration is maximum, but the smallest value of CV is suggesting that As is coming in the Indus River from effluents of the upper basin. The TDS mean and median values at M_3 is highest with larger CVs, as evident from Figure 2 and Table 2, which is a confirmation of high inorganic loading at this station because of soil erosions and agriculture activities [39, 40].

4.2. Correlation Matrix. The results of correlation analysis are given in Table 3 as a correlation matrix, which is calculated by combining the mean values of quality parameters of six regions belonging to the upper Indus Basin, i.e., from M_1 – M_6 . It can be seen from the data that most of measured parameters in the upper Indus region have a positive correlation. The strong positive correlation of pH, EC, TDS, and As and Pb concentration with DO is quite evident from the correlation matrix, and the reason for this correlation is explained in the section below where PCA of current data set is performed. In addition, EC is strongly correlated with TDS and the concentration of Pb. TDS and other inorganic matters/metals like Pb and As correlates well with EC, as reported by [35]. It is worth mentioning here that the concentration of As is positively correlated with all measured parameters with relatively strong dependence on ORP, EC, TDS, and salinity.

4.3. Cluster Analysis (CA). On the basis of similarities in water quality features, various sampling stations of UIB are

grouped into clusters. However, employing this analysis technique planning for future events with an optimum number of sampling stations is possible. In addition, this strategy is also helpful in reducing the monitoring cost with better understanding of prevailing factors involved in a system under investigation. Figure 3 shows the dendrogram obtained from hierarchy cluster analysis which generated three groups on the basis of similar characteristic features. Groups 1, 2, and 3 correspond to relatively bad, fair, and good quality regions of UIB, respectively. In aforementioned dendrogram shown in Figure 3, M_3 and M_5 formed one group, i.e., group 3 consists of comparatively less polluted site, which is attributed to the fact of almost negligible human activities at M_3 and M_5 . The water at M_3 and M_5 comes from the snow-covered peaks and glaciers, which falls into main subriver through side nallas, and most of side nallas are clear and transparent with a little or no domestic effluent. Group 2 consists of sample points belonging to M_2 and M_4 , and analysis shows that this group has slightly less quality water as compared to group 3, i.e., it is a moderately polluted group. The human excreta effluent discharge points along with dumping of domestic and commercial waste, which belongs to the population in these regions, are mainly responsible for degradation of water quality.

Group 1 which consists of sampling points belonging to M_1 , i.e., from Gilgit to Khunjerab pass, and M_6 (main Indus River) outlines the most polluted group of the upper Indus Basin. There are the following reasons for these sampling sites to be at highest polluted side:

- (i) Higher concentration of arsenic and lead
- (ii) Higher water turbidity due inclusion of silts and rocks
- (iii) Picking of herbs and shrubs for medical use and illegal cutting of forest and trees of environmental importance in an uncontrolled manner
- (iv) Higher amount of dissolved oxygen (DO)
- (v) Higher amount of oxidation reducing potential (ORP)
- (vi) Higher percentage of salinity
- (vii) Human excreta effluent discharge
- (viii) Industrial waster along the main Indus River

It is observed from analysis, however, that sampling can be done for the points/stations with similar quality parameters and human activities. Also, on the basis of cluster analysis, the upper Indus Basin can be classified as either less, moderately, or highly polluted regions. The regions M_1 (from Gilgit to Khunjerab pass which also include the sampling points of Attabad lake) and M_6 (main Indus River) are the most polluted area because of higher concentration of Arsenic which is 40 times higher than the WHO recommended limits, i.e., $10 \mu\text{g/l}$. Furthermore, a rapid and more efficient assessment of upper Indus Basin water quality is possible while using the spatial cluster analysis of various regions of the upper Indus Basin. Moreover, this analysis is also helpful for designing an optimal, more feasible, and cost-effective monitoring strategy. The sample collections

TABLE 2: Coefficient of variation (CV) in water quality parameters of the upper Indus Basin.

Quality parameters	M_1	M_2	M_3	M_4	M_5	M_6
pH	0.05862	0.03395	0.03235	0.04454	0.02798	0.10346
Do (mg/L)	0.44337	0.69481	0.90625	0.40862	0.65668	0.37309
Do (%)	0.48706	0.93223	0.93134	0.45269	0.63853	1.53101
ORP	0.32578	0.12623	0.18369	0.2137	0.35976	0.14286
Cond (ms/cm)	0.08591	0.51238	0.6919	0.13514	0.52085	0.6101
TDS (ppm)	0.08877	0.5367	0.74332	0.43104	0.49662	0.67449
Salinity (%)	0.05973	0.6935	0.66504	0.41818	0.61572	1.58771
As ($\mu\text{g/l}$)	0.01382	0.80201	1.17808	0.82926	1.74784	0.01202
Pb ($\mu\text{g/l}$)	0.08533	0.95421	0.52915	1.92162	0.64507	1.29853

TABLE 3: Correlation matrix of water quality parameters.

	pH	Do	ORP	EC	TDS	Salinity	As	Pb
pH	1							
Do	0.6642	1						
ORP	-0.5311	-0.1018	1					
EC	0.3056	0.5279	0.1066	1				
TDS	0.5924	0.6226	-0.0676	0.9394	1			
Salinity	-0.2175	0.2530	0.8862	0.04051	-0.0411	1		
As	0.0023	0.7085	0.4812	0.5967	0.4762	0.5991	1	
Pb	-0.5468	-0.9222	0.08630	-0.7916	-0.8084	-0.1233	-0.7643	1

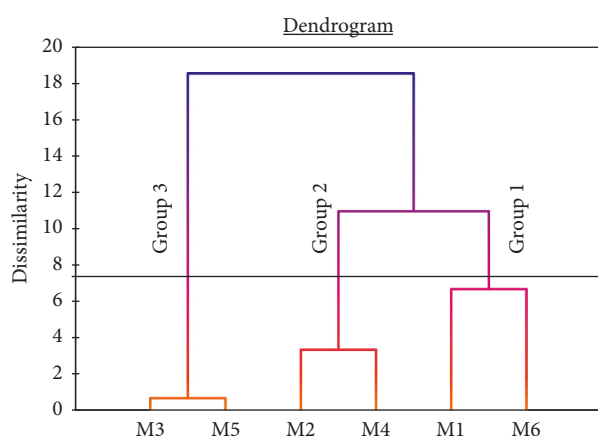


FIGURE 3: Dendrogram representing the cluster of monitoring stations.

from the upper Indus Basin is extremely difficult due to geography of this region [36, 38, 41], and this study suggests that number of monitoring stations can be reduced to only three stations instead of collecting the samples from whole upper Indus Basin.

4.4. Box Plots of Water Quality Parameters. In order to have in-depth examination of cluster analysis shown in Figure 3, a set of box plots of eight physicochemical quality parameters are shown in Figure 4. The spread of boxes for all parameters belonging to group 3 is smaller. This indicates the fact that quality parameters are less affected by environment and human activities, and water quality in this group is good which is also evident from cluster analysis shown above. The

concentration of As in samples belonging to this group is smaller and less dependent on temperature/environmental/seasonal alterations. Now coming to group 2, pH, TDS, and As concentrations have box plots with a higher spread (see Figures 4(a)–4(h)) which suggests the significant influence of environmental changes in this region. Among the abovementioned quality parameters, box plots show that pH of water in this region is more sensitive to seasonal/environmental alterations and thus results in degradation of water quality from group 2.

Group 1 box plots for EC, DO, ORP, salinity, and As concentration show largest spread of data along with bigger top and bottom whiskers for abovementioned quality parameters which is another confirmation of the fact that water quality parameters for sampling stations belonging to group 1 are more affected due to seasonal/environmental alterations. Furthermore, larger spread of data as evident from larger top and bottom whiskers also suggests that concentrations for aforementioned parameters are highest at group 1, thus confirming the role of soil erosion in degrading the water quality. The dissolved oxygen (DO) suffer more on moving from group 3 to group 1 (see Figure 4(b)) which is the confirmation of the fact that, among all three groups, group 1 is the most polluted as far as organic contents are concerned. This finding is also consistent with the box spread for salinity of samples belonging to group 1 (see Figure 4(f)) because DO and salinity are negatively correlated [38]. The soil erosion due to illegal uprooting of herbs and shrubs of medical importance, land sliding, and domestic/industrial waste are the main reasons for water pollution (as evident from cluster analysis) in this group. The results shown in Figures 3 and 4 are quite similar with the river statistical characteristics reported by number of researchers [32, 33, 38].

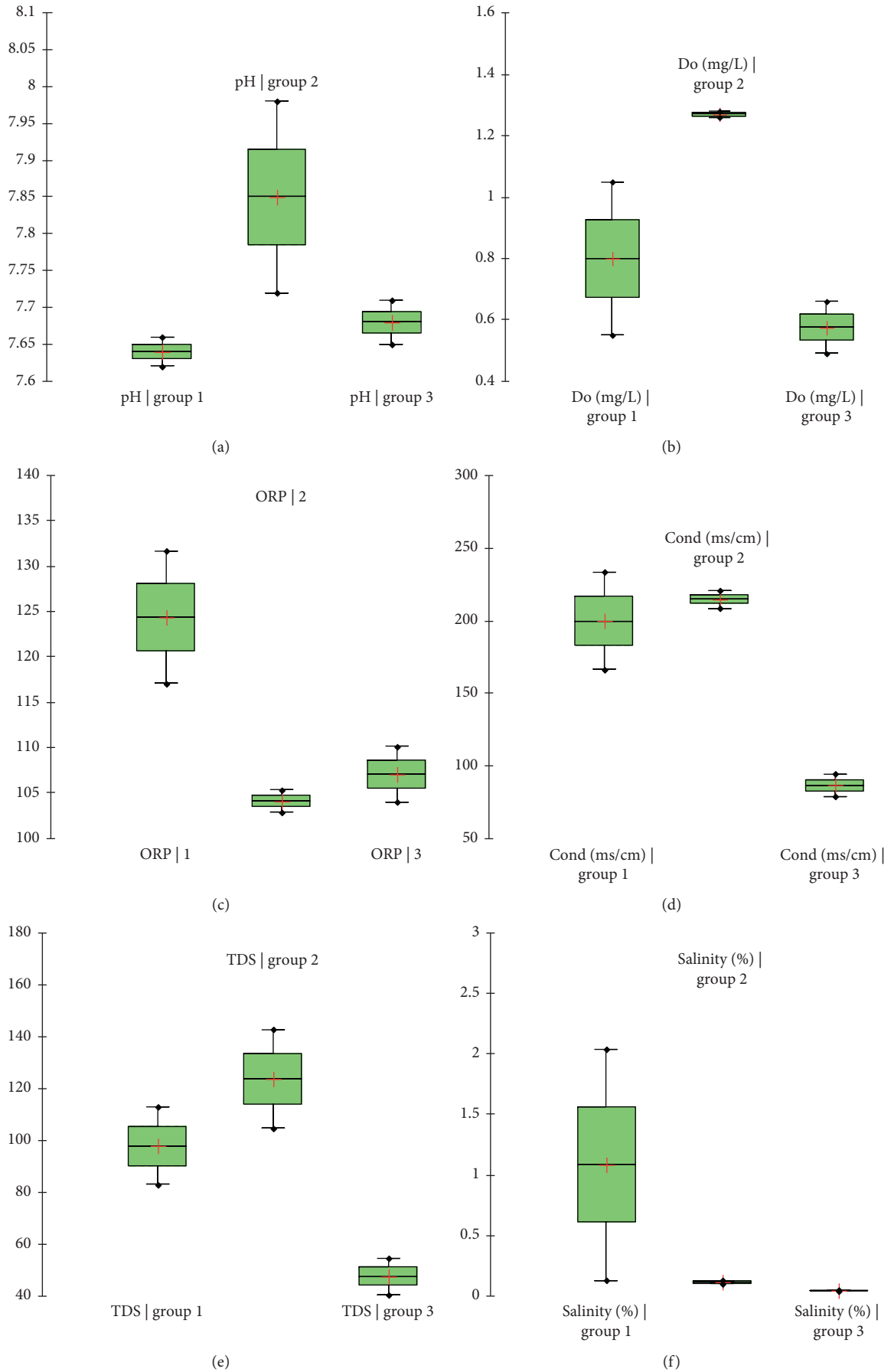


FIGURE 4: Continued.

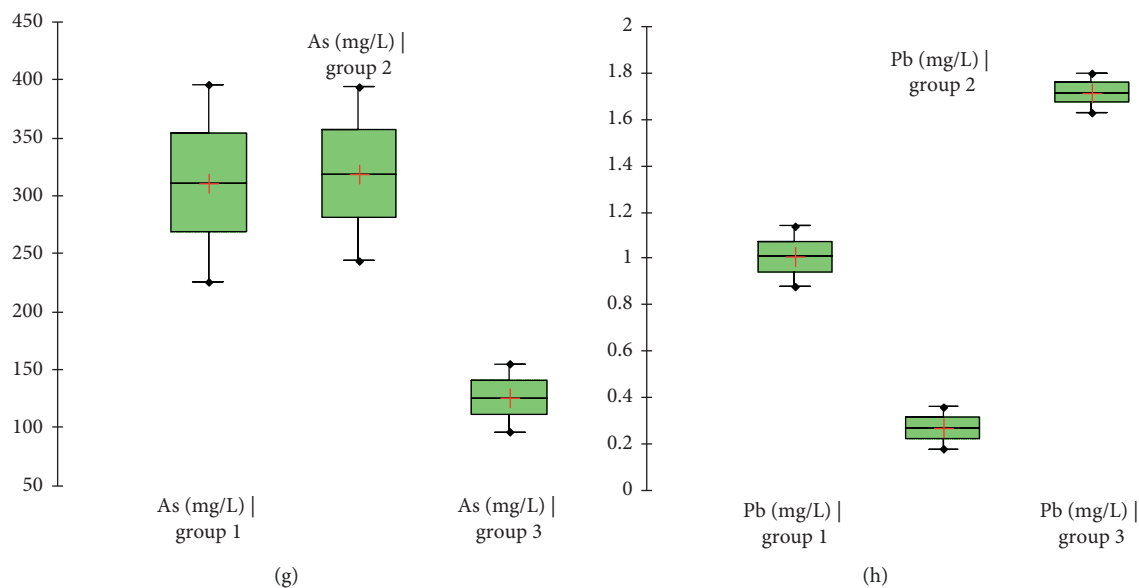


FIGURE 4: Box plots of (a) pH, (b) DO, (c) ORP, (d) EC, (e) TDS, (f) salinity, (g) As, (h) and Pb for different spatial clusters.

4.5. Principal Component Analysis (PCA) of Upper Indus River Data.

The eigenvalues obtained after performing the PCA of the quality parameters belonging to six regions, i.e., M_1 to M_6 of the upper Indus Basin, are shown in Table 4. By retaining the eigenvalues > 1 , it is evident from the results of PCA of current data that over 83% of the information of original data is explained by first two sets of eigenvalues. The variance percentage for first two eigenvalues is 83% and for the first three Eigen values is 94%. These percentages are far better than previously reported variance percentages of the first two and three eigenvalues with a focus on river quality data [32, 33, 38], thus confirming the application of PCA to the current set of data with a reasonable confidence. The eigenvalues for six regions, i.e., M_1 – M_6 , are 4.210, 2.462, 0.839, 0.464, 0.024, and < 0.024 , respectively. The higher eigenvalue for M_1 suggests the large dispersion of data for these regions. The higher concentration of As for all sampling points and significant higher dispersion in DO, ORP, salinity, and the concentration of As (as evident from the descriptive analysis and box plots) are reasons for obtaining higher eigenvalue during the PCA for this particular region. For M_2 , large dispersion of pH, TDS, and As concentration data of samples belonging to this region is responsible for obtaining the eigenvalue 2.462 (see Table 4). For region M_6 , smaller dispersion of data for all quality parameters give the lowest eigenvalue, i.e., < 0.024 .

According to PCA theory as explained by [37], parameter loadings (which are the projections of water quality parameters on PCs axes) are the correlation coefficients among variables and coefficients. The factor loading retained PCs, as shown in Table 4, and are classified as follows [38]:

- (i) Factor loading > 0.75 is classified as “strong”
- (ii) Factor loading value between 0.75 and 0.50 is classified as “moderate”

TABLE 4: Factor loadings of quality parameters.

	PCA-1	PCA-2	PCA-3
pH	-0.574	-0.617	-0.380
Do	-0.894	-0.057	-0.426
ORP	-0.036	0.965	0.118
Cond	-0.846	0.001	0.526
TDS	-0.882	-0.203	0.347
Salinity	-0.221	0.893	-0.312
As	-0.765	0.552	-0.051
Pb	0.975	0.072	0.049
Eigenvalue	4.210	2.462	0.839
Variability	52.630	30.772	10.490
Cumulative	52.630	83.402	93.892

- (iii) Factor loading value between 0.50 and 0.30 is classified as “weak”

The variance corresponding to PC-1 is 52.63% with a strong negative factor loading (> 0.7) by DO, EC, TDS, As, and Pb (positive). Parameters indicating the organic pollution are related with anthropogenic pollution sources are represented by this PC, as reported in the literature [38]. The consumption of oxygen at a larger extent during the fermentation (anaerobic) process by a higher concentration of dissolved organic matters results in formation of ammonia and organic acid which then causes a decrease of water pH because of hydrolysis. The negative loading of pH and strong positive loading of Pb shown in Table 4 are also in favor of our argument. In addition to this DO and TDS, As with strong negative loading factors confirms their negative correlation with anthropogenic pollution sources and agrees with already reported studies [24, 38]. The quality parameters strongly contributing are % salinity and ORP, while pH and the concentration of As are the moderate contributor to PC-2. This reveals the fact that this PC is the representative of seasonal variations (flow of solids from elevated

mountains and other sources during rain) and soil erosions because of illegal cutting of forests and uprooting the herbs of medical importance [36] at massive scale and agriculture activities. The negative loading of pH and strong positive loading of salinity (see Table 4) are also in favor of our argument here.

The plot of quality parameters in the first two PCs space is shown in Figure 5. From the figure, it is evident that PC-1 has strong negative loading on pH, DO, % salinity, Pb concentration, strong positive loading on the concentration of As, and moderate loading on EC and ORP. This shows that PC-1 is affected by organic and inorganic pollution due to soil erosion, interaction of Indus River water with arsenic rich bedrocks, and flowing of domestic wastewater into the Indus River through a number of creeks. The strong negative loading of PC-1 on DO and pH is quite similar to the observation reported in the literature. Zafar et al. [31, 38] confirms the presence of organic acids and DO negative correlation with organic pollutants [38]. PC-2 which is only 4.39% spread (as compared PC-1 of quality parameters has strong positive loading) on ORP, strong negative loading on As concentration, and weak to moderate negative loadings on TDS, pH, DO, and % salinity, respectively. This is the further confirmation of the fact that major source of pollution in the upper Indus region is either because of toxic heavy metal like As and Pb or anthropogenic pollution sources. In addition to these, there is some contribution of agriculture activities which have positive correlation with rain and flooding.

The negative correlations of aforementioned parameters (i.e., pH, DO, Pb, and % salinity) with inorganic/organic pollution, as shown in Figure 5, is also evident from strong negative PC-1 loading (see Figure 5) of these parameters. Both inorganic and organic pollutants mainly affect the TDS, whereas inorganic pollutants affect EC only. The moderate positive PC-1 loading of EC points to the fact that EC is mainly dependent on the concentration of As and Pb. The concentrations of As and Pb have strong positive and negative loading on PC-1, respectively (see Figure 5), thus making the loading of EC moderate. TDS has weak positive loading on PC-1 and weak positive loading on PC-2, suggesting the influence of other parameter loadings with more dominant PC-1 contributions. Figure 6 represents the projection of quality parameter on PC space with their confidence intervals and is the conclusive statement of PCA of quality parameters because it shows the true pictures about monitoring the exact number of quality parameters for water quality assessment in the upper Basin of Indus River or upper Indus Basin. According to the PCA presented in Figure 6, four parameters ORP, DO, and the concentrations of As and Pb are sufficient to have a reasonable confidence on the quality of water in the upper Indus Basin.

Figure 7 shows a bipolar plot of the quality parameters at different stations in the first two PCs space. It is evident from figure that the six regions of the upper Indus Basin, which are under investigation, form three groups: (1) M_1 and M_6 , (2) M_1 and M_6 , and (3) M_3 and M_5 . The group 3 here has strong positive loadings on PC-1, which means that 52.63% of total variance belongs to group 3. With respect to active

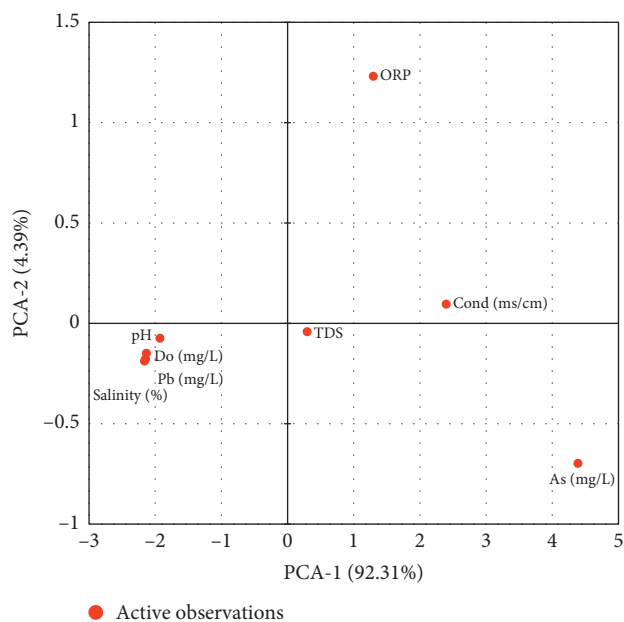


FIGURE 5: PCA-1 and PCA-2 loadings of water quality parameters.

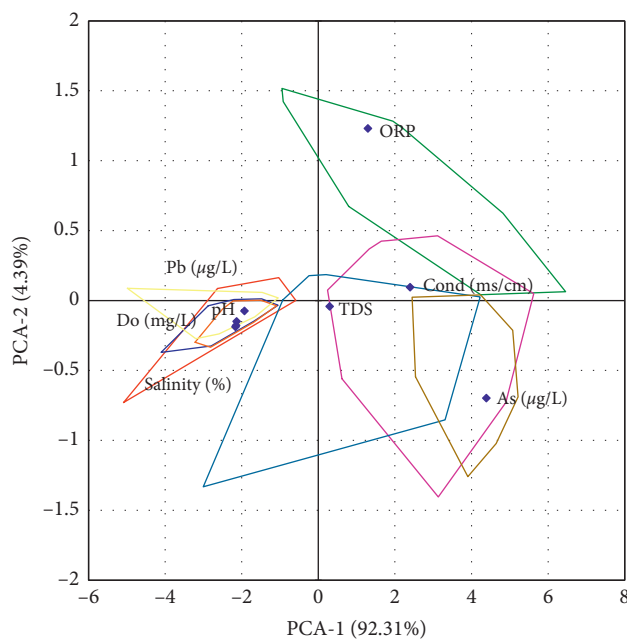


FIGURE 6: PCA-1 and PCA-2 loadings of water quality parameters with confidence intervals.

parameters, M_3 and M_5 form a least polluted group with only Pb as the notable pollutant (see Figure 7). On the contrary, group 2, which consists of M_2 and M_4 , has strong negative loadings of active variables on PC-1 and PC-2. However, out of eight physicochemical parameters EC, DO, TDS, and pH are the most prominent active variables (see Figure 7) for this group which make group 2 a moderately polluted group. M_1 active observation site/station (as shown in Figure 6) has weak positive and negative loadings on PC-1 and PC-2, but almost all the active parameters are contributing to the net

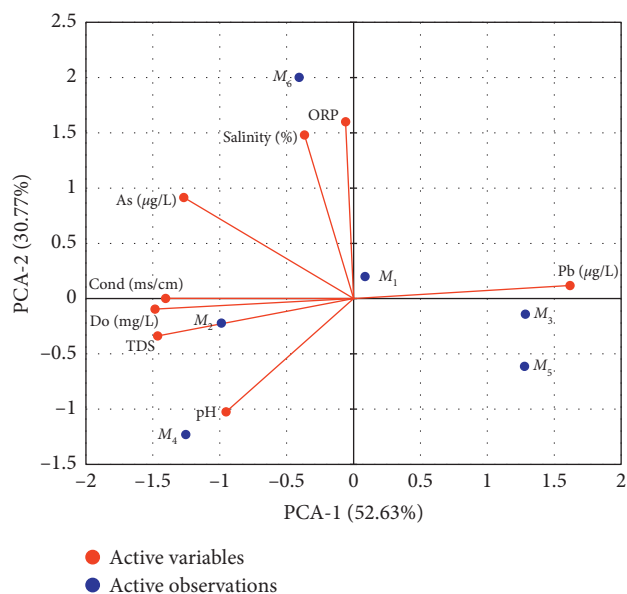


FIGURE 7: Bipolar PCA plot.

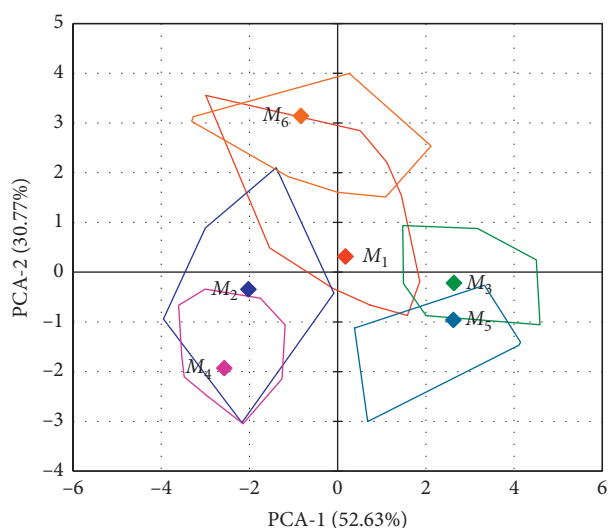


FIGURE 8: Representation of spatial behavior of the sampling network in the PC space.

pollution of M_1 , as evident from Figure 7, thus making M_1 as a member of the worst polluted group, i.e., group 1. The concentration of As and Pb, % salinity, and ORP are major contributors at M_6 (see Figure 7), thus making the M_6 active observation/site/station a very strong negative loading on 30.77% of total variance, i.e., PC-2. The higher concentration of As (i.e., $399.32 \mu\text{g/l}$, which is eight times higher than national limit and 40 times higher than the World Health Organization (WHO) permissible limits), significantly increases in % salinity due to agriculture activities along the passage of the main Indus River, and inclusion of industrial/domestic wastewater in the main Indus River is responsible for making M_6 as a member of the worst polluted group, i.e., group 1. The results of PCA shown in the bipolar plot of Figure 7 are in good agreements with the results of CA (see Figure 3) and box plots (see Figures 4(a)–4(h)).

In addition to this, Figure 8 which shows the projection of active observation sites on PC space with their confidence intervals suggests that, instead of sampling whole upper Indus Basin and Indus River, only three monitoring stations are sufficient for stating a conclusive statement about the quality of water of the upper Indus Basin and main Indus River.

5. Conclusion

CA reveals that upper Indus Basin monitoring can be done while dividing the region into three clusters, representing good quality water (M_3 and M_5), moderate quality water (M_2 and M_4), and worst quality water (M_1 and M_6) cluster, respectively. Three latent factors are responsible for explaining the 93.87% of total variance as confirmed by PCA. The parameters, which are significantly influenced by anthropogenic impact, seasonal variations, and soil erosion, are DO, EC, TDS, and concentration of As ($\mu\text{g/l}$). The concentration of Pb ($\mu\text{g/l}$) is influenced by anthropogenic sources only, while the (%) salinity and ORP are influenced due to agriculture activities and runoff, as confirmed by PCA. The box plot results are also supporting the PCA outcomes. The highest pollution is observed at M_1 and M_6 with the concentration of As being the dominant factor in making this group as the worst polluted group. The results of current study could be utilized for designing a comprehensive monitoring protocol for monitoring the Indus River, thus saving this important resource of Pakistan.

Data Availability

Data will be made available when required.

Conflicts of Interest

The authors declare that they have no conflicts of interest.

Acknowledgments

Engr. Mansoor Ahmad Baluch acknowledges the technical and moral support provided by the University of Engineering and Technology Taxila, 47050, Pakistan.

References

- [1] R. Shabbir and S. S. Ahmad, "Use of geographic information system and water quality index to assess groundwater quality in rawalpindi and islamabad," *Arabian Journal for Science and Engineering*, vol. 40, no. 7, pp. 2033–2047, 2015.
- [2] M. Kavurmaci and A. K. Üstün, "Assessment of groundwater quality using DEA and AHP: a case study in the Serflikochisar region in," *Turkey Environmental Monitoring and Assessment*, vol. 188, no. 4, p. 258, 2016.
- [3] A. Alamgir, M. A. Khan, J. Schilling, S. S. Shaukat, and S. Shahab, "Assessment of groundwater quality in the coastal area of Sindh province," *Pakistan Environmental Monitoring and Assessment*, vol. 188, no. 2, p. 78, 2016.
- [4] M. Terrado, D. Barceló, R. Tauler, E. Borrell, S. D. Campos, and D. Barceló, "Surface-water-quality indices for the analysis

- of data generated by automated sampling networks,” *TrAC Trends in Analytical Chemistry*, vol. 29, no. 1, pp. 40–52, 2010.
- [5] S. Das, M. Majumder, D. Roy, and A. Mazumdar, “Determination of urbanization impact on rain water quality with the help of water quality index and urbanization index,” in *Impact of Climate Change on Natural Resource Management*, pp. 131–142, Springer, Berlin, Germany, 2010.
 - [6] E. Fathi, R. Zamani-Ahmadmohammadi, and R. Zare-Bidaki, “Water quality evaluation using water quality index and multivariate methods, Beheshtabad River,” *Iran Applied Water Science*, vol. 8, no. 7, p. 210, 2018.
 - [7] I. Mladenović-Ranisavljević and S. Žerajić, “Comparison of different models of water quality index in the assessment of surface water quality,” *International Journal of Environmental Science and Technology*, vol. 15, no. 3, pp. 665–674, 2018.
 - [8] F. Misaghi, F. Delgosha, M. Razzaghmanesh, and B. Myers, “Introducing a water quality index for assessing water for irrigation purposes: a case study of the Ghezel Ozan River,” *Science of the Total Environment*, vol. 589, no. 4, pp. 107–116, 2017.
 - [9] S. H. Ewald, “Water quality evaluation of Al-Gharraf River by two water quality indices,” *Applied Water Science*, vol. 7, no. 7, pp. 3759–3765, 2017.
 - [10] M. T. Aalami, H. Abbasi, and V. Nourani, “Sustainable management of reservoir water quality and quantity through reservoir operational strategy and watershed control strategies,” *International Journal of Environmental Research*, vol. 12, no. 6, pp. 773–788, 2018.
 - [11] C. M. C. M. Couto, R. Ribeiro, A. R. Ribeiro et al., “Spatiotemporal distribution and sources of trace elements in Ave River (Portugal) lower basin: estuarine water, sediments and indigenous flora,” *International Journal of Environmental Research*, vol. 13, no. 2, pp. 303–318, 2019.
 - [12] M. A. Rahman, S. Kumar, A. A. Mohana, R. Islam, M. A. Hashem, and L. Chuanxiu, “Coliform bacteria and trace metals in drinking water, southwest Bangladesh: multivariate and human health risk assessment,” *International Journal of Environmental Research*, vol. 13, no. 2, pp. 395–408, 2019.
 - [13] M. Salam, M. Kabir, L. Yee, and M. Khan, “Water quality assessment of Perak River, Malaysia,” *Pollution*, vol. 5, no. 3, pp. 637–648, 2019.
 - [14] M. Barceló and E. Arslan Topal, “Monitoring of Zn and Cr in Downstream Water from Uzunçayır Dam in Turkey,” *Pollution*, vol. 5, pp. 649–655, 2019.
 - [15] S. Das Sharma, “Risk assessment and mitigation measures on the heavy metal polluted water and sediment of the Kolleru Lake in Andhra Pradesh,” *India Pollution*, vol. 5, pp. 161–178, 2019.
 - [16] M. Bhuyan, M. Bakar, A. S. M. Sharif, M. Hasan, and M. Islam, “Water quality assessment using water quality indicators and multivariate analyses of the old Brahmaputra River,” *Pollution*, vol. 4, no. 3, pp. 481–493, 2018.
 - [17] A. Karbassi, F. Mir Mohammad Hosseini, A. Baghvand, and M. Nazariha, “Development of water quality index (WQI) for Gorganrood River,” *International Journal of Environmental Research*, vol. 5, no. 4, pp. 1041–1046, 2011.
 - [18] M. Saeedi, S. Daneshvar, and A. R. Karbassi, “Role of riverine sediment and particulate matter in adsorption of heavy metals,” *International Journal of Environmental Science & Technology*, vol. 1, no. 2, pp. 135–140, 2004.
 - [19] T. Ahmad, M. A. Kahlown, A. Tahir, and H. Rashid, “Arsenic an emerging issue: experiences from Pakistan,” in *Proceedings of the 30th WEDC International Conference*, pp. 459–466, Vientiane, Laos, October 2004.
 - [20] M. M. Rahman, G. Owens, and R. Naidu, “Arsenic levels in rice grain and assessment of daily dietary intake of arsenic from rice in arsenic-contaminated regions of Bangladesh-implications to groundwater irrigation,” *Environmental Geochemistry and Health*, vol. 31, no. S1, pp. 179–187, 2009.
 - [21] T. Roychowdhury, T. Uchino, H. Tokunaga, and M. Ando, “Survey of arsenic in food composites from an arsenic-affected area of West Bengal, India,” *Food and Chemical Toxicology*, vol. 40, no. 11, pp. 1611–1621, 2002.
 - [22] A. Alamdar, S. Ali Musstjab Akber Shah Eqani, S. Waqar Ali et al., “Human Arsenic exposure via dust across the different ecological zones of Pakistan,” *Ecotoxicology and Environmental Safety*, vol. 126, pp. 219–227, 2016.
 - [23] M. H. Gholizadeh, A. M. Melesse, and L. Reddi, “Analysis of spatiotemporal trends of water quality parameters using cluster analysis in South Florida,” in *Proceedings of the World Environmental and Water Resources Congress 2016*, pp. 519–528, West Palm Beach, FL, USA, May 2016.
 - [24] X. Wang, Q. Cai, L. Ye, and X. Qu, “Evaluation of spatial and temporal variation in stream water quality by multivariate statistical techniques: a case study of the Xiangxi river basin, China,” *Quaternary International*, vol. 282, pp. 137–144, 2012.
 - [25] M. Xiao, F. Bao, S. Wang, and F. Cui, “Water quality assessment of the Huaihe River segment of Bengbu (China) using multivariate statistical techniques,” *Water Resources*, vol. 43, no. 1, pp. 166–176, 2016.
 - [26] A. H. Pejman, G. R. N. Bidhendi, A. R. Karbassi, N. Mehrdadi, and M. E. Bidhendi, “Evaluation of spatial and seasonal variations in surface water quality using multivariate statistical techniques,” *International Journal of Environmental Science & Technology*, vol. 6, no. 3, pp. 467–476, 2009.
 - [27] A. Mustapha and A. Abdu, “Application of principal component analysis & multiple regression models in surface water quality assessment,” *Journal of Environment and Earth Science*, vol. 2, no. 2, pp. 16–23, 2012.
 - [28] R. Bhattacharyya, K. Manoj, and P. Padhy, “Index analysis, graphical and multivariate statistical approaches for hydrochemical characterization of Damodar River and its canal system Durgapur, West Bengal, India,” *International Research Journal of Environment Sciences*, vol. 2, pp. 53–62, 2013.
 - [29] S. Shrestha and F. Kazama, “Assessment of surface water quality using multivariate statistical techniques: a case study of the Fuji River basin, Japan,” *Environmental Modelling & Software*, vol. 22, no. 4, pp. 464–475, 2007.
 - [30] I. Khan, A. Khan, M. S. Khan et al., “Impact of city effluents on water quality of Indus River: assessment of temporal and spatial variations in the southern region of Khyber Pakhtunkhwa,” *Pakistan Environmental Monitoring and Assessment*, vol. 190, no. 5, p. 267, 2018.
 - [31] S. Zafar, A. Khan, S. Ullah et al., “Assessing impact of effluent discharge on irrigation water quality in southern region of Khyber Pakhtunkhwa,” *Pakistan Environmental Monitoring and Assessment*, vol. 189, no. 4, p. 156, 2017.
 - [32] K. P. Kazama, A. Malik, D. Mohan, and S. Sinha, “Multivariate statistical techniques for the evaluation of spatial and temporal variations in water quality of Gomti River (India)-a case study,” *Water Research*, vol. 38, no. 18, pp. 3980–3992, 2004.
 - [33] K. R. Singh, A. P. Goswami, A. S. Kalamdhad, and B. Kumar, “Assessment of surface water quality of Pagladia, Beki and Kolong rivers (Assam, India) using multivariate statistical techniques,” *International Journal of River Basin Management*, pp. 1–10, 2019.
 - [34] Y. Zhang, Y. Li, Y. Li, W. Da, M. Yu, and Q. Quan, “Application of multivariate statistical methods in the assessment

- of water quality in selected locations in Jialing river basin in Guangyuan, China,” *Water Science and Technology: Water Supply*, vol. 19, no. 1, pp. 147–155, 2019.
- [35] D. A. Cornwell and M. L. Davis, *Introduction to environmental engineering*, Mcgraw-hill Education, Europe, 2012.
- [36] M. Ahmed, K. Nazim, A. Khan, M. F. Siddiqui, and M. U. Khan, “Arsenic and lead level from upper to lower Indus basin of Pakistan,” *FUUAST Journal of Biology*, vol. 7, pp. 183–191, 2017.
- [37] P. J. Shaw, *Multivariate Statistics for the Environmental Sciences*, Wiley, Hoboken, NJ, USA, 2009.
- [38] V. Chounlamany, M. A. Tanchuling, and T. Inoue, “Spatial and temporal variation of water quality of a segment of Marikina river using multivariate statistical methods,” *Water Science and Technology*, vol. 76, no. 6, pp. 1510–1522, 2017.
- [39] N. Yusof, A. Haraguchi, M. A. Hassan, M. R. Othman, M. Wakisaka, and Y. Shirai, “Measuring organic carbon, nutrients and heavy metals in rivers receiving leachate from controlled and uncontrolled municipal solid waste (MSW) landfills,” *Waste Management*, vol. 29, no. 10, pp. 2666–2680, 2009.
- [40] P. Kjeldsen, M. A. Barlaz, A. P. Rooker, A. Baun, A. Ledin, and T. H. Christensen, “Present and long-term composition of MSW landfill leachate: a review,” *Critical Reviews in Environmental Science and technology*, vol. 32, no. 4, pp. 297–336, 2002.
- [41] S. Akhtar, “The south Asiatic monsoon and flood hazards in the Indus river basin, Pakistan,” *Journal of Basic & Applied Sciences*, vol. 7, 2011.

Research Article

Neglect of Temperature and pH Impact Leads to Underestimation of Seasonal Ecological Risk of Ammonia in Chinese Surface Freshwaters

Zhen-Guang Yan,¹ Jun-Tao Fan,¹ Xin Zheng,¹ Shu-Ping Wang,¹ Xiao-Shan Guo,¹ Tian-Xu Zhang,¹ Su-Wen Yang ², and Yi-Zhang Zhang ¹

¹State Key Laboratory of Environmental Criteria and Risk Assessment, Chinese Research Academy of Environmental Sciences, Beijing 100012, China

²National Engineering Laboratory for Lake Pollution Control and Ecological Restoration, Chinese Research Academy of Environmental Sciences, Beijing 100012, China

Correspondence should be addressed to Su-Wen Yang; environzane@163.com and Yi-Zhang Zhang; zhangyz@craes.org.cn

Received 14 June 2019; Accepted 4 August 2019; Published 29 September 2019

Guest Editor: Yihua Xiao

Copyright © 2019 Zhen-Guang Yan et al. This is an open access article distributed under the Creative Commons Attribution License, which permits unrestricted use, distribution, and reproduction in any medium, provided the original work is properly cited.

Ammonia nitrogen (AN) is evaluated with fixed water quality standards (WQSS) in aquatic environment management in China. Since the toxicity of AN can be influenced by water parameters, the current evaluation is not rigorous and may result in problematic conclusions. The present study collected the ecotoxicity and exposure data of AN in Chinese surface freshwaters in 2017. The species sensitivity distribution of AN was established, and the ecological risk posed by AN in Chinese surface waters was assessed with Chinese AN water quality criteria. The results showed that mollusk species are the most sensitive taxa to AN. Ecological risk assessments on AN suggested that, in summer and autumn, when the water temperature and pH are high, the risk of AN may occur at some sites with good water quality (Class II or III). This poses a threat to aquatic organisms at these sites, especially highly sensitive freshwater shellfish. It suggested that neglect of water parameters impact may lead to underestimation of ecological risk of AN in Chinese basins.

1. Introduction

Ammonia nitrogen (AN) is considered one of the most concerning pollutants in aquatic environment because of its high toxicity and ubiquity in surface water systems [1]. Ammonia nitrogen is one of the most common pollutants in all watershed basins within China [2]. With the exception of the compound pollution index and chemical oxygen demand (COD), ammonia nitrogen is the only pollutant monitored and evaluated by the Chinese government for management of nation-controlled pollution sources and pollution control [3]. Ammonia nitrogen is produced for commercial fertilizers and other industrial applications, including the use as a source of hydrogen in metal treating and finishing and many other uses [4]. Natural sources of

ammonia nitrogen include the decomposition of organic matter, forest fires, biotic ammonia excretion, and nitrogen fixation [5–7].

Ammonia can enter aquatic environments via various pathways and can be highly toxic to aquatic life [8–10]; therefore, it has received considerable attention from scientists since the 1980s [11, 12]. The chemical form of ammonia in water consists of two species: the ammonium (NH_4^+) molecule and the unionized ammonia (NH_3) molecule. The ratio of the two species in a given aqueous solution is dependent upon the pH and temperature of the solution [13, 14]. As pH and temperature increase, the concentration of NH_4^+ decreases and the concentration of NH_3 increases. In general, the ratio of NH_3 to NH_4^+ in freshwater increases by 10-fold for each rise of a single pH

unit and by approximately two-fold for each 10°C rise in temperature from 0 to 30°C [14]. The concentration of ammonia nitrogen is the sum of NH_3 and NH_4^+ concentrations, and it is often expressed as total ammonia nitrogen. The toxicity of NH_3 is significantly greater than NH_4^+ toxicity, so the hypothesis that NH_3 increases with pH and temperature explains why toxicity of total ammonia also increases as pH and temperature increase [15].

Ammonia nitrogen, particularly the NH_3 , have significant toxic effects on aquatic animals. For example, the toxic effects of ammonia on fish includes gill damage [16], reduction in blood oxygen-carrying capacity [1], interference in the ability of a fish to metabolize adenosine triphosphate [17], and disruption of normal metabolic function in the liver and kidneys [18]. In order to protect aquatic organisms from ammonia hazard, the United States Environmental Protection Agency (USEPA) studied ammonia aquatic life criteria (ALC) for several decades [15, 19]. In recent years, studies have addressed the effect of ammonia toxicity on bivalves [20], particularly in freshwater mussels within the family Unionidae [21–23]; the USPEA proposed that mollusk may be the most sensitive taxa to ammonia [15], and this should be considered sufficient for the establishment of ALC for AN [24]. Following this discovery, the USEPA updated the ALC technical report and criteria values for AN in 2013 [15]. In this report, the ammonia nitrogen ALC were described as functions with two independent variables, pH and temperature. Using this framework, North American mollusks can be given sufficient protection according using the latest ALC of AN. In addition, other countries have established their own ammonia nitrogen water quality standards, such as Australia and New Zealand [25], as well as Canada [6]. Since the toxicity of ammonia nitrogen varies with the temperature and pH of the water, the standard values of ammonia nitrogen in these countries are dependent on the water quality parameters.

In order to monitor and assess surface water quality, 145 national monitoring sites were set in Chinese surface freshwaters. The water quality was assessed by comparing the monitoring data with national water quality standards (WQs). The current Chinese WQs for surface freshwater are divided into five levels according to water body function classification [26]. For example, the freshwater WQs for ammonia nitrogen were set as 0.15 mg/L (Class I), 0.5 mg/L (Class II), 1.0 mg/L (Class III), 1.5 mg/L (Class VI), and 2.0 mg/L (Class V) [26]. However, these WQs values were assigned for all Chinese surface freshwater management; no water quality parameters were considered in the WQS establishment [26]. When compared to American WQs, Chinese WQs for ammonia nitrogen are not rigorous enough to assess the ecological risks posed by ammonia or to protect aquatic organisms.

The present study collected the ecotoxicity data and assessed the species sensitivity distribution (SSD) of AN and monitoring exposure data of AN in Chinese major basins in 2017. The ecological risk posed by AN in China surface freshwaters was evaluated using the previously derived ALC of AN, and the results can provide valuable information for water environmental management in China.

2. Materials and Methods

2.1. Exposure and Toxicity Data Collection of Ammonia. Ammonia nitrogen exposure data for 145 sites in 2017 were collected weekly from surface freshwater quality monitoring reports [27]. Twenty basins (ten rivers and ten lakes) were included in the report (Figure 1).

Ammonia nitrogen ecotoxicity data were derived from both the USEPA ECOTOX database [28] and published literatures. The data were screened according to the USEPA ALC guidelines [29]. Unicellular animal toxicity data were eliminated. The toxicity test duration should be two days for *Daphnia* and chironomid larvae and four days for other aquatic animals. The accepted endpoints for an acute test are median lethal concentration (LC_{50}) or median effect concentration (EC_{50}), while the accepted endpoints for a chronic test are no observed effect concentration (NOEC) or 20% effect concentrations (EC_{20}). Both of the NOEC and the EC_{20} are acceptable chronic toxicity endpoints for ammonia according to the US ammonia criteria document [15]. For the same species, toxicity data of sensitive life stage take priority to data of the resistant life stage. The flow-through toxicity experiment data are prioritized over static or renewal experiment data, and the data produced by measuring chemical concentration are prioritized over data produced with the nominal level of chemicals. Finally, because the toxicity of ammonia can be affected by the pH and temperature of water bodies, published ammonia toxicity data that did not include pH and temperature information were abandoned.

2.2. Toxicity Data Adjustment of Ammonia Nitrogen. Temperature and pH can affect the toxicity of ammonia nitrogen; all the toxicity data were adjusted to the same baseline conditions (pH 7.0, 20°C) before data analysis. The data adjustment was performed according to the USEPA ALC document of ammonia nitrogen with the equations (1) to (4) [15]:

$$AV_{t,7} = \frac{AV_t}{\left(\frac{(0.0114)}{(1 + 10^{7.204 - \text{pH}})}\right) + \left(\frac{(1.6181)}{(1 + 10^{\text{pH} - 7.204})}\right)}, \quad (1)$$

$$\log(AV_{t,7,20}) = \log(AV_{t,7}) + 0.036(T - 20), \quad (2)$$

$$CV_{t,7} = \frac{CV_t}{\left(\frac{(0.0278)}{(1 + 10^{7.688 - \text{pH}})}\right) + \left(\frac{(1.1994)}{(1 + 10^{\text{pH} - 7.688})}\right)}, \quad (3)$$

$$\log(CV_{t,7,20}) = \log(CV_{t,7}) + 0.028(T - 20), \quad (4)$$

where AV_t and CV_t were the acute and chronic toxicity values under the given temperature and pH, respectively. $AV_{t,7}$ and $CV_{t,7}$ were the adjusted acute and chronic values under pH of 7. $AV_{t,7,20}$ and $CV_{t,7,20}$ were the adjusted values under pH of 7 and temperature of 20°C, and T was temperature.

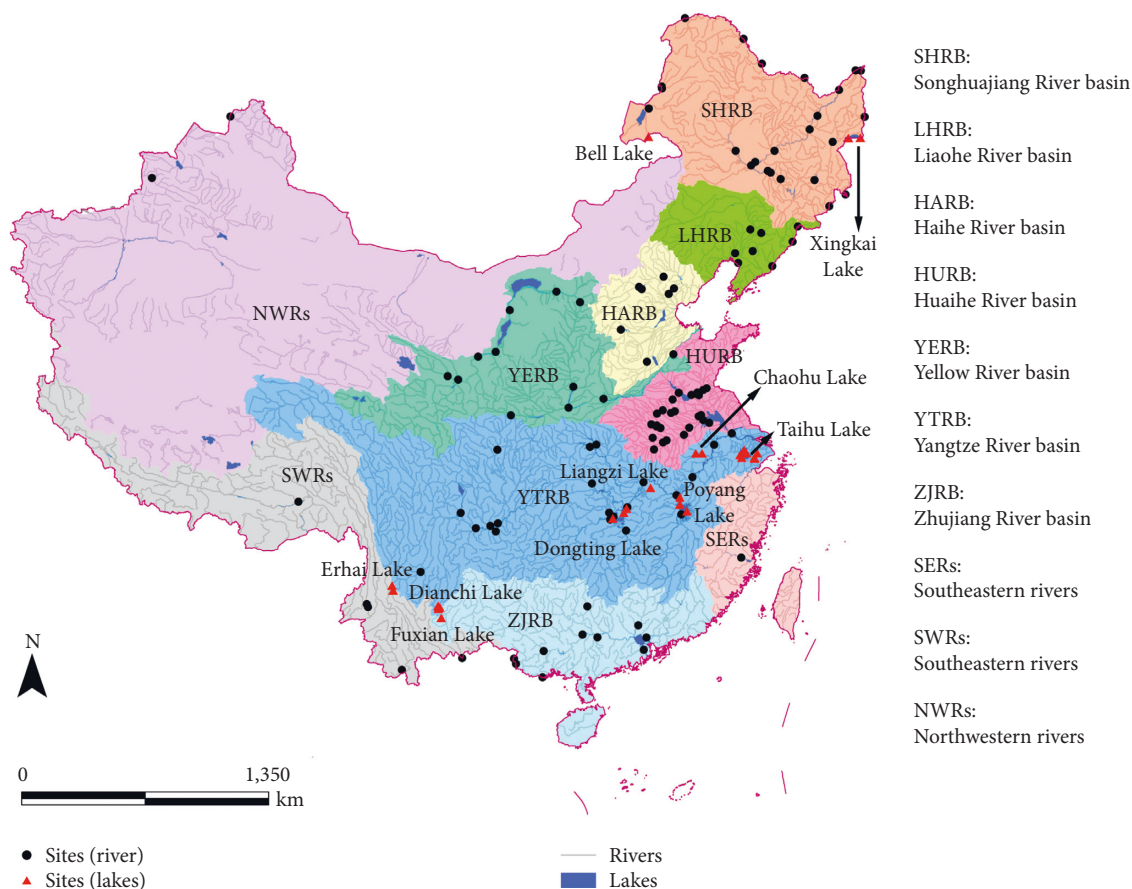


FIGURE 1: Location of national monitoring sites in Chinese surface freshwaters (ten rivers and ten lakes).

According to the document, the raw values under the given temperature and pH were transformed to an adjusted values under a pH of 7 for toxicity data of vertebrates or an adjusted value under a pH of 7 and temperature of 20°C for toxicity data of invertebrates. After adjustment, the SSD curve was established according to [30]. If the chronic ecotoxicity data are not sufficient, the acute-chronic ratio (ACR) method [15] will be used to transfer the acute data to chronic data.

2.3. Ecological Risk Assessment of Ammonia Nitrogen. The hazard quotients (HQs) method was used to assess the ecological risk of ammonia nitrogen. HQs are equal to the measured exposure concentration divided by the long-term ALC value derived in our previous study [31]. Ammonia nitrogen posed no significant risk to the environment if HQs are less than 1.0 [32]. The risk assessment was performed with exposure data in 2017 for all 145 sites (Figure 1).

The data were processed with Excel 2010 (Microsoft, USA), and the figures in this study were prepared with Origin 9.64 (OriginLab, USA) and Adobe Photoshop 8.0.1 (Adobe Systems, USA).

3. Results and Discussion

3.1. Variations of Water Parameters in Chinese Freshwater Basins. Water quality monitoring data in 2017 were collected for twenty basins. The pH and temperature data for

these basins were compared, and significant differences were observed with a range of 6.06–9.79 in pH and –1 to 33.5°C in temperature (Figure 2). The highest water pH of several basins, including Songhua River, Haihe River, and Huaihe River, was greater than 9.0, while the highest water temperature of Huaihe River, Yangtze River, Zhujiang River, Southeast rivers, and Southwest rivers was greater than 30°C (Figure 2). According to the chemical equilibrium of ammonia in water, the higher the water pH and temperature is, the more toxic the ammonia becomes [15]. Therefore, the apparent differences in pH and temperature of the twenty basins produce tremendous uncertainty if we were to assess the ecological risk of ammonia nitrogen without considering the water quality parameters in routine environmental management. Previous studies have also considered the influence of water parameters on ammonia toxicity when assessing the ecological risk of ammonia in Taihu Lake or the seven Chinese major basins [33, 34].

3.2. SSDs of Ammonia Nitrogen. A total of 565 acute ammonia nitrogen toxicity and 36 chronic ammonia nitrogen toxicity data points were collected by searching the literature (Supplemental Information Table S1). Seventy-six genus mean acute values (GMAVs) and 16 genus mean chronic values (GMCVs) of AN were obtained through calculation (Supplemental Information Table S2). The fish toxicity data set is more sufficient than other taxa with 30 GMAVs and 8

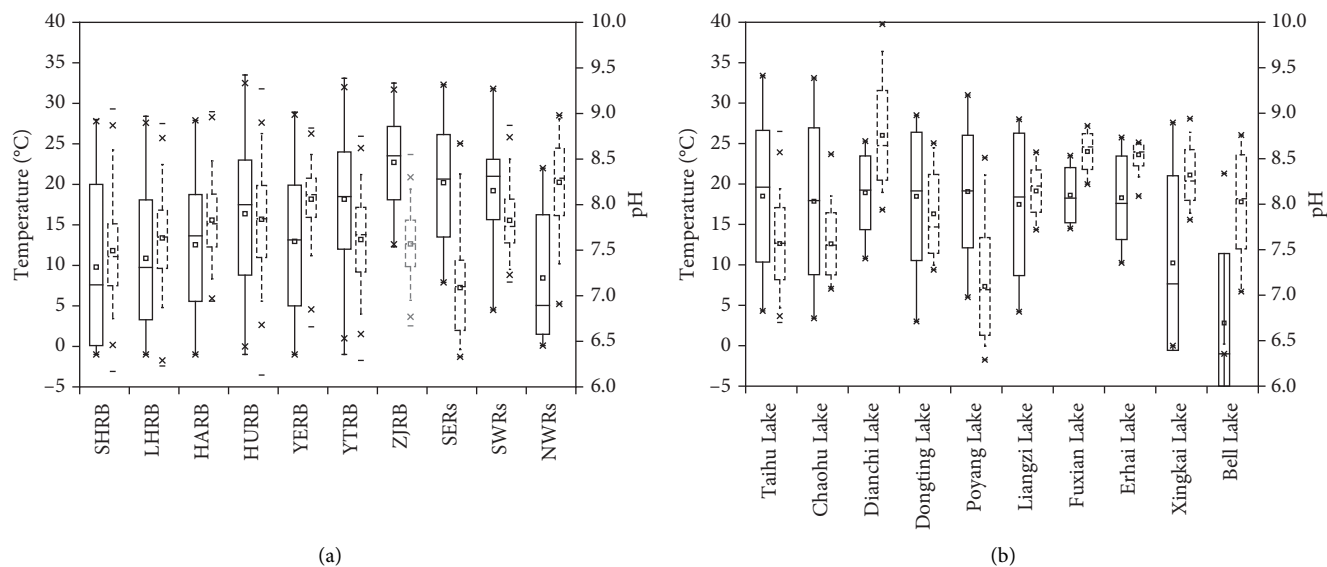


FIGURE 2: pH and temperature in twenty Chinese major basins in 2017. Dashed box indicates pH values, and solid box indicates temperature.

GMCVs. The quantities of GMCVs were relatively insufficient. In order to obtain more ammonia nitrogen GMCVs to construct the SSD, we used the ACR method to transfer the species mean acute values (SMAVs) to species mean chronic values (SMCVs). The species mean ACR values were calculated by dividing the acute value (LC_{50} or EC_{50}) with the chronic value (20% effect concentration, EC_{20}) according to the methodology provided by the ALC guidelines [29] and the ammonia nitrogen ALC technical report released by the USEPA [15]. Generally, it is desirable to use species mean ACR in the transfer process. However, species mean ACR was not always available due to the scarcity of EC_{20} toxicity data. So, the alternative ACR values were genus mean ACR, family mean ACR, class mean ACR, or phylum mean ACR in the descending priority order. The applied ACR values are shown in Supplemental Information Table S3, and total GMCVs, including the published GMCVs and the calculated ACR-based GMCVs, are shown in Supplemental Information Table S2.

All GMCVs were ranked in Figure 3. Among these 79 GMCVs, the top ten GMCVs in front were all mollusks. This suggests that mollusks are the most sensitive taxa to ammonia nitrogen. These results are consistent with the USEPA ALC technical report of ammonia nitrogen conclusions [15]. Besides mollusks, many fish species are also sensitive to ammonia nitrogen, while crustaceans and insects are relatively insensitive (Figure 3). This indicates that different organisms have different levels of sensitivity to ammonia nitrogen and results in different levels of ecological risk of ammonia nitrogen to varying organisms.

3.3. Chinese Water Quality Criteria of Ammonia Nitrogen. Study on water quality criteria is a new research hotspot in China in recent years [35–39]. Based on the sensitivity of Chinese freshwater organisms to ammonia nitrogen, we

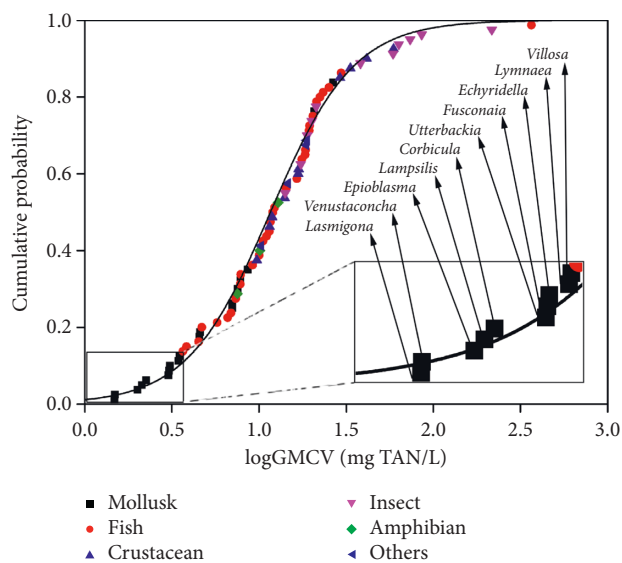


FIGURE 3: Species sensitivity distributions of ammonia nitrogen. Internal figure: top ten genera of the most sensitive species (all of them are mollusks).

have proposed China's ammonia nitrogen ALC function in the previous study [31]. The proposed short-term (CMC) and long-term (CCC) Chinese ammonia nitrogen criteria are shown in equations (5) and (6), respectively. It can be seen from the function equations that the temperature and pH of the water body are the independent variables of the two criteria functions. Therefore, the long-term and short-term criteria values of ammonia nitrogen vary with the temperature and pH of the water (Figure 4). In general, as the water temperature and pH increase, the water quality criteria value of ammonia nitrogen keeps decreasing. It suggests that when the water body temperature ranges from 0°C to 30°C, the pH value ranges from 6.5 to 9.0, and the

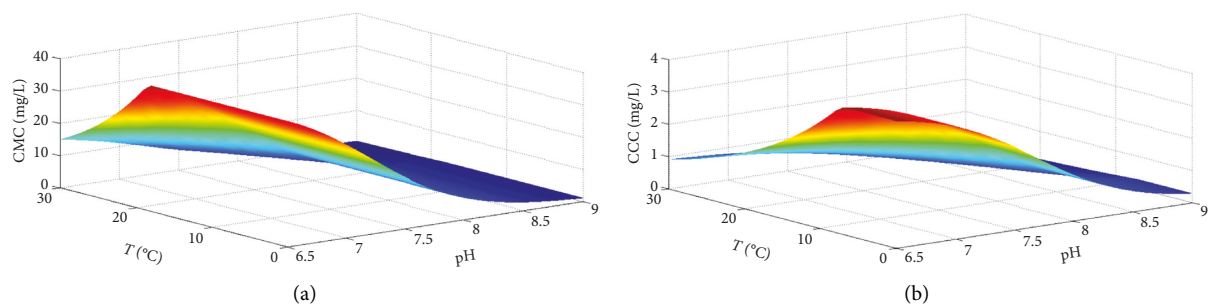


FIGURE 4: Chinese ammonia nitrogen water quality criteria vary with water temperature and pH. (a) CMC. (b) CCC.

TABLE 1: Sites with ammonia nitrogen ecological risk in summer and autumn of 2017.

Seasons	Basins	Sites	Seasonal average pH	Seasonal average temperature (°C)	Seasonal average ammonia concentration (mg/L)	Classification of water quality	WQC of ammonia (mg/L)	HQs
Summer (Jun.–Aug.)	HURB	Fuqiao brake, Luyi	8.60	29.2	0.16	II	0.14	1.14
	SWRs	Mirui, Linzhi	8.54	11.5	0.81	III	0.47	1.72
	Dianchi Lake	Luojiaying, Kunming	9.11	24.2	0.27	II	0.09	3.00
	Dianchi Lake	Dianchinan, Kunming	9.03	24.6	0.31	II	0.09	3.44
	Erhai Lake	Jinhe, Dali	8.64	24.6	0.26	II	0.17	1.53
Autumn (Sept.–Nov.)	SHRB	Songlin, Songyuan	8.57	11.8	0.73	III	0.44	1.66
	HURB	Aishanxi big bridge	8.58	19.2	0.29	II	0.27	1.07
	Dianchi Lake	Guanyinshan, Kunming	8.74	20.5	0.41	II	0.19	2.16
	Dianchi Lake	Luojiaying, Kunming	9.09	20.3	0.29	II	0.12	2.42
	Dianchi Lake	Dianchinan, Kunming	8.97	20.6	0.19	II	0.13	1.46

difference between the water quality criteria values of ammonia nitrogen can be up to dozens of times:

$$\text{CMC} = \left(\frac{0.0314}{1 + 10^{7.204 - \text{pH}}} + \frac{4.47}{1 + 10^{\text{pH} - 7.204}} \right) \times \text{MIN} \left(10.40, 6.018 \times 10^{0.036 \times (25 - T)} \right), \quad (5)$$

$$\text{CCC} = \left(\frac{0.0339}{1 + 10^{7.688 - \text{pH}}} + \frac{1.46}{1 + 10^{\text{pH} - 7.688}} \right) \times \text{MIN} \left(2.852, 0.914 \times 10^{0.028 \times (25 - \text{MAX}(T, 7))} \right). \quad (6)$$

3.4. Ecological Risk Assessment of AN. Using the derived Chinese ammonia nitrogen ALC equation (CCC), the ecological risk of ammonia nitrogen in 145 sites in Chinese surface water bodies was assessed. The results showed that the ecological risk of ammonia nitrogen was not significant at most sites, but for 20 sites with a seasonal mean pH of more than 8.5 (including 9 in summer and 11 in autumn), half (10) of the sites had excessive ammonia nitrogen concentrations, exceeding the CCC value to varying degrees. These sites includes 1 site of Songhua River, 2 sites of Huaihe River, 1 site of Southwest Rivers, 3 sites of Dianchi Lake, and 1 site of Erhai Lake (Table 1). In general, the ecological risk of ammonia nitrogen in Dianchi

Lake is the most prominent. It is worth noting that, according to the current Chinese surface water quality standards, among the above 10 risk sites, the water quality of 8 is classified as Class II and of 2 is classified as Class III. They are considered to be “good” in China aquatic environment management.

In summary, in the summer and autumn, when the water temperature and pH are high (such as temperature greater than 30°C, pH is greater than 8.5), the risk of ammonia nitrogen may occur at a site with “good” water quality (Class II or III). This poses a threat to aquatic organisms at these sites, especially highly sensitive freshwater shellfish. In recent years, investigations on benthos in Dianchi Lake have also found that benthos in Dianchi Lake is sparsely single and species diversity is significantly reduced. The dominant species of benthos in Dianchi Lake have evolved from a variety of shellfish (such as *Semisulcospira* and *Radix*) to pollution-tolerant species (*Chironomus* and *Limnodrilus*) [40]. The increase of ammonia nitrogen ecological risk may be one of the important reasons for the decline of shellfish community in Dianchi Lake.

4. Conclusions

As the exclusive chemical monitored by the Chinese government for water environment pollution control, ammonia nitrogen is evaluated with current Chinese WQS for surface

freshwater in aquatic environment management. The present study assessed the ecological risk of ammonia in 2017 in twenty basins in China with developed Chinese ALC of AN. The results indicated that, in summer and autumn, when the water temperature and pH are high, the risk of ammonia nitrogen may occur at some sites whose water quality is typically considered good. It suggested that neglecting the influence of water parameters on TAN toxicity may bring serious risk to aquatic organisms, especially for sensitive mollusk species.

Data Availability

The TAN exposure data can be derived from the weekly monitoring reports on surface water quality in China on the website <http://www.cnemc.cn/sssj/szdzjczb/>, and the other data used to support the finding of this study are included within the article.

Conflicts of Interest

The authors declare that there are no conflicts of interest regarding the publication of this paper.

Acknowledgments

This work was financially supported by the National Natural Science Foundation of China (grant nos. 31870100 and 91851111) and Major Science and Technology Program for Water Pollution Control and Treatment (2017ZX07301002).

Supplementary Materials

Table S1: the acute and chronic toxicity data of ammonia. Table S2: GMAVs and GMCVs of ammonia. Table S3: ACRs of ammonia. (*Supplementary Materials*)

References

- [1] R. C. Russo, "Ammonia, nitrite, and nitrate," in *Fundamentals of Aquatic Toxicology and Chemistry*, G. M. Rand and S. R. Petrocelli, Eds., pp. 455–471, Hemishpere Publishing Corporation, Washington, DC, USA, 1985.
- [2] MEEC, *Bulletin on the Situation of China's Ecological Environment in 2017*, Ministry of Ecology and Environment of China, Beijing, China, (in Chinese), 2018.
- [3] China State Council, *National Environmental Protection '12th Five-Year' Plan*, China State Council, Beijing, China, 2012.
- [4] M. Appl, *Ammonia: Principles and Industrial Practice*, Wiley-VCH Verlag, Weinheim, Germany, 1999.
- [5] Environment Canada, "Problem formulation for ammonia in the aquatic environment," in *Canadian Environmental Protection Act Priority Substances List 2. Version 5.0*, Environment Canada, Ottawa, Canada, 1997.
- [6] Environment Canada, "Canadian water quality guidelines for the protection of aquatic life: ammonia," in *Canadian Environmental Quality Guidelines, 1999*, Canadian Council of Ministers of the Environment, Winnipeg, Canada, 2010.
- [7] M. Geadah, "National inventory of natural and anthropogenic sources and emissions of ammonia," Environmental Protection Programs Directorate, Environmental Protection Service, Environment Canada, Gatineau, Canada Report EPS5/IC/1, 1985, 1980.
- [8] Z. Liu, X. Li, P. Tai, L. Sun, H. Yuan, and X. Yang, "Toxicity of ammonia, cadmium, and nitrobenzene to four local fishes in the Liao River, China and the derivation of site-specific water quality criteria," *Ecotoxicology and Environmental Safety*, vol. 147, pp. 656–663, 2018.
- [9] X. Xing, M. Li, L. Yuan et al., "The protective effects of taurine on acute ammonia toxicity in grass carp *Ctenopharyngodon idellus*," *Fish & Shellfish Immunology*, vol. 56, pp. 517–522, 2016.
- [10] S. Luo, B. Wu, X. Xiong, and J. Wang, "Short-term toxicity of ammonia, nitrite, and nitrate to early life stages of the rare minnow (*Gobiocypris rarus*)," *Environmental Toxicology and Chemistry*, vol. 35, no. 6, pp. 1422–1427, 2016.
- [11] J. S. Alabaster and R. Lloyd, "Ammonia," in *Water Quality Criteria for Fish*, J. S. Alabaster and R. Lloyd, Eds., pp. 85–102, Butterworths, London, UK, 1980.
- [12] USEPA, *Ambient Water Quality Criteria for Ammonia-1984*, National Technical Information Service, Springfield, VA, USA, EPA-440/5-85-001, 1985.
- [13] K. Emerson, R. C. Russo, R. E. Lund, and R. V. Thurston, "Aqueous ammonia equilibrium calculations: effect of pH and temperature," *Journal of the Fisheries Research Board of Canada*, vol. 32, no. 12, pp. 2379–2383, 1975.
- [14] R. J. Erickson, "An evaluation of mathematical models for the effects of pH and temperature on ammonia toxicity to aquatic organisms," *Water Research*, vol. 19, no. 8, pp. 1047–1058, 1985.
- [15] USEPA, *Aquatic Life Ambient Water Quality Criteria for Ammonia-Freshwater 2013*, Office of Water, Office of Science and Technology, Washington, DC, USA, EPA-822-R-13-001, 2013.
- [16] T. Lang, G. Peters, R. Hoffmann, and E. Meyer, "Experimental investigations on the toxicity of ammonia: effects on ventilation frequency, growth, epidermal mucous cells, and gill structure of rainbow trout *Salmo gairdneri*," *Diseases of Aquatic Organisms*, vol. 3, pp. 159–165, 1987.
- [17] J. A. Camargo and Á. Alonso, "Ecological and toxicological effects of inorganic nitrogen pollution in aquatic ecosystems: a global assessment," *Environment International*, vol. 32, no. 6, pp. 831–849, 2006.
- [18] A. Arillo, C. Margiocco, F. Melodia, P. Mensi, and G. Schenone, "Ammonia toxicity mechanism in fish: studies on rainbow trout (*Salmo gairdneri* Rich.)," *Ecotoxicology and Environmental Safety*, vol. 5, no. 3, pp. 316–328, 1981.
- [19] USEPA, *Quality Criteria for Water*, National Technical Information Service, Springfield, VA, USA, PB-263 943, 1976.
- [20] T. Zhang, Z. Yan, X. Zheng et al., "Transcriptome analysis of response mechanism to ammonia stress in Asian clam (*Corbicula fluminea*)," *Aquatic Toxicology*, vol. 214, Article ID 105235, 2019.
- [21] N. Wang, C. G. Ingersoll, I. E. Greer et al., "Contaminant sensitivity of freshwater mussels: chronic toxicity of copper and ammonia to juvenile freshwater mussels (Unionidae)," *Environmental Toxicology and Chemistry*, vol. 26, no. 10, pp. 2048–2056, 2007.
- [22] N. Wang, C. G. Ingersoll, D. K. Hardesty et al., "Contaminant sensitivity of freshwater mussels: acute toxicity for copper, ammonia and chlorine to glochidia and juveniles of freshwater mussels (Unionidae)," *Environmental Toxicology and Chemistry*, vol. 26, no. 10, pp. 2036–2047, 2007.
- [23] N. Wang, R. J. Erickson, C. G. Ingersoll et al., "Influence of pH on the acute toxicity of ammonia to juvenile freshwater

- mussels (fatmucket, *Lampsilis siliquoidea*),” *Environmental Toxicology and Chemistry*, vol. 27, no. 5, pp. 1141–1146, 2008.
- [24] USEPA, “Update of ambient water quality criteria for ammonia,” Office of Science and Technology, Washington, DC, USA, EPA-822-R-99-014, 1999.
- [25] ANZECC and ARMCANZ, *Australian and New Zealand Guidelines for Fresh and Marine Water Quality*, Australian and New Zealand Environment and Conservation Council and Agriculture and Resource Management Council of Australia and New Zealand, Canberra, Australia, 2000.
- [26] MEEC, *Environmental Quality Standards for Surface Water (GB3838-2002)*, Ministry of Ecology and Environment of China, Beijing, China, (in Chinese), 2002.
- [27] CNEMC, *Weekly Monitoring Reports on Surface Water Quality in China*, China National Environmental Monitoring Centre, Beijing, China, 2019, <http://www.cnemc.cn/sss/szdzjczb/>.
- [28] USEPA, *ECOTOX Database*, United States Environmental Protection Agency, Washington, DC, USA, 2019, <https://cfpub.epa.gov/ecotox/>.
- [29] USEPA, *Guidelines for Deriving Numerical National Water Quality Criteria for the Protection of Aquatic Organisms and their Uses*, Office of Research and Development, Washington DC, USA, PB85-227049, 1985.
- [30] L. Posthuma, G. W. Suter II, and T. P. Traas, *Species Sensitivity Distributions in Ecotoxicology*, CRC Press, Boca Raton, FL, USA, 2001.
- [31] Z. G. Yan, W. Mei, Z. T. Liu et al., “Development of freshwater aquatic life criteria for ammonia in China,” *Environmental Science*, vol. 32, no. 6, pp. 1564–1570, 2011, (in Chinese).
- [32] M. Constable, M. Charlton, F. Jensen, K. McDonald, G. Craig, and K. W. Taylor, “An ecological risk assessment of ammonia in the aquatic environment,” *Human and Ecological Risk Assessment: An International Journal*, vol. 9, no. 2, pp. 527–548, 2003.
- [33] Y. Li, E. G. Xu, W. Liu et al., “Spatial and temporal ecological risk assessment of unionized ammonia nitrogen in Tai Lake, China (2004-2015),” *Ecotoxicology and Environmental Safety*, vol. 140, pp. 249–255, 2017.
- [34] L. Zhang, E. G. Xu, Y. Li, H. Liu, D. E. Vidal-Dorsch, and J. P. Giesy, “Ecological risks posed by ammonia nitrogen (AN) and un-ionized ammonia (NH₃) in seven major river systems of China,” *Chemosphere*, vol. 202, pp. 136–144, 2018.
- [35] J. He, H. He, Z. Yan et al., “Comparative analysis of freshwater species sensitivity distributions and ecotoxicity for priority pesticides: implications for water quality criteria,” *Ecotoxicology and Environmental Safety*, vol. 176, pp. 119–124, 2019.
- [36] X. Jin, J. Zha, Y. Xu, Z. Wang, and S. S. Kumaran, “Derivation of aquatic predicted no-effect concentration (PNEC) for 2,4-dichlorophenol: comparing native species data with non-native species data,” *Chemosphere*, vol. 84, no. 10, pp. 1506–1511, 2011.
- [37] Z. Yan, J. Pan, F. Gao et al., “Seawater quality criteria derivation and ecological risk assessment for oil pollution in China,” *Marine Pollution Bulletin*, vol. 142, pp. 25–30, 2019.
- [38] X. Zheng, Z. Yan, P. Liu et al., “Derivation of aquatic life criteria for four phthalate esters and their ecological risk assessment in Liao River,” *Chemosphere*, vol. 220, pp. 802–810, 2019.
- [39] C. Lu, S. Yang, Z. Yan et al., “Deriving aquatic life criteria for PBDEs in China and comparison of species sensitivity distribution with TBBPA and HBCD,” *Science of the Total Environment*, vol. 640-641, pp. 1279–1285, 2018.
- [40] Y. P. Li, “Changes of zoobenthos communities in Dianchi Lake,” *Environmental Science Guide*, vol. 34, no. 6, pp. 1–3, 2015, (in Chinese).

Research Article

Modeling of Flocculation and Sedimentation Using Population Balance Equation

Zhipeng Shi ^{1,2,3}, Genguang Zhang ^{1,3}, Yuzhuo Zhang,¹ Tingting He,² and Guoliang Pei⁴

¹Key Laboratory of Agricultural Soil and Water Engineering in Arid and Semiarid Areas, Ministry of Education, Northwest A&F University, Yangling, Xianyang, Shaanxi Province 712100, China

²Jiangsu Vocational Institute of Architectural Technology, Xuzhou, Jiangsu Province 221116, China

³College of Water Resources and Architectural Engineering, Northwest A&F University, Yangling, Xianyang, Shaanxi Province 712100, China

⁴State Key Laboratory of Crop Stress Biology for Arid Areas, Northwest A&F University, Yangling, Xianyang, Shaanxi Province 712100, China

Correspondence should be addressed to Genguang Zhang; zgg64@163.com

Received 1 June 2019; Revised 19 July 2019; Accepted 12 September 2019; Published 26 September 2019

Guest Editor: Chenglian Feng

Copyright © 2019 Zhipeng Shi et al. This is an open access article distributed under the Creative Commons Attribution License, which permits unrestricted use, distribution, and reproduction in any medium, provided the original work is properly cited.

Flocculation is a special phenomenon for fine sediment or silt in reservoirs and estuaries. Flocculation usually results in changes of size, morphology, and settling velocity of sediment particles and finally changes of bed topography of reservoirs and estuaries. The process of flocculation and sedimentation was simulated based on population balance modeling (PBM) and computational fluid dynamics (CFD); the changes of particle or floc size and their settling velocities over time were examined. The results showed that flocculation is a dynamic and nonlinear process containing aggregation, breakage, reaggregation, and rebreakage between particles, microflocs, and macroflocs. Furthermore, the visual process of flocculation and sedimentation was directly created by the simulation results and is in good agreement with the results of the previous experiments.

1. Introduction

Flocculation (floc) of fine sediments is a research focus in the theory of sediment movement mechanics. Many phenomena of the settling velocity of sediment, such as sediment topography of the estuary (sediment barrier), the formation of non-Newtonian fluid, huge sediment-carrying capacity, and pulp rivers, are related to the flocculation of fine sediment [1, 2]. Flocculation has often been observed in marine and estuarine environments as well [3]. Experimental studies on the characteristics of floc and their influencing factors were conducted by many researchers, and a series of results were achieved [4–6]. In this study, we mainly investigate the mathematical modeling of flocculation and sedimentation in three dimensions.

The mathematical model of flocculation came into focus, when Witten and Sander [7] first established the diffusion-limited aggregation (DLA) model. The growth process of floc

was simulated using the DLA model in a 2D space, and three methods for calculating the fractal dimension of floc were compared by Jin et al. [8]. Qin et al. [9] developed a 3D model for the growth of floc using the DLA model as a base. The fractal dimensions of 3D DLA aggregates are higher than those of 2D DLA aggregates, according to Liu et al. [10]. However, the DLA model assumes that there is a stationary particle within the central, which is far from the actual situation. Then, Meakin [11] improved the model and proposed a diffusion-limited cluster-cluster aggregation (DLCCA) model. Gimel et al. [12] studied the process of sol-gel transition with the DLCCA by Monte Carlo simulation. Zhang and Zhang [13] found the drag forces on flocs formed by DLCCA are larger than those formed by DLA. However, there still are two assumptions of the above model that need to be improved. First, the particle is limited to a uniform sphere; second, the process of breakage is always neglected resulting in large deviations with reality. The population

balance model (PBM) [14–17], consisting of aggregation and breakage mechanisms, successfully solved the assumptions mentioned above [18, 19]. Due to the theory of collision frequency and collision efficiency, the process of aggregation and breakage can be better reflected in the PBM [20].

The aim of this study is to apply the PBM to the flocculation and sedimentation process in three dimensions. PBM was incorporated into the computational fluid dynamics (CFD) model by implementing the multiple size group model. The CFD-PBM combination is an effective method to solve the processes of flocculation and multiphase flow simultaneously [21]. In this study, the process of flocculation and sedimentation and characteristics of flocs across different time periods with validation are presented using experimental data from the literature.

2. Model Description and Methods

2.1. CFD Implementation. The process of flocculation and sedimentation is the process of a typical solid-liquid two-

phase flow interaction. Therefore, the Euler-Euler model was employed within the flocculating system [22].

2.1.1. Continuity Equation.

$$\frac{\partial}{\partial t}(\alpha_q \rho_q) + \nabla \cdot (\alpha_q \rho_q \vec{v}_q) = \sum_{p=1}^n (\dot{m}_{pq} - \dot{m}_{qp}) + S_q, \quad (1)$$

where ∇ is the Hamiltonian; S_q is the source item; α_q and ρ_q are the volume fraction and density of phase q , respectively; p and q represent different phases; \vec{v}_q is the velocity of phase q ; and \dot{m}_{pq} and \dot{m}_{qp} characterize the mass transfer within the different phases. The source term S_q on the right-hand side of equation (1) is zero by default.

2.1.2. Momentum Equation. The momentum balance for phase q yields:

$$\begin{aligned} \frac{\partial}{\partial t}(\alpha_q \rho_q \vec{v}_q) + \nabla \cdot (\alpha_q \rho_q \vec{v}_q \vec{v}_q) = & -\alpha_q \nabla \cdot P + \nabla \cdot \bar{\tau}_q + \alpha_q \rho_q \vec{g} \\ & + \sum_{p=1}^n (\vec{R}_{pq} + \dot{m}_{pq} \vec{v}_{pq} - \dot{m}_{qp} \vec{v}_{qp}) + (\vec{F}_q + \vec{F}_{\text{lift},q} + \vec{F}_{\text{wl},q} + \vec{F}_{\text{vm},q} + \vec{F}_{\text{td},q}), \end{aligned} \quad (2)$$

where $\bar{\tau}_q$ is the q^{th} phase stress-strain tensor and \vec{g} is the gravity acceleration.

$$\bar{\tau}_q = \alpha_q \mu_q \left(\nabla \vec{v}_q + \nabla \vec{v}_q^T \right) + \alpha_q \left(\lambda_q - \frac{2}{3} \mu_q \right) \nabla \cdot \vec{v}_q \bar{I}, \quad (3)$$

where μ_q and λ_q are the shear and bulk viscosity of phase q , \vec{F}_q is an external body force, $\vec{F}_{\text{lift},q}$ is a lift force, $\vec{F}_{\text{wl},q}$ is a wall lubrication force, $\vec{F}_{\text{vm},q}$ is a virtual mass force, and $\vec{F}_{\text{td},q}$

is a turbulent dispersion force (in the case of turbulent flows only). \vec{R}_{pq} is an interaction force between phases, and p is the pressure shared by all phases. Finally, \vec{v}_{pq} is the interphase velocity.

2.1.3. Turbulence Modeling. A standard $k - \varepsilon$ turbulence model was employed because it reduces the computational effort and increases the reasonable accuracy of the model [23, 24].

$$\begin{aligned} \frac{\partial}{\partial t}(\rho k) + \frac{\partial}{\partial x_i}(\rho k u_i) = \frac{\partial}{\partial x_j} \left[\left(\mu + \frac{\mu_t}{\sigma_k} \right) \frac{\partial k}{\partial x_j} \right] + G_k + G_b - \rho \varepsilon - Y_M + S_q, \\ \frac{\partial}{\partial t}(\rho \varepsilon) + \frac{\partial}{\partial x_i}(\rho \varepsilon u_i) = \frac{\partial}{\partial x_j} \left[\left(\mu + \frac{\mu_t}{\sigma_\varepsilon} \right) \frac{\partial \varepsilon}{\partial x_j} \right] + C_{1\varepsilon} \frac{\varepsilon}{k} (G_k + C_{3\varepsilon} G_b) - C_{2\varepsilon} \rho \frac{\varepsilon^2}{k} + S_q. \end{aligned} \quad (4)$$

In these equations, k is the turbulence kinetic energy; ε is the turbulent energy dissipation rate; and G_k represents the generation of turbulence kinetic energy due to the mean velocity gradients. G_b is the generation of turbulence kinetic energy due to buoyancy. Y_M represents the contribution of the fluctuating dilatation in compressible turbulence to the overall dissipation rate. $C_{1\varepsilon}$, $C_{2\varepsilon}$, and $C_{3\varepsilon}$ are constants. σ_k

and σ_ε are the turbulent Prandtl numbers for k and ε , respectively. S_q is the user-defined source term.

2.2. Population Balance Model. Assuming that ϕ is the particle volume, the transport equation for the number density function is given as

$$\begin{aligned}
& \frac{\partial}{\partial t} [n(V, t)] + \nabla \cdot [\vec{u}n(V, t)] + \underbrace{\nabla_v \cdot [G_v n(V, t)]}_{\text{grown term}} \\
& = \underbrace{\frac{1}{2} \int_0^V \alpha(V - V', V') n(V - V', t) n(V', t) dV'}_{\text{birth due to aggregation}} - \underbrace{\int_0^\infty \alpha(V, V') n(V, t) n(V', t) dV'}_{\text{death due to aggregation}} + \underbrace{\int_{\Omega_v} pg(V') \beta(V | V') n(V', t) dV'}_{\text{birth due to breakage}} \\
& \quad - \underbrace{g(V) n(V, t)}_{\text{death due to breakage}}, \tag{5}
\end{aligned}$$

where $n(V, t)$ is the number density of particles of volume V at time t ; ∇ is the Hamiltonian; \vec{u} is the particle velocity; G is the linear growth rate; and $G = \partial L / \partial t$; B_{ag} , D_{ag} , B_{br} , D_{br} represent the birth and death rates due to aggregation and breakage respectively [25, 26]. They are given as [27]

$$\begin{aligned}
B_{\text{ag}} &= \frac{1}{2} \int_0^V \alpha(V - V', V') n(V - V') n(V') dV', \\
D_{\text{ag}} &= \int_0^\infty \alpha(V, V') n(V) n(V') dV', \\
B_{\text{br}} &= \int_{\Omega_v} Ng(V') \beta(V | V') n(V') dV', \\
D_{\text{br}} &= g(V) n(V), \tag{6}
\end{aligned}$$

where particles of volume $V - V'$ aggregate with particles of volume V' to form particles of volume V . The factor 1/2 is included to avoid accounting for each collision event twice. $g(V') n(V') dV'$ particles of volume V' break per unit time, producing $pg(V') n(V') dV'$ particles, of which a fraction $\beta(V | V') dV$ represent particles of volume V . N is the number of child particles produced per parent particle.

The Luo and Ghadiri models were adopted to study the aggregation and breakage processes between particles, respectively [28].

2.3. Experimental. Flocculation and sedimentation experiments were performed on particles diluted to 5 g/L and 15 g/L solid in deionized water in a 1000 ml graduated cylinder. Particles, with a mean diameter of 39.63 μm , were used as the model suspension. They were obtained from Luohe aqueduct in the Yellow River. Deionized (DI) water with a pH of 7.1 was employed for all experimental work. All experiments were carried out in two steps. First, particles were dispersed by vigorous stirring at 200 rpm for 3 minutes to prepare the suspensions, followed by 5 minutes of slow stirring. The settling velocity of floc was recorded during the process. The settling velocity was calculated using the distance traveled by a floc and the travel time measured by a digital-display stopwatch. Second, the floc suspension was transferred to glass slides with a pipet (8 mm inner diameter mouth) and then freeze-dried. Finally, images of the flocs were captured by a microscope imaging system and analyzed by the Image pro Plus 6.0 software; this is how the size of the floc was measured. The

detailed results for the flocculation and sedimentation experiments are presented previously [29].

2.4. Numerical Details. The Ansys Fluent 15.0 software was used to solve the equations of mass, momentum, and population balance equations. Considering that the previous experiment of flocculation and sedimentation were carried out in a 1000 ml graduated cylinder, the three-dimensional geometry of this cylinder was built with a 0.068 m diameter and 0.44 m height. The details of the experimental data can be found in the cited references [29]. Meshing was implemented using a structural mesh of 0.04 mm grid sizes. The total number of nodes is 1,642,170. Figure 1 shows the geometry with the mesh.

Water was chosen as the growth medium liquid phase. Considering the range of the initial particle diameter, the solid dispersed phase was divided into 6 groups (Table 1). Each group was considered as having an individual percentage. The floc was formed by collision within particles, along with the interaction of the velocity and flow fields. A coupled solver was used to solve the momentum and pressure items. A second-order backward scheme was adopted for temporal discretization. The convergence criteria were set to 0.0001 for all variables. Based on the previous experiment, the boundary conditions of the inlet were defined as the velocity inlet, and other parts were defined as the wall. All procedures explained were conducted by using the Ansys Fluent 15.0 software package [24].

3. Results and Discussion

3.1. Flocculation and Sedimentation. The critical size of flocculation between particles is 0.01~0.03 mm for different water quality and particle properties [30]. The specific value should be determined by the local environment conditions. For example, in estuary coastal areas, when fine sediment particles occupy a large proportion, even if the particle size is greater than 0.03 mm, we should consider the influence of flocculation. Two conditions must be met for flocculation: first, there must be a certain collision frequency during the process; second, the collision efficiency is also very important. Brownian motion, applied shear and differential sedimentation are three mechanisms for the collisions. The process of flocculation and sedimentation between particles or flocs is shown in Figure 2.

The phenomenon of aggregation and breakage can be clearly observed during the process of flocculation and sedimentation, as shown in Figure 2. For example, the aggregation of particles is more clearly reflected in the images

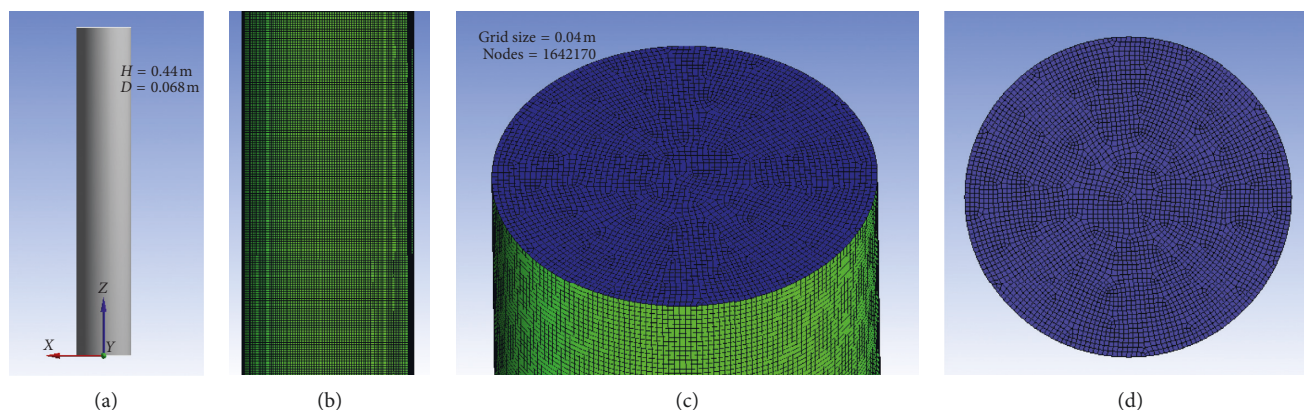


FIGURE 1: Three-dimensional geometry and grid measurements with meshing. (a) geometry; (b) $\times 20$ times; (c) $\times 40$ times; (d) $\times 30$ times.

TABLE 1: Particle size groups.

No.	Bin 0	Bin 1	Bin 2	Bin 3	Bin 4	Bin 5
Size ($\times 10^{-3}$ m) (d_{50})	0.031	0.032	0.038	0.026	0.007	0.021
Volume concentration (%)	10	20	20	20	20	10

of $T = 5$ s and $T = 10$ s. The particle size and number of flocs increase significantly. Breakage of macroflocs is also more clearly reflected from the image of $T = 30$ s. This is the result of effective collisions between the particles. There are three different states during the flocculation and sedimentation process: particles, microflocs, and macroflocs. According to Manning and Dyer [31], 0.16 mm is the critical size of microflocs and macroflocs. Although they have three different states, they are not fixed. The process of flocculation and sedimentation is a dynamic and nonlinear process of aggregation, breakage, reaggregation and rebreakage.

It can also be seen from Figure 2 that aggregation takes place as a result of particle-particle, particle-microflocs, or microflocs-microflocs collisions, leading to the formation of macroflocs. Additionally, the flocs are all highly irregular in shape and structure. Lee et al. [32] believe that there are four typical processes of flocculation in two-class PBM: (1) aggregation between microflocs, (2) aggregation between microflocs and macroflocs, (3) aggregation between macroflocs, and (4) breakage of macroflocs. Gregory and Zabel [33] also conceived the morphology of flocs during sedimentation, and compared to their regimes, the calculation results of flocculation and sedimentation in Figure 2 are indeed correct.

3.2. Particle or Floc Size. The time series of the particle or floc size during flocculation and sedimentation is predicted with CFD-PBM, as shown in Figure 3. It can be observed from Figure 3 that the size profiles of the particles or flocs initially decrease and then increase, especially for the first three Bins (Bin 0~Bin 2). The reason is that there were a large number of particles with a high collision frequency in the first 10 s resulting in a large shearing effect. However, as the collision frequency increased, the collision efficiency also gradually increased. Then after 10 s, the floc size began to increase. Around 15 s, the curves show a maximum point. Microflocs

gradually appeared. The stage of 15~24 s is a relatively stable stage. Relative to the initial phase, the size increased significantly. However, after 24 s, the curve increased dramatically, indicating that macroflocs gradually appeared. The volume of macroflocs is larger than that of a sphere because macroflocs usually have an irregular and porous structure [34]. Combined with Figure 2, the process of flocculation and sedimentation can be summarized into three stages: first, 0~15 s, which is primarily the interaction between particles; second, 15~24 s, which is primarily the interaction between microflocs; third, 24~30 s, which is primarily the interaction between macroflocs. The photos and size of the flocs as shown in Figure 4 were obtained based on the previous experiments, which were measured using a research grade microscope imaging system (U-HGLGPS, OLYMPUS company, Japan) and Image Pro Plus 6.0 software. Particles, microflocs, and macroflocs are three different states with a huge difference in size. The average and maximum size of flocs in the experiments were $174.84\ \mu\text{m}$ and $364.49\ \mu\text{m}$, respectively, which may correspond to the size of microflocs and macroflocs. Additionally, the size of flocs in the model described quite well with the variation of the experimental flocs size. It is confirmed that the proposed model offers a good approximation for the flocculation and sedimentation.

The collision frequency between particles can result from Brownian motions, shear flow, or differential settling [35]. In this study, the shear flow and differential settling are the main causes of particle or floc collision. Vajihinejad and Soares [34] observed the same trend as in Figure 3. They believed that there is a dispersal time for particles or polymer within the suspension before flocculation occurs. After that time, they grow quickly to a maximum value, and then reach an equilibrium stage [36]. Heath et al. [37] believed that the size decrease was caused by polymer degradation. From the results of this study, we believe that this phenomenon can be explained by shear effect and differential settling. Shear effect focuses on the early stage, while differential settling influences the later stage. In addition, an increase of the curve results from the aggregation of particles or flocs, while the fluctuation of the curve is a symbol of equilibrium. During the equilibrium stage (fluctuation stage between 25 s~30 s),

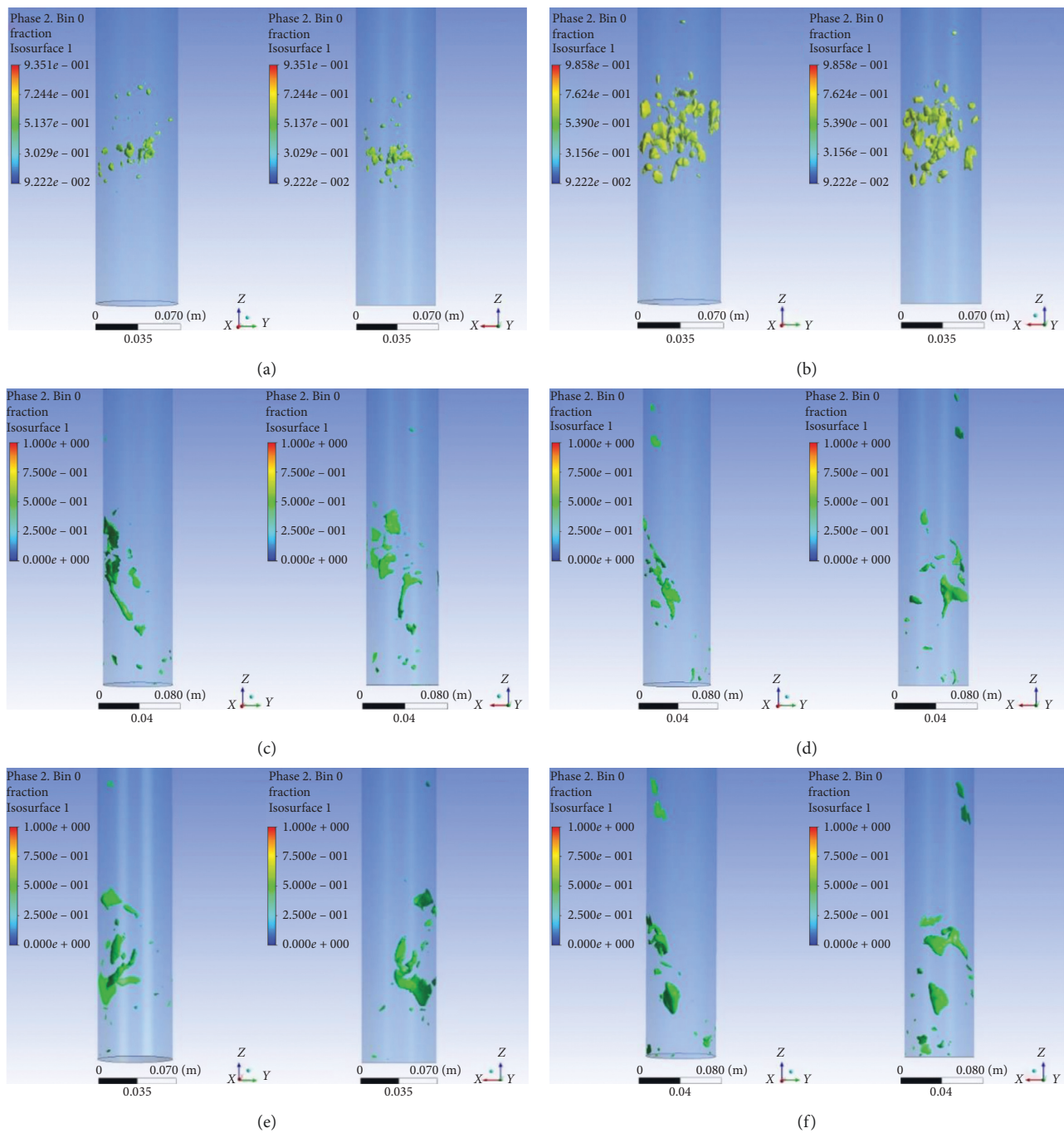
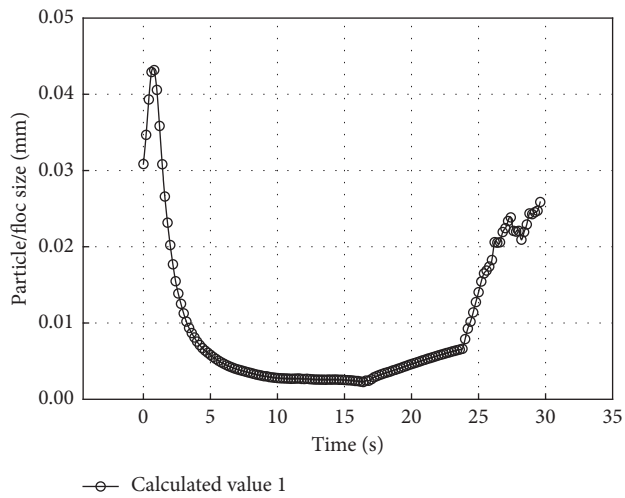


FIGURE 2: The process of flocculation and sedimentation between particles or flocs. Note that (a) and (b) represent the process of flocculation and sedimentation between particles at 5 s and 10 s, respectively. Images (c) and (d) represent the process of flocculation and sedimentation between microflocs at 15 s and 20 s, respectively. Finally, (e) and (f) represent the process of flocculation and sedimentation between macroflocs at 25 s and 30 s, respectively. (a) Time = 5 s (particles). (b) Time = 10 s (particles). (c) Time = 15 s (microflocs). (d) Time = 20 s (microflocs). (e) Time = 25 s (macroflocs). (f) Time = 30 s (macroflocs).

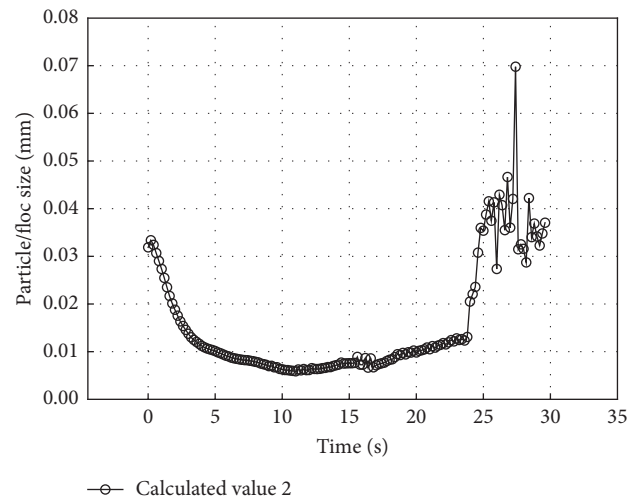
although both aggregation and breakage occurred, their effects were neutralized within one another.

3.3. Particle or Floc Settling Velocity. The settling velocity is a key parameter in modeling the settlement process in sedimentation analysis and sediment transport. For noncohesive

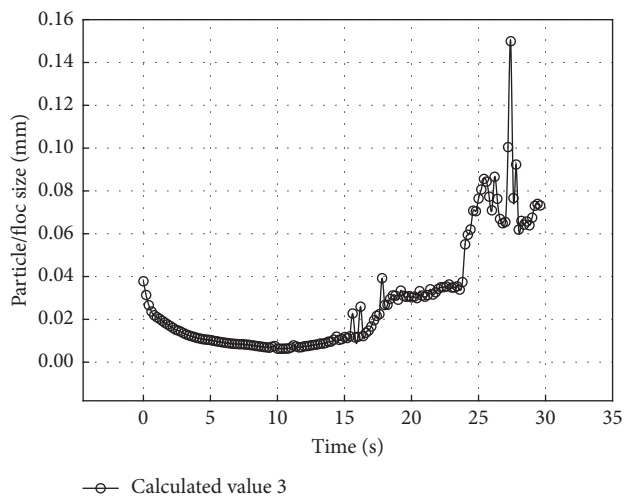
particles, the settling velocity is dependent on the individual particle size, gravity, and particle shape, which substantially differs from the settling velocity of floc. For example, due to the process of flocculation, muds are often changed to flocs during suspension in estuary coastal areas [38]. For such flocs, the size, shape, and settling velocity all become a dynamic process. Therefore, it is necessary to know the



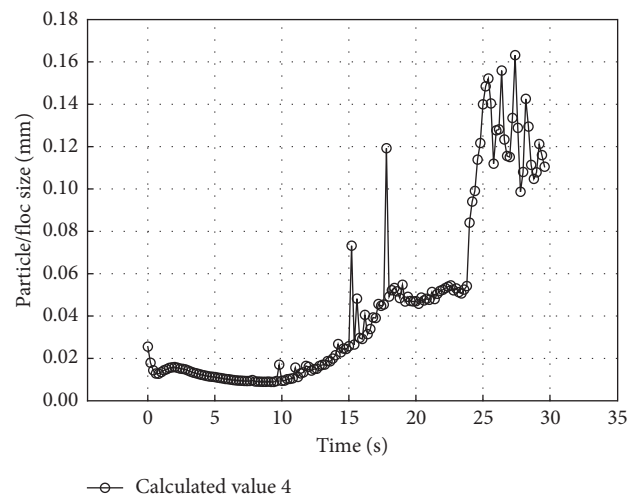
(a)



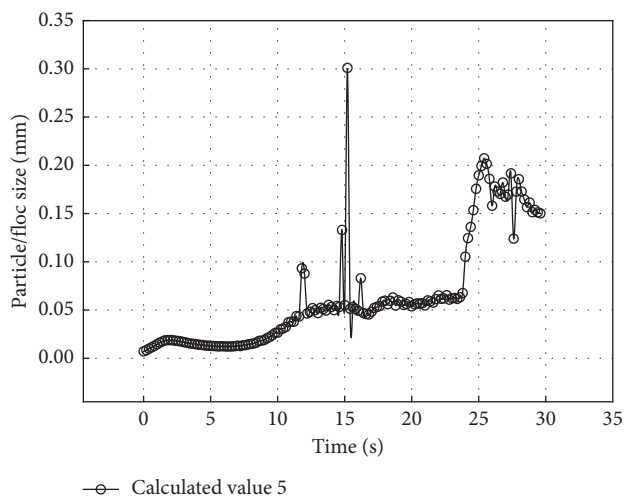
(b)



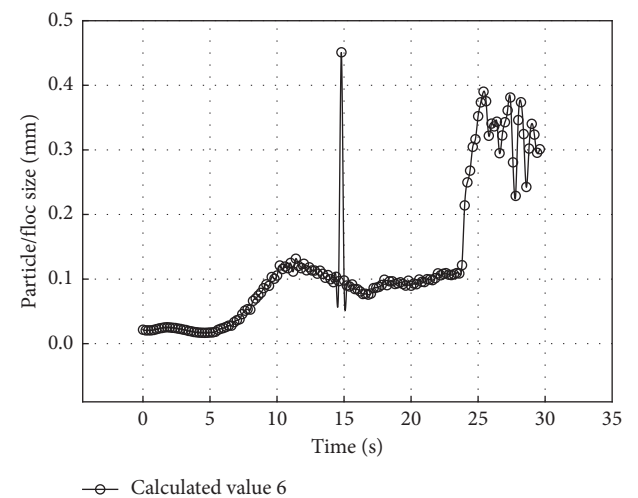
(c)



(d)



(e)



(f)

FIGURE 3: Time series of the particle or floc size of each bin: (a) Bin 0. (b) Bin 1. (c) Bin 2. (d) Bin 3. (e) Bin 4. (f) Bin 5.

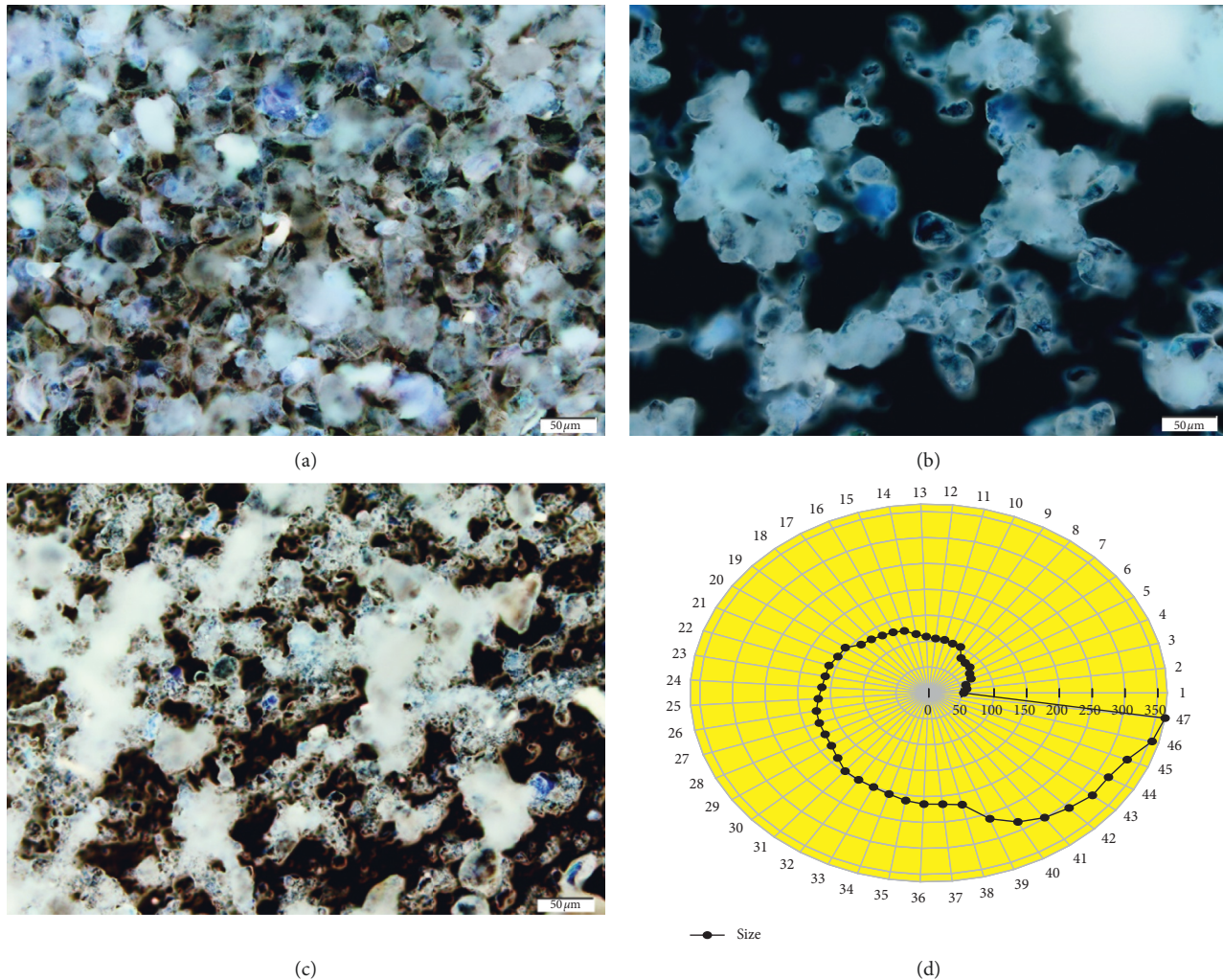


FIGURE 4: Three states and sizes of flocs during flocculation and sedimentation in experiments: (a) Particles. (b) Microflocs. (c) Macroflocs. (d) Size in experiments (μm).

dynamic treatment of the settling velocity in order to more accurately evaluate and predict the sediment transport processes. However, most of the research on this topic is mainly concerned with the relationship between the floc settling velocity and its size, while there remain only a few studies on the time series of the floc settling velocity. We examined the differences in settling velocity functionality with time and the differences of settling velocities in different directions, as shown in Figure 5. Note that $N = 33$ in Figure 5 means the total number of settling velocities obtained from the experiments is 33.

It should be noted that from Figure 5, the curve of the settling velocity decreased in 0~15 s and then increased in 15~30 s regardless of the direction. The main reason for this phenomenon is that the collision frequency was higher at the beginning, resulting in a large shear effect. Due to the shearing effect, the floc began to experience breakage, resulting in decreasing size. Another reason is that there is a resistance effect from the particles on the lower position to the particles on the upper position. Li et al. [39] believe that a rigid network was formed by aggregated particles, resulting

in a sharp decrease of the settling velocity. As mentioned above, after 15 s, the collision efficiency increased. The effect of aggregation was more powerful than the effect of breakage, resulting in an increase of the settling velocity. It can also be observed from Figure 4 that the settling velocity of u is significantly greater than the settling velocities of either v or w . The effect of the boundary of the settlement area is negligible. Experimental studies were also conducted on the flocculation of cohesive sand suspensions [29]. The settling velocities of the flocs in those experiments were $0.003\sim 0.011\text{ m}\cdot\text{s}^{-1}$ for particles whose concentration is 5 g/L and $0.005\sim 0.015\text{ m}\cdot\text{s}^{-1}$ for particles whose concentration is 15 g/L, while the calculated settling velocity used in this study is $0.0038\sim 0.012\text{ m}\cdot\text{s}^{-1}$ in 15 s~30 s (Figure 5). The calculated data is much closer to the experimental results.

For the variation of the curve in 0~15 s, some authors [40, 41] believe that an uneven distribution of the shear rate is the main reason for the decrease of floc size. Selomulya et al. [20] suggest that size reduction is caused by the irregular and porous structure of flocs, making their structures more compact. The settling velocity is a function of size and

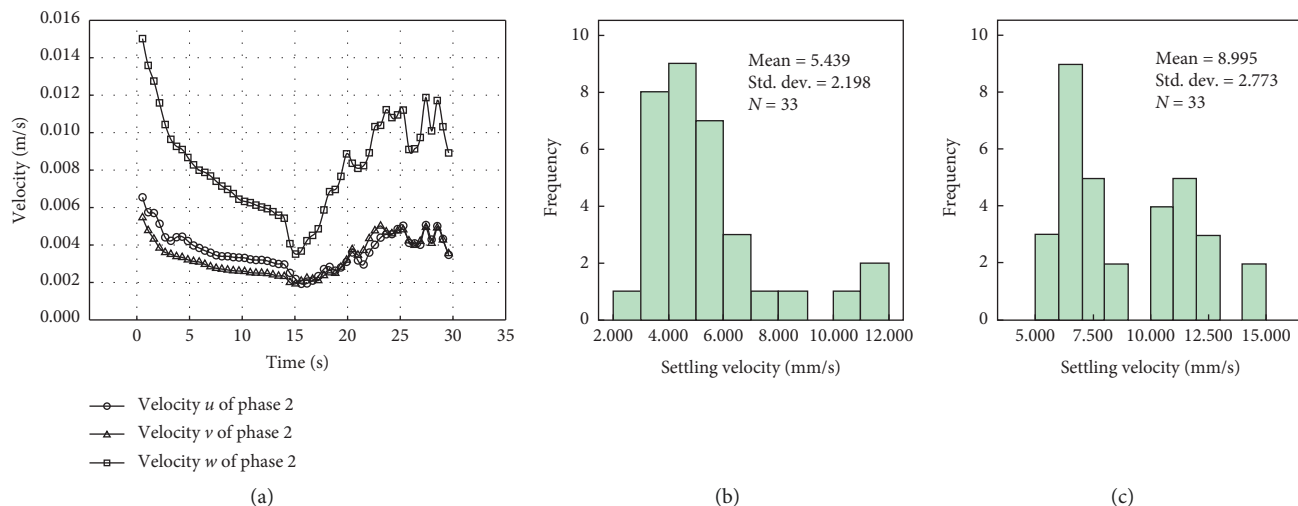


FIGURE 5: Settling velocities of particle or floc in model and experiments. (a) Time series of the settling velocities, phase 2 represents particles or flocs. u is the direction of settlement; v and w are the radial directions perpendicular to u . (b) Statistics of the settling velocities in experiments when the particle concentration in suspension is 5 g/L. (c) Statistics of the settling velocities in experiments when the particle concentration in suspension is 15 g/L. (a) Model. (b) Experiments (particle concentration = 5 g/L). (c) Experiments (particle concentration = 15 g/L).

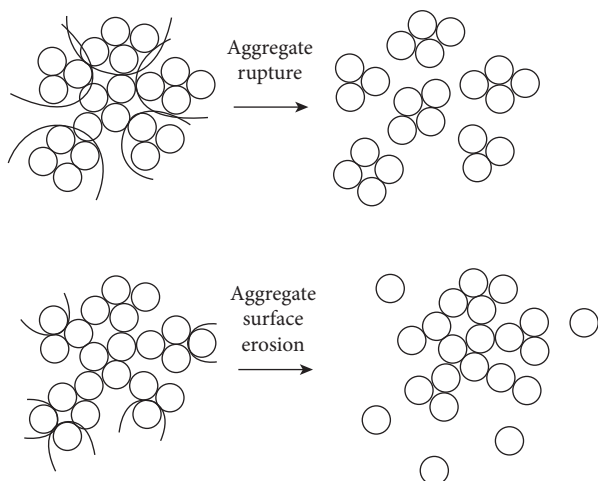


FIGURE 6: Mechanisms of different breakage modes of flocs. In the case of an aggregate rupture, both size and the perimeter change significantly. In the case of aggregate surface erosion, only the perimeter changes, and size remains almost constant.

density, and they have the same change law. We believe that aggregate rupture was the main reason for the curve decreasing in 0~15 s, while aggregate surface erosion was the main reason for the curve fluctuation in 25~30 s, as shown in Figure 6. In the early phase, due to the aggregate rupture, the number of flocs increased, but the size decreased. On the contrary, in the later phase due to the aggregate surface erosion, the size of floc increased significantly [42]. The results presented in this paper confirm both hypotheses.

4. Conclusions

PBM was proven to be a more advanced model that is capable of approximating flocculation and sedimentation of

particles better than previous versions. In contrast to the DLA or DLCCA model, the PBM can simultaneously simulate both the aggregation and breakage processes between microflocs and macroflocs with irregular shape. The presented results lead to the following conclusions:

- (1) Particles, microflocs, and macroflocs are the three important states during the process of flocculation and sedimentation. This process is a dynamic and nonlinear process of aggregation, breakage, re-aggregation, and rebreakage.
- (2) There are three stages in the process of flocculation and sedimentation corresponding to the three above states. Shear effect focuses on the decrease of floc size, while differential settling influences the increase of floc size. Eventually, the equilibrium phase appears in which the breakage rate is equal to the aggregation rate.
- (3) The process of flocculation and sedimentation can be reasonably described by aggregate rupture and aggregate surface erosion. They are two different mechanisms important for the settling velocity decreasing in the early stage and fluctuating in the late stage.

Finally, CFD-PBM is an effective method to study the dynamics of flocs and their influence on flocculation and sedimentation, in order to not only gain a deeper understanding of flocculation dynamics, but also to improve the theory of sediment movement.

Nomenclature

∇ :	the Hamiltonian
S_q :	source item
α_q :	volume fraction of phase q

ρ_q :	density of phase q
\vec{v}_q :	velocity of phase q
\dot{m}_{pq} :	mass transfer within phase p to q
\dot{m}_{qp} :	mass transfer within phase q to p
$\bar{\tau}_q$:	q^{th} phase stress-strain tensor
\vec{F}_q :	external body force
$\vec{F}_{\text{lift},q}$:	lift force
$\vec{F}_{\text{wl},q}$:	wall lubrication force
$\vec{F}_{\text{vm},q}$:	virtual mass force
$\vec{F}_{\text{td},q}$:	turbulent dispersion force
\vec{R}_{pq} :	interaction force between phases
P :	pressure
\vec{v}_{pq} :	interphase velocity
\vec{g} :	gravity acceleration, $9.81 \text{ m}\cdot\text{s}^{-2}$.
k :	the turbulence kinetic energy
ε :	turbulent energy dissipation rate
G_k :	generation of turbulence kinetic energy due to the mean velocity gradients
G_b :	generation of turbulence kinetic energy due to buoyancy.
Y_M :	contribution of the fluctuating dilatation in compressible turbulence to the overall dissipation rate
$C_{1\varepsilon}, C_{2\varepsilon}, C_{3\varepsilon}$:	constants, 1.44, 1.92, 0.09.
σ_k :	turbulent Prandtl numbers for k , 1.0.
σ_ε :	turbulent Prandtl numbers for ε , 1.3.
$n(V, t)$:	number density of particles of volume V at time t
\vec{u} :	particle velocity
G :	the linear growth rate
B_{ag} :	birth rate of aggregation
D_{ag} :	death rate of aggregation
B_{br} :	birth rate of breakage
D_{br} :	death rate of breakage
V' :	particle volume
V :	floc volume
N :	number of particles

Data Availability

The model description and Figure 2 used to support the findings of this study were supplied by Northwest A&F University under license and so cannot be made freely available. Requests for access to these data should be made to Professor Zhang Gengguang with email zgg@64.com. The data of Figures 3–5 used to support the findings of this study may be released upon application to the Northwest A&F University, who can be contacted at zgg@64.com.

Conflicts of Interest

The authors declare no conflicts of interest.

Authors' Contributions

Z. P. S. and G. G. Z. performed conceptualization and methodology. Y. Z. Z., G. L. P., and Z. P. S performed

investigation and data collection. Z. P. S wrote the original draft. G. G. Z and T. T. H reviewed and edited the draft. G. G. Z supervised the study. G. G. Zhang and Z. P. Shi were responsible for funding acquisition.

Acknowledgments

The authors thanks Prof. Onyx W. H. Wai from the civil and environmental engineering department of the Hong Kong Polytechnic University for his kind advice which helped us prepare a better manuscript. This work was supported by the Jiangsu Overseas Visiting Scholar Program for University Prominent Young & Middle-aged Teachers and Presidents (2018), National Natural Science Foundation of China (grant no. 51879227), Qing Lan Project (2016), and Science and Technology Project of Department of Housing and Urban-Rural Development of Jiangsu province (grant no. 2016ZD80).

References

- [1] R. L. Xia, G. L. Yang, and L. S. Liu, "Simulation for fine sediment flocculating settlement in flowing water and its influential factors," *Engineering Journal of Wuhan University*, vol. 46, no. 2, pp. 149–153, 2013.
- [2] T. S. Yang, F. Li, and C. H. Lian, "Computer simulation of flocculation growth for cohesive sediment in still water," *Journal of Sediment Research*, vol. 4, pp. 14–20, 2005.
- [3] A. J. Manning, P. L. Friend, N. Prowse, and C. L. Amos, "Estuarine mud flocculation properties determined using an annular mini-flume and the LabSFLOC system," *Continental Shelf Research*, vol. 27, no. 8, pp. 1080–1095, 2007.
- [4] D. Bouyer, A. Line, and A. Cockx, "Experimental analysis of floc size distribution and hydrodynamics in a jar-test," *Chemical Engineering Research & Design*, vol. 79, no. 8, pp. 1017–1024, 2001.
- [5] B. G. Li, D. Eisma, Q. C. Xie, J. Kalf, Y. Li, and X. Xia, "Concentration, clay mineral composition and Coulter counter size distribution of suspended sediment in the turbidity maximum of the Jiaojiang river estuary, Zhejiang, China," *Journal of Sea Research*, vol. 42, no. 2, pp. 105–116, 1999.
- [6] D. Orange, A. García-García, T. Lorenson et al., "Shallow gas and flood deposition on the Po Delta," *Marine Geology*, vol. 222–223, pp. 159–177, 2005.
- [7] T. A. Witten and L. M. Sander, "Diffusion-limited aggregation, a kinetic critical phenomenon," *Physical Review Letters*, vol. 47, no. 19, pp. 1400–1403, 1981.
- [8] P. K. Jin, X. C. Wang, and K. Guo, "DLA Simulation of fractal flocs and calculation of fractal dimension," *Environmental Chemistry*, vol. 26, no. 1, pp. 5–9, 2007.
- [9] Z. Y. Qin, Z. M. Qiu, and W. Y. Chen, "Simulation on flocs using three dimensional DLA model," *Journal of Nanchang University*, vol. 32, no. 2, pp. 122–126, 2010.
- [10] D. J. Liu, W. G. Zhou, X. Song, and Z. M. Qiu, "Fractal simulation of flocculation processes using a diffusion-limited aggregation model," *Fractal and Fractional*, vol. 1, no. 12, pp. 1–14, 2017.
- [11] P. Meakin, "Formation of fractal clusters and networks by irreversible diffusion-limited aggregation," *Physical Review Letters*, vol. 51, no. 13, pp. 1119–1122, 1983.
- [12] J. C. Gimel, D. Durand, and T. Nicolai, "Transition between flocculation and percolation of a diffusion-limited cluster-

- cluster aggregation process using three-dimensional Monte Carlo simulation," *Physical Review B*, vol. 51, no. 17, pp. 11348–11357, 1995.
- [13] J. Zhang and Q. Zhang, "Direct simulation of drag force on fractal flocs during settling," *Journal of Coastal Research*, vol. 73, no. 1, pp. 753–757, 2015.
- [14] C. A. Biggs and P. A. Lant, "Modelling activated sludge flocculation using population balances," *Powder Technology*, vol. 124, no. 3, pp. 201–211, 2002.
- [15] P. Garrido, R. Burgos, F. Concha, and R. Bürger, "Software for the design and simulation of gravity thickeners," *Minerals Engineering*, vol. 16, no. 2, pp. 85–92, 2003.
- [16] Y. Liao, D. Lucas, E. Krepper, and M. Schmidtke, "Development of a generalized coalescence and breakup closure for the inhomogeneous MUSIG model," *Nuclear Engineering and Design*, vol. 241, no. 4, pp. 1024–1033, 2011.
- [17] I. Nopens, D. Beheydt, and P. A. Vanrolleghem, "Comparison and pitfalls of different discretised solution methods for population balance models: a simulation study," *Computers & Chemical Engineering*, vol. 29, no. 2, pp. 367–377, 2005.
- [18] M. Petitti, M. Vanni, D. L. Marchisio, A. Buffo, and F. Podenzani, "Simulation of coalescence, break-up and mass transfer in a gas-liquid stirred tank with CQMOM," *Chemical Engineering Journal*, vol. 228, pp. 1182–1194, 2013.
- [19] O. P. Prat and J. J. Ducoste, "Modeling spatial distribution of floc size in turbulent processes using the quadrature method of moment and computational fluid dynamics," *Chemical Engineering Science*, vol. 61, no. 1, pp. 75–86, 2006.
- [20] C. Selomulya, G. Bushell, R. Amal, and T. D. Waite, "Understanding the role of restructuring in flocculation: the application of a population balance model," *Chemical Engineering Science*, vol. 58, no. 2, pp. 327–338, 2003.
- [21] L. F. L. R. Silva, R. B. Damian, and P. L. C. Lage, "Implementation and analysis of numerical solution of the population balance equation in CFD packages," *Computers & Chemical Engineering*, vol. 32, no. 12, pp. 2933–2945, 2008.
- [22] D. N. Thomas, S. J. Judd, and N. Fawcett, "Flocculation modelling: a review," *Water Research*, vol. 33, no. 7, pp. 1579–1592, 1999.
- [23] A. Amokrane, S. Maass, F. Lamadie, F. Puel, and S. Charton, "On droplets size distribution in a pulsed column. Part I: in-situ measurements and corresponding CFD-PBE simulations," *Chemical Engineering Journal*, vol. 296, pp. 366–376, 2016.
- [24] M. Golzarjalal, F. Z. Ashtiani, and B. Dabir, "Modeling of microalgal shear-induced flocculation and sedimentation using a coupled CFD-population balance approach," *Biotechnology Progress*, vol. 34, no. 1, pp. 160–174, 2018.
- [25] Z. L. Li, "Population balance model for the flocculation process: a research review," *Journal of Chongqing University of Education*, vol. 26, no. 3, pp. 8–12, 2013.
- [26] Y. Zhou, T. Lei, Z. M. Zheng, G. X. Zheng, J. J. Xu et al., "Flocculation reaction model based on population balance principle," *China Water and Wastewater*, vol. 30, no. 21, pp. 54–57, 2014.
- [27] P. Somasundaran and V. Runkana, "Modeling flocculation of colloidal mineral suspensions using population balances," *International Journal of Mineral Processing*, vol. 72, no. 1–4, pp. 33–55, 2003.
- [28] Z.-e. Ruan, C.-p. Li, and C. Shi, "Numerical simulation of flocculation and settling behavior of whole-tailings particles in deep-cone thickener," *Journal of Central South University*, vol. 23, no. 3, pp. 740–749, 2016.
- [29] Z. P. Shi, G. G. Zhang, J. C. Liu, and T. T. He, "Predicting the floc characteristics and settling velocity of flocs under various polyacrylamide concentration treatments," *Taiwan Water Conservancy*, vol. 64, no. 2, pp. 77–90, 2016.
- [30] A. X. Fan, N. J. Turro, and P. Somasundaran, "A study of dual polymer flocculation," *Colloids and Surfaces A-Physico-chemical and Engineering Aspects*, vol. 162, no. 1–3, pp. 141–148, 2000.
- [31] A. J. Manning and K. R. Dyer, "Mass settling flux of fine sediments in Northern European estuaries: measurements and predictions," *Marine Geology*, vol. 245, no. 1–4, pp. 107–122, 2007.
- [32] B. J. Lee, E. Toorman, F. J. Molz, and J. Wang, "A two-class population balance equation yielding bimodal flocculation of marine or estuarine sediments," *Water Research*, vol. 45, no. 5, pp. 2131–2145, 2011.
- [33] R. Gregory and T. F. Zable, "Sedimentation and flotation," in *Water Quality and Treatment: A Handbook of Community Water Supplies*, McGraw-Hill, New York, NY, USA, 1999.
- [34] V. Vahid and J. B. P. Soares, "Monitoring polymer flocculation in oil sands tailings: a population balance model approach," *Chemical Engineering Journal*, vol. 346, pp. 447–457, 2018.
- [35] M. J. Hounslow, R. L. Ryll, and V. R. Marshall, "A discretized population balance for nucleation, growth, and aggregation," *AIChE Journal*, vol. 34, no. 11, pp. 1821–1832, 1988.
- [36] R. I. Jeldres, F. Concha, and P. G. Toledo, "Population balance modelling of particle flocculation with attention to aggregate restructuring and permeability," *Advances in Colloid and Interface Science*, vol. 224, pp. 62–71, 2015.
- [37] A. R. Heath, P. A. Bahri, P. D. Fawell, and J. B. Farrow, "Polymer flocculation of calcite: population balance model," *AIChE Journal*, vol. 52, no. 5, pp. 1641–1653, 2006.
- [38] G. J. Hong and T. S. Yang, "3D simulation of flocculation settling of cohesive fine sediment," *Journal of Hydraulic Engineering*, vol. 37, no. 2, pp. 172–177, 2006.
- [39] D. M. Li, T. G. Jing, Z. S. Li, and W. C. Tan, "The effect of concentration of high molecular weight flocculants on fractal structures of bridging flocculated aggregates for sediments," *Journal of Guangdong University of Technology*, vol. 23, no. 3, pp. 40–45, 2006.
- [40] C. Selomulya, R. Amal, G. Bushell, and T. D. Waite, "Evidence of shear rate dependence on restructuring and breakup of latex aggregates," *Journal of Colloid and Interface Science*, vol. 236, no. 1, pp. 67–77, 2001.
- [41] P. T. Spicer and S. E. Pratsinis, "Shear-induced flocculation: the evolution of floc structure and the shape of the size distribution at steady state," *Water Research*, vol. 30, no. 5, pp. 1049–1056, 1996.
- [42] P. Bubakova, M. Pivokonsky, and P. Filip, "Effect of shear rate on aggregate size and structure in the process of aggregation and at steady state," *Powder Technology*, vol. 235, pp. 540–549, 2013.

Research Article

Effect of Colloidal Silicate on the Migration Behaviour of Strontium in Groundwater Environment of Geological Disposal Candidate Site

Rui Zuo ^{1,2}, Kexue Han ^{1,2}, Rongtao Shi,^{1,2} Fei Ding,³ Li Liu,^{1,2} Jinsheng Wang,^{1,2} Yanguo Teng,^{1,2} Jie Yang,^{1,2} and Xin Liu^{1,2}

¹College of Water Sciences, Beijing Normal University, Beijing 100875, China

²Engineering Research Center of Groundwater Pollution Control and Remediation, Ministry of Education, Beijing 100875, China

³Key Laboratory of Beijing for Water Quality Science and Water Environment Recovery Engineering, College of Architecture and Civil Engineering, Beijing University of Technology, Beijing 100124, China

Correspondence should be addressed to Rui Zuo; zuo1101@163.com

Received 12 June 2019; Accepted 6 August 2019; Published 23 September 2019

Guest Editor: Chenglian Feng

Copyright © 2019 Rui Zuo et al. This is an open access article distributed under the Creative Commons Attribution License, which permits unrestricted use, distribution, and reproduction in any medium, provided the original work is properly cited.

Various colloids are present in the natural groundwater environment, and colloids act on the processes involved when radionuclides leak from a repository in a high-level waste disposal site. This paper investigates the effect of colloidal silicate in natural groundwater environments on the migration behaviour of Sr(II). Three different experimental cases have been designed: (1) effect in the presence of colloidal silicate, (2) effect in the presence of a porous medium, and (3) effect in the presence of both colloidal silicate and porous medium (referred to as CS, PM, and PC, respectively). Batch experiments were used to study the effect of influencing factors on Sr(II) migration behaviour, such as the amount of CS, solid-to-liquid ratio, pH, contact time, and initial concentration of Sr(II). The experiments showed that the effect of PC on the migration behaviour of Sr(II) was greatest, and the presence of CS enhanced the sorption. The colloid amount, pH, and solid-to-liquid ratio significantly affected the migration behaviour. The more the colloids were added, the better the adsorption effect. The optimal pH and solid-to-liquid ratio were 6 and 20 : 1, respectively. The alkaline environment is more conducive to colloid sorption. When the solid-to-liquid ratio was 20 : 1, the sorption percentage of PC is 0.5 times larger than PM. Although the PC has a longer adsorption equilibrium time, the percentage of adsorption can be larger than that in the other two cases. The kinetics and isotherms of Sr(II) were best described by the pseudo-second-order and Langmuir models. It was inferred that strong chemical interactions and/or surface complexation contributed primarily to Sr(II) sorption, and the process was on the monolayer adsorption of the outer surface. These findings provide valuable information for the migration behaviour of strontium in groundwater environments of geological disposal site. At the same time, it provides information for the implementation of permeable reactive barrier technology to control the transport of radioactive Sr(II) and its species in natural surface and groundwater.

1. Introduction

Since the development and utilization of nuclear energy, the nuclear industry has developed rapidly, and a large amount of nuclear waste has been created [1–3]. Presently, high-level waste is being managed by immobilizing it in solid form (glass and synroc), which is to be buried in deep geological repositories in the near future. However, over thousands of years, there is a finite probability of these minor radionuclides

entering the geosphere, through earthquakes, volcanic eruptions, leaching, and corrosion of the waste form, and underground water movement [4]. It is therefore imperative to study the migration behaviour of these minor radionuclides in the aquatic environment.

Strontium (Sr) is an important product of nuclear fission and is among the typical components of radioactive waste [5, 6]. Sr(II) has good mobility and a half-life of 28.8 years. Its migration speed in geological media is faster than many

actinide, fission, and transuranic nuclides [7, 8]. It is a regulatory object that needs special attention in geological disposal and has been ranked by the US Department of Energy as the third most important nuclear element that can be easily transferred to the environment [9–11]. The chemical properties of Sr(II) are similar to those of Ca or Ba. However, the ability of the human body to distinguish between Sr(II) and Ca(II) is not strong. Sr(II) can easily replace Ca(II) and accumulate in the human body, resulting in osteosarcoma, leukaemia, and other diseases [12, 13]. Therefore, there is high value in taking Sr(II) as the research representative to study the effect of colloids on the migration of nuclides in the groundwater environment for the geological disposal of radioactive nuclides.

At present, many studies have been conducted on the migration of heavy metal elements in aqueous solution or soil medium. Some materials, such as illite [14–16], attapulgite [17], natural clayey sandstone [18], kaolinite [19], montmorillonite [20], and Na-rectorite [21], may play an important role in the migration behaviour of heavy metal elements. Furthermore, colloids have been found to have a significant influence on the migration of radionuclides in the water environment. Yu et al. [20] and Zhao et al. [21] showed that the presence of HA enhances $^{90}\text{Sr(II)}$ sorption on Na-montmorillonite at $\text{pH} < 7.0$ but reduces $^{90}\text{Sr(II)}$ sorption at $\text{pH} > 7.0$. Feng et al. [22] found that the adsorption behaviour of arsenic on soils was strongly dependent on the concentrations of Fe(OH)_3 and H_2SiO_3 colloid. Arsenic adsorption on soils increased significantly with decreasing H_2SiO_3 colloid concentration, but the effect of Fe(OH)_3 colloid on the adsorption behaviour of arsenic in soils is complicated.

The common colloids present in natural water are based on oxides of Si, Al, and Fe [23, 24]. Ultrafiltration analysis confirmed that the elemental composition of colloids in the groundwater of the study area was Si, Fe, Na, etc. In the treatment of wastewater containing radionuclides, silica gel is often used as a sorbent [25]. Many studies have shown that silica gel has sorption properties for nuclides [26, 27]. Lu and Mason [28] found that the isotope exchange behaviour of radioactive Sr(II) onto montmorillonite and silica colloids is an important pathway for the transport of Sr(II) and its species in aqueous systems. At present, one of the important aspects, which is not clearly understood, is the effect of CS in groundwater environment on the migration behaviour of Sr(II). Various authors have reported the influence of colloids or a single component of PM on the migration behaviour of nuclides. Luo et al. [29] studied the sorption behaviour of V(V) onto natural soil colloids and found that the adsorption capacity has different changes with changing environmental conditions such as temperature and pH. Kaygun et al. [17] studied the adsorption behaviour of Sr and Cs onto attapulgite, and the adsorption efficiency was quite high at pH levels from 4 to 8. Therefore, research on the effect of colloids in groundwater environment on the migration behaviour of Sr can make up for this deficiency.

The effect of CS in natural groundwater environments on the migration behaviour of Sr(II) was studied by batch experiments, which explored the impact of various factors

(colloid amounts, solid-liquid ratio, pH, initial concentration of Sr(II), and contact time). The sorption mechanism, sorption kinetics, and isotherms of CS and PM on Sr(II) were discussed. The results provide information for the implementation of permeable reactive barrier technology to control the transport of Sr(II) and its species in natural surface and groundwater.

2. Materials and Methods

2.1. Materials. Study area and reagent source: the study area is in a preselected high-level waste disposal area in Beishan, Gansu Province, China. The sampling location is $41^\circ 49' 17''$ N and $97^\circ 00' 50''$ E. Soil and groundwater samples were collected from the area. Inductively coupled plasma mass spectrometry (ICP-MS) (NexION 300X, PerkinElmer Inc., USA) was used to examine the elements in groundwater. Inductively coupled plasma emission spectrometry (ICP-ES) (Spectro Arcos Eop, Spectro Analytical Instruments GmbH, USA) was used to detect the metal components in the soil samples. Nanosilica was purchased from Sinopharm Group Chemical Reagent Co., Ltd., China. Strontium nitrate was obtained from Tianjin Guangfu Fine Chemical Research Institute, China. Hydrochloric acid and sodium hydroxide were purchased from Beijing Beihua Fine Chemicals Co., Ltd., China. All chemicals used in this study were analytically pure.

Preparation of CS: 50 mg of nanosilica is taken into a 500 ml volumetric flask and dilute with groundwater to a final volume of 500 ml. It is placed into a sonicator for a 30 min ultrasonic bath to evenly disperse the sample and filtered through a $0.45\ \mu\text{m}$ membrane. The concentration of CS was $100\ \text{mg L}^{-1}$.

Preparation of Sr(II) stock solution: 1.2 g of $\text{Sr(NO}_3)_2$ is placed into a volumetric flask and diluted with groundwater to a final volume of 500 ml. The concentration of Sr(II) in the solution was determined to be $500\ \text{mg L}^{-1}$.

2.2. Batch Tests. The influencing factors including the amount of CS, solid-to-liquid ratio, pH, contact time, and initial concentration were investigated using the batch technique. The volume of the solution was 100 ml for all experiments (when the amount of colloid was 100 ml, the solution volume was 100 ml by default). In the process, the experimental time was 1440 min, the pH values of the solutions were carefully adjusted by either 0.1 M HCl or 0.1 M NaOH, and the solid-to-liquid ratio was controlled by adding different amounts of PM. The initial concentrations of Sr(II) varied from 0.5 to $1000\ \text{mg L}^{-1}$, and the amount of colloid varied from 0 to 100 ml. The variable quantity of Sr(II) was determined from the difference between the initial and final concentrations of Sr(II). Experimental conditions were changed by changing specific experimental parameters; other parameters remained unchanged. The different controlled conditions are shown in Table 1. Three groups of controls were designed for each part of the experiment. The experimental results were taken as the average of the three groups.

TABLE 1: Controlled and various factors of experiments.

Various factors	Colloid amounts (ml)	Contact time (min)	pH	Sr(II) initial concentration (mg L ⁻¹)	Solid-to-liquid ratio (g L ⁻¹)
Colloid amounts (ml)	10, 50, 100	1440	6	10	20
Contact time (min)	10	10, 20, 60, 120, 300, 600, 1440, 2880, 4320	6	10	20
pH	10	1440	3, 4, 5, 6, 7, 8, 9, 10	10	20
Sr(II) initial concentration (mg L ⁻¹)	10	1440	6	0.5, 1, 5, 10, 50, 100, 200, 500, 800, 1000	20
Solid-to-liquid (g L ⁻¹)	10	1440	6	10	1:1, 2:1, 5:1, 10:1, 20:1, 100:1

3. Results and Discussion

3.1. Composition of the Water and Soil Samples. ICP-MS was used to determine the trace elements in groundwater. The pH of groundwater was 7.3, and the chemical composition is summarized in Table 2. The purpose of this step is to further understand whether the composition of groundwater will have an unnecessary effect on the experimental results. The metal components in the soil samples were determined by ICP-ES. The chemical composition of the soil samples is summarized in Table 3. Similarly, the detection of chemical composition in soil samples is to determine whether there are silicic colloids in the samples to affect the experimental results.

3.2. Characterization of Soil Samples. In Figure 1, it can be seen that the loose porous mineral skeleton of the soil samples is basically bare, and the soil is mainly composed of small particles of approximately 150 nm in size. The mineral skeleton is covered and filled with the clay material, and it is difficult to separate with no certain shape. The surface micropores and pores are relatively numerous and have a strong adsorption effect on metals and radionuclides.

3.3. Effect of Colloid Amount. When PM worked alone, the amount of PM was 1 g, 5 g, and 10 g. When CS worked alone and PC worked, the volume of CS was 10 ml, 50 ml, and 100 ml, and the amount of PM was 1 g. The results are shown in Figures 2–4.

When CS worked alone, the equilibrium time of each addition amount to Sr(II) was approximately 10 h, which was not affected by the amount of CS. The sorption percentage was approximately 28%, 31%, and 36%, respectively. The reason may be that Sr(II) contacts with sorption sites on the surface of colloid [30]. First, there is the outer layer of complexation and ion exchange. Then, there is the inner complexation [30]. Ultimately, the sorption reaches equilibrium within 10 h.

When PM worked alone, the equilibrium time of each amount to Sr(II) was approximately 10 h, which was not affected by the amount of PM. The sorption percentage was approximately 33%, 41%, and 46%, respectively. When CS and PM worked together, the experimental equilibrium time did not vary with the amount of colloid and was always

TABLE 2: Chemical composition of groundwater.

Test items	Mass concentration (mg L ⁻¹)
K	6.42
Na	159
Ga	82.7
Mg	22.4
Fe	<0.005
Sr	1.39
Mn	0.0067
B	0.265
Ba	0.0685
Fluoride	0.0904
Chloride	223
Nitrate	1.82
Sulphate	524
CO ₃ ²⁻	0
HCO ₃ ⁻	182

TABLE 3: Chemical composition of soil samples.

Test items	Mass concentration (mg/kg)
K	20355.50
Na	13726.50
Ga	18111.80
Mg	3652.82
Al	49402.50
Fe	15279.00
Sr	114.58
Si	467.56

approximately 24 h. The sorption percentage was approximately 80%, 87%, and 91%, respectively.

By comparison, when CS interacted with PM, the equilibrium time was longer than CS or PM alone.

3.4. Effect of Solid-to-Liquid Ratio. The experiments were designed with solid-to-liquid ratios of 1:1, 2:1, 5:1, 10:1, 20:1, and 100:1 (g L⁻¹), and the amount of Sr(II) in the sample was 1 mg. With the presence or absence of CS, the results of three media on the sorption of Sr(II) are shown in Figure 5.

When the solid-to-liquid ratio was less than 20:1 and with increasing solid-to-liquid ratio, the amount of Sr(II) removal and the sorption percentage increased gradually.

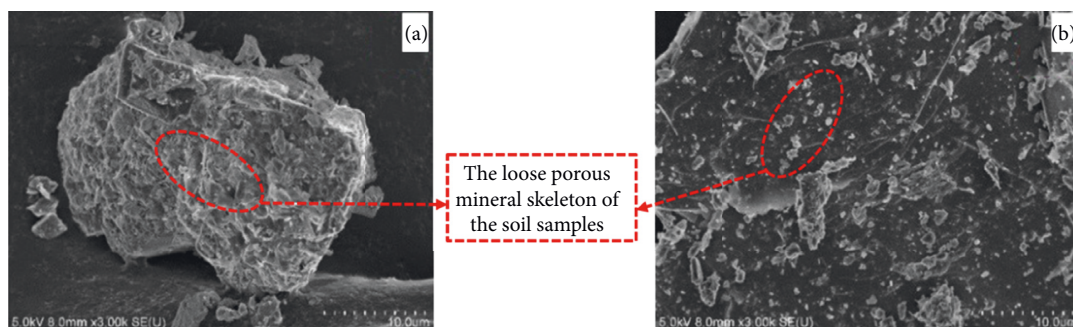


FIGURE 1: SEM of soil samples.

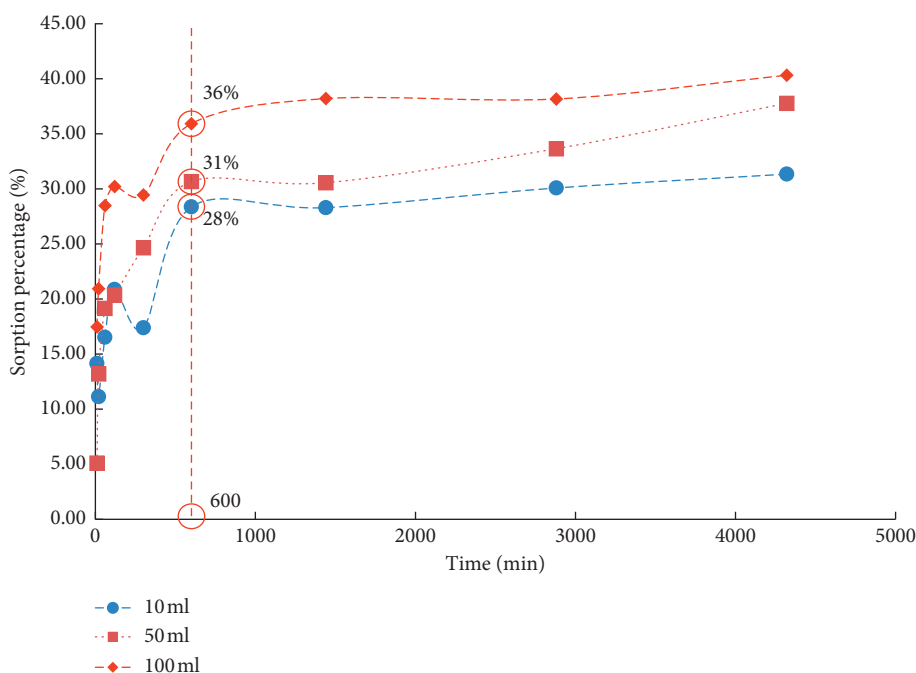


FIGURE 2: Effect of CS addition on equilibrium time: each of the red circles is the point where the experimental phenomenon changes significantly, and the data are the sorption percentage and time of the points.

When the solid-to-liquid ratio was greater than 20:1, the sorption tended to be stable. The sorption percentage affected by CS increased from 29% to 81%. When CS and PM worked together, the trendline was similar to PM alone. However, the effect of sorption increased by approximately 0.5 times. With the increasing solid-to-liquid ratio, the amount of PM in the system increased, as did the total amount of sorption sites [31, 32]. In other words, PM can provide a certain amount of sorption sites. Therefore, the sorption increased correspondingly in the solid phase media [33]. When the solid-to-liquid ratio was greater than 20:1, Sr(II) and the sorption points fully contacted, so the sorption percentage no longer increased.

3.5. Effect of pH. The designed pH levels of the experiment were 3, 4, 5, 6, 7, 8, 9, and 10, and the error was less than 0.1. The amount of Sr(II) in the sample was 1 mg. In each case, the effect of pH on the Sr(II) sorption is shown in Figure 6.

When CS worked alone and $\text{pH} < 6$, with the increasing pH, the sorption percentage increased from 11% to 36%. When $\text{pH} > 6$, the sorption percentage decreased to 14% with the increasing pH. In general, the neutral and alkaline environments are more conducive to colloid sorption [12, 34]. The reason may be that when pH is low, H^+ of higher concentration adsorbs competitively with Sr^{2+} , and the effect of sorption on Sr(II) is poor. With the increasing pH and the decreasing concentration of H^+ , competition decreases. The colloid plays a more important role, and the adsorption amount of Sr(II) increases. The alkaline environment can dissolve the colloid, which is not conducive to the colloid sorption [35]. At the same time, the concentration of OH^- in strong alkaline environment is higher, which reacts with Sr(II) in solution, forming precipitate of $\text{Sr}(\text{OH})_2$. Under the combined action, Sr(II) in solution is removed to a certain extent.

When PC worked and $\text{pH} < 4$, the sorption percentage of Sr(II) increased slowly from 40% to 60%. In general, the

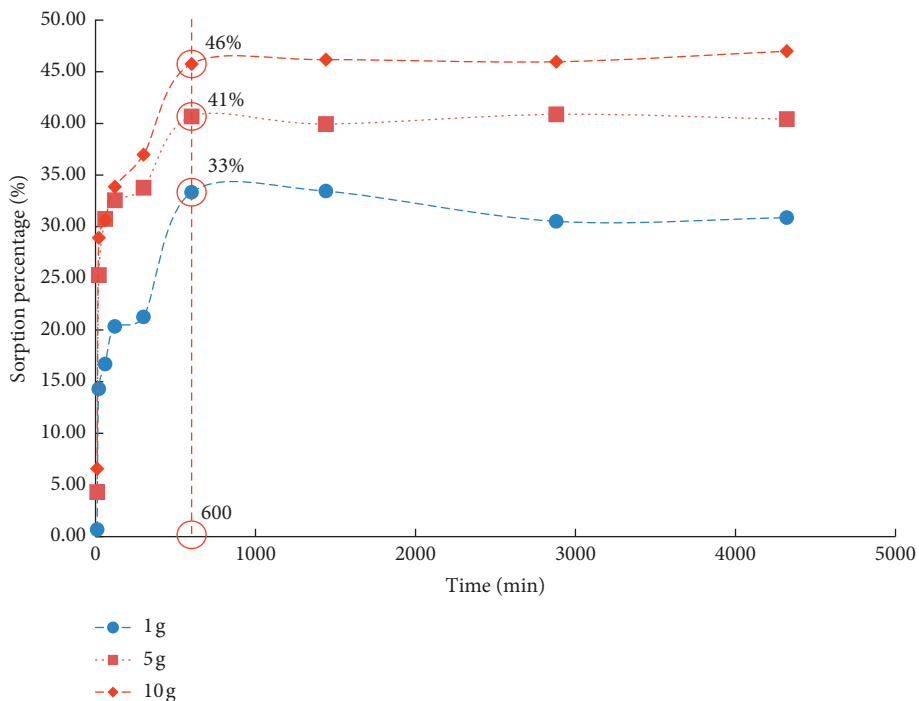


FIGURE 3: Effect of PM addition on equilibrium time: each of the red circles is the point where the experimental phenomenon changes significantly, and the data are the sorption percentage and time of the points.

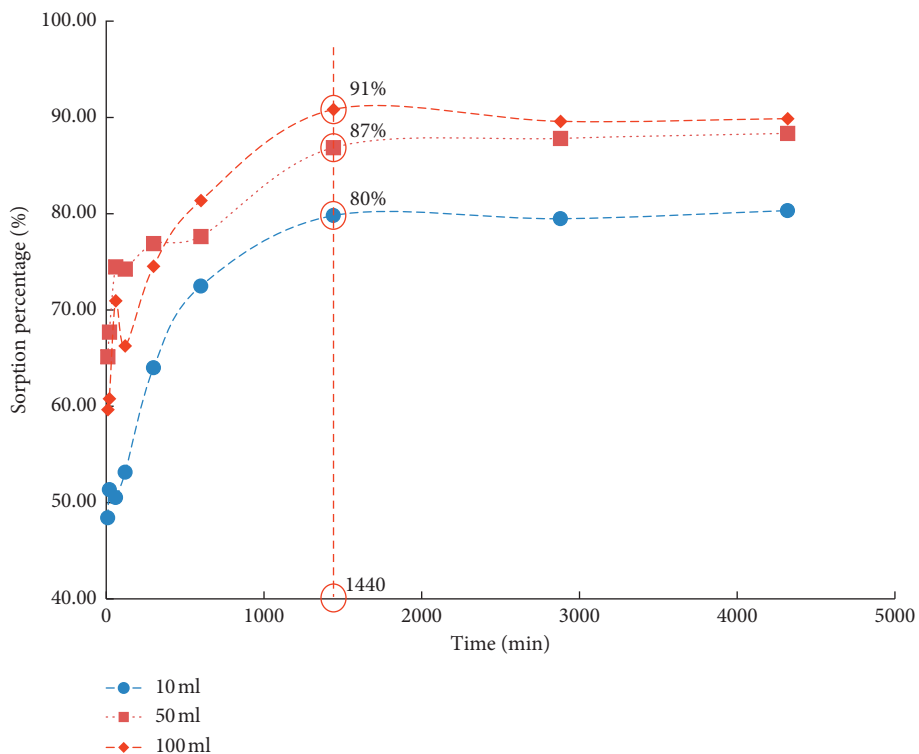


FIGURE 4: Effect of PC addition on equilibrium time: each of the red circles is the point where the experimental phenomenon changes significantly, and the data are the sorption percentage and time of the points.

alkaline environment is more conducive to colloid sorption. The reason is the same as above, but the difference is that PM may be complex with CS forming macromolecules to adsorb Sr(II) [36]. The effect of sorption is better.

In contrast, the sorption of CS and PM is strongly influenced by pH, and the effect of pH on the PC is relatively small. The combined effect increases by approximately 0.5 times relative to PM alone.

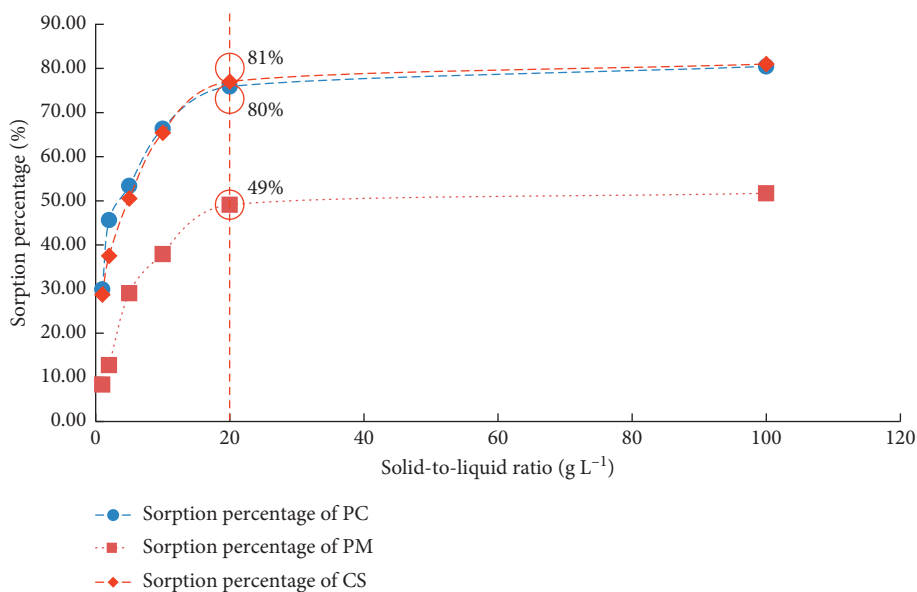


FIGURE 5: Sorption percentage changes with solid-to-liquid ratio.

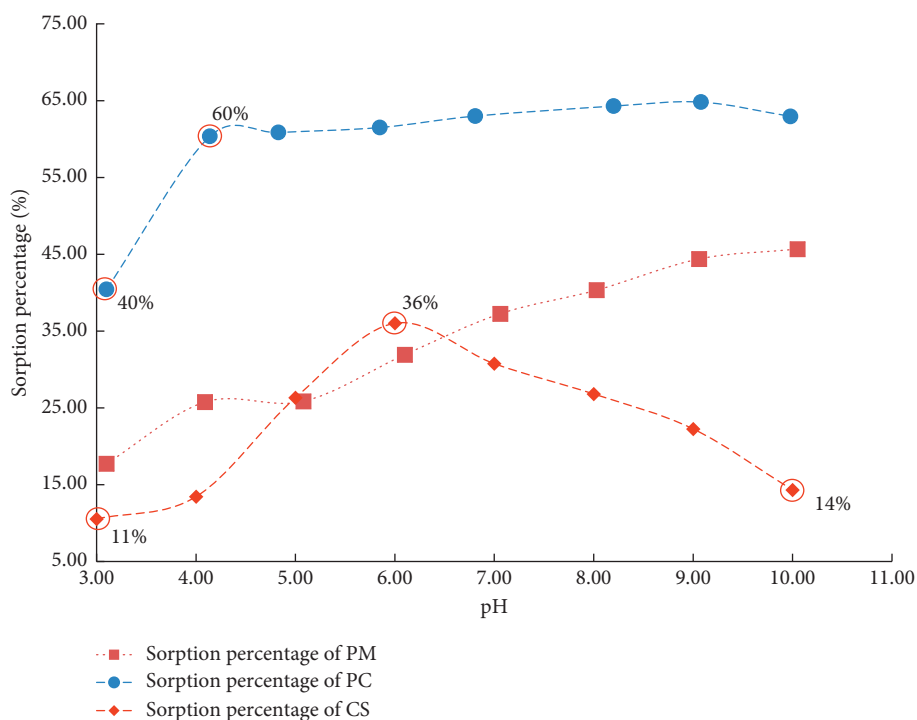


FIGURE 6: Sorption percentage changes with pH.

3.6. *Effect of Sorption Time.* Under the same experimental control conditions, the oscillation times were varied to 10, 20, 60, 120, 300, 600, 1440, 2880, 4320, and 5760 min per sample, and the Sr(II) element content was determined. In each case, the effect of experimental time is shown in Figure 7.

When CS worked alone, the sorption percentage of Sr(II) increased rapidly within 10 h and no longer increased after 10 h. At this time, it was up to sorption equilibrium. The sorption percentage increased from 14% to 31%. The reason

is that Sr(II) contacts with sorption sites on the surface of colloids. First, there is the outer layer of complexation and ion exchange. Then, there is the inner complexation [30]. Ultimately, the sorption reaches equilibrium within 10 h.

Under the combined action of CS and PM, the removal rate of Sr(II) and the sorption percentage increased rapidly within 10 h, increased slowly after 10 h, and no longer increased after 24 h. It tended to equilibrium. The sorption percentage increased from 48% to 70%. The reason is the same as above.

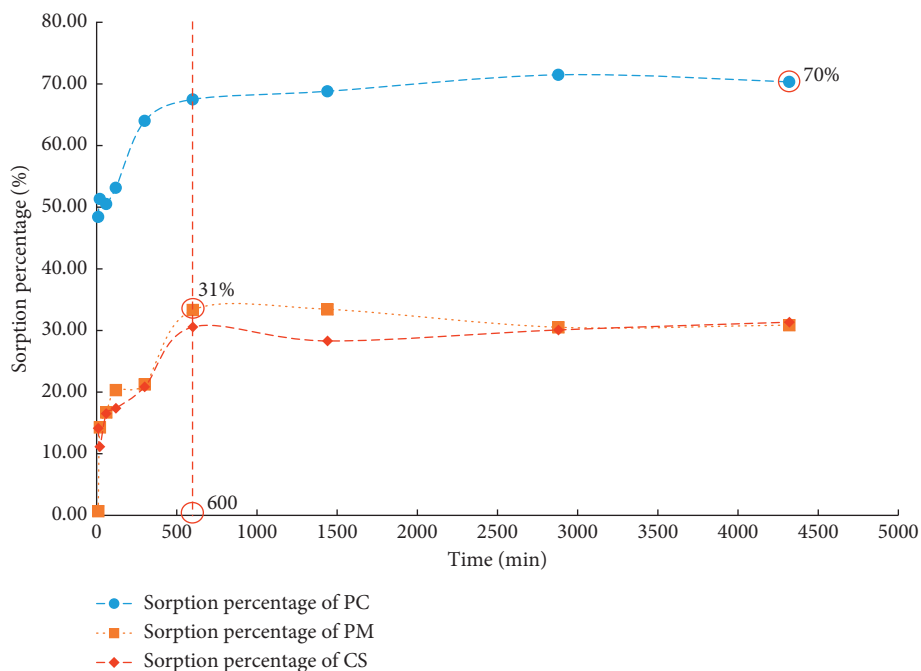


FIGURE 7: Sorption percentage changes with experimental time.

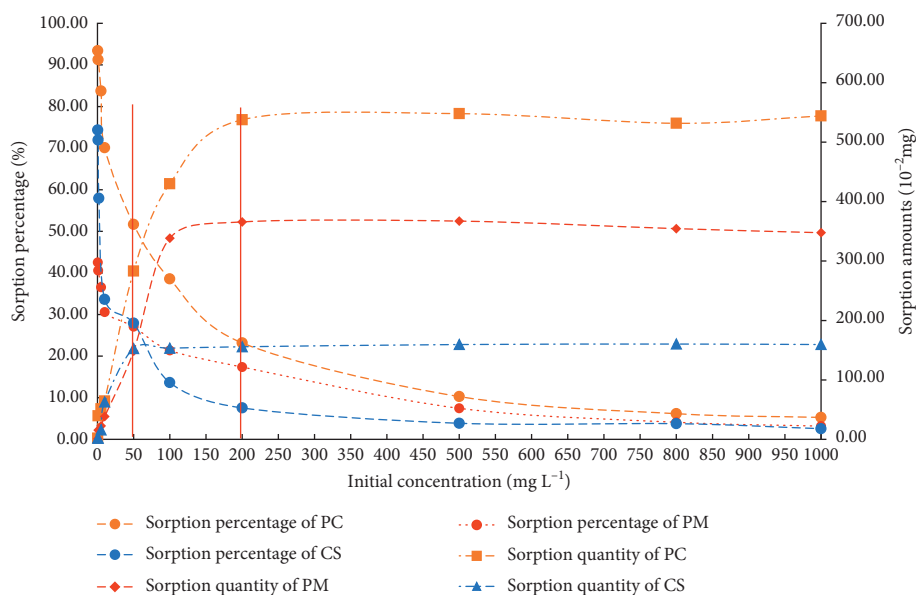


FIGURE 8: Sorption percentage and amounts of Sr(II) change with initial concentration.

By comparison, when PC alone worked, the equilibrium time was the same as CS alone and longer than PM alone. However, the sorption effect is approximately 2.3 times that of PM alone.

3.7. Effect of Initial Concentration. The initial concentration of Sr(II) was 0.5, 1, 5, 10, 50, 100, 200, 500, 800, and 1000 mg L⁻¹. The initial concentration of Sr(NO₃)₂ solution was determined after the sample was prepared. In each case, the effect of Sr(II) initial concentration is shown in Figure 8.

When CS worked alone and the initial concentration of Sr(II) was less than 50 mg L⁻¹, the sorption percentage of Sr(II) increased with increasing concentration. When the concentration was greater than 50 mg L⁻¹, the sorption percentage decreased from the initial 28% to 3%. As the initial concentration increases, the chance of Sr(II) and CS contacting increases and Sr(II) adsorption quantity increases [30]. At the same time, the competition between Sr²⁺ is strengthened, so the sorption percentage decreases [37].

Under the combined action of CS and PM, the adsorption quantity of Sr(II) increased rapidly with increasing

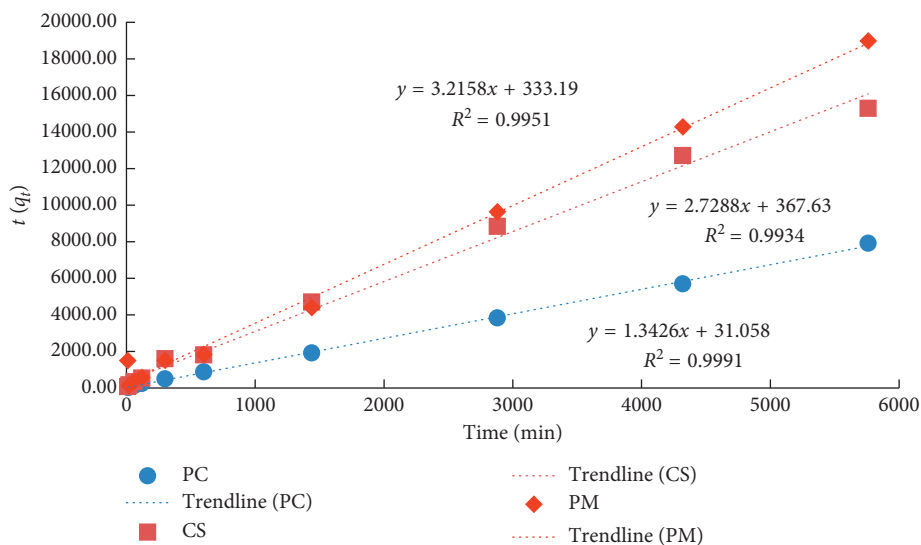


FIGURE 9: Pseudo-second-order kinetic model Sr(II) in the three media.

initial concentration when it was less than 200 mg L^{-1} . The reason is that as the initial concentration increased, the higher binding energy points were fully utilized. At the same time, the sites with lower binding energy also gradually functioned [37, 38]. When the initial concentration was greater than 200 mg L^{-1} , the sorption reached equilibrium. At this time, all points adsorbing Sr(II) in the solution could be in full use. The amount of sorption and desorption was balanced. As the concentration increased, the sorption percentage decreased from 93% to 5% and the competitive sorption between Sr^{2+} intensified.

The sorption effect when CS interacts with PM is obviously better than the cases of the two substances alone. When PC worked, the adsorption of Sr(II) increased by approximately 0.5 times relative to PM alone. With the presence of PM, the adsorptive saturation concentration increased from 50 mg L^{-1} to 100 mg L^{-1} . When PC worked, it was more suitable for a high-concentration Sr(II) environment than PM or CS alone.

3.8. Sorption Kinetics. To study the sorption mechanism of CS on Sr(II), the experimental data were processed by pseudo-first-order and second-order kinetic equations to describe the kinetic behaviour of the reaction.

The pseudo-first-order model is as follows [39]:

$$\ln(q_1 - q_t) = \ln q_1 - K_1 t. \quad (1)$$

The pseudo-second-order model is as follows [40]:

$$\frac{t}{q_t} = \frac{1}{K_2 q_2^2} + \frac{t}{q_2}, \quad (2)$$

$$h = K_2 q_2^2,$$

where K_1 (min^{-1}) and K_2 (min^{-1}) are the adsorption rate constants, which reflect the speed of adsorption and are proportional to the speed of the adsorption reaction; q_1 , q_2 , and q_t represent the amounts (mg/g) of Sr(II) adsorbed at

equilibrium and at time t , respectively; and h is the initial adsorption rate (mg/g-min).

Based on the results of the experimental data, we found that the correlation coefficients (R^2) fitted by the pseudo-second-order kinetic equation were larger. The results are shown in Figure 9. R^2 was greater than 0.99 in all three cases, reaching a significant correlation ($P < 0.0001$). We speculate that the sorption process is mainly chemical sorption [41].

3.9. Sorption Isotherm. Freundlich and Langmuir isotherm sorption equations were used to fit the sorption process of the three media on Sr(II).

The Langmuir isotherm sorption equation is as follows [42]:

$$\frac{q_e}{q_m} = \frac{K_L C_e}{1 + K_L C_e}. \quad (3)$$

The Freundlich isotherm sorption equation is as follows [37]:

$$q_e = K_F C_e^{1/n}, \quad (4)$$

where q_e is the sorption capacity of Sr(II) under different initial mass concentrations, mg/g; C_e is the mass concentration of residual Sr(II) in the solution at equilibrium sorption, mg L^{-1} ; q_m is the maximal saturated sorption capacity, mg/g; K_L is the Langmuir constant, mg^{-1} ; and K_F and n are empirical constants.

As can be seen from Figure 10, the correlation coefficients (R^2) of PC, PM, and CS adsorbed Sr(II) fitted by the Freundlich model are 0.9152, 0.93, and 0.7596, respectively. As shown in Figure 11, the comparison of R^2 between the Langmuir and Freundlich models showed that the Langmuir model exhibited a better fit for the experimental data than the Freundlich model. The Langmuir isotherm sorption equation assumes that the surface of the adsorbent is homogeneous and that there is no interaction between the adsorbates, and it is monolayer sorption. Sorption occurs only

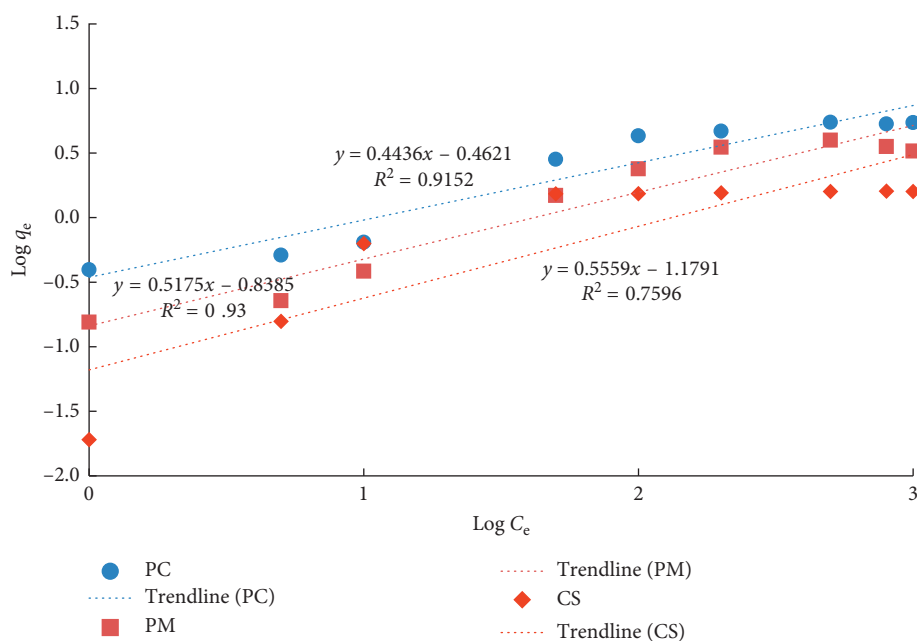


FIGURE 10: Freundlich model of Sr(II) in the three media.

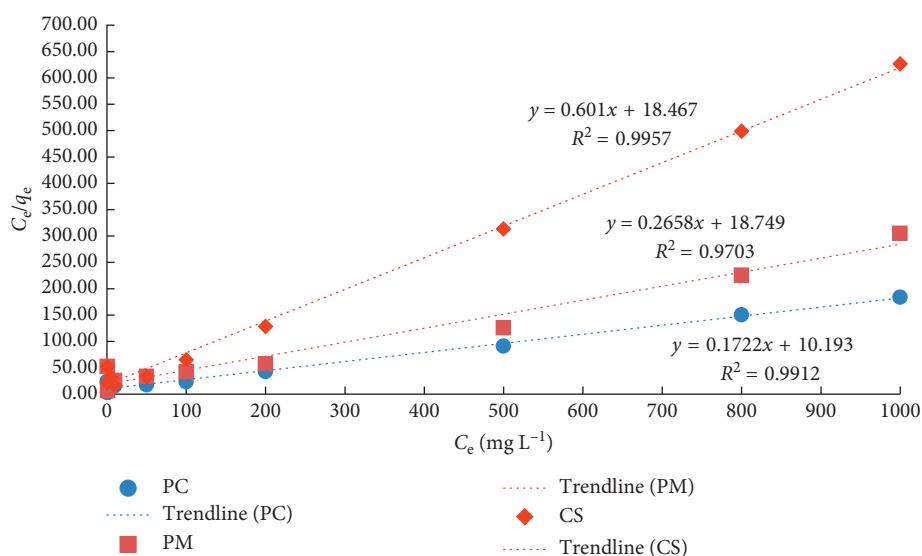


FIGURE 11: Langmuir model of Sr(II) in the three media.

on the outer surface of the adsorbent. The Freundlich isotherm sorption equation can be applied to both single-layer sorption and nonuniform surface sorption [36, 43]. In the present study, the results indicated that the binding sites of the sorbent were distributed uniformly on its surface and the adsorption of Sr(II) was regarded as monolayer adsorption. The characteristics of the adsorption isotherms in this study were consistent with those in previous reports [36, 43].

4. Conclusion

The results suggest that CS promoted the sorption of Sr(II) in groundwater environment. The adsorption amount of Sr(II) was highly dependent on the amount of CS, solid-to-liquid

ratio, and pH. The best solid-to-liquid ratio was 20:1. The sorption percentage reached a maximum at pH=6 and decreased as the acidity or alkalinity of the solution increased. The sorption time studies showed that PC adsorbed approximately 2.67 more Sr(II) than PM and CS. Moreover, the solid-to-liquid ratio and equilibrium times (24 h for PC and 10 h for PM and CS) revealed that PM was the dominant force for adsorbing Sr(II). The initial concentration studies showed that PC worked with a higher sorption saturated concentration (500 mg L⁻¹) compared with PM working alone (200 mg L⁻¹), which indicated that PC was more suitable for a high concentration of Sr(II). The sorption behaviour of Sr(II) followed the pseudo-second-order kinetic model and the Langmuir isotherm, demonstrating that

the adsorption of Sr(II) and the adsorbent was mainly chemical adsorption and formed a monolayer on the outer surface. This study confirmed that the presence of CS in groundwater environment promotes the adsorption of Sr(II), and the results provide information for the implementation of permeable reactive barrier technology to control the transport of radioactive Sr(II) and its species in natural surface and groundwater.

Data Availability

All of the data used in this article support the findings of the study.

Conflicts of Interest

The authors declare that they have no conflicts of interest.

Acknowledgments

This study was supported by the National Natural Science Foundation of China (Grant nos. 41672228 and 41877181) and the National Water Pollution Control and Treatment Science and Technology Major Project (Grant no. 2018ZX07109-003).

References

- [1] N. A. Beresford, S. Fesenko, A. Konoplev, L. Skuterud, J. T. Smith, and G. Voigt, "Thirty years after the Chernobyl accident: what lessons have we learnt?," *Journal of Environmental Radioactivity*, vol. 157, pp. 77–89, 2016.
- [2] M. Gavrilescu, L. V. Pavel, and I. Cretescu, "Characterization and remediation of soils contaminated with uranium," *Journal of Hazardous Materials*, vol. 163, no. 2-3, pp. 475–510, 2009.
- [3] Y. He, Y. G. Chen, and W. M. Ye, "Equilibrium, kinetic, and thermodynamic studies of adsorption of Sr(II) from aqueous solution onto GMZ bentonite," *Environmental Earth Sciences*, vol. 75, no. 9, p. 807, 2016.
- [4] A. S. Kar, S. Kumar, B. S. Tomar, and V. K. Manchanda, "Sorption of curium by silica colloids: effect of humic acid," *Journal of Hazardous Materials*, vol. 186, no. 2-3, pp. 1961–1965, 2011.
- [5] S. Komarneni, N. Kozai, and W. J. Paulus, "Superselective clay for radium uptake," *Nature*, vol. 410, no. 6830, p. 771, 2001.
- [6] H. Qi, H. Liu, and Y. Gao, "Removal of Sr(II) from aqueous solutions using polyacrylamide modified graphene oxide composites," *Journal of Molecular Liquids*, vol. 208, pp. 394–401, 2015.
- [7] H. Faghiihan, M. Iravani, and M. Moayed, "Application of PAN-NaY composite for CS⁺ and SR²⁺ adsorption: kinetic and thermodynamic studies," *Environmental Progress & Sustainable Energy*, vol. 34, no. 4, pp. 999–1008, 2015.
- [8] J. Li, Z. Shao, C. Chen, and X. Wang, "Hierarchical GOs/Fe₃O₄/PANI magnetic composites as adsorbent for ionic dye pollution treatment," *RSC Advances*, vol. 4, no. 72, pp. 38192–38198, 2014.
- [9] F. Liu, Y. Liu, Y. Xu et al., "Efficient static and dynamic removal of Sr(II) from aqueous solution using chitosan ion-imprinted polymer functionalized with dithiocarbamate," *Journal of Environmental Chemical Engineering*, vol. 3, no. 2, pp. 1061–1071, 2015.
- [10] R. Sureda, X. Martínez-Lladó, M. Rovira, J. de Pablo, I. Casas, and J. Giménez, "Sorption of strontium on uranyl peroxide: implications for a high-level nuclear waste repository," *Journal of Hazardous Materials*, vol. 181, no. 1–3, pp. 881–885, 2010.
- [11] R. Zuo, Y. Teng, and J. Wang, "Sorption and retardation of strontium in fine-particle media from a VLLW disposal site," *Journal of Radioanalytical and Nuclear Chemistry*, vol. 279, no. 3, pp. 893–899, 2009.
- [12] M. Wang, L. Xu, J. Peng, M. Zhai, J. Li, and G. Wei, "Adsorption and desorption of Sr(II) ions in the gels based on polysaccharide derivatives," *Journal of Hazardous Materials*, vol. 171, no. 1–3, pp. 820–826, 2009.
- [13] W. E. Cabrera, I. Schrooten, M. E. De Broe, and P. C. D'Haese, "Strontium and bone," *Journal of Bone and Mineral Research*, vol. 14, no. 5, pp. 661–668, 1999.
- [14] T. Missana, M. Garcia-Gutierrez, and U. Alonso, "Sorption of strontium onto illite/smectite mixed clays," *Physics and Chemistry of the Earth, Parts A/B/C*, vol. 33, pp. S156–S162, 2008.
- [15] A. Wissocq, C. Beaucaire, and C. Latrille, "Ca and Sr sorption on Ca-illite: experimental study and modelling," *Procedia Earth and Planetary Science*, vol. 17, pp. 662–665, 2017.
- [16] V. Montoya, B. Baeyens, M. A. Glaus et al., "Sorption of Sr, Co and Zn on illite: batch experiments and modelling including Co in-diffusion measurements on compacted samples," *Geochimica et Cosmochimica Acta*, vol. 223, pp. 1–20, 2018.
- [17] A. K. Kaygun, M. Eral, and S. A. Erenturk, "Removal of cesium and strontium using natural attapulgite: evaluation of adsorption isotherm and thermodynamic data," *Journal of Radioanalytical and Nuclear Chemistry*, vol. 311, no. 2, pp. 1459–1464, 2017.
- [18] A. Wissocq, C. Beaucaire, and C. Latrille, "Application of the multi-site ion exchanger model to the sorption of Sr and Cs on natural clayey sandstone," *Applied Geochemistry*, vol. 93, pp. 167–177, 2018.
- [19] E. Başçetin and G. Atun, "Adsorption behavior of strontium on binary mineral mixtures of montmorillonite and kaolinite," *Applied Radiation and Isotopes*, vol. 64, no. 8, pp. 957–964, 2006.
- [20] S. Yu, H. Mei, X. Chen et al., "Impact of environmental conditions on the sorption behavior of radionuclide 90 Sr(II) on Na-montmorillonite," *Journal of Molecular Liquids*, vol. 203, pp. 39–46, 2015.
- [21] Y. Zhao, Z. Shao, C. Chen, J. Hu, and H. Chen, "Effect of environmental conditions on the adsorption behavior of Sr(II) by Na-rectorite," *Applied Clay Science*, vol. 87, pp. 1–6, 2014.
- [22] Q. Feng, Z. Zhang, Y. Chen, L. Liu, Z. Zhang, and C. Chen, "Adsorption and desorption characteristics of arsenic on soils: kinetics, equilibrium, and effect of Fe(OH)₃ colloid, H₂SiO₃ colloid and phosphate," *Procedia Environmental Sciences*, vol. 18, pp. 26–36, 2013.
- [23] A. S. Saleh, J.-Y. Lee, Y. Jo, and J.-I. Yun, "Uranium(VI) sorption complexes on silica in the presence of calcium and carbonate," *Journal of Environmental Radioactivity*, vol. 182, pp. 63–69, 2018.
- [24] D. M. Singer, H. Guo, and J. A. Davis, "U(VI) and Sr(II) batch sorption and diffusion kinetics into mesoporous silica (MCM-41)," *Chemical Geology*, vol. 390, pp. 152–163, 2014.
- [25] J. R. Lead and K. J. Wilkinson, "Aquatic colloids and nanoparticles: current knowledge and future trends," *Environmental Chemistry*, vol. 3, no. 3, pp. 159–171, 2006.
- [26] X. L. Li, C. L. Chen, P. P. Chang, S. M. Yu, W. S. Wu, and X. K. Wang, "Comparative studies of cobalt sorption and

- desorption on bentonite, alumina and silica: effect of pH and fulvic acid,” *Desalination*, vol. 244, no. 1–3, pp. 283–292, 2009.
- [27] F. Huber, U. Noseck, and T. Schäfer, “Colloid/nanoparticle formation and mobility in the context of deep geological nuclear waste disposal,” Project Kollorado-2 Final report. Wissenschaftliche Berichte Fzka 7515, pp. 1–180, Karlsruhe Institute of Technology, Karlsruhe, Germany, 2010.
- [28] N. Lu and C. F. V. Mason, “Sorption-desorption behavior of strontium-85 onto montmorillonite and silica colloids,” *Applied Geochemistry*, vol. 16, no. 14, pp. 1653–1662, 2002.
- [29] X. Luo, L. Yu, C. Wang et al., “Sorption of vanadium (V) onto natural soil colloids under various solution pH and ionic strength conditions,” *Chemosphere*, vol. 169, pp. 609–617, 2017.
- [30] Z. Ma, Q. Li, Q. Yue et al., “Adsorption removal of ammonium and phosphate from water by fertilizer controlled release agent prepared from wheat straw,” *Chemical Engineering Journal*, vol. 171, no. 3, pp. 1209–1217, 2011.
- [31] Q. Fan, D. Shao, Y. Lu, W. Wu, and X. Wang, “Effect of pH, ionic strength, temperature and humic substances on the sorption of Ni(II) to Na-attapulgite,” *Chemical Engineering Journal*, vol. 150, no. 1, pp. 188–195, 2009.
- [32] M. S. Murali and J. N. Mathur, “Sorption characteristics of Am(III), Sr(II) and Cs(I) on bentonite and granite,” *Journal of Radioanalytical and Nuclear Chemistry*, vol. 254, no. 1, pp. 129–136, 2002.
- [33] L. Tan, X. Wang, X. Tan et al., “Bonding properties of humic acid with attapulgite and its influence on U(VI) sorption,” *Chemical Geology*, vol. 464, pp. 91–100, 2017.
- [34] B. Ivanova and M. Spiteller, “Adsorption of uranium complexes onto saltrock oxides—experimental and theoretical study,” *Journal of Environmental Radioactivity*, vol. 135, pp. 75–83, 2014.
- [35] Z. R. Komy, A. M. Shaker, S. E. M. Heggy, and M. E. A. El-Sayed, “Kinetic study for copper adsorption onto soil minerals in the absence and presence of humic acid,” *Chemosphere*, vol. 99, pp. 117–124, 2014.
- [36] C. Kütahyalı, B. Çetinkaya, M. B. Acar, N. O. Işık, and İ. Cireli, “Investigation of strontium sorption onto kula volcanics using central composite design,” *Journal of Hazardous Materials*, vol. 201–202, pp. 115–124, 2012.
- [37] R. M. Ali, H. A. Hamad, M. M. Hussein, and G. F. Malash, “Potential of using green adsorbent of heavy metal removal from aqueous solutions: adsorption kinetics, isotherm, thermodynamic, mechanism and economic analysis,” *Ecological Engineering*, vol. 91, pp. 317–332, 2016.
- [38] S. Yang, J. Li, Y. Lu, Y. Chen, and X. Wang, “Sorption of Ni(II) on GMZ bentonite: effects of pH, ionic strength, foreign ions, humic acid and temperature,” *Applied Radiation and Isotopes*, vol. 67, no. 9, pp. 1600–1608, 2009.
- [39] Y. S. Ho and G. McKay, “Kinetic models for the sorption of dye from aqueous solution by wood,” *Process Safety and Environmental Protection*, Institution of Chemical Engineers, vol. 76, no. 2, pp. 183–191, 1998.
- [40] B. K. Nandi, A. Goswami, and M. K. Purkait, “Adsorption characteristics of brilliant green dye on kaolin,” *Journal of Hazardous Materials*, vol. 161, no. 1, pp. 387–395, 2009.
- [41] I. Langmuir, “The adsorption of gases on plane surfaces of glass, mica and platinum,” *Journal of the American Chemical Society*, vol. 40, no. 9, pp. 1361–1403, 1918.
- [42] R. Donat, A. Akdogan, E. Erdem, and H. Cetisli, “Thermodynamics of Pb²⁺ and Ni²⁺ adsorption onto natural bentonite from aqueous solutions,” *Journal of Colloid and Interface Science*, vol. 286, no. 1, pp. 43–52, 2005.
- [43] Q. H. Fan, W. S. Wu, X. P. Song, J. Z. Xu, J. Hu, and Z. W. Niu, “Effect of humic acid, fulvic acid, pH and temperature on the sorption-desorption of Th(IV) on attapulgite,” *Radiochimica Acta*, vol. 96, no. 3, pp. 159–165, 2008.

Research Article

Distribution and Bioaccumulation of Perfluoroalkyl Acids in Xiamen Coastal Waters

Zhineng Dai^{1,2} and Fansheng Zeng³

¹School of Environmental Science and Engineering, Xiamen University of Technology, 361024 Xiamen, China

²Key Laboratory of Environmental Biotechnology (XMUT), Fujian Province University, Xiamen, China

³Yiyang Medical College, 413002 Yiyang, China

Correspondence should be addressed to Zhineng Dai; daizn@xmut.edu.cn

Received 30 June 2019; Accepted 5 August 2019; Published 20 August 2019

Guest Editor: Chunjiang An

Copyright © 2019 Zhineng Dai and Fansheng Zeng. This is an open access article distributed under the Creative Commons Attribution License, which permits unrestricted use, distribution, and reproduction in any medium, provided the original work is properly cited.

Since perfluoroalkyl acids (PFAs) are widely used and harmless to organisms, they have attracted great attention in recent years. The distribution of PFAs in the oceans all around the world is well documented. However, the study of PFAs in Xiamen could be a beneficial complement, for its unique geologies of no rivers that originate from other cities to influence the concentration of PFAs in this area. In this paper, six PFAs were analyzed in water, sediments, and organisms from both freshwater and seawater and the bioaccumulation factors (BAFs) were calculated with the quantity of PFAs in different trophic levels of aquatic organisms. The results showed that the Σ PFAs concentrations ranged from 7.66 to 11.98 ng·L⁻¹ for seawater samples and from 2.12 to 8.61 ng·L⁻¹ for freshwater. The concentration of Σ PFAs in sediments was 7.43–12.89 ng·g⁻¹ and 4.53–5.80 ng·g⁻¹ in seawater and freshwater, respectively. The PFA concentration in water is highly positive correlated with the PFA concentration in sediments ($R^2 = 0.85$). The calculated bioaccumulation factors (BCFs) were 6412–14254 L·kg⁻¹ and 2927–7959 L·kg⁻¹ for perfluorooctanoic acid (PFOA) and perfluorooctane sulfonates (PFOS), respectively. PFOA seems more bioaccumulative than PFOS in seawater. The results illustrated the PFA pollution in the Xiamen sea area, and it is useful for the protection and control of the organic pollutants in this area.

1. Introduction

Perfluorinated acids (PFAs) have emerged as a new class of global environmental pollutants and have a wide range of industrial applications, such as fire-fighting foams, pesticides, and consumer applications including surface coatings for carpets, furniture, and paper products [1]. The unique physicochemical properties of perfluorinated compounds, such as high surface activity, thermal stability, and amphipathicity, are responsible for their industrial value, but they also contributed to the compounds' persistence in the environment and accumulation in biota [2, 3]. PFAs persist in the environment as persistent organic pollutants, but unlike PCBs, they are not known to degrade by any natural processes due to the strength of the carbon-fluorine bond [4, 5].

Due to their high water solubility, PFAs are ubiquitous in various kinds of waters and the aqueous phase is considered as a major sink for PFAs [4–7]. About 40 perfluorinated compounds (PFCs) have been found in ocean water collected from a number of locations, including remote marine locations such as the Arctic and the Antarctic Oceans [8–12].

Many researchers have investigated the pollution of PFCs in major rivers, lakes, reservoirs, and other environments in China and obtained relatively comprehensive pollution situation of PFCs in freshwater environment [13–16]. Studies on PFAs pollution in marine environment of China mainly include the reports on PFA pollution in sediments in the East China Sea, Yellow Sea, and Bohai Sea [17]. In addition, there are also some reports on the amount of PFAs in offshore seawater and sediments in Dalian [10], Shenzhen [18], and Wenzhou [19], as well as reports on the

pollution situation in the estuaries of the Yangtze River, Huangpu River, and Pearl River [20, 21]. Survey shows that nearly all samples have different concentrations of PFAs detected. Generally, compared with other parts of the world, PFAs pollution in China is in the intermediate level among the world. As we know, the aqueous phase is considered as a major sink for PFAs, especially in the oceans. Considering the very long coastline and broad maritime territory of China, the research studies about the distribution of PFAs in the ocean are obviously insufficient. The objective of this research is to study the distribution of PFAs in Xiamen coastal waters. The water, sediment, and organism samples were collected from different sampling sites in Xiamen. In addition, the concentrations of PFAs of several organisms were analyzed, and the bioaccumulation factors were calculated. The purpose of this study is to support basic information about the pollution of PFAs in Xiamen coastal water for the risk assessment and control of PFAs.

2. Materials and Methods

2.1. Chemicals. PFOS (98%) was purchased from Tokyo Chemical Industries (Tokyo, Japan); PFOA (96%), perfluorononanoic acid (PFNA, 97%), perfluorodecanoic acid (PFDA, 98%), perfluoroundecanoic acid (PFUnA, 95%), and perfluorododecanoic acid (PFDoA, 95%) were obtained from Acros Organics (New Jersey, US), and a purity corrected equimass stock standard solution containing these perfluorinated acids was prepared in a 80:20 (v/v) methanol/water solution with the concentration of 200 mg·L⁻¹ for each PFAs. The methanol was purchased from J. T. Baker (chromatography grade, Phillipsburg, NJ, USA). [1,2,3,4-¹³C₄]Perfluorooctanoic acid (MPFOA) (purity > 99%) was obtained from Wellington Laboratories (Guelph, Canada), and it was used as an internal standard. Ammonium acetate (98%), methyl-*tert*-butyl ether (MTBE, 99.5%), and tetrabutylammonium hydrogensulfate (TBA) were purchased from Sigma-Aldrich Chemical Co. (St. Louis, US), and they were used to extract PFAs from aquatic organisms.

2.2. Sample Collection. Six surface seawater samples were collected from Xinglin Bay, Fenglin, Zhenzhu Bay, Gulf Park, Convention Center, Wuyuan Bay, and Jimei Bridge (Figure 1). Four freshwater samples were collected from Bantou Reservoir (two samples: one is from the tail and one is from the middle of the reservoir), Beixi River, and Jiangdong Reservoir (Figure 1). Samples were collected using a clean stainless steel grab sampler and stored in 1 L polypropylene containers. The containers were rinsed with methanol, deionized water, and water from the particular sampling location prior to use. The amount of suspended matter was kept to a minimum. The samples were extracted within 24 h after collection. All of the water samples were collected during March to May, 2018.

The sediment samples were collected from the same sites that the water samples were collected at the same time. About 1 kg sediments were collected at each site by the



FIGURE 1: Sampling locations of PFAs in Xiamen (1, Bantou Reservoir (middle); 2, Bantou Reservoir (tail area); 3, Xinglin Bay; 4, Fenglin; 5, Jimei Bridge; 6, Gulf Park; 7, Zhenzhu Bay; 8, Convention Center; 9, Wuyuan Bay).

clean stainless steel grab sampler and stored in 1 L polypropylene containers. The samples were extracted within 24 h after collection.

Aquatic organisms, including crab, oyster, hermit crab, fish, and kelp, were collected from Jimei Bridge, Fenglin, Wuyuan Bay, Haiwan Bay, and Bantou Reservoir. Since the organisms were difficult to sample, it took almost one month to collect all of them. So the earlier collected organisms were stored at -20°C until analysis. Fish were caught by a fishing net, and all species were coastal fishes.

2.3. Extraction and Analysis of PFAs. The PFAs in sediments and organisms were extracted by the ion-pairing agent extracted method with some modifications [22–24]. A total of 2 mL of Na₂CO₃ (0.25 M), 1 mL of the ion-pairing agent tetrabutylammonium hydrogensulfate (0.5 M, adjusted to pH 10), 2 mL of MTBE, and 100 μL (10 ng) of MPFOA (as an internal standard) were added into the centrifuge tubes containing the samples in turn. These tubes were shaken vigorously by an oscillator with the speed of 150 rpm for 12 h and then sonicated for 30 min, followed by centrifugation to isolate the organic phase. The MTBE supernatant was collected in a separate polypropylene tube. This extraction process was repeated twice except the shaken time was reduced to 2 h for the second time. The supernatants were combined and blown to dryness under high-purity nitrogen gas, and the analytes were dissolved in 1 mL of 80:20 (v/v) methanol: water solution. The extraction of water samples was similar to that described before [25]. The key step is the

filtration of water samples by 10 g solid-phase extraction (SPE) C18 cartridges.

PFCs, including PFOA, PFNA, PFOS, PFDA, PFDoA, and PFUnA, were analyzed by liquid chromatography-tandem mass spectrometry (LC-MS/MS; Dionex Ultimate 3000 and Applied Biosystems API 3200) in the electrospray negative ionization mode. The methods used in our previous study [26] and those used by Martin et al. were modified to analyze PFAs in this study [27]. In brief, a 10 μL aliquot of sample was injected into a 4.6 \times 150 mm Acclaim 120 C18 column. The mobile phase was 5 mM ammonium acetate and methanol for tubes A and B, respectively, and the gradient eluting procedure was adopted with a flow rate of 1 $\text{mL}\cdot\text{min}^{-1}$. In brief, the mobile phase gradient was ramped from 70% to 95% methanol in 4 min, held at 95% methanol for 3 min, and then ramped down to 70% methanol in 3 min.

2.4. Quality Assurance and Quality Control (QA/QC). The concentrations of all target analytes were quantified from calibration curves drawn using external standards, and the correlation coefficients of the standard curves were higher than 0.98. The limits of quantification (LOQs) were defined as the lowest amount of the PFA concentrations that can be quantitatively determined with a signal-to-noise ratio greater than 7, and the deviations were within $\pm 20\%$ from theoretical values of the duplicate injection. The LOQs of the target chemicals were in the range of 0.01–0.05 $\text{ng}\cdot\text{mL}^{-1}$, and the corresponding detection limits for biological samples were 0.05–0.10 $\text{ng}\cdot\text{g}^{-1}$ wet weight. Concentrations below the LOQ were set to zero.

The recoveries of PFAs and the internal standard (MPFOA) in water and biological samples ranged from 82% to 93%. Polypropylene or polyethylene containers were used for all stock solutions and test vessels, and glass and Teflon containers were avoided due to the sorption of PFAs on them. The results showed that the PFAs were not detected in blanks.

2.5. Data Processes. One-way analysis of variance and Tukey's honestly significant difference test were performed using PASW statistic 18.0 for Windows (SPSS). The graphs were drawn by Origin Pro 8 and Microsoft Excel 2016.

3. Results and Discussion

3.1. PFA Distribution in Water. All six PFAs were detected in both freshwater and seawater samples (Table 1). The ΣPFA concentrations ranged from 7.66 to 11.98 $\text{ng}\cdot\text{L}^{-1}$ for seawater samples and from 2.12 to 8.61 $\text{ng}\cdot\text{L}^{-1}$ for freshwater. In addition, only PFOA, PFOS, and PFNA were detected in Bantou Reservoir and Jiangdong Reservoir. PFOS was the predominated PFAs with its contribution ranging from 15% to 45%, followed by PFOA, with its contribution ranged from 11% to 18% (Figure 2). PFAs such as PFOS, PFHS, PFOA, and PFOSA have been found in ocean water collected from a number of locations, including remote marine locations such as the Arctic and the

Antarctic Oceans. The concentration of PFAs in Xiamen coastal water is in the middle level when compared to other bays. For example, the PFOA and PFOS concentration ranges from 0.9 to 1.4 $\text{ng}\cdot\text{L}^{-1}$ and 1.07 to 5.37 $\text{ng}\cdot\text{L}^{-1}$; however, it ranges from 0.73 to 5.5 $\text{ng}\cdot\text{L}^{-1}$ and 0.09 to 3.1 $\text{ng}\cdot\text{L}^{-1}$ in Hong Kong, 0.24 to 320 $\text{ng}\cdot\text{L}^{-1}$ and 0.04 to 730 $\text{ng}\cdot\text{L}^{-1}$ in Korea, 0.17 to 37.55 $\text{ng}\cdot\text{L}^{-1}$ and <0.10 to 2.25 $\text{ng}\cdot\text{L}^{-1}$ in Dalian, and 1.8 to 192 $\text{ng}\cdot\text{L}^{-1}$ and 0.34 to 58 $\text{ng}\cdot\text{L}^{-1}$ in Tokyo, respectively [7, 9, 10, 25, 28, 29].

In most cases, the concentration of PFAs in seawater samples and freshwater samples is close to each other, and they are below 10 $\text{ng}\cdot\text{L}^{-1}$, except the sample from Wuyuan Bay. The sampling site of Wuyuan Bay is close to a municipal sewage outfall. As we know, the PFA is one kind of synthetic compounds, and its pollution is all comes from human activities. So maybe that is the reason why the concentration of PFAs in Wuyuan Bay is higher than other sampling sites. In fact, the other sampling locations that have a relatively higher concentration, such as Fenglin and Xinglin Bay, were all near the domestic sewage outfalls or industrial effluents outfalls. In addition, as described above, only 3 PFAs were detected in two reservoirs. The results may attribute to the reason that these reservoirs are drinking water sources, and they have been protected for several years. So, little pollutants were introduced to the reservoirs and led to the low concentration of PFAs.

The special distribution of 9 PFCs from the East to South China Sea was investigated by Cai et al. The results showed that the ΣPFC concentrations ranged from 0.13 ng/L to 3.320 ng/L , with PFOA (0.037–1.54 ng/L), PFBS (0.023–0.94 ng/L), and PFHpA (0–0.42 ng/L) as dominant compounds [30]. These samples were gathered in coastal waters along Shanghai, Ningbo, Taizhou, and Xiamen and along coastal cities of Guangdong Province. The relatively lower PFC concentration may ascribe to the sampling location when compared to this study. The water samples were collected by the research vessel Snow Dragon a few kilometers way from the coast, but in this study, they were collected about 100 m away from the coast. Since the PFCs were man-made pollutants, their concentrations decrease from the coast to the open sea area.

In addition, the PFC concentrations in Jiulong River have been investigated, and the results showed that total content of 17 PFCs in the water sample from Jiulong River watershed estuary was in the range of 5.31–463.16 ng/L in dry season, 3.14–155.16 ng/L in medium season, and 3.57–42.96 ng/L in wet season [31]. Jiulong River is close to Xiamen, and the relatively higher PFC concentration in Jiulong River watershed estuary indicated that that the PFCs could migrate along the river and accumulate in the lower course of river.

The concentration of PFAs from seawater samples is higher than the concentration from freshwater samples, and the only exception is the sample from Beixi Channel. Beixi Channel is an aqueduct made by concrete. The relatively high concentration of PFAs may attribute to the construction material. Otherwise, the water in Beixi Channel comes from Jiulong River, which has been polluted by various kinds of pollutants.

TABLE 1: Distribution of PFAs in surface waters around Xiamen.

Location	Temperature (°C)	Sampling depth (m)	<i>n</i>	ΣPFAs (ng·L ⁻¹)
<i>Seawater</i>				
Xinglin Bay	18.5	0.2	3	8.36–8.73
Fenglin	18.8	0.2	3	8.77–9.96
Zhenzhu Bay	17.9	0.2	3	7.66–7.77
Gulf Park	18.2	0.2	3	7.98–8.26
Convention Center	18.1	0.2	3	7.68–7.79
Wuyuan Bay	18.5	0.2	3	9.86–11.98
Jimei Bridge	18.4	0.2	3	7.99–8.32
<i>Freshwater</i>				
Bantou Reservoir (middle)	19.3	0.2	3	2.12–2.36
Bantou Reservoir (tail area)	19.1	0.2	3	2.96–3.52
Jiangdong Reservoir	18.8	0.2	2	3.16–4.24
Beixi Channel	18.1	0.2	2	8.01–8.61

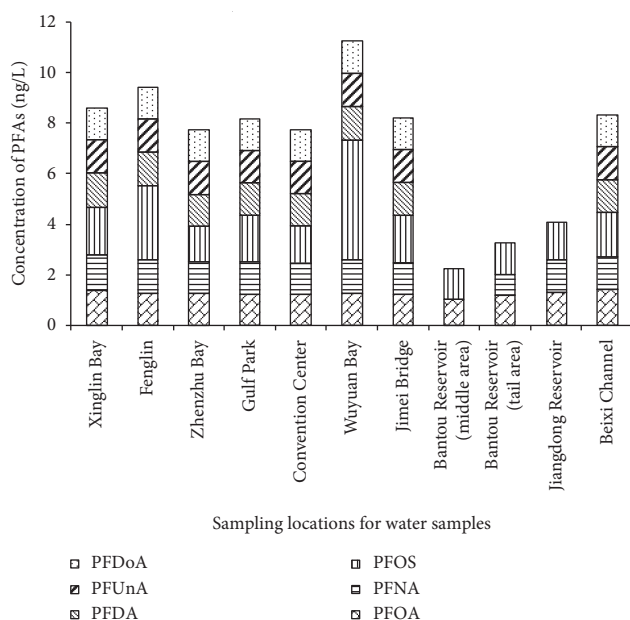


FIGURE 2: Concentration of six PFAs in water samples from Xiamen (the concentration of PFAs represents the mean value).

3.2. PFA Distribution in Sediments. The concentration of ΣPFAs in sediments of seawater is ranged from 7.43 to 12.89 ng·g⁻¹ (Table 2). The Wuyuan Bay has the highest concentration, while the Convention Center has the lowest. In addition, the concentration of ΣPFAs in sediments of freshwater are ranged from 5.53 to 16.70 ng·g⁻¹. It seems like that the concentration of PFAs in sediments is corresponding to the concentration in water; e.g., the sample with the highest concentration of PFAs in water and sediments is both from Wuyuan bay, while the sample with lowest concentration is both from the Convention Center. Although we also found the domestic sewage outfalls exist in the Convention Center, the concentration of PFAs in there is not as higher as it is predicted. The reason may attribute to the location of this site. As shown in the map in Figure 1, the Convention Center is located at the east of Xiamen Island, it faces the relatively broad Taiwan Strait, and the current in the strait may dilute the concentration of PFCs in this site.

The concentration of ΣPFAs in sediments of the freshwater is ranging from 4.53 to 5.80 ng·g⁻¹ (Table 2). Obviously, the less polluted sampling sites, reservoirs, have the lowest concentration of PFAs. The ΣPFA concentration from the sediments of the Daliao River system in northeast China were determined in the range of 0.29–1.03 ng·g⁻¹ dry weight, and the concentrations of PFOS and PFOA, dominant PFA contaminants in sediment samples, were ranging between <LOQ and 0.37 ng·g⁻¹ dry weight and from <LOQ to 0.17 ng·g⁻¹ dry weight, respectively [32]. However, the ΣPFA concentration (C2–C14) in sediments from Shanghai is in the range of 62.5–276.9 ng·g⁻¹ [33]. Lin et al. has investigated the sediment from the Science Park of Taiwan, and the results showed that, in sediment samples, predominant contaminants were PFOS (1.5–78 ng/g), PFOA (0.5–5.6 ng/g), and perfluorododecanoic acid (PFDoA) (n.d.-5.4 ng/g) [34]. Generally speaking, when compared to other sediments, the PFA concentration levels in Xiamen are in a relatively lower level.

As shown in Figure 3, the PFA concentration in water is highly positive correlated with the PFA concentration in sediment, with the correlation coefficient as higher as 0.85. It means that the PFAs could migrate between water and sediment, and the migration has a significant linear correlation. According to the previous studies, the major factor that controls the migration and transportation is the organic matter in water and sediments [22, 35].

3.3. PFA Distribution in Organisms. As shown in Table 3, all six PFAs were detected in the organism in Xiamen both from seawater and freshwater. The total concentration of PFAs ranges from 7.68 to 17.56 ng·g⁻¹. It is obvious that the organism from Gulf Park and Wuyuan Bay have the relatively higher PFA concentration. Based on above results, we know that the water and sediment samples from Gulf Park and Wuyuan Bay also have relatively higher PFA concentrations. It seems like that the PFA concentration in organisms correlated with the concentration in the environment where they are living in.

According to previous studies, PFOA and PFOS are always the dominant pollutants of PFAs. In the muscle samples of fish from the Keya River and the Keelung River in

TABLE 2: Distribution of PFAs in sediments.

Location	Water temperature (°C)	<i>n</i>	PFOA (ng·g ⁻¹)	PFOS (ng·g ⁻¹)	ΣPFAs (ng·g ⁻¹)
<i>Seawater</i>					
Xinglin Bay	18.5	3	1.05	1.23	8.14–8.61
Fenglin	18.8	3	1.47	2.09	8.58–8.8
Gulf Park	18.2	3	1.32	2.17	8.66–10.26
Convention Center	18.1	3	1.11	1.15	7.43–7.45
Wuyuan Bay	18.5	3	1.89	1.18	12.13–12.89
Jimei Bridge	18.4	3	1.21	1.30	8.11–8.71
<i>Freshwater</i>					
Bantou Reservoir (middle)	19.3	3	1.09	1.17	4.53–5.37
Bantou Reservoir (tail area)	19.1	3	1.41	1.16	4.93–5.80

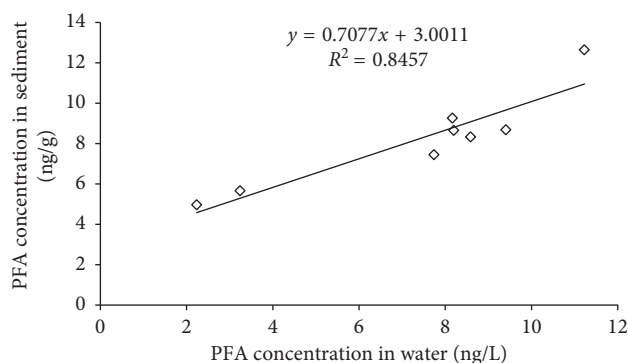


FIGURE 3: Relationship between PFA concentration in water and sediment.

TABLE 3: Concentrations of PFAs in aquatic organism.

Location	Species	<i>n</i>	PFOA* (ng·g ⁻¹)	PFOS* (ng·g ⁻¹)	ΣPFAs (ng·g ⁻¹)
<i>Seawater</i>					
Fenglin	Kelp (<i>Thallus laminariae</i>)	3	1.64	1.42	8.15–8.92
	Ocypode stimpsoni (<i>Ocypode stimpsoni</i> Ortmann)	3	1.34	2.47	7.82–12.91
Jimei Bridge	Kelp (<i>Thallus laminariae</i>)	3	1.69	1.62	8.34–8.80
	Ocypode stimpsoni (<i>Ocypode stimpsoni</i> Ortmann)	3	1.44	1.26	7.78–8.03
	Ostrea gigas (<i>Crassostrea gigas</i>)	3	1.39	1.22	7.68–7.97
	<i>Clibanarius infraspinus</i>	3	1.42	1.22	7.73–8.06
Gulf Park	Kelp (<i>Thallus laminariae</i>)	3	1.70	3.58	8.66–10.26
	Ostrea gigas (<i>Crassostrea gigas</i>)	3	1.85	1.32	16.41–17.56
	<i>Tridentiger trignocephalus</i>	3	3.11	1.66	10.97–12.93
Wuyuan Bay	Kelp (<i>Thallus laminariae</i>)	3	4.36	3.05	12.13–12.89
<i>Freshwater</i>					
Bantou Reservoir	Grass carp (<i>Ctenopharyngodon idellus</i>)	3	1.57	1.67	8.87–10.66

*The value in this column is in mean value.

Taiwan, PFOS accounted for 76–84% and 55–64% of all PFAAs, respectively, and the concentration of PFOA is in the second position [36]. However, in this study, the concentration of PFOA and PFOS are only a little higher than other 4 PFAs. The concentration of PFOS in oysters in this study was higher than that in mussels and oysters from south China and Japan from 0.113 to 0.586 ng·g⁻¹·ww [37]. Other studies reported the concentration of PFOA and PFNA in mussels from a tidal flat area of Ariake Sea in Japan is 9.5 and 1.6 ng·g⁻¹·ww [38]. Generally speaking, the reported PFA concentrations in oysters were in the same magnitude, and the reason may ascribe to the similar pollution situation.

The concentration of PFOS in the fish from Keya River and Keelung River was 1,828 and 113 ng/g, respectively, which a thousand and a hundred times of the concentration in the fish from Bantou Reservoir in this study. Schuetze et al. have investigated the concentration of PFOS and PFOA in wild fish caught from different German waters, and the results showed that PFOA was not found in any of the investigated samples above the limit of quantitation of 0.27 μg·kg⁻¹ fresh weight (fw.), whereas PFOS was found in the filet samples caught from densely populated regions at levels between 8.2 and 225 μg·kg⁻¹·fw [39].

As shown in Table 4, the BCF of some organisms in Xiamen freshwater and seawater was listed. The values of

TABLE 4: Bioconcentration factors of some organisms in Xiamen freshwater and seawater.

Locations	BCF ($\times 10^3$ L/kg)							
	Kelp		<i>Ostrea gigas</i>		<i>Ocyropsis stimpsoni</i>		<i>Grass carp</i>	
	PFOA	PFOS	PFOA	PFOS	PFOA	PFOS	PFOA	PFOS
Fenglin	6.66	2.93			7.44	3.27		
Gulf Park			9.68	6.43			9.68	6.43
Wuyuan Bay	14.25	3.79						
Jimei Bridge	7.00	4.57	6.41	4.18	6.49	4.24		
Bantou Reservoir (tail)							8.16	7.96

BCF were calculated with the concentration of PFAs in organisms and the water where they live in. The calculated BCF values of PFOS were at the same order of magnitude with the values from literatures. The reported BCF value of PFOS is 4.50×10^2 in fathead minnow [40], 1.10×10^3 in rainbow trout [27], and 1.8×10^3 in zebrafish [41]. However, the BCF of PFOA in this study is much higher than that reported before. According to the literature, the BCF of PFOA is 4 in rainbow trout [41] and 3.1~9.4 in carp [9].

The previous studies indicated that only the PFAs with the carbon chain length more than 7 could accumulate in organism, and the BCF increases with the increasing carbon chain length [42]. The significant differences of the BCF value of PFOA between this study and reported values may attribute to the difference of water concentration of PFOA. The reported BCF values of PFOA were obtained from experiment that the water concentration of PFOA was set in the level of microgram per liter. However, the value in this study is calculated by the concentration of organisms and the natural water where they live in, and in most cases, the water concentration of PFOA is in nanograms per liter. Therefore, the significant difference of the PFA concentration in water leads to the significant difference of the BCF value. In addition, the environmental factors, like dissolved organic matter or salinity [43], and the different chain length of PFAs could both affect the bioaccumulation of PFAs [44]. So the data from the other area are just used as a reference.

4. Conclusion

All six PFAs were detected in water, sediments, and organisms from both freshwater samples and seawater samples. The Σ PFA concentrations ranged from 7.66 to 11.98 ng·L⁻¹ for seawater samples and from 2.12 to 8.61 ng·L⁻¹ for freshwater. The concentration of Σ PFAs in sediments was 7.43–12.89 ng·g⁻¹ and 4.53–5.80 ng·g⁻¹ in seawater and freshwater, respectively. The PFA concentration in water is highly positive correlated with the PFA concentration in sediments ($R^2=0.85$). The calculated bioaccumulation (BCF) was 6412–14254 L·kg⁻¹ and 2927–7959 L·kg⁻¹ for PFOA and PFOS, respectively. PFOA seems more bioaccumulative than PFOS in seawater.

Data Availability

The data used to support the findings of this study are available from the corresponding author upon request.

Conflicts of Interest

The authors declare that they have no conflicts of interest.

Acknowledgments

This study was supported by the Key Laboratory of Environmental Biotechnology (XMUT), Fujian Province University (EBL2018003), and Xiamen Science and Technology Planning Project (3502Z20183064).

References

- [1] E. Kissa, "Fluorinated surfactants and repellents: second edition, revised and expanded surfactant science series," *Journal of the American Chemical Society*, vol. 123, no. 36, p. 8882, 2001.
- [2] S. Banzhaf, M. Filipovic, J. Lewis, C. J. Sparrenbom, and R. Barthel, "A review of contamination of surface-, ground-, and drinking water in Sweden by perfluoroalkyl and polyfluoroalkyl substances (PFASs)," *Ambio*, vol. 46, no. 3, pp. 335–346, 2017.
- [3] H. P. H. Arp, C. Niederer, and K.-U. Goss, "Predicting the partitioning behavior of various highly fluorinated compounds," *Environmental Science & Technology*, vol. 40, no. 23, pp. 7298–7304, 2006.
- [4] B. Bhatarai and P. Gramatica, "Prediction of aqueous solubility, vapor pressure and critical micelle concentration for aquatic partitioning of perfluorinated chemicals," *Environmental Science & Technology*, vol. 45, no. 19, pp. 8120–8128, 2011.
- [5] J. P. Giesy and K. Kannan, "Global distribution of perfluorooctane sulfonate in wildlife," *Environmental Science & Technology*, vol. 35, no. 7, pp. 1339–1342, 2001.
- [6] K. Kannan, L. Tao, E. Sinclair, S. D. Pastva, D. J. Jude, and J. P. Giesy, "Perfluorinated compounds in aquatic organisms at various trophic levels in a great lakes food chain," *Archives of Environmental Contamination and Toxicology*, vol. 48, no. 4, pp. 559–566, 2005.
- [7] K. H. Harada and A. Koizumi, "Environmental and biological monitoring of persistent fluorinated compounds in Japan and their toxicities," *Environmental Health and Preventive Medicine*, vol. 14, no. 1, pp. 7–19, 2009.
- [8] S. Rayne and K. Forest, "Perfluoroalkyl contaminants in an Arctic marine food web: trophic magnification and wildlife exposure," *Environmental Science & Technology*, vol. 43, no. 15, p. 6112, 2009.
- [9] N. Yamashita, K. Kannan, S. Taniyasu, Y. Horii, G. Petrick, and T. Gamo, "A global survey of perfluorinated acids in oceans," *Marine Pollution Bulletin*, vol. 51, no. 8–12, pp. 658–668, 2005.

- [10] X. Ju, Y. Jin, K. Sasaki, and N. Saito, "Perfluorinated surfactants in surface, subsurface water and microlayer from Dalian coastal waters in China," *Environmental Science & Technology*, vol. 42, no. 10, pp. 3538–3542, 2008.
- [11] C. J. Young, V. I. Furdul, J. Franklin, R. M. Koerner, D. C. G. Muir, and S. A. Mabury, "Perfluorinated acids in Arctic snow: new evidence for atmospheric formation," *Environmental Science & Technology*, vol. 41, no. 10, pp. 3455–3461, 2007.
- [12] S. B. Nash, S. R. Rintoul, S. Kawaguchi et al., "Perfluorinated compounds in the antarctic region: ocean circulation provides prolonged protection from distant sources," *Environmental Pollution*, vol. 158, no. 9, pp. 2985–2991, 2010.
- [13] P. Zhao, X. Xia, J. Dong et al., "Short- and long-chain perfluoroalkyl substances in the water, suspended particulate matter, and surface sediment of a turbid river," *Science of the Total Environment*, vol. 568, pp. 57–65, 2016.
- [14] Y. H. Jin, H. M. Qin, Y. X. Ma et al., "The status quo of perfluorooctane sulfonate (PFOS) pollution in tap water and different waters in partial areas of China," *China Environmental Science*, vol. 24, no. 2, pp. 166–169, 2004.
- [15] S. Chen, X.-C. Jiao, N. Gai et al., "Perfluorinated compounds in soil, surface water, and groundwater from rural areas in eastern China," *Environmental Pollution*, vol. 211, pp. 124–131, 2016.
- [16] W. Liu, W. He, J. Wu, N. Qin, Q. He, and F. Xu, "Residues, bioaccumulations and biomagnification of perfluoroalkyl acids (PFAAs) in aquatic animals from lake Chaohu, China," *Environmental Pollution*, vol. 240, pp. 607–614, 2018.
- [17] Y. Gao, J. Fu, L. Zeng et al., "Occurrence and fate of perfluoroalkyl substances in marine sediments from the Chinese Bohai sea, yellow sea, and east China sea," *Environmental Pollution*, vol. 194, no. 6, pp. 60–68, 2014.
- [18] B. L. Liu, H. Zhang, L. W. Xie et al., "Pollution characteristics of perfluorinated compounds in offshore marine area of Shenzhen," *Environmental Science*, vol. 36, no. 6, pp. 2028–2037, 2015.
- [19] S. J. Zhao, C. Pei, C. K. Zhu et al., "Pollution characteristics of PFOS and PFOA in water and sediment samples from Wenzhou inshore," *Marine Environmental Science*, vol. 31, no. 4, pp. 221–224, 2012.
- [20] R. Sun, M. Wu, L. Tang et al., "Perfluorinated compounds in surface waters of Shanghai, China: source analysis and risk assessment," *Ecotoxicology and Environmental Safety*, vol. 149, pp. 88–95, 2018.
- [21] M. K. So, Y. Miyake, W. Y. Yeung et al., "Perfluorinated compounds in the Pearl River and Yangtze River of China," *Chemosphere*, vol. 68, no. 11, pp. 2085–2095, 2007.
- [22] K. J. Hansen, L. A. Clemen, M. E. Ellefson, and H. O. Johnson, "Compound-specific, quantitative characterization of organic fluorochemicals in biological matrices," *Environmental Science & Technology*, vol. 35, no. 4, pp. 766–770, 2001.
- [23] S. Taniyasu, K. Kannan, M. K. So et al., "Analysis of fluorotelomer alcohols, fluorotelomer acids, and short- and long-chain perfluorinated acids in water and biota," *Journal of Chromatography A*, vol. 1093, no. 1-2, pp. 89–97, 2005.
- [24] S. Barreca, M. Busetto, M. Vitelli, L. Colzani, L. Clerici, and P. Dellavedova, "Online solid-phase extraction LC-MS/MS: a rapid and valid method for the determination of perfluorinated compounds at sub ng-L⁻¹ level in natural water," *Journal of Chemistry*, vol. 2018, Article ID 3780825, 9 pages, 2018.
- [25] S. Taniyasu, N. Yamashita, K. Kannan et al., "Perfluorinated carboxylates and sulfonates in open ocean waters of the Pacific and Atlantic oceans," *Organohalogen Compounds*, vol. 66, pp. 4035–4039, 2004.
- [26] Z. Dai, X. Xia, J. Guo, and X. Jiang, "Bioaccumulation and uptake routes of perfluoroalkyl acids in *Daphnia magna*," *Chemosphere*, vol. 90, no. 5, pp. 1589–1596, 2013.
- [27] J. W. Martin, S. A. Mabury, K. R. Solomon, and D. C. G. Muir, "Bioconcentration and tissue distribution of perfluorinated acids in rainbow trout (*Oncorhynchus mykiss*)," *Environmental Toxicology & Chemistry*, vol. 22, no. 1, pp. 196–204, 2010.
- [28] D. Skutlarek, M. Exner, and H. Frber, "Perfluorierte Tenside (PFT) in der aquatischen Umwelt und im Trinkwasser," *Environmental Sciences and Pollutant Research*, vol. 18, no. 3, pp. 151–154, 2006.
- [29] K. Kannan, J.-W. Choi, N. Iseki et al., "Concentrations of perfluorinated acids in livers of birds from Japan and Korea," *Chemosphere*, vol. 49, no. 3, pp. 225–231, 2002.
- [30] M. Cai, Z. Zhao, H. Yang et al., "Spatial distribution of per- and polyfluoroalkyl compounds in coastal waters from the east to south China sea," *Environmental Pollution*, vol. 161, no. 1, pp. 162–169, 2012.
- [31] S. Zheng, B. Chen, X. Qiu, M. Chen, Z. Ma, and X. Yu, "Distribution and risk assessment of 82 pesticides in Jiulong River and estuary in south China," *Chemosphere*, vol. 144, pp. 1177–1192, 2016.
- [32] J. Bao, W. Liu, L. Liu, Y. Jin, X. Ran, and Z. Zhang, "Perfluorinated compounds in urban river sediments from Guangzhou and Shanghai of China," *Chemosphere*, vol. 80, no. 2, pp. 123–130, 2010.
- [33] F. Li, C. Zhang, Y. Qu et al., "Quantitative characterization of short- and long-chain perfluorinated acids in solid matrices in Shanghai, China," *Science of the Total Environment*, vol. 408, no. 3, pp. 617–623, 2010.
- [34] Y. C. Lin, W. P. Lai, H. H. Tung, and Y. C. Lin, "Occurrence of pharmaceuticals, hormones, and perfluorinated compounds in groundwater in Taiwan," *Environmental Monitoring & Assessment*, vol. 187, no. 5, pp. 1–19, 2015.
- [35] M. Haitzer, S. Höss, W. Traunspurger, and C. Steinberg, "Effects of dissolved organic matter (DOM) on the bioconcentration of organic chemicals in aquatic organisms—a review—," *Chemosphere*, vol. 37, no. 7, pp. 1335–1362, 1998.
- [36] A. Y.-C. Lin, S. C. Panchangam, Y.-T. Tsai, and T.-H. Yu, "Occurrence of perfluorinated compounds in the aquatic environment as found in science park effluent, river water, rainwater, sediments, and biotissues," *Environmental Monitoring and Assessment*, vol. 186, no. 5, pp. 3265–3275, 2014.
- [37] M. K. So, S. Taniyasu, P. K. S. Lam, G. J. Zheng, J. P. Giesy, and N. Yamashita, "Alkaline digestion and solid phase extraction method for perfluorinated compounds in mussels and oysters from south China and Japan," *Archives of Environmental Contamination and Toxicology*, vol. 50, no. 2, pp. 240–248, 2006.
- [38] H. Nakata, K. Kannan, T. Nasu, H.-S. Cho, E. Sinclair, and A. Takemura, "Perfluorinated contaminants in sediments and aquatic organisms collected from shallow water and tidal flat areas of the Ariake sea, Japan: environmental fate of perfluorooctane sulfonate in aquatic ecosystems," *Environmental Science & Technology*, vol. 40, no. 16, pp. 4916–4921, 2006.
- [39] A. Schuetz, T. Heberer, S. Effkemann, and S. Juergensen, "Occurrence and assessment of perfluorinated chemicals in wild fish from northern Germany," *Chemosphere*, vol. 78, no. 6, pp. 647–652, 2010.
- [40] G. Ankley, D. Kuehl, M. Kahl et al., "Reproductive and developmental toxicity and bioconcentration of

perfluorooctanesulfonate in a partial life-cycle test with the fathead minnow (*Pimephales promelas*),” *Environmental Toxicology & Chemistry*, vol. 24, no. 9, pp. 2316–2324, 2010.

- [41] W. Wen, X. Xia, D. Zhou et al., “Bioconcentration and tissue distribution of shorter and longer chain perfluoroalkyl acids (PFAAs) in zebrafish (*Danio rerio*): effects of perfluorinated carbon chain length and zebrafish protein content,” *Environmental Pollution*, vol. 249, pp. 277–285, 2019.
- [42] J. M. Conder, R. A. Hoke, W. D. Wolf, M. H. Russell, and R. C. Buck, “Are PFCAs bioaccumulative? A critical review and comparison with regulatory criteria and persistent lipophilic compounds,” *Environmental Science & Technology*, vol. 42, no. 4, pp. 995–1003, 2008.
- [43] Z. N. Dai, A. L. Yang, and H. Y. Fu, “Study on the effects of DOM on the bioaccumulation of perfluorinated acids in *Daphnia magna*,” *IOP Conference Series: Earth and Environmental Science*, vol. 146, article 012067, 2018.
- [44] W. Wen, X. Xia, D. Hu et al., “Long-chain perfluoroalkyl acids (PFAAs) affect the bioconcentration and tissue distribution of short-chain PFAAs in zebrafish (*Danio rerio*),” *Environmental Science & Technology*, vol. 51, no. 21, pp. 12358–12368, 2017.